International
Progress Report

IPR-04-05

Äspö Hard Rock Laboratory

Analysis of overcoring stress data at the Äspö HRL, Sweden

Analysis of overcoring rock stress measurements preformed using the Borre Probe

Daniel Ask, KTH/LTU, Sweden

Francois H. Cornet, IPGP, France

Ove Stephansson, GFZ, Germany

December 2002

Svensk Kärnbränslehantering AB
Swedish Nuclear Fuel
and Waste Management Co
Box 5864
SE-102 40 Stockholm Sweden
Tel 08-459 84 00
+46 8 459 84 00
Fax 08-661 57 19
+46 8 661 57 19

Äspö Hard Rock
Laboratory

Report no.
IPR-04-05
No.
F86K
Author
Daniel Ask
Francois H. Cornet
Ove Stephansson
Date
Dec. 2002
Checked by
Rolf Christiansson
Date
Approved
Christer Svemar
Date
2004-06-09

Äspö Hard Rock Laboratory

Analysis of overcoring stress data at the Äspö HRL, Sweden

Analysis of overcoring rock stress measurements preformed using the Borre Probe

Daniel Ask, KTH/LTU, Sweden

Francois H. Cornet, IPGP, France

Ove Stephansson, GFZ, Germany

December 2002

Keywords: Rock stress, overcoring, Borre Probe, Äspö HRL

Abstract

This report describes a detailed analysis of existing overcoring rock stress data from the Borre Probe at the Äspö HRL and central Oskarshamn, Sweden. The aim of the study is to create a new overcoring strain database on which future work and stress determinations will be based. For this purpose, a new analysis method for overcoring strain data has been developed. In principle, the method involves detailed analysis of the strain versus time curves recorded approximately 30 minutes before and 20 minutes after the overcoring phase. The uncertainty of each strain gauge is based on: (1) the stability of the strain gauges before and after the overcoring phase; and (2) the difference between the calculated and observed strain.

The biaxial tests for determination of the elastic parameters E and ν have also been analyzed in detail. These parameters have been determined using the secant modulus and unloading curves and at pressures as close to the measured *in situ* stress values as possible.

The analysis of Borre Probe data presented in this report revealed that 64 strain gauges out of 729 are erroneous. Furthermore, 252 strain gauges are of doubtful quality, 22 measurement points requires temperature corrections (mainly borehole KK0045G01) and another 11 measurement points indicate a high temperature in the test section (borehole KAS05 not included in analysis). However, the temperature variation is difficult to correct for since the data file is incomplete. During the measurements in borehole KA0093A01 and most data from KOV01 the temperature-measuring device was malfunctioning. Borehole KAS05 was excluded because the raw data was not found.

Based on the results from the re-analysis of the Borre Probe stress data, following recommendation for future testing are made: (1) The borehole bottom should always be flattened before drilling of the pilot hole commences and the guiding cylinders used to centralize the pilot hole should be in good condition. This will reduce the risk for a decentralized, non-axial pilot hole as well as possible misplacing of the cell during installation; (2) The analysis should include verification of glue bonding between the rosettes and the rock and glue hardening; (3) The core should be investigated and documented thoroughly with respect to glue bonding, position of strain rosettes, grain size distribution, fractures etc, and with respect to possible decentralized or non-axial pilot hole; (4) The relatively thin core used is sensitive to drilling induced microfracturing and the maximum applicable load during the biaxial test is 10 MPa (which may be significantly lower than the measured *in situ* stresses). Thus, an overcoring drill bit giving a thicker core will reduce these deficits; (5) Due to the position of the temperature measuring device, the flushing water temperature is recorded and not the temperature at the position of the strain gauges. It is therefore important that the temperature, prior to core break, is constant and preferably at the same level as the *in situ* rock mass temperature before overcoring start.

After re-analysis, a standard least squares program was used to determine the stresses in single measurement points and the results are compared with the published material. The stress calculation using re-analyzed data indicates in general slightly lower principal and horizontal stress magnitudes compared to the published material. An exception is borehole KOV01, where larger magnitudes were found. The orientations of the principal and horizontal stresses were not significantly different.

Sammanfattning

Denna rapport innehåller en detaljerad analys av existerande överborrningdata vid Äspö HRL, Sverige. Målet med studien är att etablera en ny töjningsdatabas på vilken framtida arbete och spänningsbestämningar kommer att vara baserade. För detta ändamål har en ny analysmetod utvecklats. Metoden består i princip av att analysera töjningsdata ca 30 minuter före och 20 minuter efter överborrningsfasen. Kvalitén för varje töjningsgivare bestäms av två delar: (1) stabiliteten av givare före och efter överborrningsfasen samt (2) skillnaden mellan beräknad och uppmätt töjning.

Biaxialtesterna som används för bestämning av de elastiska parametrarna E och ν har också detaljstuderats. Dessa parametrar har bestämts med sekantmetoden på avlastningskurvorna och med laster som ligger så nära spänningsnivån *in situ* som möjligt.

Analysen av Borre Probe data har visat att 64 givare av 729 inte fungerat samt 252 givare är förknippade med osäkerheter. Vidare kräver 22 mätpunkter temperaturkorrektion (främst borrhål KK0045G01) och ytterligare 11 punkter indikerar en hög temperatur i testsektionen. Temperaturkorrektionen är dock svår att genomföra eftersom datafilerna inte är kompletta. Under mätningarna i KF0093A01 och flertalet mätpunkter i borrhål KOV01 fungerade inte temperaturgivaren varför tempereturеffekter ej kunde studeras. Borrhål KAS05 har ej omtolkats eftersom rådata inte lokaliserats.

Baserat på resultaten från omtolkningarna av Borre Probe data, kan följande rekommendationer göras: (1) Innan borrning av pilothålet inleds bör botten av hålet vara planat och styrcylindrarna som centraliserar pilothålet bör vara i god kondition. I kombination reducerar dessa förslag risken för decentraliserade och icke-axiella pilothål liksom risken för felplacering av töjningsrosetter; (2) Analysen av data bör inkludera verifiering av härdning av limmet och en korrekt limningen mellan töjningsrosetter och berg; (3) Kärnan bör studeras och dokumenteras noga med avseende på limning, position av töjningsrosetter, kornstorleksfördelning, sprickor mm. Pilothålets orientering bör också dokumenteras, speciellt om hålet är decentralicerat och/eller icke-axialt; (4) Den relativt tunna kärnan är känslig för inducering av microsprickor och biaxialtesterna kan enbart utföras med maximal last av 10 MPa. Det senare innebär att elastiska parameterar utvärderas vid lägre tryck än vad som ev. uppmäts *in situ*. En större överborrningsdiameter skulle reducera dessa problem; (5) På grund av att temperaturgivaren mäter spolvattentemperaturen och inte bergtemperaturen vid töjningsgivarna, är det av stor vikt att mätcellen lämnas kvar i hålet tills temperaturen är konstant och helst har nått samma nivå som innan testet började.

Efter omtolkning av data användes ett standard minsta-kvadrat program för att bestämma spänningarna i enskilda mätpunkter. De nya spänningsberäkningarna indikerar generellt något mindre magnituder för huvud- och horisontalspänningarna jämfört med publicerade resultat. Ett undantag utgör mätningarna i borrhål KOV01, där högre magnituder erhölls. Orienteringarna av huvud- och horisontalspänningarna påverkas obetydligt av applicerad analys.

Table of contents

1 Introduction

1.1 General

The Äspö Hard Rock Laboratory (HRL) of the Swedish Nuclear Fuel and Waste Management Co. (SKB) has been a geoscientific research area since 1986 (Fig. 1-1). The underground laboratory provides an implementation and operation test site for a future deep repository in Sweden. The vast number of research projects conducted has enabled valuable development and verification of site characterization methods from ground surface, boreholes and underground excavations, among them *in situ* rock stress measurements.

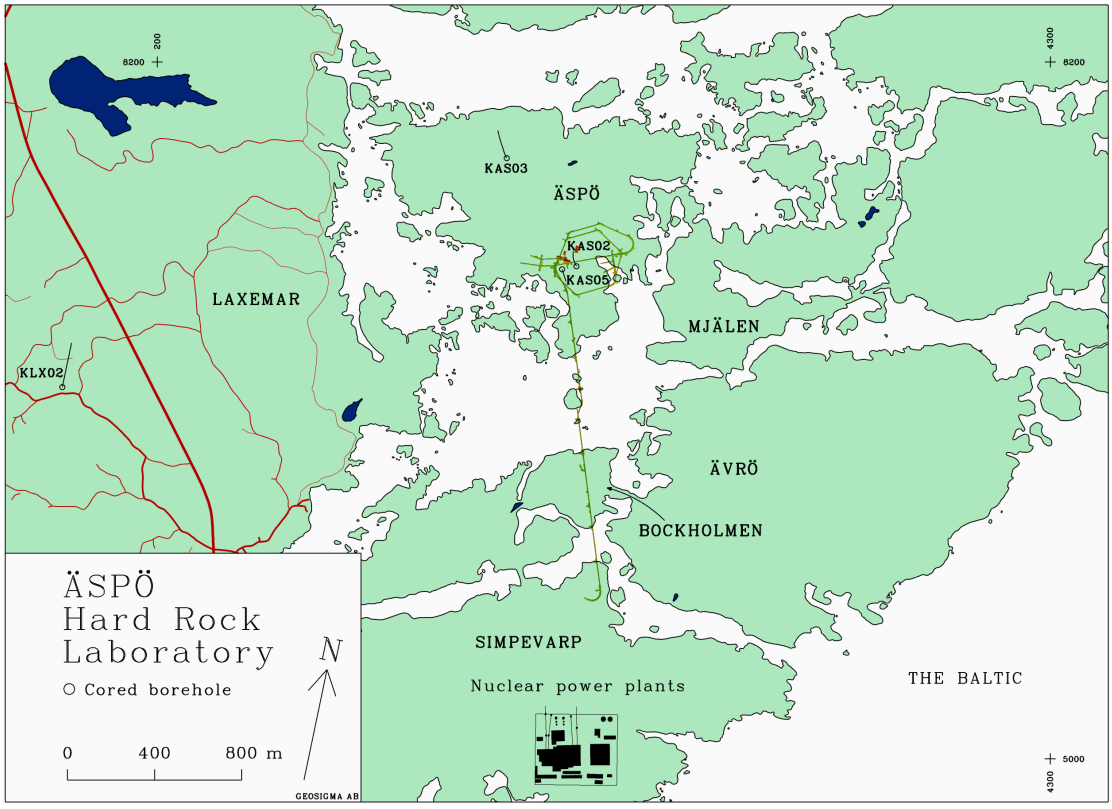

Figure 1-1. *Surface borehole locations in the Äspö region where rock stress measurements have been conducted (Modified after Ekman (2001)).*

A detailed knowledge of the *in situ* stress field is important for several rock-engineering aspects, including investigation, design, construction, and performance of engineered structures built on, in or of rock. Storage facilities for hazardous waste, e.g. spent nuclear fuel are suggested to be located in rock at great depth. A full understanding of the stresses is essential in order to provide (i) boundary conditions for the storage facility; (ii) means to make a proper design and to analyze the mechanical response and possible failure of the rock mass; and (iii) insight on how fluids flow underground (Stephansson, 1997).

Generally, in-situ stress measuring techniques consist of disrupting the rock. The response associated with the disturbance, and often also the process of the disturbance itself, is measured (strain, displacement or hydraulic pressure record) and analyzed by making several assumptions about the rock's constitutive behavior. Over the past 30 years, numerous techniques have been developed and improved. These may be divided into six main groups: hydraulic methods, relief methods, jacking methods, strain recovery methods, borehole breakout methods, and others (Amadei and Stephansson, 1997).

Hydraulic stress measurements record the state of stress in boreholes using fluid pressure to open, generate, propagate and reopen fractures in rock. The directions of the in-situ stresses using hydraulic methods are inferred by inversion techniques or by observing or measuring the orientation of hydraulically induced fractures. The hydraulic methods may be divided into three subgroups: hydraulic fracturing measurements (HF), sleeve fracturing, and hydraulic test in pre-existing fractures (HTPF).

The general idea behind overcoring, or relief, methods are to isolate a rock sample, partially or wholly, from the stress field in the surrounding rock volume and to measure its response (Merrill, 1964; Amadei and Stephansson, 1997). The stresses are inferred from strain or displacement measurements created by the stress relief. A number of assumptions have to be made in order to determine the stress field: (1) the rock behaves as an ideally linear elastic material; (2) the rock is isotropic (anisotropic solution exists for some cells); (3) the material is continuous and subjected to a homogeneous stress field in the volume of interest. The assumption regarding an elastic and isotropic rock material implies that elastic theory applies, hence the deformation of the core sample during overcoring is assumed identical in magnitude to that by the *in situ* stress field but of opposite sign. Application of elastic theory also requires knowledge of the elastic parameters of the rock, Young's modulus, E, and Poisson's ratio, ν.

1.2 Background

The results of the *in situ* hydraulic stress measurements at Äspö indicate a non-linear stress distribution versus depth and the magnitudes seems influenced by discontinuities (Bjarnason et al., 1989; Leijon, 1995; Hansson et al., 1995; Ljunggren and Klasson, 1997; Ekman, 1997; Ekman et al., 1997; Ask, 2001; Ask et al., 2001a and 2001b; Christiansson and Jansson, 2002; Hudson, 2002; Hakami et al., 2002; Ask et al, 2003), see also Figs. 1-3 to 1-9.

When comparing the hydraulic and overcoring stress measurement results, there is a considerable difference in the stress magnitudes. Generally, the overcoring stress measurements (all cells) indicate larger or even much larger magnitudes compared to the hydraulic stress measurements. The orientation of the maximum horizontal stress is though rather consistent for both methods, NW-SE.

The discrepancies between the hydraulic and overcoring measurements at Äspö have been investigated by Ljunggren et al. (1998), based on statistical analyses of the Äspö stress data (Andersson, 1996 and 1997), and a comparison of the Äspö stress data with the data in the Fennoscandian Rock Stress Data Base (FRSDB) (Ljunggren and Persson, 1995). The results also indicate that the variance of the stresses at Äspö differs significantly between the methods. To some extent, this could be explained by depth-dependency, but the remaining variance is large for the two methods and presumably Gaussian distributed. However, in average, the difference is quite small (Ljunggren et al., 1998).

This report is the first of a series in which attempts to seek explanation to the observed variability in stress magnitudes are made, see Ch. 1.4.

1.3 Existing rock stress data at ÄSPÖ HRL

At Äspö the in-situ rock stress measurements consists of hydraulic fracturing stress measurements (HF), hydraulic tests in pre-existing fractures (HTPF) and overcoring stress measurements. Totally, the in-situ rock stress data consist of about 110 HF, 5 HTPF and 140 overcoring stress measurement points (including data in borehole KOV01 in central Oskarshamn), Table 1-1 and Appendix 1.

The overcoring rock stress data have been collected in 21 boreholes. KAS05 and KOV01 (in central Oskarshamn) are the only surface drilled boreholes and the remaining 19 boreholes were drilled from the underground laboratory below the island of Äspö, Fig. 1-2. Four different cells have been used: (1) The Swedish State Power Boards (SSPB) Borre Probe; (2) Three different CSIRO (Commonwealth Scientific and Industrial Research Organization) Hollow Inclusion cells (9 and 12 strain gauges respectively, the latter with thick and thin hollow inclusions); and (3) The Atomic Energy of Canada (AECL) Doorstopper. Of the total 140 measurement points, about 30 are likely to be influenced by the underground excavation (Table 1-1).

The applied data analysis is based on existing overcoring rock stress data from the Borre Probe, which have been extracted and re-evaluated from raw data and from reports (Bjarnason et al., 1989; Ljunggren and Klasson, 1996; Ljunggren and Klasson, 1997; Ljunggren and Bergsten, 1998; Klasson et al., 2001; Klasson and Andersson, 2002; Klasson et al., 2002). A number of reports relating to the rock stress data have also been reviewed (Leijon, 1995; Ekman, 1997; Ekman et al., 1997; Myrvang, 1997; Lundholm, 2000a and 2000b; Christiansson, 2000; Ask, 2001; Ask et al., 2001a and 2001b; Christiansson and Jansson, 2002; Hudson, 2002; Hakami et al., 2002). Figures 1-3 and 1-9 present the reported results from the Äspö region. The results from the above references will be used for comparison with the results obtained in the present study.

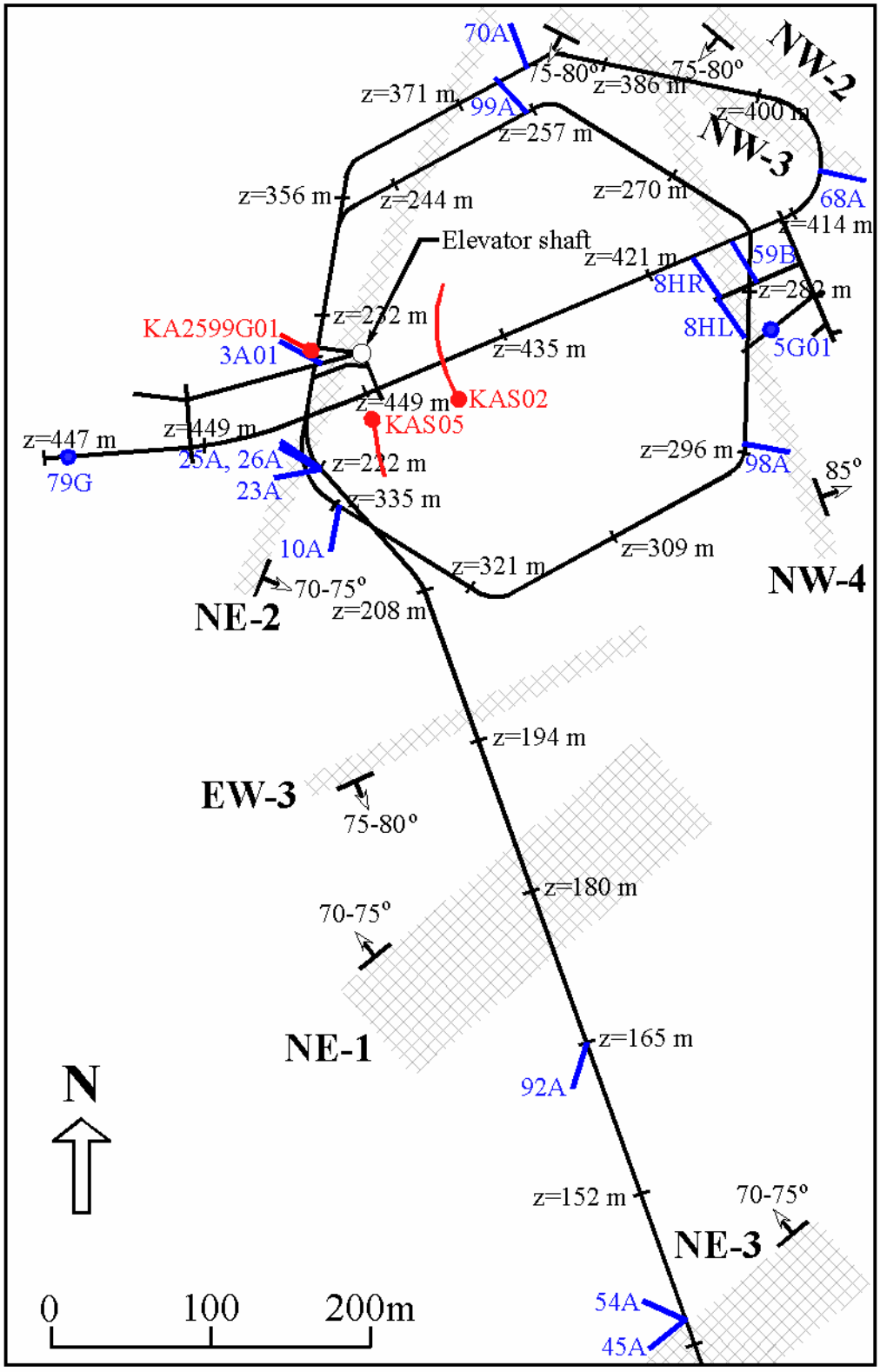

Figure 1-2. *Detailed map of the Äspö HRL showing stress measurement boreholes and major fracture zones at tunnel intersection depth. Overcoring and hydraulic fracturing boreholes are represented by solid blue and red lines, respectively. Note that the blue-marked borehole 3A01 also includes hydraulic fracturing stress data. Vertical boreholes are marked with circles and sub-vertical boreholes with circles and solid line in the borehole direction (Modified after Rhén et al, 1997).*

Table 1-1. Stress measurements performed in the Äspö region (Bjarnason et al., 1989; Lee et al., 1993; Lee et al., 1994; Litterbach et al., 1994; Ljunggren and Klasson, 1996; Ljunggren and Klasson, 1997; Ekman, 1997; Ekman et al., 1997; Nilsson et al., 1997; Ljunggren and Bergsten, 1998; Klasson et al., 2001; Klasson and Andersson, 2001; Klasson et al., 2002).

Borehole	Hydraulic data		Overcoring data			
	HF (number)	HTPF (number)	BP (number)	CHI_9 (number)	CHI_12 (number)	AECL (number)
KAS02	22	-	-	-	-	-
KAS03	21	-	-	-	-	-
KAS05	-	-	7	-	-	-
KLX02	37	5	-	-	-	-
KOV01	19	-	9	-	-	-
KA1045A	-	-	-	3	-	-
KA1054A	-	-	-	3	-	-
KA1192A	-	-	-	-	3	-
KA1623A	-	-	-	-	3	-
KA1625A	-	-	-	-	3	-
KA1626A	-	-	-	-	3	-
KA1899A	-	-	-	-	5	-
KA2198A	-	-	-	-	4	-
KA2510A	-	-	-	-	6	-
KA2870A	-	-	-	-	5	-
KA3068A	-	-	-	-	4	-
KZ0059B	-	-	-	-	6	-
KXZSD8HR	-	-	23	-	-	-
KXZSD81HR	-	-	4	-	-	-
KXZSD8HL	-	-	4	-	-	-
KK0045G01	-	-	19	-	-	-
KA2599G01	6	-	-	-	-	4
KF0093A01	6	-	4	-	-	3
KA3579G	-	-	11	-	-	-
SUM	111	5	81	6	42	7

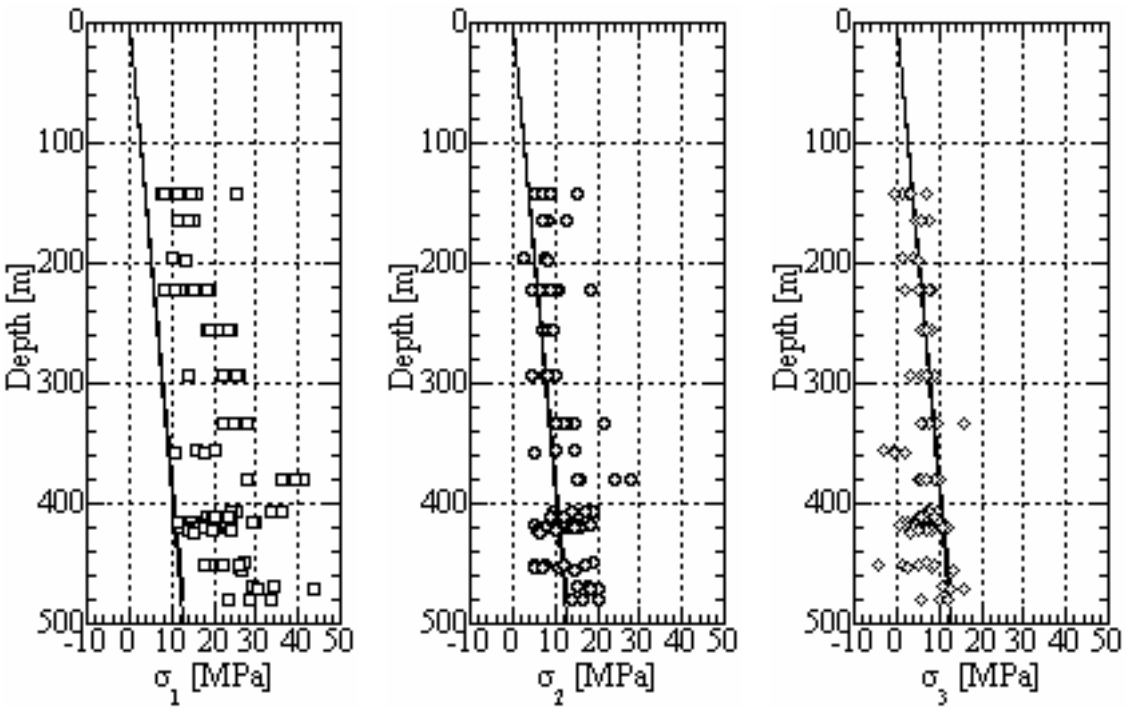

Figure 1-3. *Compilation of principal stress magnitudes versus depth from overcoring rock stress data at the Äspö HRL.*

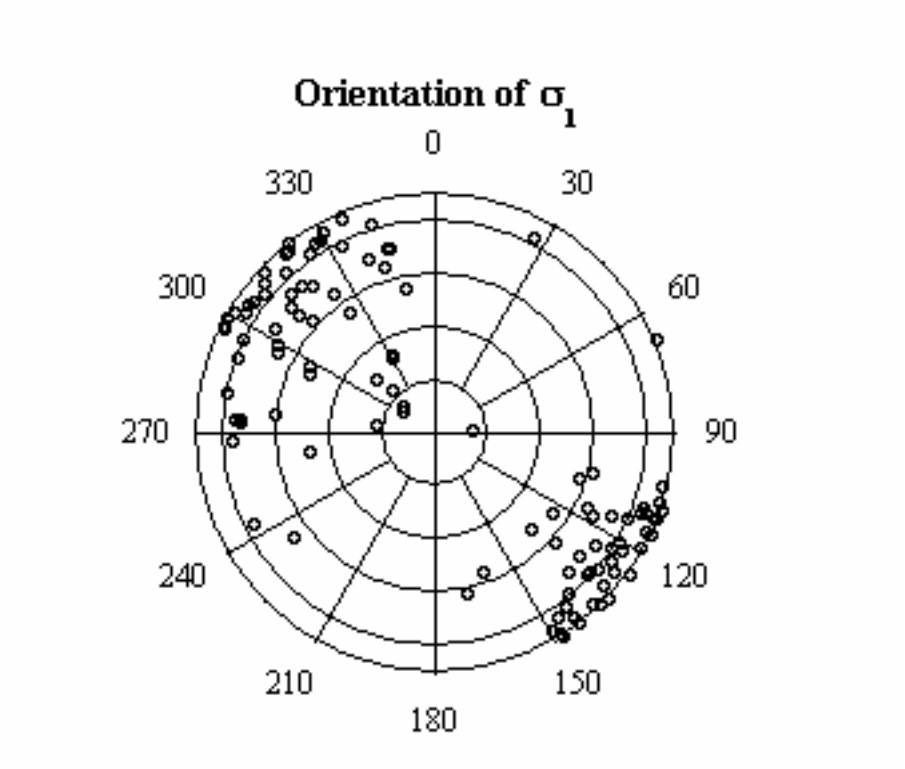

Figure 1-4. *Compilation of orientation of σ_1 between 140 to 480 m depth from overcoring rock stress measurements at the Äspö HRL.*

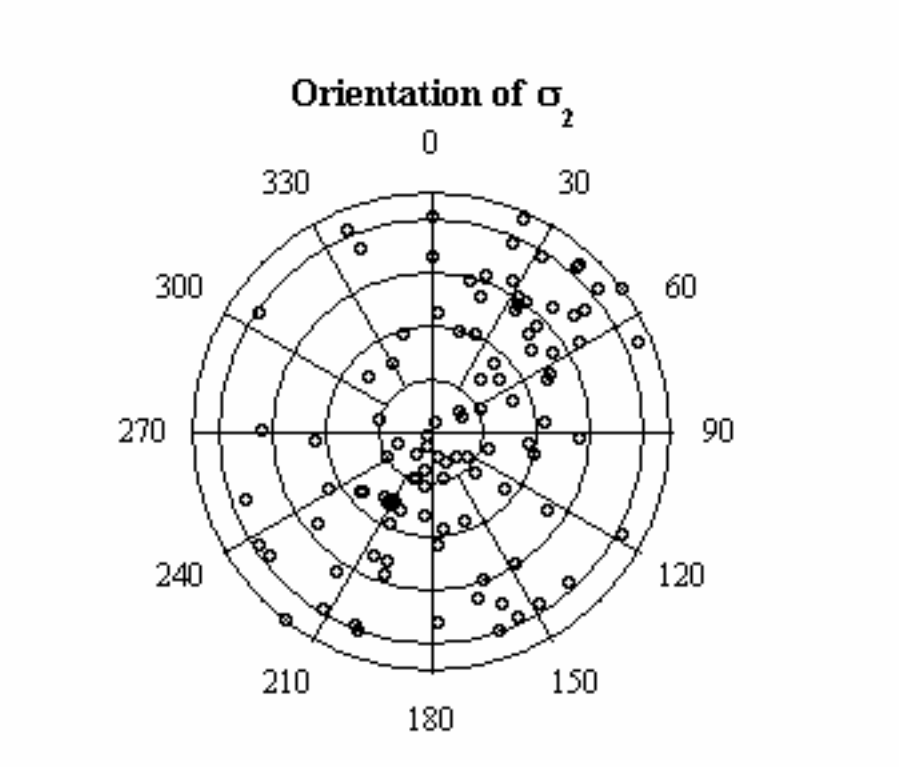

Figure 1-5. *Compilation of orientation of σ_2 between 140 to 480 m depth from overcoring rock stress measurements at the Äspö HRL.*

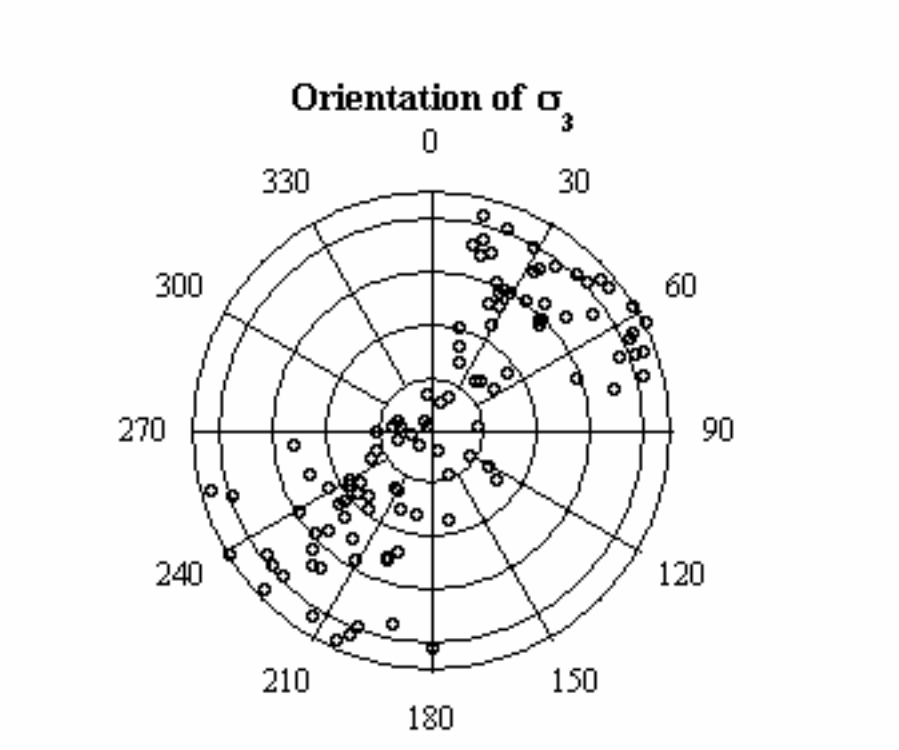

Figure 1-6. *Compilation of orientation of σ_3 between 140 to 480 m depth from overcoring rock stress measurements at the Äspö HRL.*

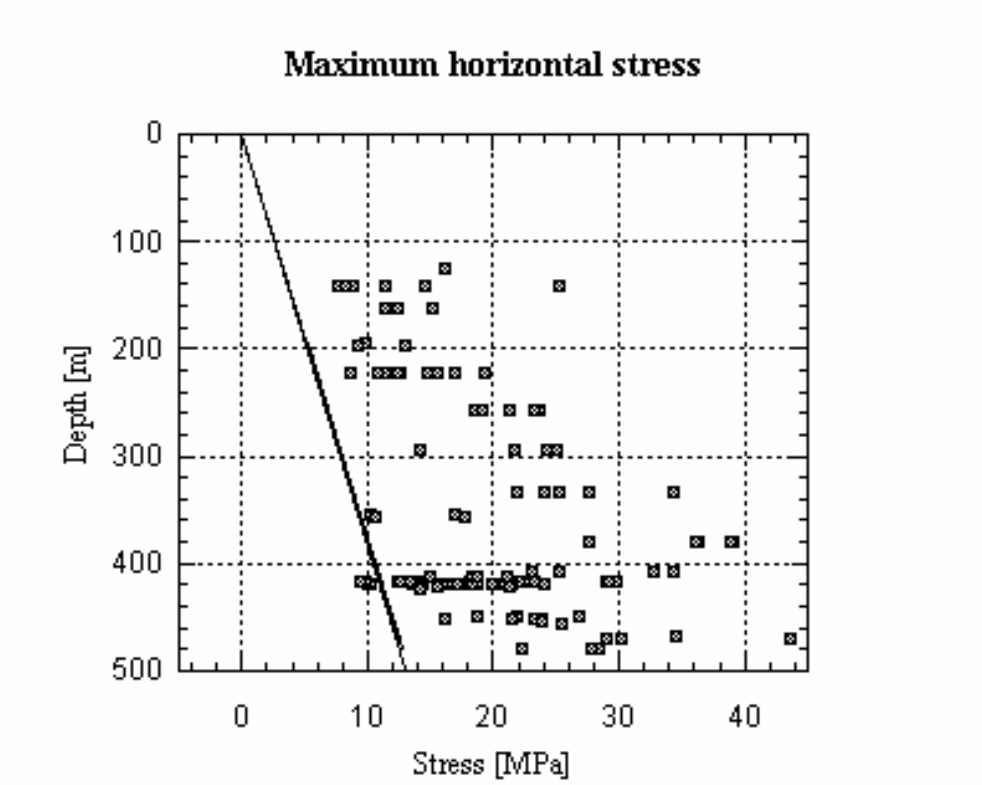

Figure 1-7. *Compilation of maximum horizontal stress magnitude versus depth from overcoring rock stress measurements at the Äspö HRL.*

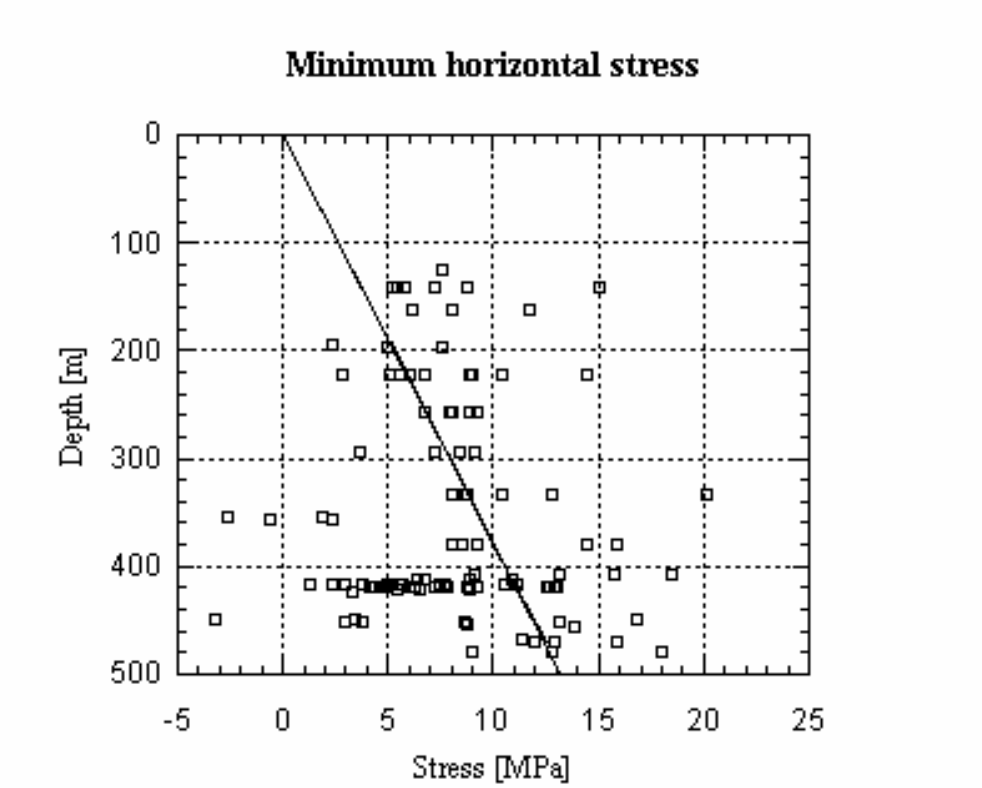

Figure 1-8. *Compilation of minimum horizontal stress magnitude versus depth from overcoring rock stress measurements at the Äspö HRL.*

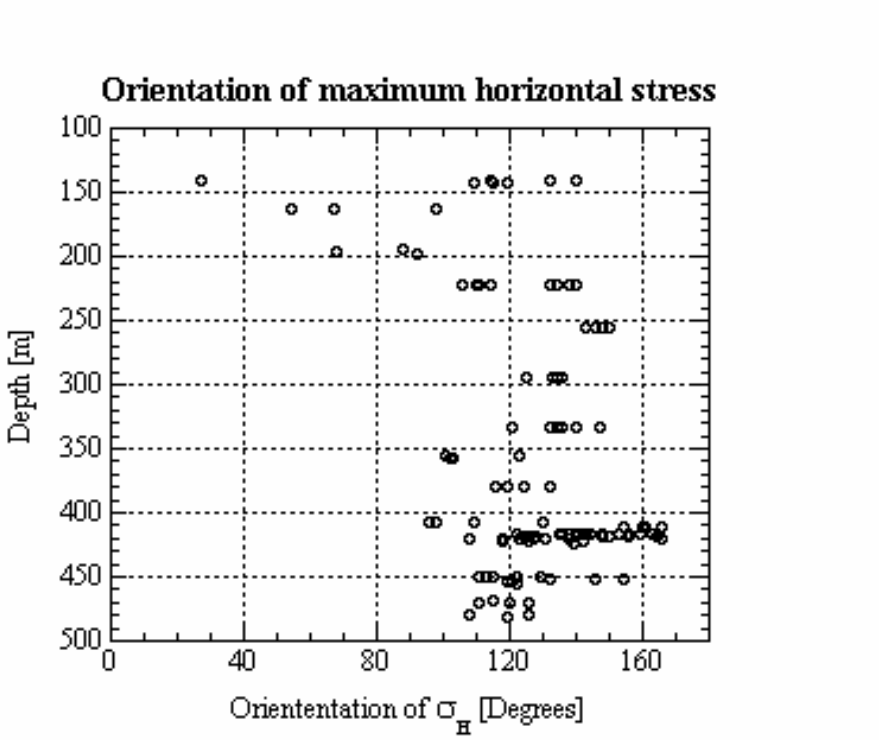

Figure 1-9. *Compilation of orientation of maximum horizontal stress versus depth from overcoring rock stress measurements at the Äspö HRL.*

1.4 Aim of study

The present study aims at improving the quality of the existing overcoring rock stress database in the Äspö region. The detailed analysis of overcoring rock stress data aim at eliminating doubtful strain gauges and thereby improve and receive a more reliable overcoring strain database. The re-analyzed strain database will be used for stress calculations at different scales and to evaluate the observed variability between different measuring techniques at Äspö HRL and improve the consistency between methods.

In this report, the overcoring strain data from the Borre Probe will be analyzed. The stress data may be grouped according to three different scales: (1) The single test scale; (2) The measuring location scale, which includes results from one or more boreholes; and (3) The application scale, representing results from a larger rock volume for a particular rock engineering problem, i.e. following the work by Gray and Toews (1974) and Leijon (1989). However, in this report, the overcoring stress data will be analyzed only as individual test points. The re-analyzed strains are also used for stress calculation using a standard least squares program and the results are compared with the published material. The other scales will be dealt with in a future studies.

This report is the second of a series in which the inversion method developed by Cornet and Valette (1984); Cornet (1993) is applied. The first report dealt with the hydraulic stress data in boreholes KAS02, KAS03 and KLX02 (Ask et al., 2001b). The third report will deal with the CSIRO HI overcoring stress data (Ask et al., in press.) and a fourth with stress determinations using the re-evaluated overcoring strain database and stress calculation programs based on the Integrated Stress Determination Method (ISDM), see e.g. Cornet (1993).

2 The overcoring cells used in the ÄSPÖ region

2.1 General

The measurements performed at the Äspö HRL are so-called borehole relief methods (Amadei and Stephansson, 1997). The relief process is in this case accomplished by drilling a large borehole concentric with an existing borehole (pilot hole), in which the measurement cell is located (see Fig. 2-1).

2.2 The Swedish state power board's Borre Probe

2.2.1 General

The Borre Probe is a CSIR-type (Council for Scientific and Industrial Research) of triaxial strain cell developed by Leeman and Hayes (1966). The automatic Borre Probe is a development of the non-automatic Hiltscher SSPB-probe (Hiltscher et al., 1979; Hallbjörn, 1986). The Borre probe is the only three-dimensional overcoring cell that permits measurements in deep, water-filled boreholes. The methodology for the automatic Borre Probe is described in Hallbjörn et al. (1989 and 1990).

2.2.2 Techniques, equipment and procedures

The Borre Probe technique is based on coring a ϕ76 mm borehole (Craelius T2-76) over a coaxial small-diameter (ϕ36 mm) pilot hole, usually 50 cm deep, in which the strain-measuring instrument is located, Fig. 2-1. The resulting outer and inner cylinder diameter is 62 and 36 mm respectively.

The Borre Probe has recently been upgraded to employ wireline drilling (Hagby WL-76) for the pilot hole, thus reducing time requirements drastically for deep measurements. The overcoring is though core drilled with conventional technique (Sjöberg and Klasson, 2002).

The probe automatically measures the strain and temperature before, during and after overcoring. The measurement interval is normally 1 minute (valid for all tests analyzed in this report). Recently, the Borre Probe was also upgraded with a new logger which has two recording modes: (1) sparse recording (every 15 minutes) during time of activation and selected time for dense recording; and (2) dense recording in user-specified intervals between 3 and 60 seconds. For both recordings, strain gauge values are being sampled during a 20 ms period (64 discrete readings) which then are averaged to filter low-frequency noise in gauges, A/D-converters, etc (Sjöberg and Klasson, 2002).

The strain and the temperature values are stored in a logger unit without connection to the ground surface. In the latest version of the Borre Probe, an automatic temperature compensation is included (this was previously done during post-processing of the data). The probe also contains a magnetic compass giving the orientation of the probe downhole. The compass contains a fluid, which freezes at temperatures below 15° C thereby fixing the position of the compass needle. A detailed description of the cell is presented in Fig. 2-2.

The probe includes three strain rosettes attached to plastic cantilever arms, 120° apart, at the lower end of the probe, which is the only part of the instrument that enters into the pilot hole (Fig. 2-3). These must be attached properly to the rock before overcoring, which is done with an adhesive. The adhesive used is a two-component acrylic resin when the rock temperature is between 5-10 °C. At higher temperatures or when cementing is done overnight, a two-component epoxy resin is used. The glue is kept in a glue pot (Fig. 2-2) in which the strain tongues are submerged when lowering into the borehole. During installation in the pilothole, the glue pot is automatically pushed away when the adaptor reaches the bottom of the hole.

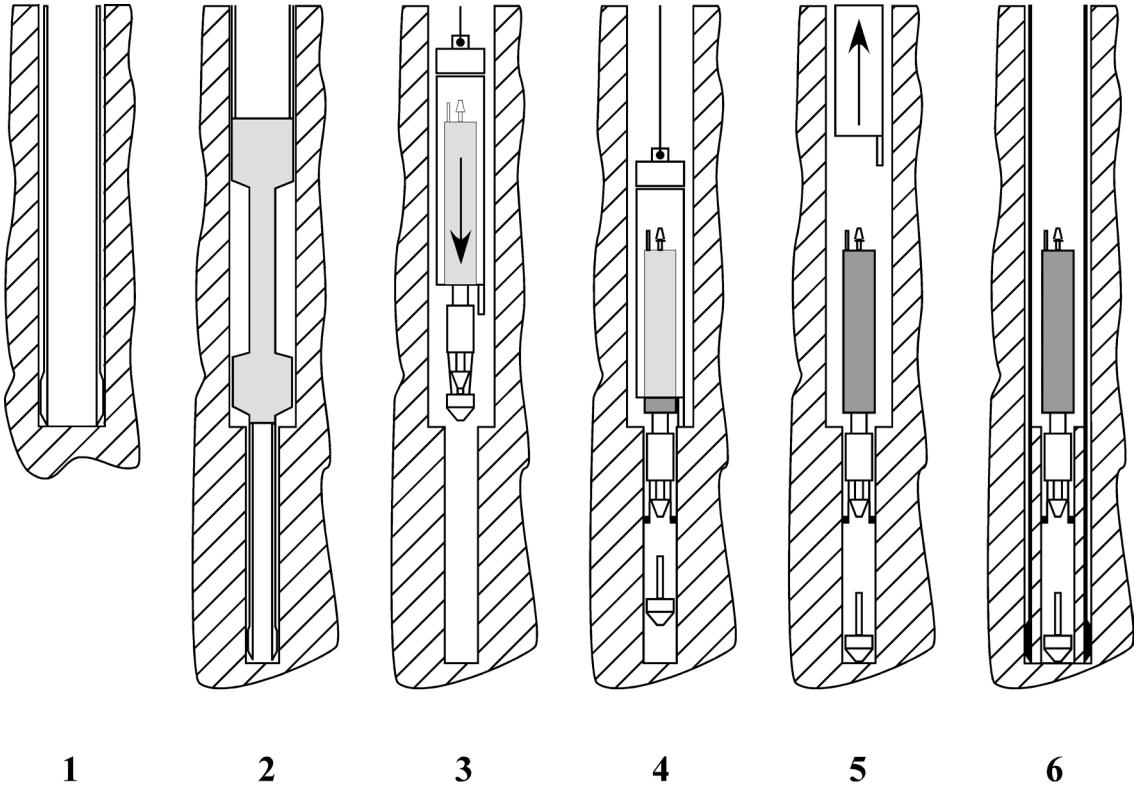

Figure 2-1. *Measurement procedure for the Borre Probe (After Ljunggren and Klasson, 1996). (1) Advance of main borehole to measurement depth; (2) drill ϕ 36 mm pilot hole and recover core for appraisal; (3) lower Borre Probe in installation tool down hole; (4) probe releases from installation tool. Strain gauges bond to pilot-hole wall under pressure from the cone; (5) raise installation tool. Probe/gauges bonded in place; and (6) overcore the Borre Probe and recover hollow cylinder to surface in core barrel.*

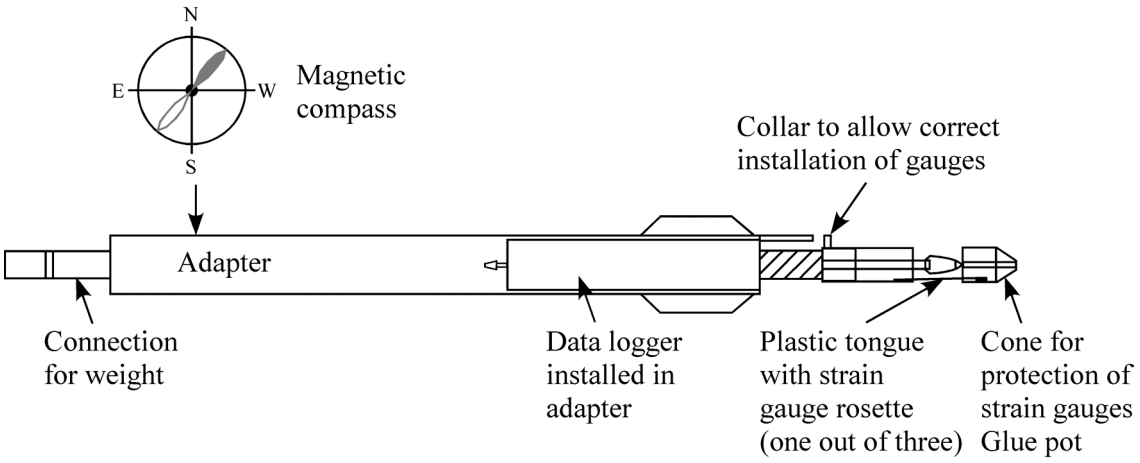

Figure 2-2. *Detailed description of the Borre Probe (After Hallbjörn, 1986)*

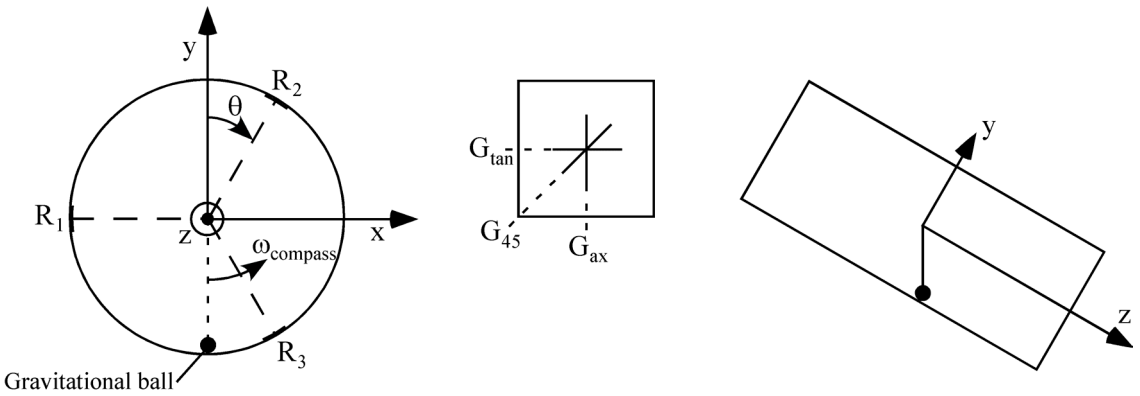

Figure 2-3. *Strain gauge configuration for the Borre Probe (After Hitscher et al., 1979)*

A typical time between installing the cell and overcoring is about 2 hours using acrylic and 10-15 hours using epoxy resin.

2.2.3 Remarks

The Borre Probe is one of few overcoring cells capable of measuring the complete stress tensor in one single borehole down to 1000 m (also in water-filled boreholes).

Hiltscher et al (1979) mentioned a number of problems that may occur during measurement.

- A geometrical problem is the difficulty to correlate the cylindrical surface of the borehole and the strain rosettes/tongues exactly. This may be overcome using an intermediate layer of rubber or a deformable substance. However, if rubber is used, the pressure on the glue will not be uniform and result in bad quality bonding.

- A correct bonding also requires clean and smooth walls free from undulations.

Other problems may be

- Decentralizing of the borehole if the guiding/steering cylinders are not in good condition. If the borehole is not made flat before drilling of the pilot hole, the borehole may not be co-axial and end effect may be introduced if the strain rosettes are not lowered deep enough into the pilot hole (should be lowered 16 cm into the pilot hole). However, a more important fact is that a decentralized and non-axial pilothole may have great influence on the calculated stresses as the core for the Borre Probe is thin (approximately 12 mm)

- The thin core when using the Borre technique implies that it is sensitive to possible drilling induced microfractures. A recommended drilling speed is 3-4 cm/min. Another consequence is that the biaxial testing allows a maximum load of 10 MPa, which may be considerably lower than the measured stress magnitudes.

- As in all overcoring measurements, grain size, joints and core discing may cause problem in the measurement and interpretation.

- The temperature gauge is not located at the position of the strain gauges. This implies that the measured temperatures are a measure of the flush water temperature and thus may not be representative for the strain gauges, Fig. 2-4.

- A recent study concerning the effect of glue thickness on the determination of Young's modulus using aluminum cylinders (Sjöberg and Klasson, 2002) showed that the applied glue thickness significantly affects the result. It was concluded that the current field practice, using 0.1-0.2 mm, gave the most reliable results. Thicker glue resulted in lower values and even malfunctioning gauges due to poor bonding.

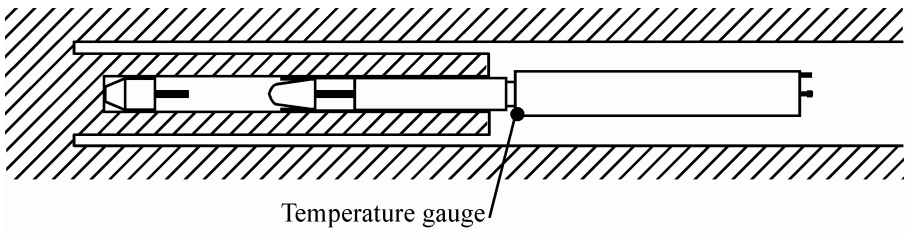

Figure 2-4. *The temperature gauge in relation to the strain gauges for the Borre Probe.*

2.3 The CSIRO HI cells

The CSIRO HI cells are described in detail in a separate SKB-report (Ask et al., in press.) and are not further commented here.

3 Analysis of existing overcoring rock stress data

3.1 General

The general idea behind overcoring, or relief, methods are to isolate a rock sample, partially or wholly, from the stress field in the surrounding rock volume and to measure its response (Merrill, 1964; Amadei and Stephansson, 1997). The stresses are inferred from strain or displacement measurements created by the stress relief. A number of assumptions have to be made in order to determine the stress field: (1) the rock behaves as an ideally linear elastic material; (2) the rock is isotropic (anisotropic solution exists for some cells); (3) the material is continuous and subjected to a homogeneous stress field in the volume of interest.

The assumption regarding an elastic and isotropic rock material implies that elastic theory applies, hence the deformation of the core sample during overcore is assumed identical in magnitude to that by the *in situ* stress field but of opposite sign. Application of elastic theory also requires knowledge of the elastic parameters of the rock, Young's modulus, E, and Poisson's ratio, ν.

The measurements performed at the Äspö HRL are so called borehole relief methods (Amadei and Stephansson, 1997). The relief process is in this case accomplished by drilling a large borehole concentric with an existing borehole (pilot hole), in which the measurement cell is located (see Fig. 2-1).

The Borre Probe has been used in 7 different boreholes in the Äspö HRL. In total, 72 measurement points are available (see Table 1.1). Of these, only 57 are reported successful due to a variety of reasons. Borehole KOV01 in central Oskarshamn includes 9 measurements of which only 3 were judged reliable (Klasson and Andersson, 2001).

The 9 gauge CSIRO Hollow Inclusion cell were used in the early stages of the construction of the Äspö HRL. They are therefore located at rather shallow depth (approx. 140 m). The 9 gauge was exchanged with the 12 gauge CSIRO HI cell primarily for measurements in the ramp of the HRL, except for the measurements conducted at the Zedex area. In total, 7 measurement points are available with the 9 gauge cell and 42 points with the 12 gauge version. During the entire measurement campaign, both the thick and thin versions of the 12-gauge cell have been used. The CSIRO HI data will be dealt with in an individual study and is not commented further in this report.

3.2 Methodology

The overcoring strain data is analyzed at three different scales: (1) the single test scale; (2) the measuring location scale, which includes results from one or more boreholes; and (3) the application scale, representing results from a larger rock volume for a particular rock engineering problem or site, i.e. following the work by Gray and Toews (1974) and Leijon (1989). However, in this report, the overcoring stress data will be analyzed only as individual test points. The combined borehole scale will be dealt with in a future studies.

3.3 Brief theory of overcoring rock stress measurements

3.3.1 General

The theory of relief methods are generally based on elastic theory and it is normally assumed that the rock behaves in a linearly, isotropically elastic manner. Hence, the deformation of the core sample during stress relief is assumed identical in magnitude to that produced by the *in situ* stress field but opposite in sign. It is assumed that the rock mass is both continuous and homogeneous. Furthermore, the measuring probe is assumed to be mounted far enough from the end of the probe, to ensure that no stress/strain variations exist along the axis of the probe (Amadei and Stephansson, 1997).

Consider a hole in a plate composed of an ideally elastic and isotropic material. If the material is subjected to a homogeneous stress field, stress will concentrate around the hole. The corresponding displacements around the borehole are given by:

$$u_r = \frac{1+\nu}{2E} r \left[\begin{array}{l} \dfrac{R^2}{r^2}\left(\sigma_x + \sigma_y\right) + \left\{1 + 4(1-\nu)\dfrac{R^2}{r^2} - \dfrac{R^4}{r^4}\right\}\left\{\left(\sigma_x - \sigma_y\right)\cos 2\theta + 2\tau_{xy}\sin 2\theta\right\} \\ + \left\{\dfrac{1-\nu}{1+\nu}\left(\sigma_x + \sigma_y\right) - 2\dfrac{\nu}{1+\nu}\sigma_z\right\} \end{array} \right] \quad (3\text{-}1)$$

$$u_\theta = \frac{1+\nu}{2E} r \left[\left\{1 + 2(1-2\nu)\frac{R^2}{r^2} + \frac{R^4}{r^4}\right\}\left\{\left(\sigma_x - \sigma_y\right)\sin 2\theta - 2\tau_{xy}\cos 2\theta\right\} \right] \quad (3\text{-}2)$$

$$u_z = \frac{1+\nu}{2E} \left[2r\left\{1 + \frac{R^2}{r^2}\right\}\left(\tau_{yz}\sin\theta + \tau_{zx}\cos\theta\right) + \frac{z}{1+\nu}\left\{\sigma_z - \nu\left(\sigma_x + \sigma_y\right)\right\} \right] \quad (3\text{-}3)$$

where R is the borehole radius, r is the radial distance to the measurement point.

3.3.2 The Borre Probe

The Borre Probe data includes three strain rosettes 120° apart (one axial strain gauge, one tangential, and one inclined 45° in each rosette), thus totally nine strain gauges in each measurement point (Fig. 2-3). The following relationships are valid:

$$\varepsilon_\theta = \frac{1}{R}\left\{(u_r)_{r=R} + \left(\frac{\partial u_\theta}{\partial \theta}\right)_{r=R}\right\} \tag{3-4}$$

$$\varepsilon_z = \left(\frac{\partial u_z}{\partial z}\right)_{r=R} \tag{3-5}$$

$$\gamma_{\theta z} = \frac{1}{R}\left(\frac{\partial u_z}{\partial \theta}\right)_{r=R} \tag{3-6}$$

$$\varepsilon_{45^\circ} = \frac{1}{2}(\varepsilon_z + \varepsilon_\theta + \gamma_{\theta z}) \tag{3-7}$$

where

$$\left(\frac{\partial u_\theta}{\partial \theta}\right)_{r=R} = -\frac{4(1-\nu^2)}{E} R\left[(\sigma_x - \sigma_y)\cos 2\theta + 2\tau_{xy}\sin 2\theta\right] \tag{3-8}$$

$$\left(\frac{\partial u_z}{\partial z}\right)_{r=R} = \frac{1}{E}\left[\sigma_z - \nu(\sigma_x + \sigma_y)\right] \tag{3-9}$$

$$\left(\frac{\partial u_z}{\partial \theta}\right)_{r=R} = \frac{R}{E}\left[4(1+\nu)(\tau_{yz}\cos\theta - \tau_{zx}\sin\theta)\right] \tag{3-10}$$

Combining Eqs. 3-8 to 3-14, using r = R, gives the final solution

$$\varepsilon_\theta = \left[(\sigma_X^\infty + \sigma_Y^\infty) - 2(1-\nu^2)\{(\sigma_X^\infty - \sigma_Y^\infty)\cos 2\theta + 2\tau_{XY}\sin 2\theta\} - \nu\sigma_Z^\infty\right]/E \tag{3-11}$$

$$\varepsilon_z = \left[\sigma_Z^\infty - \nu(\sigma_X^\infty + \sigma_Y^\infty)\right]/E \tag{3-12}$$

$$\gamma_{\theta z} = \left[4(1+\nu)(\tau_{YZ}^\infty\cos\theta - \tau_{ZX}^\infty\sin\theta)\right]/E \tag{3-13}$$

$$\varepsilon_{45^\circ} = \frac{1}{2}(\varepsilon_z + \varepsilon_\theta + \gamma_{\theta z}) \tag{3-14}$$

3.4 Analysis of the recorded strains

3.4.1 Determination of strains

Generally, when determining the observed strains from overcoring, a stable value before overcoring starts and after overcoring stops is preferential. The difference between these values is assumed to correspond to the strain relief involved in the overcoring process. Further, the value after overcoring stop is chosen in such a manner that temperature effect is minimized. In practice, this means that flushing is continued until the temperature in the test section is close to the *in situ* rock mass temperature. However, in some cases, this is not possible and temperature corrections are necessary (if more than 1°C), see Chap. 3.4.3.

One method to verify that the strain rosettes have been glued properly, is to investigate the strain gauge response in connection to start of flushing of drilling water. The flushing normally starts 5-10 minutes before overcoring and is a valuable means to identify malfunctioning gauges/rosettes, Fig. 3-1. Verification of the glue hardening process is also conducted which involves strain analysis for a period of about 30 minutes prior to the overcoring.

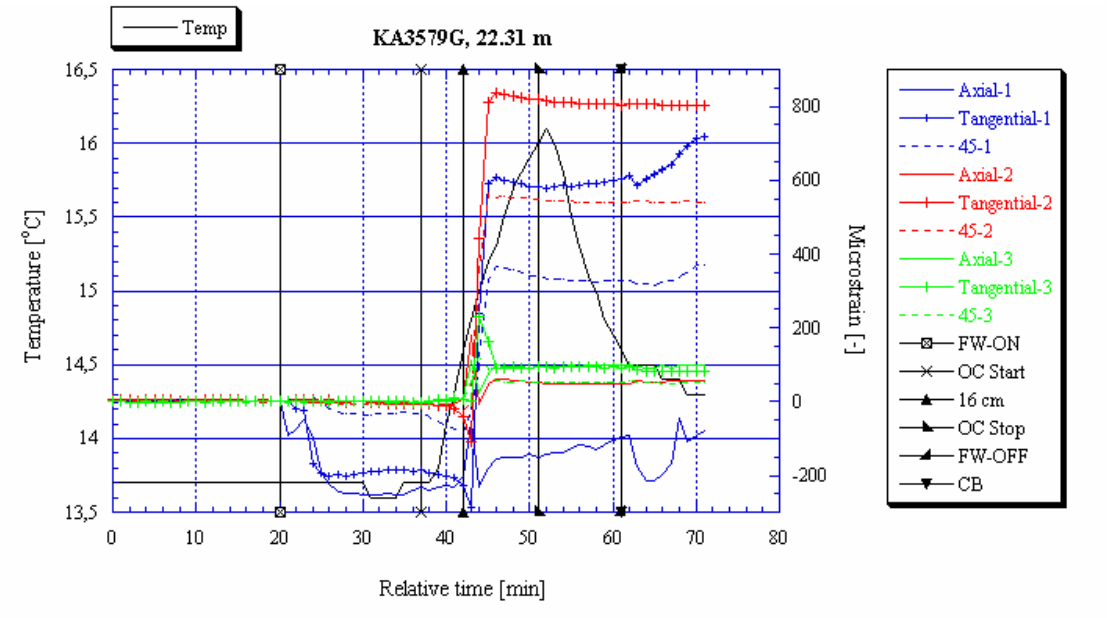

Figure 3-1. *Typical strain gauge response during overcoring. In this measurement point at 22.31 m in KA3579G, strain rosette 1 is obviously not glued properly as the gauges reacts strongly when the flushing water is turned on.*

3.4.2 Determination of standard deviation of strains

The analysis of the strain data is based on the assumption that all errors obey Gaussian distribution. The analysis may be divided in two steps:

1. The stability of the strain gauge readings

2. The difference between calculated and observed strain

The strain gauge readings should be stable, if the gauges are properly attached to the rock, and if there are small or no fluctuations of the temperature of the drilling water. The strain variations 20 minutes before flushing starts, and the variation between the end of overcoring and core break/end of flushing is determined and averaged (Fig. 3-2). The resulting interval is assumed to be equal to a 99 % confidence interval, and is used to determine the first part of the standard deviation for the strain gauge, denominated SD^{gauge}.

The difference between the calculated and observed strain values may be used to determine the standard deviation for each strain gauge (Fig. 3-3). For calculation of the strains, a standard least-squares program was developed. The calculation is based on: (1) individual measurement points; (2) average values for a number of measurement points in one borehole that has been judged to represent the same *in-situ* stress field; and (3) average values for a number of measurement points in multiple boreholes that has been judged to represent the same *in-situ* stress field. The resulting interval is assumed

to be equal to a 99 % confidence interval and is used to determine the second part of the standard deviation for the strain gauge, denominated $SD^{diff,\ ind}$, $SD^{diff,\ avsb}$ and $SD^{diff,\ avmb}$ for the **ind**ividual; **av**erage for **s**ingle **b**orehole; and **av**erage for **m**ultiple **b**oreholes, respectively.

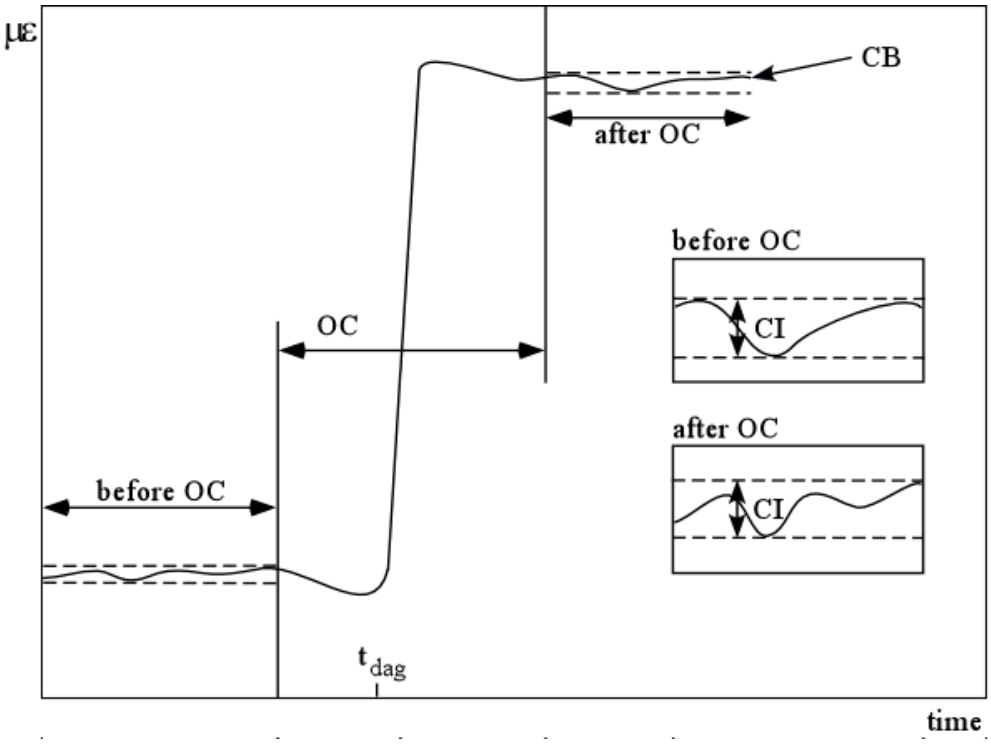

Figure 3-2. *Schematic response of a tangential strain gauge during overcoring. The strongest strain gauge response occurs at t_{dag}, i.e. when the **d**rill bit is **a**t the **g**auge position. The dotted lines show the 99 % confidence intervals (CI) before and after overcoring (OC). CB denotes core break. This interval is averaged and used for determination of standard deviation.*

The final standard deviation for the gauge is the sum of these sources, $SD = SD^{gauge} + SD^{diff}$, i.e. giving maximum three values according to the classification above. The reason for this choice of standard deviation is that the least squares solution may give zero standard deviation when based solely on the difference between measured and calculated strain, i.e. $SD^{Diff}=0$, although one strain rosette is malfunctioning.

If a strain gauge is judged unreliable (malfunctioning or removed based Chauvenet's criteria for outlyers) and hence excluded during the later stress calculation, the strain gauge is removed and a new set of standard deviations is calculated (only SD^{diff} and SD will change). Note that only one measurement at the time is removed (the most erroneous). Thus, a stepwise procedure will be conducted during stress determinations.

The methodology for the determination of strains and their standard deviation to be included in the stress analysis is presented in Fig. 3-4. Strain gauges are discarded when obvious problems have occurred (e.g. unglued rosettes) or when the difference between calculated and measured strains exceed the empirical Chauvenet's criteria for outlyers.

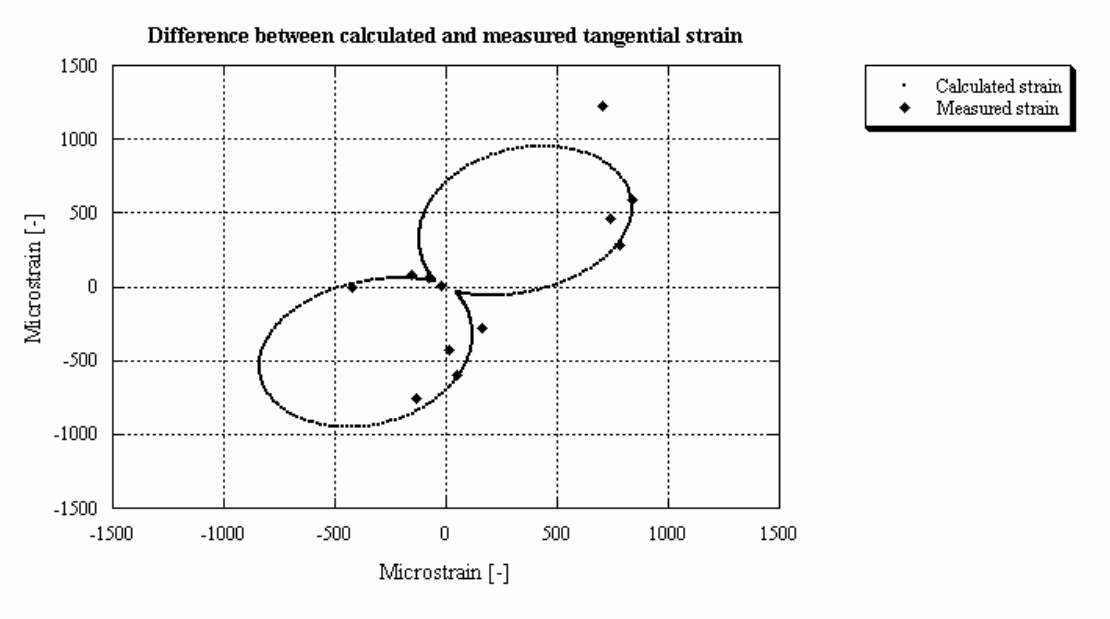

Figure 3-3. *Difference between calculated and measured tangential strain for the deeper measurement points in borehole KA3579G, Prototype Repository. This difference is assumed equal to a 99% confidence interval, giving* SD^{Diff} *for each strain gauge.*

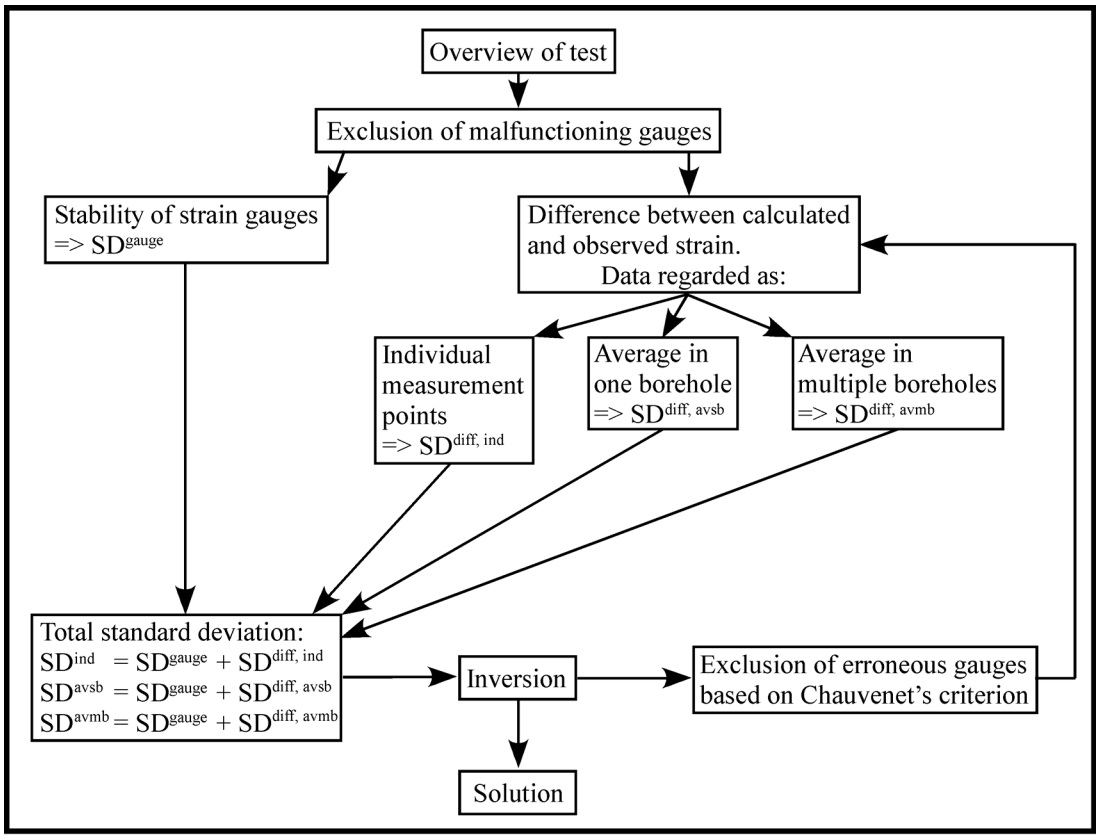

Figure 3-4. *Flow chart showing the steps included in the determination of strains.*

3.4.3 Temperature effects

The temperature correction may be determined using following equation (Leijon, 1988):

$$\alpha_M^{Theoretical} = \alpha_A + \alpha_s \tag{3-15}$$

where $\alpha_M^{Theoretical}$ is the recorded heating response per unit temperature (με/°C); α_A is the thermal expansion coefficient for the rock; α_S is the inherent thermal expansion compensation factor of the strain gauges. The inherent thermal expansion compensation factor is by the manufacturer to –10.8 με/°C for the Borre Probe.

The thermal expansion coefficient for two Äspö rocks, diorite and granite, have been determined by Larsson (2001) for a temperature interval between 20° and 70°C. The average thermal expansion coefficient, α_A, for diorite and granite within this interval was found to be $4.5 \cdot 10^{-6}$/°C. Larsson used both loaded and unloaded samples and found that the axial thermal expansion coefficient was independent of loading condition. Thus, both these data types may be combined, see Fig. 3-5.

The temperature interval is considerably larger than the temperature experienced during overcoring, but may be used for extrapolation to the temperature interval of interest (10°-20°C). Extrapolation, using both loaded and unloaded samples, gives an average thermal expansion (diorite and granite) between 2.9 to 3.2 με/°C (Fig. 3-5) between 10° and 20°C.

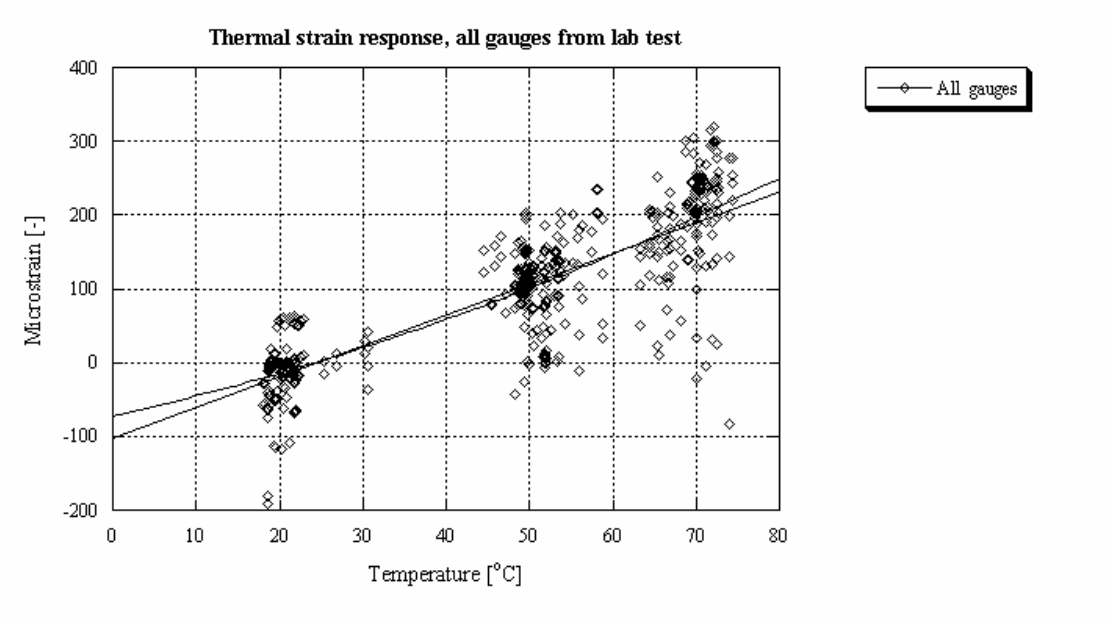

Figure 3-5. *Average thermal response (diorite and granite) using laboratory data (Larsson, 2001). The lines are linear and 2nd degree polynomial fitted curves, respectively.*

The *in situ* overcoring strain gauge response is composed of short data readings, e.g strains readings between 12.5°-13.2°C and 14.5°-12.8°C before and after the overcoring phases, respectively. Thus, all data cover different temperature ranges that are often overlapping. The thermal expansion coefficient for the *in situ* strain data is presented in Fig. 3-6. The data obviously is very scattered but when discarding unrealistic values of the thermal expansion coefficient, thus looking only at the interval 0 to 10 με/°C, α_A varies between 1-3 με/°C. This approach is though regarded as very uncertain.

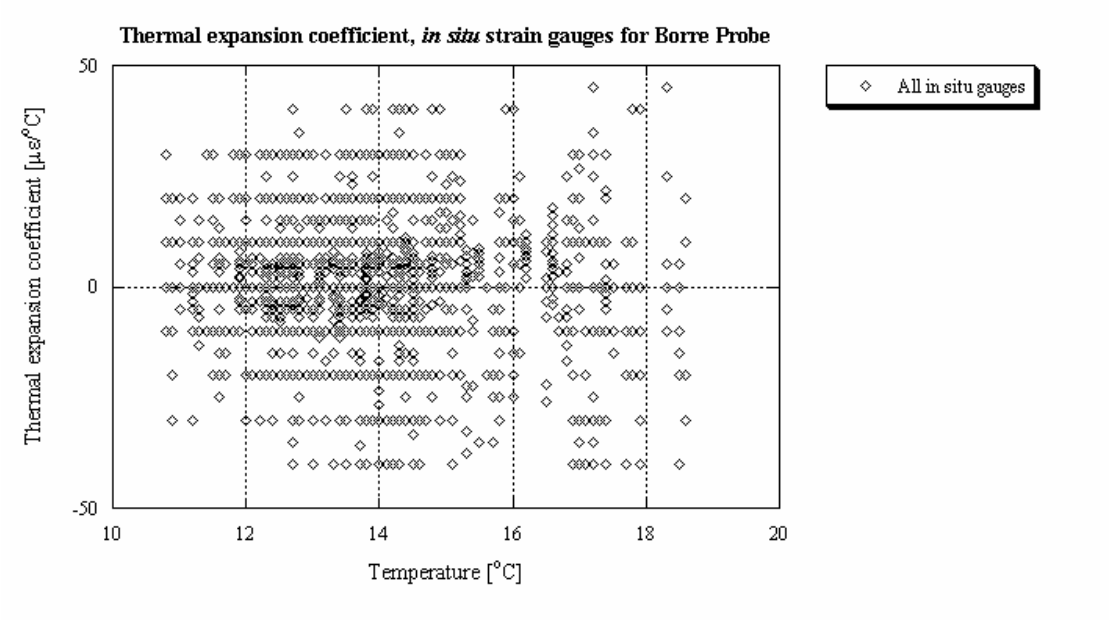

Figure 3-6. *Average thermal response using* in situ *overcoring strain gauge data.*

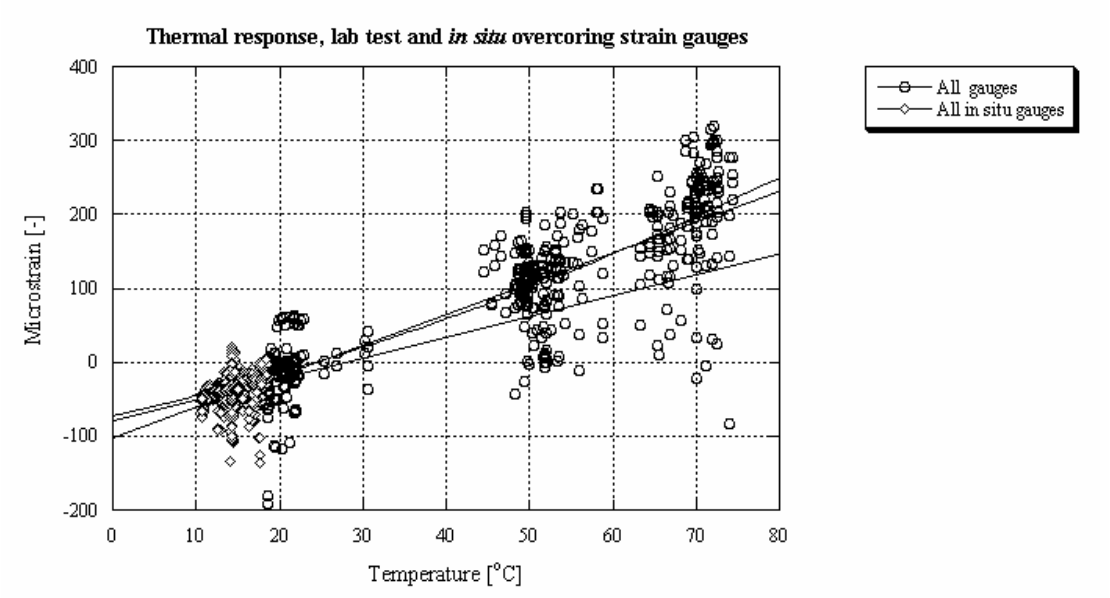

Figure 3-7. *Average thermal response (diorite and granite) using laboratory data and* in situ *overcoring strain gauge data.*

Normalizing the *in situ* data using the average of the fitted linear and 2nd degree polynomial curves of the data from Larsson (2001) gives a more reliable result (Fig. 3-7). The combined data gives linear thermal expansion coefficient between 10°-20°C equal to $\alpha_A = 3.0$ με/°C. Conclusively, the temperature correction factor for the overcoring strain gauges is

$$\alpha_M^{Theoretical,\,Borre\,\Pr obe} = 3 - 10.8 \approx -8\mu\varepsilon / °C \qquad (3\text{-}16)$$

i.e. if the temperature is 1°C higher during the strain reading after overcoring compared to the temperature during the reading before overcoring, 8 με should be added to all strain gauges.

As mentioned in Ch. 2, the position of the temperature gauge for the Borre Probe introduces a large uncertainty. In current position, only the flushing water temperature is monitored and the temperature in the rock at the position of the strain gauges is unknown. In Fig. 3-8, the strain gauge response at 8.00 m depth in KA3579G is presented. The rapid temperature increase after the flushing water has been turned off indicates a very high rock temperature and it is likely that large temperature-induced stresses are included in the analysis. In this case, data are available a few minutes after the flushing water has been turned off, but this is rare. Thus, all Borre Probe data include a great uncertainty regarding temperature-induced stresses. To overcome this problem in the future, the final strain reading should be taken when the rock temperature has been lowered to the initial *in situ* rock temperature.

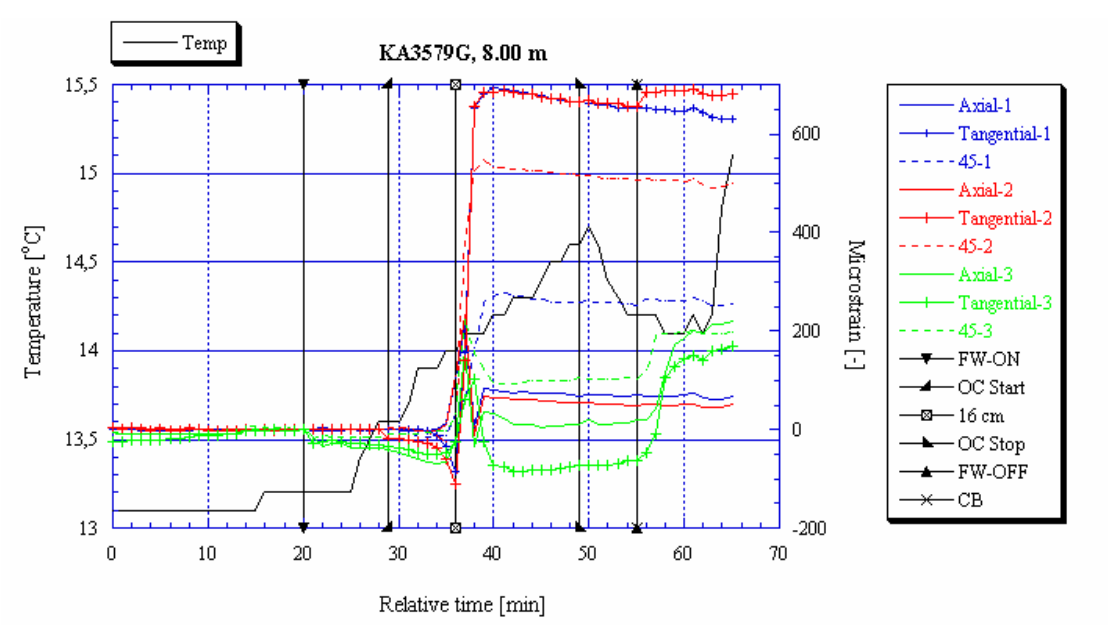

Figure 3-8. *Strain gauge response during overcoring at 8.00 m depth in KA3579G (After Ljunggren and Bergsten, 1998).*

The elastic parameters are also influenced by temperature (e.g. Lama and Vutukuri (1978); Heuze (1983)). However, the effect on the elastic parameters for the small temperature variations in this study is assumed to be negligible.

3.4.4 Special case

Due to malfunctioning equipment, the strain rosettes are not always glued in the correct position in the pilot hole. This may lead to erroneous calculated stresses unless malfunctions are accounted for. Following example is based on a close examination of a measuring point at a depth of 31.67 m in borehole KK0045G01 of the Demo Tunnel in Äspö HRL. At this measuring point, strain rosette #1 has displaced 10-15° towards strain rosette #2, most probably due to bending of the rosette holder during installation of the Borre Probe. This further implies that the three strain gauges in rosette #1 have been offset by an angle $\xi=\phi$. To investigate the effect of misplaced strain rosettes on the state of stress, a sensitivity analysis was conducted. The analysis was conducted for the following three cases (Fig. 3-9), using offset angles ξ and ϕ equal to 12.5°:

A) The holder of rosette #1 is in correct location ($\phi=0$), but the strain gauges in rosette #1 are offset at an angle ξ;

B) The holder of rosette #1 is bent and offsets rosette #1 by an angle ϕ, but the orientation of the strain gauges in rosette #1 are unaffected ($\xi=0$); and

C) The holder of rosette #1 is bent and offsets rosette #1 by an angle ϕ, and the strain gauges in rosette #1 are offset at an angle $\xi=\phi$.

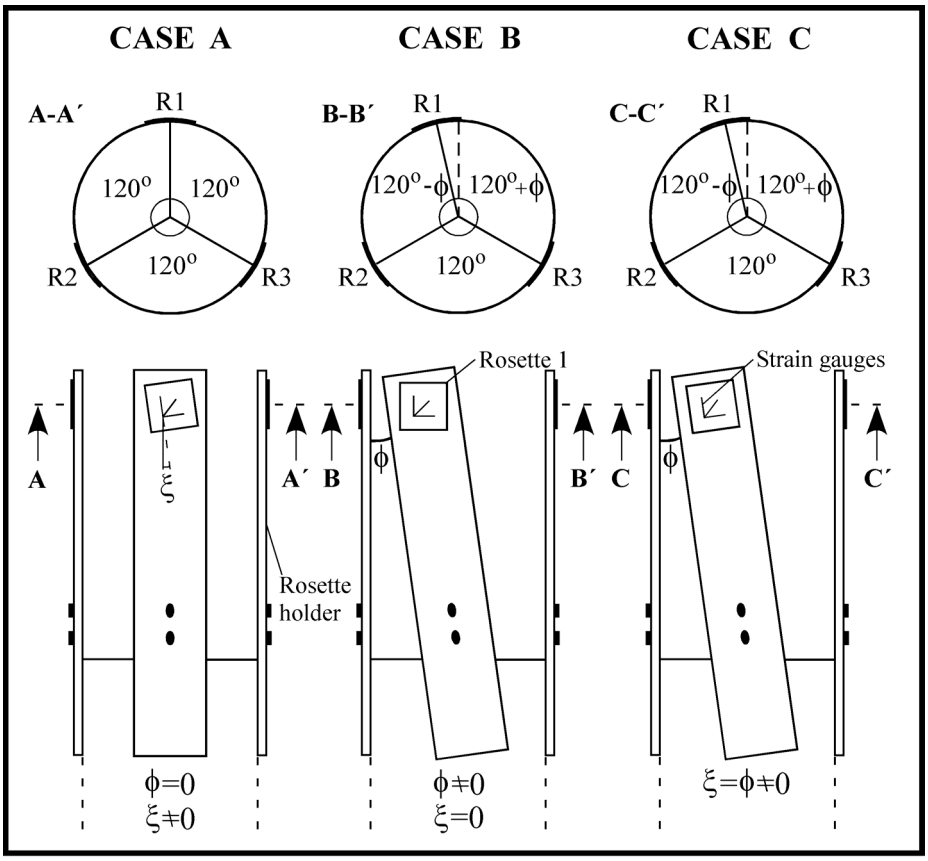

Figure 3-9. *Schematic view of the three cases studied in the sensitivity analysis. The value of offset angle is 12.5°.*

By resolving of the strains in from Fig. 2-3, the relations between the strains e_A, e_B, and e_C measured by the strain gauges G_A, G_B, and G_C are given by:

$$e_A = e_X \cos^2 \phi_A + e_Y \sin^2 \phi_A + \gamma_{XY} \sin \phi_A \cos \phi_A \quad (3\text{-}17)$$

$$e_B = e_X \cos^2 \phi_B + e_Y \sin^2 \phi_B + \gamma_{XY} \sin \phi_B \cos \phi_B \quad (3\text{-}18)$$

$$e_C = e_X \cos^2 \phi_C + e_Y \sin^2 \phi_C + \gamma_{XY} \sin \phi_C \cos \phi_C \quad (3\text{-}19)$$

Combining Eqs. 3-17 to 3-19 with Eqs. 3-11 to 3-13 gives:

$$e_A = A \cos^2 \phi_A + B \sin^2 \phi_A + C \sin \phi_A \cos \phi_A \quad (3\text{-}20)$$

$$e_B = A \cos^2 \phi_B + B \sin^2 \phi_B + C \sin \phi_B \cos \phi_B \quad (3\text{-}21)$$

$$\gamma_{AB} = A \cos^2 \phi_C + B \sin^2 \phi_C + C \sin \phi_C \cos \phi_C \quad (3\text{-}22)$$

and

$$e_{45} = \frac{1}{2}\left(e_A + e_B + \gamma_{AB}\right) \quad (3\text{-}23)$$

where A, B, and C are the right hand side in Eqs. 3-11 to 3-13. Equations 3-20 to 3-23 thus involves both the orientation of the strain rosette in the tangential direction, θ, and the individual orientation of the strain gauges, ϕ_A-ϕ_C, thereby enabling the sensitivity analysis of a misplaced strain rosette.

Table 3-1 shows the results from the sensitivity analysis of a misplaced strain rosette. The results are presented as the relative difference between the original result, i.e. assuming no displacement of rosette #1. For each case A, B, and C, the state of stress has been calculated using two angles of offset. The results are based on re-analyzed strains (including a temperature correction of 3°C) and elastic parameters.

As the most probable cause of event is that the holder of rosette #1 was bent during installation of the measuring Probe, Case C gives the most probable state of stress in the measuring point of interest. Based on the corrected stresses, the corresponding strains may be determined (Table 3-2). These corrected strains will be used for future stress field determination.

Table 3-1. Corrected principal stresses at borehole depth 31.67 m in borehole KK0045G01 assuming 12.5° offset of rosette #1 for Case A-C and including a 3°C temperature correction.

Results assuming no displacement of rosette 1									
$\phi=\xi$ (Degr.)	**Magn. σ_1 (MPa)**	**Strike σ_1 (Degr.)**	**Dip σ_1 (Degr.)**	**Magn. σ_2 (MPa)**	**Strike σ_2 (Degr.)**	**Dip σ_2 (Degr.)**	**Magn. σ_3 (MPa)**	**Strike σ_3 (Degr.)**	**Dip σ_3 (Degr.)**
0	28.4	71	18	23.9	321	48	7.1	175	37
CASE A									
12.5	28.6	67	31	25.7	302	43	6.0	178	31
CASE B									
12.5	29.8	63	22	24.3	311	43	9.1	172	39
CASE C									
12.5	29.9	60	34	25.8	297	39	8.1	175	33

Table 3-2. Corrected strains at borehole depth 31.67 m in borehole KK0045G01 assuming 12.5° offset of rosette #1 for Case C. The brackets includes the original result (Klasson et al., 2001).

Corrected strains at borehole depth 31.67 m in borehole KK0045G01									
Case	Axial 1 [-]	Tang 1 [-]	45 1 [-]	Axial 2 [-]	Tang 2 [-]	45 2 [-]	Axial 3 [-]	Tang 3 [-]	45 3 [-]
C	44 (82)	427 (368)	590 (593)	215 (207)	1163 (1082)	551 (542)	116 (195)	438 (312)	1 (38)

3.5 Analysis of elastic parameters

3.5.1 General

Application of elastic theory also requires knowledge of the elastic parameters of the rock material, i.e. Young's modulus, E, and Poisson's ratio, υ. The elastic parameters are determined using biaxial tests. During testing the induced strains in the sample are monitored. The test sequence includes both loading and unloading, which allows examination of possible inelastic behavior of the rock sample. The elastic parameters are determined from the unloading parts of the load cycles, as it reflects the overcoring test. Preferably, the maximum applied load should correspond to the measured stress magnitudes. However, to avoid cracking of the thin-walled cylinder sample, the maximum applied load is 10 MPa for the Borre Probe (see calculation example in Appendix 2). The load/unload increment is equal to 1 MPa. The results are plotted as strains versus applied pressure (Fig. 3-10).

Theoretically, the strain gauges within each group (i.e. axial, tangential, and 45° inclined) should respond identically to loading/unloading. The elastic properties are derived using the theory for an infinitely long, thick-walled hollow cylinder subject to uniform external pressure, and the assumption that plane stress applies:

$$E = K_1 \frac{p}{\varepsilon_\theta} \frac{2}{1 - \left(\frac{D_i}{D_o}\right)^2} \tag{3-24}$$

and

$$\nu = -K_1 \frac{\varepsilon_z}{\varepsilon_\theta} \tag{3-25}$$

where E is Young's modulus; p is applied load, ε_θ and ε_z are tangential and axial strain, respectively (on inner surface); D_i and D_o are inner and outer diameter, respectively, of the cylinder; and K_1 is a correction factor (K_1 = 1 for the Borre Probe).

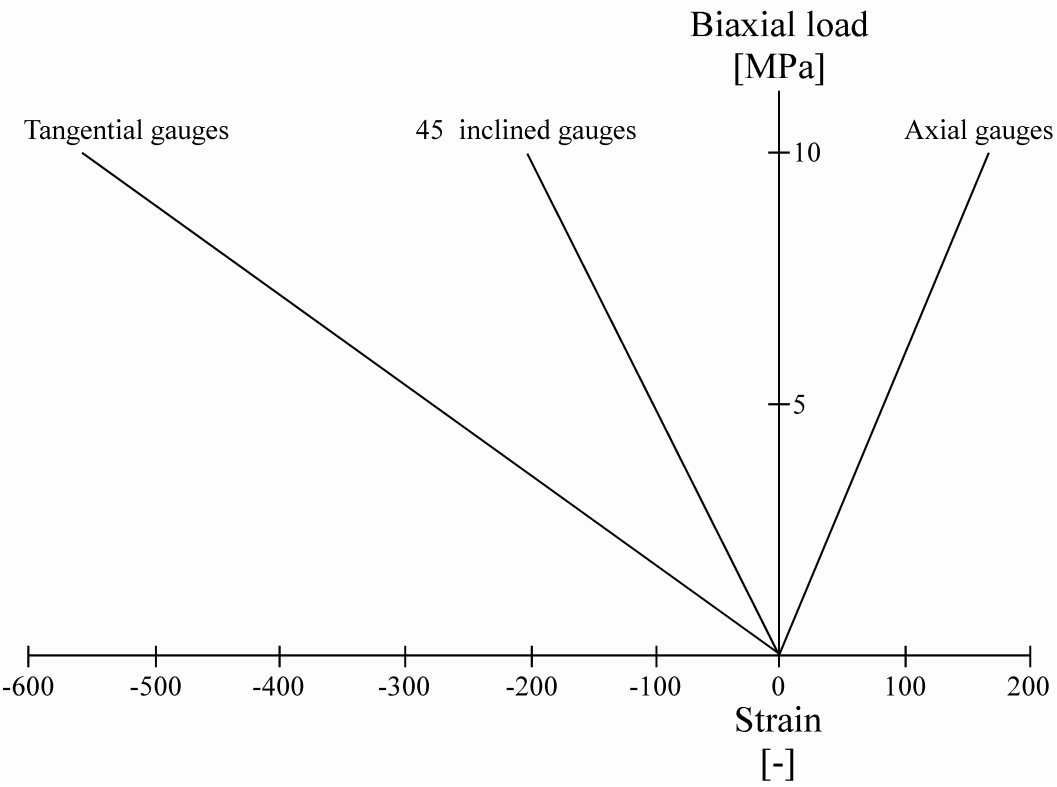

Figure 3-10. *Hypothetical result from biaxial testing of an ideal material (After Ljunggren and Bergsten, 1998).*

3.5.2 Determination of elastic parameters

The values of E and υ are determined as secant values, calculated from the strain data during the unloading of the core sample. The unloading phase was chosen because this phase is fully elastic and because it mimics the stress relief of the overcoring sample (Amadei and Stephansson, 1997). The secant values from zero loads to pressures between 8 and 10 MPa are chosen as this is most representative for the stress magnitudes *in situ*. The calculation is based on: (1) individual measurement points; (2) average values for a single borehole; and (3) average values for several boreholes.

The Borre Probe gives 3 different values for E and ν. This may be used for estimation of anisotropy. Anisotropy may also be investigated though comparison of the 45° inclined strain gauges with the tangential and axial strain gauges (Worotnicki and Walton, 1979). If the rock is isotropic, the three tangential strain gauges, $\varepsilon_{\theta,i}$ (i=1 to 5), must be equal and following relationship must hold:

$$\varepsilon_{45,i} = \frac{1}{2}\left(\varepsilon_{z,i} + \varepsilon_{\theta,i}\right) \tag{3-26}$$

However, due to e.g. gauge debonding these rules are seldom strictly satisfied and Worotnicki (1993) suggested that deviation up to ±20% should be accepted before inferring rock anisotropy.

Amadei (1983a and 1983b) recommended, as a rule of thumb, that when the ratio E_{max}/E_{min} exceeds 2, the anisotropy should be regarded in the analysis.

3.6 Uncertainties in existing overcoring data

3.6.1 General

The uncertainties in the analysis of overcoring strain data involve: (1) natural (intrinsic, inherent) uncertainty; (2) measurement related uncertainties; and (3) uncertainties associated with the analysis of the stress measurement data (Amadei and Stephansson, 1997).

The natural uncertainties mainly involve the variation of the rock material (fabric, geological structures etc), which may result in varying stresses even at small distances or volumes. The variation of the rock material also affects the elastic parameters. The calculated *in situ* rock stresses are directly related to the Young's modulus while the effect of varying Poisson's ratio is more complex but usually of less importance compared to Young's modulus.

Measurement related uncertainties are errors or mistakes due to the construction of the instrument used to measure the stresses. These involve poor installation of cell, malfunctioning of strain gauges, creep of glue, temperature effects (environment, drilling water, and heat generated during drilling), electrical problems, borehole eccentricity, borehole oversize etc.

Data analysis related uncertainties involve the assumption of a linearly elastic, isotropic and homogeneous continuum material (neglecting effects of grain size, anisotropy, nonlinear or inelastic response, time-dependent response, yielding of rock after drilling, inhomogeneities at the scale of the overcore sample). It is further assumed that the diameter of overcoring does not influence the results, that the relieved stresses during overcoring are equal to the stresses in its precoring condition, and that the rock deforms in plane strain or plane stress. The latter implies that the measurement points must be in a plane distant from the overcore ends by three to four times the borehole diameter (i.e. for a 38 mm borehole a minimum total overcore length of 300 mm).

The determination of the elastic parameters is also subject to some errors. The biaxial test loading cycle should preferably reach the magnitudes measured *in situ*. However, the Borre Probe uses a maximum load of 10 MPa, which may be considerably less than the measured stress magnitudes.

A comparative study of overcore samples using both biaxial and triaxial tests revealed 20% lower Young's modulus, more scattered, and on average twice as large Poisson's ratio for the biaxial tests compared to the triaxial tests (Leijon and Stillborg, 1986). Because Leijon and Stillborg (1986) did not observe such a difference between the biaxial and triaxial tests on aluminum cylinders, they attributed that the discrepancy in the elastic parameters to the rock material. Possibly, the results achieved by Leijon and Stillborg (1986) could be related to the fact that that biaxial test does not fully mimic the situation in-situ. The overcore sample expands in all directions as the stresses are removed during the overcoring and relief process, whereas it is forced contract in the radial direction and to expand in the axial direction in the biaxial testing (e.g. Sandström, 1999; Fig. 3-11).

The results from Leijon and Stillborg (1986) were based on rock samples from the Luossavaara Mine, within the Kiruna iron ore fields in Northern Sweden, and were constituted of quartz and syenite porphyry, and magnetite. The rock samples proved to have non-ideal mechanical characteristics and with Poisson's ratios from the biaxial tests ranging between about 0.27 to 0.66. The non-ideal rock properties and suspect values of Poisson's ratio from the biaxial tests thus reduce the confidence of the results presented by Leijon and Stillborg (1986).

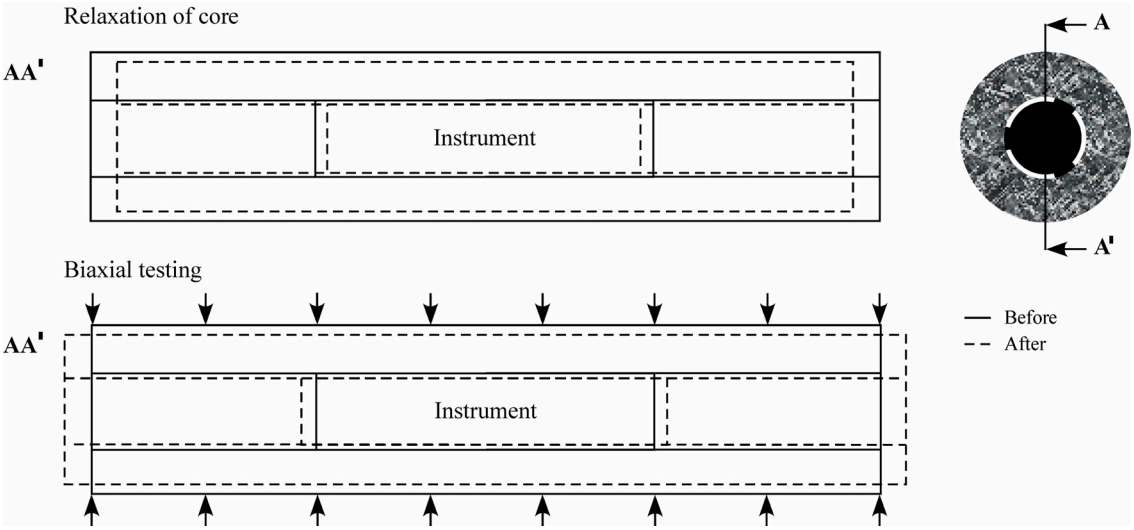

Figure 3-11. *Effect of core relaxation and reloading during biaxial testing (After Sandström, 1999).*

3.6.2 Uncertainties in this study

In this report, the recorded strains and calculated elastic parameters are assumed to follow Gaussian distribution. The preliminary data analysis in this study is based on the following assumptions: (1) the strain gauge response immediately before and after overcoring; and (2) the difference between calculated and measured strains. It is assumed that other sources of uncertainty are incorporated using this method.

The assumption that the strain data follows Gaussian distribution may be roughly estimated by plotting histograms and cumulative frequency plots of the strain deviation, i.e. difference between observed and calculated strain (Worotnicki, 1993). The results for the raw data and re-analyzed data (excluding borehole KOV01) indicate that the strain data are reasonably consistent with the assumed Gaussian distribution (Figs. 3-12 to 3-13). As would be expected, the average deviation for both the raw data and the re-analyzed data is close to zero ($1.9 \cdot 10^{-3}$ and $5.4 \cdot 10^{-4}$, respectively). The re-analyzed data seems to apply better to the Gaussian distribution compared to the raw data. This could perhaps be explained by the fact that the raw data commonly, to some degree, are re-calculated. Thus the data are not entirely "raw". This could explain the large amount of data concentrated around the central zero value.

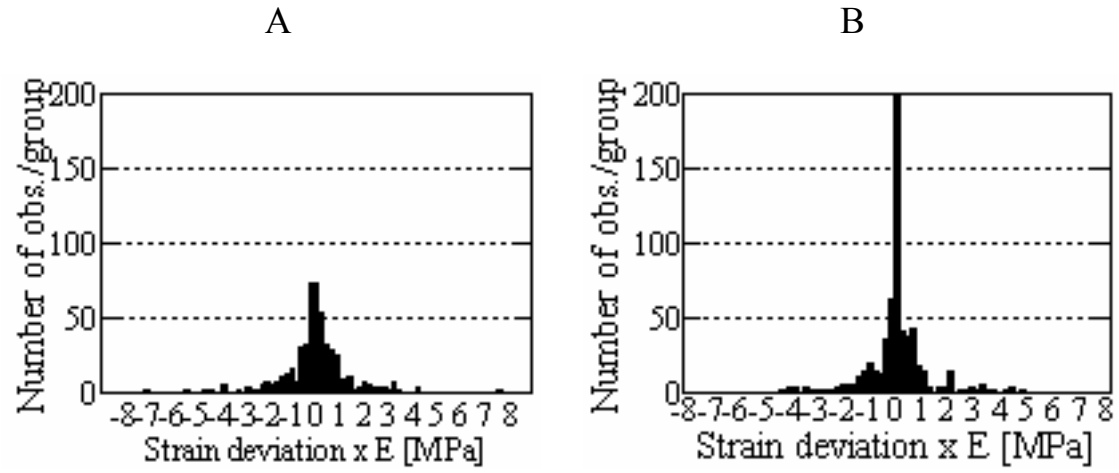

Figure 3-12. *Histogram of the strain deviation x E using strains measured with the Borre Probe; A and B are re-analyzed and raw data, respectively.*

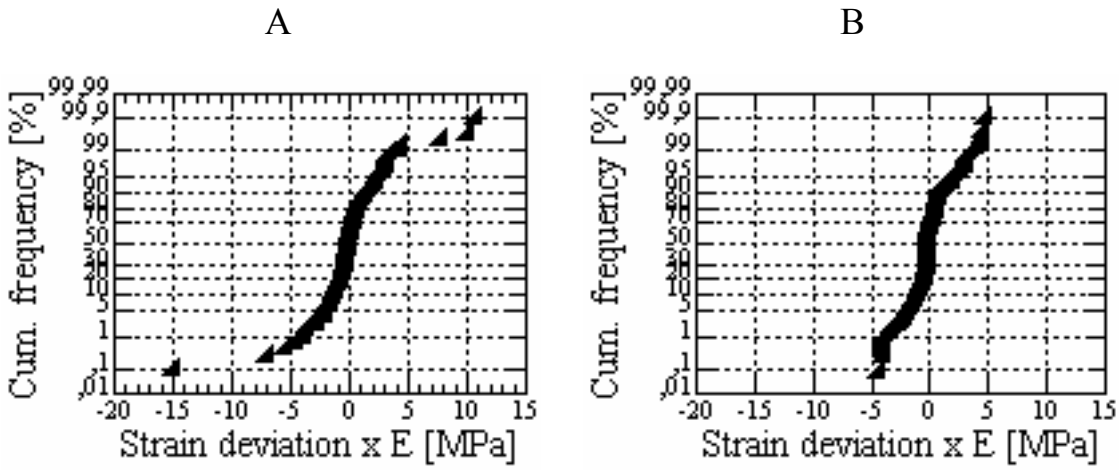

Figure 3-13. *Cumulative frequency distribution using strains measured with the Borre Probe; A and B are re-analyzed and raw data, respectively.*

4 Analysis example

4.1 General

In this chapter, an analysis example using data from the Borre Probe in borehole KA3579G, Prototype Repository, Äspö HRL, is presented. The results from the other boreholes are presented in appendices 3 to 5.

4.2 Borehole KA3579G, Prototype Repository

These example only involve the deeper measurements conducted in borehole KA3579G, i.e. between 468.4 to 470.7 m depth. The evaluated strains and their standard deviation are presented in Table 4-1 and the corresponding elastic parameters in Table 4-2. None of the measurement points needed temperature corrections and anisotropy was not evident according to Amadei's rule of thumb. Note that SD^{ind} includes all data, i.e. also strain gauges that are likely to be erroneous.

Table 4-1. Strains and associated standard deviation for the deeper measurement points in borehole KA3579G. Data analyzed as individual measurement points, i.e. SD^{gauge}, $SD^{diff,ind}$, and the resulting SD^{ind}. Numbers in italic indicates malfunctioning and rejected gauges based on Chauvenet's criteria for outliers are indicated by ^{C}. The values in brackets are the strain determination by Ljunggren and Bergsten (1998).

Depth	Microstrains [-]								
	Rosette 1			Rosette 2			Rosette 3		
[m]	Ax.	Tang.	45°	Ax.	Tang.	45°	Ax.	Tang.	45°
20.06	36 (60)	603 (622)	318 (333)	26^{C} (47)	1009 (1013)	512 (550)	*36* (31)	*68* (23)	*64* (62)
21.21	-9 (-4)	867 (902)	454 (477)	-13 (-14)	184 (178)	-11 (41)	*50*^{C} (90)	*346* (435)	*271* (276)
21.50	61 (62)	423 (423)	267 (261)	25 (21)	311 (312)	249 (253)	56 (56)	*1364* (1427)	802 (833)
22.31	*-90*^{C} (82)	*612* (785)	*329* (393)	50 (66)	806 (843)	542 (562)	97 (95)	94 (93)	55 (52)
[m]	SD^{gauge} [-]								
20.06	9	2	1	7	9	6	*15*	*10*	*3*
21.21	2	3	3	1	1	1	*7*	*13*	*6*
21.50	2	1	1	1	1	1	4	*11*	12
22.31	*36*	*29*	*8*	2	3	2	1	1	1
[m]	$SD^{diff, ind}$ [-]								
20.06	1	2	1	0	0	0	*0*	*0*	*0*
21.21	6	7	7	0	0	0	*0*	*0*	*0*
21.50	3	15	4	7	7	7	15	*15*	15
22.31	*42*	*5*	*21*	5	5	5	10	10	10

Table 4-1. Continued.

Depth	Microstrains [-]								
	Rosette 1			Rosette 2			Rosette 3		
[m]	Ax.	Tang.	45°	Ax.	Tang.	45°	Ax.	Tang.	45°
	SD^{ind} [-]								
20.06	10	4	2	7	9	6	*15*	*10*	*3*
21.21	8	10	10	1	1	1	*7*	*13*	*6*
21.50	5	16	5	8	8	8	19	*26*	27
22.31	*78*	*34*	*29*	7	8	7	11	11	11

Table 4-2. Elastic parameters and their standard deviation for the deeper measurement points in borehole KA3579G. Values in brackets include erroneous gauges.

Depth	Elastic parameters			
[m]	E^{ind}	δE^{ind}	υ^{ind}	$\delta\upsilon^{ind}$
20.06	70.4 (68.8)	6.7 (5.8)	0.28 (0.28)	0.02 (0.02)
21.21	72.5 (72.6)	4.7 (3.7)	0.32 (0.35)	0.02 (0.05)
21.50	72.7	3.2	0.26	0.02
22.31	61.7 (64.9)	8.8 (8.5)	0.31 (0.31)	0.07 (0.06)
	E^{avsb}	δE^{avsb}	υ^{avsb}	$\delta\upsilon^{avsb}$
21.27	69.7 (69.8)	7.1 (6.4)	0.29 (0.30)	0.04 (0.05)

5 Stress calculations

5.1 General

In this chapter, results from stress calculations based on a standard least squares program are presented. The results are based on viewing the overcoring data as individual measurement points. The results are also presented in Appendix 6.

The re-analyzed strain data have been used which includes all strain gauges except the gauges rejected by the empirical Chauvenet's criterion. This means that strain gauges that are somewhat suspicious or likely erroneous are still included. However, this chapter is solely dedicated to visualize the differences between the calculated stresses in existing literature (referred to as raw data) and the calculated stresses.

The raw data is found in the following publications: Bjarnason et al. (1989), Ljunggren and Klasson (1996), Ljunggren and Klasson (1997), Ljunggren and Bergsten (1998), Klasson et al. (2001), Klasson and Andersson (2001), and Klasson et al. (2002).

5.2 Borehole KXZSD8HR, ZEDEX test site

The stress analysis and comparison with raw data in borehole KXZSD8HR includes 16 measurement points of which seven include questionable strain gauge readings (Figs. 5-1 to 5-5). Thus, these results are regarded as uncertain and preliminary. The re-calculated principal and horizontal stresses are in general a few MPa lower compared to the raw data (Ljunggren and Klasson, 1996). This difference is due to both lower strain gauge readings and lower values on the elastic parameters. Both data sets indicate a decrease in stress magnitudes from 20 m borehole length, especially for σ_1 and σ_2.

The re-calculated principal stress orientations are in general the same as the raw data. Possibly, the re-calculated data gives slightly more consistent orientations for σ_1 and σ_2.

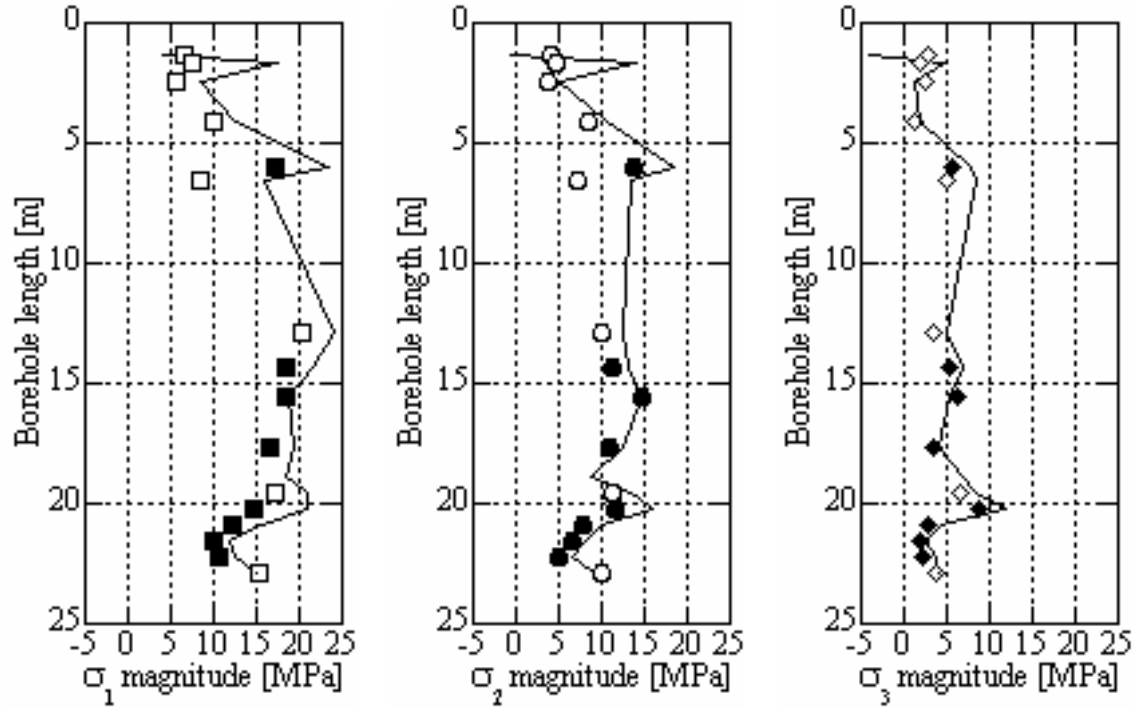

Figure 5-1. *Principal stress magnitudes in borehole KXZSD8HR. The principal stresses are represented with unfilled and filled symbols for uncertain and more reliable result, respectively. The raw data found in literature are represented with full lines.*

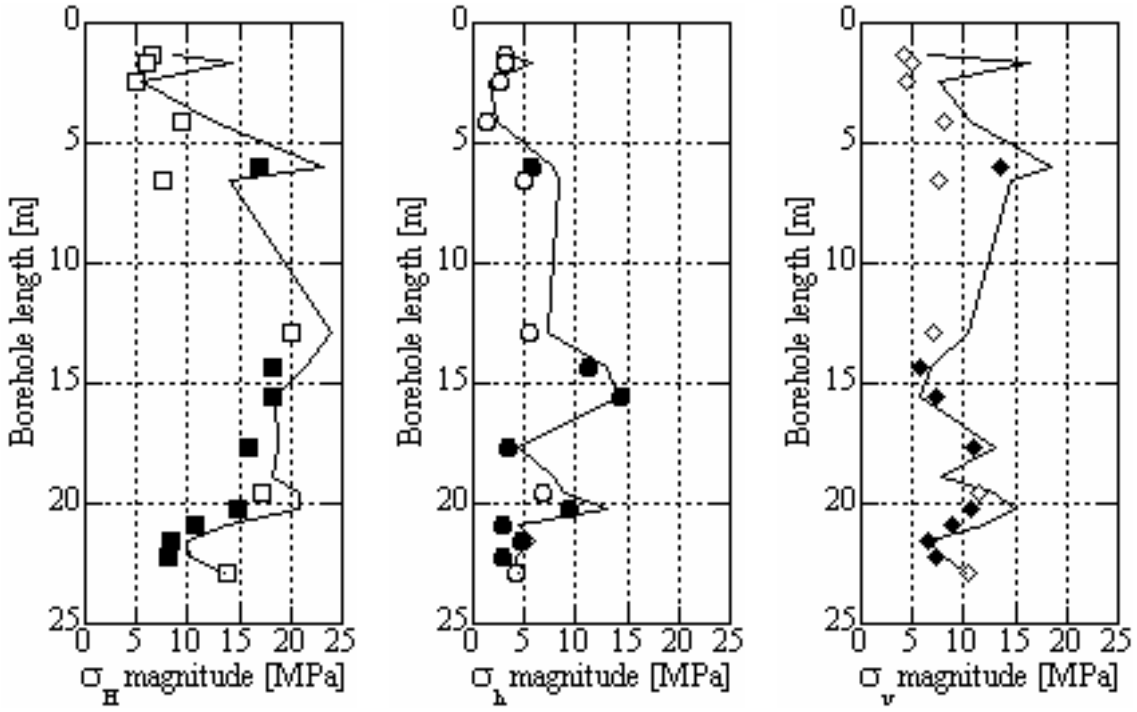

Figure 5-2. *Horizontal stress magnitudes in borehole KXZSD8HR. The horizontal stresses are represented with unfilled and filled symbols for uncertain and more reliable result, respectively. The raw data found in literature are represented with full lines.*

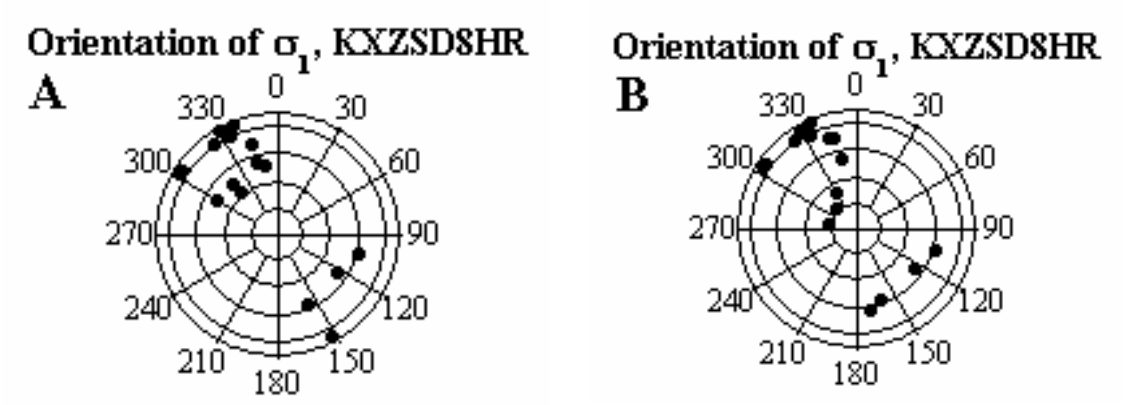

Figure 5-3. *Orientation of maximum principal stress in borehole KXZSD8HR. A and B are the re-calculated stresses and the raw data, respectively.*

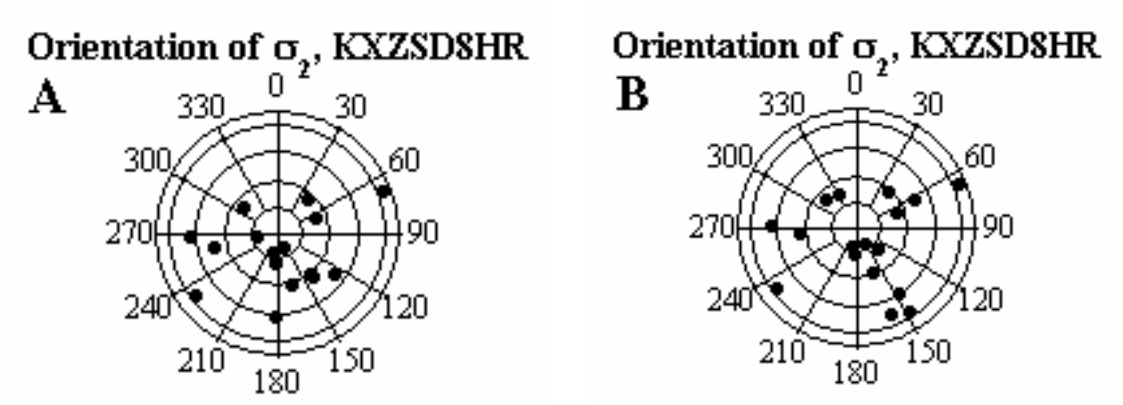

Figure 5-4. *Orientation of intermediate principal stress in borehole KXZSD8HR. A and B are the re-calculated stresses and the raw data, respectively.*

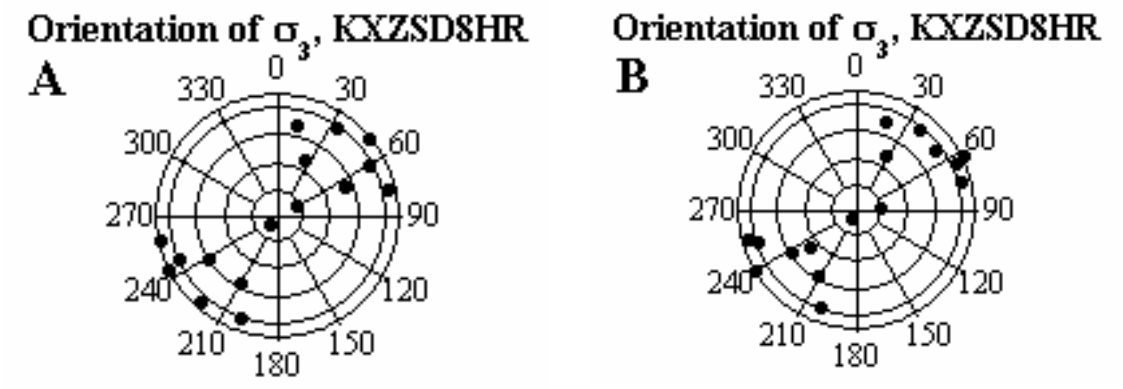

Figure 5-5. *Orientation of minimum principal stress in borehole KXZSD8HR. A and B are the re-calculated stresses and the raw data, respectively.*

5.3 Borehole KXZSD81HR, ZEDEX test site

The stress analysis and comparison with raw data in borehole KXZSD81HR includes 4 measurement points of which two include questionable strain gauge readings (0.86 and 1.43 m; Figs. 5-6 to 5-10). Thus, these results are regarded as uncertain and preliminary. The re-calculated principal and horizontal stresses are in general a few MPa lower compared to the raw data (Ljunggren and Klasson, 1996). This difference is due to both lower strain gauge readings and lower values on the elastic parameters.

The re-calculated principal stress orientations are in general the same as the raw data.

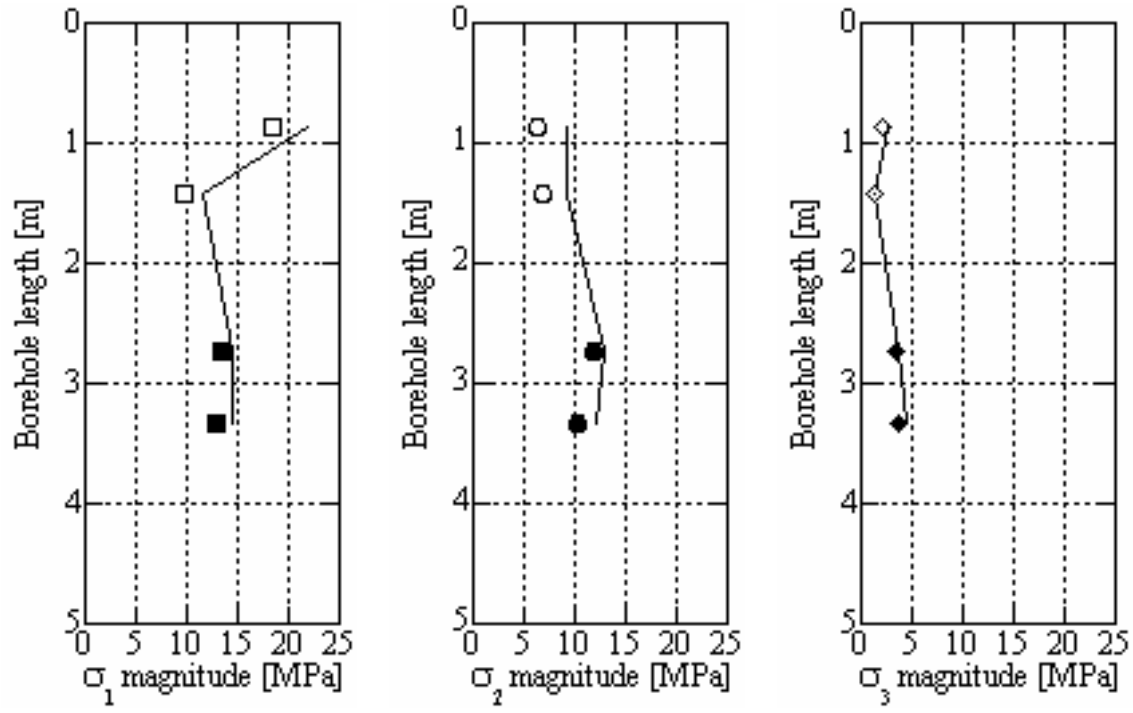

Figure 5-6. *Principal stress magnitudes in borehole KXZSD81HR. The principal stresses are represented with unfilled and filled symbols for uncertain and more reliable result, respectively. The raw data found in literature are represented with full lines.*

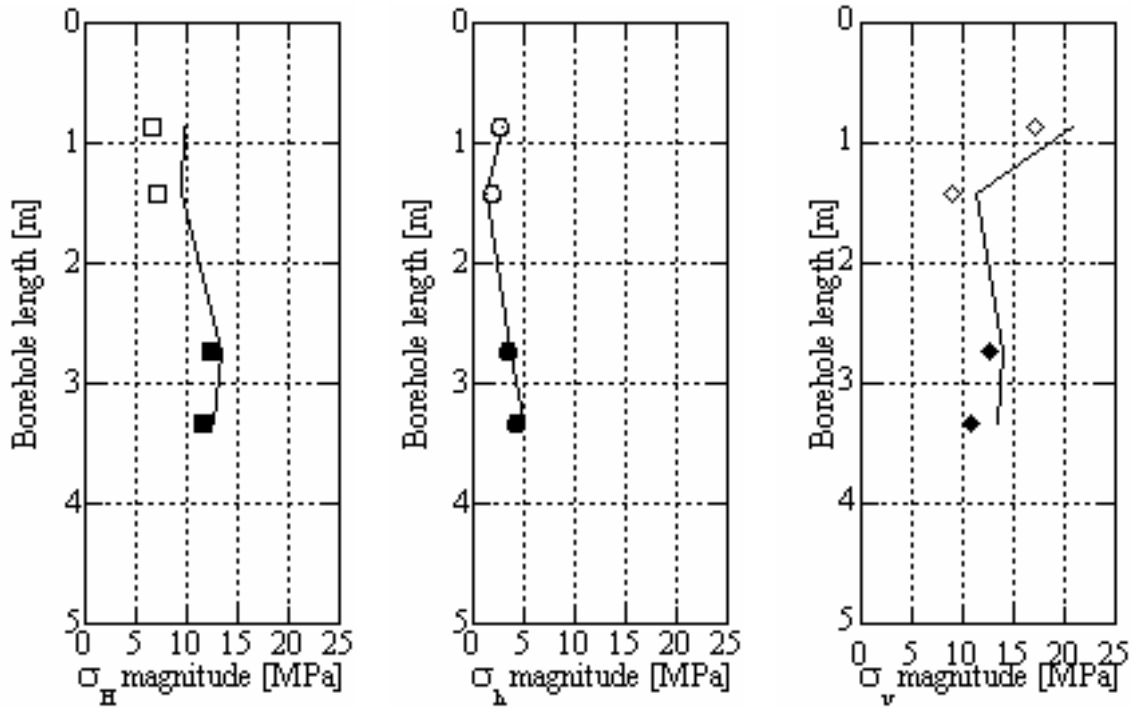

Figure 5-7. *Horizontal stress magnitudes in borehole KXZSD81HR. The horizontal stresses are represented with unfilled and filled symbols for uncertain and more reliable result, respectively. The raw data found in literature are represented with full lines.*

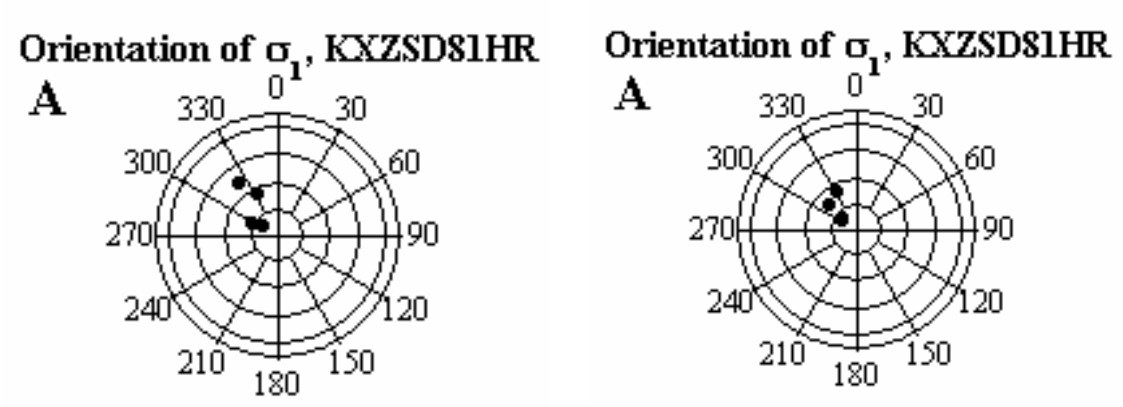

Figure 5-8. *Orientation of maximum principal stress in borehole KXZSD81HR. A and B are the re-calculated stresses and the raw data, respectively.*

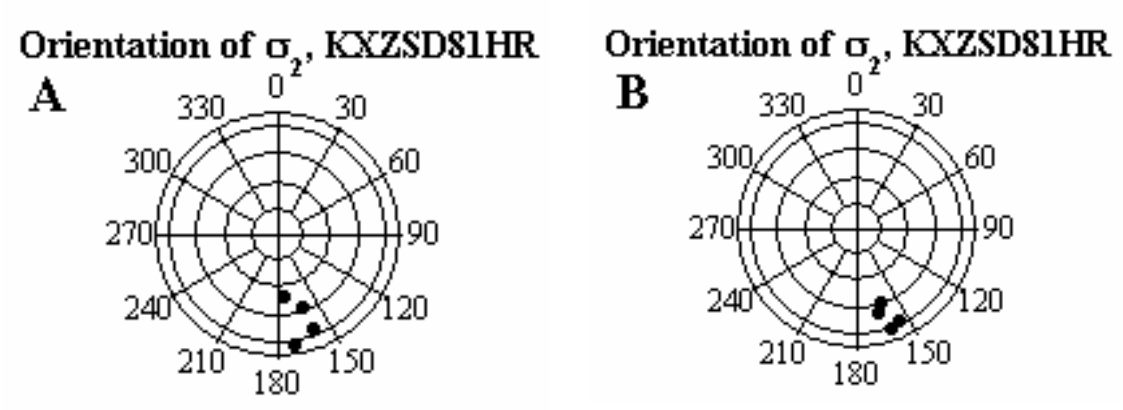

Figure 5-9. *Orientation of intermediate principal stress in borehole KXZSD81HR. A and B are the re-calculated stresses and the raw data, respectively.*

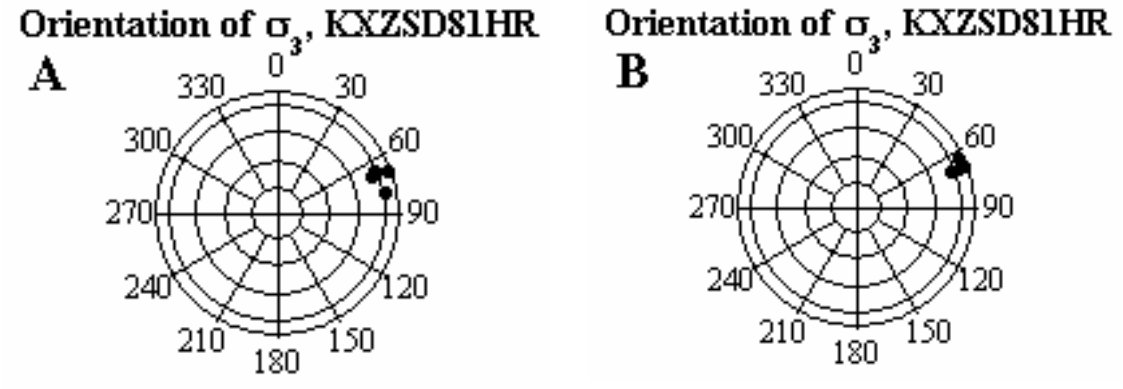

Figure 5-10. *Orientation of minimum principal stress in borehole KXZSD81HR. A and B are the re-calculated stresses and the raw data, respectively.*

5.4 Borehole KXZSD8HL, ZEDEX test site

The stress analysis and comparison with raw data in borehole KXZSD8HL includes 4 measurement points of which two include questionable strain gauge readings (23.37 and 24.06 m; Figs. 5-11 to 5-15). Thus, these results are regarded as uncertain and preliminary. The re-calculated principal and horizontal stresses are in general a few MPa lower compared to the raw data (Ljunggren and Klasson, 1996). This difference is due to both lower strain gauge readings and lower values on the elastic parameters.

The re-calculated principal stress orientations are in general the same as the raw data. The measurement point at 25.44 m seems to be an outlier when looking at the orientation of σ_2 and σ_3, giving swapped values for these two orientations. This may be explained by the similarity in σ_2 and σ_3 magnitudes.

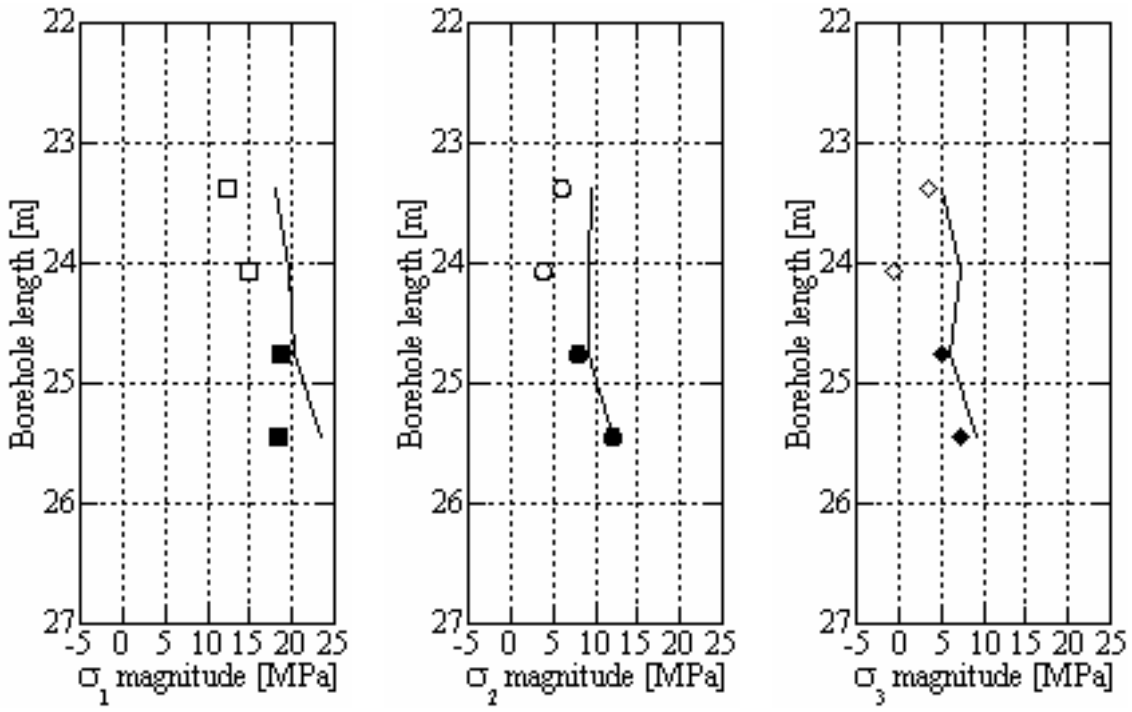

Figure 5-11. *Principal stress magnitudes in borehole KXZSD8HL. The principal stresses are represented with unfilled and filled symbols for uncertain and more reliable result, respectively. The raw data found in literature are represented with full lines.*

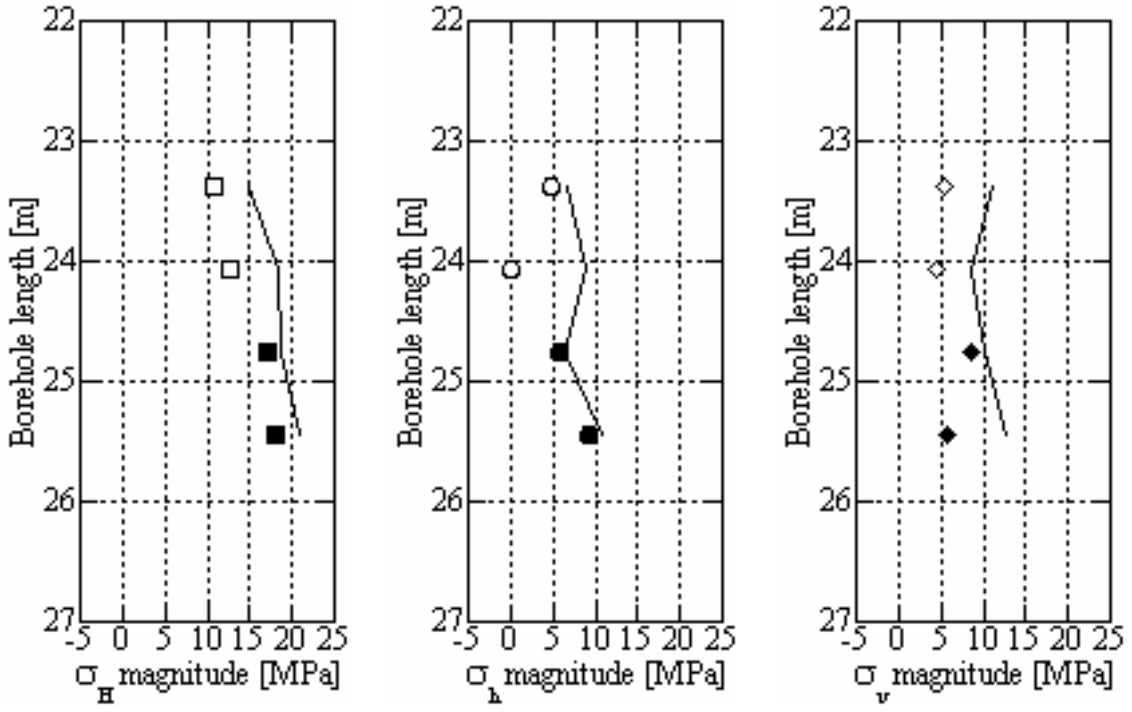

Figure 5-12. *Horizontal stress magnitudes in borehole KXZSD8HL. The horizontal stresses are represented with unfilled and filled symbols for uncertain and more reliable result, respectively. The raw data found in literature are represented with full lines.*

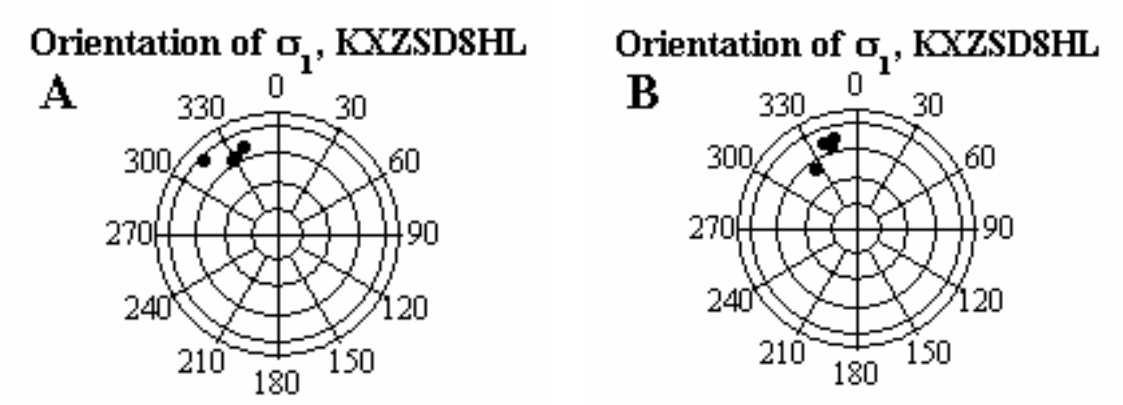

Figure 5-13. *Orientation of maximum principal stress in borehole KXZSD8HL. A and B are the re-calculated stresses and the raw data, respectively.*

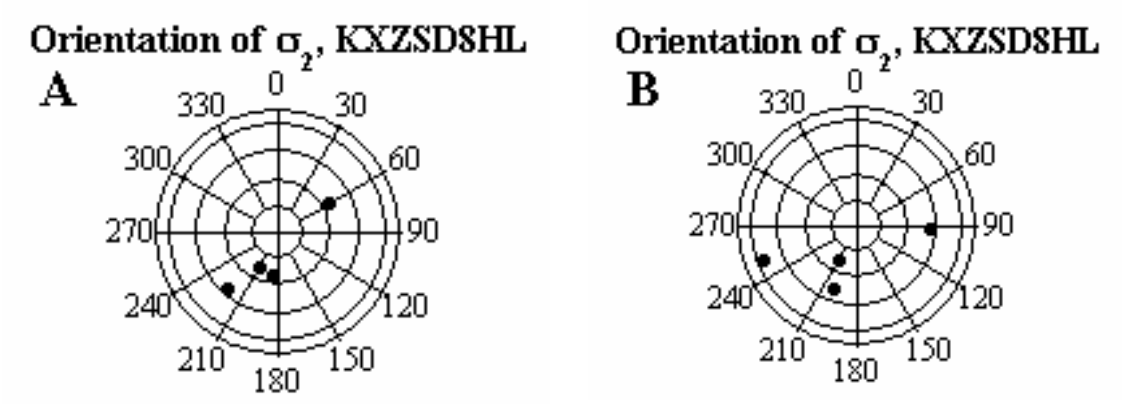

Figure 5-14. *Orientation of intermediate principal stress in borehole KXZSD8HL. A and B are the re-calculated stresses and the raw data, respectively.*

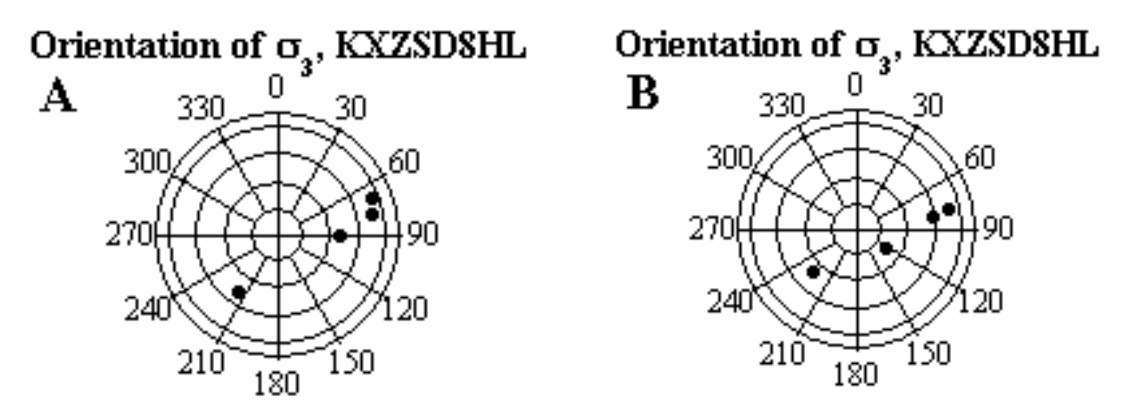

Figure 5-15. *Orientation of minimum principal stress in borehole KXZSD8HL. A and B are the re-calculated stresses and the raw data, respectively.*

5.5 Borehole KK0045G01, demo tunnel

The stress analysis and comparison with raw data in borehole KK0045G01 includes 15 measurement points of which eleven include questionable strain gauge readings (Figs. 5-16 to 5-23). Thus, these results are regarded as uncertain. The re-calculated principal and horizontal stresses are in general the same as the raw data (Klasson et al., 2001). The re-analyzed elastic parameters in this borehole are in general lower compared to the raw data. This is balanced by smaller strain gauge readings, resulting in similar stress magnitudes.

The re-calculated principal stress orientations are in somewhat different. Both data sets indicate a rather large spread of the stress orientations. For both data sets, the measurement point at 31.67 m seems to be an outlier. For the raw data (not included in plots), this was to be expected as strain rosette 1 is misplaced about 12.5 degrees. For the re-analyzed data, this rotation has been taken into account, but it seems that this procedure did not improve the reliability of the datum. In general, the results from borehole 5G01 are judged to be of poor quality. At 450m depth, 60% of the gauges were suspect or malfunctioning (e.g. improper glue mix) and all measurement points needed temperature corrections. At 480 m depth, two out of three tests were of questionable quality due to drifting gauges (probably improper glue mix) and also required temperature correction.

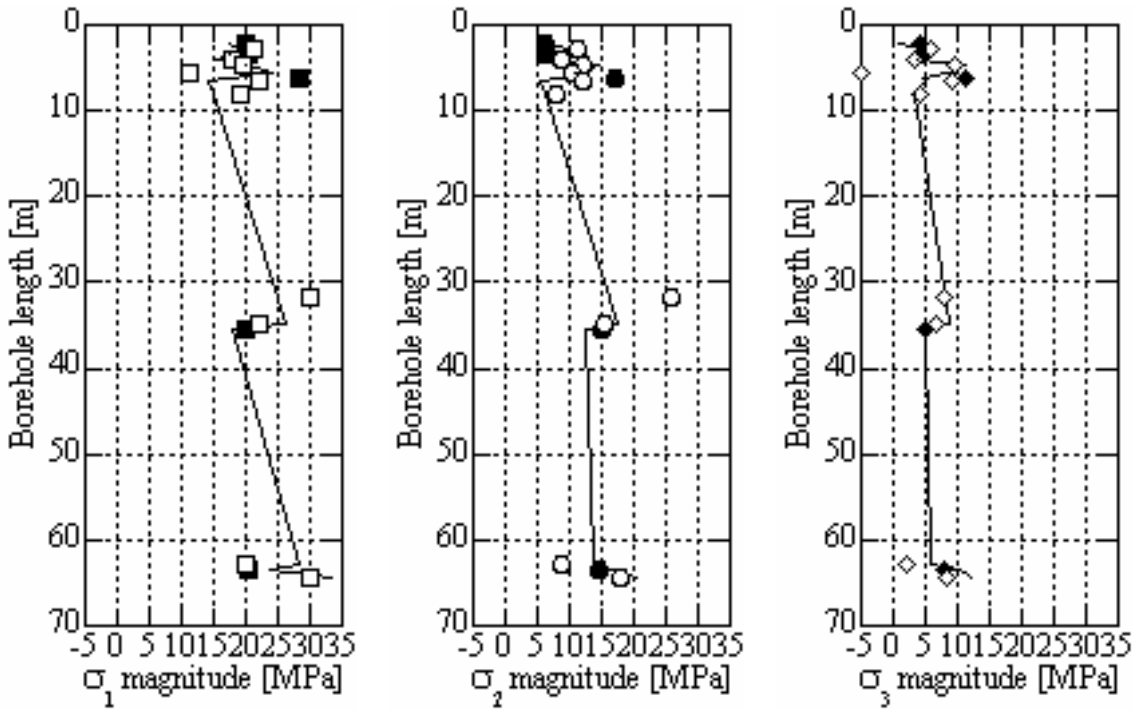

Figure 5-16. *Principal stress magnitudes in borehole KK0045G01. The principal stresses are represented with unfilled and filled symbols for uncertain and more reliable result, respectively. The raw data found in literature are represented with full lines.*

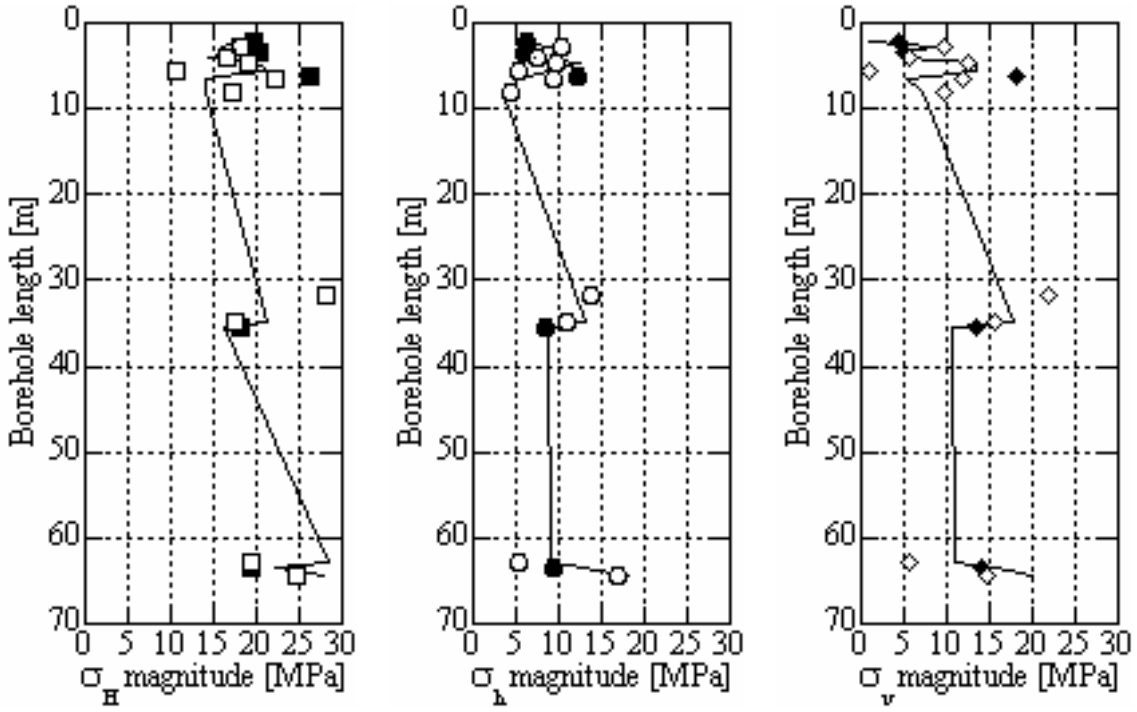

Figure 5-17. *Horizontal stress magnitudes in borehole KK0045G01. The horizontal stresses are represented with unfilled and filled symbols for uncertain and more reliable result, respectively. The raw data found in literature are represented with full lines.*

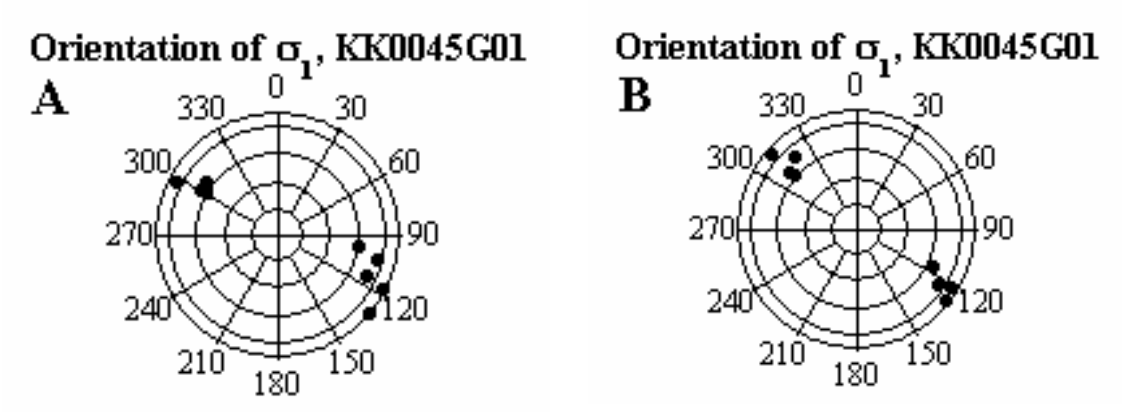

Figure 5-18. *Orientation of maximum principal stress using shallow measurement data in borehole KK0045G01 (2.24-8.16 m). A and B are the re-calculated stresses and the raw data, respectively.*

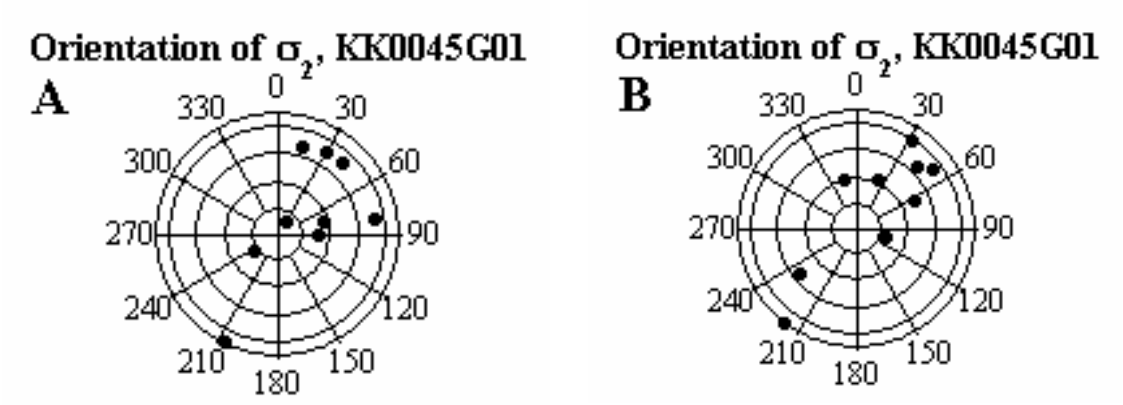

Figure 5-19. *Orientation of intermediate principal stress using shallow measurement data in borehole KK0045G01 (2.24-8.16 m). A and B are the re-calculated stresses and the raw data, respectively.*

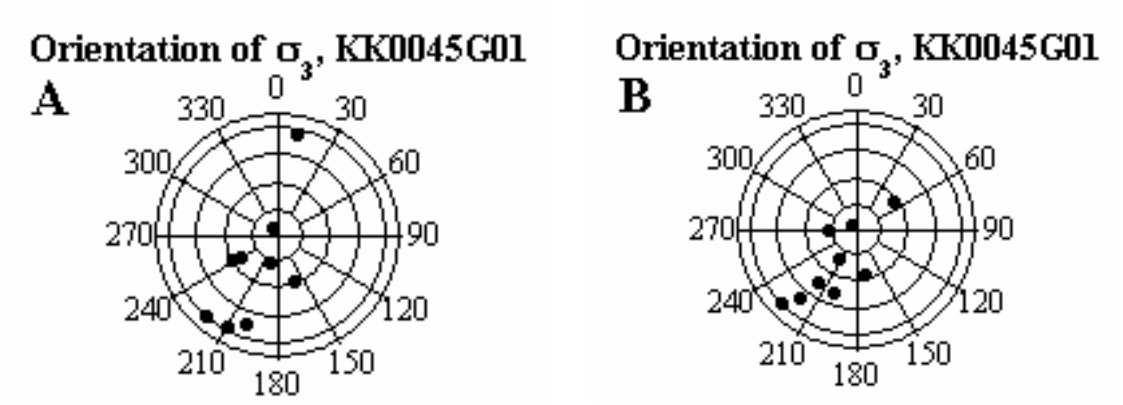

Figure 5-20. *Orientation of minimum principal stress using shallow measurement data in borehole KK0045G01 (2.24-8.16 m). A and B are the re-calculated stresses and the raw data, respectively.*

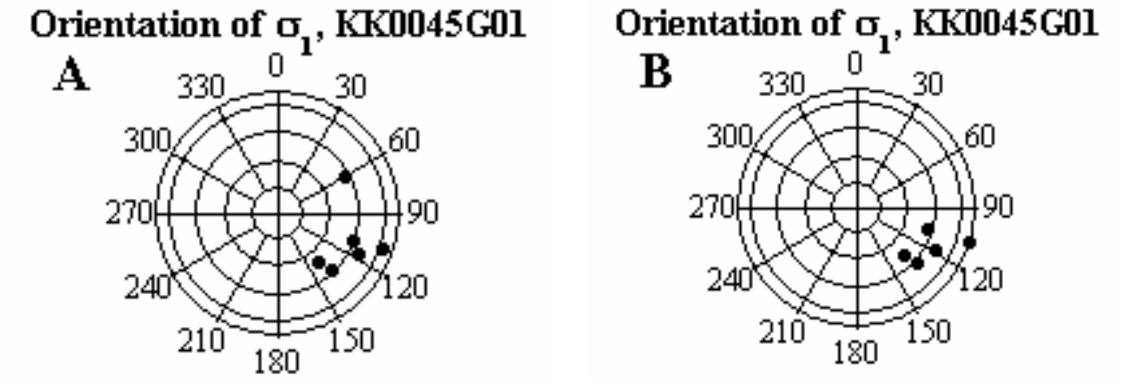

Figure 5-21. *Orientation of maximum principal stress using deeper measurement data in borehole KK0045G01 (31.67-64.51 m). A and B are the re-calculated stresses and the raw data, respectively.*

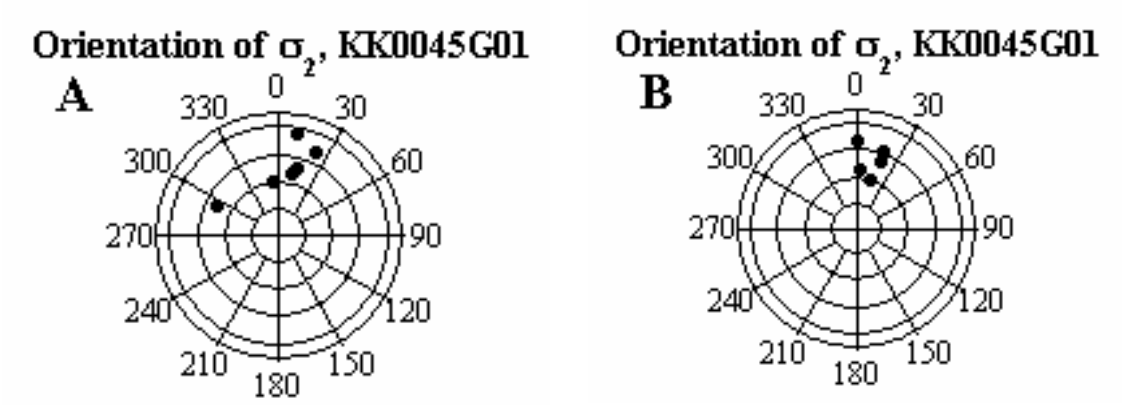

Figure 5-22. *Orientation of intermediate principal stress using deeper measurement data in borehole KK0045G01 (31.67-64.51 m). A and B are the re-calculated stresses and the raw data, respectively.*

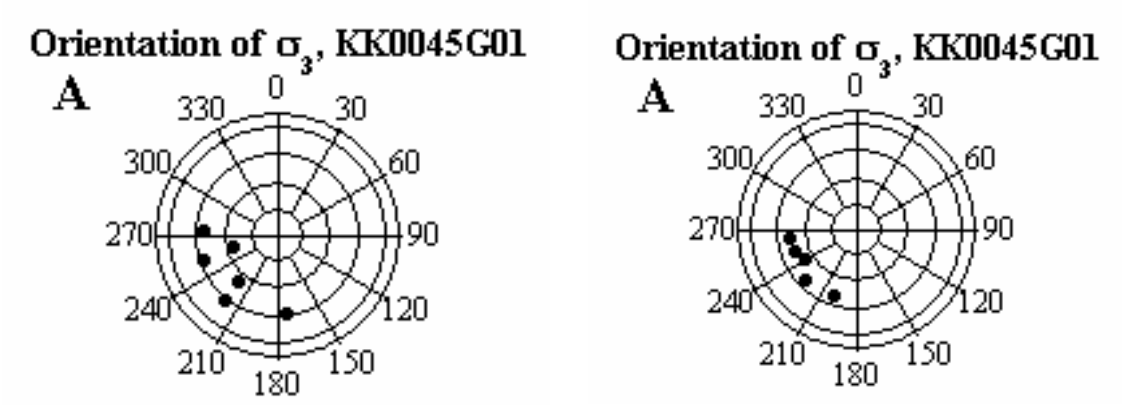

Figure 5-23. *Orientation of minimum principal stress using deeper measurement data in borehole KK0045G01 (31.67-64.51 m). A and B are the re-calculated stresses and the raw data, respectively.*

5.6 Borehole KF0093A01, F-tunnel

The stress analysis and comparison with raw data in borehole KF0093A01 includes 3 measurement points of which all data are questionable (Figs. 5-24 to 5-28). All measurement data in borehole KF0093A01 are suspect when comparing with the diagnostic strain curves of Blackwood (1978), especially concerning the significant strain drops at the end of the overcoring phase. To some extent, the observed strain drop may represent a temperature effect, but because the temperature gauge was not operating during the measurements a quantification of such an effect could not be made. Furthermore, the strain drop seemed to be too large to be solely a temperature effect. In two of the three tests, the axial and 45°-gauges increased with time at the end and after the overcoring phase, suggesting boundary yield between the cell and the rock (Irvin et al., 1987). Three axial gauges also indicate strains which seem too high for this depth (340 to 360 μstrain), whereas four gauges indicate axial strains of 200 μstrain or less.

However, a correction for boundary yield between the cell and the rock would lower the stress magnitudes even further and it is therefore more likely that the rock walls have also yielded.

The re-calculated principal and horizontal stresses are as a result considerably lower compared to the raw data (Klasson and Andersson, 2001). Hydraulic fracturing stress measurements in the same borehole (horizontal) gave σ_h = 11.0±1.2 MPa and σ_v = 19.5±1.1 MPa and a nearby vertical borehole (KA2599G01) gave σ_h = 11.0±0.9 MPa and σ_H = 21.8±2.9 MPa (Klee and Rummel, 2001). The raw data fits these values much better than the re-analyzed data. This is explained by the difference in strain reading, and in this case, the final reading gives a great difference as the strains are dropping significantly during the later phase of the overcoring. The re-analyzed data takes the stop value just before core break, while the raw data involves a reading approximately when the drilling has progressed 40 cm, i.e. during the drilling phase.

Conclusively, in this case with strains dropping significantly during overcoring, it is clearly better to make an early reading, at least in comparison with the hydraulic stress data. Interestingly, the re-analyzed data gives σ_v = 11.6 MPa (with great uncertainty though, and excluding the lower point), i.e. close to the theoretical vertical stress (~12.0 MPa). The re-calculated principal stress orientations are in general the same as the raw data.

The biaxial testing also reveals non-linear strains versus applied load leading to the conclusion that the data in borehole 3A01 are unreliable.

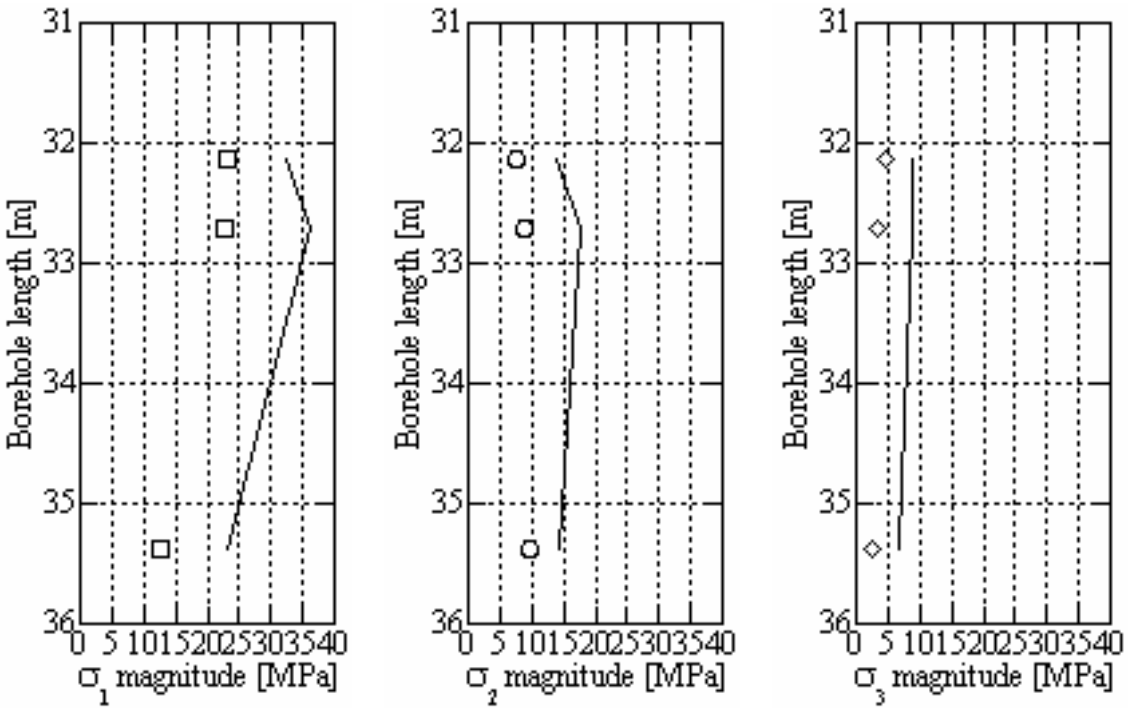

Figure 5-24. *Principal stress magnitudes in borehole KF0093A01. The principal stresses are represented with unfilled and filled symbols for uncertain and more reliable result, respectively. The raw data found in literature are represented with full lines.*

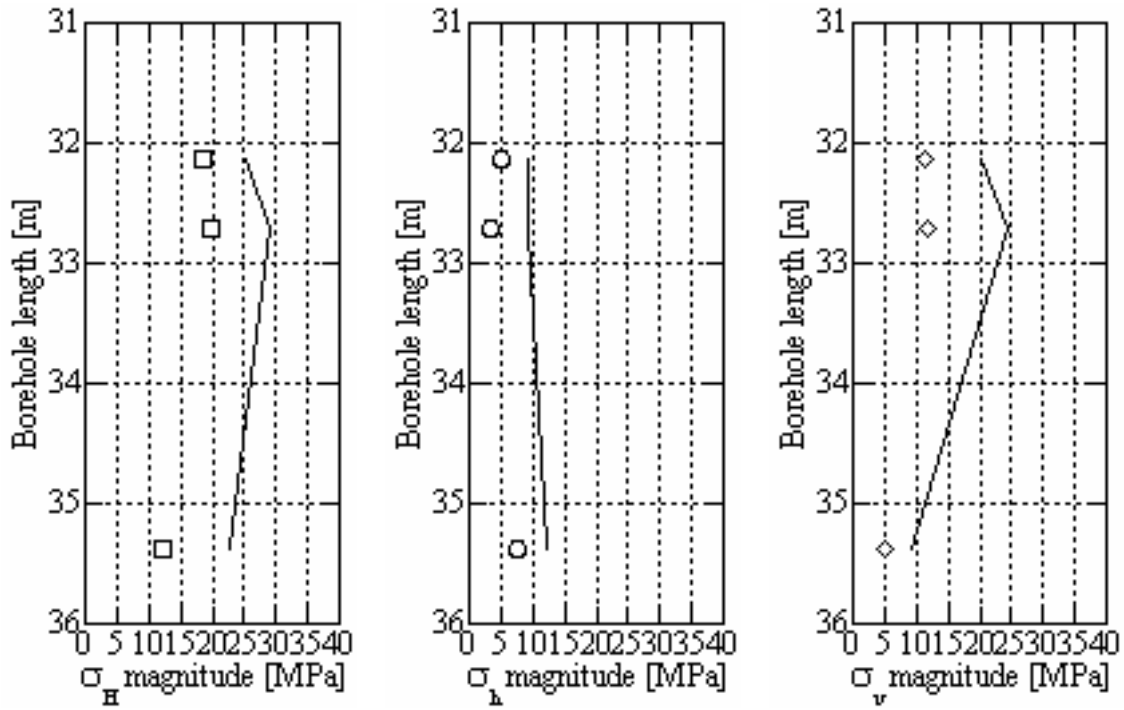

Figure 5-25. *Horizontal stress magnitudes in borehole KF0093A01. The horizontal stresses are represented with unfilled and filled symbols for uncertain and more reliable result, respectively. The raw data found in literature are represented with full lines.*

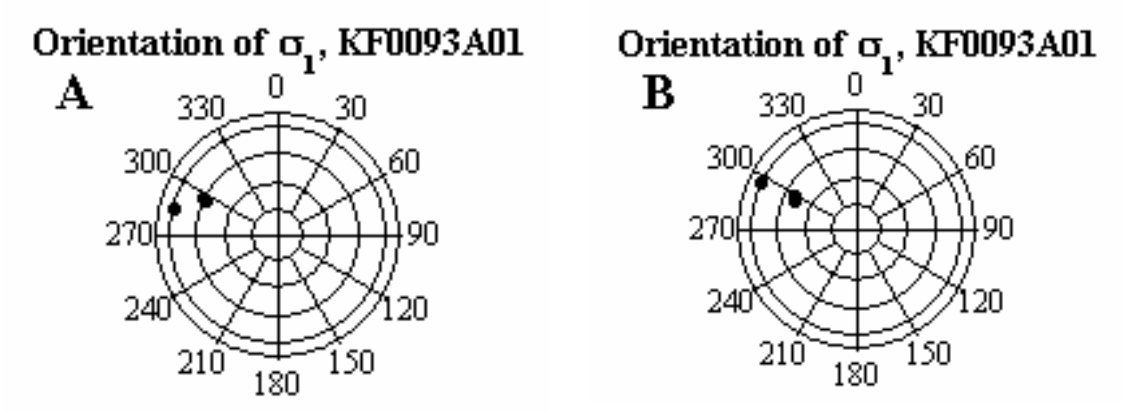

Figure 5-26. *Orientation of maximum principal stress in borehole KF0093A01. A and B are the re-calculated stresses and the raw data, respectively.*

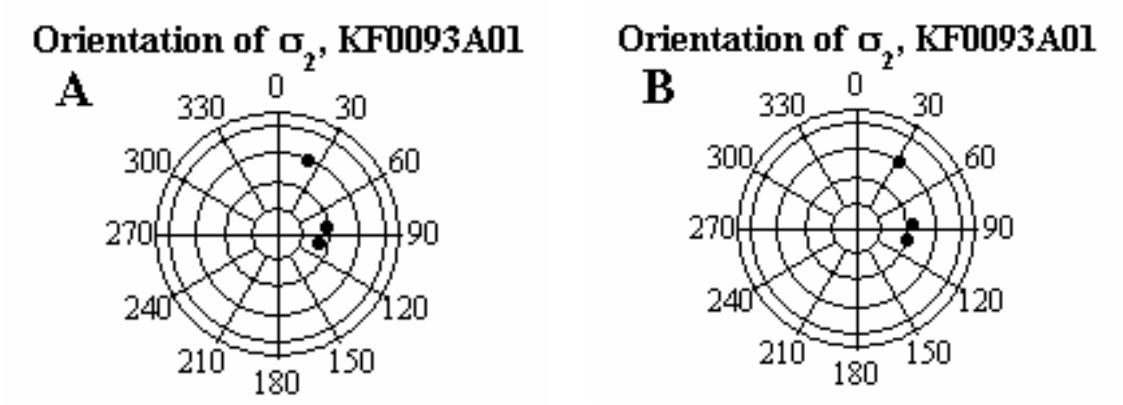

Figure 5-27. *Orientation of intermediate principal stress in borehole KF0093A01. A and B are the re-calculated stresses and the raw data, respectively.*

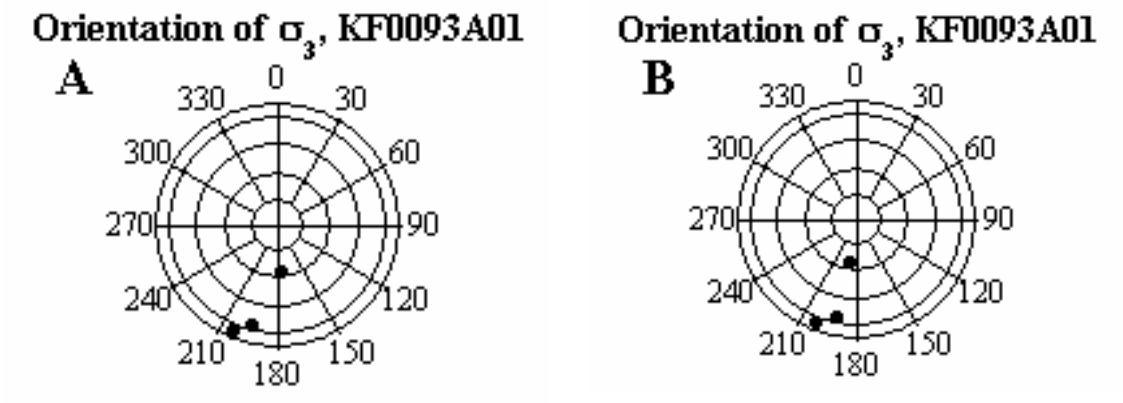

Figure 5-28. *Orientation of minimum principal stress in borehole KF0093A01. A and B are the re-calculated stresses and the raw data, respectively.*

5.7 Borehole KA3579G, Prototype Repository

The stress analysis and comparison with raw data in borehole KA3579G includes 9 measurement points (Figs. 5-29 to 5-33). Of these, the re-interpretation gave that 5 test points involves questionable strain gauge readings (unfilled symbols in the stress magnitude plots). Thus, these measurement points are regarded as uncertain and preliminary.

The re-calculated principal and horizontal stresses are in general a few MPa lower compared to the raw data (Ljunggren and Bergsten, 1998). This difference is due to both lower strain gauge readings and lower values on the elastic parameters. The principal stress orientations are in general unaffected, except for the measurement point at 8.00 m. For this measurement point, the re-analysis indicates a better fit with the overall data, especially regarding orientation of σ_2 and σ_3. Note that the measurement point is still regarded as uncertain due to suspect behavior of rosette 3.

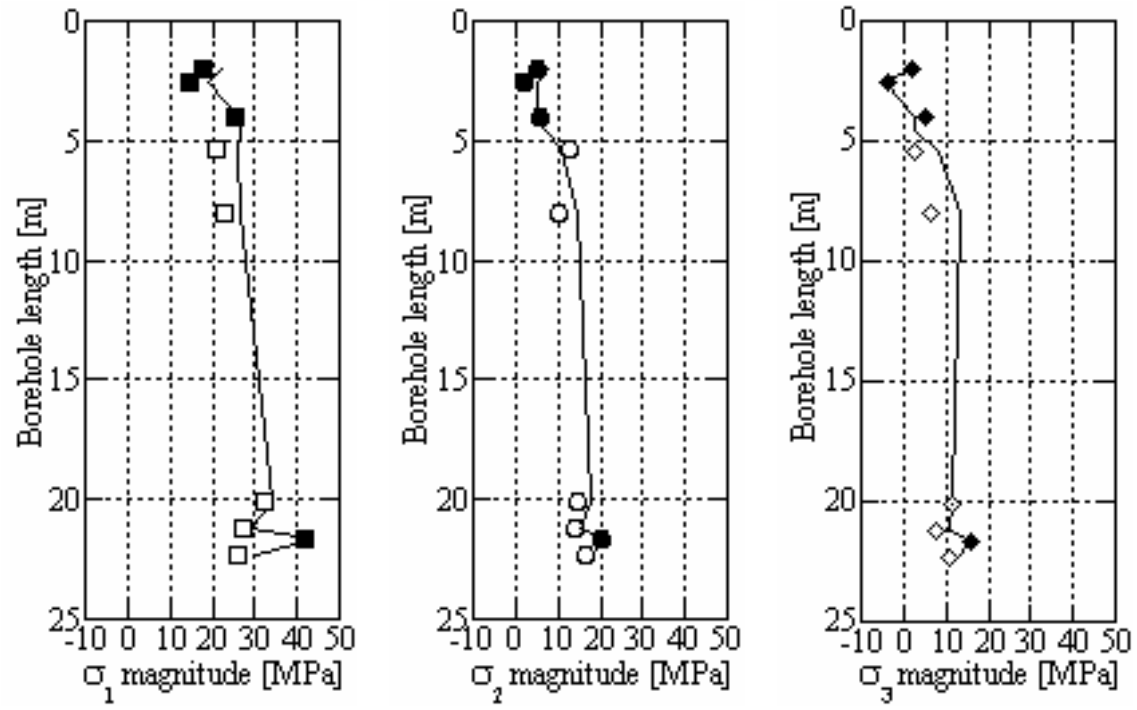

Figure 5-29. *Principal stress magnitudes in borehole KA3579G. The principal stresses are represented with unfilled and filled symbols for uncertain and more reliable result, respectively. The raw data found in literature are represented with full lines.*

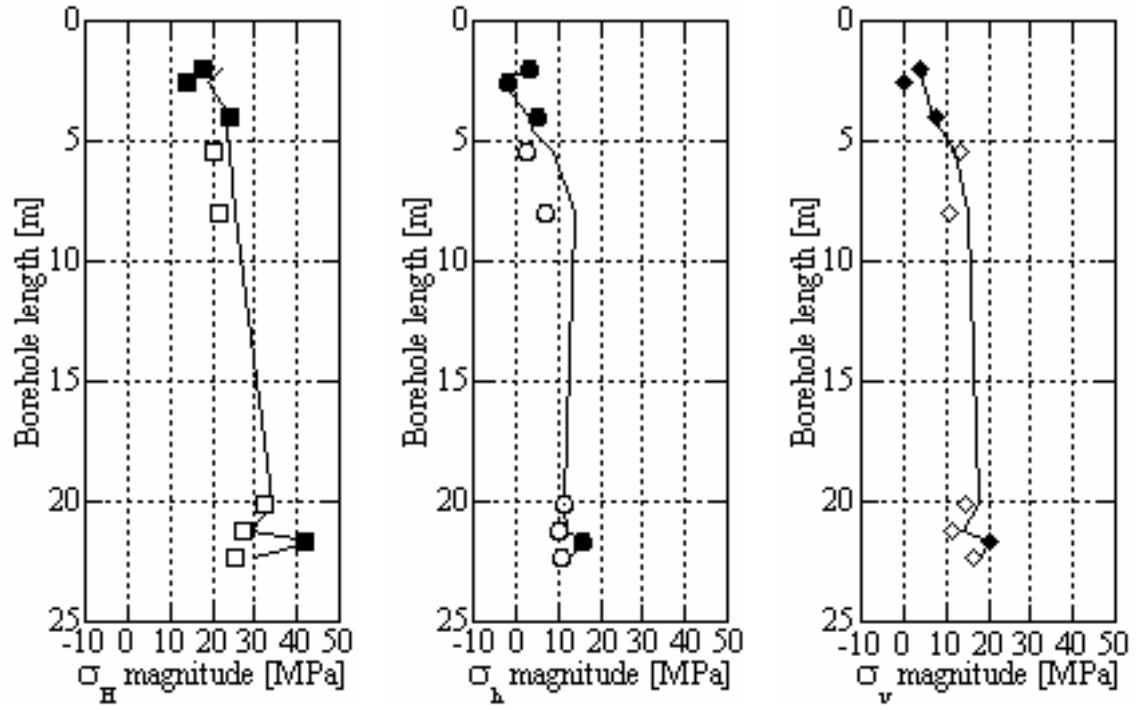

Figure 5-30. *Horizontal stress magnitudes in borehole KA3579G. The horizontal stresses are represented with unfilled and filled symbols for uncertain and more reliable result, respectively. The raw data found in literature are represented with full lines.*

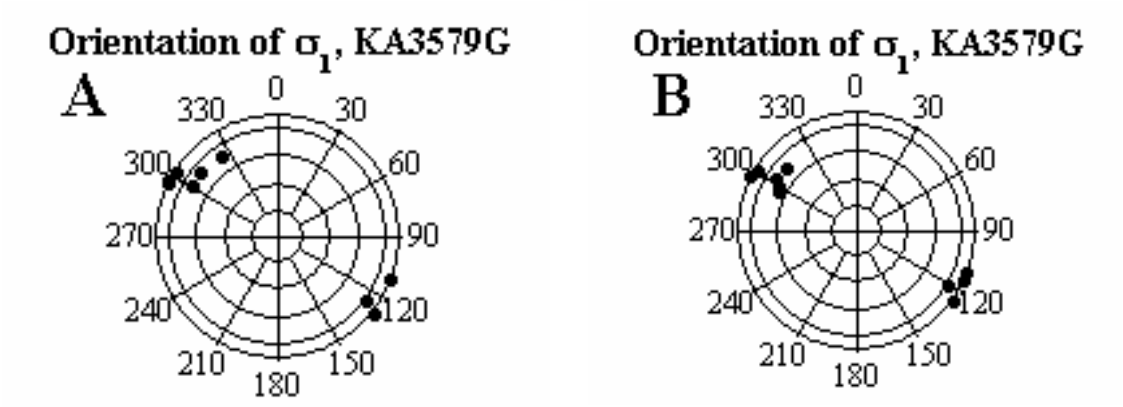

Figure 5-31. *Orientation of maximum principal stress in borehole KA3579G. A and B are the re-calculated stresses and the raw data, respectively.*

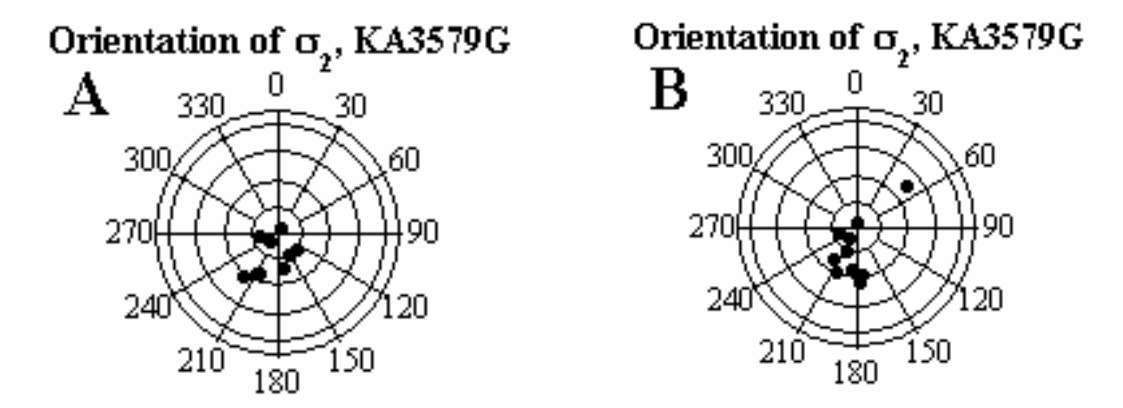

Figure 5-32. *Orientation of intermediate principal stress in borehole KA3579G. A and B are the re-calculated stresses and the raw data, respectively.*

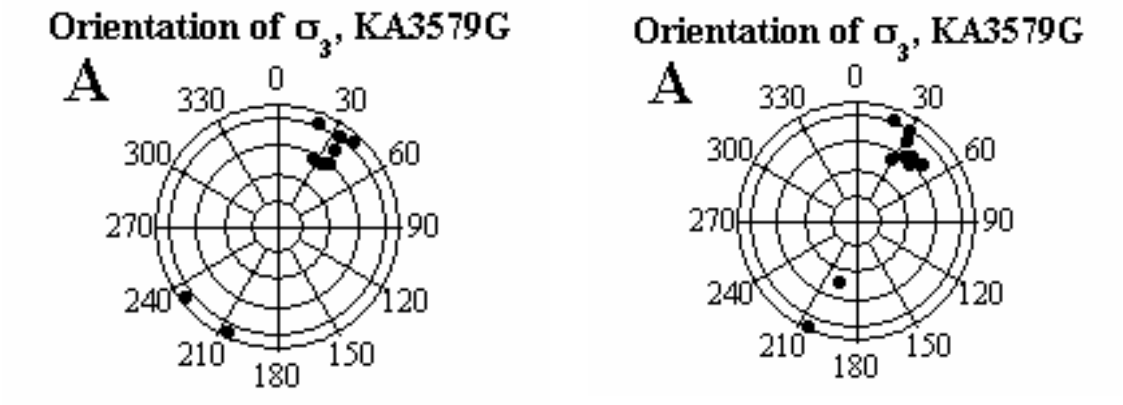

Figure 5-33. *Orientation of minimum principal stress in borehole KA3579G. A and B are the re-calculated stresses and the raw data, respectively.*

5.8 Borehole KOV01, central Oskarshamn

The stress analysis and comparison with raw data in borehole KK0045G01 includes 9 measurement points of which seven include questionable strain gauge readings (Figs. 5-34 to 5-40). However, all data from KOV01 are to be regarded as uncertain due to problems with correct gluing of the strain rosettes due to that mud-sized drill cutting could not be fully removed.

The re-calculated principal and horizontal stresses are in general a few MPa larger than the raw data (Klasson et al., 2002). The re-analyzed elastic parameters and strain readings in this borehole are in general larger compared to the raw data. The re-calculated result fits better to the hydraulic fracturing data in the same borehole giving σ_h and σ_H equal to 11.5 and 22.4 MPa, respectively, at the 300 m level, and 13.2 and 28.0 MPa, respectively, at the 500 m level (Rummel et al., 2001). The corresponding from the re-analyzed data gives σ_h and σ_H equal to 8.0 and 25.6 MPa (325.83 m), respectively at the 300 m level, and the average σ_h and σ_H equal to 8.5 and 29.4 MPa (excluding 511.78, 516.89, and 519.84 m), respectively, at the 500 m level.

The re-calculated principal stress orientations are in general the same as the raw data. For both data sets, the measurement points at 290.31 and 527.46 m seems to be outliers.

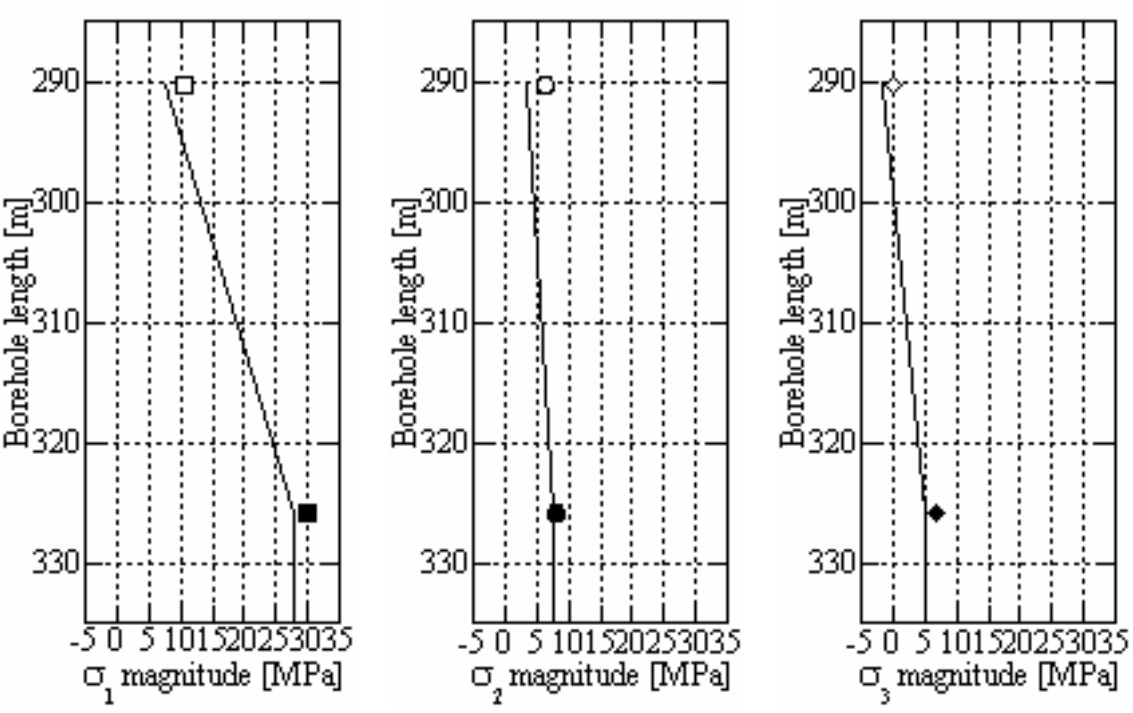

Figure 5-34. *Principal stress magnitudes at the 300 m level in borehole KOV01. The principal stresses are represented with unfilled and filled symbols for uncertain and more reliable result, respectively. The raw data found in literature are represented with full lines.*

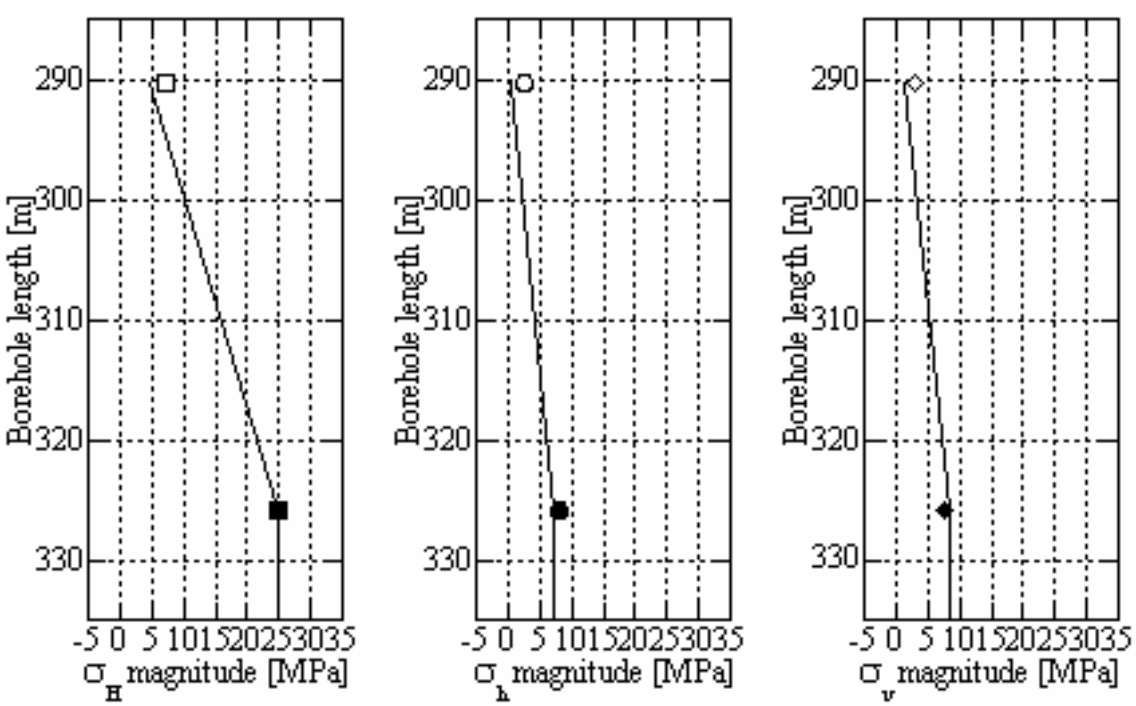

Figure 5-35. *Horizontal stress magnitudes at the 300 m level in borehole KOV01. The horizontal stresses are represented with unfilled and filled symbols for uncertain and more reliable result, respectively. The raw data found in literature are represented with full lines.*

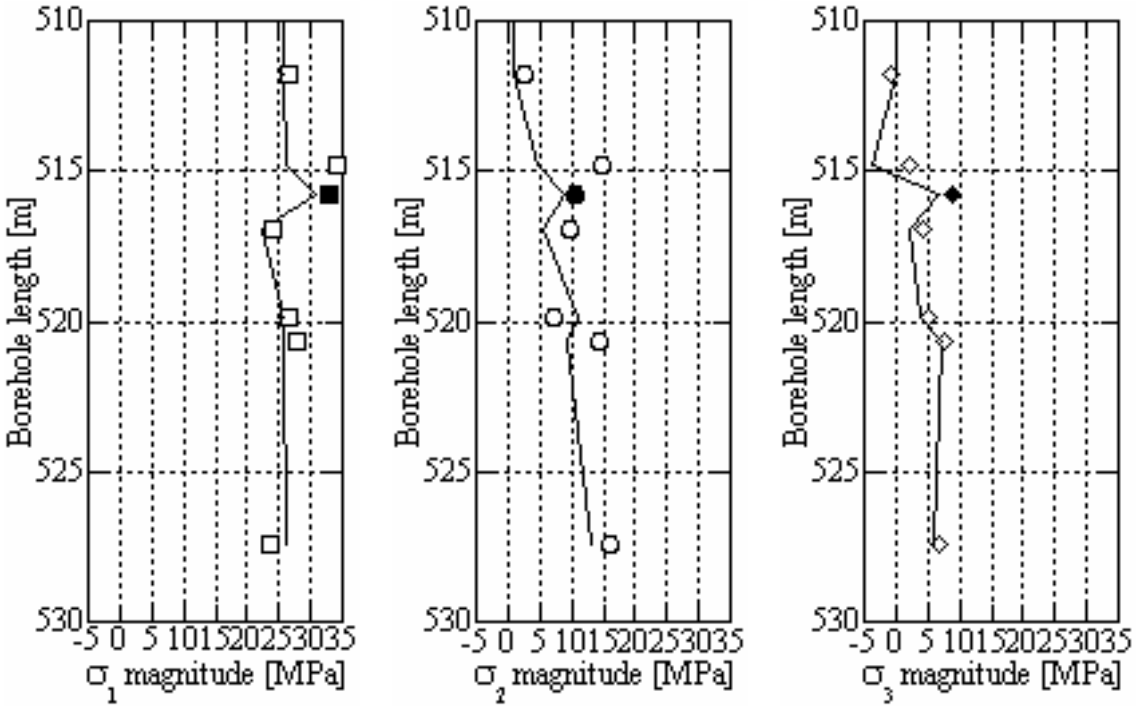

Figure 5-36. *Principal stress magnitudes at the 500 m level in borehole KOV01. The principal stresses are represented with unfilled and filled symbols for uncertain and more reliable result, respectively. The raw data found in literature are represented with full lines.*

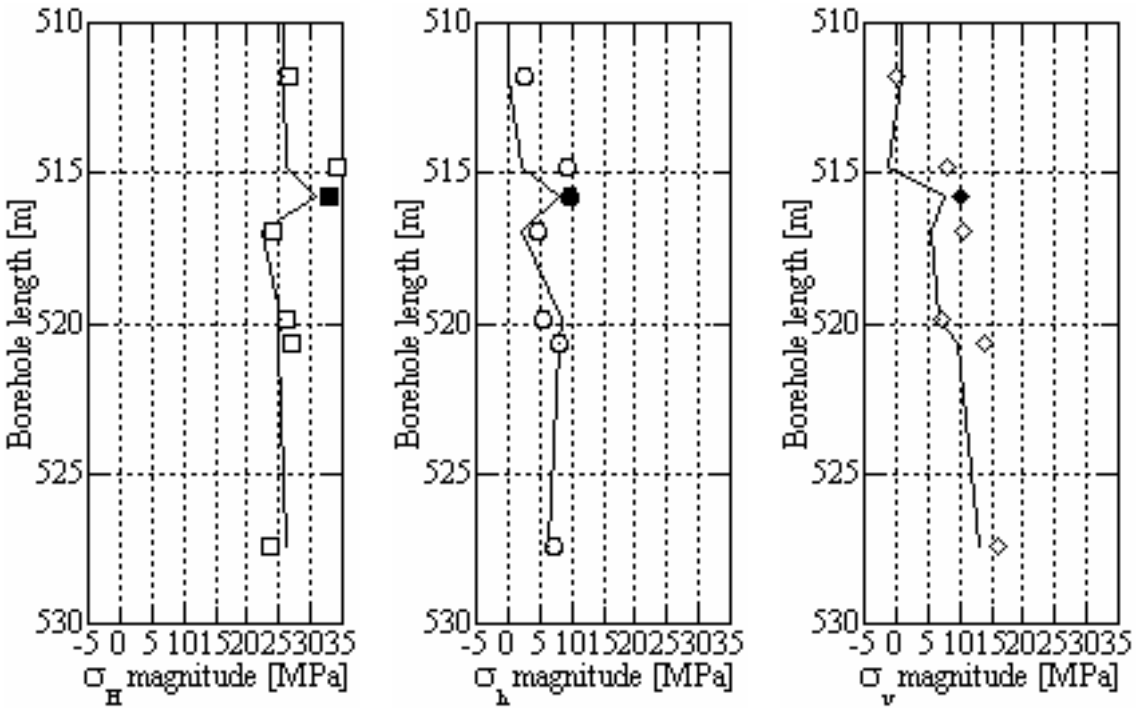

Figure 5-37. *Horizontal stress magnitudes at the 500 m level in borehole KOV01. The horizontal stresses are represented with unfilled and filled symbols for uncertain and more reliable result, respectively. The raw data found in literature are represented with full lines.*

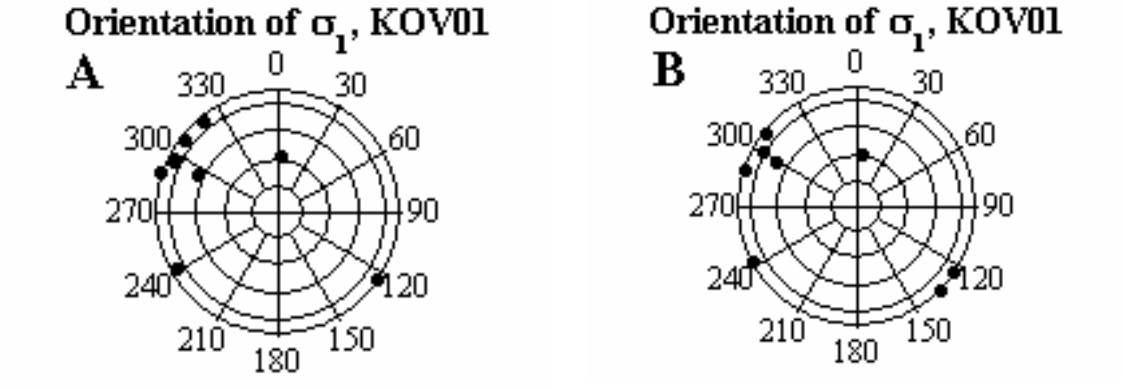

Figure 5-38. *Orientation of maximum principal stress in borehole KOV01. A and B are the re-calculated stresses and the raw data, respectively.*

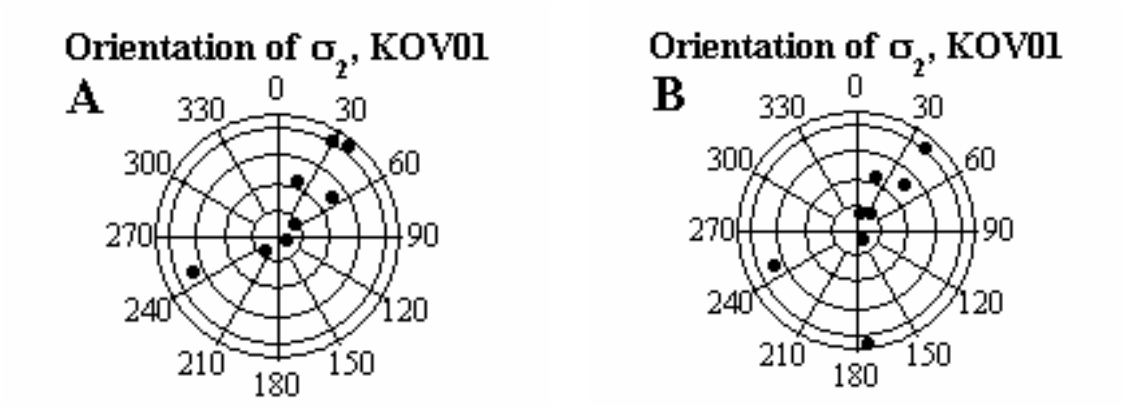

Figure 5-39. *Orientation of intermediate principal stress in borehole KOV01. A and B are the re-calculated stresses and the raw data, respectively.*

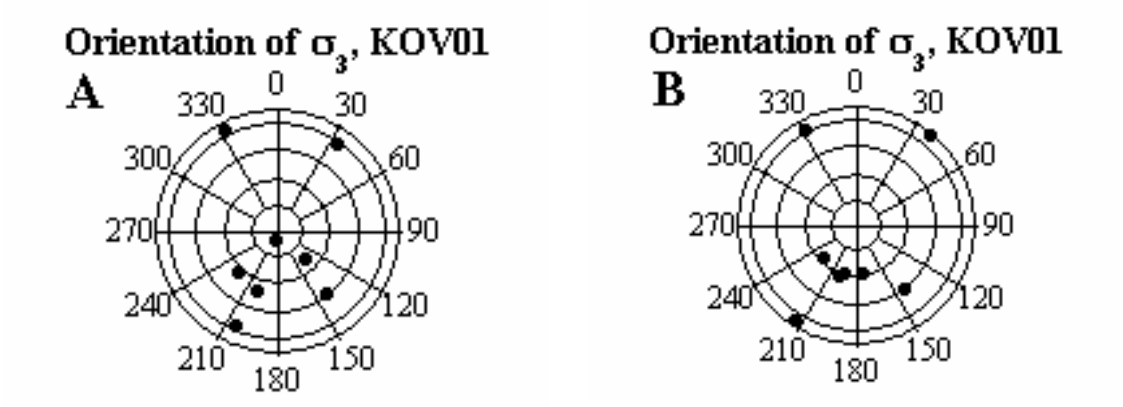

Figure 5-40. *Orientation of minimum principal stress in borehole KOV01. A and B are the re-calculated stresses and the raw data, respectively.*

6 Results

6.1 General

In this chapter, a summary of the analysis results is presented. The results are presented as tables indicating erroneous or questionable strain gauges for each measurement point. Because this study deals with stress measurements at the single test scale, erroneous or questionable strain rosettes are still included (in order to calculate the stress). The detailed results of the data analysis are presented in appendices 3 to 5.

6.2 Results from data analysis

The analysis of the overcoring data using the Borre Probe is presented in Table 6-1 (see also Appendix 3). In total, 64 strain gauges are excluded out of totally 729. Furthermore, 252 strain gauges are of doubtful quality and are likely to be excluded in the future stress analysis. 22 measurement points requires temperature corrections (mainly borehole KK0045G01) and another 11 measurement points indicate a high temperature in the test section (borehole KAS05 not included). However, the latter is difficult to correct for because the data records are incomplete. During the measurements in borehole KA0093A01 and most tests in borehole KOV01 the temperature-measuring device was malfunctioning.

Table 6-1. Results from analysis of strain data during the overcoring test using the Borre Probe. Doubtful gauges/rosettes expressed as R1(1,2,3), i.e. axial, tangential and 45 strain gauges in rosette 1. Temperature corrections and probable temperature induced strains indicated by T and T?, respectively.

Borehole	Borehole depth [m]	Excluded	Questionable data	Temp Effects
KXZSD8HR	1.29		R1, R2, R3	T
	1.66		R1, R2, R3	T?
	2.40		R2, R3	T?
	3.18	R1(1), R2(1), R3(1)		T?
	4.07		R1, R2, R3	
	5.96			
	6.61		R3	
	11.49	R1, R2, R3		
	12.28			
	12.93		R3?	
	13.59		R1, R2, R3	

Table 6-1. Continued.

Borehole	Borehole depth [m]	Excluded	Questionable data	Temp Effects
KXZSD8HR	14.30			
	15.60			
	16.96	R1	R2, R3	
	17.62			
	18.27		R1, R2, R3	
	18.92		R1, R2, R3	
	19.57		R1?	
	20.22			
	20.85			
	21.50			
	22.21			T?
	22.94	R3		
KXZSD81HR	0.86		R1, R2, R3	T?
	1.43		R2, R3	T?
	2.73			T?
	3.34			T?
KXZSD8HL	23.37	R2	R1, R3	T
	24.06	R2	R1	
	24.75			
	25.44			
KK0045G01	1.20			T
	2.24			T
	2.70	R2		T
	3.33			T
	4.12		R2, R3	T
	4.53		R3	T
	4.97	R3	R1, R2	T
	5.51	R1		T
	6.07			T
	6.50		R1, R3	T
	8.16	R1(1)	R2	T
	31.67		R3 (R1 misplaced)	T
	32.48		R1, R2, R3	T
	33.35	R1, R2, R3		T
	34.77		R2	T
	35.48	R1(2), R2(2), R3(1)		T
	62.82		R1, R2, R3	
	63.59			T
	64.51		R1, R2, R3	T
KA0093A01	32.14		R1, R2, R3	Malfunc.
	32.70		R1, R2, R3	Malfunc.
	33.23	R1, R2, R3		Malfunc.
	35.38		R1, R2, R3	Malfunc.

Table 6-1. Continued.

Borehole	Borehole depth [m]	Excluded	Questionable data	Temp Effects
KA3579G	0.88	R1, R2, R3		
	2.04			
	2.53			T
	3.99			T?
	4.54		R2	T?
	5.41		R1	T?
	8.00		R3	T
	20.06		R1, R2, R3	
	21.21		R3	
	21.70			
	22.31		R1	
KOV01	290.31		R1, R2, R3	
	325.83			
	511.78		R1, R2, R3	Malfunc.
	514.79		R1, R2, R3	Malfunc.
	515.80			Malfunc.
	516.89		R1, R2, R3	Malfunc.
	519.84		R1, R2, R3	Malfunc.
	520.71		R1, R2, R3	Malfunc.
	527.46		R3	Malfunc.

The analysis of the biaxial data using the Borre Probe is presented in Table 6-2 (see also Appendix 4). Almost all biaxial tests indicate hysteresis and some degree of anisotropy. The latter is however not large enough to require correction according to Amadei's rule of thumb (1983a and 1983b). In total, 13 measurement points did not include a following biaxial test. 4 biaxial tests indicate fracturing of the core, and 7 biaxial tests include one or more gauges with clearly nonlinear responses.

The elastic parameters were evaluated both with and without doubtful strain gauges for comparison (see Appendix 5).

Table 6-2. Results from analysis of strain data during the biaxial test using the Borre Probe. Doubtful gauges/rosettes expressed as R1(1,2,3), i.e. axial, tangential and 45 strain gauges in rosette 1.

Borehole	Borehole depth [m]	Excluded	Questionable data
KXZSD8HR	1.29		R1, R2, R3
	1.66		R1, R2, R3
	2.40		R2, R3
	3.18	Not tested in biax	
	4.07		R1, R2, R3. Fractures at 6 MPa
	5.96		Several gauges nonlinear
	6.61		R3
	11.49	Not tested in biax	
	12.28	Not tested in biax	
	12.93		R3
	13.59	Not tested in biax	
	14.30		Several gauges nonlinear
	15.60		Core fractures during unloading? R1, R2, R3
	16.96	Not tested in biax	
	17.62		
	18.27		R1, R2, R3
	18.92	Not tested in biax	
	19.57		R1
	20.22	R2	R1
	20.85		
	21.50		
	22.21	R2	
	22.94		R3
KXZSD81HR	0.86		R1, R2, R3. R2(1,2), R3(1,2) nonlinear
	1.43		R2, R3. R3 nonlinear
	2.73		
	3.34		R1(2), R3(2) nonlinear
KXZSD8HL	23.37	R2	R1, R3.
	24.06	R2	R1
	24.75		
	25.44		
KK0045G01	1.20		
	2.24		R1
	2.70	R2	R1
	3.33		R1, R2, R3
	4.12	Not tested in biax	
	4.53		R3
	4.97	Not tested in biax	

Table 6-2. Continued.

Borehole	Borehole depth [m]	Excluded	Questionable data
KK0045G01	5.51	R1	
	6.07		R1, R2, R3
	6.50		R1, R2, R3
	8.16	R1(1)	R1, R2, R3
	31.67		R3 (R1 misplaced)
	32.48		R1, R2, R3. Unstable axial gauges
	33.35	Not tested in biax	
	34.77		R2
	35.48	R1(2), R2(2), R3(1)	
	62.82		R1, R2, R3
	63.59		
	64.51		R1, R2, R3
KA0093A01	32.14		R1, R2, R3. Core fractures at 5-6 MPa
	32.70		R1, R2, R3
	33.23	Not tested in biax	
	35.38		R1, R2, R3
KA3579G	0.88	Not tested in biax	
	2.04		R1, R2, R3
	2.53		R1, R2, R3. R1(1) indicates fracturing
	3.99		
	4.54		R1, R2, R3
	5.41		R1
	8.00		R3. R1(1,2), R2(1,2) nonlinear
	20.06		R1, R2, R3.
	21.21		R3
	21.70		
	22.31		R1
KOV01	290.31	R3	R1, R2
	325.83		R1, R2, R3
	511.78	R3	R1, R2
	514.79	Not tested in biax	
	515.80	R2, R3	R1
	516.89		R1, R2, R3
	519.84		R1, R2, R3
	520.71		R1, R2, R3
	527.46	Not tested in biax	

6.3 Results from stress calculation using the re-analysed strain data

6.3.1 Summary of stress calculation results

The stress calculation using re-analyzed data indicates, apart from borehole KOV01, lower principal and horizontal stress magnitudes. This could be explained by lower values on both the strain gauge readings and the elastic parameters. The horizontal and vertical stress magnitudes for the in-situ measurements points at the Äspö HRL (i.e. excluding excavation disturbed points and borehole KOV01) are displayed in Figs. 6-1 to 6-3 and the orientation of maximum horizontal stress in Fig. 6-4. The results should be regarded as preliminary as many measurement points include strain gauges that have a suspicious response during overcoring (unfilled symbols). Only the data with all gauges seemingly functioning should be regarded as final or "as good as it gets" (filled symbols). Removing the suspicious/erroneous gauges implies that the data must be integrated in order to solve the state of stress. However, this is outside the scope of this report and this will be presented in future studies.

The average elastic parameters at Äspö HRL (excluding borehole KAS05) using all gauges are E=62.3±5.8 GPa and υ=0.25±0.03, whereas exclusion of data influenced by the tunnel gives E=60.9±6.9 GPa and υ=0.25±0.03.

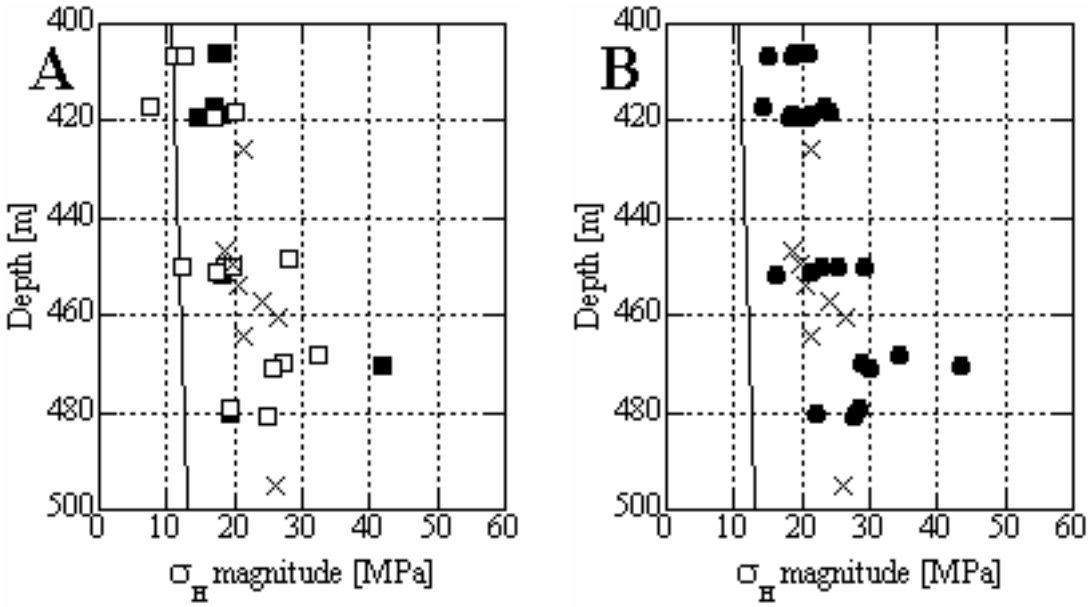

Figure 6-1. *Maximum horizontal stress magnitude for in-situ stress measurement points at the Äspö HRL. The stresses are in A represented with unfilled and filled squares for uncertain and more reliable result, respectively. The original results in B are represented by filled circles. Crosses are results from hydraulic fracturing stress measurements and the full line represents the theoretical vertical stress.*

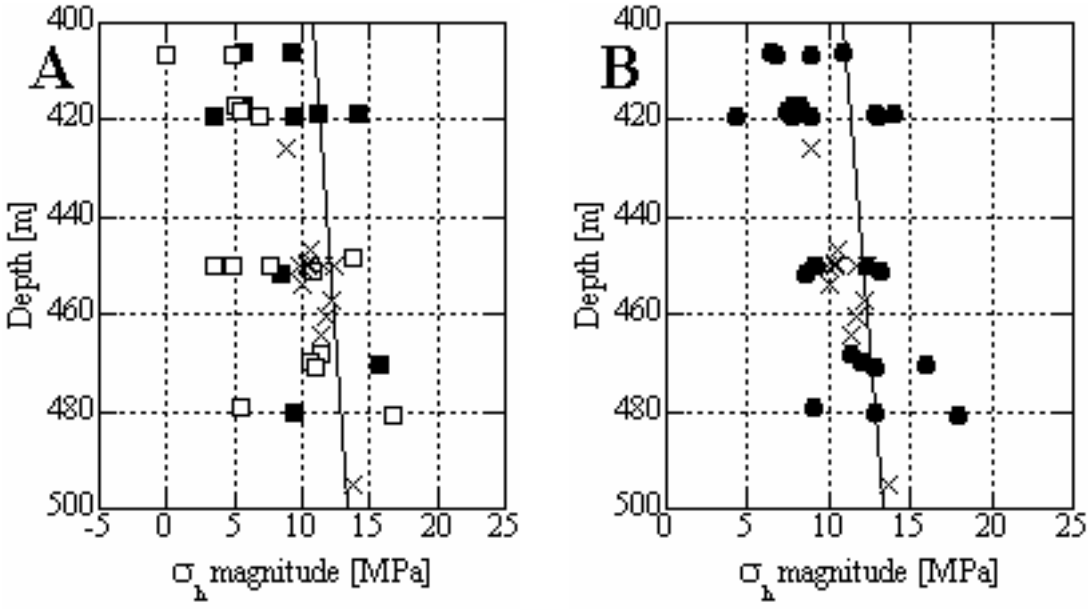

Figure 6-2. *Minimum horizontal stress magnitude for in-situ stress measurement points at the Äspö HRL. The stresses are in A represented with unfilled and filled squares for uncertain and more reliable result, respectively. The original results in B are represented by filled circles. Crosses are results from hydraulic fracturing stress measurements and the full line represents the theoretical vertical stress.*

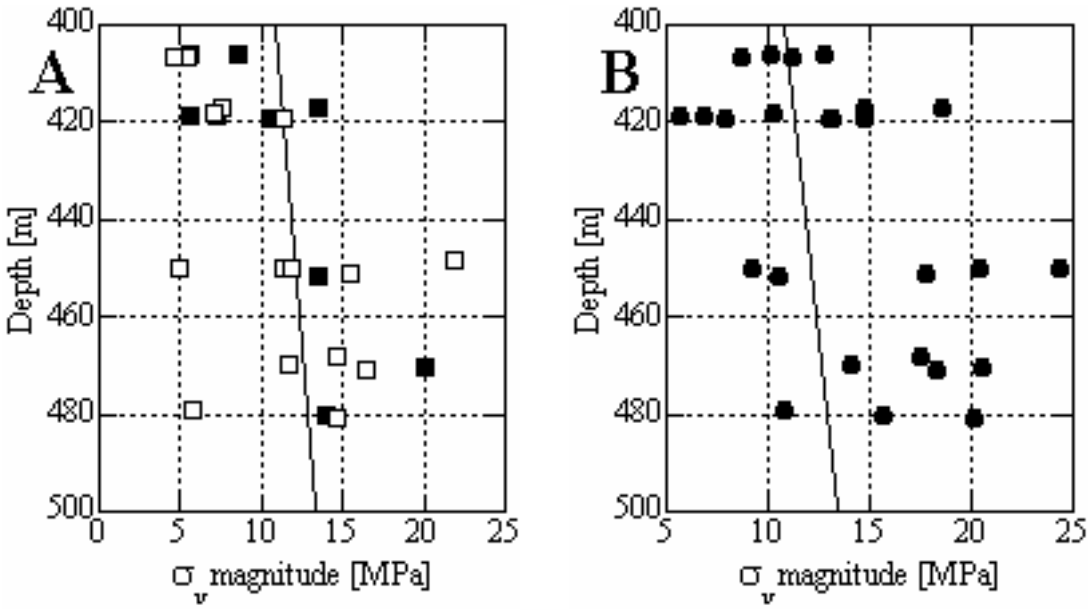

Figure 6-3. *Vertical stress magnitude for in-situ stress measurement points at the Äspö HRL. The stresses are in A represented with unfilled and filled squares for uncertain and more reliable result, respectively. The original results in B are represented by filled circles. Crosses are results from hydraulic fracturing stress measurements and the full line represents the theoretical vertical stress.*

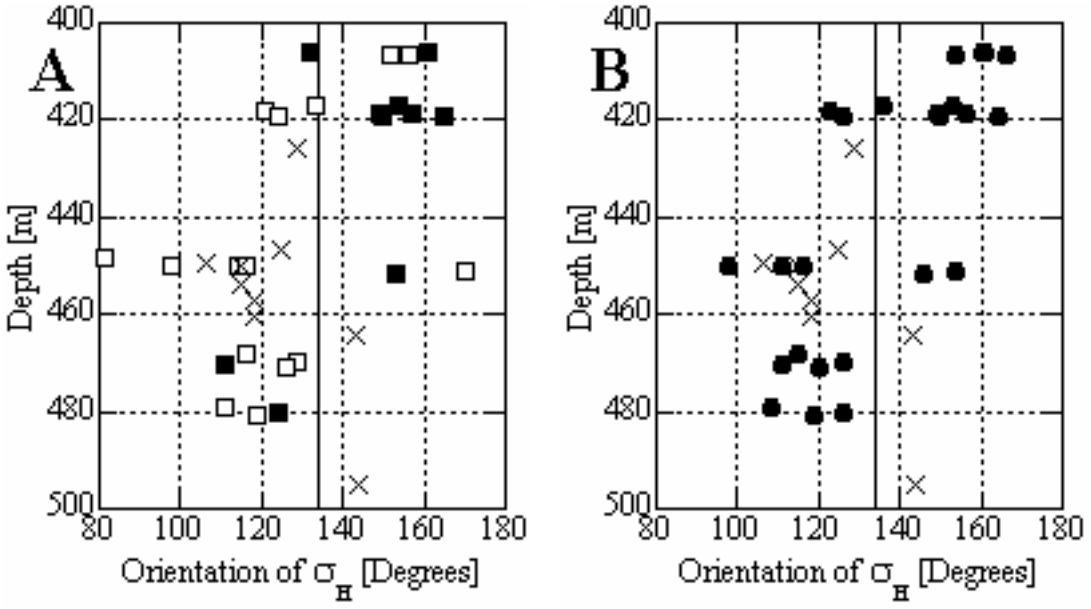

Figure 6-4. *Orientation of maximum horizontal stress for in-situ stress measurement points at the Äspö HRL. The stresses are in A represented with unfilled and filled squares for uncertain and more reliable result, respectively. The original results in B are represented by filled circles. Crosses are results from hydraulic fracturing stress measurements and the full line represents the average Borre Probe orientation of* σ_H *(134±22°N).*

6.3.2 Difference between re-analyzed and original strain interpretations

The difference in strain gauge readings between the re-analyzed data and the raw data are generally caused by that the start reading is taken well before overcoring start (1 minute before flushing water is turned on) and the stop value is taken well after overcoring stop (at core break/flush water stop or 1 minute before this). The former is motivated by the fact that the flushing water sometimes affects the gauges and should preferably be avoided. Gauges are in many cases clearly jumping to another strain level when flush water is turned on. By taking the strain stop value at core break or immediately before this, a strain reading unaffected by the flushing process is achieved. At the same time, temperature effects are minimized as the temperature at the strain gauges normally is close to the *in situ* rock temperature (or as close as they can get). In some cases though, temperature corrections have been made. The differences in the calculated stresses between the original interpretation and the results in this study (and [28]) can be attributed to the choice of final strains.

The final strain readings in the original interpretation were taken immediately after the strains have reached their maximum strain value. This implies that the rock cylinder may not be fully relieved from the in-situ stress field and, because drilling is still ongoing, the drilling operation itself may induce stresses into the overcore cylinder. In addition, the original analyses included re-calculation of individual strain gauges (eq. 2 in [33]). At the single test scale, one can argue against this approach for the following reasons: (1) the Borre Probe cell uses seven strains to determine the six unknowns of the stress tensor (the three axial strain gauges may be regarded as one). The re-calculation

of strains thus have a great impact on the calculated stresses; (2) the analysis presented in this study indicate that suspect data concern entire strain rosettes rather than individual strain gauges; and (3) the choice of functioning strain gauges is subjective.

The difference in elastic parameters between the two data sets is mainly cased by the different biaxial pressures used for interpretation of the secant modulus. The re-analyzed data uses the unloading curves as close to the *in situ* raw stress magnitudes as possible, i.e. in general between the unloading from 10 to 8 MPa, whereas the original interpretation uses pressures between 3 and 10 MPa. The elastic parameters for the re-analyzed and original data are displayed in Fig. 6.5.

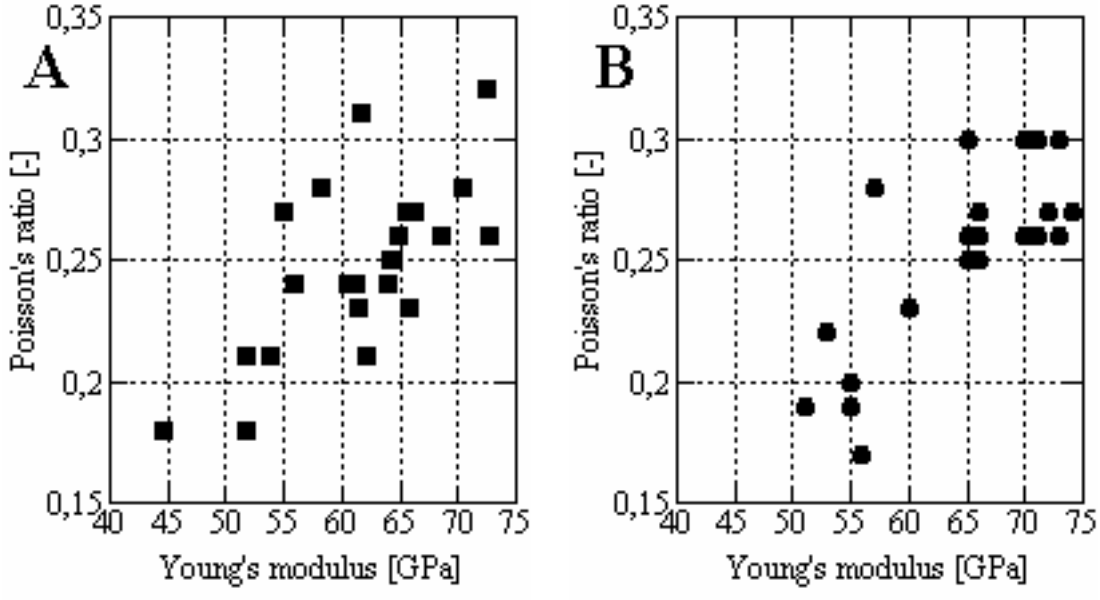

Figure 6-5. *Young's modulus versus Poisson's ratio for re-analyzed (A) and original (B) overcoring stress data.*

6.3.3 Remarks regarding the hydraulic fracturing stress data

We would like to make a comment on the recent hydraulic fracturing stress data in boreholes KF0093A01, KA2599G01, and KOV01. Ito et al. (1999) and Rutqvist et al. (2000) showed that the classical hydraulic fracturing equation, giving σ_v (in KF0093A01) and σ_H (in KA2599G01 and KOV01) equal to 3 times the shut-in pressure minus the re-opening pressure, is not valid. In practice, the classical formula gives σ_v (in the horizontal borehole) and σ_H (in the vertical borehole) as two times σ_h. In borehole KF0093A01, σ_v = 19.5±1.1 MPa which may be compared with $2\cdot\sigma_h$ = 22.0 MPa. In borehole KA2599G01, σ_H = 21.8±2.9 MPa which may be compared with $2\cdot\sigma_h$ = 22.0 MPa. In borehole KOV01, σ_H = 22.4 MPa which may be compared with $2\cdot\sigma_h$ = 23.0 MPa at the 300 m level, and σ_H = 28.0 MPa which may be compared with $2\cdot\sigma_h$ = 26.4 MPa at the 500 m level. Conclusively, this implies that only σ_h is reliable in these boreholes.

6.3.4 Remarks considering the overcoring stress data from the Borre Probe

The calculated stresses based on re-analyzed data call for clarifying remarks mainly for borehole KF0093A01, KK0045G01, and KOV01.

The strain data at about 450 m depth in borehole KF0093A01 have a suspect behaviour versus time compared to the diagnostic strain curves of Blackwood (1978) and with significant strain drops at the end of the overcoring phase. The applied analysis consequently gives very low stress magnitudes compared to the original result. To some extent, the observed strain drop may represent a temperature effect, but because the temperature gauge was not operating during the measurements a quantification of such an effect could not be made. Furthermore, the strain drop seemed to be too large to be solely a temperature effect. In two of the three tests, the axial and 45°-gauges increased with time at the end and after the overcoring phase, suggesting boundary yield between the cell and the rock (e.g. Irvin et al., 1987). Three axial gauges also indicate strains which seem too high for this depth (340 to 360 μstrain) compared to the remainder of the data (four gauges indicate axial strains of 200 μstrain or less in the same borehole). However, a correction for boundary yield between the cell and the rock would lower the stress magnitudes even further and it is therefore more likely that the rock walls have also yielded. The biaxial testing also reveals non-linear strains versus applied load leading to the conclusion that the data in borehole 3A01 are less reliable.

The results from borehole KK0045G01 (two levels at about 450 and about 480 m depth) were also judged to be of poor quality, especially those from 480 m depth. At 450m depth, 60% of the gauges were suspect or malfunctioning (e.g. improper glue mix) and all measurement points needed temperature corrections. At 480 m depth, two out of three tests were of questionable quality due to drifting gauges (probably improper glue mix) and also required temperature correction. Corrections for glue creep can be roughly estimated before overcoring start and sometimes after overcoring stop (data is normally sparse). Because the glue creep before and after overcoring are quite different, implying that the glue creep is non-linear versus time, the estimated glue creep was judged unreliable and corrections were not applied.

The measurements in borehole KOV01 suffered from poor flushing capacity before gluing of rosettes leaving drill cuttings in the borehole. This implies that the gluing of the rosettes was affected and the results are therefore less reliable.

7 Recommendations for future overcoring stress measurements

Based on the re-analysis of existing Borre Probe rock stress data, a number of recommendations are made which may improve the results in future testing:

1. The borehole bottom should always be flattened before drilling of the pilot hole commences (is currently usually performed). This will reduce the risk for a decentralized pilot hole and possible misplacing the cell during installation.

2. The guiding cylinders used when drilling the pilot hole should be checked for wear. If these are in bad condition, the pilot hole may be non-axial which may have great consequences for the stress determination in particular for the Borre Probe with the relatively thin-walled core.

3. The analysis should include verification of glue bonding between the rosettes and the rock and glue hardening. Thus, the analysis should include some 30 minutes prior to the overcoring start.

4. After each overcoring test, the core at the position of the strain rosettes should be investigated thoroughly and documented. The quality of the gluing, position of the rosettes and geology (grain sizes, fractures) at the gauges should be documented. The position and orientation of the pilot hole should also be determined and well documented (if decentralized and/or non-axial).

5. The relatively thin core used is sensitive to drilling induced microfracturing. It also implies that the maximum pressure during the biaxial test is set to 10 MPa. This pressure may be significantly lower than the measured *in situ* stresses. Thus, an overcoring drill bit giving a thicker core is preferable.

6. Due to the position of the temperature measuring device, which measures only the flushing water temperature, care should be taken during field work. Before core break, the temperature reading should be constant and preferably at the same level as the *in situ* rock mass temperature before overcoring start.

8 Acknowledgements

The study was financially supported by the Swedish Nuclear Fuel and Waste Management Co. (SKB). We would acknowledge Mr. Hans Klasson, SwedPower Co, for sharing raw data and for an excellent record keeping of the Borre Probe data. We would also like to acknowledge MSc. Kristina Larsson for sharing the thermal expansion data on Äspö rocks and for valuable comments. We also would like to acknowledge Mr. Rolf Christiansson, SKB, Mr. Janne Malmtorp, JLM Tunnelkonsult, Dr. Christer Ljunggren, SwedPower Co., and Dr. Maria Ask, Luleå University of Technology, for reviewing the manuscript. Finally, Mr. Lennart Ekman, LE Geokonsult, and Mr. Tommy Nilsson, Centralverkstaden LTU, is acknowledged for valuable comments.

References

Andersson, J. Statistisk analys av bergspänningsdata - En inledande studie av vertikalspänningars och töjningars djupberoende på Äspö. SKB Utveckling, Arbetsrapport U-96-33, Stockholm, 1996, 21 p.

Andersson, J. Statistiska ansatser för att studera skillnader mellan hydraulisk spräckning och överborrning. SKB Utveckling, Arbetsrapport U-97-04, Stockholm, 1997, 12 p.

Amadei, B. and Stephansson, O. *Rock Stress and Its Measurements*, Chapman and Hall Publ., London, 1997, 490 p.

Amadei, B. *Rock anisotropy and the theory of stress measurements*, Lecture notes in Engineering, Springer-Verlag, 1983a.

Amadei, B. Number of boreholes to measure the state of stress in-situ by overcoring. *Proc. 24th U.S. Rock Mechanics Symposium,* College Station, USA. Association of Eng. Geologists Publ., 1983a, pp.87-98.

Ask, D. Inversion and interpretation of hydraulic and overcoring stress measurements in the Äspö region. Licentiate Thesis, Royal Institute of Technology, Stockholm, 2001, 101 p.

Ask, D., Stephansson, O., and Cornet, F.H. Analysis of overcoring rock stress data in the Äspö region. *Proc. 38th U.S. Rock Mechanics Symposium,* Washington, USA. A.A. Balkema Publisher, 2001a, pp 1401-1405.

Ask, D., Stephansson, O., and Cornet, F.H. Integrated stress analysis of hydraulic and overcoring rock stress data in the Äspö region. Analysis of hydraulic fracturing stress measurements and hydraulic tests in pre-existing fractures (HTPF) in boreholes KAS02, KAS03, and KLX02. SKB International Progress Report IPR-01-26, Stockholm, 2001b, 155 p.

Ask, D., Stephansson, O., and Cornet, F.H. Analysis of overcoring stress data at the Äspö HRL, Sweden. Analysis of overcoring rock stress measurements using the CSIRO HI cell. SKB Report in press. 2003.

Blackwood, R.L. Diagnostic stress-relief curves in stress measurement by overcoring. *Int. J. Rock Mech. Min. Sci. & Geomech. Abstr.*, **15**, 1978, pp. 205-209.

Bjarnason, B., Klasson, H., Leijon, B., Strindell, L. and Öhman, T. Rock stress measurements in boreholes KAS02, KAS03 and KAS05 on Äspö. SKB Progress Report 25-89-17, Stockholm, 1989, 59 p.

Christiansson, R. Rock stress measurements by overcoring. Quality control of overcoring data from the Äspö HRL with special emphasis on the properties of intact rock and geological influence. SKB Technical Document TD-00-01, 2000, 2000, 19 p.

Christiansson, R., and Jansson, T. Test with three different stress measurement methods in two orthogonal boreholes. *Proc. 38th North American Rock Mechanics Symposium,* Toronto, Canada, pp. 1429-1436.

Cornet, F.H. and Valette, B. In situ determination from hydraulic injection test data. *J. Geophys. Res.*, **89**, 1984, pp. 11527-37.

Cornet, F.H. The HTPF and the integrated stress determination methods. *Comprehensive Rock Engineering*, Vol **3**. (J. Hudson, Ed.). Pergamon Press, Oxford, 1993a, pp. 413-432.

Ekman, L. Project deep drilling KLX02 - Phase 2. Methods, scope of activities and results. Summary report. SKB Technical Report TR-01-11, Stockholm, 2001, 188 p.

***Ekman, D.** Rock stress, hydraulic conductivity and stiffness of fracture zones in the Laxemar borehole, Småland, Sweden. Master of Science Thesis, Royal Institute of Technology, Stockholm, Sweden, 1997, 52 pp.

***Ekman, D., Rutqvist, J. and Ljunggren, C.** Determination of hydromechanical parameters down to 1 340 m depth in borehole KLX02 in Laxemar, Sweden. Rock Mechanics Meeting in Stockholm March 12, 1997 (Ed. C. Bachman). Swedish Rock Engineering Research (SveBeFo), Stockholm, 1997a, pp. 39-61.

Gray, W.M., and Toews, N.A. Optimization of the design and use of a triaxial strain cell for stress determination, in *Field Testing and Instrumentation of Rock*, ASTM STP 554, 1974, pp. 116-33.

Hakami, E., Hakami, H., and Cosgrove, J. Strategy for rock mechanics site descriptive model. Development and testing of an approach to modeling the state of stress. SKB Report R-02-03, Stockholm, 2002, 129 p.

Hallbjörn, L., Ingevald, K., Martna, J., and Strindell, L. A new automatic probe for the measurment of triaxial rock stresses in deep boreholes. Proc. Rock mechanics meeting, Stockholm, 26 Jan, 1989, BeFo, Stockholm, pp 57-64.

Hallbjörn, L., Ingevald, K., Martna, J., and Strindell, L. New automatic probe for measuring triaxial stresses in deep boreholes. *Tunneling Underground Space Technology*, Vol. **5**, No. 1/2, 1990, pp. 141-145.

Hallbjörn, L. Rock stress measurements performed by Swedish State Power Board. *Proc. Int. Symp. On Rock Stress and Rock Stress Measurements*, Stockholm, Centek Publ. Luleå, 1986, pp. 197-205.

Hansson, H., Stephansson, O. and Shen, B. Site-94, Far-field rock mechanics modelling for nuclear waste disposal. SKI Report 95:40, Stockholm, 1995, 83 p.

Heuze, F.E. High-temperature mechanical, physical and thermal properties of granitic rocks – A review. *Int. J. Rock Mech. Min. Sci& Geomech. Abstr.*, **20** (1), 1983, pp. 3-10.

*Ekman, D., now Ask, D.

Hiltscher, R., Martna, J,. and Strindell, L. The measurement of triaxial rock stresses in deep holes and the use of rock stress measurements in the design and construction of rock openings. *Proc. 4th Cong. Int. Soc. Rock Mech.* (ISRM), Montreaux, Balkema, Rotterdam, Vol 2, 1979, pp. 227-34.

Hudson, J.A. Strategy for rock mechanics site descriptive model. A test case based on data from the Äspö HRL. SKB Report R-02-04, Stockholm, 2002, 123 p.

Irvin, R.A., Garritty, P., and Farmer, I.W. The effect of boundary yield on the results of in-situ stress measurements using overcoring techniques. *Int. J. Rock Mech. Min. Sci. & Geomech. Abstr.*, **24**, 1987, pp. 87-93.

Ito, T., Evans, K., Kawai, K., and Hayashi, K. Hydraulic fracturing reopening pressure and the estimation of maximum horizontal stress. *Int. J. Rock Mech. & Geomech. Abstr.*, **36**, 1999, 811-26.

Klasson, H. and Andersson, S. 3D overcoring rock stress measurements in borehole KF0093A01 at the Äspö HRL. SKB Report in press, 2001.

Klasson, H., Persson, M., Ljunggren, C., and Bergsten, K-Å. SKB Report in press, 2001.

Klasson, H., Lindblad, K., Lindfors, U., and Andersson, S. Overcoring rock stress measurements in borehole KOV01, Oskarshamn. SKB Report in press, 2002.

Klee, G. and Rummel, F. Rock stress measurements at the Äspö HRL. Hydraulic fracturing in boreholes KA2599G01 and KF0093A01. SKB International Progress Report IPR-02-02, Stockholm, 2002, 33 p.

Lama, R.D., and Vutukuri, V.S. *Handbook on mechanical properties of rocks – Testing techniques and results, volume II*, Series on rock and soil mechanics (vol. 3), no 1. Trans. Tech Publ., Clasusthal, 1978.

Larsson, K. Determination of the coefficient of thermal expansion for two Äspö rocks, diorite and granite. MSc Thesis, Luleå University of Technology, Luleå, 2001, 35 p.

Lee, M. and Stillborg, B. Äspö virgin stress measurement results in sections 1050, 1190 and 1620 m of the access ramp. SKB Progress Report 25-93-02, Stockholm, 1993, 117 p.

Lee, M., Hewitt, T. and Stillborg, B. Äspö virgin stress measurement results. Measurements in boreholes KA1899A, KA2198A and KA2510A. In SKB Progress Report 25-94-02, Stockholm, 1994, 66 p.

Leeman, E.R., and Hayes, D.J. A technique for determining the complete state of stress in rock using a single borehole. In *Proc. 1st Cong. Int. Soc. Rock mech.* (ISRM), Lisbon, Lab Nac. De eng. Civil, Lisbon, vol 2, 1966, pp. 17-24.

Leijon, B. A. Relevance of pointwise rock stress measurements – an analysis of overcoring data. *Int. J. Rock Mech. Min. Sci. & Geomech. Abstr.*, **26**, 1989, pp. 61-68.

Leijon, B.A. Rock stress measurements using the LUT-gauge overcoring method. PhD Thesis, Luleå University of Technology, Luleå, 1988, 25 p.

Leijon, B. A. Summary of rock stress data from Äspö. SKB Progress Report 25-95-15, Stockholm, 1995, 12 p.

Leijon, B. A., and Stillborg, B.L. A comparative study between two rock stress measurement techniques at Loussavaara mine. *Rock Mech. Rock Eng.*, **19**, 1986, pp. 143-63.

Litterbach, N., Lee, M. Struthers, M. and Stillborg, B. Virgin stress measurement results in boreholes KA2870A and KA3068A. SKB Progress Report 25-94-32, Stockholm, 1994, 26 p.

Ljunggren, C. and Bergsten, K-Å. Rock stress measurements in KA3579G, prototype repository. SKB Progress Report HRL-98-09, Stockholm, 1998, 25 p.

Ljunggren, C., Chang, Y. och Andersson, J. Bergspänningsmätningars representativitet - Mätnoggrannhet och naturliga variationer vid hydraulisk spräckning och överborrning. SveBeFo Rapport 37, Stockholm, 1998, 79 p.

Ljunggren, C. and Klasson, H. Deep hydraulic fracturing rock stress measurements in borehole KLX02, Laxemar, Drilling KLX02-Phase 2, Lilla Laxemar, Oskarshamn. SKB Utveckling, Project Report U-97-27, Stockholm, 1997, 33 p.

Ljunggren, C. and Klasson H. Rock stress measurements at Zedex test area, Äspö HRL. Äspö Hard Rock Laboratory, Technical Note TN-96-08z, Stockholm, 1996, 34 p.

Ljunggren, C. and Persson, M. Beskrivning av databas – Bergspänningsmätningar i Sverige. SKB Djupförvar, Projektrapport PR D-95-017, Stockholm, 1995, 21p.

Lundholm, B. Analysis of rock stress and rock stress measurements with application to Äspö HRL. Licentiate Thesis, Luleå University of Technology, Luleå, 2000a, 125 p.

Lundholm, B. Rock stress and rock stress measurements at Äspö HRL. SKB International Progress Report IPR-00-24, Stockholm, 2000b, 64 p.

Myrvang, A.M. Evaluation of in-situ rock stress measurements at the Zedex test area. SKB, Progress Report HRL-97-22, 1997, 14 p.

Merril, R.H. In situ determination of stress by relief techniques. *Proc. Int. Conf. State of stress in the Earth's crust*, Santa Monica, Elsevier, New York, 1964, pp 343-69.

Nilsson, G., Litterbach, N., Lee, M., and Stillborg, B. Virgin stress measurement results, borehole KZ0059B. Äspö Hard Rock Laboratory, Technical Note TN-97-25g, Stockholm, 1997, 3 p.

Rhén, I., Gustafson, G., Stanfors, R. and Wikberg, P. Äspö HRL – geoscientific evaluation 1997/5. Models based on site characterization 1986-1995. SKB Technical Report, TR-97-06, Stockholm, 1997.

Rutqvist, J., Tsang, C.-F., and Stephansson, O. Uncertainty in the principal stress estimated from hydraulic fracturing measurements due to the presence of the induced fracture. *Int. J. Rock Mech. & Geomech. Abstr.*, **37**, 2000, 107-20.

Rummel, F., Klee, G., and Weber, U. Rock stress measurements in Oskarshamn. Hydraulic fracturing and core testing in boreholes KOV01. SKB International Progress Report IPR-02-01, Stockholm, 2002, 62 p.

Sandström, D. Utvärdering av genomförda bergspänningsmätningar i Kiirunavvaara. MSc Thesis, Luleå university of Technology, Luleå, 1999, 48 p.

Savin, G.N. *Stress concentrations around holes*, Pergamon Press, Oxford, 1961, pp. 241-296.

Sjöberg, J. and Klasson, H. Stress measurements in deep boreholes using the Borre (SSPB) probe. Submitted to *Int. J. Rock Mech. Min. Sci. & Geomech. Abstr.*, 2002.

SKB. Numerical modelling, acoustic emission and velocity studies of the excavation disturbed zone at the hard rock laboratory. SKB Technical Note TN-97-02z, Stockholm, 1996.

Stacey, T.R. A simple extension strain criterion for fracture of brittle rock. *Int. J. Rock Mech. Min. Sci. & Geomech. Abstr.*, 18, 1981, pp. 469-74.

Stephansson, O. The importance of rock stress measurement and it's interpretation for rock disposal of hazardous waste. *Proc. Int. Symp. on Rock Stress*, Kumamoto, Japan. A.A. Balkema Publisher, 1997, pp. 3-13.

Worotniki, G., and Walton, R.J. Triaxial hollow inclusion gauges for determination of rock stresses in situ. In *Investigation of stresses in rock; Advances in stress measurements* (A.J. Hargraves, Ed.), p. 8, Institute of Engineers, Sydney, 1976.

Worotnicki, G. CSIRO triaxial stress measurement cell. *Comprehensive Rock Engineering*, Vol **3**. (J. Hudson, Ed.). Pergamon Press, Oxford, 1993, pp. 329-94.

Appendix 1

Boreholes coordinates

Borehole	Bearing [°]	Dip [°]	X	Y	Z	Measurement depth [m]
KAS05*	150	84.9	6367768.06	1551359.34	-8.68	195.31
						196.61
						197.41
						355.01
						356.91
						356.81
						357.74
KXZSD8HR	336.6	9.60	7280.356	2255.772	416.144	0.84
						1.29
						1.66
						2.40
						3.18
						4.07
						5.96
						6.61
						11.49
						12.28
						12.93
						13.59
						14.30
						15.43
						15.60
						16.96
						17.62
						18.27
						18.92
						19.57
						20.22
						20.85
						21.50
						22.21
						22.94
KXZSD81HR	339.82	8.91	7280.252	2255.373	416.020	0.86
						1.43
						2.73
						3.34
KXZSD8HL	157.88	9.14	7275.406	2257.122	415.509	23.37
						24.06
						24.75
						25.44
KK0045G01	135	89.84	6367798.101	1551557.298	416.398	1.20
						2.70
						3.33
						4.12
						4.53
						4.97
						5.51
						6.07
						6.50
						8.16
						31.67

Borehole	Bearing [°]	Dip [°]	X	Y	Z	Measurement depth [m]
KK0045G01						32.48
						33.35
						34.77
						35.48
						62.82
						63.59
						64.51
KF0093A01	298	-2	7297.50	1997.00	451.00	32.14
						32.70
						33.23
						35.38
KA3579G	266.94	89.4	7274.422	1886.684	448.366	0.88
						2.04
						2.53
						3.99
						4.54
						5.41
						8.00
						20.06
						21.21
						21.70
						22.31
KOV01*	202.7	77.3	6348516.013	1539942.059	-3.052	290.31
						325.83
						511.78
						514.79
						515.80
						516.89
						519.84
						520.71
						527.46

Dip positive downwards, depth positive downwards. *RT38-RH00 system, and the rest according to the Äspö local coordinate system.

Appendix 2

Influence of the biaxial test on the rock core – A calculation example

This appendix is based on Sandström (1999).

A2.1 Calculation prerequisites

The calculation example is based on the following prerequisites:
σ_H = 23.0 MPa; σ_h = 10.0 MPa; σ_v = 36.0 MPa
E = 65.0 GPa; υ = 0.25
This corresponds to the average values for borehole KA3579G, Prototype Repository, Äspö HRL.

A2.2 Calculation of strains

The strains become
ε_{axial} = [(36.0-0.25*(23.0+10.0)]/65000 = 427 μstrain;
ε_H = [(23.0-0.25*(36.0+10.0)]/65000 = 177 μstrain;
ε_h = [10.0-0.25*(36.0+23.0)]/65000 = -73 μstrain;

A2.3 Stresses in the rock core

The thick pipe solution gives:

$$\sigma_r = p\frac{D^2}{D^2 - d^2}\left(1 - \frac{d^2}{r^2}\right) \quad \text{(A5-1)}$$

$$\sigma_\theta = p\frac{D^2}{D^2 - d^2}\left(1 + \frac{d^2}{r^2}\right) \quad \text{(A5-2)}$$

$$\sigma_{axial} = 0 \quad \text{(A5-3)}$$

where p is the applied biaxial pressure, D and d are the outer and inner diameter respectively, and r is the radius. The stresses at D becomes:

$$\sigma_r = p \quad \text{(A5-4)}$$

$$\sigma_\theta = p\frac{D^2 + d^2}{D^2 - d^2} \quad \text{(A5-5)}$$

$$\sigma_{axial} = 0 \quad \text{(A5-6)}$$

and at d:

$$\sigma_r = 0 \quad \text{(A5-7)}$$

$$\sigma_\theta = 2p\frac{D^2}{D^2 - d^2} \quad \text{(A5-8)}$$

$$\sigma_{axial} = 0 \quad \text{(A5-9)}$$

The least strain (axial) becomes:

At outer wall, D

$$\varepsilon_{axial} = \frac{1}{E}\left[\sigma_{axial} - \upsilon\left(\sigma_r + \sigma_\theta\right)\right] = -\frac{2p\upsilon}{E}\frac{D^2}{D^2 - d^2} \tag{A3-10}$$

and at dinner wall, d

$$\varepsilon_{axial} = \frac{1}{E}\left[\sigma_{axial} - \upsilon\left(\sigma_r + \sigma_\theta\right)\right] = -\frac{2p\upsilon}{E}\frac{D^2}{D^2 - d^2} \tag{A3-11}$$

During biaxial testing, the Borre Probe allows a maximum pressure of 10 MPa, whereas the CSIRO HI cores are loaded up to 20 MPa. The approximate dimensions for the cells are D_{BP}=62 mm; d_{BP}=37 mm and D_{CHI}=72 mm; d_{CHI}=38 mm, respectively. This gives (neglecting correction factors for the CSIRO HI cell):

At D,d

Borre Probe $\varepsilon_{axial,\ 10\ MPa}$ = -119 μstrain

CSIRO HI $\varepsilon_{axial,\ 10\ MPa}$ = -107 μstrain

$\varepsilon_{axial,\ 15\ MPa}$ = -160 μstrain

$\varepsilon_{axial,\ 20\ MPa}$ = -213 μstrain

According to Stacey (1981), the tension crack initiation strain in granite is approximately 125 μstrain and macroscopic tensional cracks at approximately 250 μstrain. For the Äspö diorite, the crack initiation begins at approximately 60 MPa and that this level is only somewhat dependent on confining stress (SKB, 1997). Using the average in-situ Young's modulus of 60.9 GPa obtained from biaxial tests on Borre Probe cores, results in a crack initiation strain of about 100 μstrain for the Äspö diorite. Thus, this calculation indicates that the biaxial test may be exposed to a critical tensional strain and microcrack generation.

Appendix 3

Overcoring graphs and interpretation

A3 Overcoring data from the Borre Probe

A3.1 Borehole KAS05

Raw data not found.

A3.2 Borehole KXZSD8HR

1.29 m
Rosette 3 not glued properly. Test questionable. Indication of high temperature in the test section at the end of the test. 3°C temperature correction necessary.

1.66 m
Unstable gauges before overcoring. Test questionable. Indication of high temperature in the test section at the end of the test.

2.40 m
Rosettes 2 and 3 not glued properly. The temperature is increasing rapidly as the flushing water is turned off, thus induced temperature effect probable.

3.18 m
Borre twisted in borehole during overcore leading to shortcutting of axial gauges. Test questionable. The temperature is increasing rapidly as the flushing water is turned off, thus induced temperature effect probable.

4.07 m
Suspect jump before overcoring start, possibly an effect of the drill bit passing the overcoring cell. Questionable gluing of rosettes.

5.96 m
Test ok.

6.61 m
Rosette 3 not glued properly.

11.49 m
Test failed and not included in the analysis.

12.28 m
Test ok.

12.93 m
Poor gluing of rosette 3? Drilling process too fast.

13.59 m
Rosettes not glued properly. Axial fracture in core. Test questionable.

14.30 m
Test ok.

15.60 m
Test ok.

16.96 m
Suspect jump before overcoring start, possibly an effect of the drill bit passing the overcoring cell. Rosette 1 malfunctioning. Fracture in core makes biaxial test impossible. Test questionable.

17.62 m
Test ok.

18.27 m
Questionable result due to soft glue.

18.92 m
Glue not fully hardened.

19.57 m
Rosette 1 not glued properly?

20.22 m
Test ok.

20.85 m
Test ok.

21.50 m
Test ok.

22.21 m
The temperature is increasing rapidly as the flushing water is turned off, thus induced temperature effect probable.

22.94 m
Rosette 3 malfunctioning.

A3.3 Borehole KXZSD81HR

0.86 m
Rosette 1 not glued properly. Unstable gauges overall. Indication of high temperature in the test section at the end of the test.

1.43 m
Rosettes 2 and 3 questionable. The temperature is increasing rapidly as the flushing water is turned off, thus induced temperature effect probable.

2.73 m
The temperature is increasing rapidly as the flushing water is turned off, thus induced temperature effect probable.

3.34 m
The temperature is increasing as the flushing water is turned off, thus induced temperature effect probable.

A3.4 Borehole KXZSD8HL

23.37 m
Rosette 2 malfunctioning. Unstable gauges before overcoring. 2°C temperature correction necessary.

24.06 m
Rosettes 1 not glued properly and rosette 2 malfunctioning.

24.75 m
Test ok.

25.44 m
Test ok.

A3.5 Borehole KK0045G01

All tests in borehole KK0045G01 includes temperature induced strains/stresses.

1.20 m
2.5°C temperature correction necessary.

2.24 m
4°C temperature correction necessary.

2.70 m
Rosette 2 malfunctioning. 3°C temperature correction necessary.

3.33 m
Test ok. 2°C temperature correction necessary.

4.12 m
Rosettes 2 and 3 not glued properly. 2.5°C temperature correction necessary.
4.53 m
Rosette 3 not glued properly. 5°C temperature correction necessary.

4.97 m
Rosette 3 malfunctioning. 3.5°C temperature correction necessary.

5.51 m
Rosette 1 malfunctioning. 4°C temperature correction necessary.

6.07 m
Test ok. 4°C temperature correction necessary.

6.50 m
Rosettes 1 and 3 questionable. 3.5°C temperature correction necessary.

8.16 m
Rosette 2 not glued properly, axial strain gauge in rosette 1 malfunctioning. 4°C temperature correction necessary.

31.67 m
Rosette 3 not glued properly. Rosette 1 misplaced by 12.5 degrees (see Ch. 3.4.4). 3°C temperature correction necessary.

32.48 m
Unstable gauges during the entire test. 3°C temperature correction necessary.

33.35 m
Rosette 3 and axial strain gauge in rosette 2 malfunctioning due to fracturing of core. 3°C temperature correction necessary. Excluded in the analysis.

34.77 m
Rosette 2 questionable. 2.5°C temperature correction necessary.

35.48 m
Tangential gauges in rosettes 1 and 2, axial gauge in rosette 3 malfunctioning. 2°C temperature correction necessary.

62.82 m
Glue not fully hardened?

63.59 m
Test ok. The temperature is increasing rapidly as the flushing water is turned off, thus induced temperature effect probable. 2.5°C temperature correction necessary.

64.51 m
Glue not fully hardened? 2°C temperature correction necessary.

A3.6 Borehole KA0093A01

During the field campaign it was found that the vibrations during drilling fractured the pilot core, rendering difficulties is determining if the pilot hole was free from fractures. The temperature measuring device was malfunctioning during all tests.

32.14 m
Gauges dropping strongly after overcoring. Possibly due to temperature effects or core yielding.

32.70 m
Gauges dropping strongly after overcoring. Possibly due to temperature effects or core yielding.

33.23 m
Test failed and not included in the analysis.

35.38 m
Suspect behavior of rosette 3 between overcoring stop and core break. Strains dropping after overcoring. Possibly due to temperature effects or core yielding.

A3.7 Borehole KA3579G

0.88 m
Test failed and not included in the analysis.

2.04 m
Test ok.

2.53 m
2°C temperature correction necessary.

3.99 m
The temperature is increasing rapidly as the flushing water is turned off, thus induced temperature effect probable.

4.54 m
Rosette 2 not glued properly. The temperature is increasing rapidly as the flushing water is turned off, thus induced temperature effect probable.

5.41 m
Rosette 1 not glued properly. The temperature is increasing rapidly as the flushing water is turned off, thus induced temperature effect probable.

8.00 m
Rosette 3 not glued properly. The temperature is increasing rapidly as the flushing water is turned off, thus induced temperature effect probable. 2°C temperature correction necessary.

20.06 m
Rosette 3 not glued properly. Unstable gauges before overcoring start.

21.21 m
Rosette 3 not glued properly.

21.70 m
Test ok.

22.31 m
Rosette 1 not glued properly.

A3.1.8 Borehole KOV01

290.31 m
All gauges drifting.

325.83 m
Test ok.

511.78 m
All gauges suspect. The temperature measuring device was malfunctioning during the test.

514.79 m
All gauges drifting. The temperature measuring device was malfunctioning during the test.

515.80 m
Test ok. The temperature measuring device was malfunctioning during the test.

516.89 m
All gauges suspect. The temperature measuring device was malfunctioning during the test.

519.84 m
All gauges suspect. The temperature measuring device was malfunctioning during the test.

520.71 m
All gauges suspect, especially rosette 2. The temperature measuring device was malfunctioning during the test.

527.46 m
Rosette 3 not glued properly? The temperature measuring device was malfunctioning during the test.

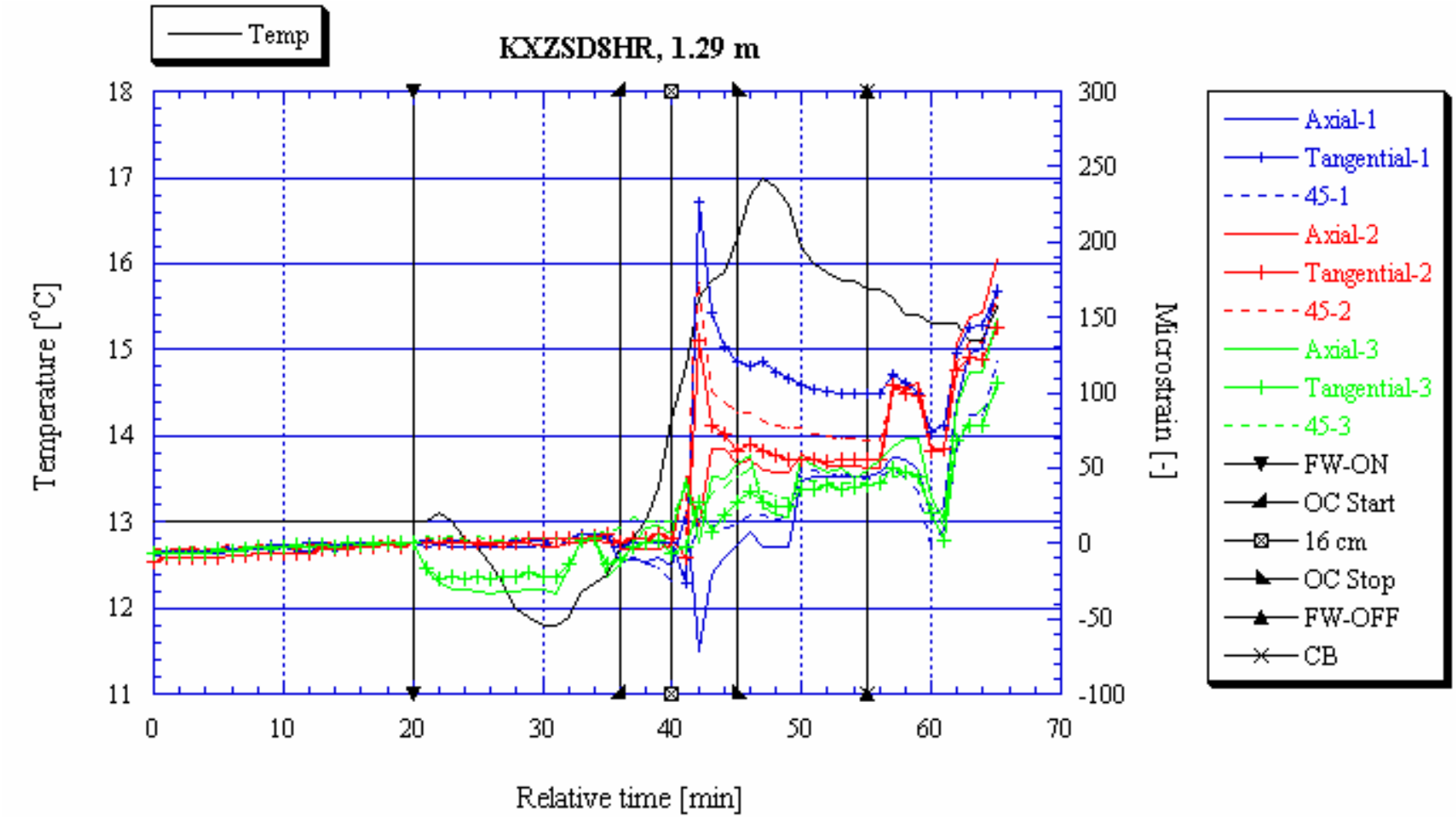
Temp
KXZSD8HR, 1.29 m
Temperature [°C]
Microstrain [-]
Relative time [min]
18
17
16
15
14
13
12
11
300
250
200
150
100
50
0
-50
-100
0
10
20
30
40
50
60
70
Axial-1
Tangential-1
45-1
Axial-2
Tangential-2
45-2
Axial-3
Tangential-3
45-3
FW-ON
OC Start
16 cm
OC Stop
FW-OFF
CB

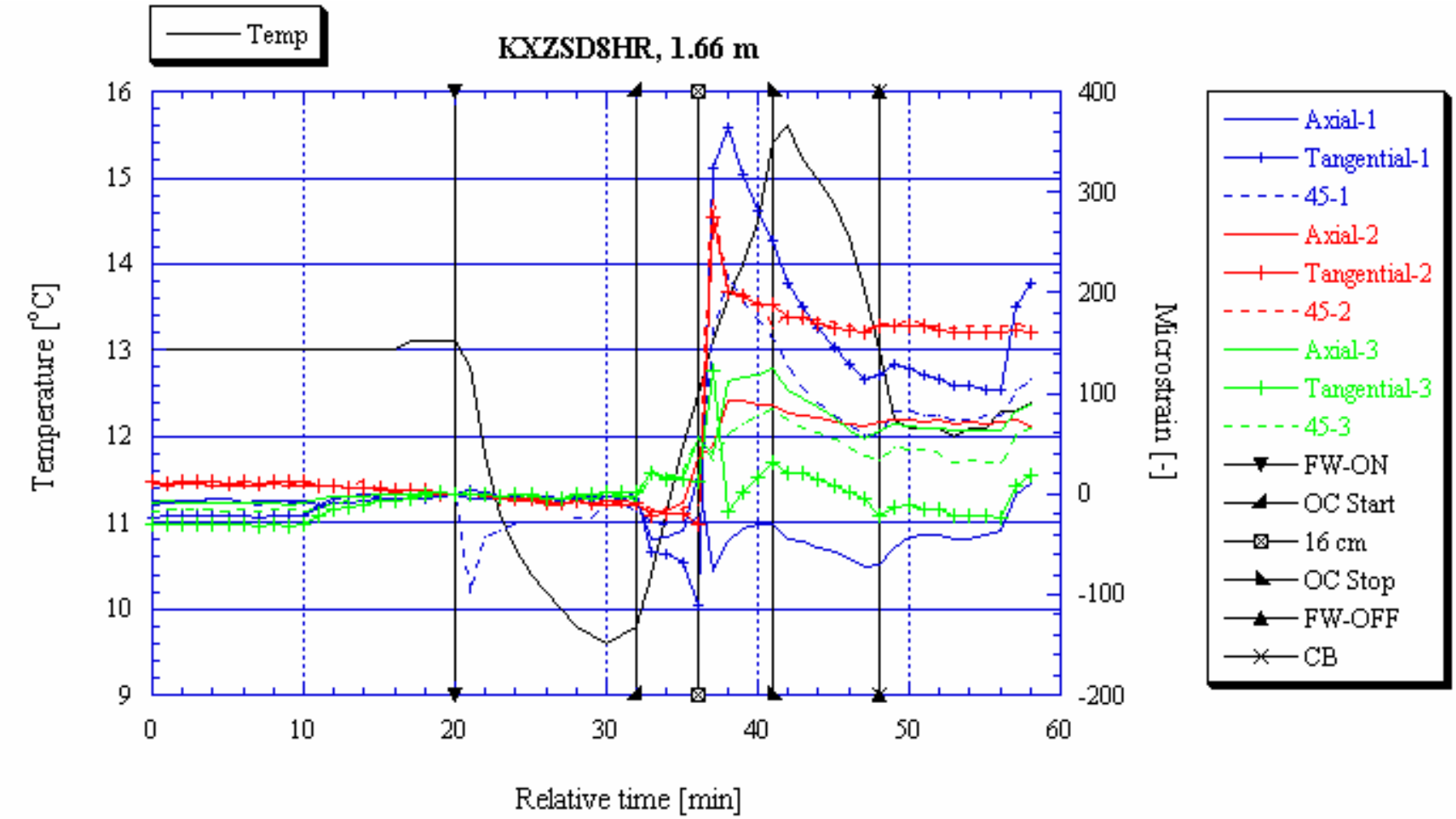
Temp
KXZSD8HR, 1.66 m
Temperature [°C]
Microstrain [-]
Relative time [min]
16
15
14
13
12
11
10
9
400
300
200
100
0
-100
-200
0
10
20
30
40
50
60
Axial-1
Tangential-1
45-1
Axial-2
Tangential-2
45-2
Axial-3
Tangential-3
45-3
FW-ON
OC Start
16 cm
OC Stop
FW-OFF
CB

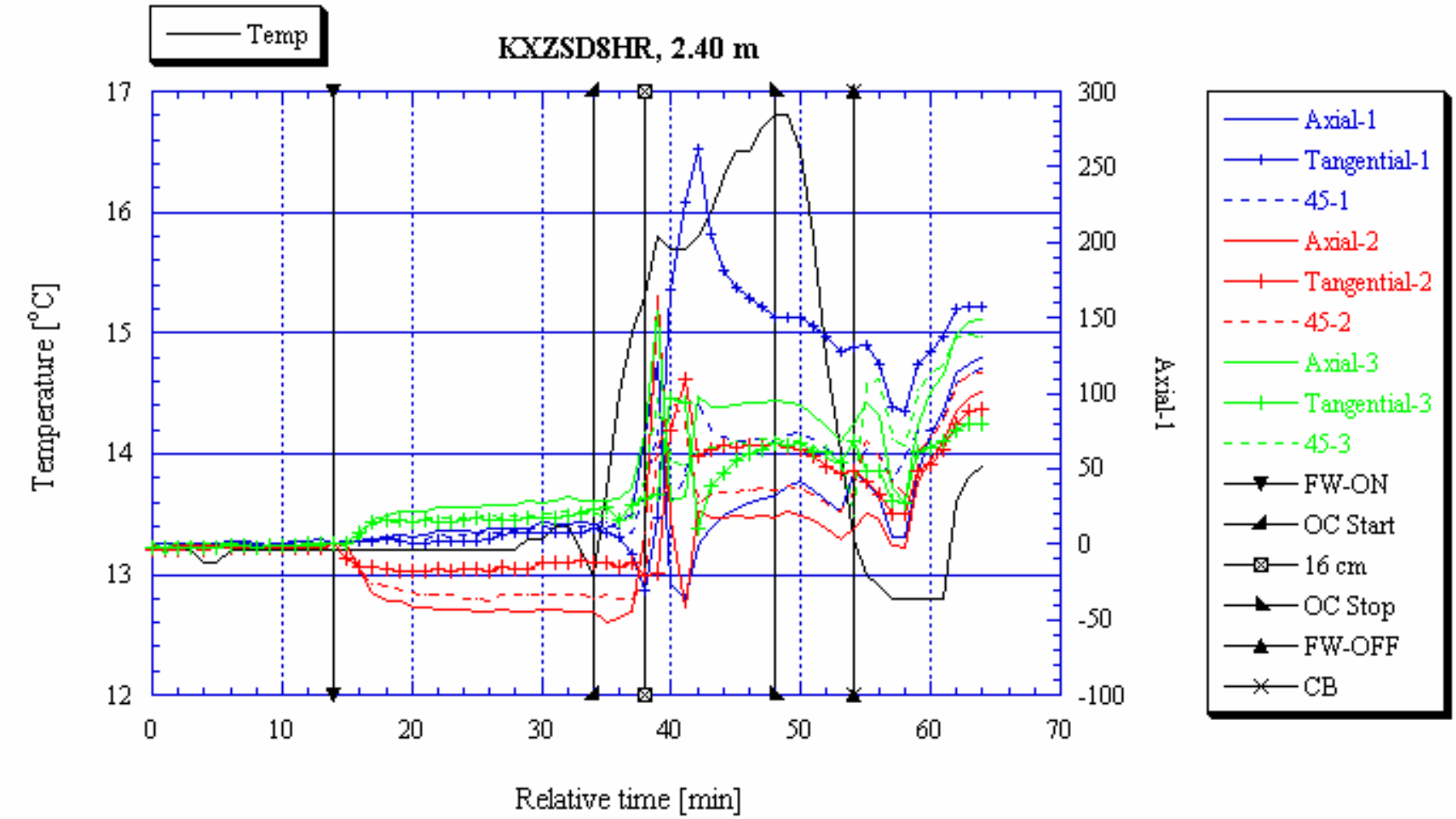
Temp
KXZSD8HR, 2.40 m
Temperature [°C]
17
16
15
14
13
12
0
10
20
30
40
50
60
70
Relative time [min]
300
250
200
150
100
50
0
-50
-100
Axial-1
Axial-1
Tangential-1
45-1
Axial-2
Tangential-2
45-2
Axial-3
Tangential-3
45-3
FW-ON
OC Start
16 cm
OC Stop
FW-OFF
CB

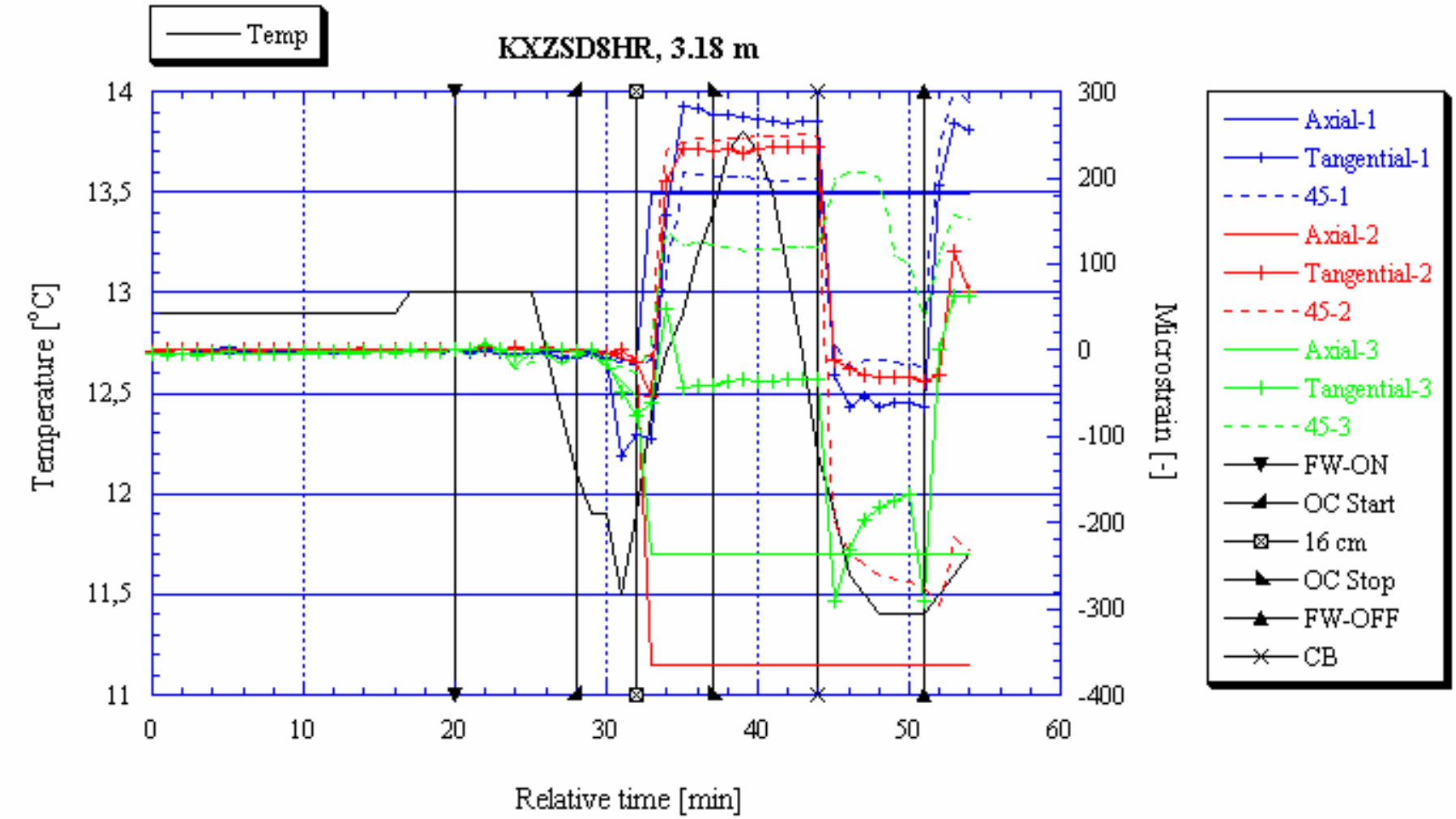
Temp
KXZSD8HR, 3.18 m
Temperature [°C]
Microstrain [-]
Relative time [min]
14
13,5
13
12,5
12
11,5
11
300
200
100
0
-100
-200
-300
-400
0
10
20
30
40
50
60
Axial-1
Tangential-1
45-1
Axial-2
Tangential-2
45-2
Axial-3
Tangential-3
45-3
FW-ON
OC Start
16 cm
OC Stop
FW-OFF
CB

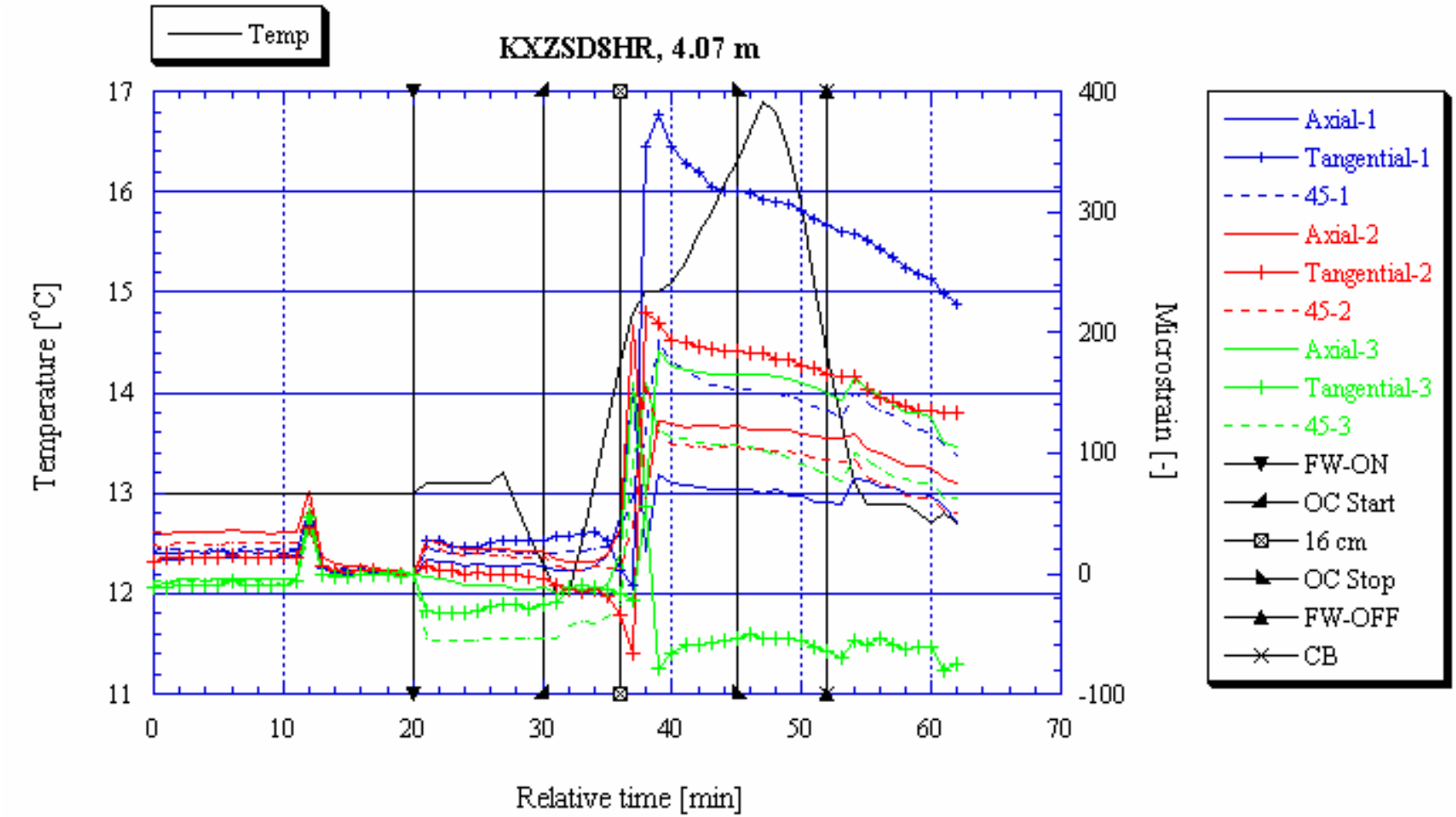
Temp
KXZSD8HR, 4.07 m
Temperature [°C]
Microstrain [-]
Relative time [min]
17
16
15
14
13
12
11
400
300
200
100
0
-100
0
10
20
30
40
50
60
70
Axial-1
Tangential-1
45-1
Axial-2
Tangential-2
45-2
Axial-3
Tangential-3
45-3
FW-ON
OC Start
16 cm
OC Stop
FW-OFF
CB

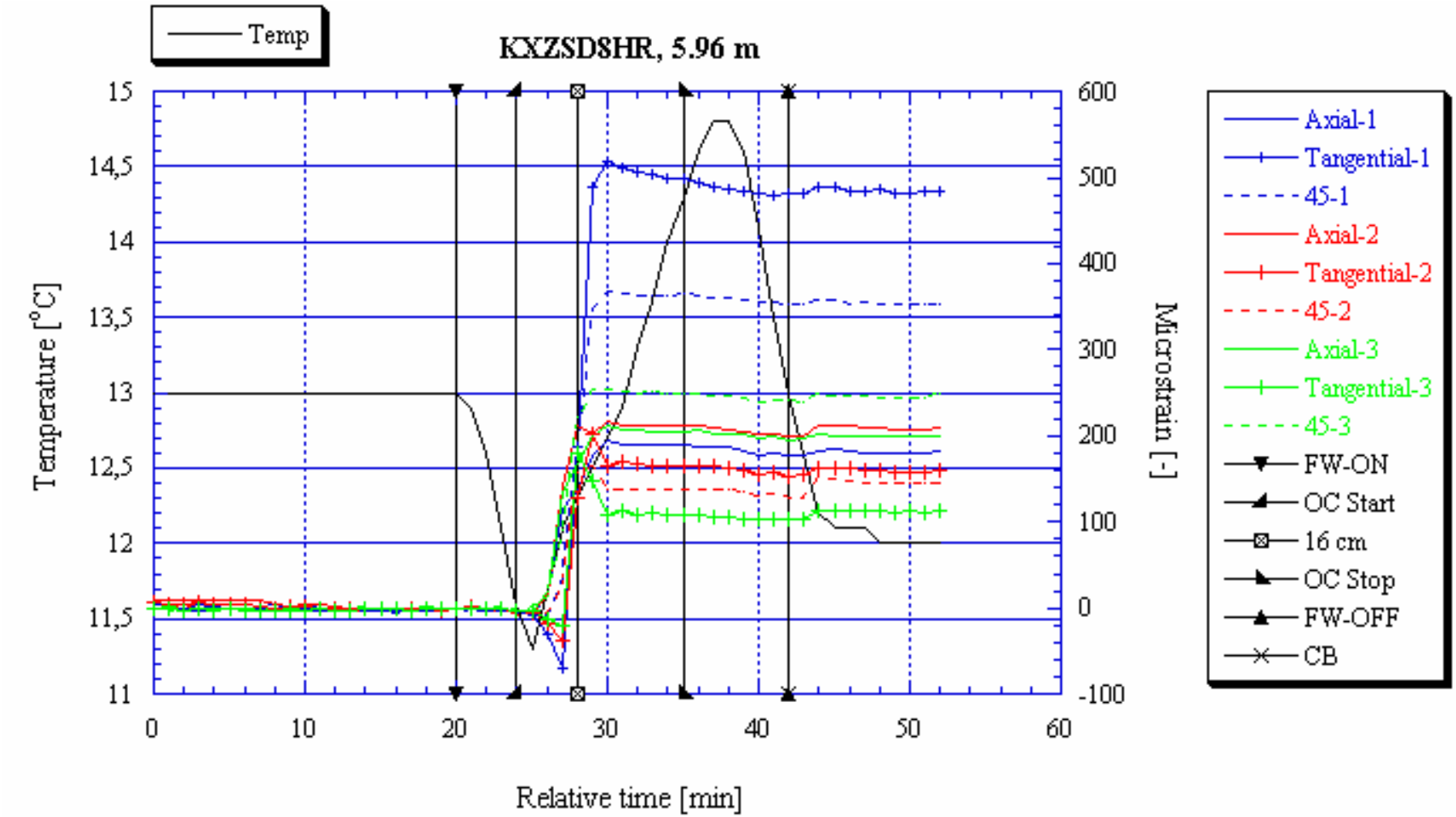
Temp
KXZSD8HR, 5.96 m
Temperature [°C]
15
14,5
14
13,5
13
12,5
12
11,5
11
0
10
20
30
40
50
60
Relative time [min]
600
500
400
300
200
100
0
-100
Microstrain [-]
Axial-1
Tangential-1
45-1
Axial-2
Tangential-2
45-2
Axial-3
Tangential-3
45-3
FW-ON
OC Start
16 cm
OC Stop
FW-OFF
CB

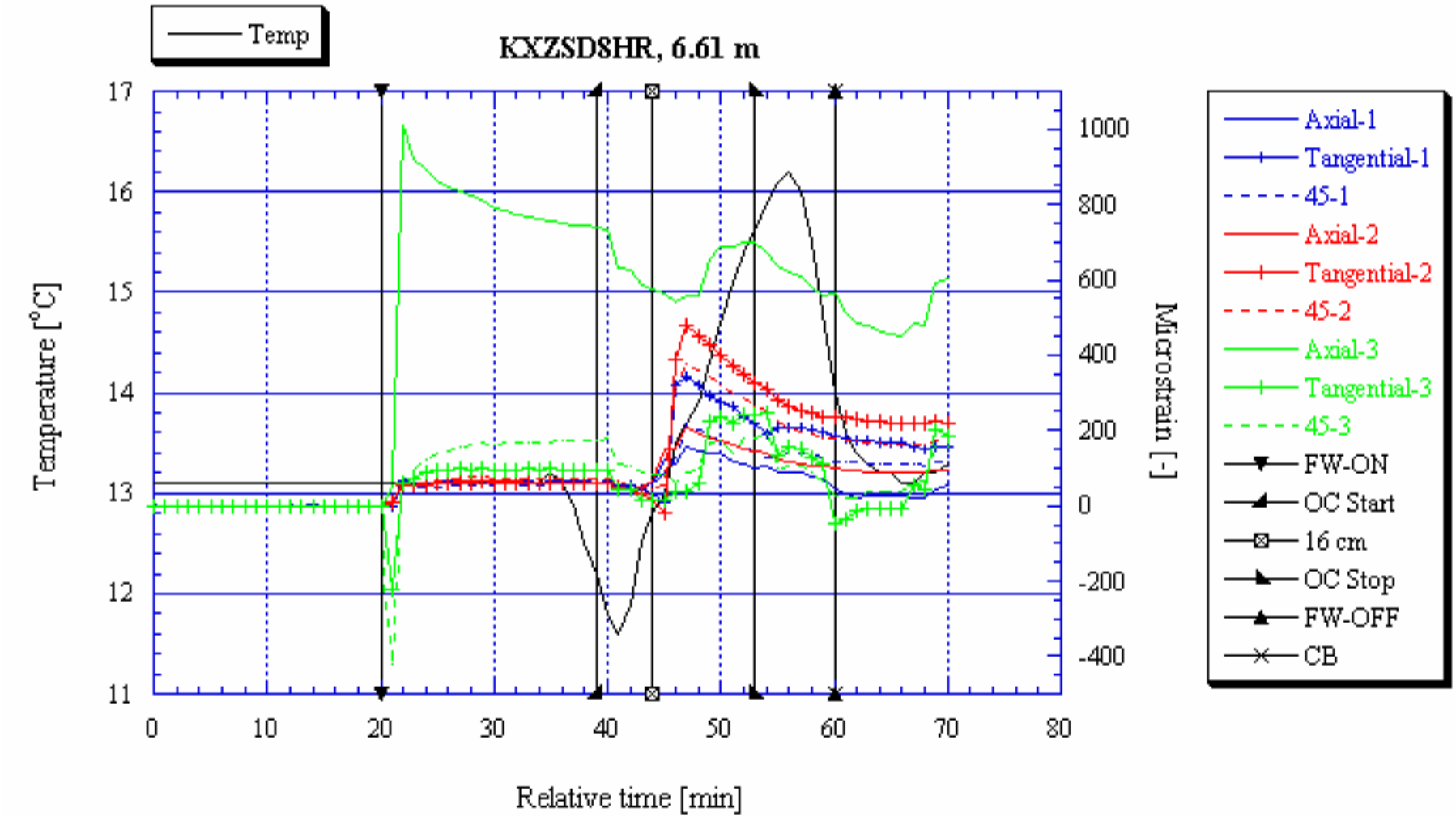
Temp
KXZSD8HR, 6.61 m
Temperature [°C]
Microstrain [-]
Relative time [min]
17
16
15
14
13
12
11
1000
800
600
400
200
0
-200
-400
0
10
20
30
40
50
60
70
80
Axial-1
Tangential-1
45-1
Axial-2
Tangential-2
45-2
Axial-3
Tangential-3
45-3
FW-ON
OC Start
16 cm
OC Stop
FW-OFF
CB

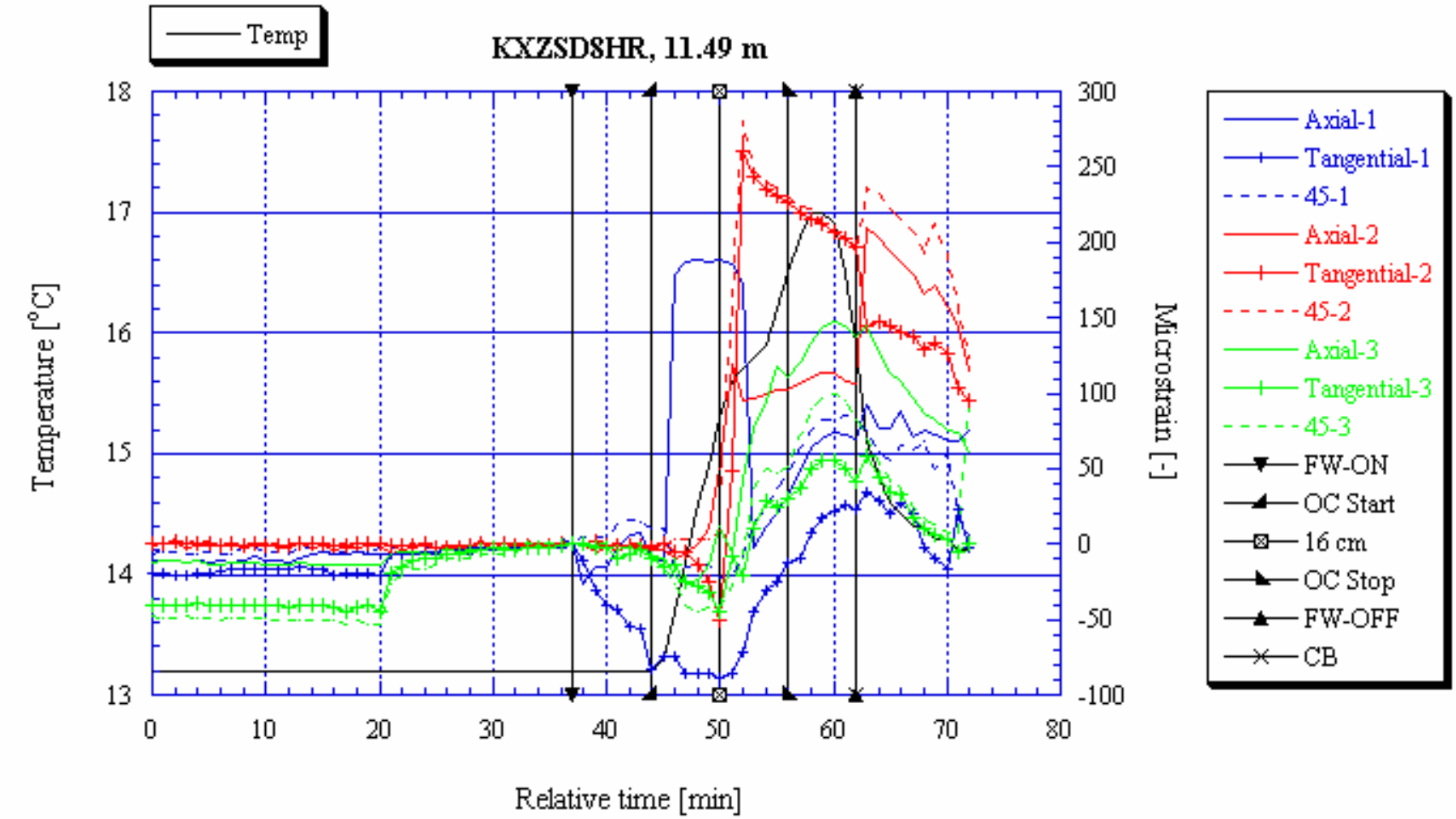
Temp
KXZSD8HR, 11.49 m
Temperature [°C]
Microstrain [-]
Relative time [min]
18
17
16
15
14
13
300
250
200
150
100
50
0
-50
-100
0
10
20
30
40
50
60
70
80
Axial-1
Tangential-1
45-1
Axial-2
Tangential-2
45-2
Axial-3
Tangential-3
45-3
FW-ON
OC Start
16 cm
OC Stop
FW-OFF
CB

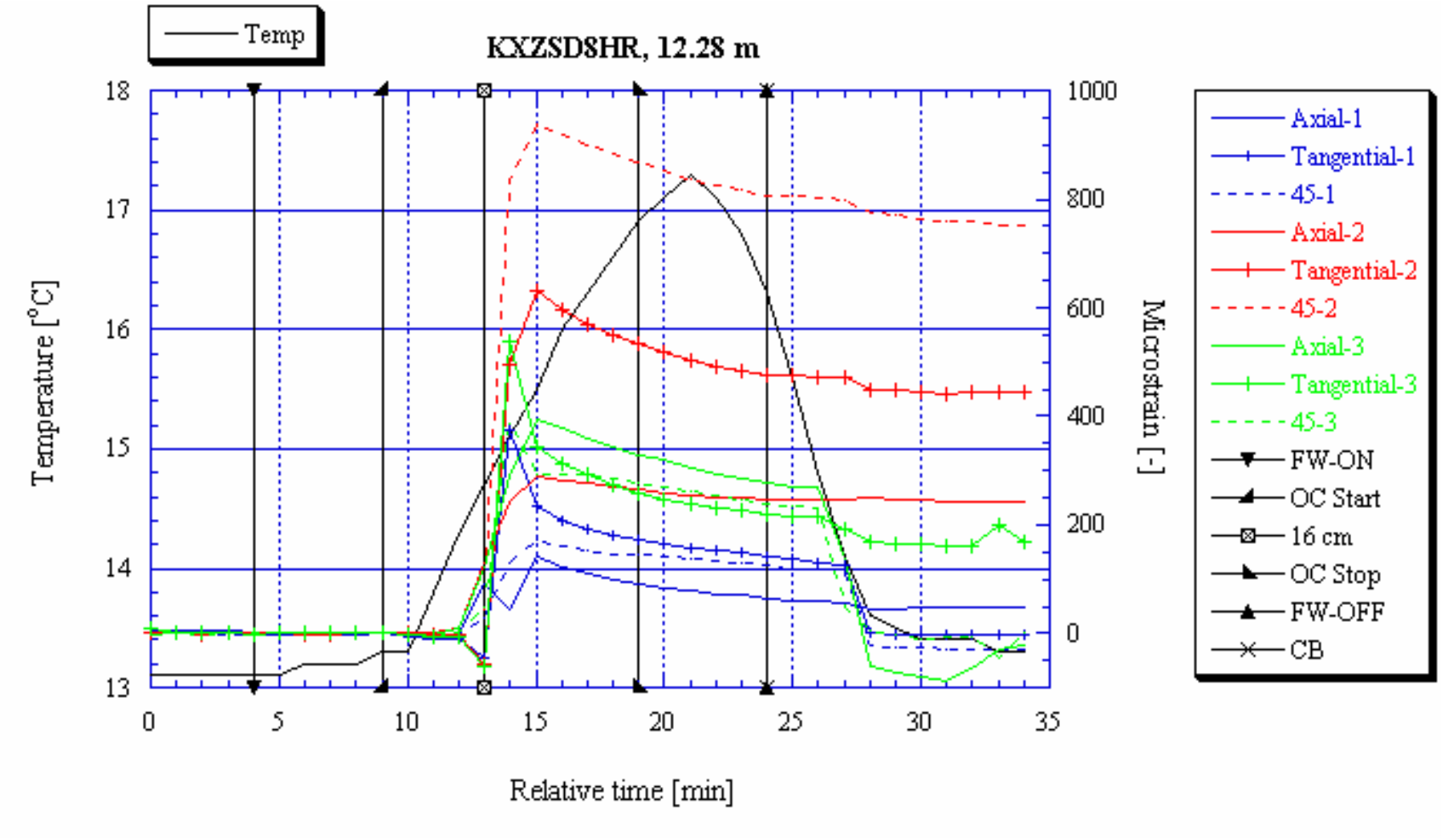
Temp
KXZSD8HR, 12.28 m
Temperature [°C]
Microstrain [-]
Relative time [min]
18
17
16
15
14
13
1000
800
600
400
200
0
0
5
10
15
20
25
30
35
Axial-1
Tangential-1
45-1
Axial-2
Tangential-2
45-2
Axial-3
Tangential-3
45-3
FW-ON
OC Start
16 cm
OC Stop
FW-OFF
CB

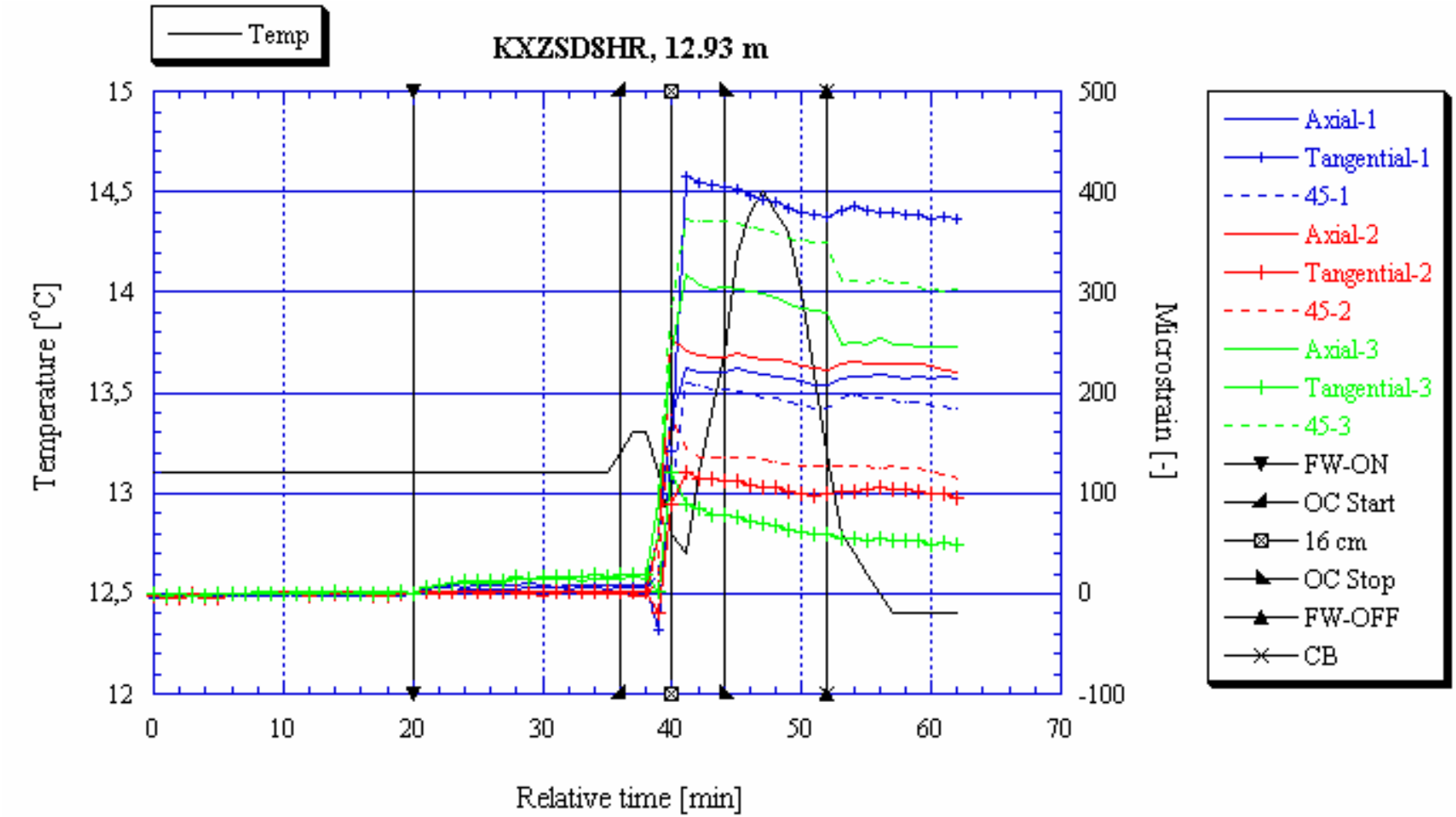
Temp
KXZSD8HR, 12.93 m
Temperature [°C]
15
14,5
14
13,5
13
12,5
12
0
10
20
30
40
50
60
70
Relative time [min]
500
400
300
200
100
0
-100
Microstrain [-]
Axial-1
Tangential-1
45-1
Axial-2
Tangential-2
45-2
Axial-3
Tangential-3
45-3
FW-ON
OC Start
16 cm
OC Stop
FW-OFF
CB

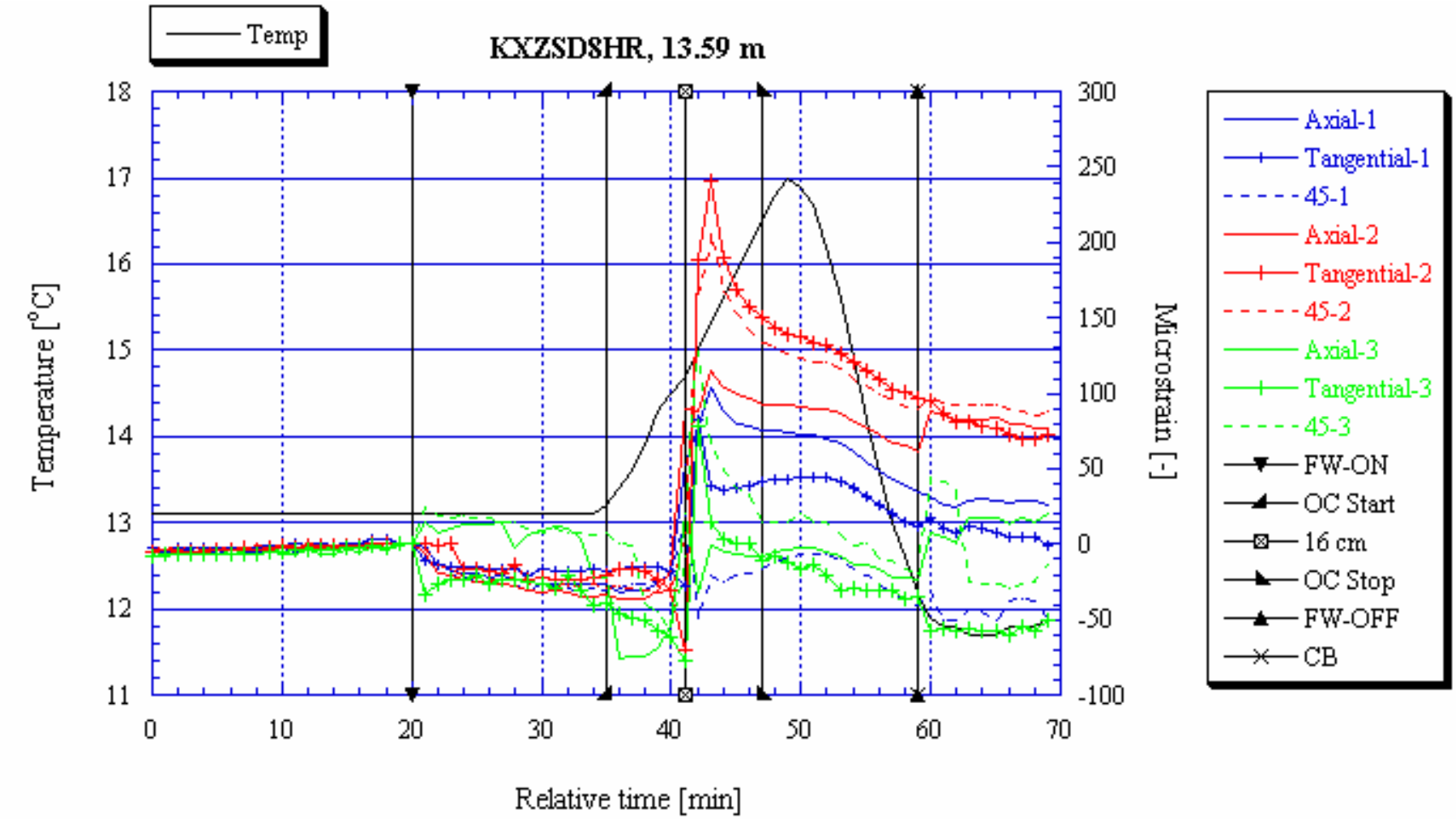
Temp
KXZSD8HR, 13.59 m
Temperature [°C]
Microstrain [-]
Relative time [min]
18
17
16
15
14
13
12
11
300
250
200
150
100
50
0
-50
-100
0
10
20
30
40
50
60
70
Axial-1
Tangential-1
45-1
Axial-2
Tangential-2
45-2
Axial-3
Tangential-3
45-3
FW-ON
OC Start
16 cm
OC Stop
FW-OFF
CB

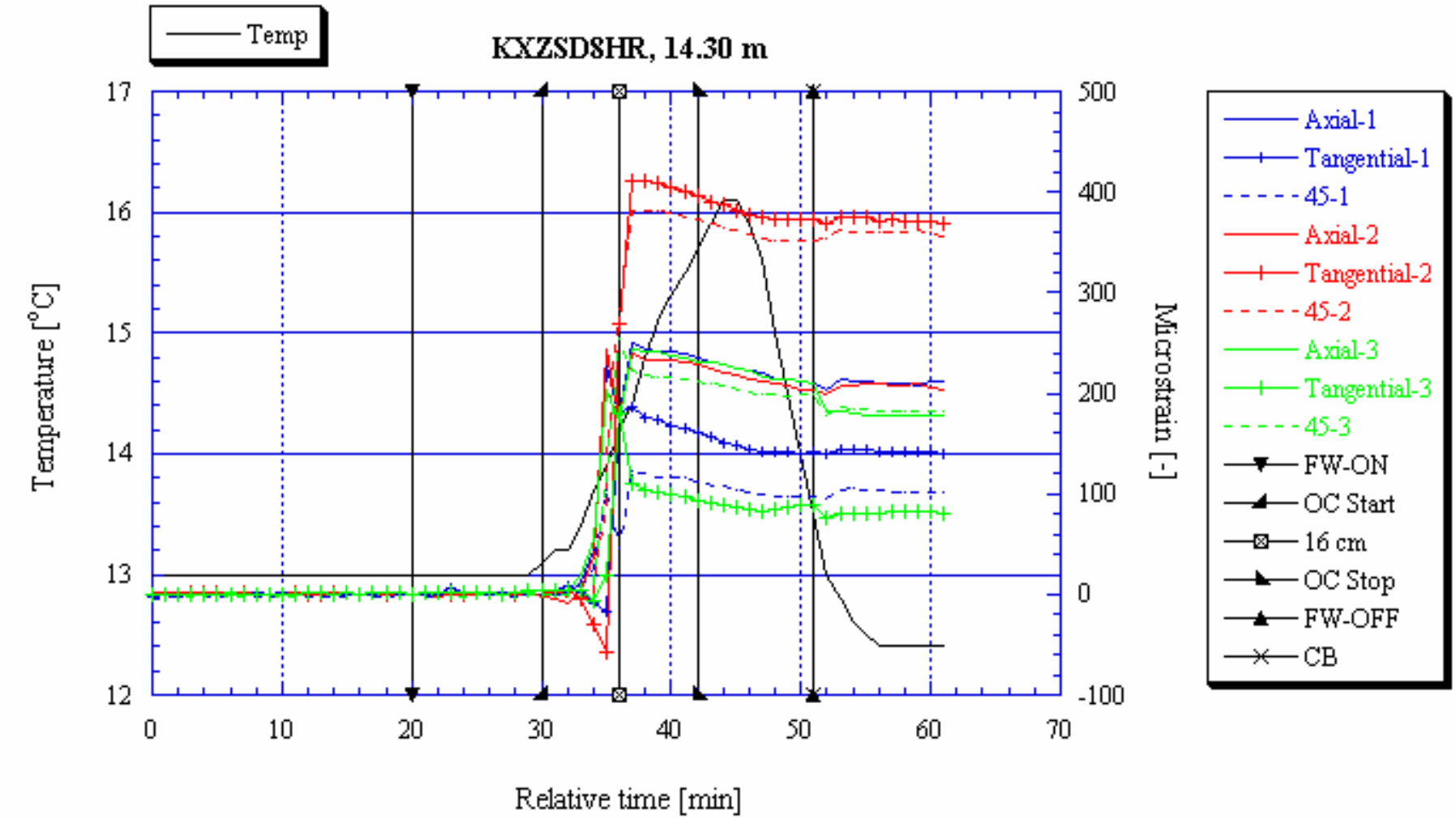
Temp
KXZSD8HR, 14.30 m
Temperature [°C]
Microstrain [-]
Relative time [min]
17
16
15
14
13
12
500
400
300
200
100
0
-100
0
10
20
30
40
50
60
70
Axial-1
Tangential-1
45-1
Axial-2
Tangential-2
45-2
Axial-3
Tangential-3
45-3
FW-ON
OC Start
16 cm
OC Stop
FW-OFF
CB

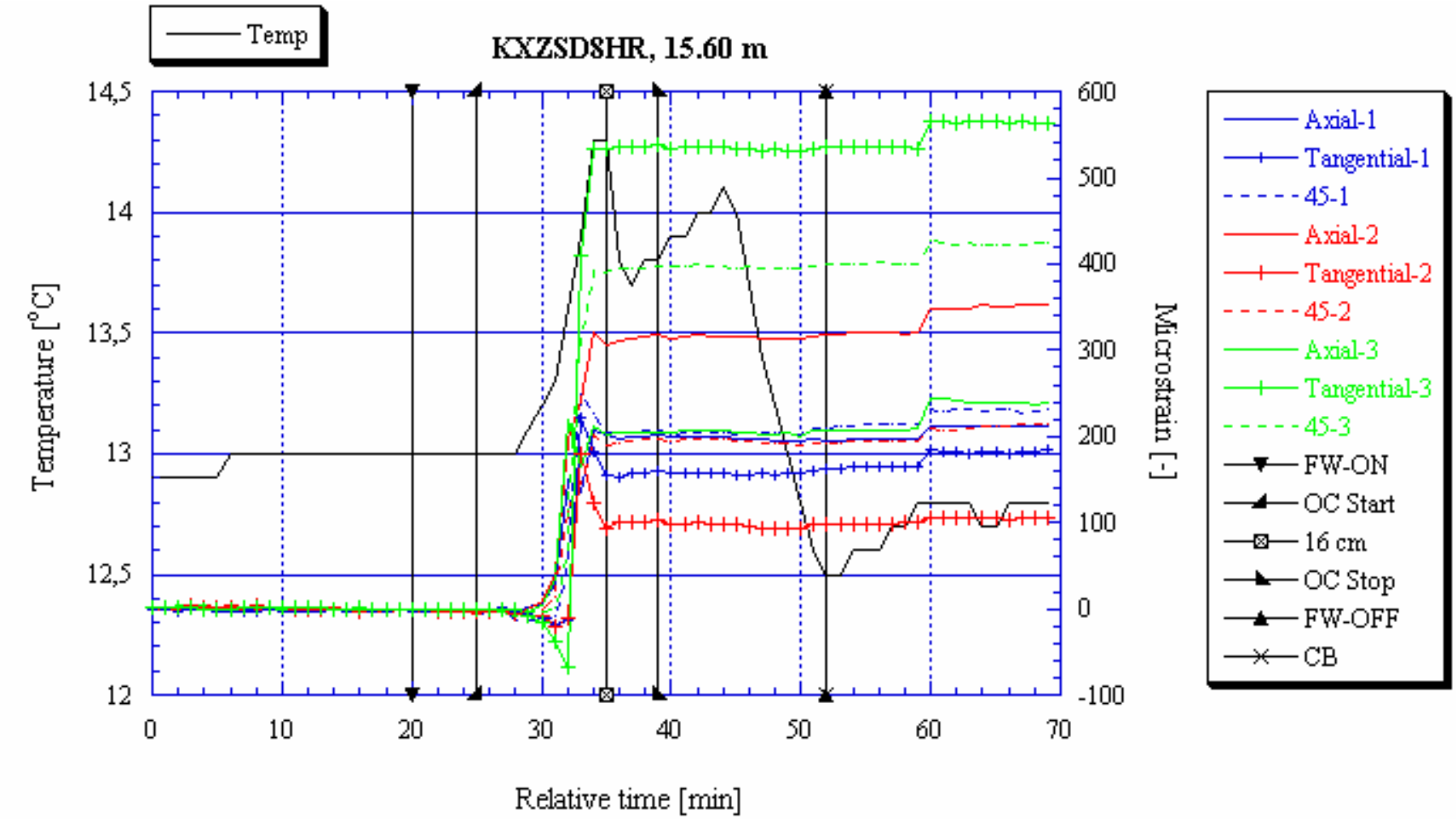
Temp
KXZSD8HR, 15.60 m
Temperature [°C]
14,5
14
13,5
13
12,5
12
0
10
20
30
40
50
60
70
Relative time [min]
600
500
400
300
200
100
0
-100
Microstrain [-]
Axial-1
Tangential-1
45-1
Axial-2
Tangential-2
45-2
Axial-3
Tangential-3
45-3
FW-ON
OC Start
16 cm
OC Stop
FW-OFF
CB

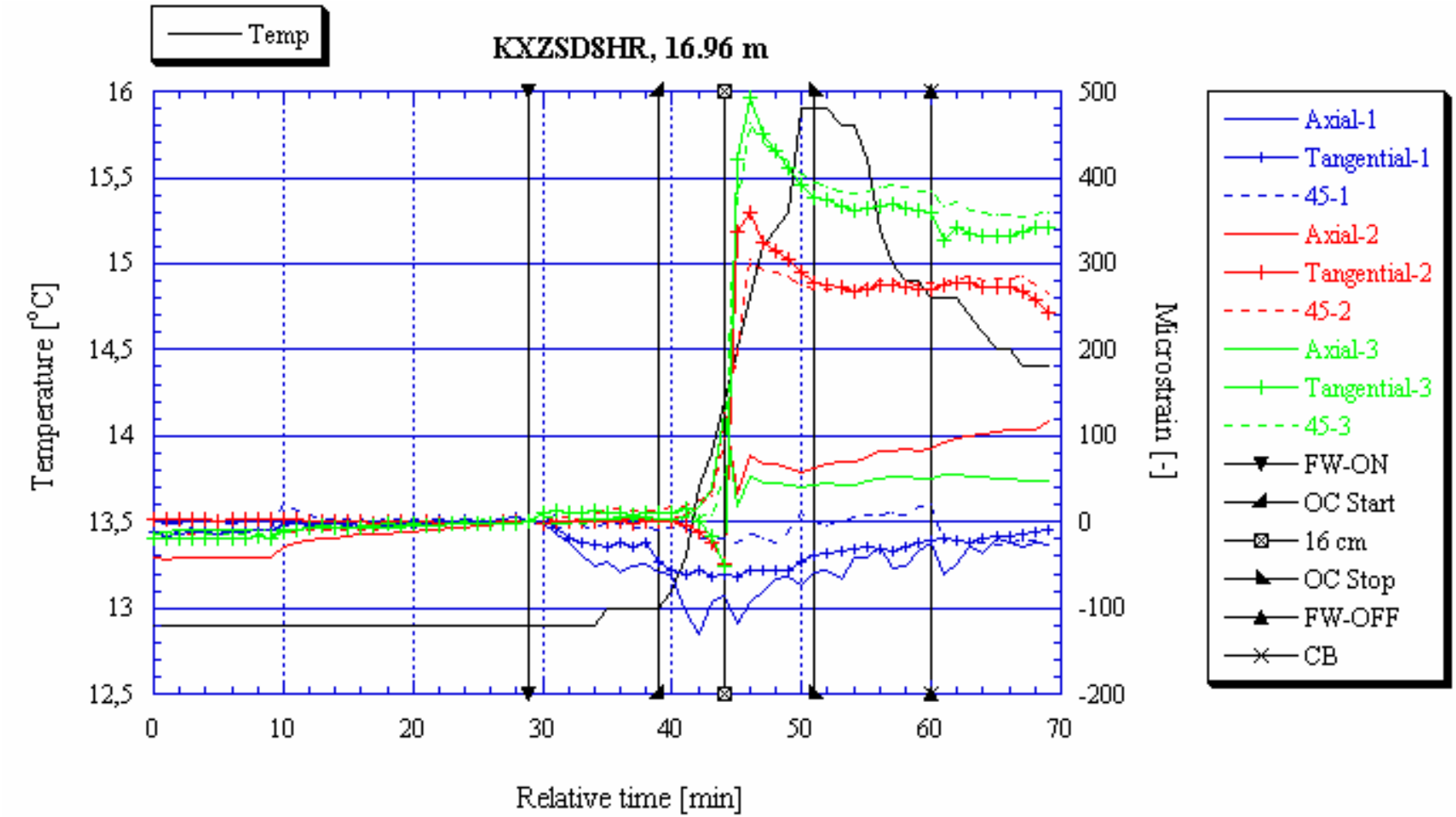
Temp
KXZSD8HR, 16.96 m
Temperature [°C]
16
15,5
15
14,5
14
13,5
13
12,5
0
10
20
30
40
50
60
70
Relative time [min]
500
400
300
200
100
0
-100
-200
Microstrain [-]
Axial-1
Tangential-1
45-1
Axial-2
Tangential-2
45-2
Axial-3
Tangential-3
45-3
FW-ON
OC Start
16 cm
OC Stop
FW-OFF
CB

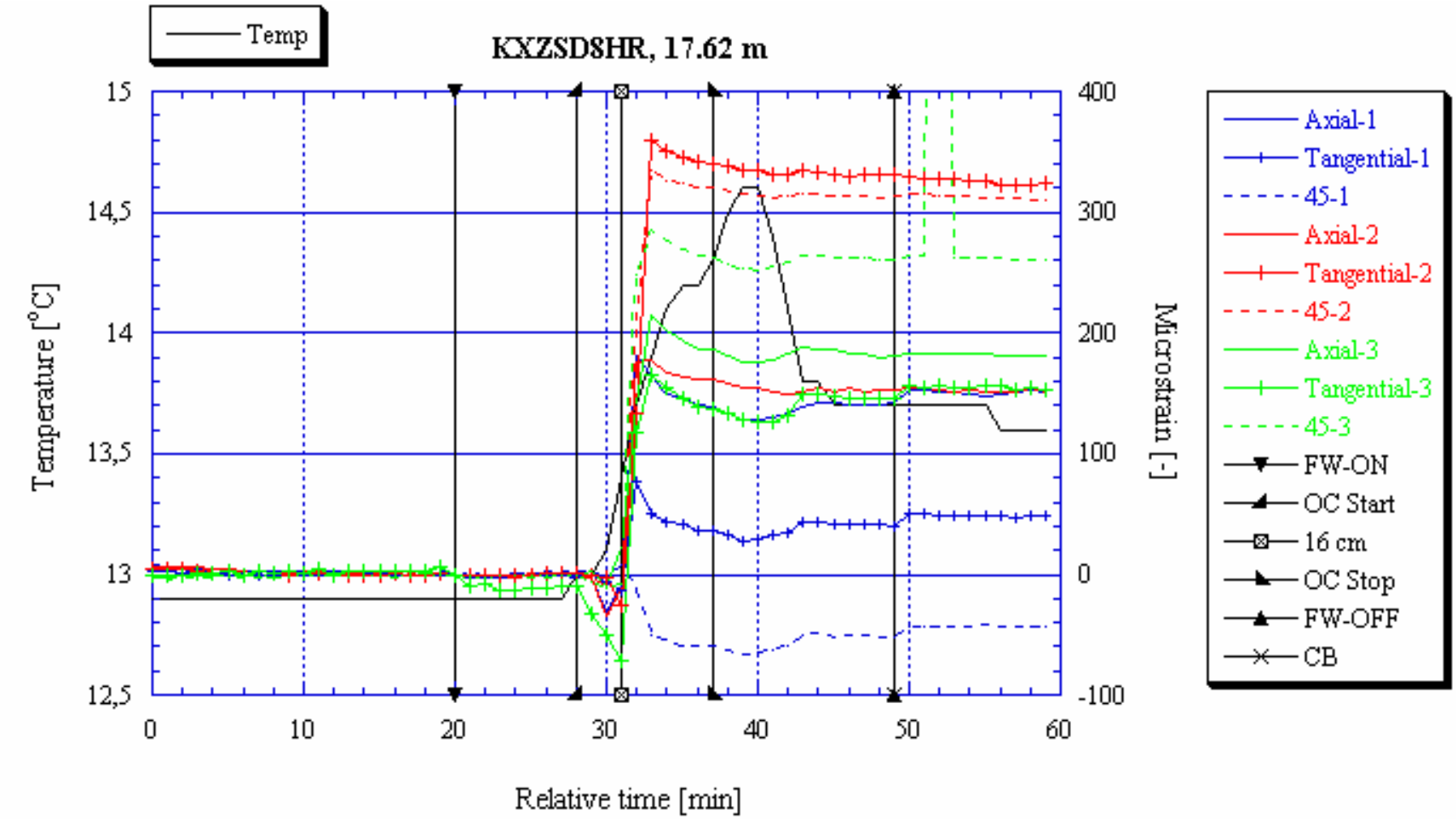
Temp
KXZSD8HR, 17.62 m
Temperature [°C]
15
14,5
14
13,5
13
12,5
0
10
20
30
40
50
60
Relative time [min]
400
300
200
100
0
-100
Microstrain [-]
Axial-1
Tangential-1
45-1
Axial-2
Tangential-2
45-2
Axial-3
Tangential-3
45-3
FW-ON
OC Start
16 cm
OC Stop
FW-OFF
CB

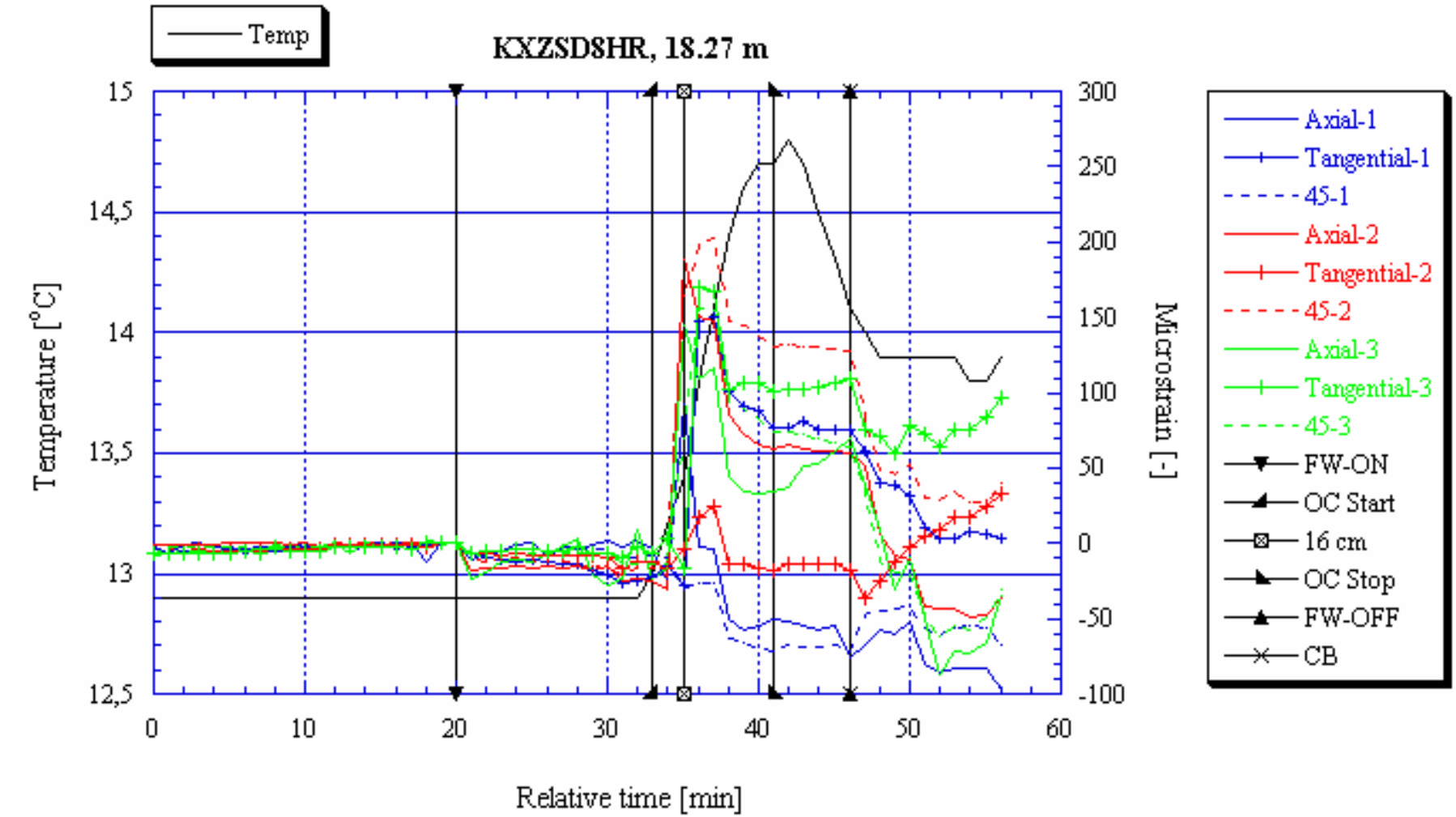
Temp
KXZSD8HR, 18.27 m
Temperature [°C]
15
14,5
14
13,5
13
12,5
0
10
20
30
40
50
60
Relative time [min]
300
250
200
150
100
50
0
-50
-100
Microstrain [-]
Axial-1
Tangential-1
45-1
Axial-2
Tangential-2
45-2
Axial-3
Tangential-3
45-3
FW-ON
OC Start
16 cm
OC Stop
FW-OFF
CB

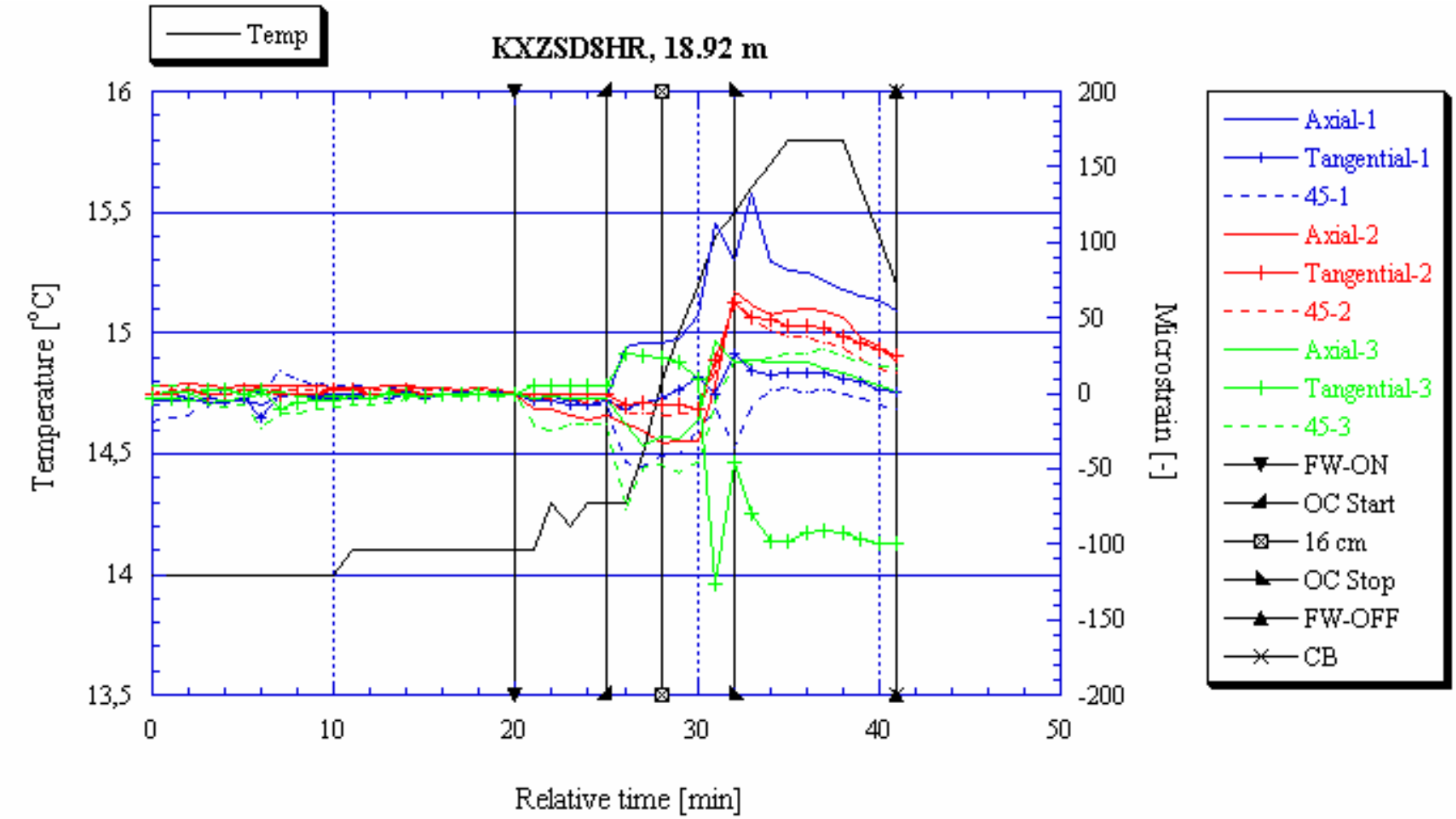
Temp
KXZSD8HR, 18.92 m
Temperature [°C]
16
15,5
15
14,5
14
13,5
Microstrain [-]
200
150
100
50
0
-50
-100
-150
-200
0
10
20
30
40
50
Relative time [min]
Axial-1
Tangential-1
45-1
Axial-2
Tangential-2
45-2
Axial-3
Tangential-3
45-3
FW-ON
OC Start
16 cm
OC Stop
FW-OFF
CB

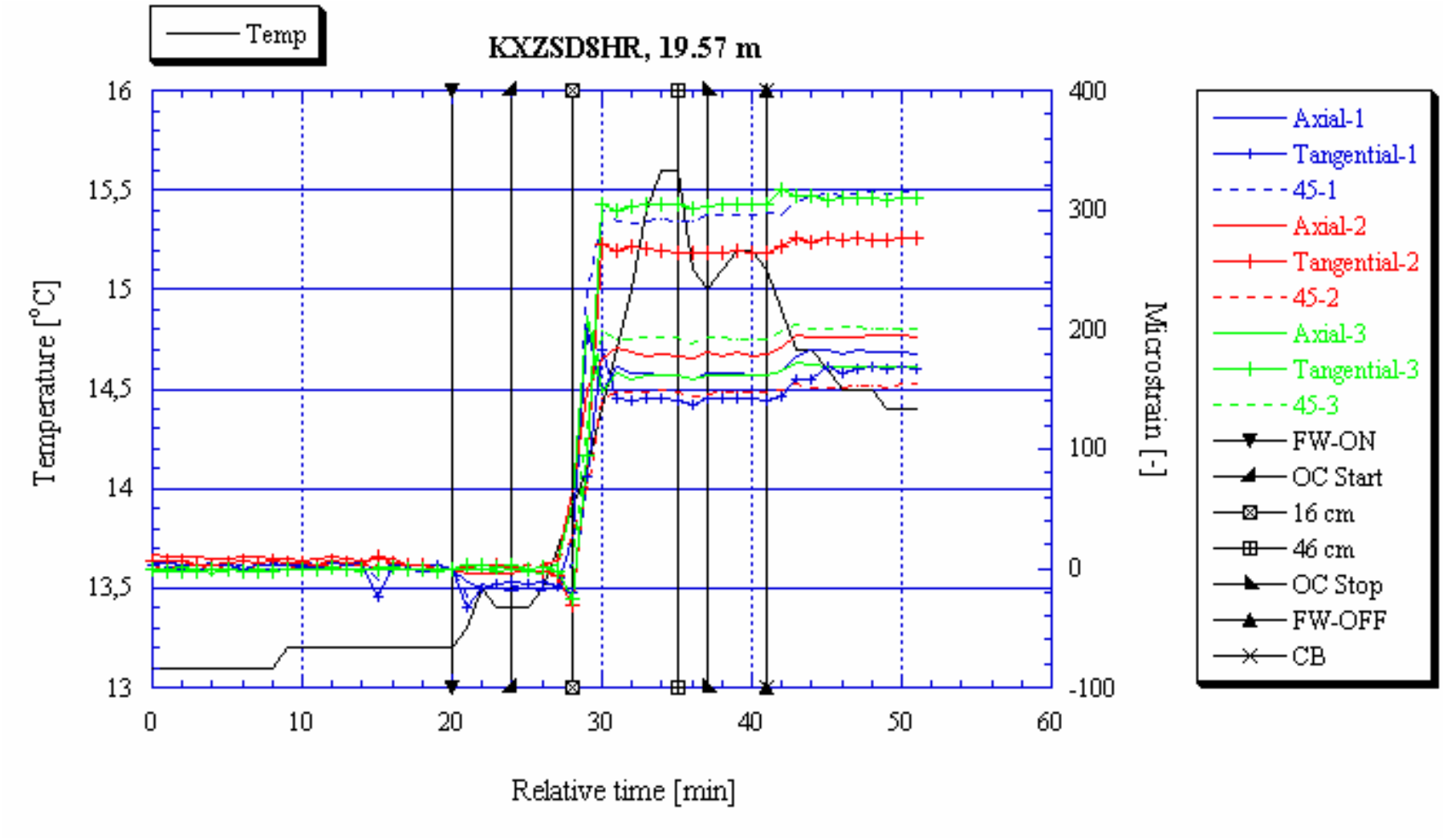
Temp
KXZSD8HR, 19.57 m
Temperature [°C]
16
15,5
15
14,5
14
13,5
13
Microstrain [-]
400
300
200
100
0
-100
0
10
20
30
40
50
60
Relative time [min]
Axial-1
Tangential-1
45-1
Axial-2
Tangential-2
45-2
Axial-3
Tangential-3
45-3
FW-ON
OC Start
16 cm
46 cm
OC Stop
FW-OFF
CB

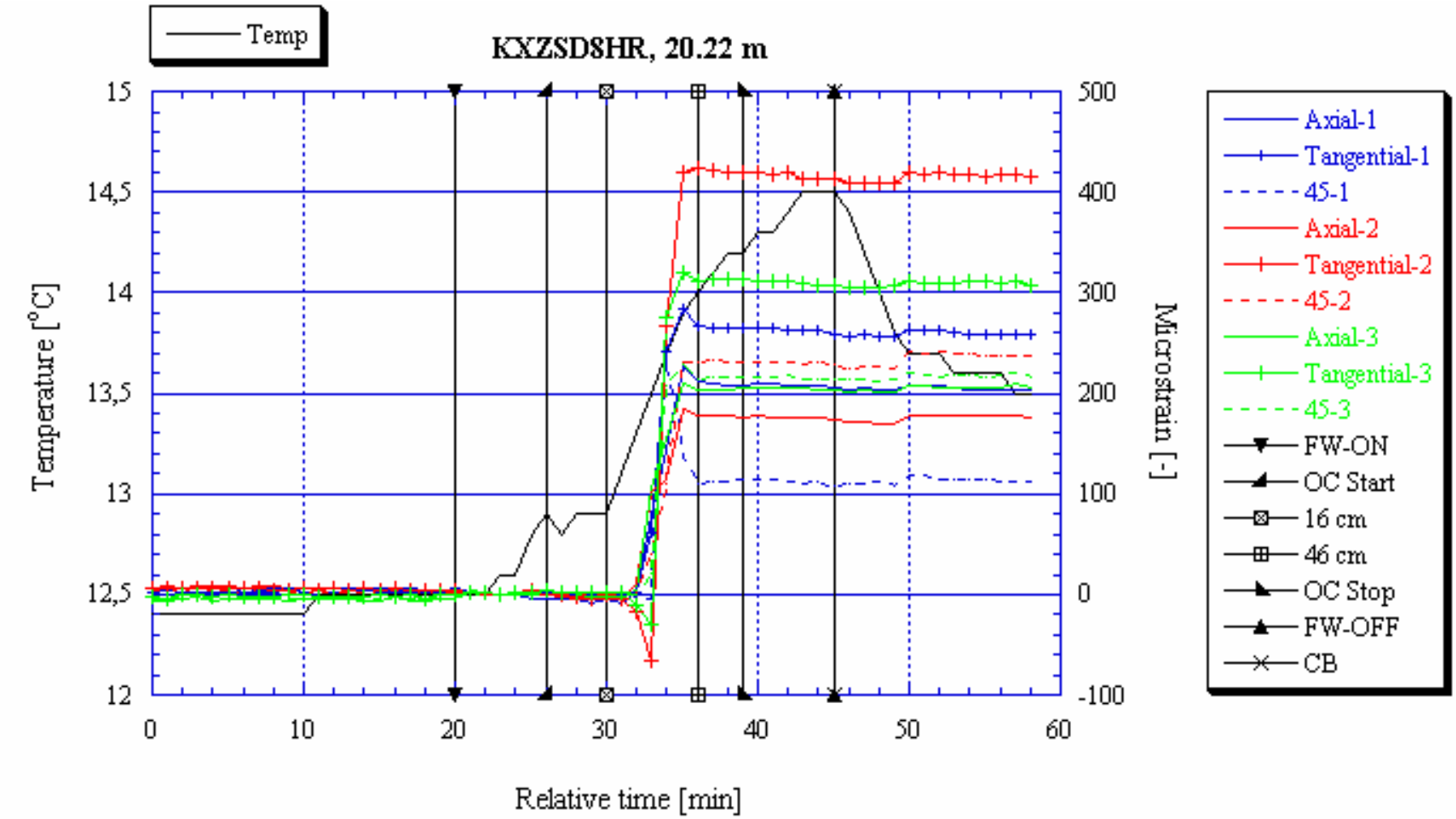
Temp
KXZSD8HR, 20.22 m
Temperature [°C]
15
14,5
14
13,5
13
12,5
12
0
10
20
30
40
50
60
Relative time [min]
500
400
300
200
100
0
-100
Microstrain [-]
Axial-1
Tangential-1
45-1
Axial-2
Tangential-2
45-2
Axial-3
Tangential-3
45-3
FW-ON
OC Start
16 cm
46 cm
OC Stop
FW-OFF
CB

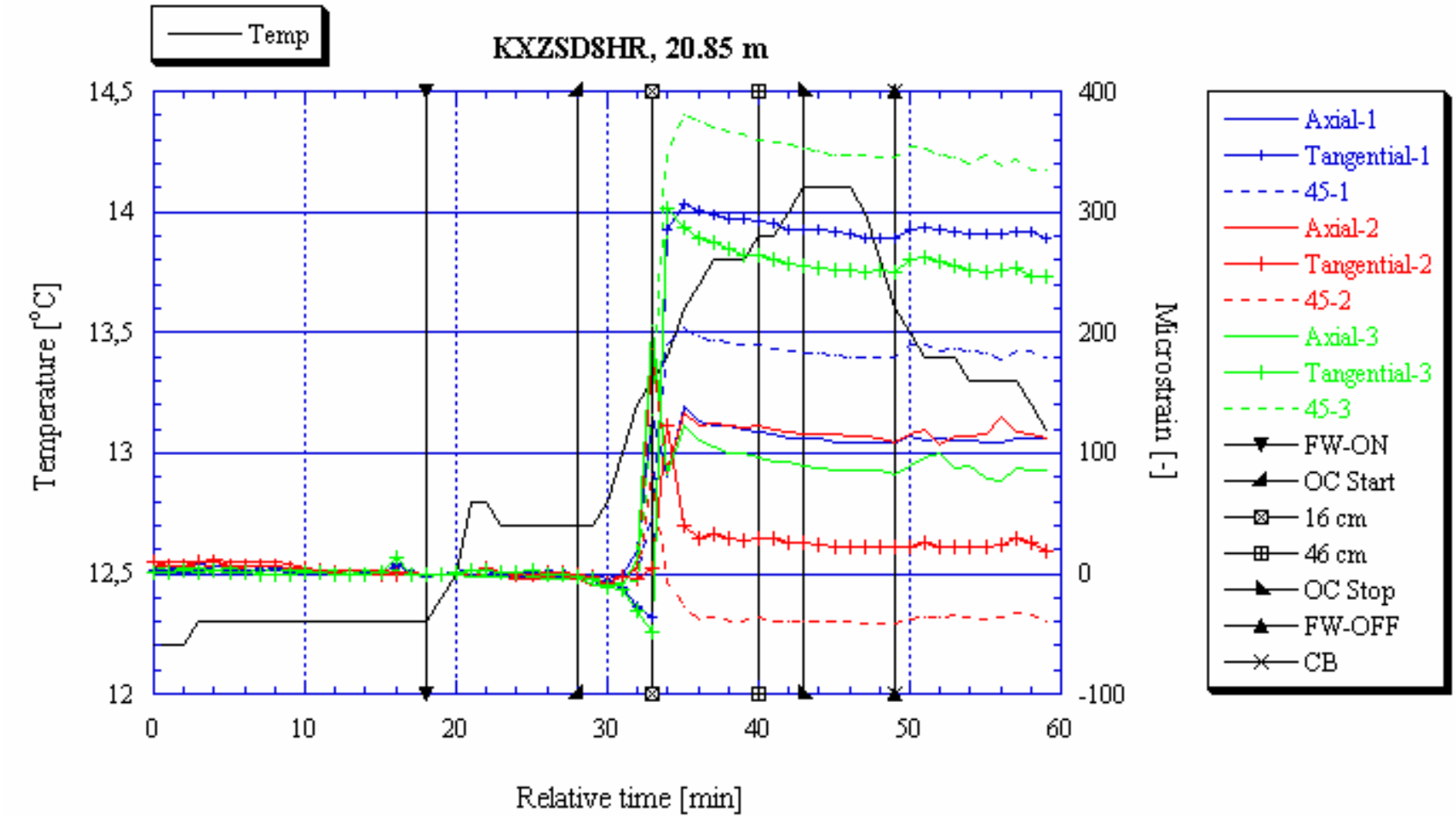
Temp
KXZSD8HR, 20.85 m
Temperature [°C]
14,5
14
13,5
13
12,5
12
0
10
20
30
40
50
60
Relative time [min]
400
300
200
100
0
-100
Microstrain [-]
Axial-1
Tangential-1
45-1
Axial-2
Tangential-2
45-2
Axial-3
Tangential-3
45-3
FW-ON
OC Start
16 cm
46 cm
OC Stop
FW-OFF
CB

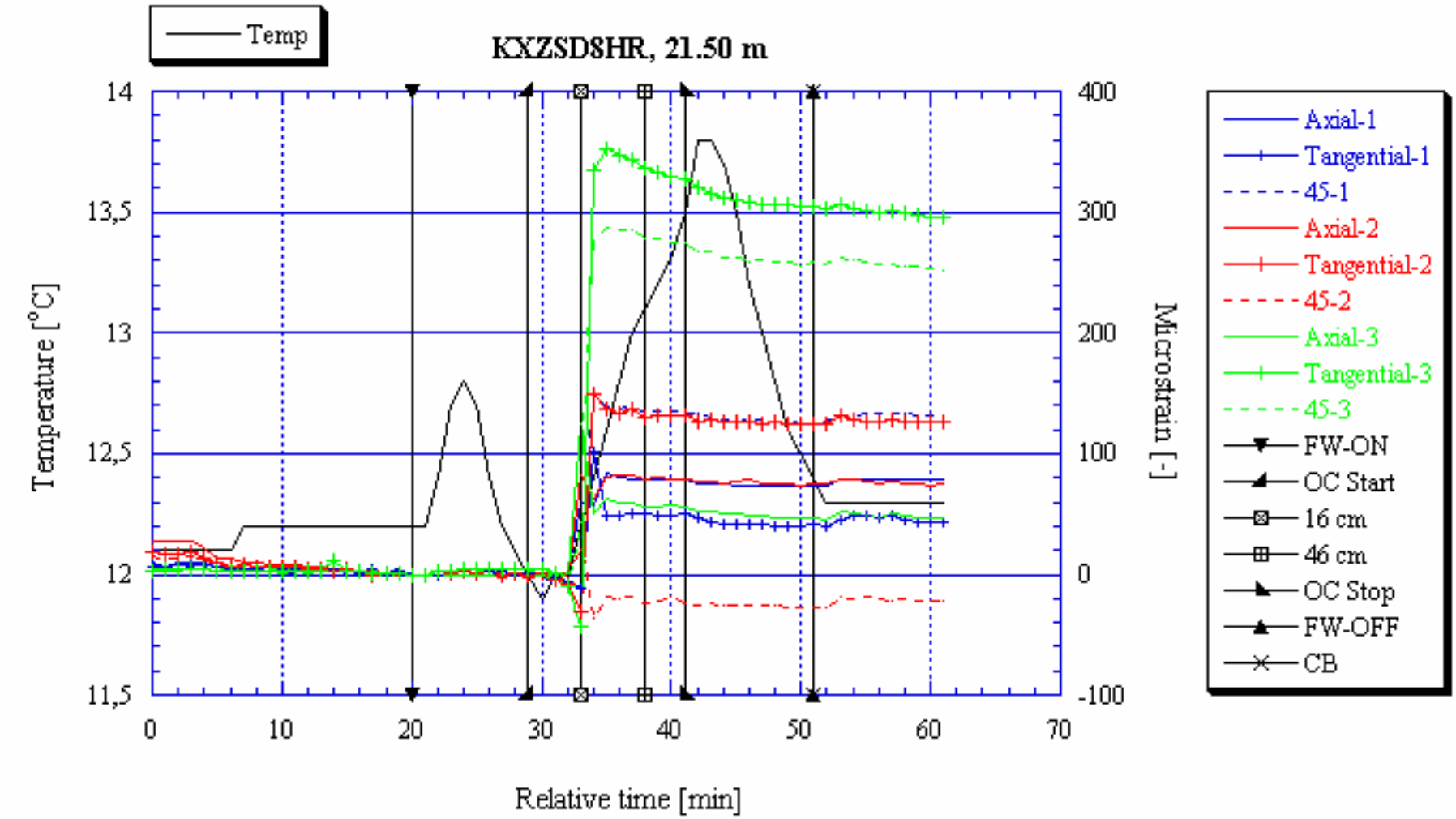
Temp
KXZSD8HR, 21.50 m
Temperature [°C]
14
13,5
13
12,5
12
11,5
0
10
20
30
40
50
60
70
Relative time [min]
400
300
200
100
0
-100
Microstrain [-]
Axial-1
Tangential-1
45-1
Axial-2
Tangential-2
45-2
Axial-3
Tangential-3
45-3
FW-ON
OC Start
16 cm
46 cm
OC Stop
FW-OFF
CB

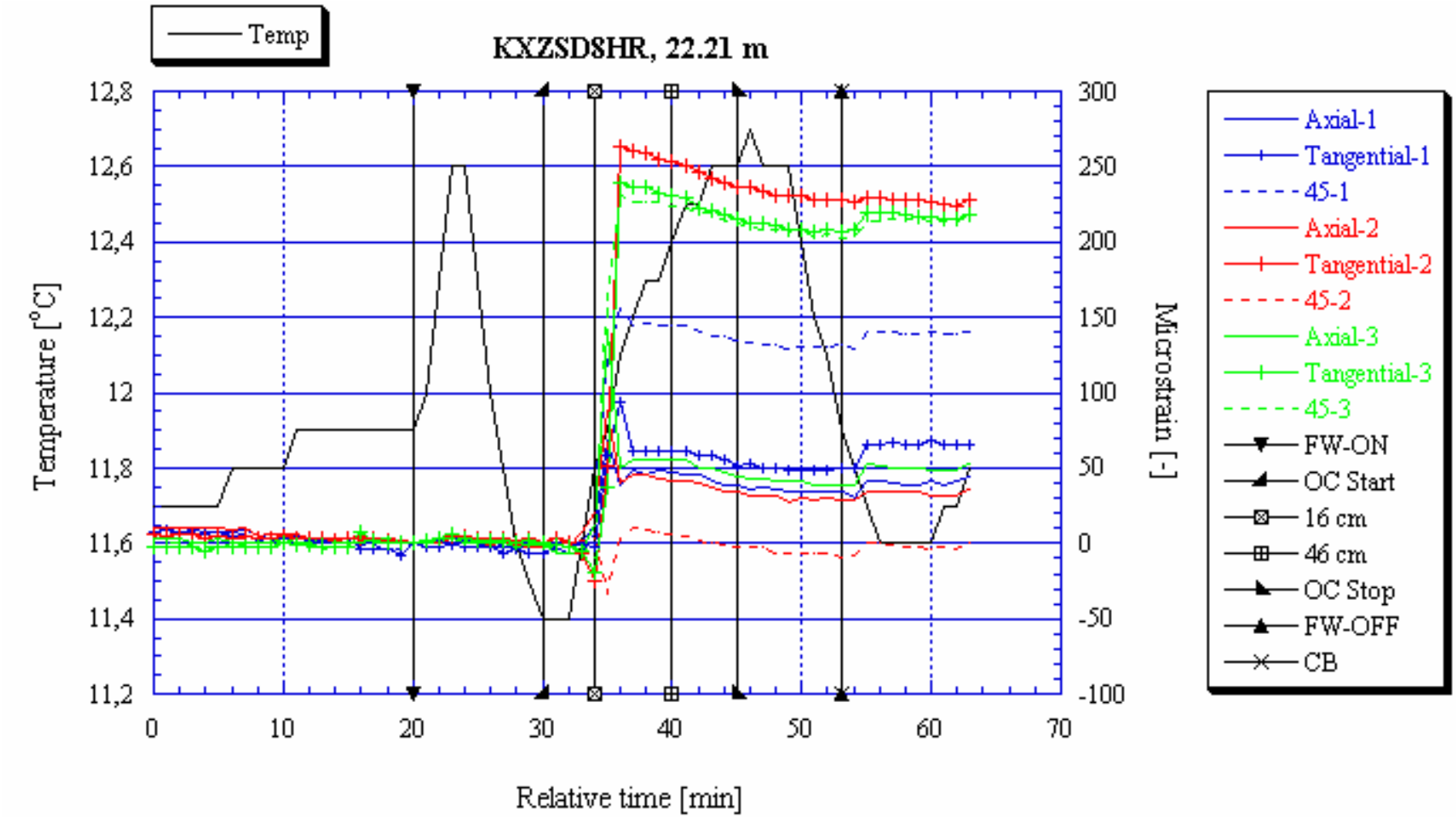
Temp
KXZSD8HR, 22.21 m
Temperature [°C]
12,8
12,6
12,4
12,2
12
11,8
11,6
11,4
11,2
Microstrain [-]
300
250
200
150
100
50
0
-50
-100
0
10
20
30
40
50
60
70
Relative time [min]
Axial-1
Tangential-1
45-1
Axial-2
Tangential-2
45-2
Axial-3
Tangential-3
45-3
FW-ON
OC Start
16 cm
46 cm
OC Stop
FW-OFF
CB

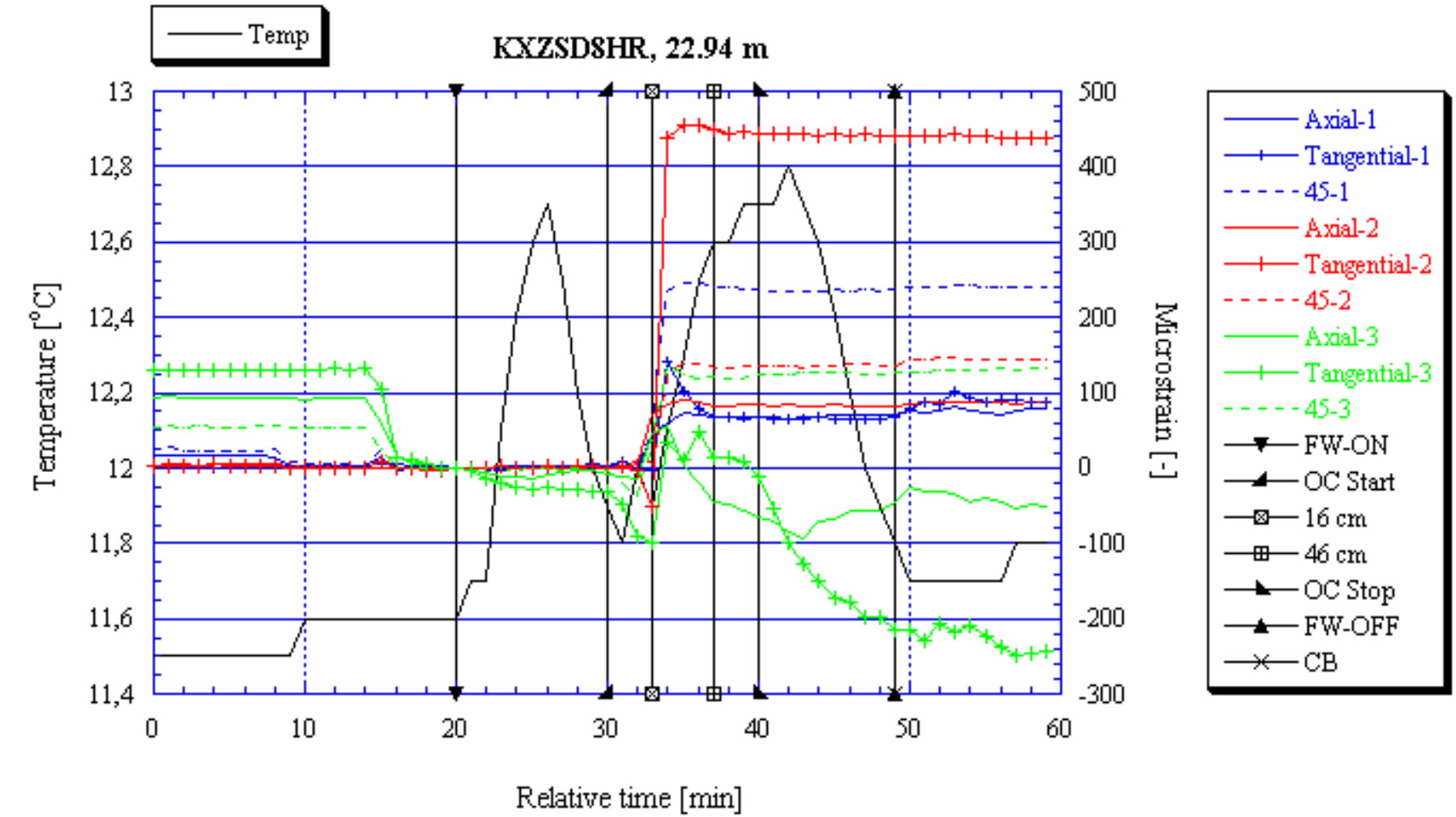
Temp
KXZSD8HR, 22.94 m
Temperature [°C]
13
12,8
12,6
12,4
12,2
12
11,8
11,6
11,4
Microstrain [-]
500
400
300
200
100
0
-100
-200
-300
0
10
20
30
40
50
60
Relative time [min]
Axial-1
Tangential-1
45-1
Axial-2
Tangential-2
45-2
Axial-3
Tangential-3
45-3
FW-ON
OC Start
16 cm
46 cm
OC Stop
FW-OFF
CB

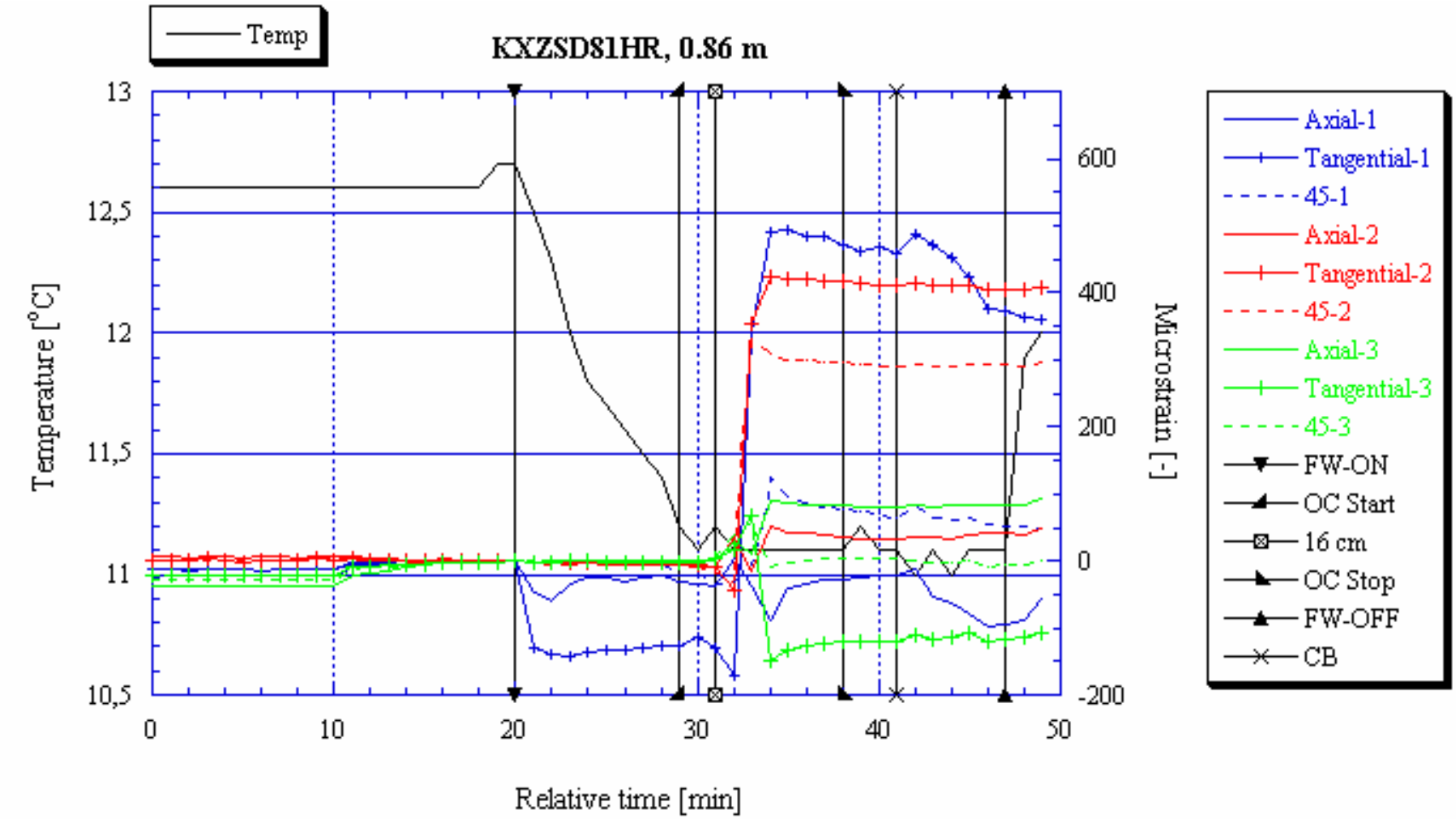
Temp
KXZSD81HR, 0.86 m
Temperature [°C]
13
12,5
12
11,5
11
10,5
0
10
20
30
40
50
Relative time [min]
600
400
200
0
-200
Microstrain [-]
Axial-1
Tangential-1
45-1
Axial-2
Tangential-2
45-2
Axial-3
Tangential-3
45-3
FW-ON
OC Start
16 cm
OC Stop
FW-OFF
CB

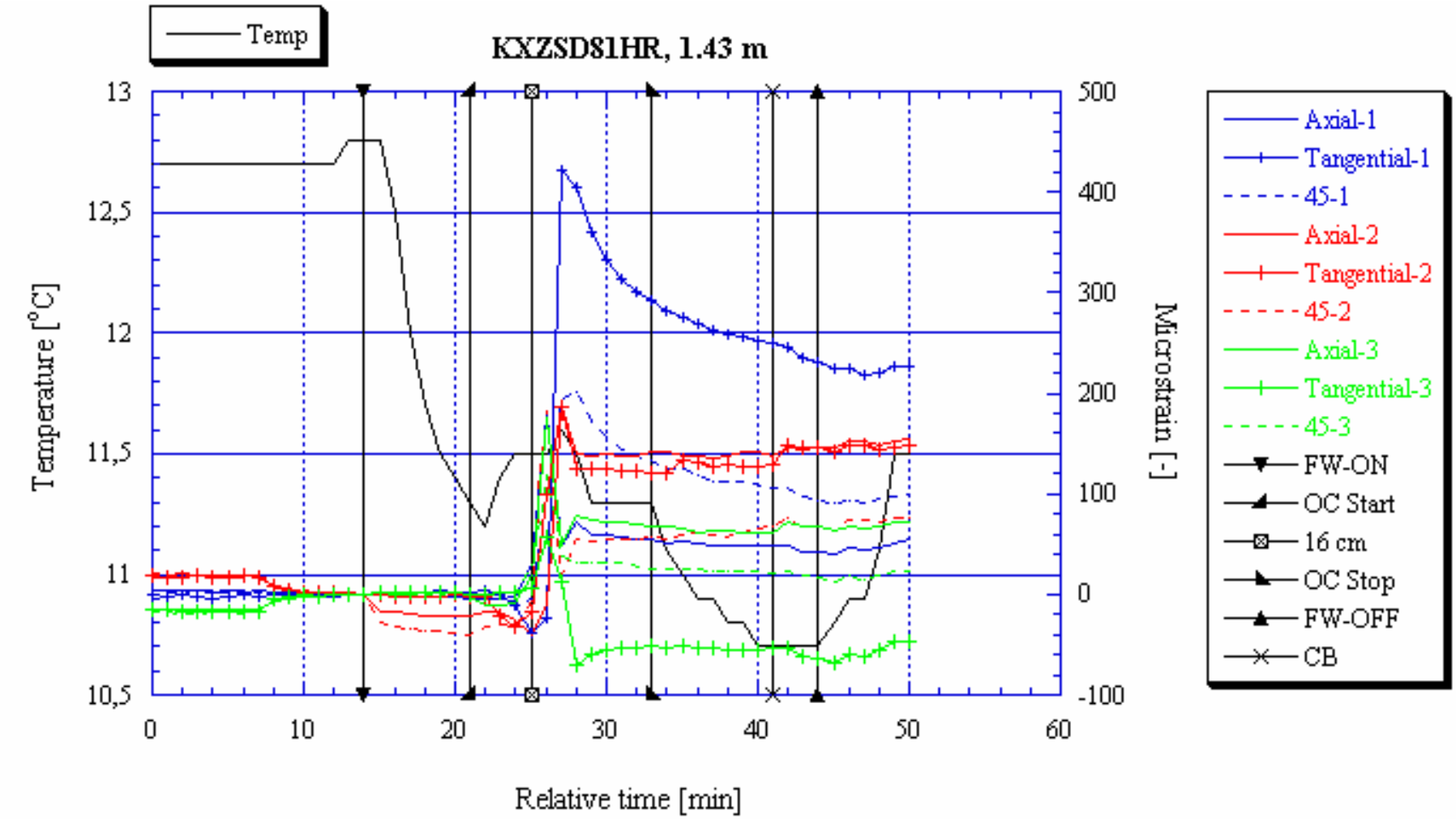
Temp
KXZSD81HR, 1.43 m
Temperature [°C]
13
12,5
12
11,5
11
10,5
Microstrain [-]
500
400
300
200
100
0
-100
0
10
20
30
40
50
60
Relative time [min]
Axial-1
Tangential-1
45-1
Axial-2
Tangential-2
45-2
Axial-3
Tangential-3
45-3
FW-ON
OC Start
16 cm
OC Stop
FW-OFF
CB

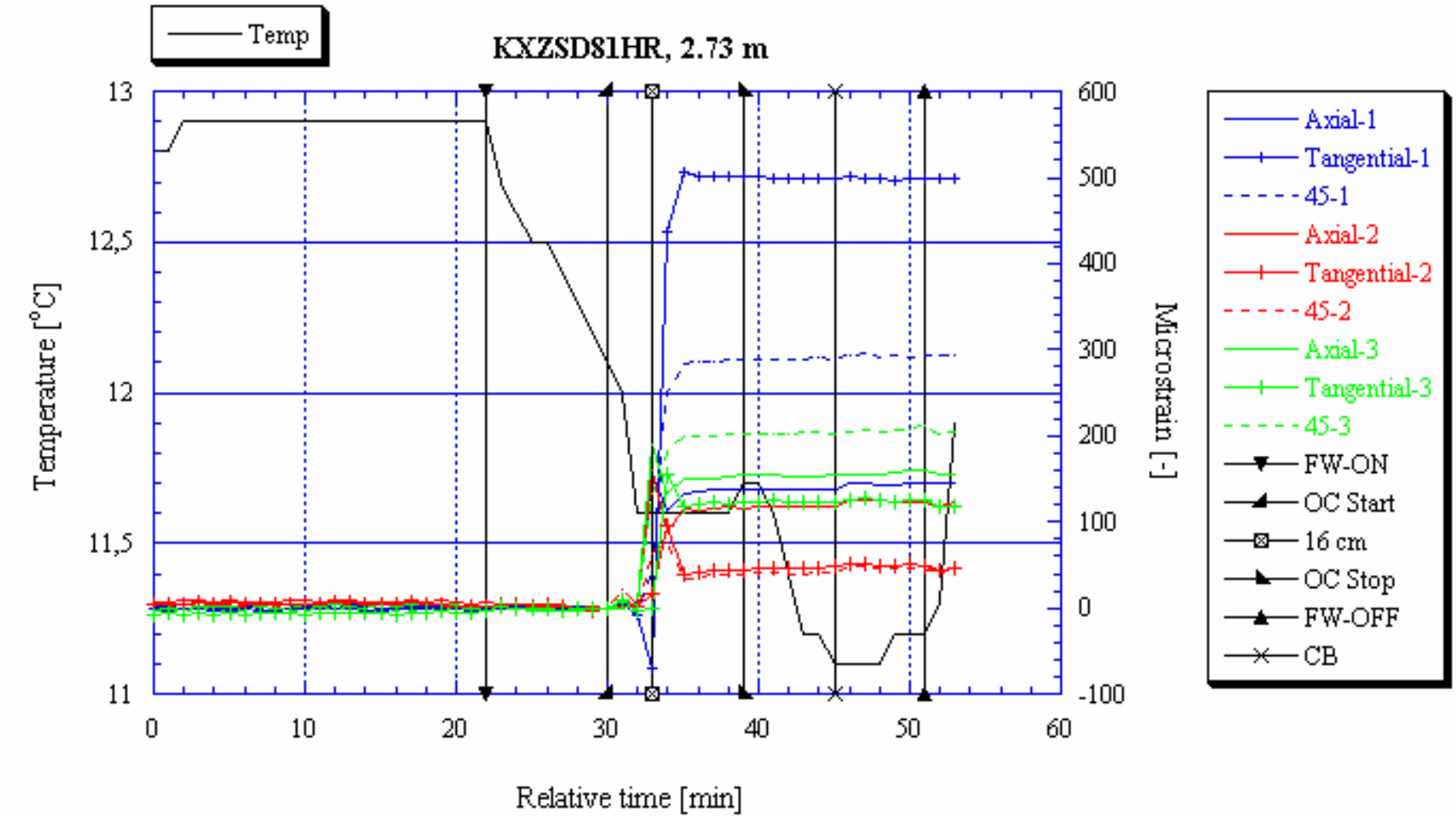
Temp
KXZSD81HR, 2.73 m
Temperature [°C]
13
12,5
12
11,5
11
Microstrain [-]
600
500
400
300
200
100
0
-100
0
10
20
30
40
50
60
Relative time [min]
Axial-1
Tangential-1
45-1
Axial-2
Tangential-2
45-2
Axial-3
Tangential-3
45-3
FW-ON
OC Start
16 cm
OC Stop
FW-OFF
CB

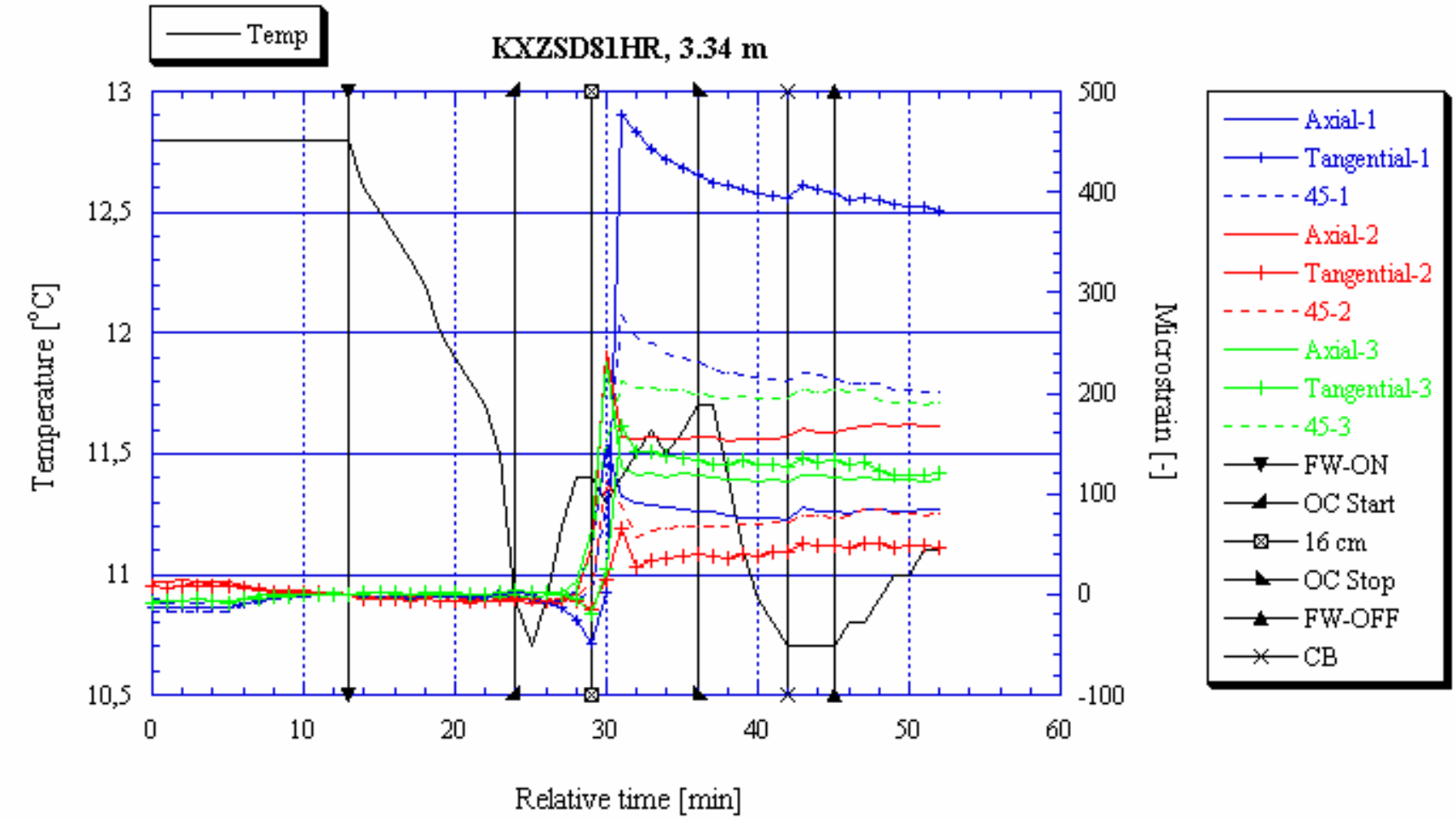
Temp
KXZSD81HR, 3.34 m
Temperature [°C]
13
12,5
12
11,5
11
10,5
0
10
20
30
40
50
60
Relative time [min]
500
400
300
200
100
0
-100
Microstrain [-]
Axial-1
Tangential-1
45-1
Axial-2
Tangential-2
45-2
Axial-3
Tangential-3
45-3
FW-ON
OC Start
16 cm
OC Stop
FW-OFF
CB

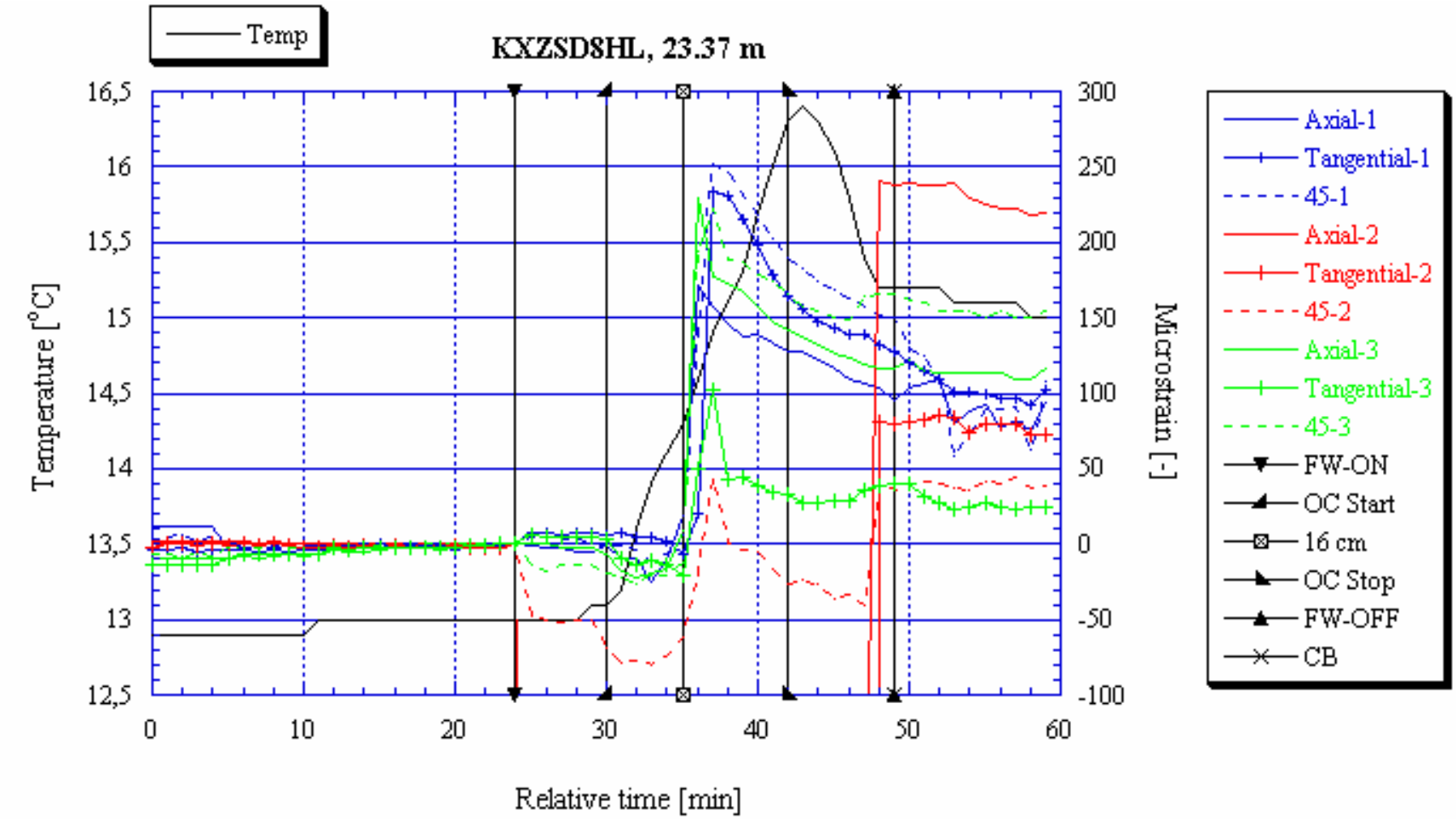
Temp
KXZSD8HL, 23.37 m
Temperature [°C]
16,5
16
15,5
15
14,5
14
13,5
13
12,5
0
10
20
30
40
50
60
Relative time [min]
300
250
200
150
100
50
0
-50
-100
Microstrain [-]
Axial-1
Tangential-1
45-1
Axial-2
Tangential-2
45-2
Axial-3
Tangential-3
45-3
FW-ON
OC Start
16 cm
OC Stop
FW-OFF
CB

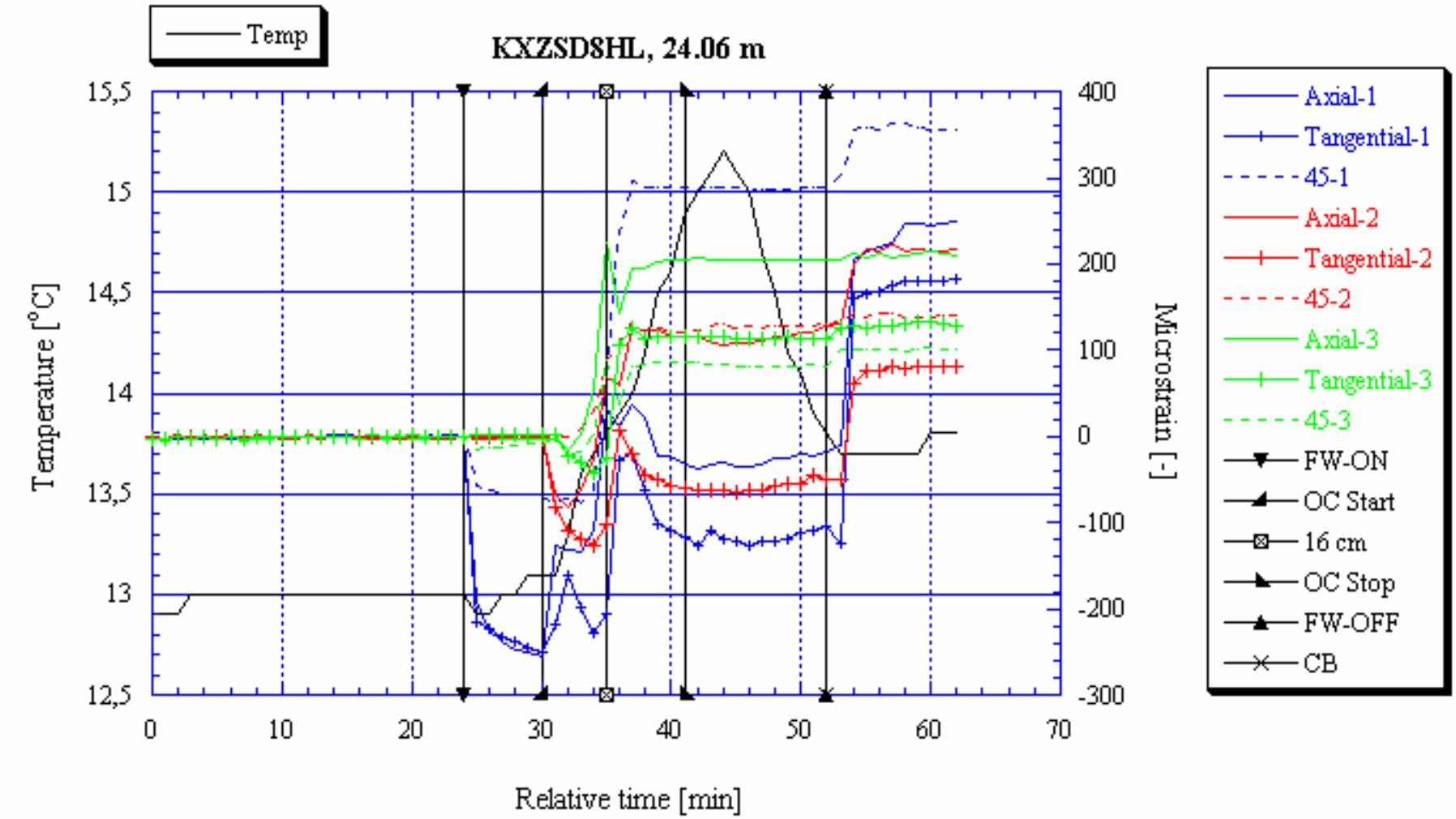
Temp
KXZSD8HL, 24.06 m
Temperature [°C]
15,5
15
14,5
14
13,5
13
12,5
0
10
20
30
40
50
60
70
Relative time [min]
400
300
200
100
0
-100
-200
-300
Microstrain [-]
Axial-1
Tangential-1
45-1
Axial-2
Tangential-2
45-2
Axial-3
Tangential-3
45-3
FW-ON
OC Start
16 cm
OC Stop
FW-OFF
CB

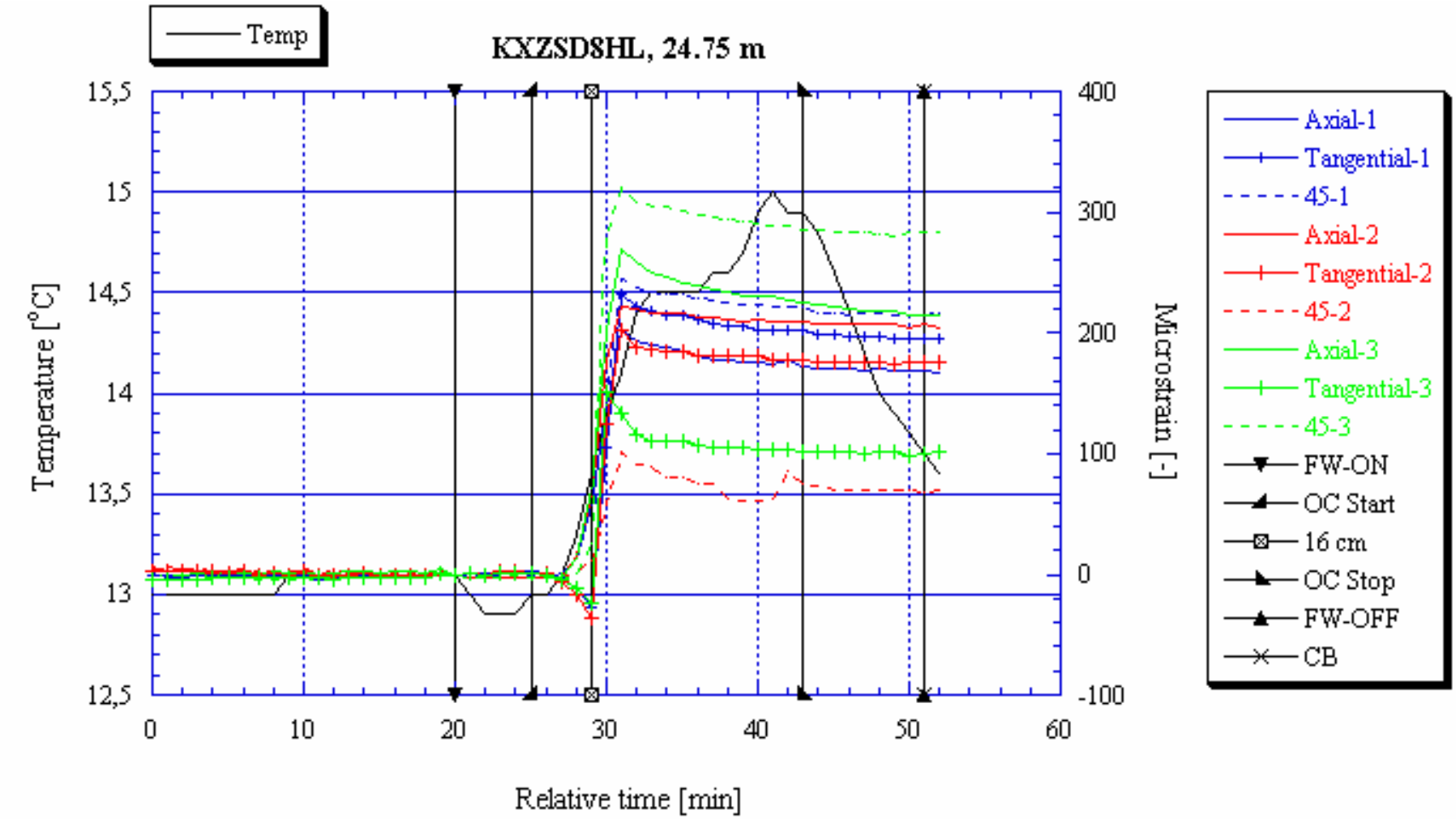
Temp
KXZSD8HL, 24.75 m
15,5
15
14,5
14
13,5
13
12,5
Temperature [°C]
400
300
200
100
0
-100
Microstrain [-]
0
10
20
30
40
50
60
Relative time [min]
Axial-1
Tangential-1
45-1
Axial-2
Tangential-2
45-2
Axial-3
Tangential-3
45-3
FW-ON
OC Start
16 cm
OC Stop
FW-OFF
CB

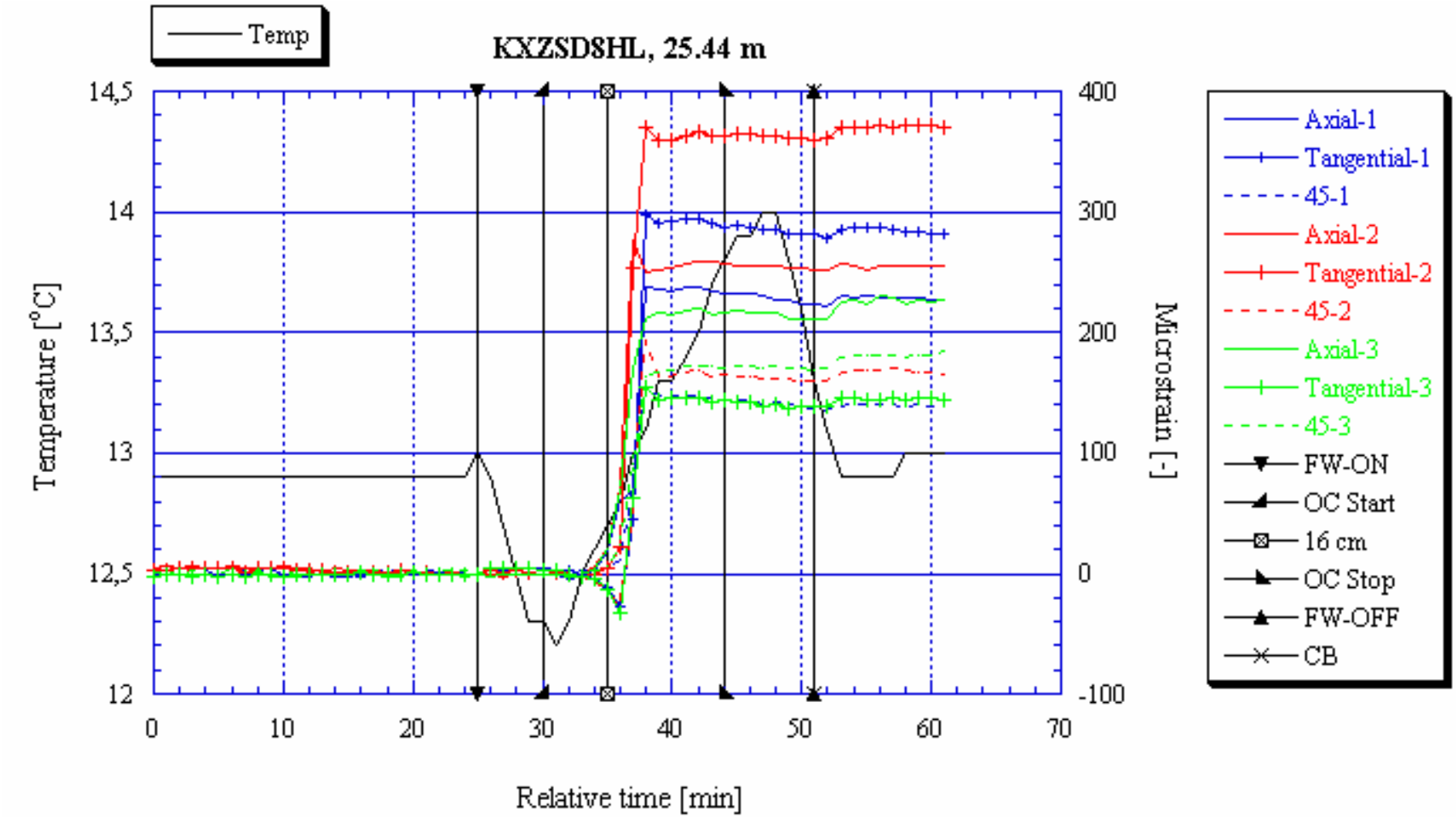
Temp
KXZSD8HL, 25.44 m
Temperature [°C]
14,5
14
13,5
13
12,5
12
Microstrain [-]
400
300
200
100
0
-100
0
10
20
30
40
50
60
70
Relative time [min]
Axial-1
Tangential-1
45-1
Axial-2
Tangential-2
45-2
Axial-3
Tangential-3
45-3
FW-ON
OC Start
16 cm
OC Stop
FW-OFF
CB

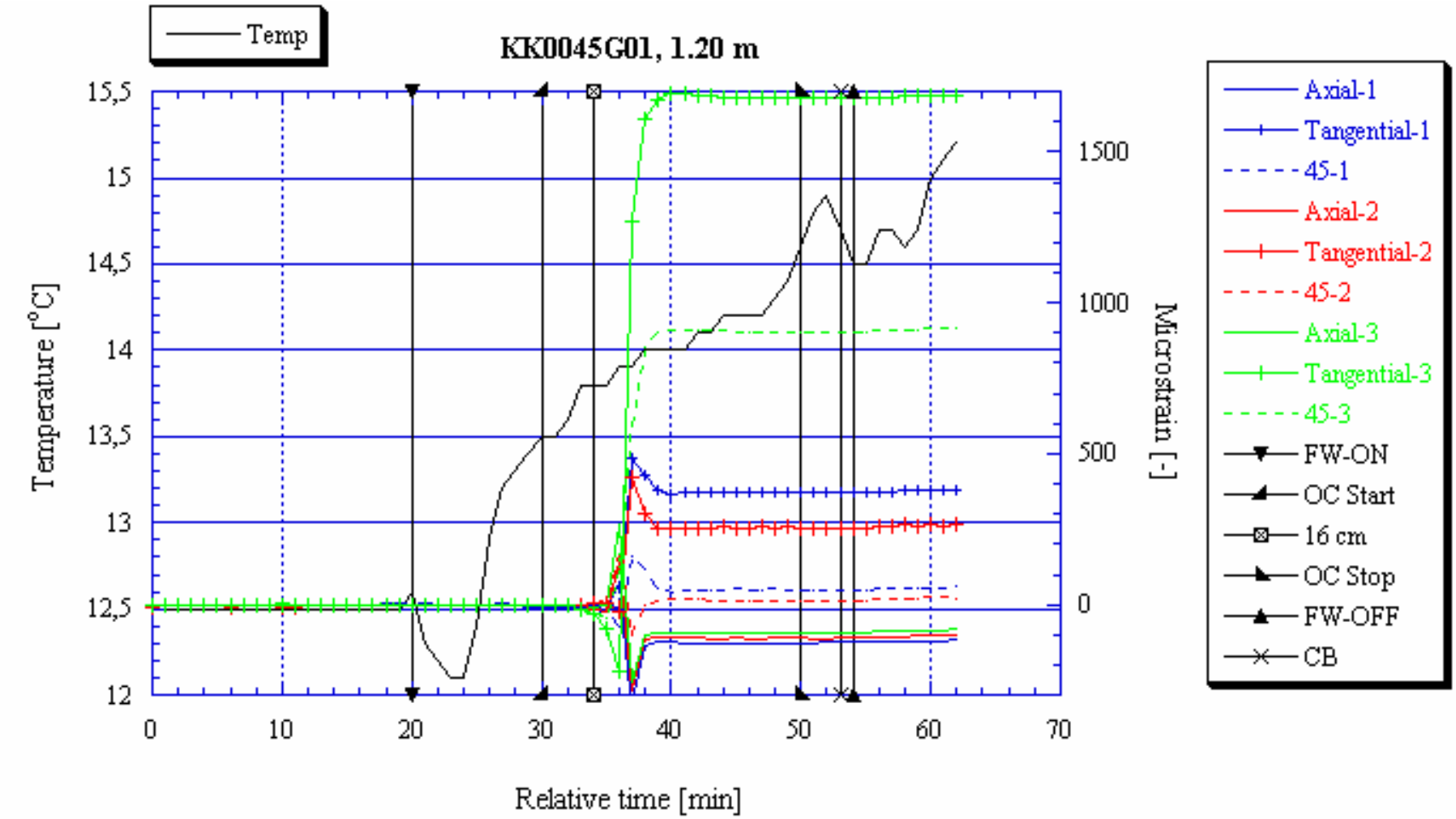
Temp
KK0045G01, 1.20 m
Temperature [°C]
15,5
15
14,5
14
13,5
13
12,5
12
0
10
20
30
40
50
60
70
Relative time [min]
1500
1000
500
0
Microstrain [-]
Axial-1
Tangential-1
45-1
Axial-2
Tangential-2
45-2
Axial-3
Tangential-3
45-3
FW-ON
OC Start
16 cm
OC Stop
FW-OFF
CB

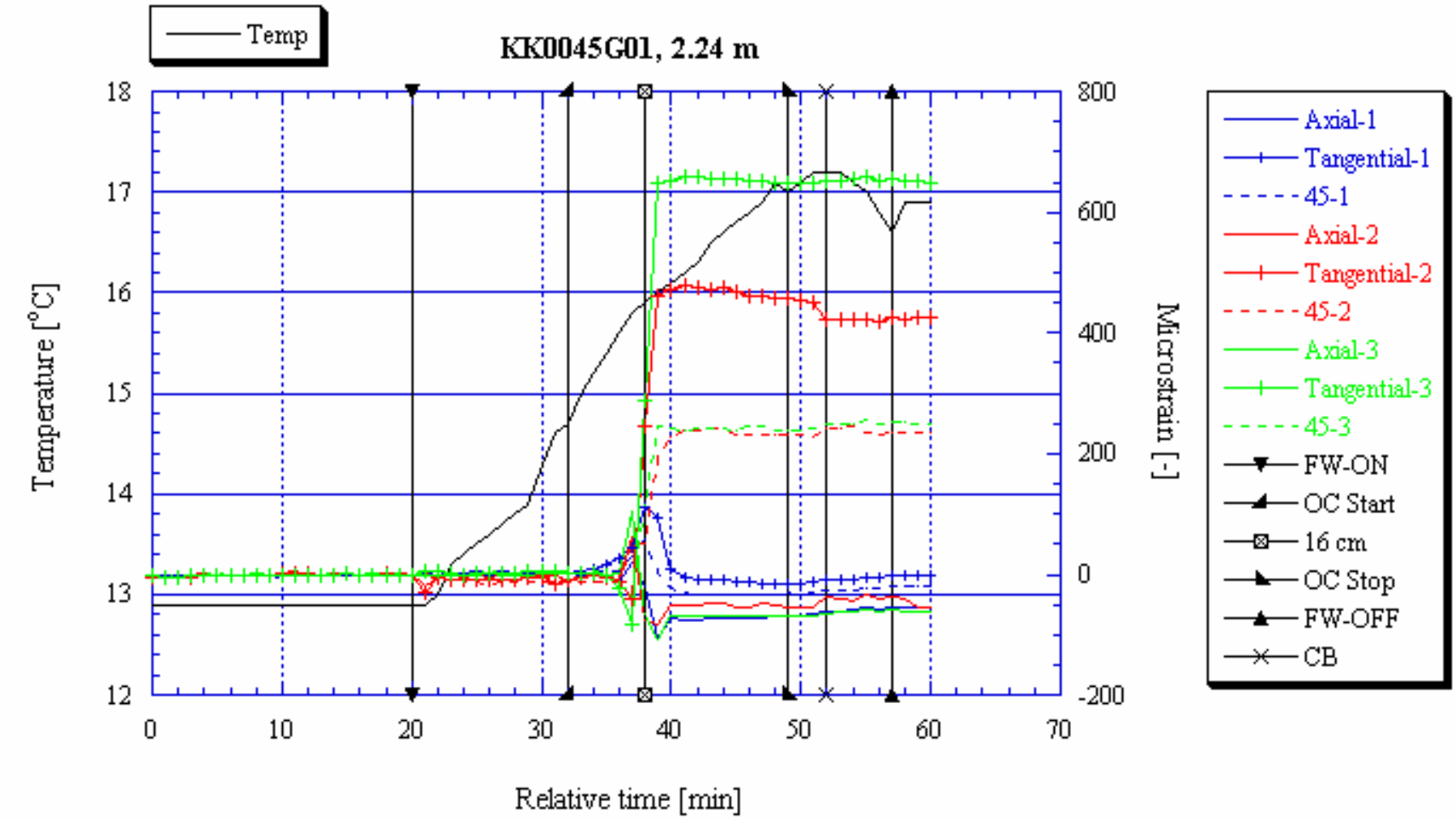
Temp
KK0045G01, 2.24 m
Temperature [°C]
Microstrain [-]
Relative time [min]
18
17
16
15
14
13
12
800
600
400
200
0
-200
0
10
20
30
40
50
60
70
Axial-1
Tangential-1
45-1
Axial-2
Tangential-2
45-2
Axial-3
Tangential-3
45-3
FW-ON
OC Start
16 cm
OC Stop
FW-OFF
CB

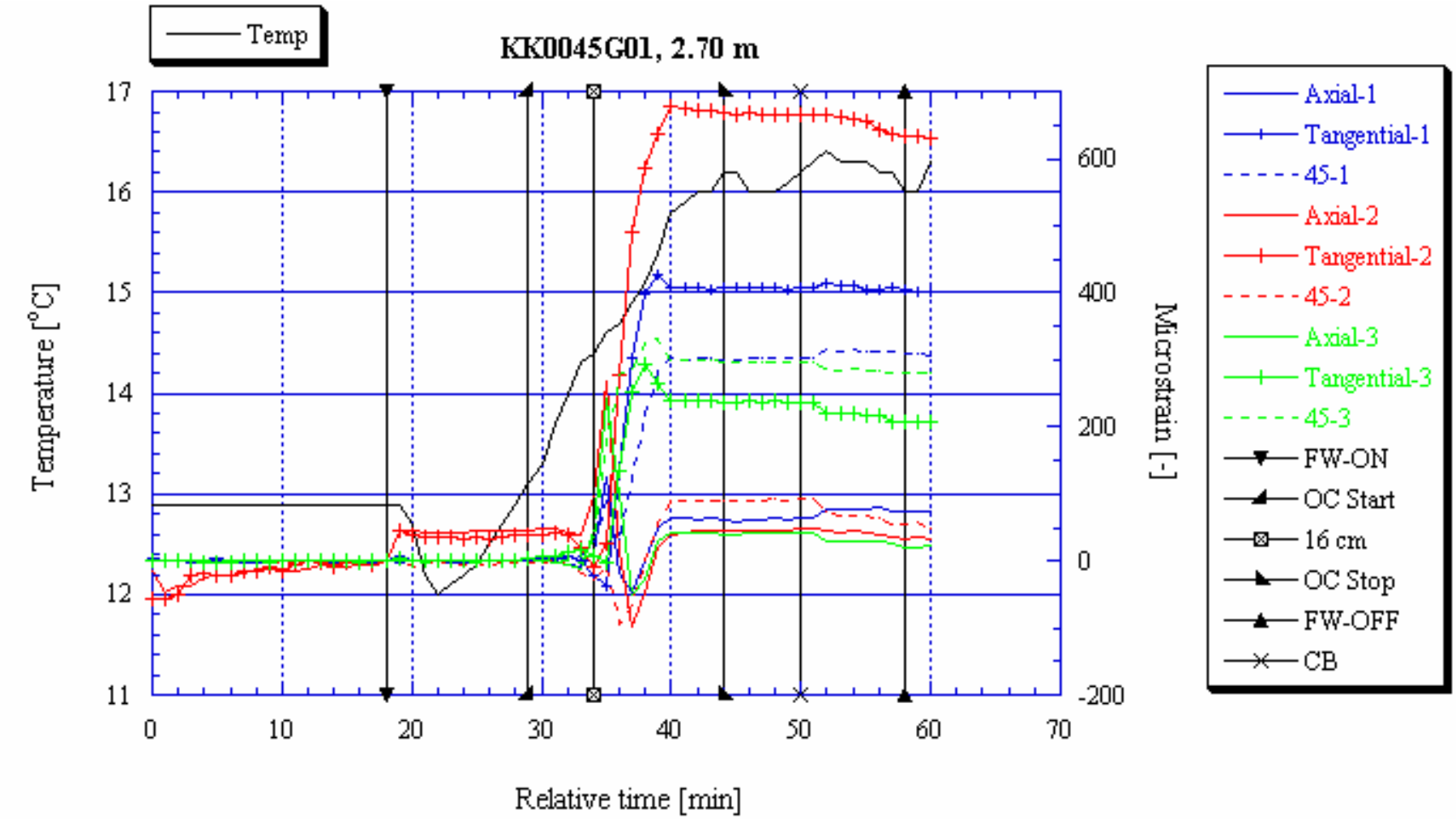
Temp
KK0045G01, 2.70 m
Temperature [°C]
17
16
15
14
13
12
11
0
10
20
30
40
50
60
70
Relative time [min]
600
400
200
0
-200
Microstrain [-]
Axial-1
Tangential-1
45-1
Axial-2
Tangential-2
45-2
Axial-3
Tangential-3
45-3
FW-ON
OC Start
16 cm
OC Stop
FW-OFF
CB

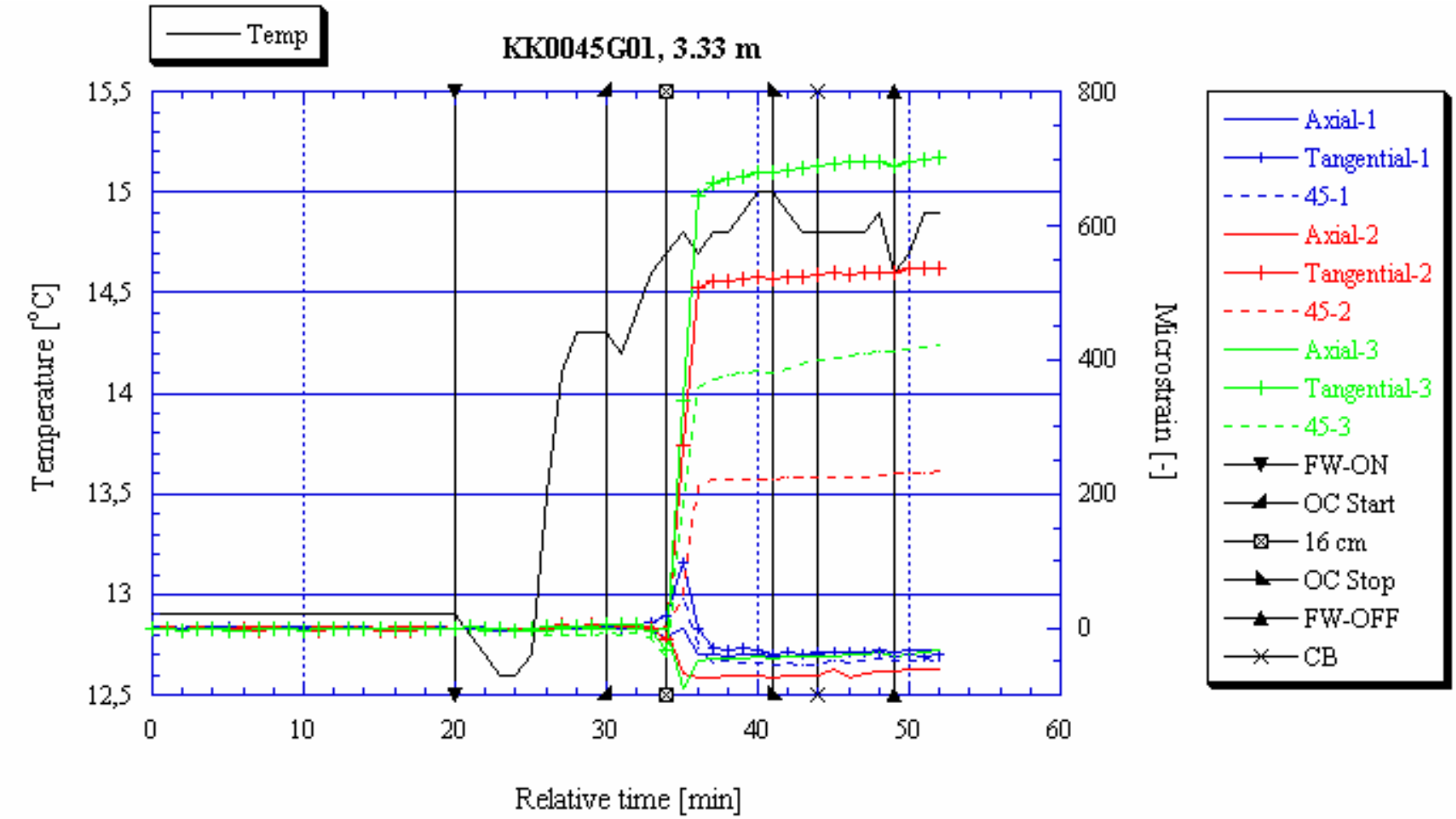
Temp
KK0045G01, 3.33 m
Temperature [°C]
15,5
15
14,5
14
13,5
13
12,5
Microstrain [-]
800
600
400
200
0
0
10
20
30
40
50
60
Relative time [min]
Axial-1
Tangential-1
45-1
Axial-2
Tangential-2
45-2
Axial-3
Tangential-3
45-3
FW-ON
OC Start
16 cm
OC Stop
FW-OFF
CB

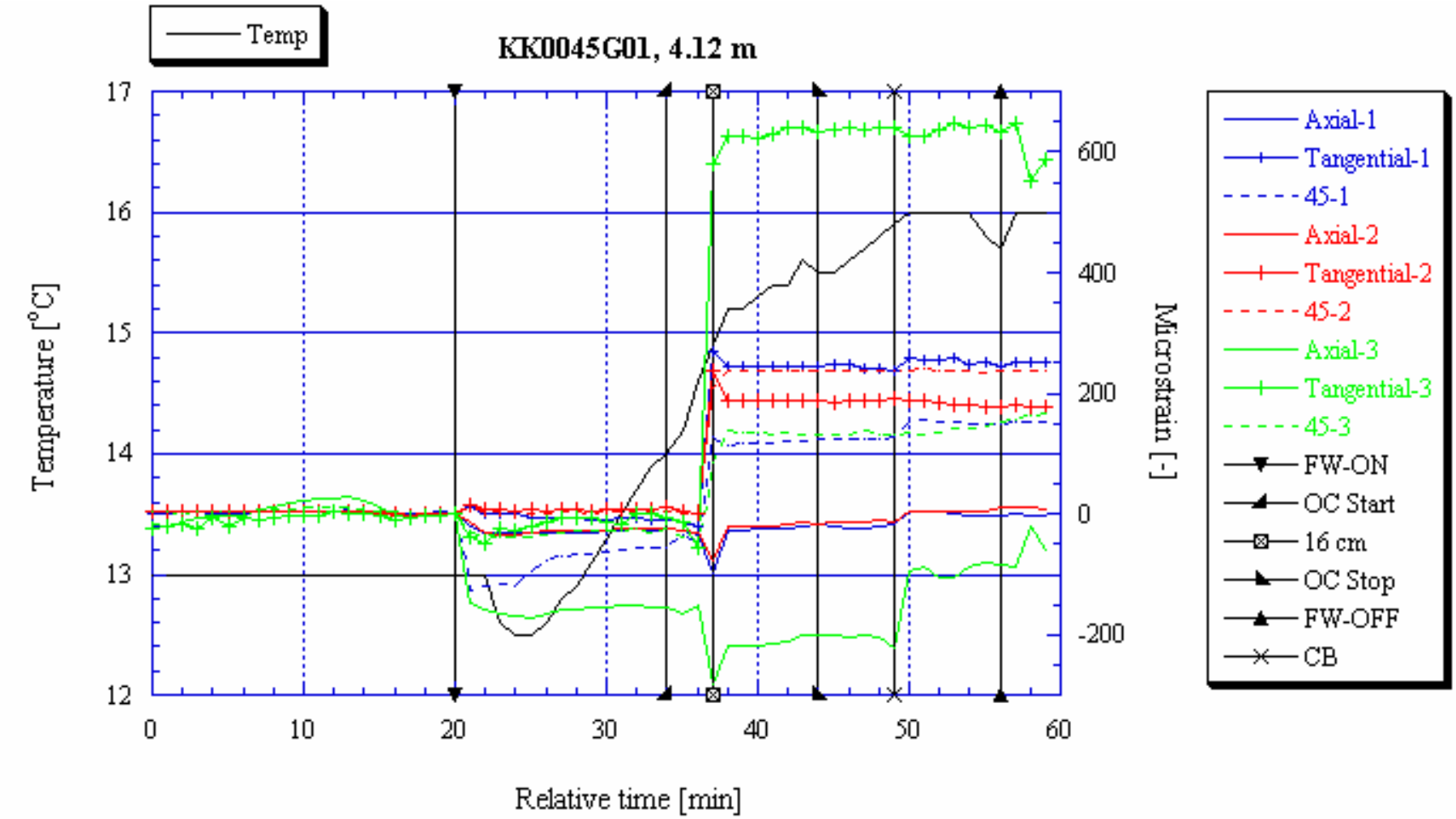
Temp
KK0045G01, 4.12 m
Temperature [°C]
17
16
15
14
13
12
0
10
20
30
40
50
60
Relative time [min]
600
400
200
0
-200
Microstrain [-]
Axial-1
Tangential-1
45-1
Axial-2
Tangential-2
45-2
Axial-3
Tangential-3
45-3
FW-ON
OC Start
16 cm
OC Stop
FW-OFF
CB

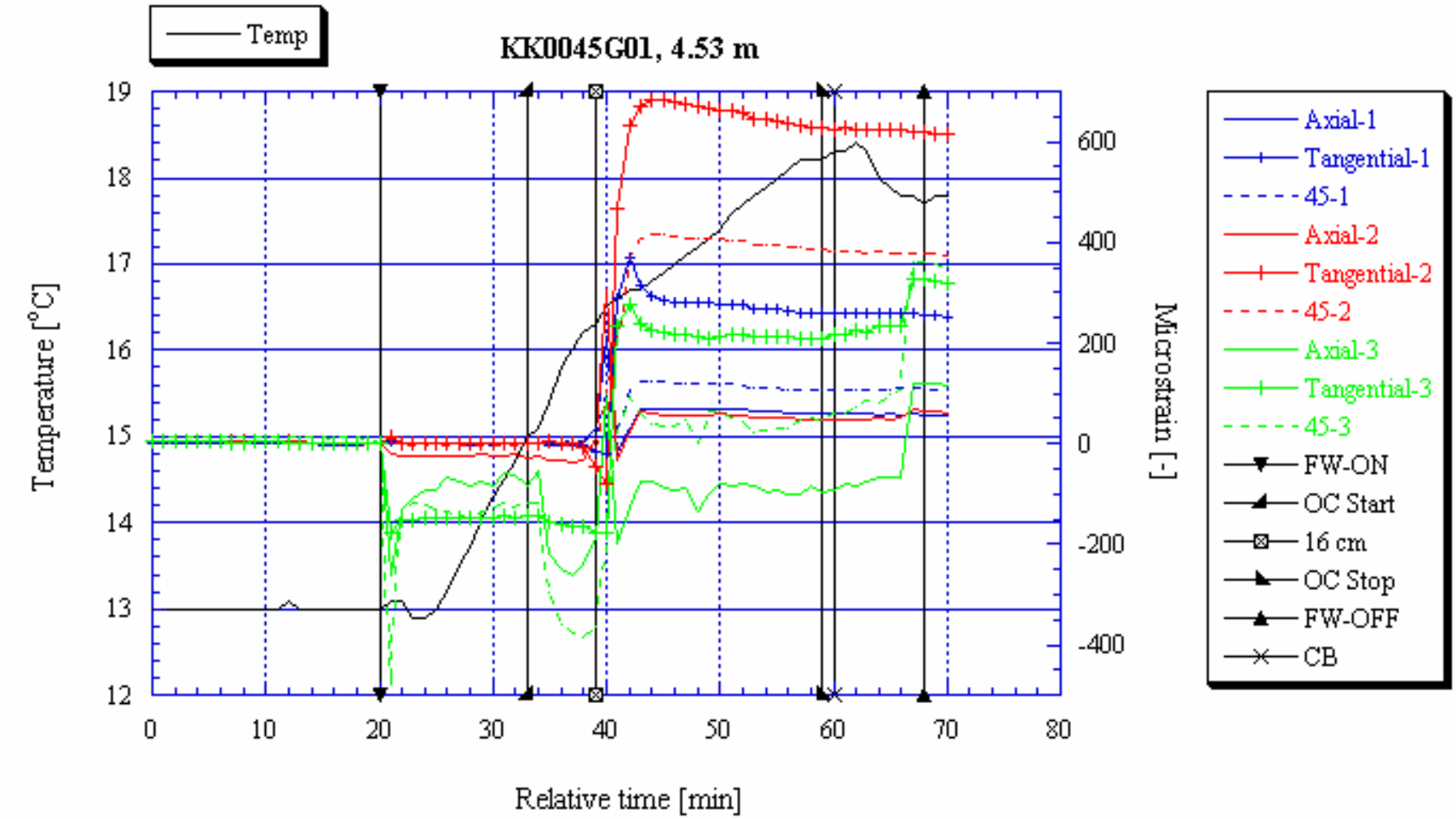
Temp
KK0045G01, 4.53 m
Temperature [°C]
Microstrain [-]
Relative time [min]
19
18
17
16
15
14
13
12
600
400
200
0
-200
-400
0
10
20
30
40
50
60
70
80
Axial-1
Tangential-1
45-1
Axial-2
Tangential-2
45-2
Axial-3
Tangential-3
45-3
FW-ON
OC Start
16 cm
OC Stop
FW-OFF
CB

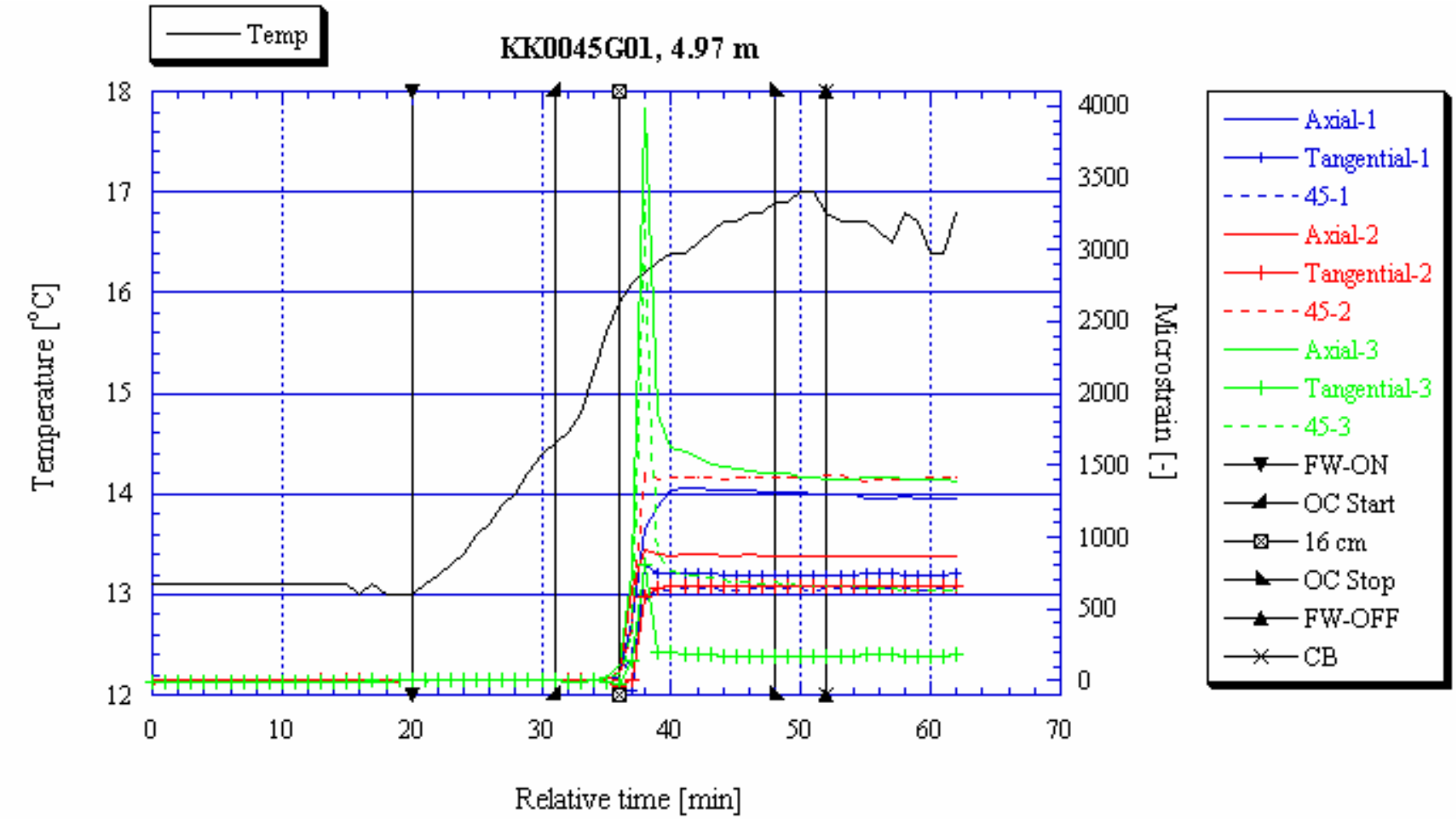
Temp
KK0045G01, 4.97 m
Temperature [°C]
Microstrain [-]
Relative time [min]
18
17
16
15
14
13
12
4000
3500
3000
2500
2000
1500
1000
500
0
0
10
20
30
40
50
60
70
Axial-1
Tangential-1
45-1
Axial-2
Tangential-2
45-2
Axial-3
Tangential-3
45-3
FW-ON
OC Start
16 cm
OC Stop
FW-OFF
CB

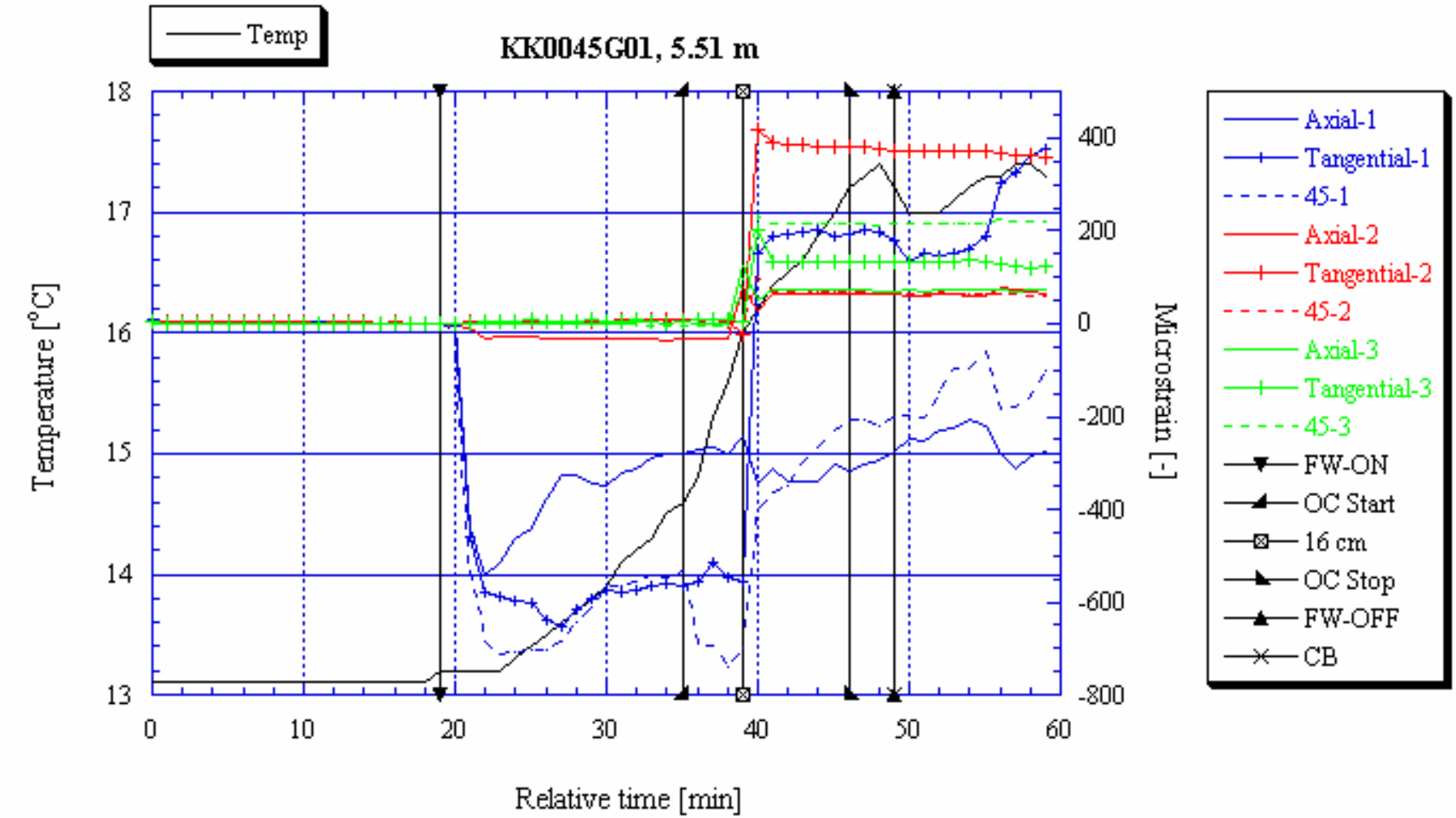
Temp
KK0045G01, 5.51 m
Temperature [°C]
Microstrain [-]
Relative time [min]
18
17
16
15
14
13
0
10
20
30
40
50
60
400
200
0
-200
-400
-600
-800
Axial-1
Tangential-1
45-1
Axial-2
Tangential-2
45-2
Axial-3
Tangential-3
45-3
FW-ON
OC Start
16 cm
OC Stop
FW-OFF
CB

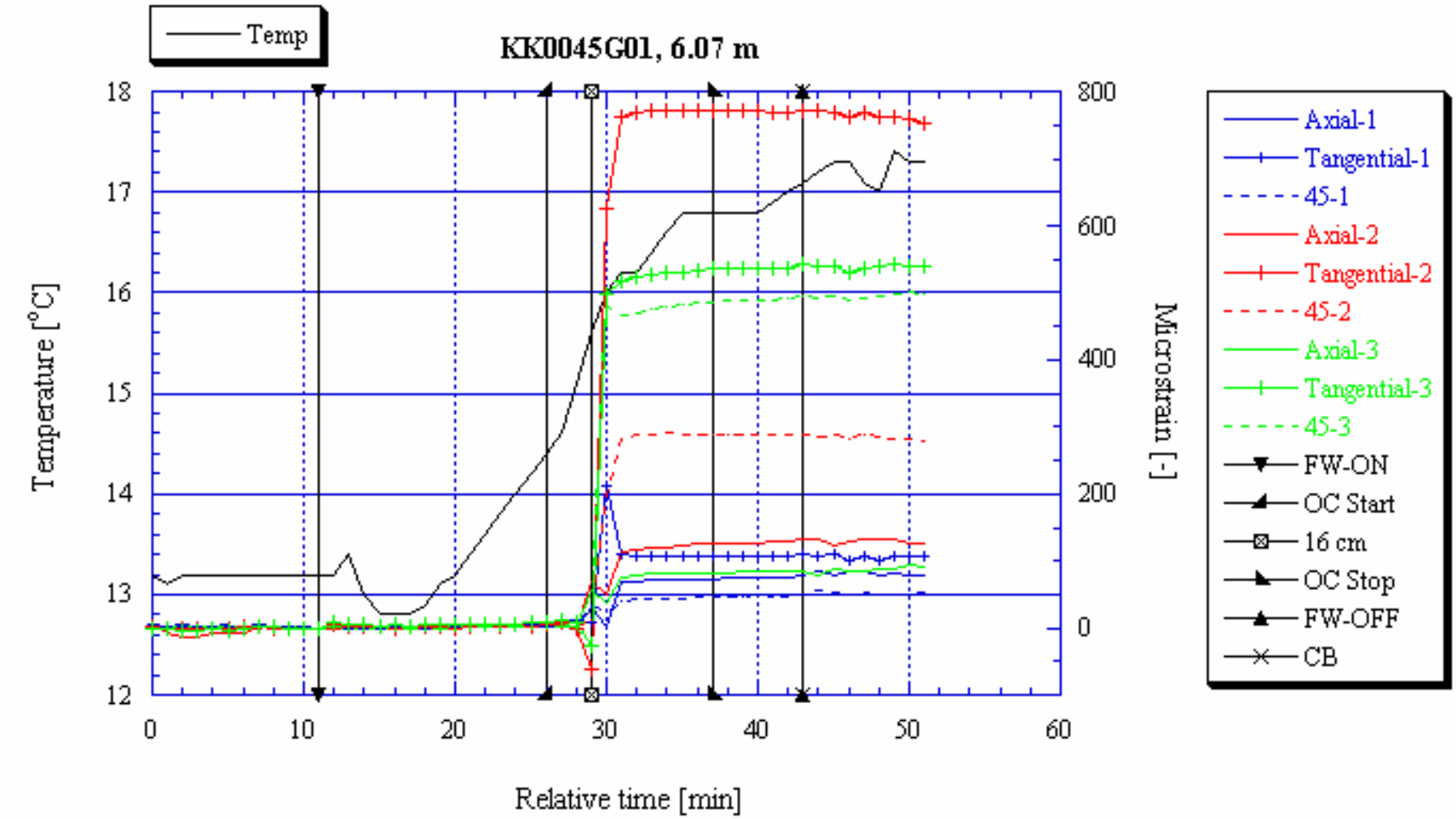
Temp
KK0045G01, 6.07 m
Temperature [°C]
Microstrain [-]
Relative time [min]
18
17
16
15
14
13
12
800
600
400
200
0
0
10
20
30
40
50
60
Axial-1
Tangential-1
45-1
Axial-2
Tangential-2
45-2
Axial-3
Tangential-3
45-3
FW-ON
OC Start
16 cm
OC Stop
FW-OFF
CB

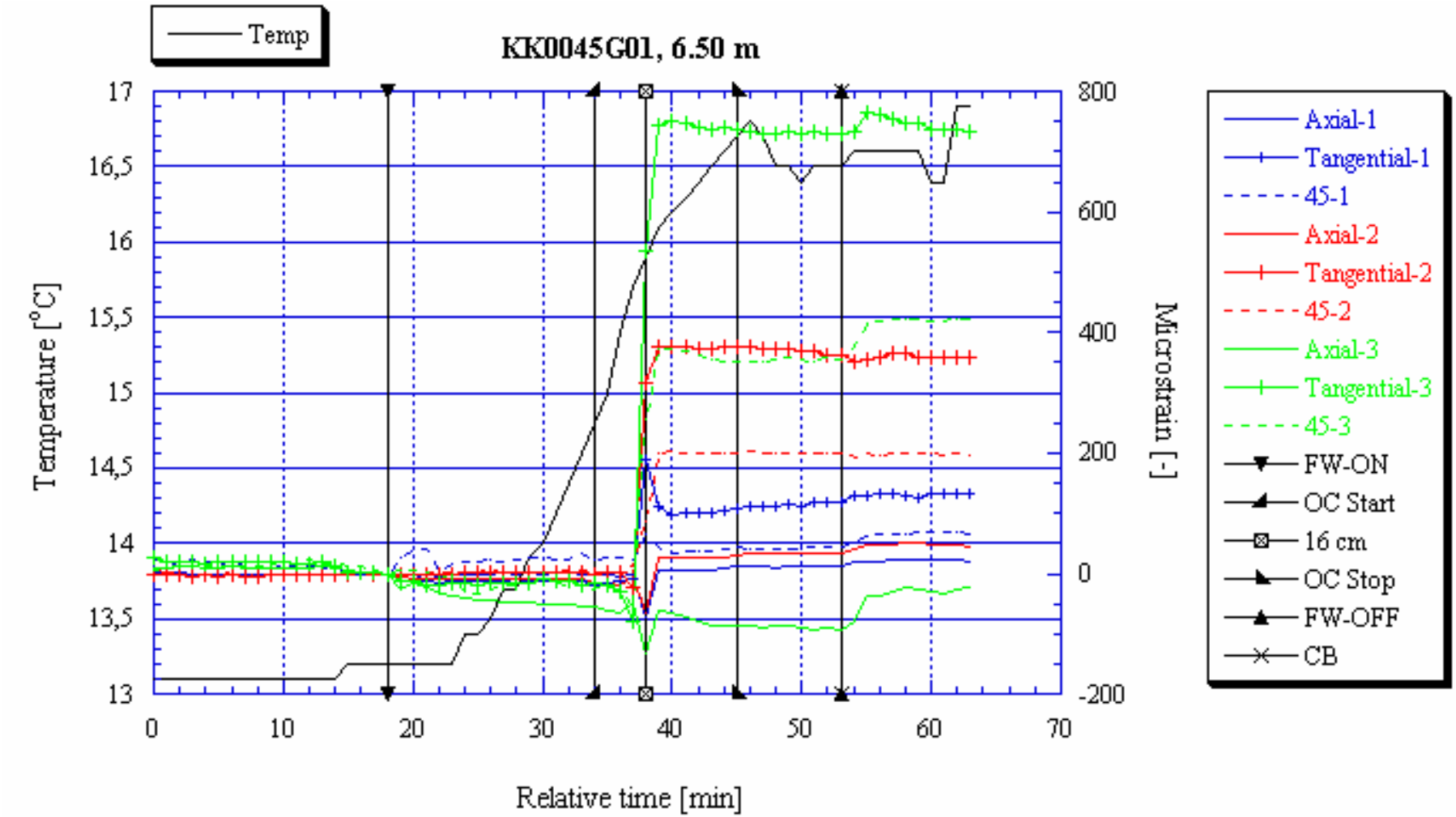
Temp
KK0045G01, 6.50 m
Temperature [°C]
17
16,5
16
15,5
15
14,5
14
13,5
13
Microstrain [-]
800
600
400
200
0
-200
0
10
20
30
40
50
60
70
Relative time [min]
Axial-1
Tangential-1
45-1
Axial-2
Tangential-2
45-2
Axial-3
Tangential-3
45-3
FW-ON
OC Start
16 cm
OC Stop
FW-OFF
CB

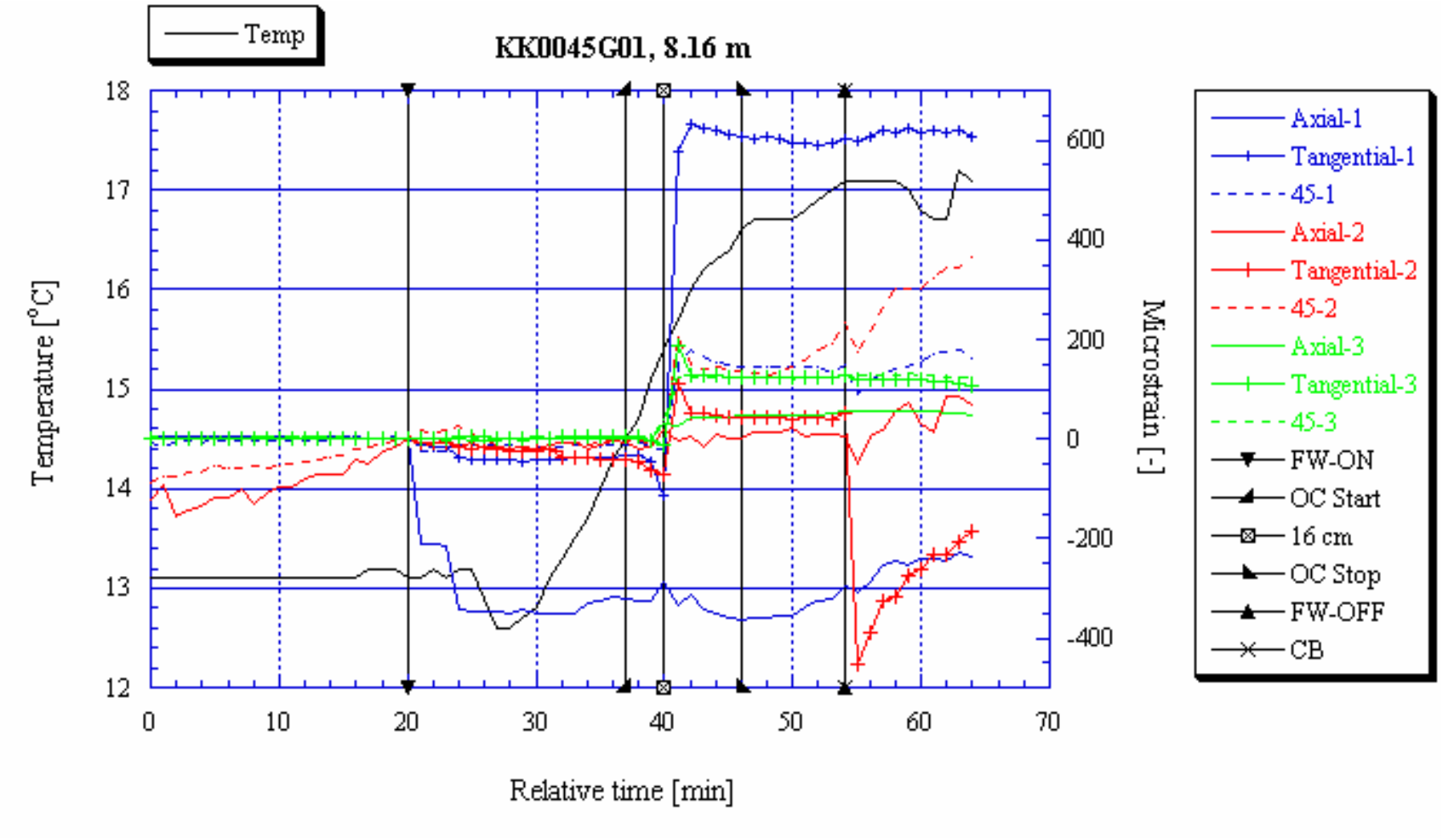
Temp
KK0045G01, 8.16 m
Temperature [°C]
Microstrain [-]
Relative time [min]
18
17
16
15
14
13
12
600
400
200
0
-200
-400
0
10
20
30
40
50
60
70
Axial-1
Tangential-1
45-1
Axial-2
Tangential-2
45-2
Axial-3
Tangential-3
45-3
FW-ON
OC Start
16 cm
OC Stop
FW-OFF
CB

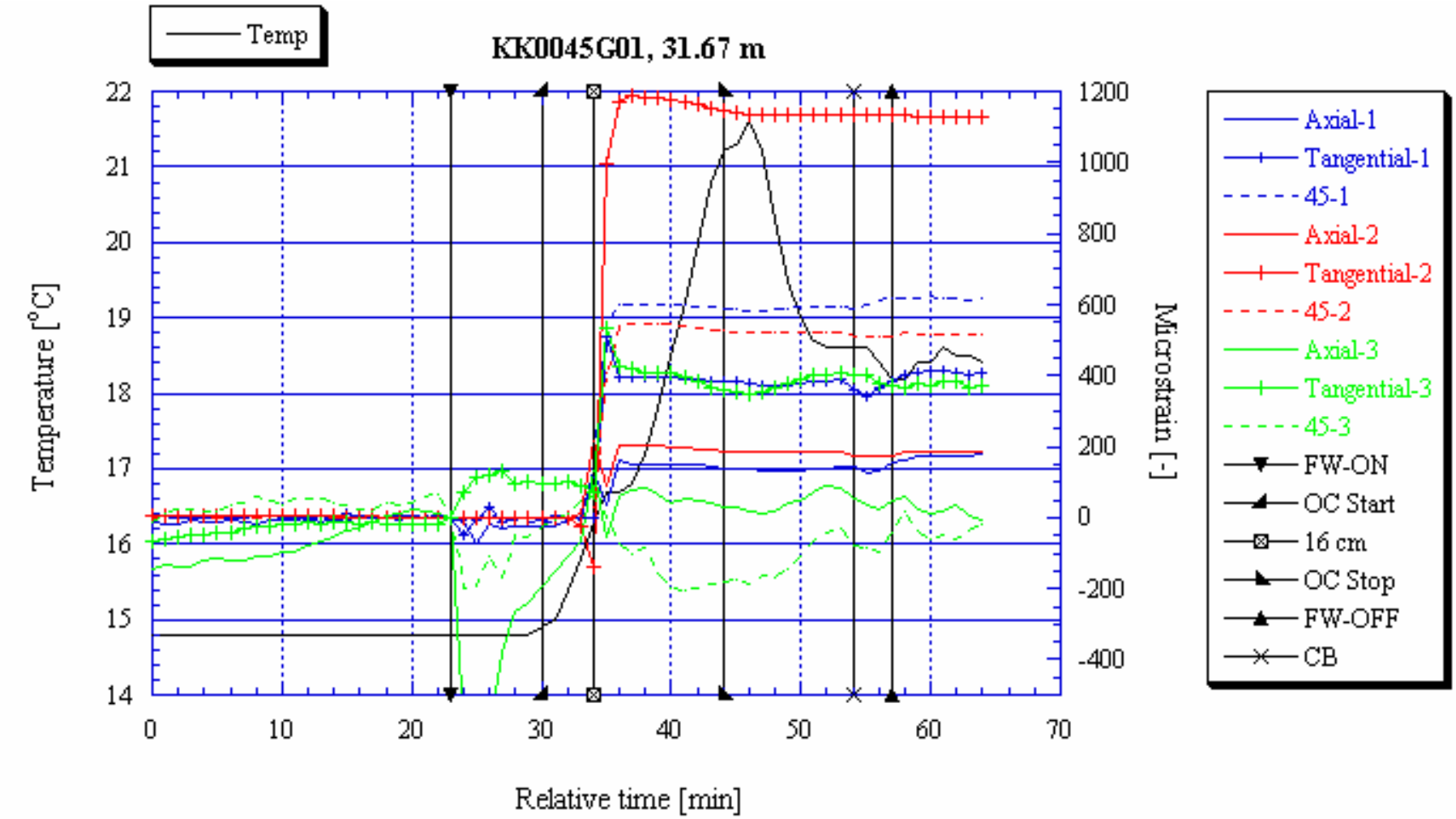
Temp
KK0045G01, 31.67 m
Temperature [°C]
Microstrain [-]
Relative time [min]
22
21
20
19
18
17
16
15
14
1200
1000
800
600
400
200
0
-200
-400
0
10
20
30
40
50
60
70
Axial-1
Tangential-1
45-1
Axial-2
Tangential-2
45-2
Axial-3
Tangential-3
45-3
FW-ON
OC Start
16 cm
OC Stop
FW-OFF
CB

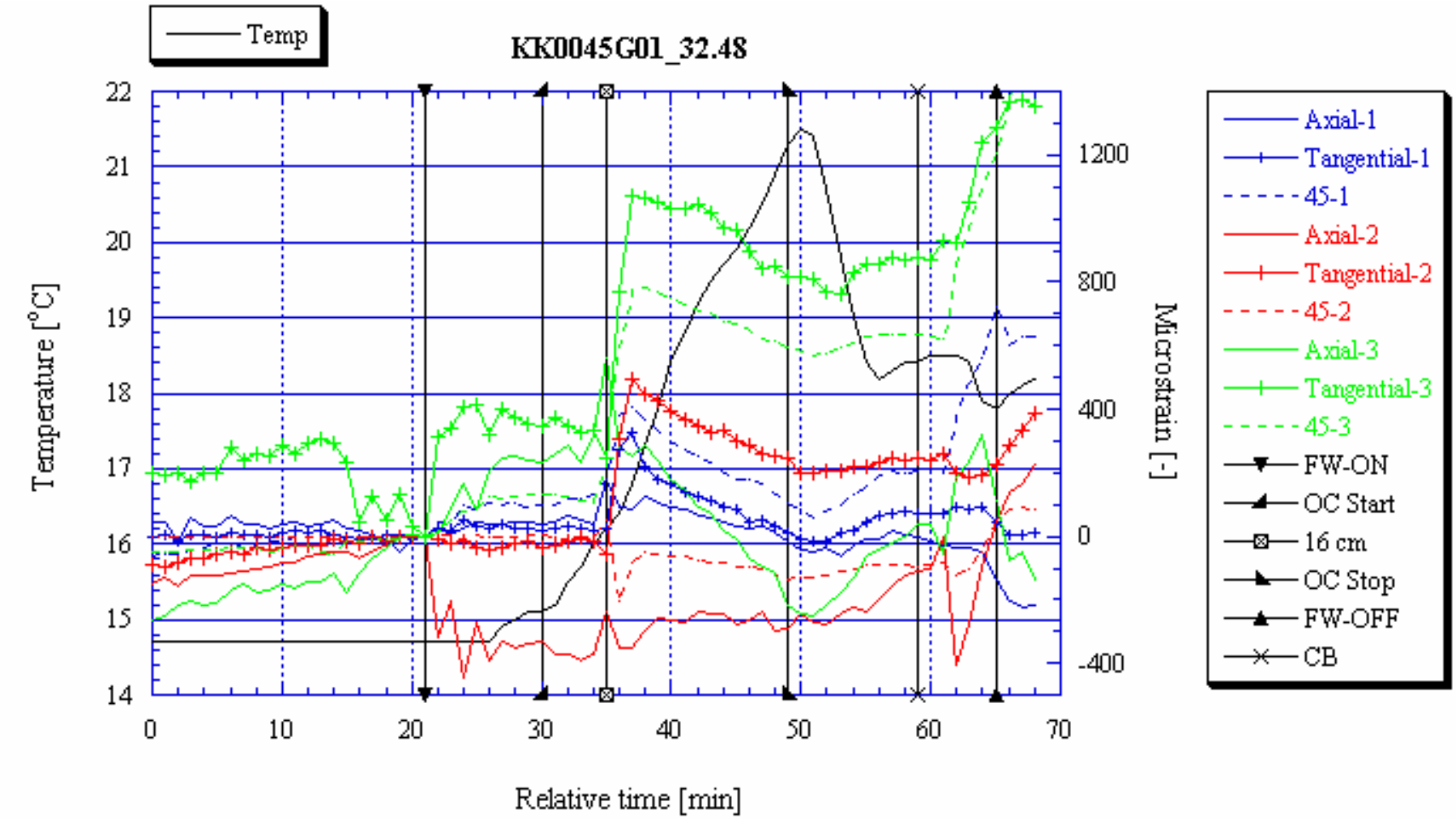
Temp
KK0045G01_32.48
Temperature [°C]
Microstrain [-]
Relative time [min]
22
21
20
19
18
17
16
15
14
1200
800
400
0
-400
0
10
20
30
40
50
60
70
Axial-1
Tangential-1
45-1
Axial-2
Tangential-2
45-2
Axial-3
Tangential-3
45-3
FW-ON
OC Start
16 cm
OC Stop
FW-OFF
CB

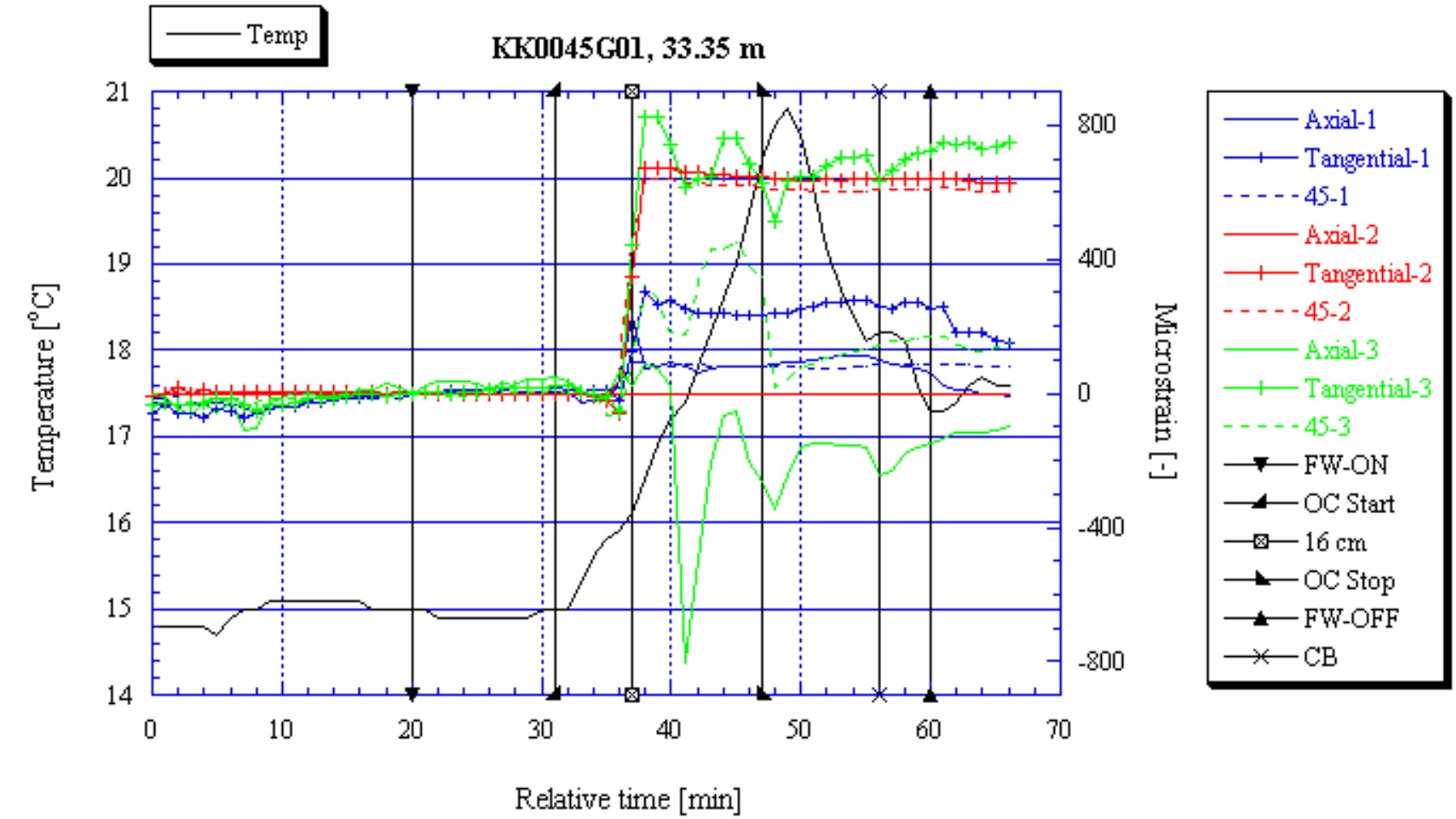
Temp
KK0045G01, 33.35 m
Temperature [°C]
Microstrain [-]
Relative time [min]
21
20
19
18
17
16
15
14
800
400
0
-400
-800
0
10
20
30
40
50
60
70
Axial-1
Tangential-1
45-1
Axial-2
Tangential-2
45-2
Axial-3
Tangential-3
45-3
FW-ON
OC Start
16 cm
OC Stop
FW-OFF
CB

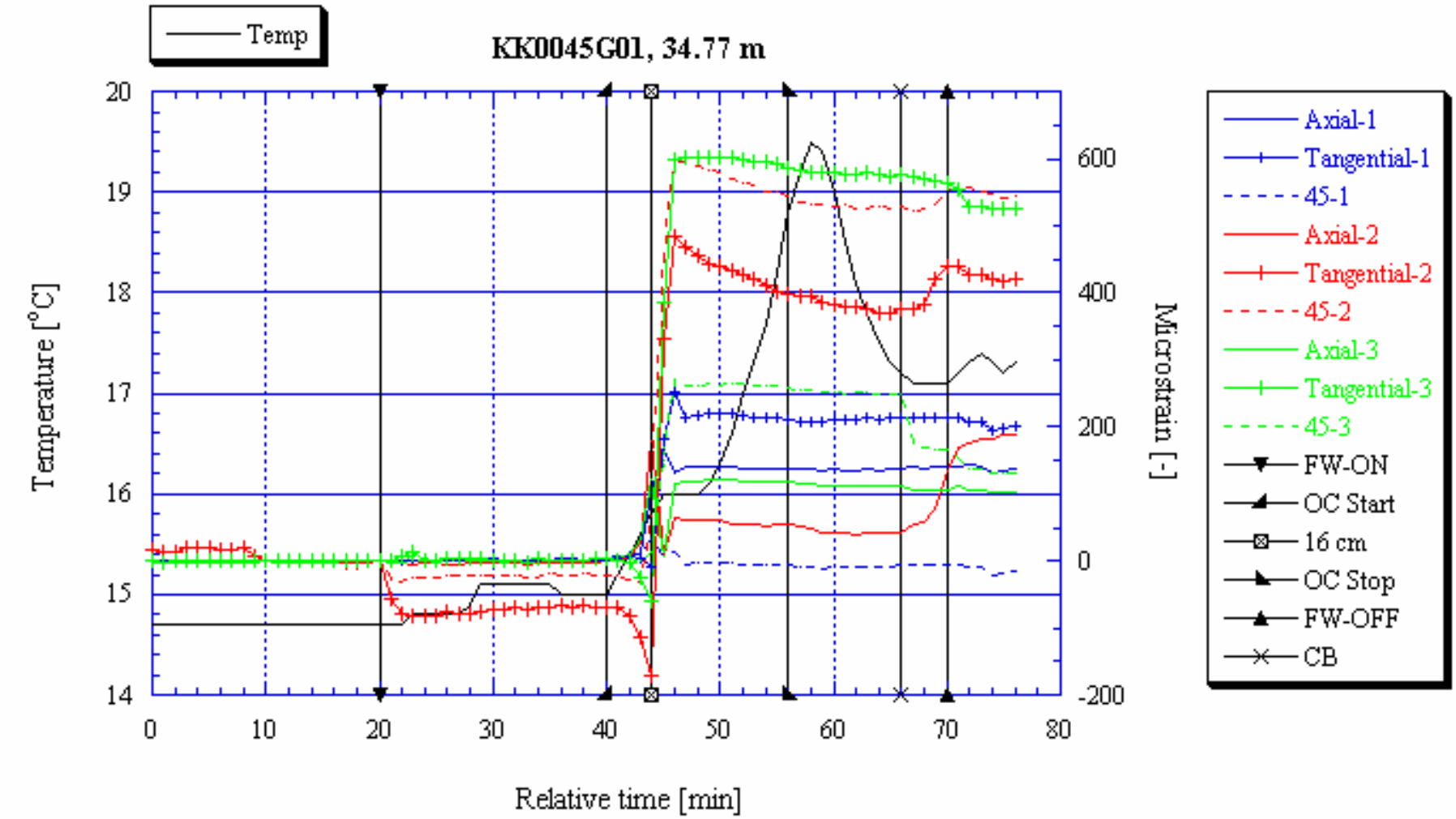
Temp
KK0045G01, 34.77 m
Temperature [°C]
Microstrain [-]
Relative time [min]
20
19
18
17
16
15
14
600
400
200
0
-200
0
10
20
30
40
50
60
70
80
Axial-1
Tangential-1
45-1
Axial-2
Tangential-2
45-2
Axial-3
Tangential-3
45-3
FW-ON
OC Start
16 cm
OC Stop
FW-OFF
CB

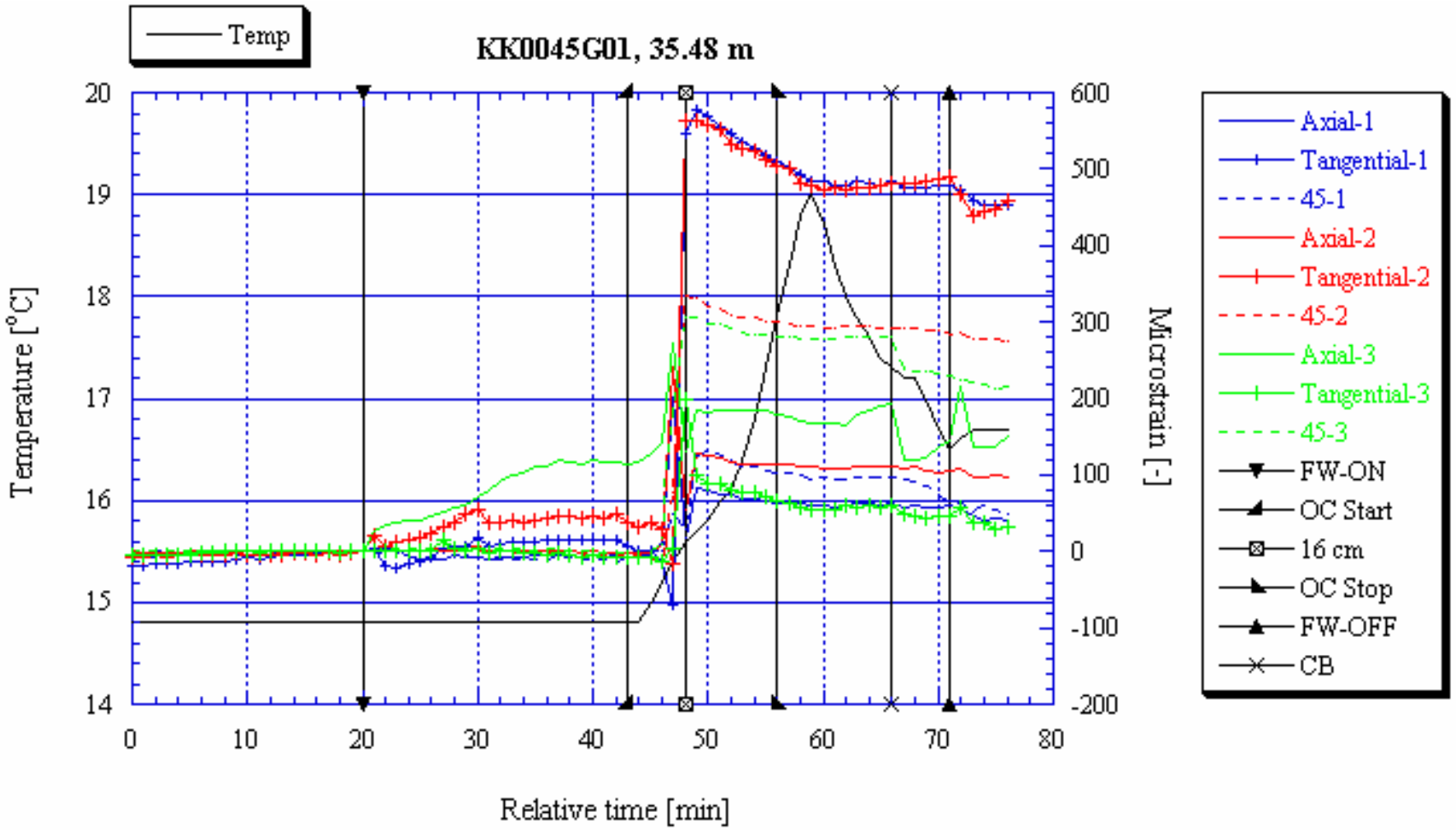
Temp
KK0045G01, 35.48 m
Temperature [°C]
Microstrain [-]
Relative time [min]
20
19
18
17
16
15
14
600
500
400
300
200
100
0
-100
-200
0
10
20
30
40
50
60
70
80
Axial-1
Tangential-1
45-1
Axial-2
Tangential-2
45-2
Axial-3
Tangential-3
45-3
FW-ON
OC Start
16 cm
OC Stop
FW-OFF
CB

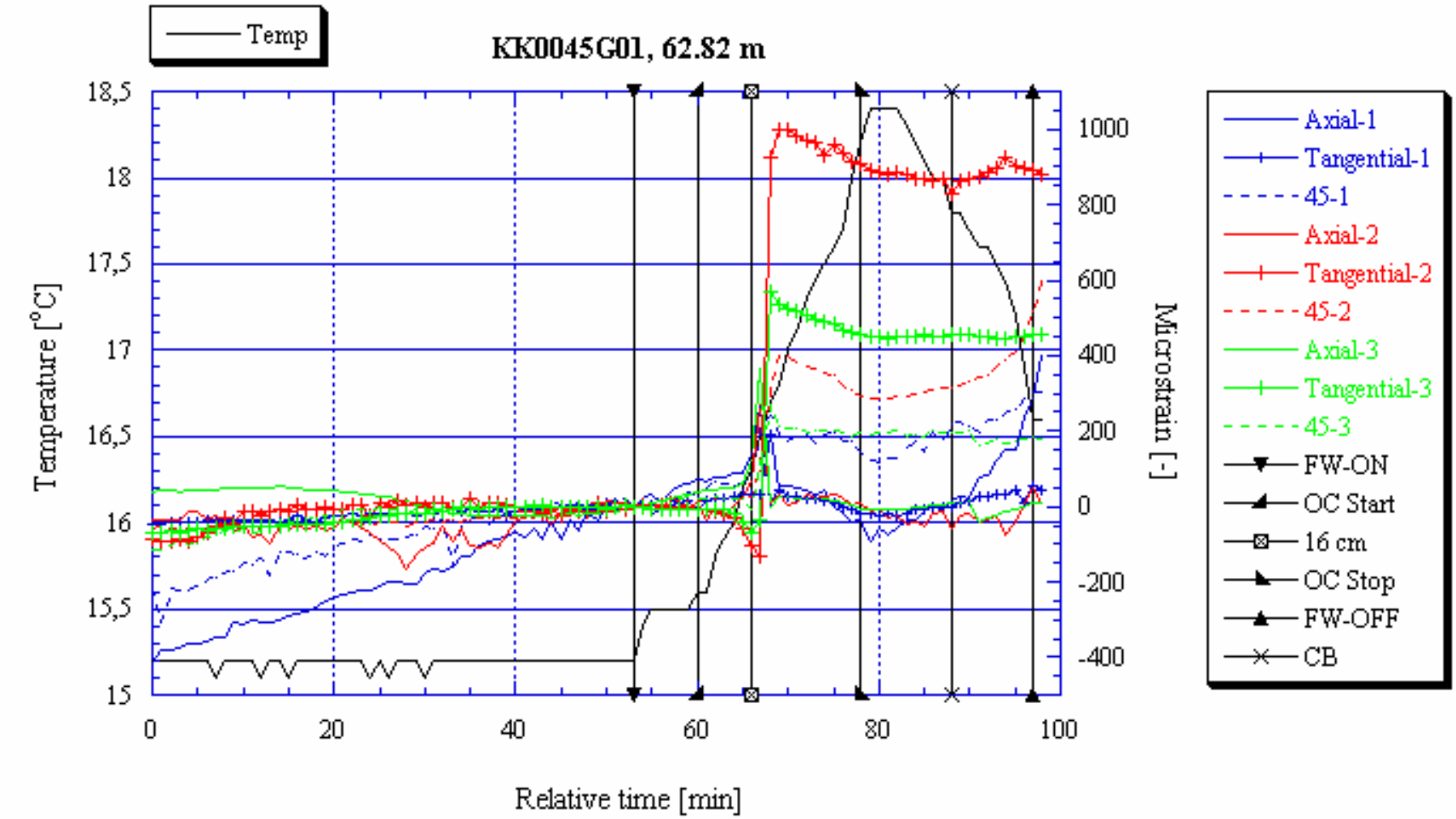
Temp
KK0045G01, 62.82 m
Temperature [°C]
18,5
18
17,5
17
16,5
16
15,5
15
0
20
40
60
80
100
Relative time [min]
1000
800
600
400
200
0
-200
-400
Microstrain [-]
Axial-1
Tangential-1
45-1
Axial-2
Tangential-2
45-2
Axial-3
Tangential-3
45-3
FW-ON
OC Start
16 cm
OC Stop
FW-OFF
CB

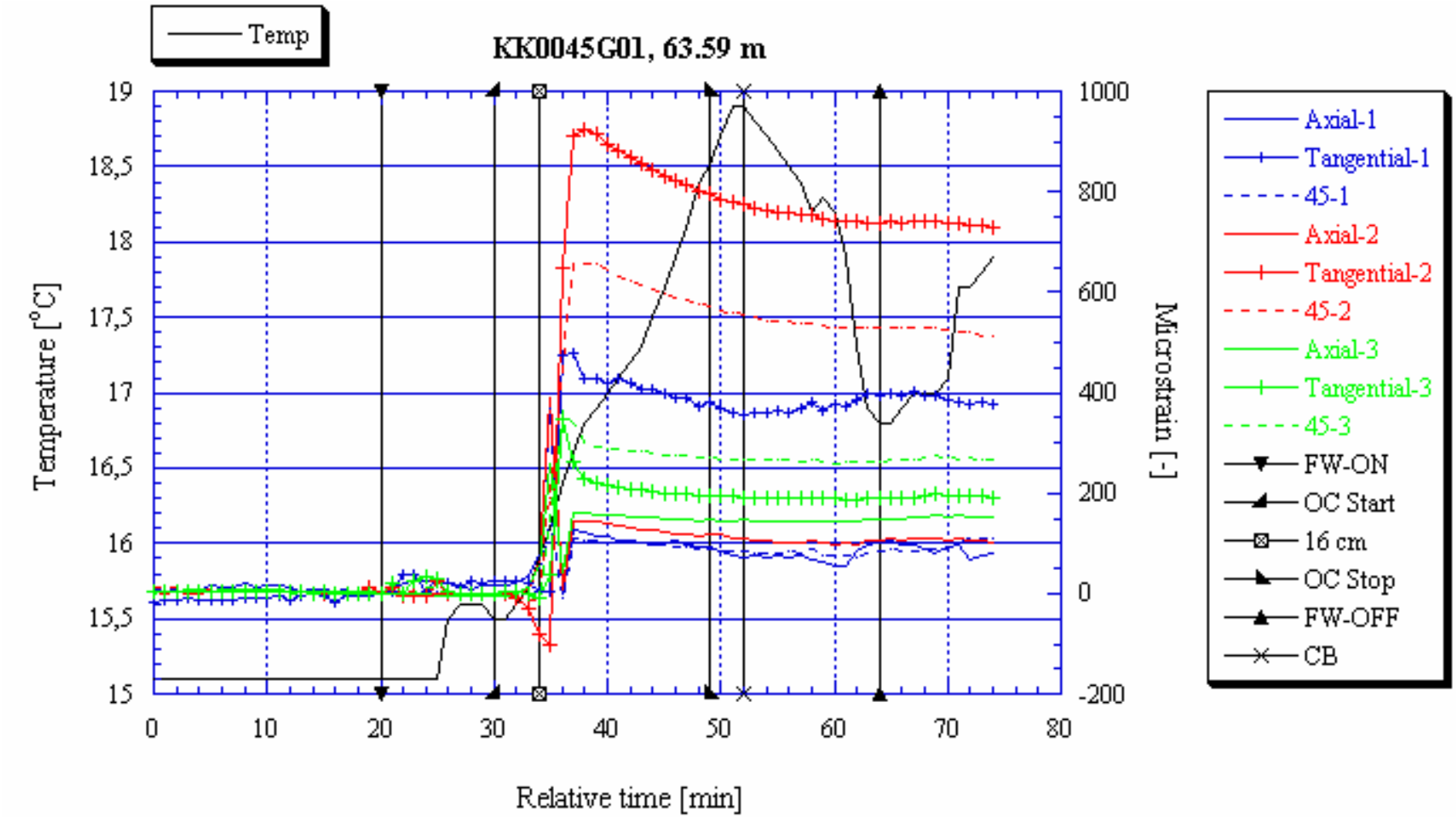
Temp
KK0045G01, 63.59 m
Temperature [°C]
Microstrain [-]
Relative time [min]
19
18,5
18
17,5
17
16,5
16
15,5
15
1000
800
600
400
200
0
-200
0
10
20
30
40
50
60
70
80
Axial-1
Tangential-1
45-1
Axial-2
Tangential-2
45-2
Axial-3
Tangential-3
45-3
FW-ON
OC Start
16 cm
OC Stop
FW-OFF
CB

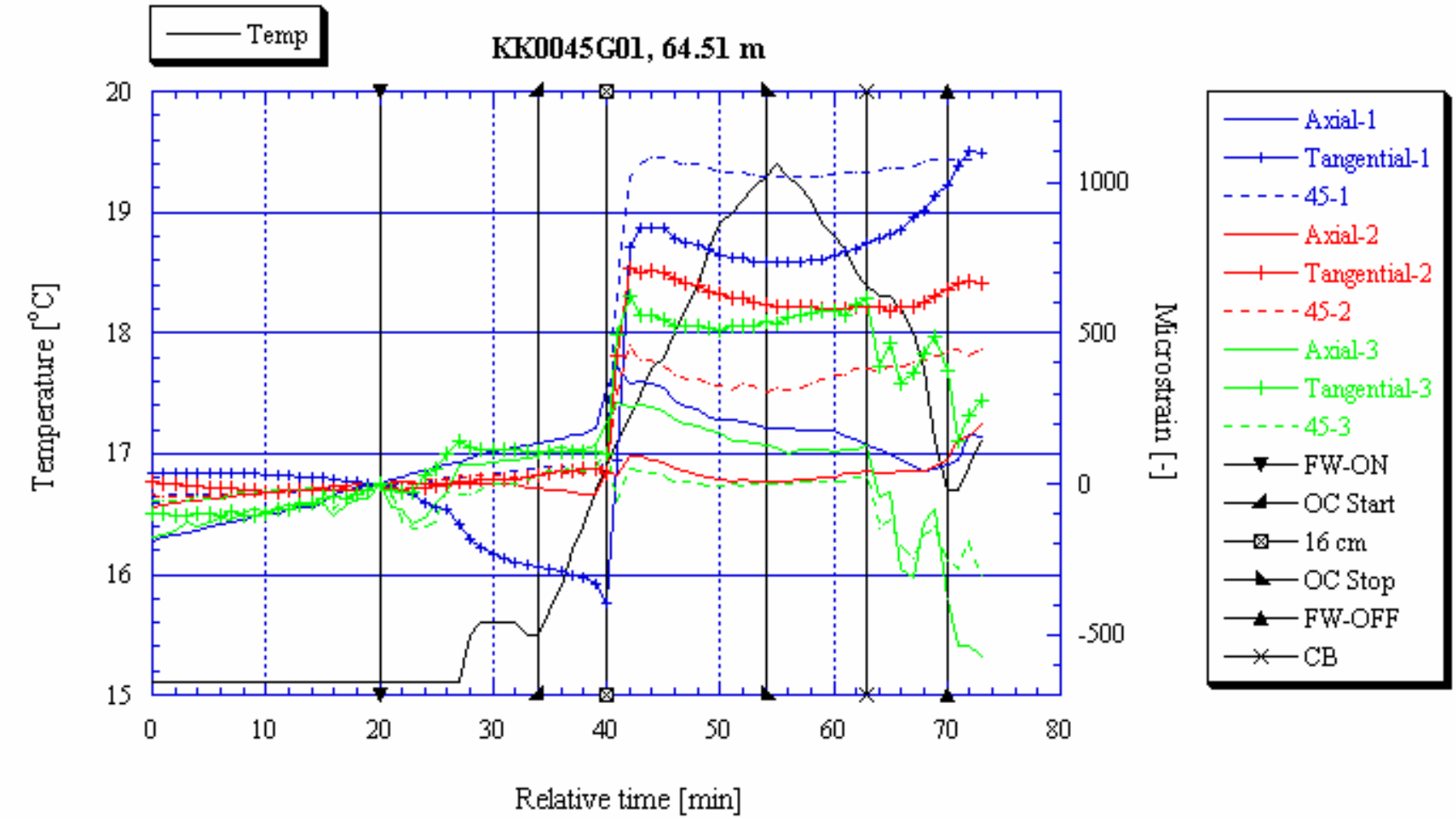
Temp
KK0045G01, 64.51 m
Temperature [°C]
Relative time [min]
Microstrain [-]
20
19
18
17
16
15
0
10
20
30
40
50
60
70
80
1000
500
0
-500
Axial-1
Tangential-1
45-1
Axial-2
Tangential-2
45-2
Axial-3
Tangential-3
45-3
FW-ON
OC Start
16 cm
OC Stop
FW-OFF
CB

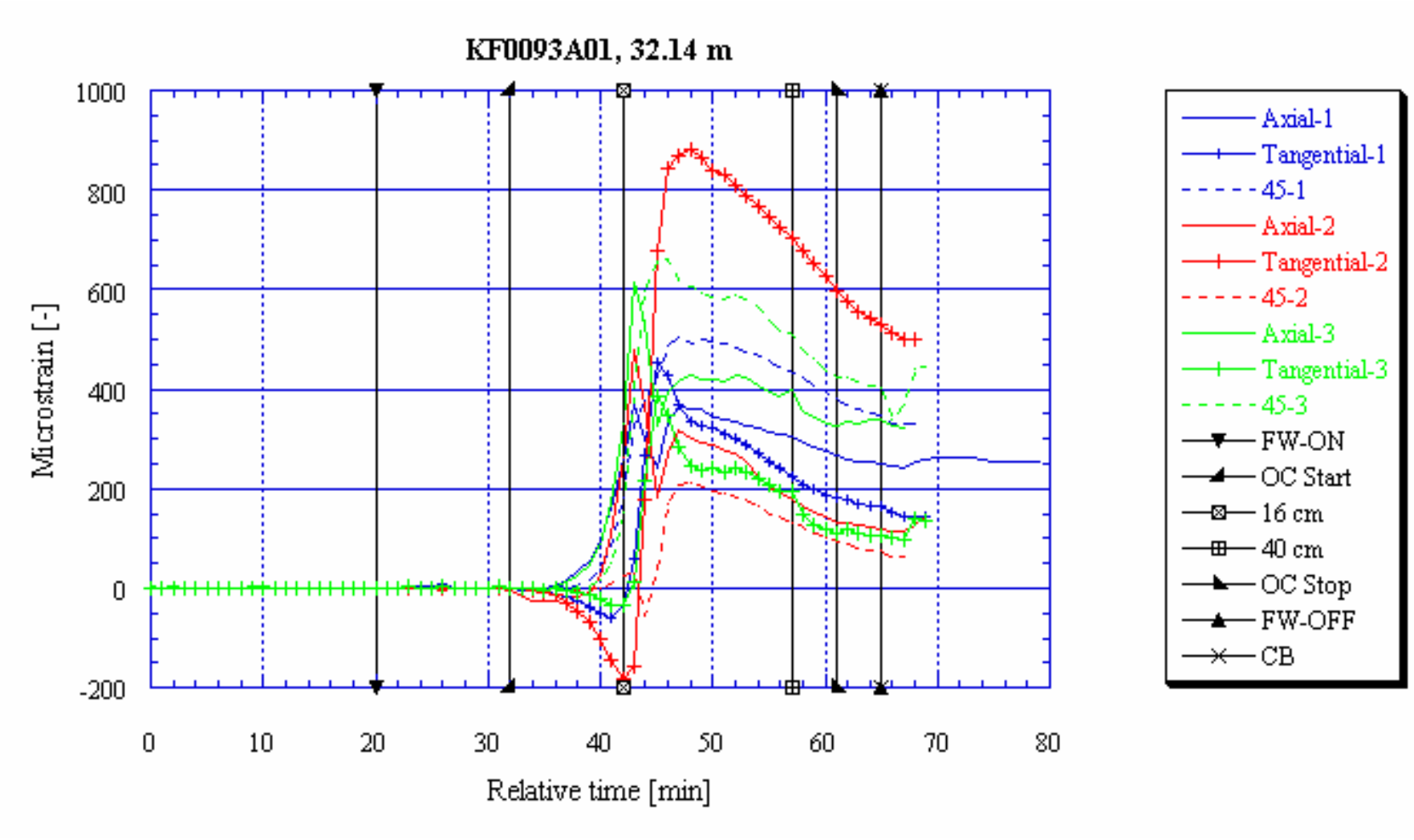
KF0093A01, 32.14 m
Microstrain [-]
1000
800
600
400
200
0
-200
0
10
20
30
40
50
60
70
80
Relative time [min]
Axial-1
Tangential-1
45-1
Axial-2
Tangential-2
45-2
Axial-3
Tangential-3
45-3
FW-ON
OC Start
16 cm
40 cm
OC Stop
FW-OFF
CB

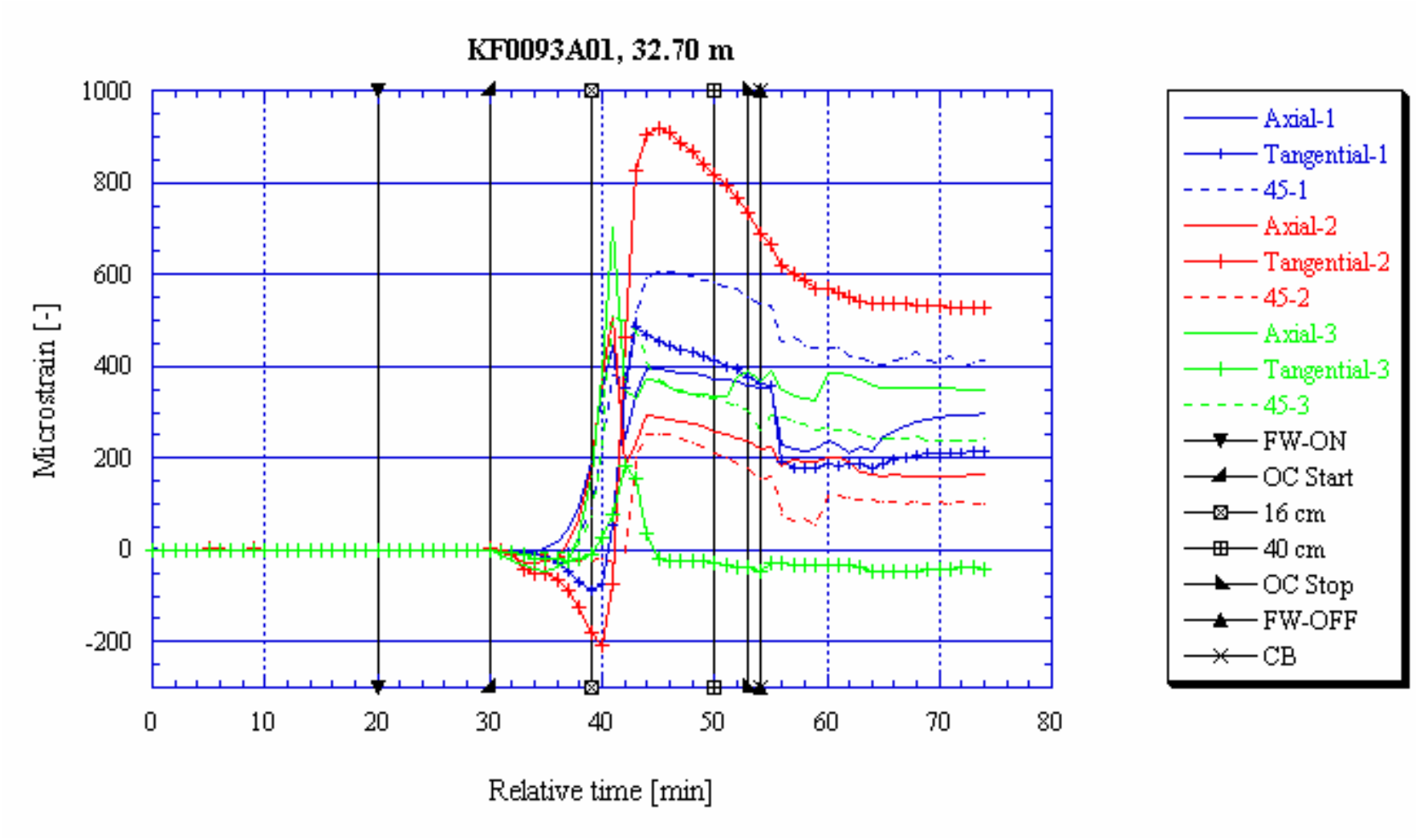
KF0093A01, 32.70 m
Microstrain [-]
1000
800
600
400
200
0
-200
0
10
20
30
40
50
60
70
80
Relative time [min]
Axial-1
Tangential-1
45-1
Axial-2
Tangential-2
45-2
Axial-3
Tangential-3
45-3
FW-ON
OC Start
16 cm
40 cm
OC Stop
FW-OFF
CB

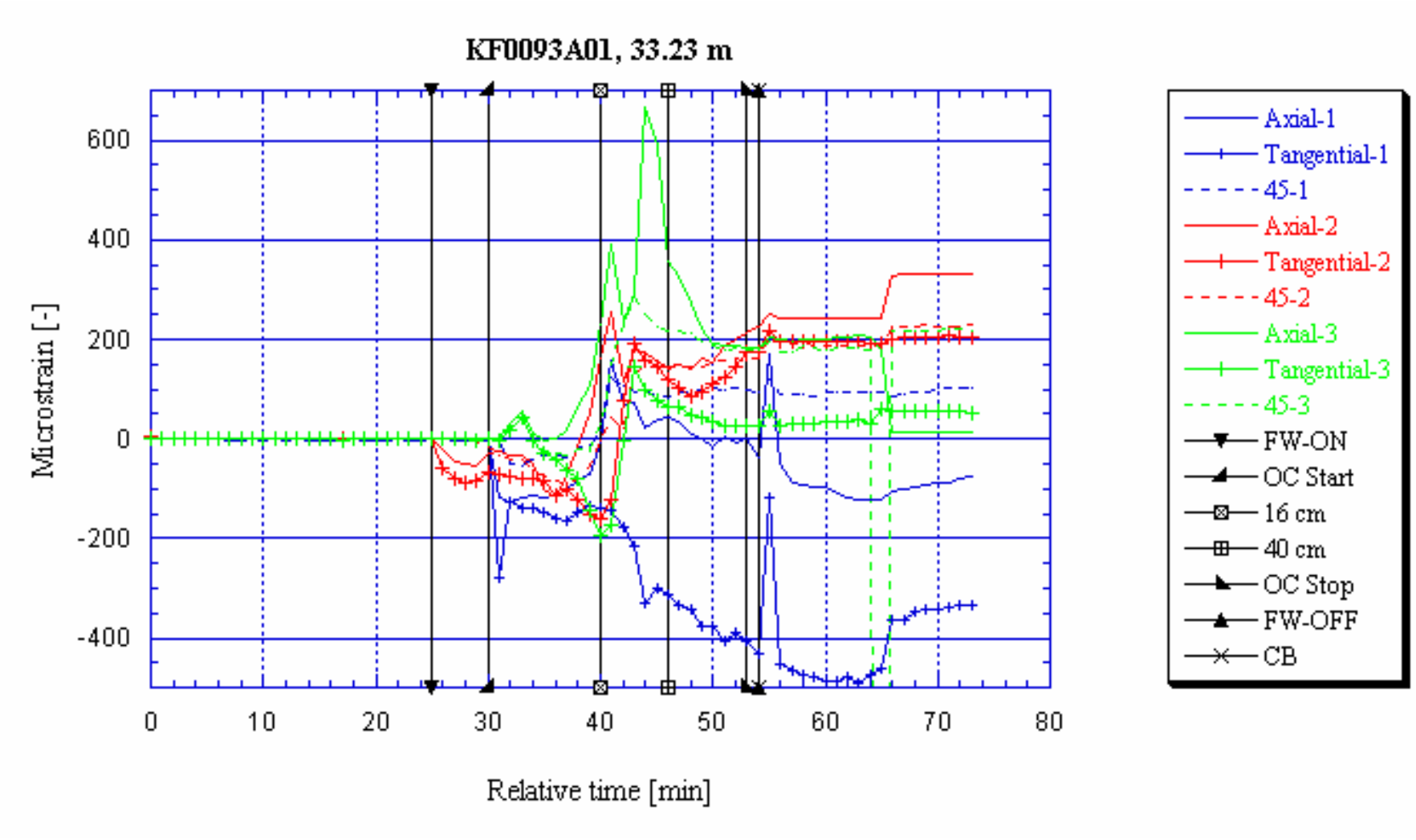
KF0093A01, 33.23 m
Microstrain [-]
600
400
200
0
-200
-400
0
10
20
30
40
50
60
70
80
Relative time [min]
Axial-1
Tangential-1
45-1
Axial-2
Tangential-2
45-2
Axial-3
Tangential-3
45-3
FW-ON
OC Start
16 cm
40 cm
OC Stop
FW-OFF
CB

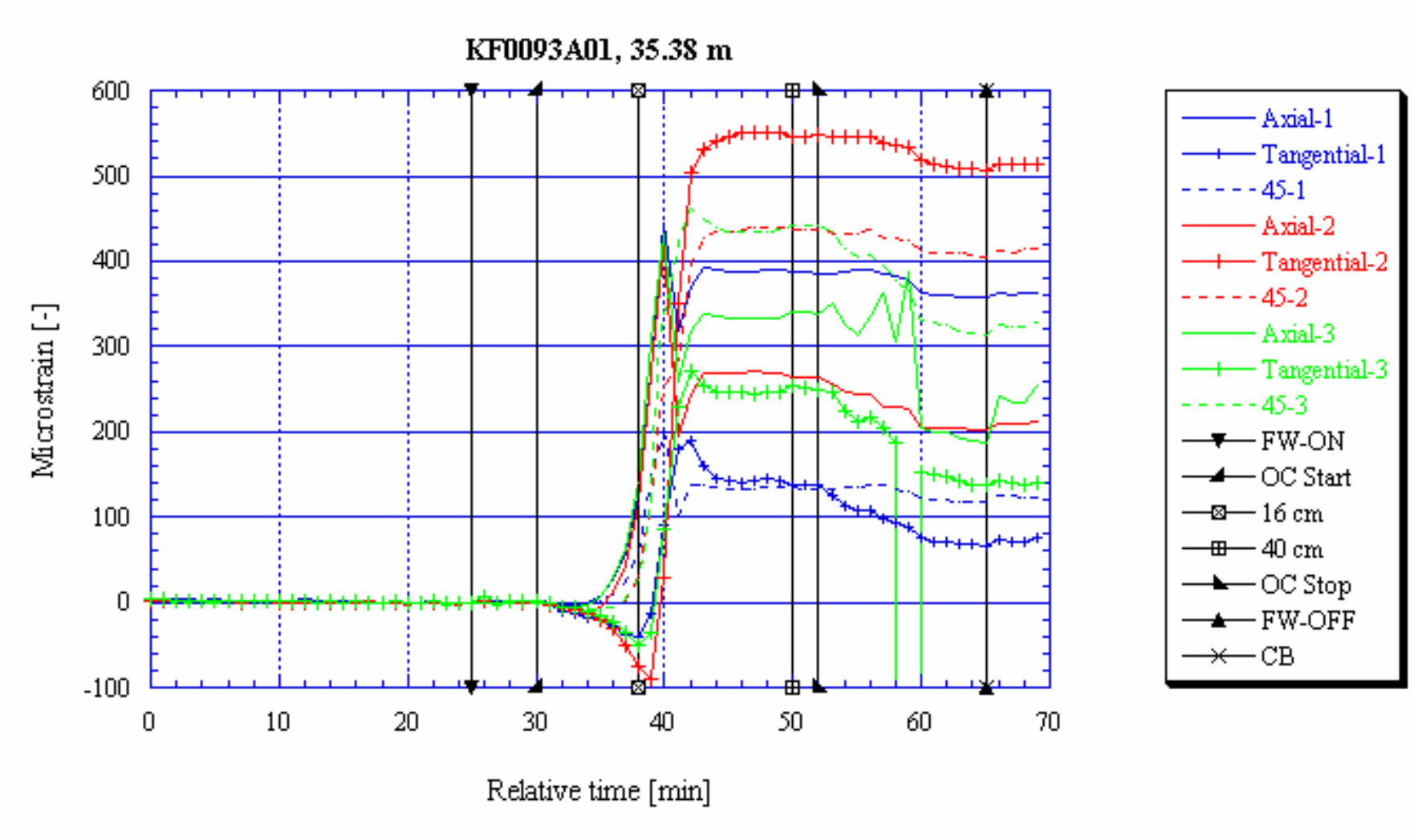
KF0093A01, 35.38 m
Microstrain [-]
600
500
400
300
200
100
0
-100
0
10
20
30
40
50
60
70
Relative time [min]
Axial-1
Tangential-1
45-1
Axial-2
Tangential-2
45-2
Axial-3
Tangential-3
45-3
FW-ON
OC Start
16 cm
40 cm
OC Stop
FW-OFF
CB

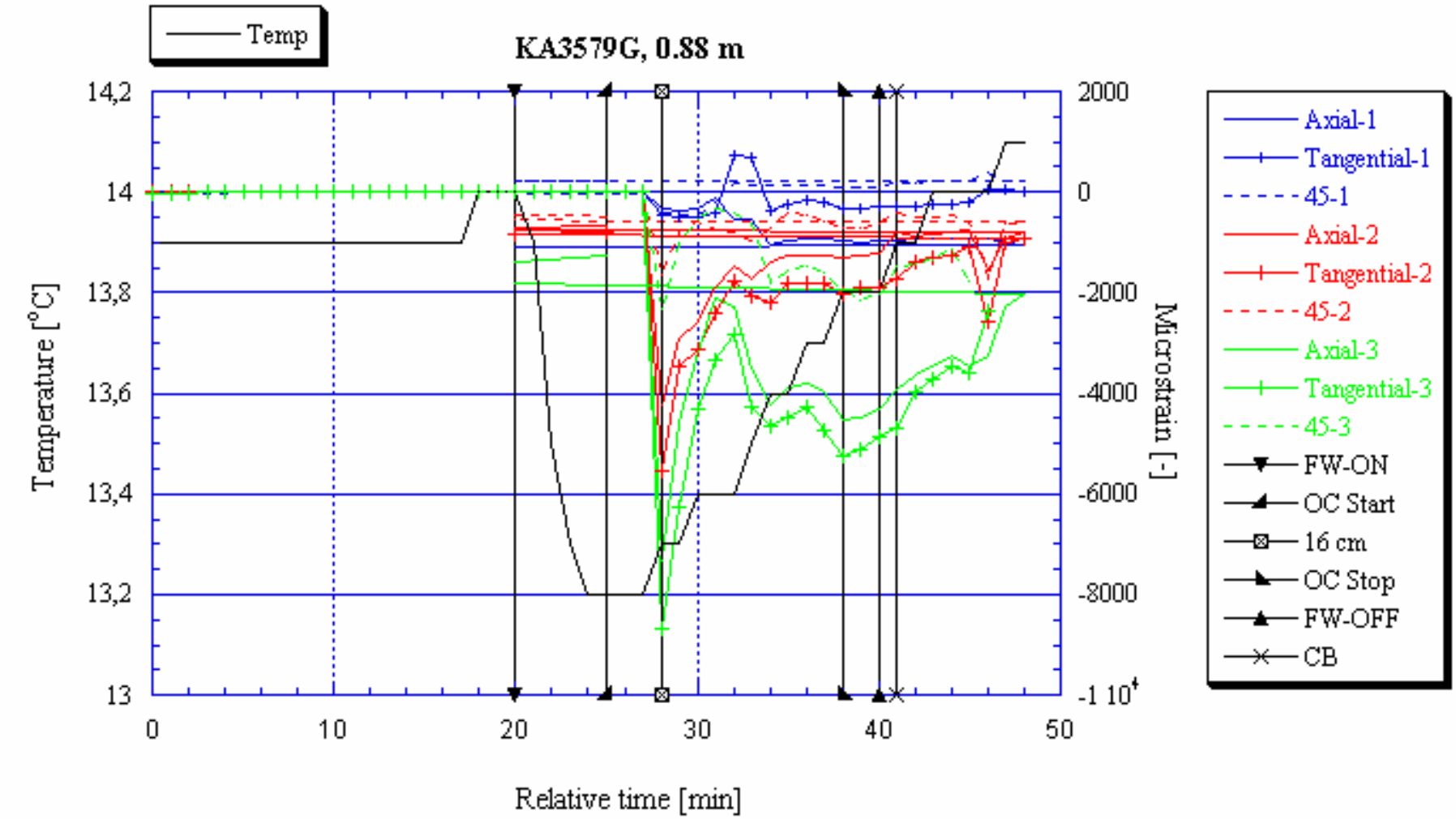
Temp
KA3579G, 0.88 m
14,2
14
13,8
13,6
13,4
13,2
13
Temperature [°C]
2000
0
-2000
-4000
-6000
-8000
-1 10⁴
Microstrain [-]
0
10
20
30
40
50
Relative time [min]
Axial-1
Tangential-1
45-1
Axial-2
Tangential-2
45-2
Axial-3
Tangential-3
45-3
FW-ON
OC Start
16 cm
OC Stop
FW-OFF
CB

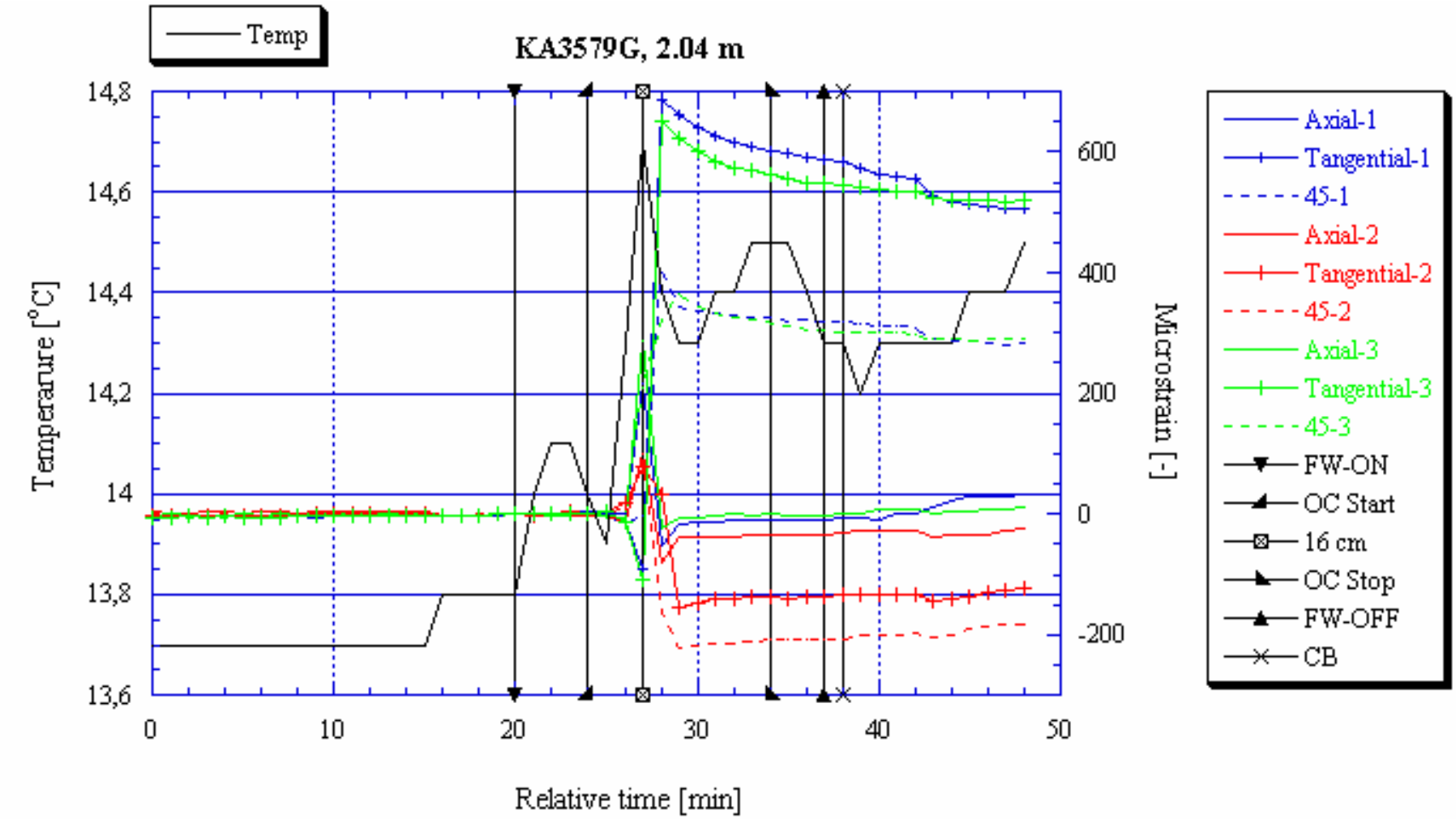
Temp
KA3579G, 2.04 m
Temperarure [°C]
14,8
14,6
14,4
14,2
14
13,8
13,6
0
10
20
30
40
50
Relative time [min]
600
400
200
0
-200
Microstrain [-]
Axial-1
Tangential-1
45-1
Axial-2
Tangential-2
45-2
Axial-3
Tangential-3
45-3
FW-ON
OC Start
16 cm
OC Stop
FW-OFF
CB

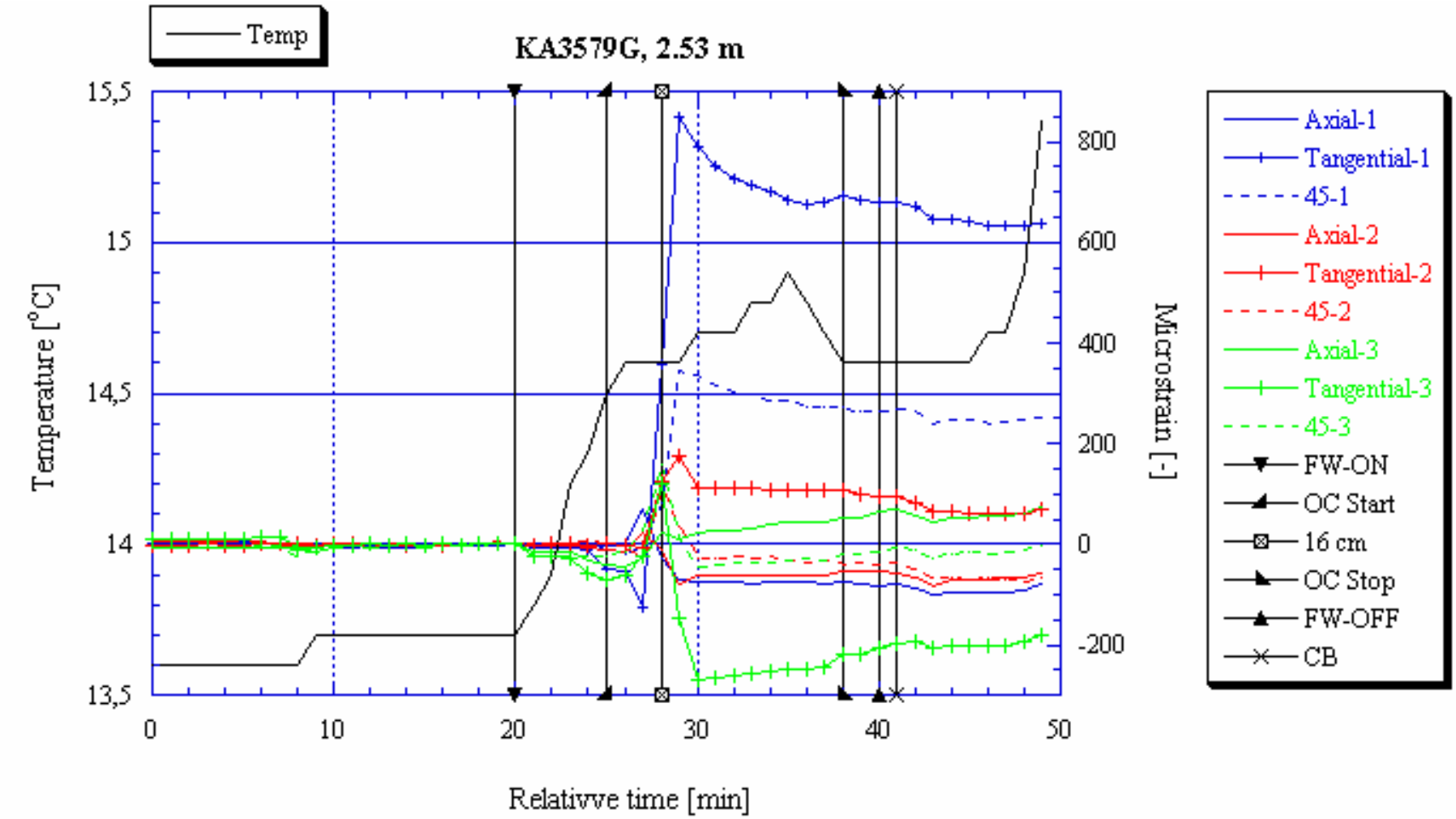
Temp
KA3579G, 2.53 m
15,5
15
14,5
14
13,5
Temperature [°C]
0
10
20
30
40
50
Relativve time [min]
800
600
400
200
0
-200
Microstrain [-]
Axial-1
Tangential-1
45-1
Axial-2
Tangential-2
45-2
Axial-3
Tangential-3
45-3
FW-ON
OC Start
16 cm
OC Stop
FW-OFF
CB

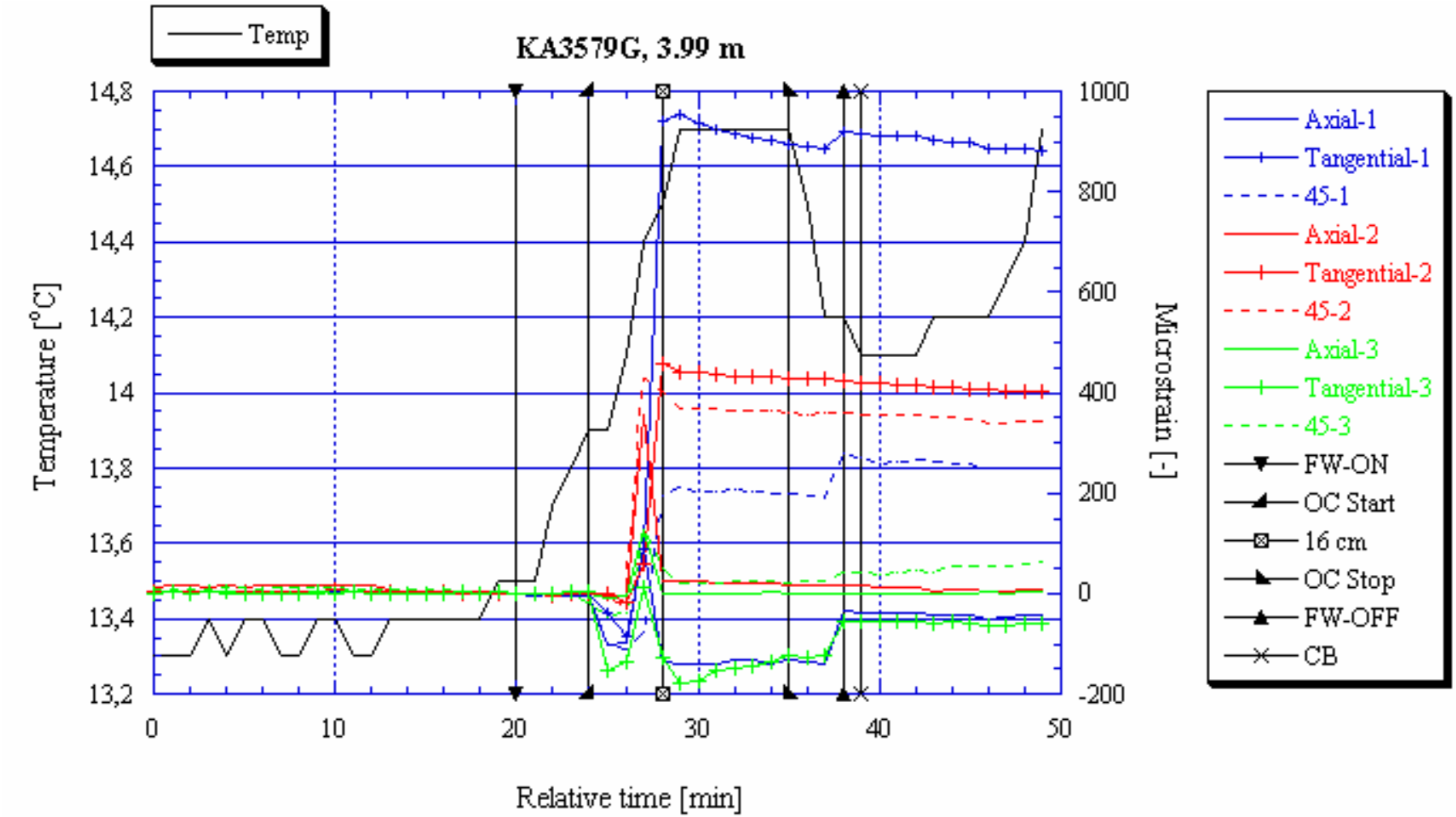
Temp
KA3579G, 3.99 m
Temperature [°C]
14,8
14,6
14,4
14,2
14
13,8
13,6
13,4
13,2
1000
800
600
400
200
0
-200
Microstrain [-]
0
10
20
30
40
50
Relative time [min]
Axial-1
Tangential-1
45-1
Axial-2
Tangential-2
45-2
Axial-3
Tangential-3
45-3
FW-ON
OC Start
16 cm
OC Stop
FW-OFF
CB

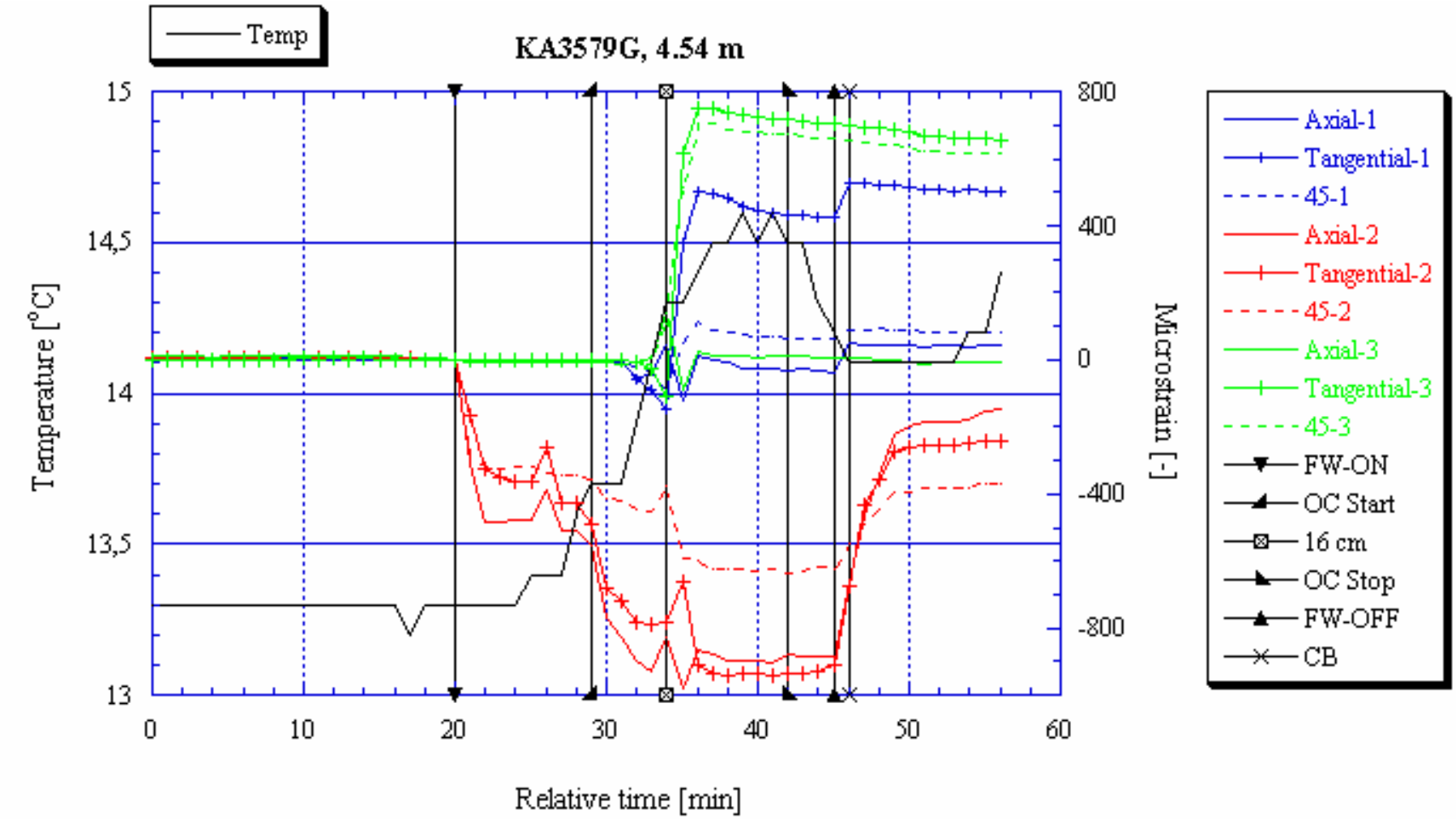
Temp
KA3579G, 4.54 m
Temperature [°C]
15
14,5
14
13,5
13
0
10
20
30
40
50
60
Relative time [min]
800
400
0
-400
-800
Microstrain [-]
Axial-1
Tangential-1
45-1
Axial-2
Tangential-2
45-2
Axial-3
Tangential-3
45-3
FW-ON
OC Start
16 cm
OC Stop
FW-OFF
CB

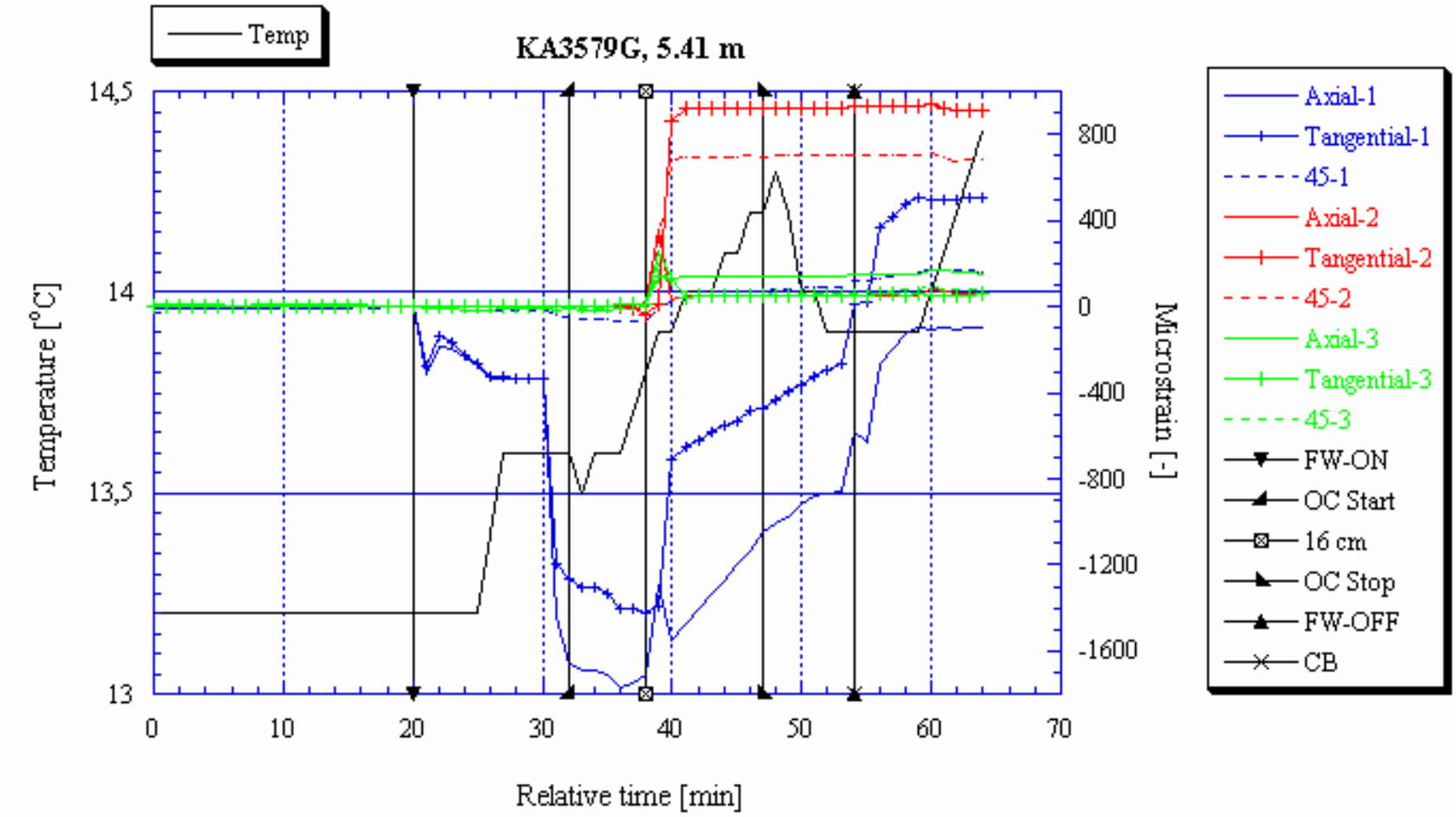
Temp
KA3579G, 5.41 m
14,5
14
13,5
13
Temperature [°C]
800
400
0
-400
-800
-1200
-1600
Microstrain [-]
0
10
20
30
40
50
60
70
Relative time [min]
Axial-1
Tangential-1
45-1
Axial-2
Tangential-2
45-2
Axial-3
Tangential-3
45-3
FW-ON
OC Start
16 cm
OC Stop
FW-OFF
CB

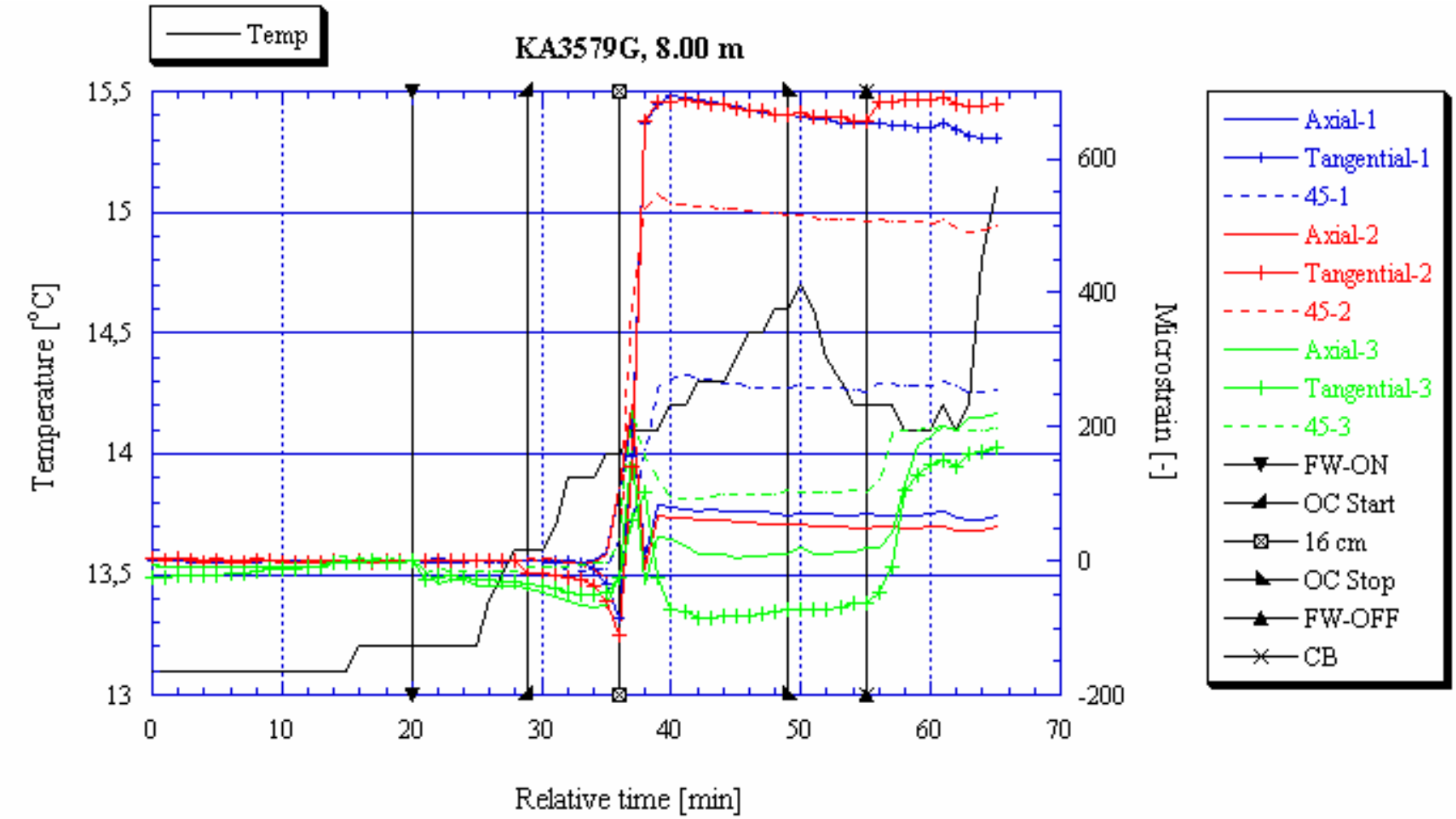
Temp
KA3579G, 8.00 m
15,5
15
14,5
14
13,5
13
Temperature [°C]
600
400
200
0
-200
Microstrain [-]
0
10
20
30
40
50
60
70
Relative time [min]
Axial-1
Tangential-1
45-1
Axial-2
Tangential-2
45-2
Axial-3
Tangential-3
45-3
FW-ON
OC Start
16 cm
OC Stop
FW-OFF
CB

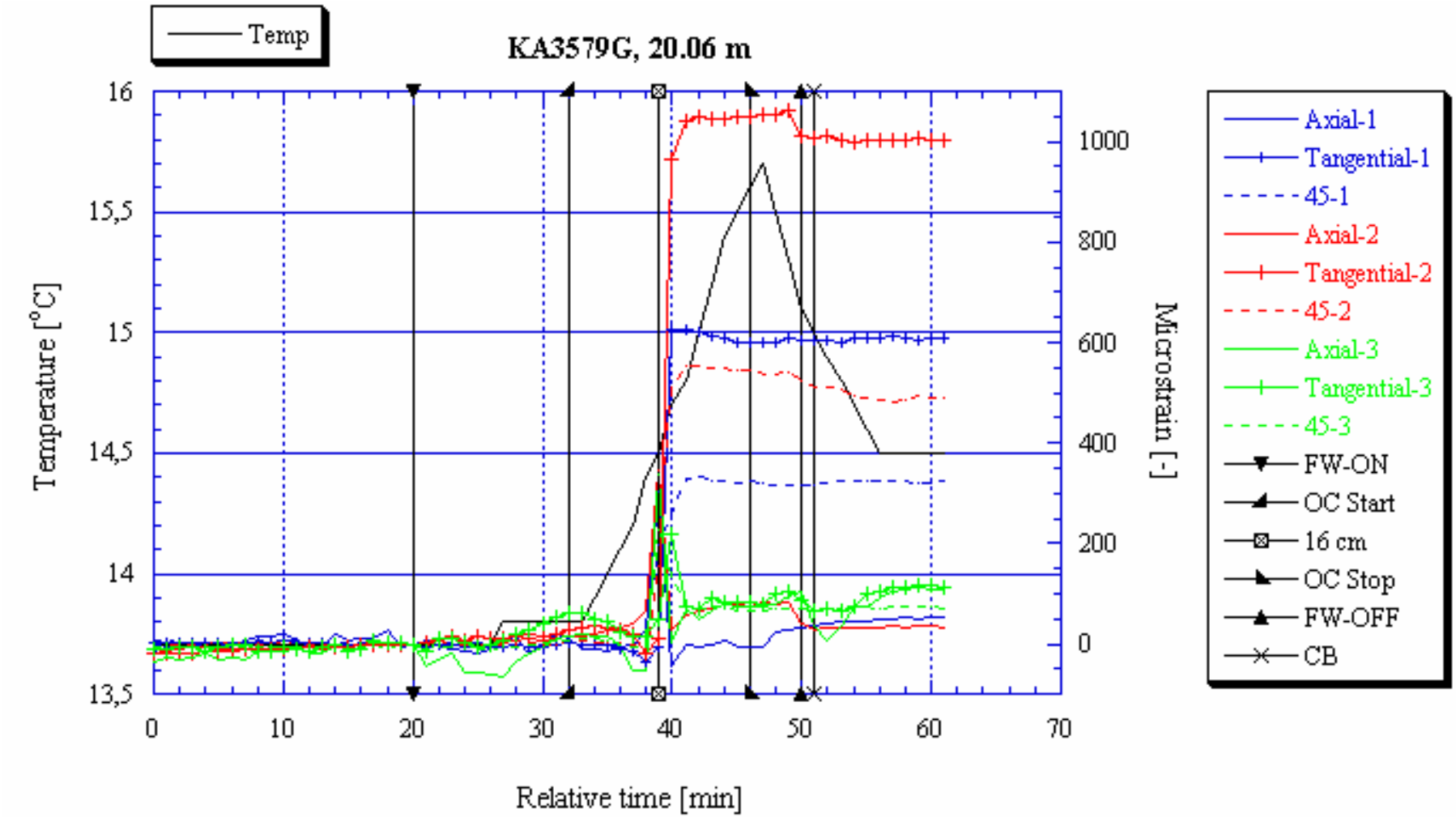
Temp
KA3579G, 20.06 m
Temperature [°C]
16
15,5
15
14,5
14
13,5
0
10
20
30
40
50
60
70
Relative time [min]
1000
800
600
400
200
0
Microstrain [-]
Axial-1
Tangential-1
45-1
Axial-2
Tangential-2
45-2
Axial-3
Tangential-3
45-3
FW-ON
OC Start
16 cm
OC Stop
FW-OFF
CB

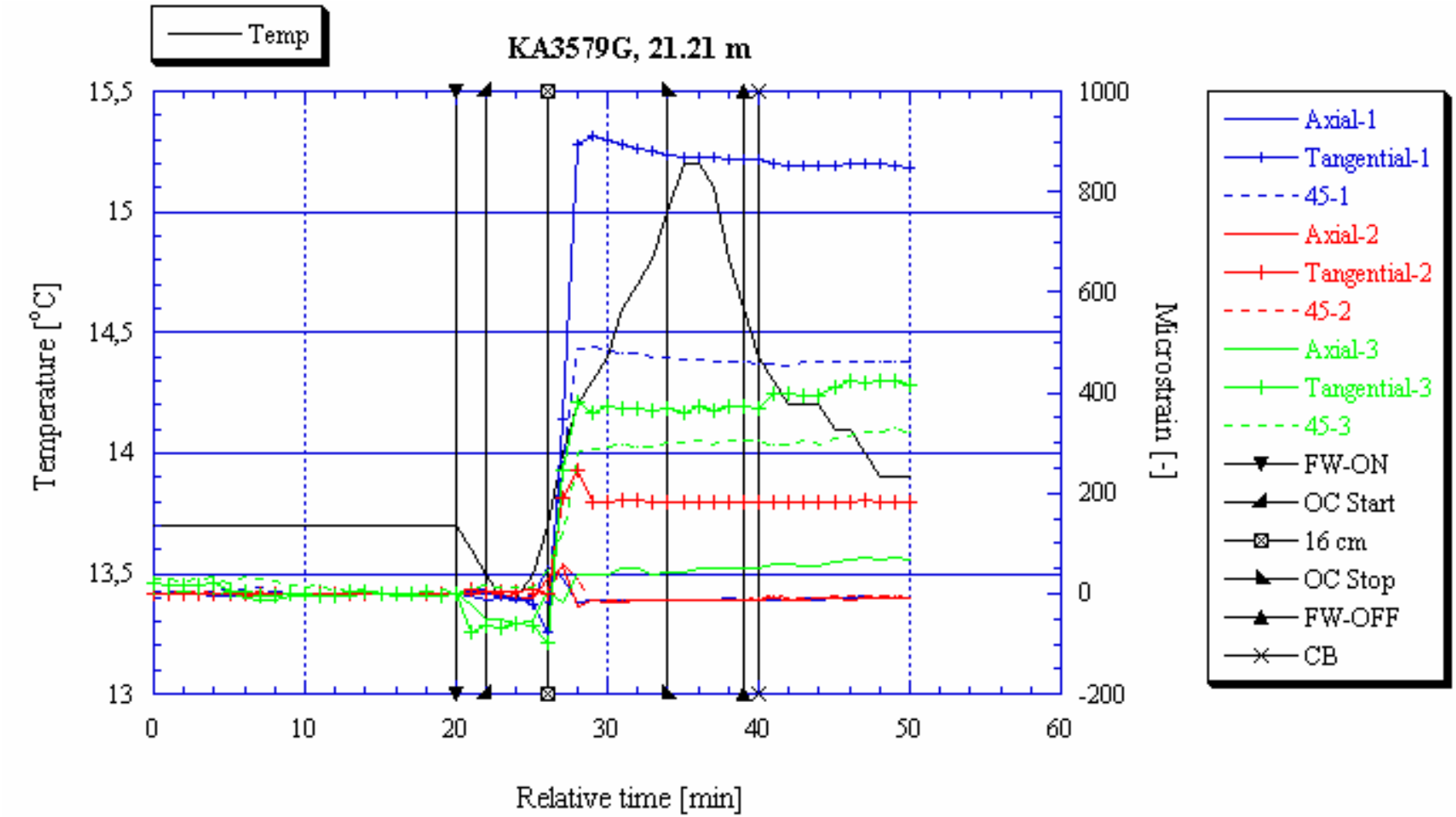
Temp
KA3579G, 21.21 m
Temperature [°C]
15,5
15
14,5
14
13,5
13
1000
800
600
400
200
0
-200
Microstrain [-]
0
10
20
30
40
50
60
Relative time [min]
Axial-1
Tangential-1
45-1
Axial-2
Tangential-2
45-2
Axial-3
Tangential-3
45-3
FW-ON
OC Start
16 cm
OC Stop
FW-OFF
CB

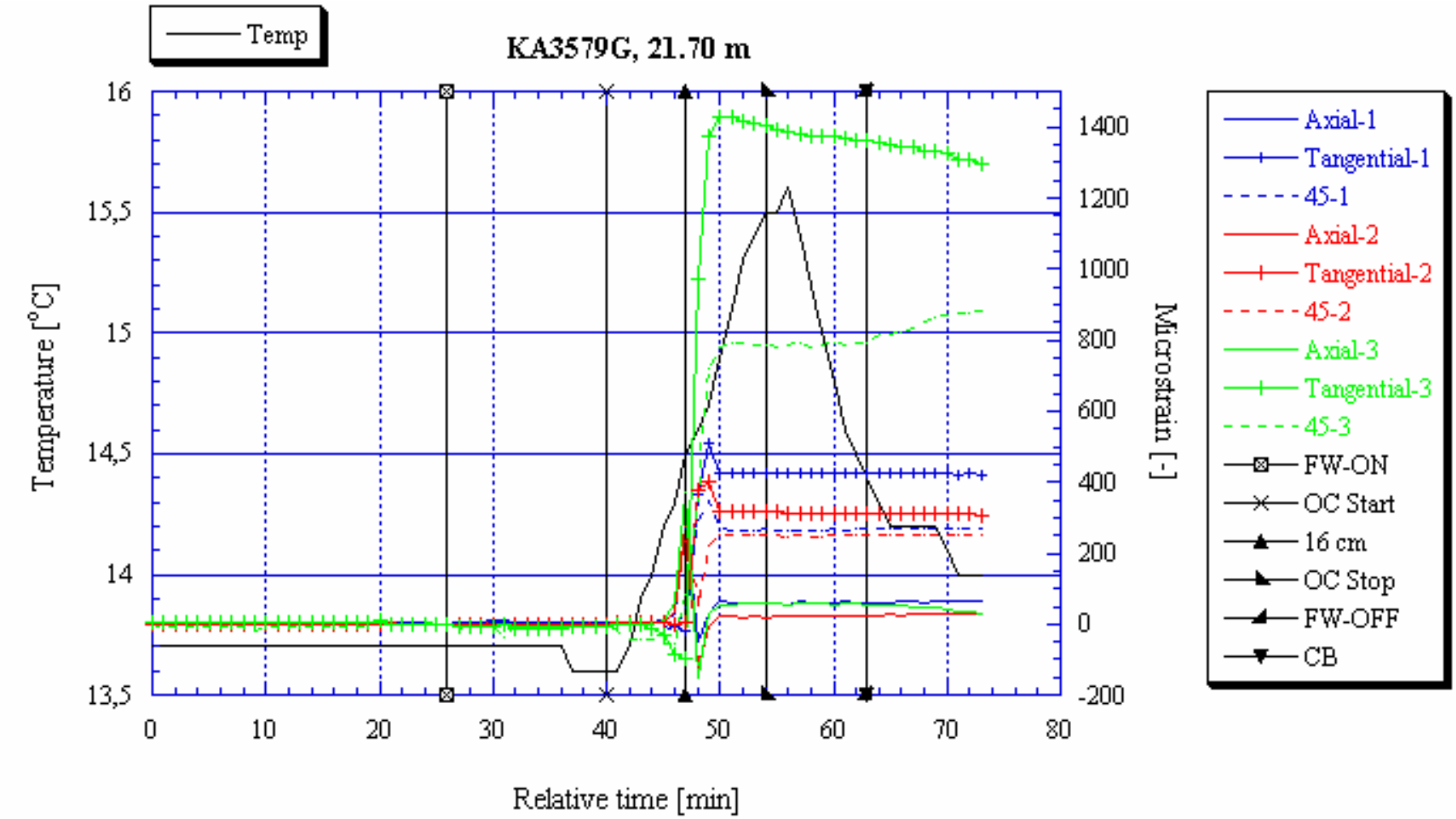
Temp
KA3579G, 21.70 m
Temperature [°C]
16
15,5
15
14,5
14
13,5
0
10
20
30
40
50
60
70
80
Relative time [min]
1400
1200
1000
800
600
400
200
0
-200
Microstrain [-]
Axial-1
Tangential-1
45-1
Axial-2
Tangential-2
45-2
Axial-3
Tangential-3
45-3
FW-ON
OC Start
16 cm
OC Stop
FW-OFF
CB

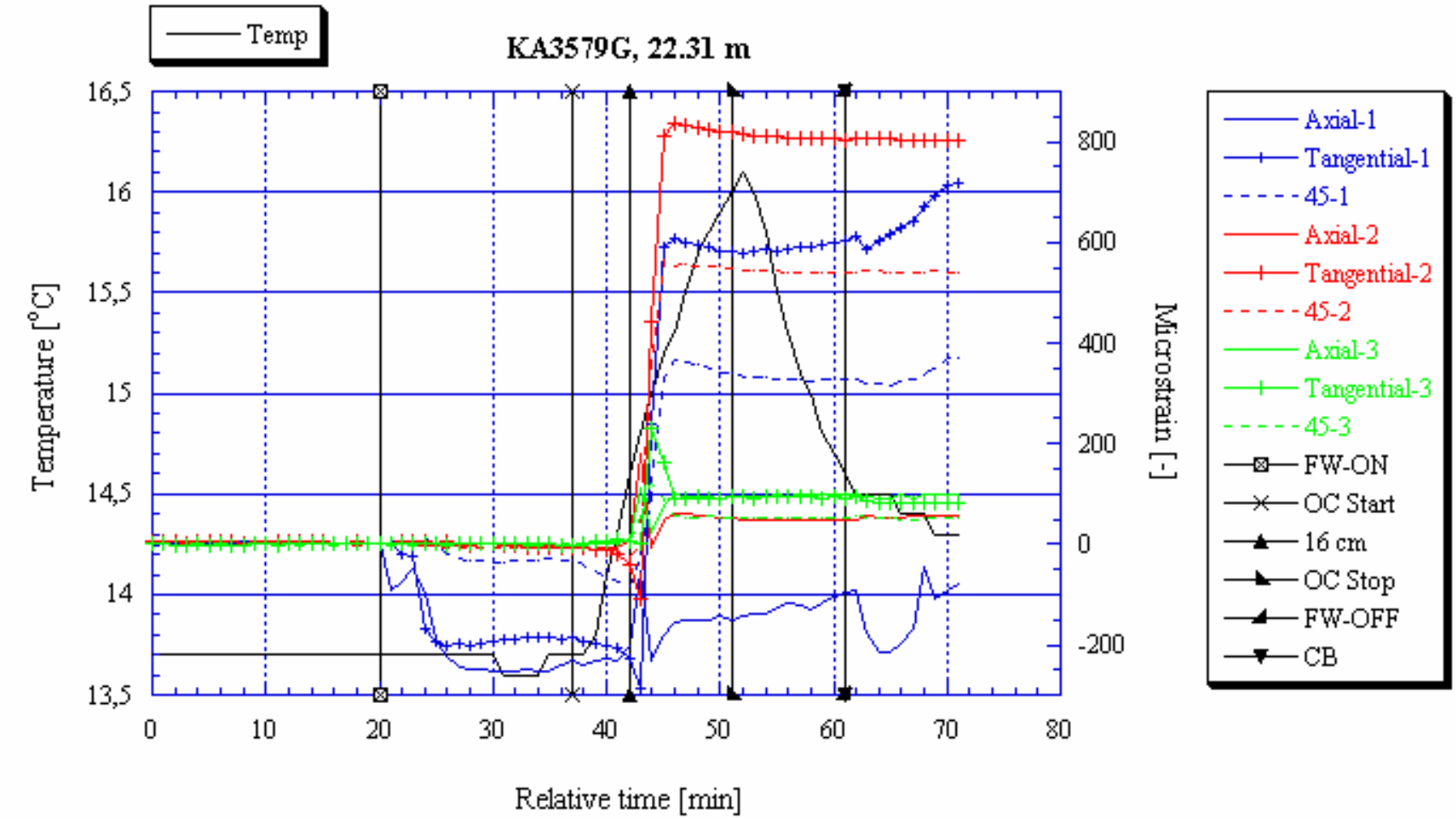
Temp
KA3579G, 22.31 m
16,5
16
15,5
15
14,5
14
13,5
Temperature [°C]
800
600
400
200
0
-200
Microstrain [-]
0
10
20
30
40
50
60
70
80
Relative time [min]
Axial-1
Tangential-1
45-1
Axial-2
Tangential-2
45-2
Axial-3
Tangential-3
45-3
FW-ON
OC Start
16 cm
OC Stop
FW-OFF
CB

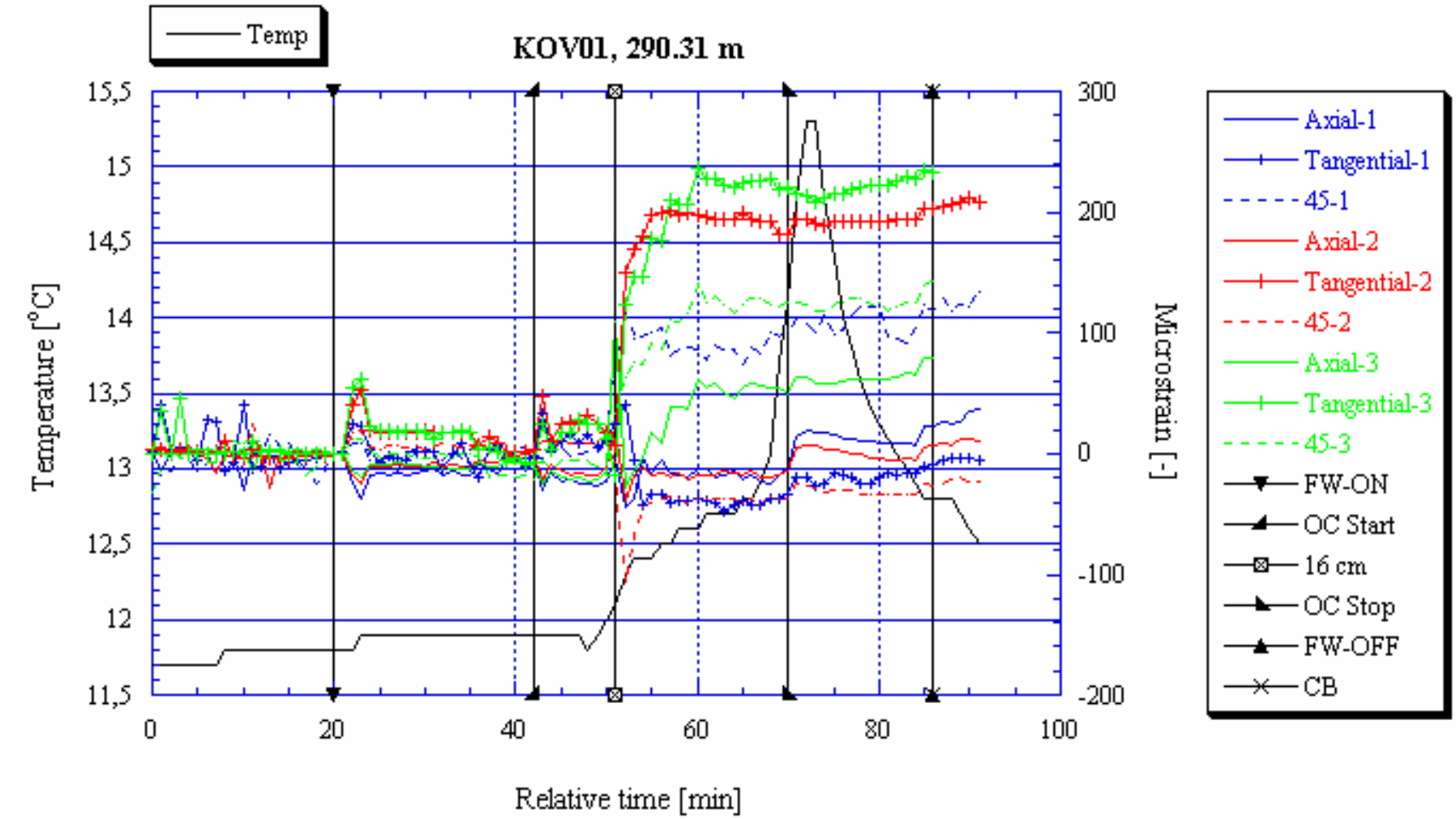
Temp
KOV01, 290.31 m
15,5
15
14,5
14
13,5
13
12,5
12
11,5
Temperature [°C]
300
200
100
0
-100
-200
Microstrain [-]
0
20
40
60
80
100
Relative time [min]
Axial-1
Tangential-1
45-1
Axial-2
Tangential-2
45-2
Axial-3
Tangential-3
45-3
FW-ON
OC Start
16 cm
OC Stop
FW-OFF
CB

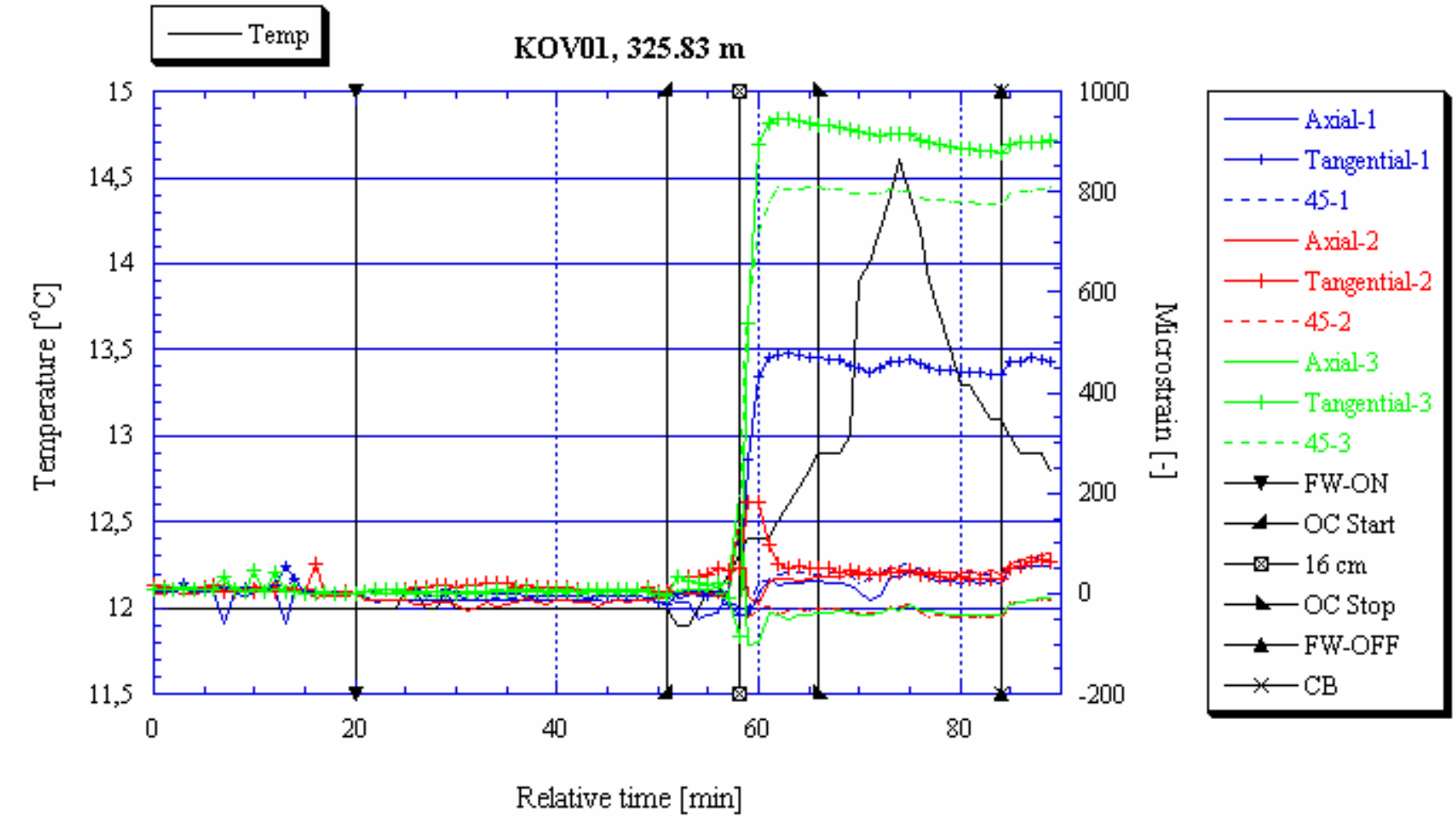
Temp
KOV01, 325.83 m
Temperature [°C]
15
14,5
14
13,5
13
12,5
12
11,5
0
20
40
60
80
Relative time [min]
1000
800
600
400
200
0
-200
Microstrain [-]
Axial-1
Tangential-1
45-1
Axial-2
Tangential-2
45-2
Axial-3
Tangential-3
45-3
FW-ON
OC Start
16 cm
OC Stop
FW-OFF
CB

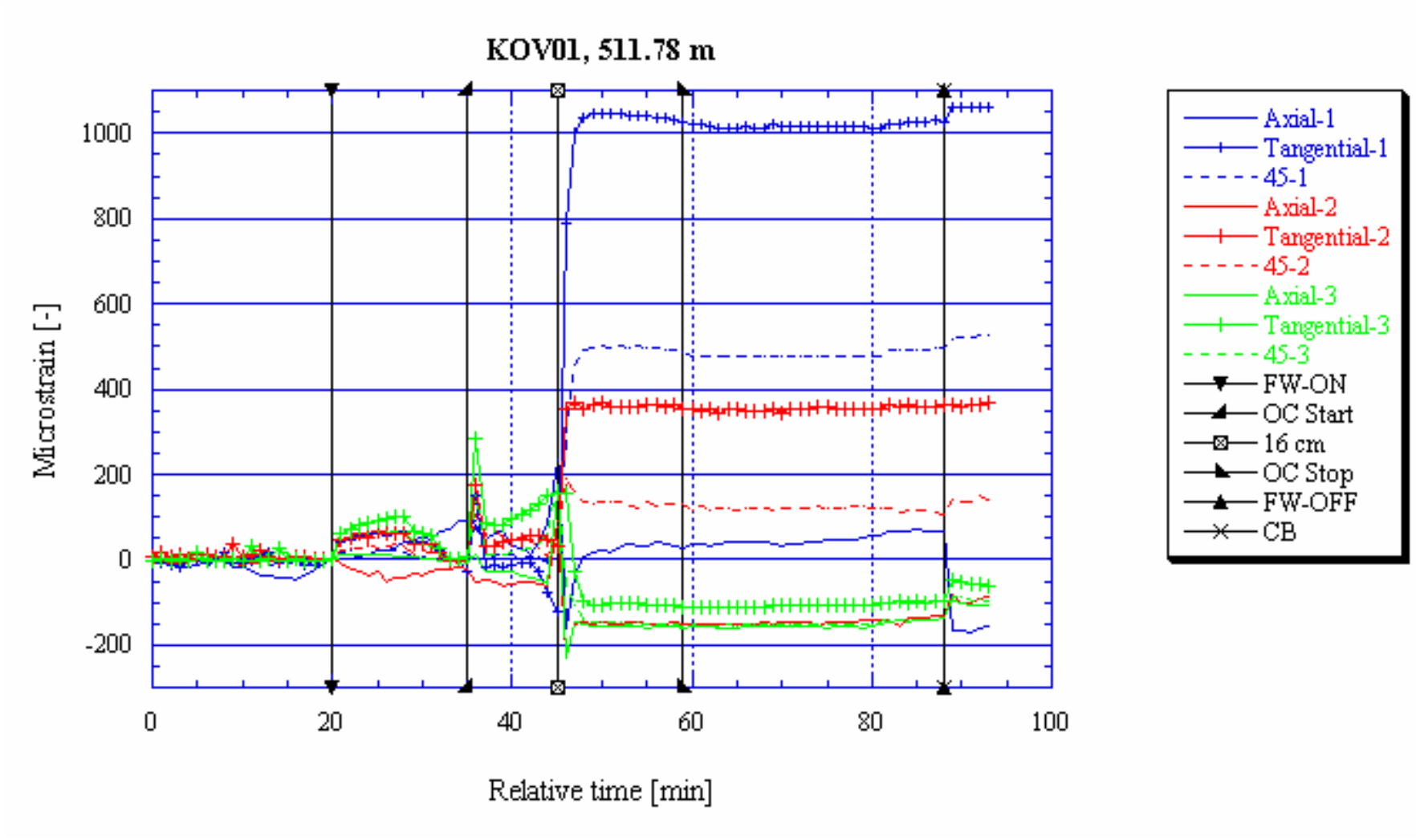
KOV01, 511.78 m
Microstrain [-]
1000
800
600
400
200
0
-200
0
20
40
60
80
100
Relative time [min]
Axial-1
Tangential-1
45-1
Axial-2
Tangential-2
45-2
Axial-3
Tangential-3
45-3
FW-ON
OC Start
16 cm
OC Stop
FW-OFF
CB

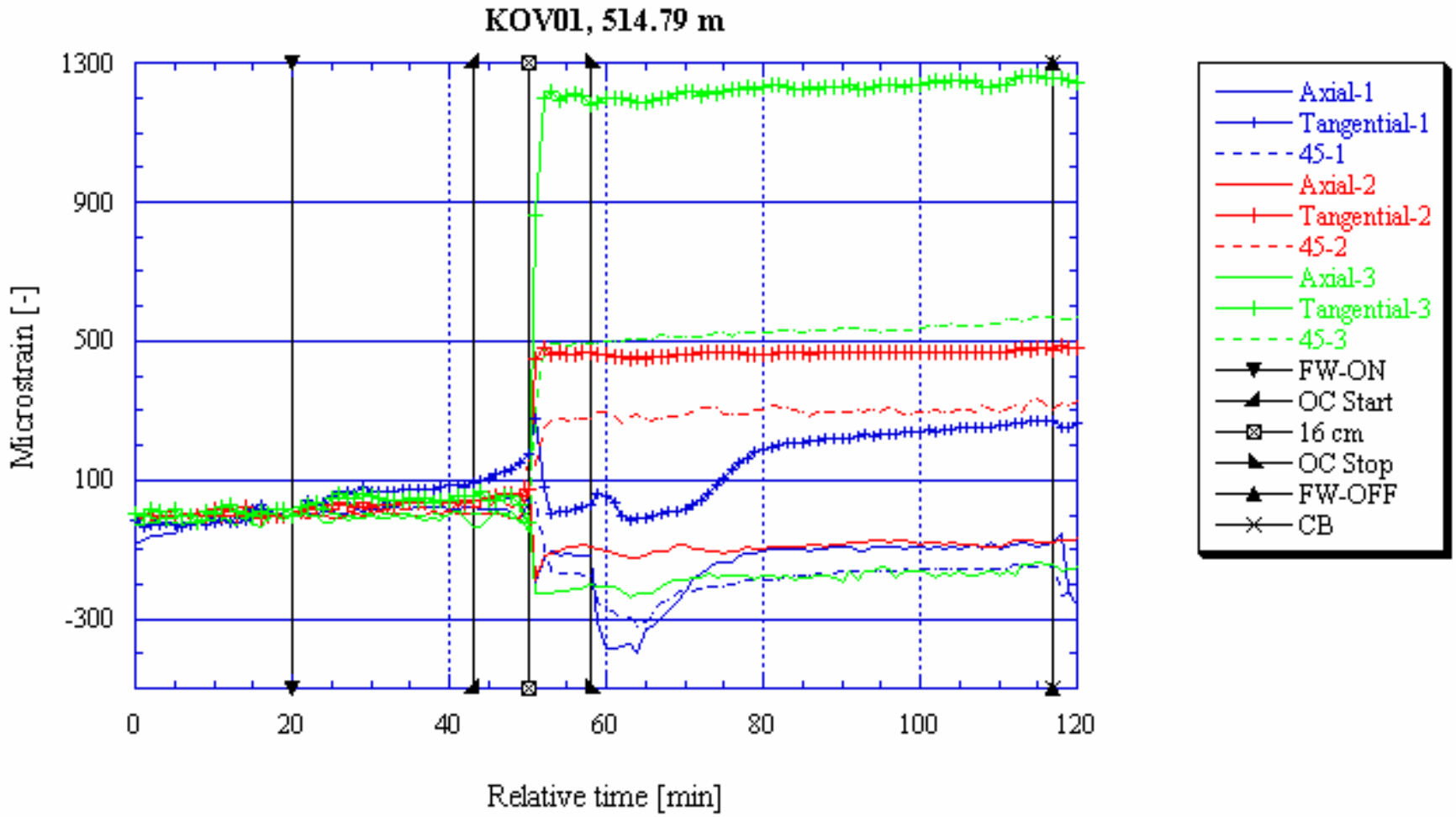
KOV01, 514.79 m
Microstrain [-]
1300
900
500
100
-300
0
20
40
60
80
100
120
Relative time [min]
Axial-1
Tangential-1
45-1
Axial-2
Tangential-2
45-2
Axial-3
Tangential-3
45-3
FW-ON
OC Start
16 cm
OC Stop
FW-OFF
CB

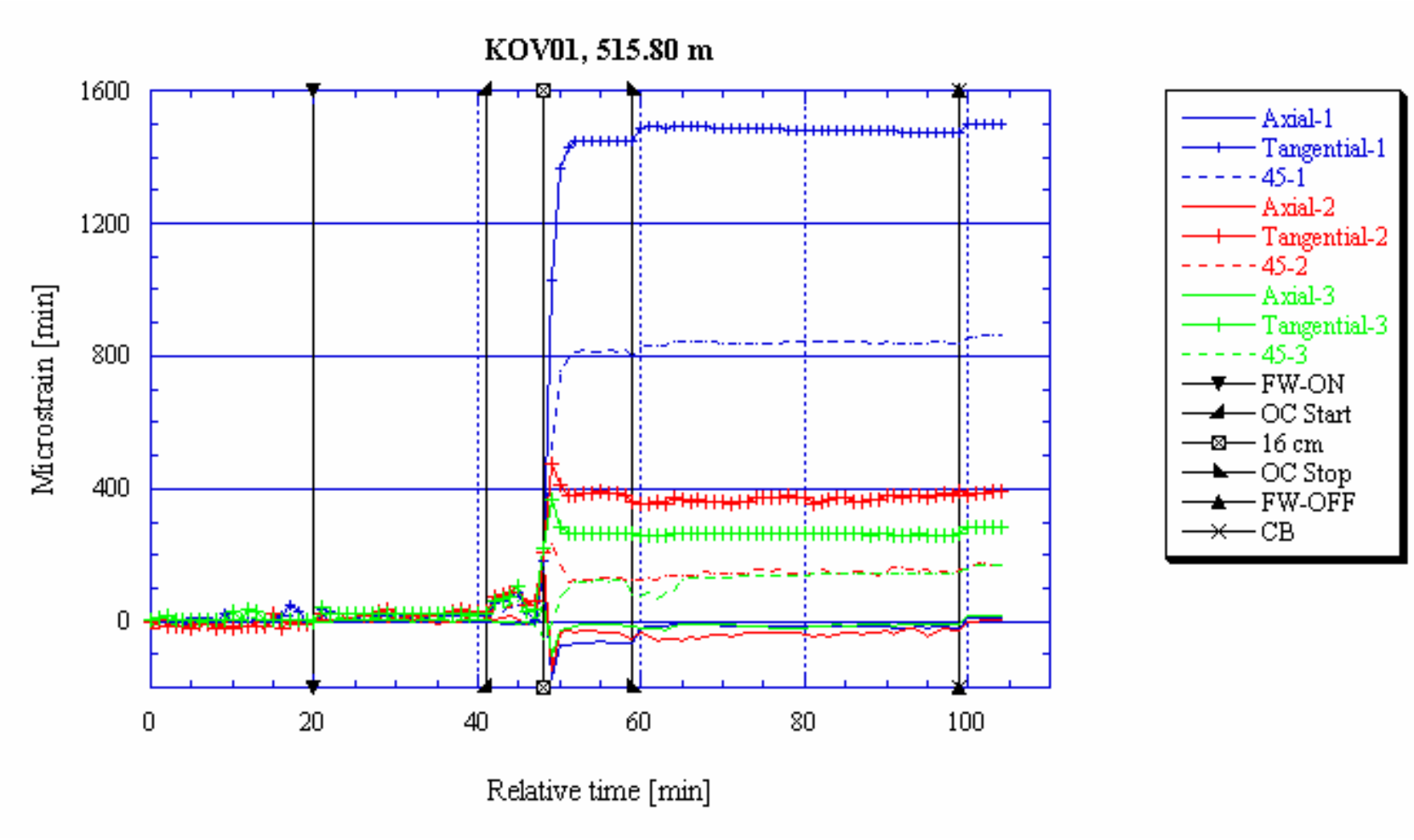
KOV01, 515.80 m
Microstrain [min]
1600
1200
800
400
0
0
20
40
60
80
100
Relative time [min]
Axial-1
Tangential-1
45-1
Axial-2
Tangential-2
45-2
Axial-3
Tangential-3
45-3
FW-ON
OC Start
16 cm
OC Stop
FW-OFF
CB

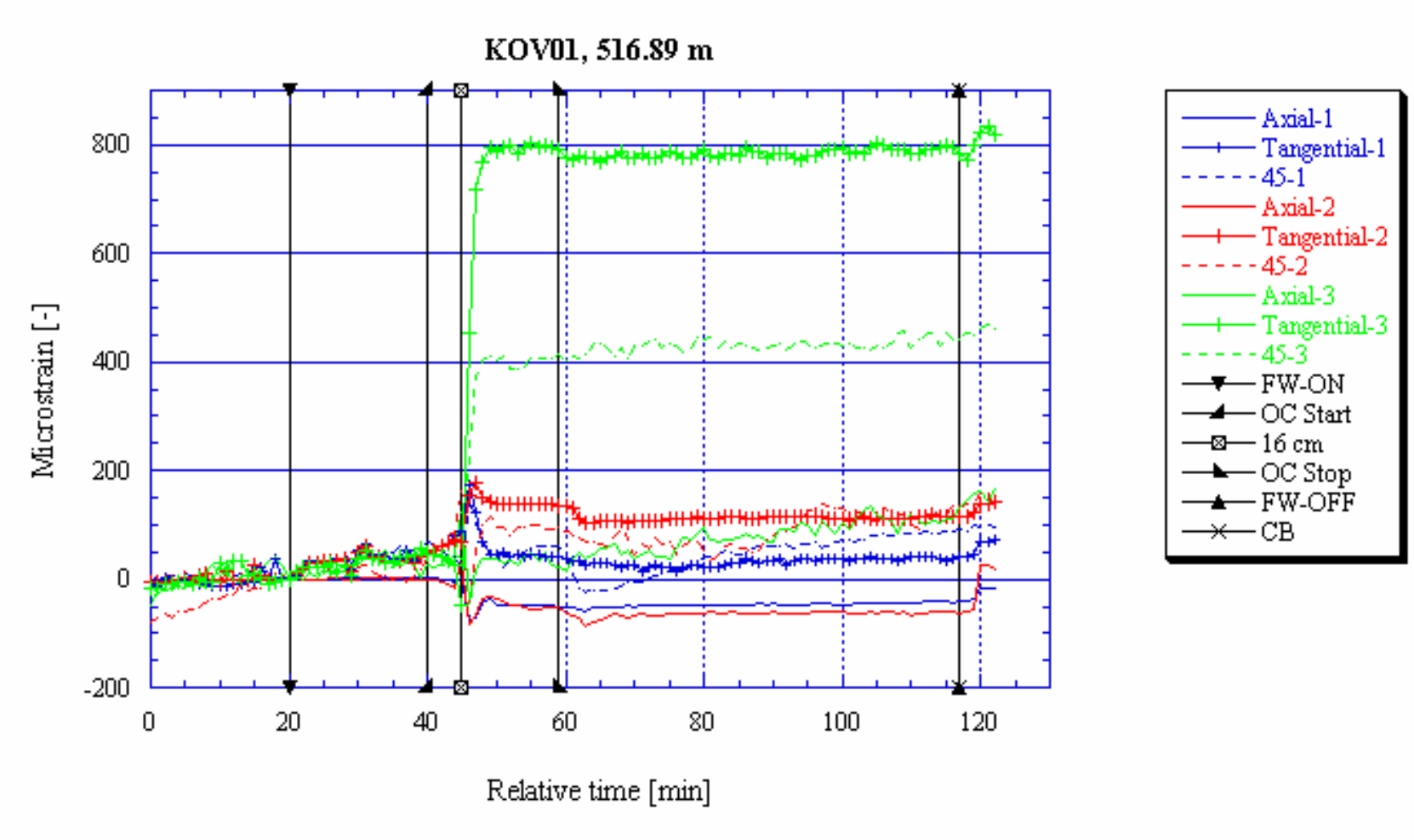
KOV01, 516.89 m
Microstrain [-]
800
600
400
200
0
-200
0
20
40
60
80
100
120
Relative time [min]
Axial-1
Tangential-1
45-1
Axial-2
Tangential-2
45-2
Axial-3
Tangential-3
45-3
FW-ON
OC Start
16 cm
OC Stop
FW-OFF
CB

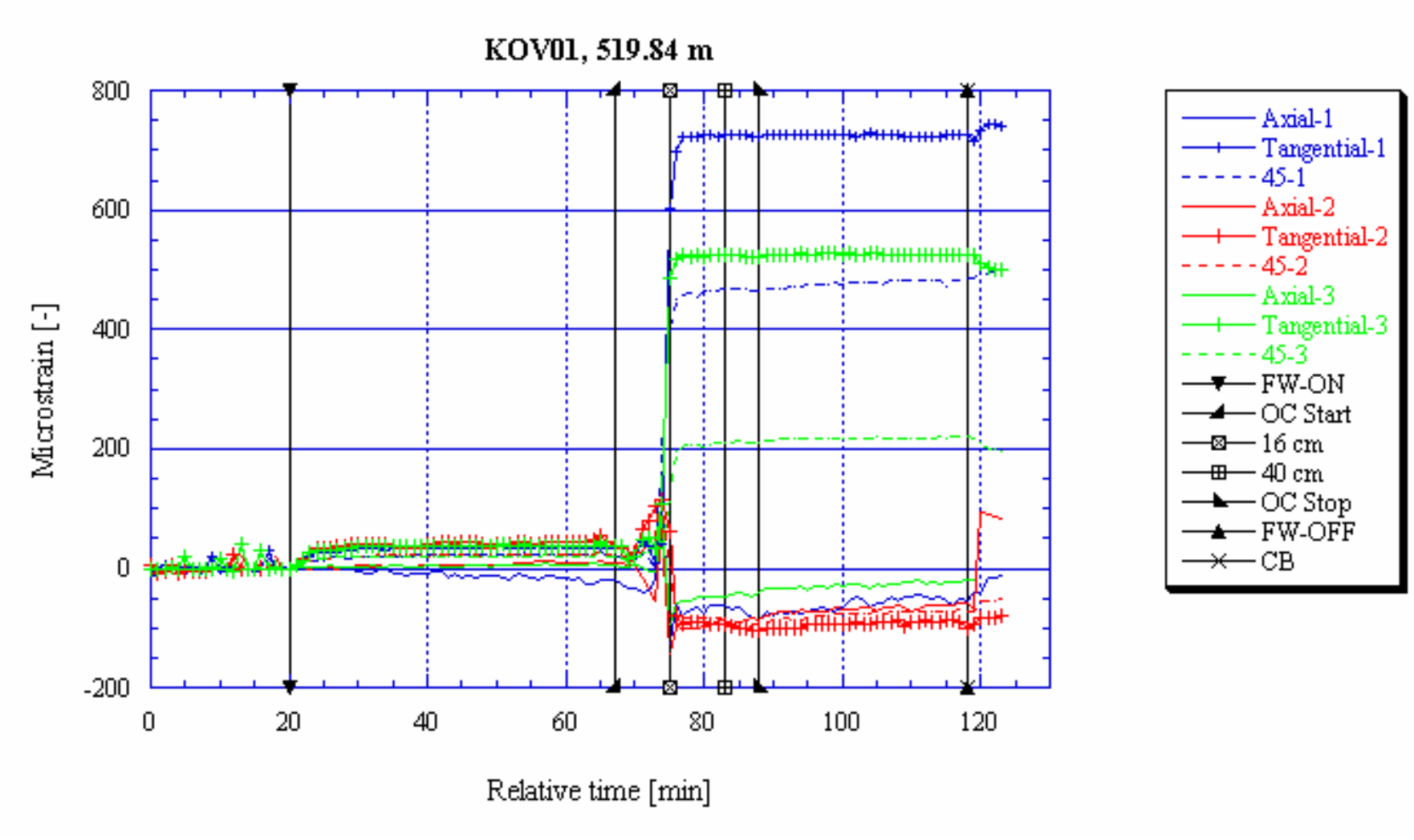
KOV01, 519.84 m
Microstrain [-]
800
600
400
200
0
-200
0
20
40
60
80
100
120
Relative time [min]
Axial-1
Tangential-1
45-1
Axial-2
Tangential-2
45-2
Axial-3
Tangential-3
45-3
FW-ON
OC Start
16 cm
40 cm
OC Stop
FW-OFF
CB

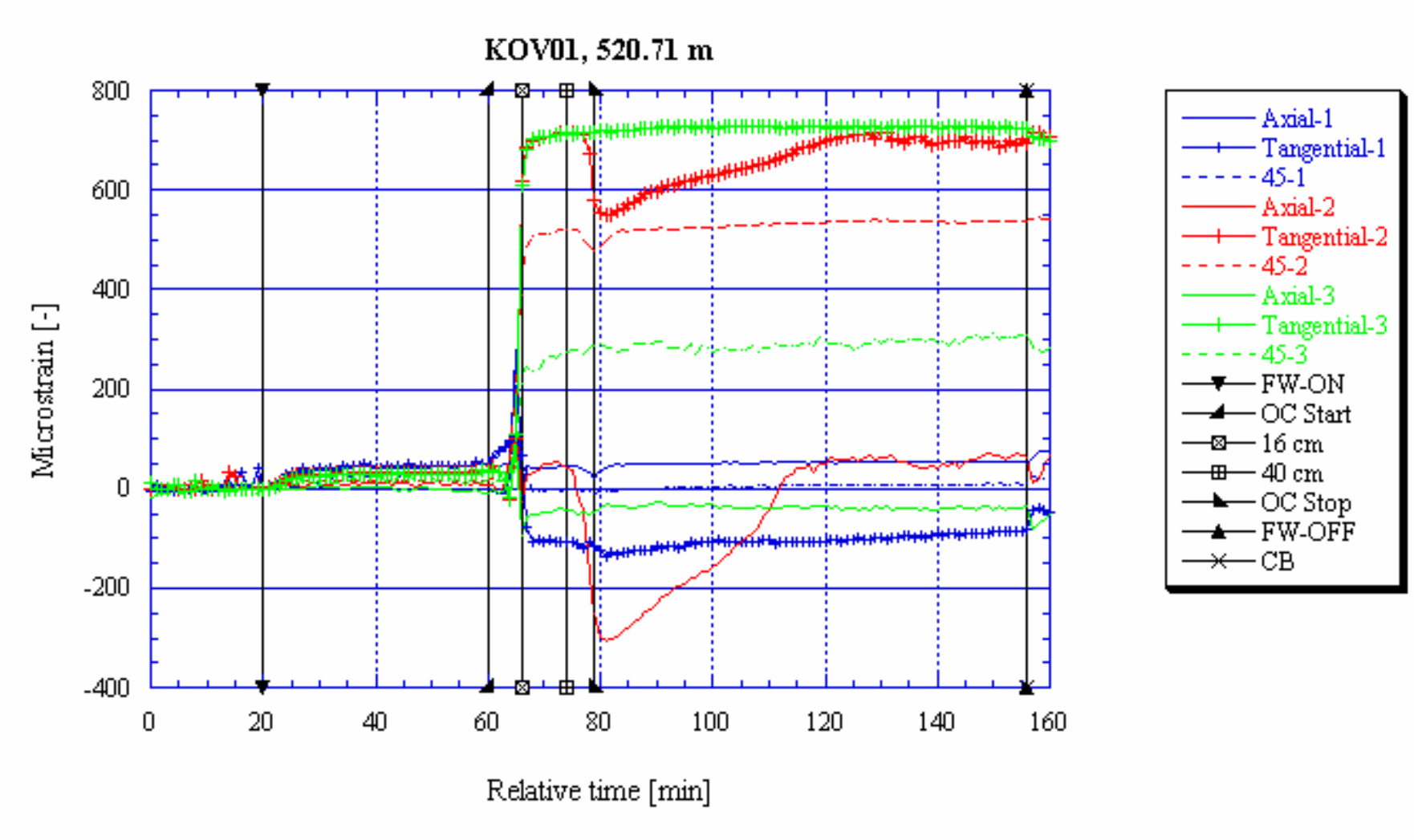
KOV01, 520.71 m
Microstrain [-]
800
600
400
200
0
-200
-400
0
20
40
60
80
100
120
140
160
Relative time [min]
Axial-1
Tangential-1
45-1
Axial-2
Tangential-2
45-2
Axial-3
Tangential-3
45-3
FW-ON
OC Start
16 cm
40 cm
OC Stop
FW-OFF
CB

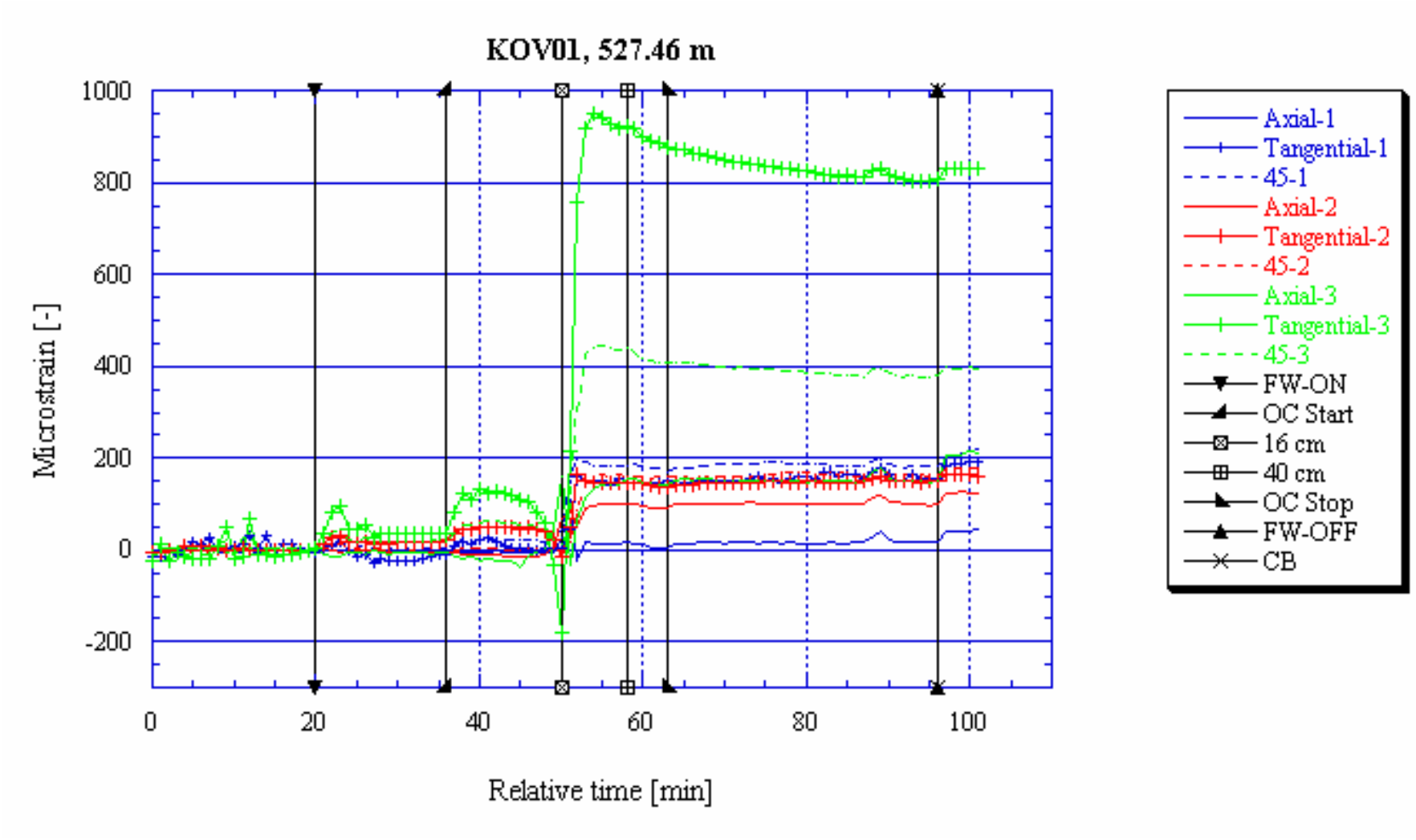
KOV01, 527.46 m
Microstrain [-]
1000
800
600
400
200
0
-200
0
20
40
60
80
100
Relative time [min]
Axial-1
Tangential-1
45-1
Axial-2
Tangential-2
45-2
Axial-3
Tangential-3
45-3
FW-ON
OC Start
16 cm
40 cm
OC Stop
FW-OFF
CB

Appendix 4

A4 Biaxal data from the Borre Probe

A4.1 Borehole KAS05

Raw data not found.

A4.2 Borehole KXZSD8HR

1.29 m
Test questionable as indicated by overcoring test. Rosettes 1 and 2 questionable according to biaxial test. Hysteresis and some degree of anisotropy.

1.66 m
Test questionable as indicated by overcoring test. Rosettes 1 and 3 questionable according to biaxial test. Hysteresis and some degree of anisotropy.

2.40 m
Rosettes 2 and 3 questionable indicated by overcoring test.

4.07 m
Core fractures at 6 MPa? Rosettes 1 and 3 questionable as indicated by overcoring test.

5.96 m
Several gauges are nonlinear. Hysteresis and some degree of anisotropy.

6.61 m
Rosette 3 questionable indicated by overcoring test. Hysteresis and some degree of anisotropy.

12.93 m
Rosette 3 questionable indicated by overcoring test. Gauges in rosettes 1 and 2 are nonlinear over the entire pressure interval. Rosettes 1 and 3 questionable as indicated by overcoring test. Hysteresis and some degree of anisotropy.

14.30 m
Several gauges are slightly nonlinear.

15.60 m
Core fractures during unloading? Biaxial test unreliable.

17.62 m
Test ok.

18.27 m
Questionable result due to soft glue indicated by overcoring test. The effect of the soft glue on the biaxial test result is difficult to evaluate. Thus, the biaxial result is regarded as very uncertain.
19.57 m
Rosette 1 not glued properly indicated by overcoring and biaxial test. Hysteresis and some degree of anisotropy.

20.22 m
Rosette 2 malfunctioning? Rosette 1 questionable according to biaxial test. Hysteresis and some degree of anisotropy.

20.85 m
Test ok. Hysteresis and some degree of anisotropy.

21.50 m
Test ok. Hysteresis and some degree of anisotropy.

22.21 m
Rosette 2 malfunctioning? Hysteresis and some degree of anisotropy.

22.94 m
Rosette 3 malfunctioning indicated by overcoring and biaxial test. Hysteresis and some degree of anisotropy.

A4.3 Borehole KXZSD81HR

0.86 m
Rosette 1 questionable as indicated from overcoring test. Axial and tangential strain gauges in rosettes 2 and 3 are slightly nonlinear for the entire pressure interval. Hysteresis apparent in tangential gauges and all gauges indicate some degree of anisotropy. Rosettes 1 and 3 questionable according to biaxial test.

1.43 m
Rosettes 2 and 3 questionable as indicated from overcoring test. Gauges in rosette 3 are slightly nonlinear.

2.73 m
Test ok. Hysteresis apparent in tangential gauges and all gauges indicate some degree of anisotropy.

3.34 m
Test ok. Hysteresis apparent in tangential gauges and all gauges indicate some degree of anisotropy. Tangential gauges in rosettes 1 and 3 are slightly nonlinear.

A4.4 Borehole KXZSD8HL

23.37 m
Rosette 2 malfunctioning and rosettes 1 and 3 questionable as indicated from overcoring test. Rosette 1 questionable in biaxial test. All gauges are slightly nonlinear over the entire pressure interval.

24.06 m
Rosette 2 malfunctioning and rosette 1 questionable as indicated from overcoring test. All gauges are slightly nonlinear over the entire pressure interval. Unreliable biaxial test.

24.75 m
All gauges are slightly nonlinear over the entire pressure interval.

25.44 m
All gauges are slightly nonlinear over the entire pressure interval.

A4.5 Borehole KK0045G01

1.20 m
Test ok.

2.24 m
Rosette 1 questionable according to biaxial test result.

2.70 m
Rosette 2 malfunctioning indicated by overcoring test. Rosette 1 questionable according to biaxial test result.

3.33 m
Biaxial result questionable.

4.53 m
Rosettes 3 not glued properly indicated by overcoring test.

5.51 m
Rosette 1 malfunctioning indicated by overcoring test.

6.07 m
Biaxial test indicates that rosette 3 is unreliable and the entire test result is questionable.

6.50 m
Rosettes 1 and 3 questionable indicated by overcoring test. Biaxial test indicates that rosettes 1 and 3 is unreliable and the entire test result is questionable.

8.16 m
Rosette 2 not glued properly, axial strain gauge in rosette 1 malfunctioning indicated by overcoring test. Biaxial test indicates that rosette 2 is unreliable and the entire test result is questionable.

31.67 m
Rosette 3 not glued properly indicated by overcoring test. Rosette 1 misplaced by 12.5 degrees (see Ch. 3.4.4).

32.48 m
Unstable axial gauges during the test. Rosette 3 questionable according to biaxial test result.

34.77 m
Rosette 2 questionable indicated by overcoring and biaxial test.

35.48 m
Tangential gauges in rosettes 1 and 2, axial gauge in rosette 3 malfunctioning indicated by overcoring test.

62.82 m
Glue not fully hardened indicated by overcoring test. The effect of the soft glue on the biaxial test result is difficult to evaluate. Thus, the biaxial result is regarded as very uncertain.

63.59 m
Test ok.

64.51 m
Glue not fully hardened indicated by overcoring test. The effect of the soft glue on the biaxial test result is difficult to evaluate. Thus, the biaxial result is regarded as very uncertain.

A4.6 Borehole KA0093A01

32.14 m
All rosettes questionable indicated from overcoring test. Core fractures between 5-6 MPa?

32.70 m
All rosettes questionable indicated from overcoring test. Hysteresis apparent in tangential gauges and all gauges indicate some degree of anisotropy.

35.38 m
Rosette 3 questionable indicated from overcoring and biaxial test. Hysteresis apparent in tangential gauges and all gauges indicate some degree of anisotropy.

A4.7 Borehole KA3579G

2.04 m
Test questionable according to biaxial test. Hysteresis apparent in all gauges and some degree of anisotropy.

2.53 m
Axial gauge in rosette 1 indicates fracturing. Test questionable according to biaxial test. Hysteresis apparent in tangential gauges and all gauges indicate some degree of anisotropy.
3.99 m
Test ok, some indications of anisotropy.

4.54 m
Rosette 2 questionable as indicated on overcoring test. Test questionable according to biaxial test. Hysteresis apparent in all gauges.

5.41 m
Test ok. Hysteresis apparent in tangential gauges and all gauges indicate some degree of anisotropy.

8.00 m
Rosette 3 questionable indicated from overcoring test. Axial and tangential gauges in rosettes 1 and 2 are nonlinear at low pressures. Hysteresis apparent in tangential gauges and all gauges indicate some degree of anisotropy.

20.06 m
All rosettes questionable indicated from overcoring test. Hysteresis apparent in tangential gauges and all gauges indicate some degree of anisotropy.

21.21 m
Error in output file for axial gauge in rosette 3 or a result of that rosette 3 is not glued properly, as indicated from the overcoring test. Biaxial test indicates that rosette 3 is questionable.

21.70 m
Test ok.

22.31 m
Rosette 1 questionable indicated from overcoring and biaxial test.

A4.8 Borehole KOV01

290.31 m
Rosette 3 malfunctioning and rosette 1 and 2 are unsteady but sub-linear.

325.83 m
Rosettes 2 and 3 non-linear at low pressures.

511.78 m
Rosette 3 malfunctioning and rosette 1 and 2 are unsteady but sub-linear.

515.80 m
Rosette 2 and 3 malfunctioning.

516.89 m
All rosettes are unsteady but sub-linear.

519.84 m
All rosettes are unsteady but sub-linear.

520.71 m
All rosettes are non-linear at low pressures but at higher pressures unsteady but sub-linear.

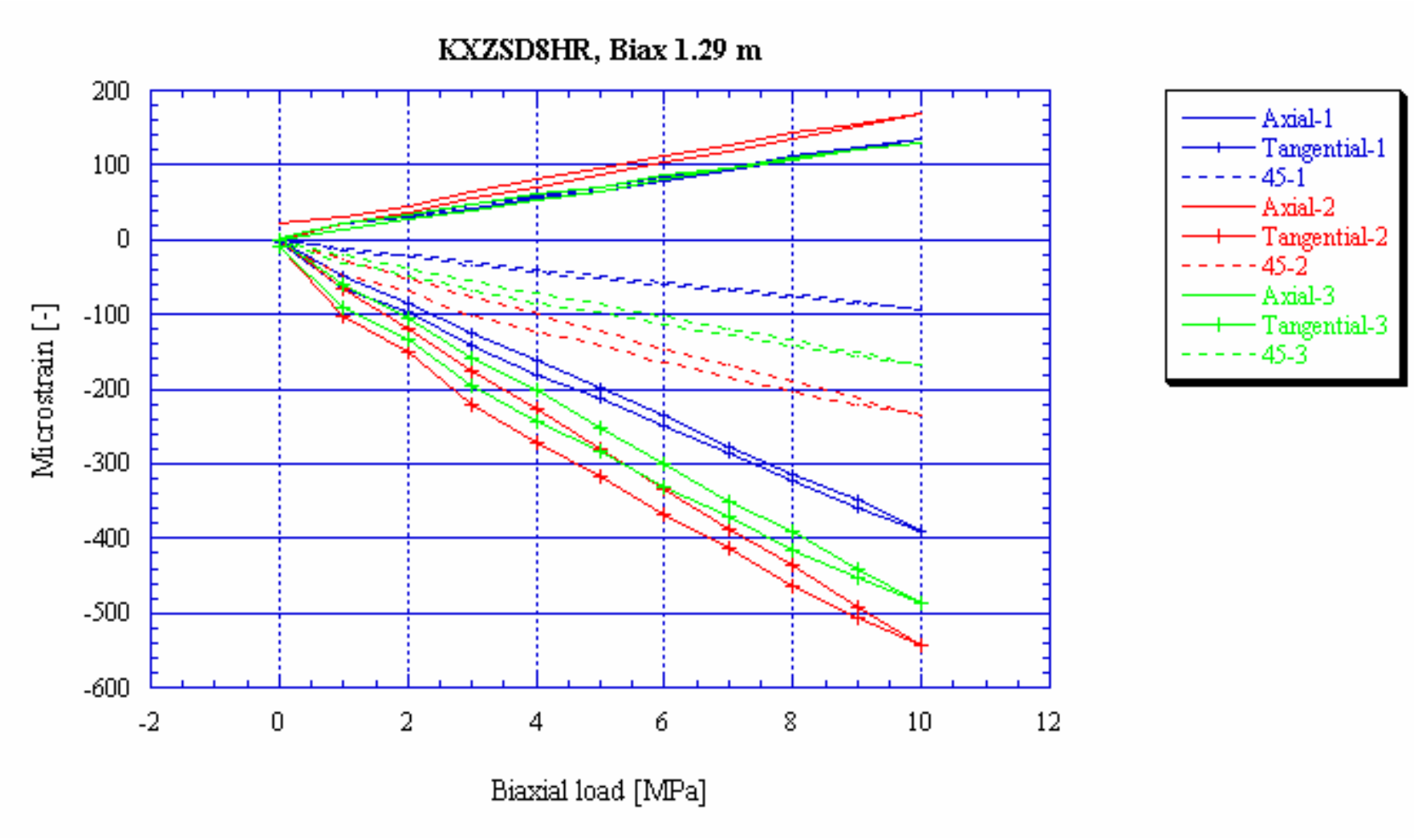
KXZSD8HR, Biax 1.29 m
Microstrain [-]
200
100
0
-100
-200
-300
-400
-500
-600
-2
0
2
4
6
8
10
12
Biaxial load [MPa]
Axial-1
Tangential-1
45-1
Axial-2
Tangential-2
45-2
Axial-3
Tangential-3
45-3

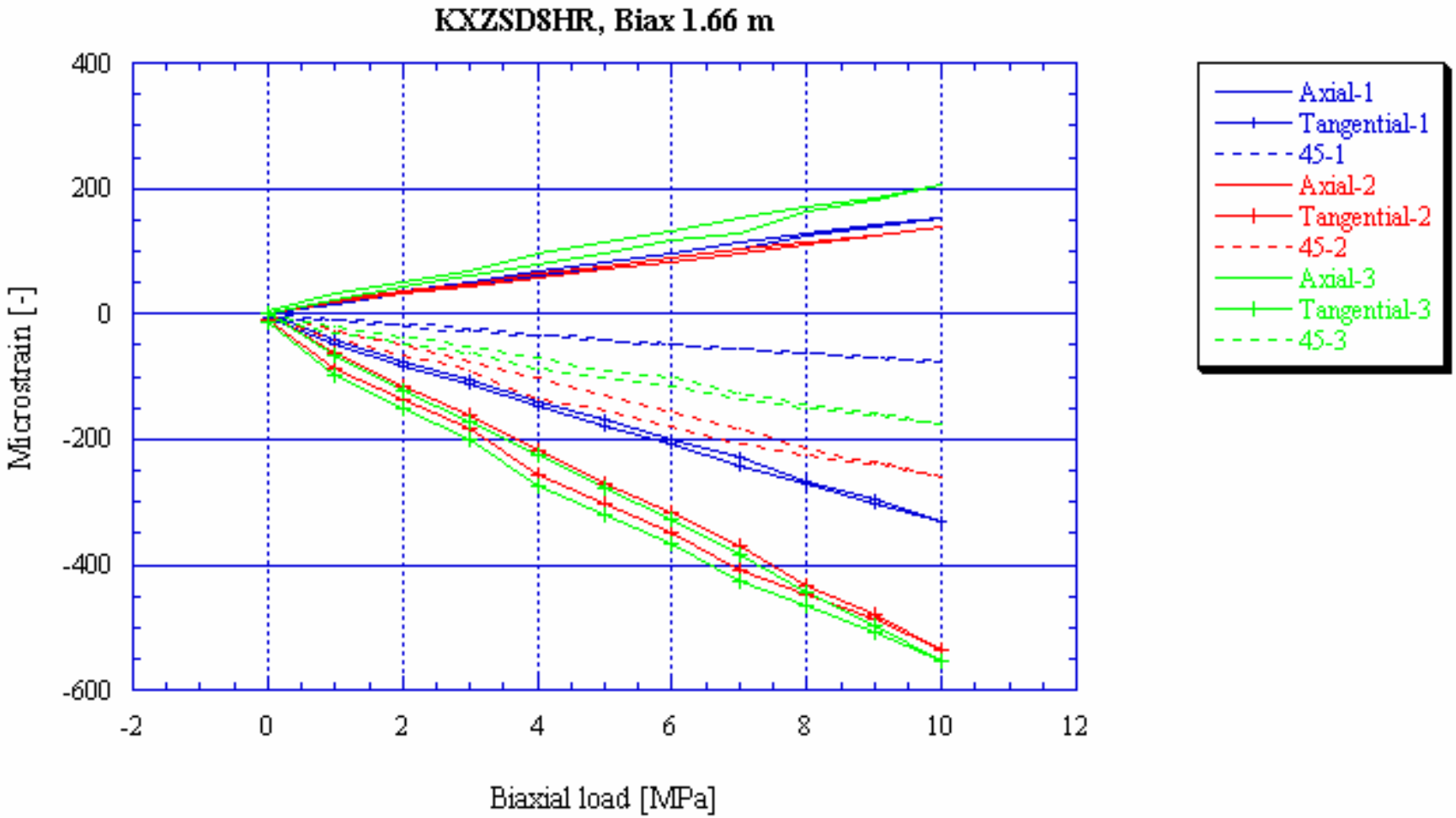
KXZSD8HR, Biax 1.66 m
Microstrain [-]
400
200
0
-200
-400
-600
-2
0
2
4
6
8
10
12
Biaxial load [MPa]
Axial-1
Tangential-1
45-1
Axial-2
Tangential-2
45-2
Axial-3
Tangential-3
45-3

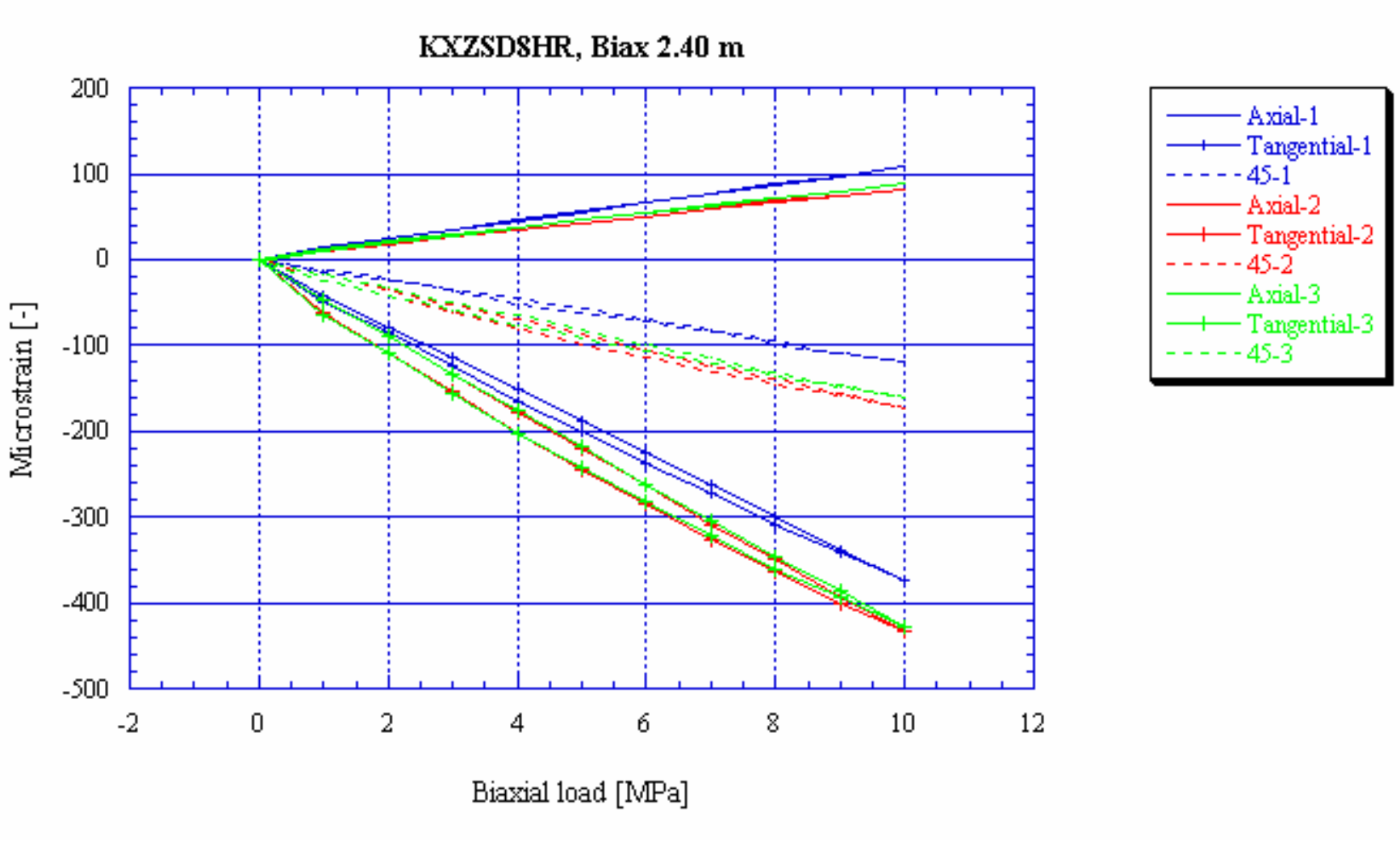
KXZSD8HR, Biax 2.40 m
Microstrain [-]
200
100
0
-100
-200
-300
-400
-500
-2
0
2
4
6
8
10
12
Biaxial load [MPa]
Axial-1
Tangential-1
45-1
Axial-2
Tangential-2
45-2
Axial-3
Tangential-3
45-3

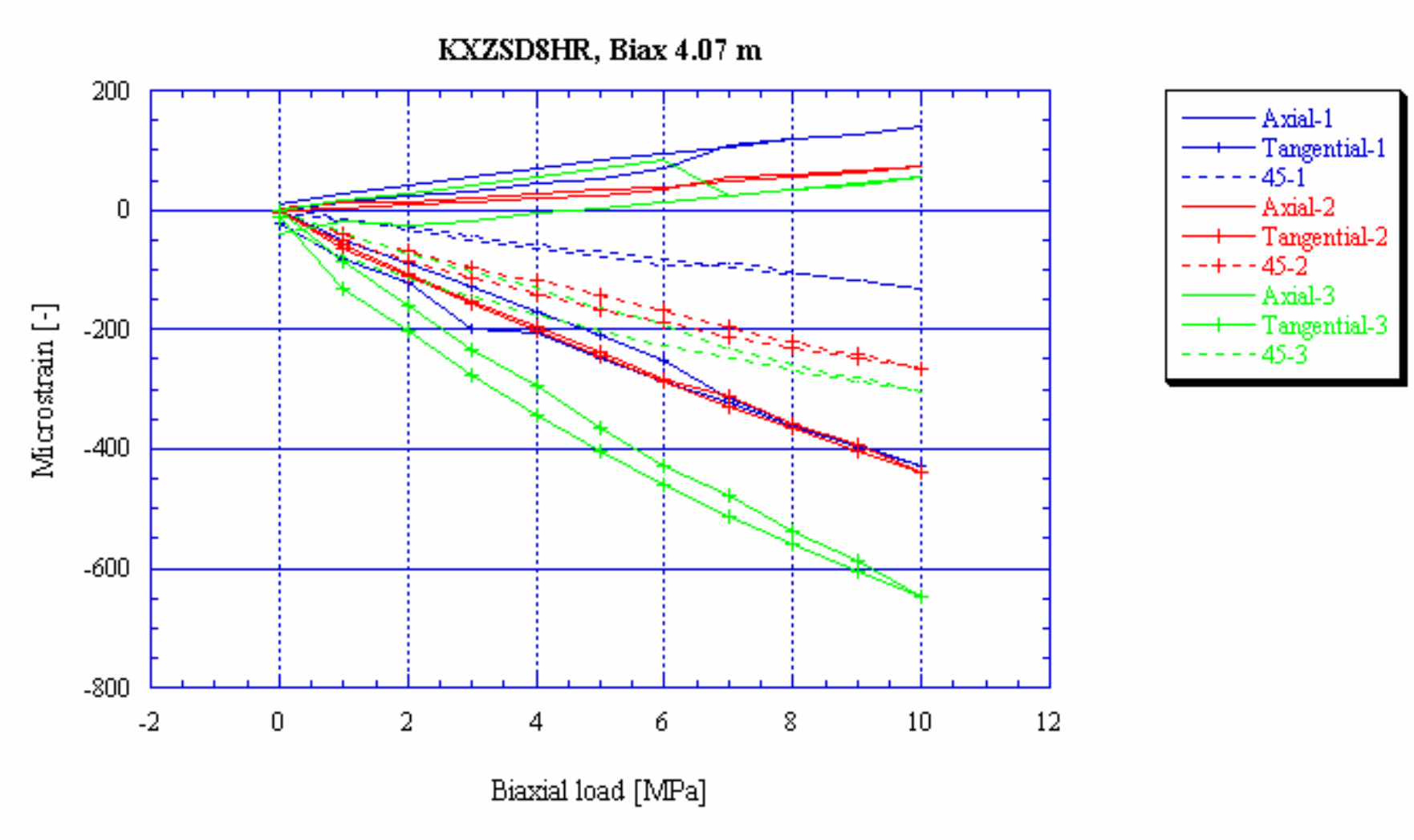
KXZSD8HR, Biax 4.07 m
Microstrain [-]
200
0
-200
-400
-600
-800
-2
0
2
4
6
8
10
12
Biaxial load [MPa]
Axial-1
Tangential-1
45-1
Axial-2
Tangential-2
45-2
Axial-3
Tangential-3
45-3

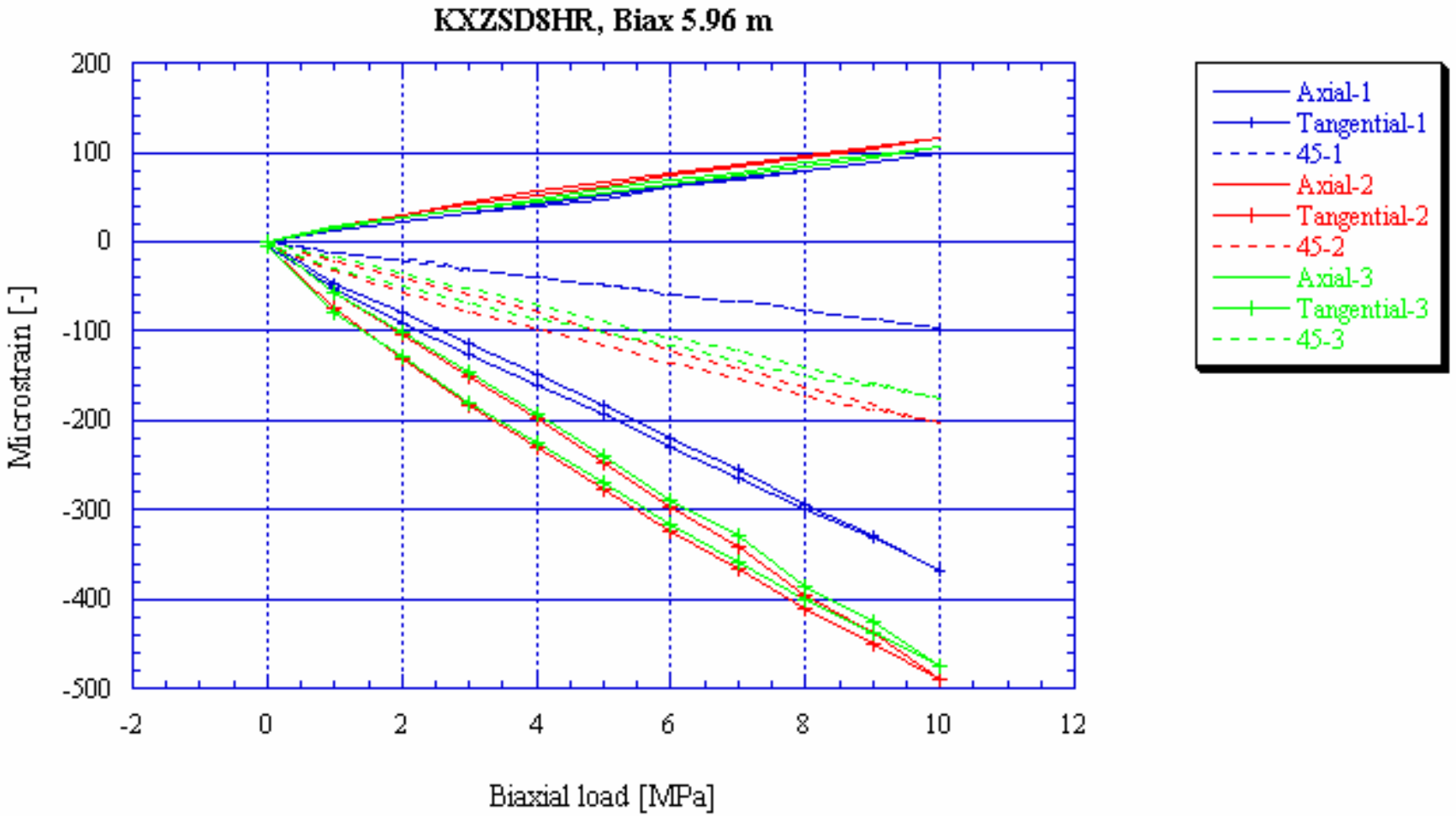
KXZSD8HR, Biax 5.96 m
Microstrain [-]
200
100
0
-100
-200
-300
-400
-500
-2
0
2
4
6
8
10
12
Biaxial load [MPa]
Axial-1
Tangential-1
45-1
Axial-2
Tangential-2
45-2
Axial-3
Tangential-3
45-3

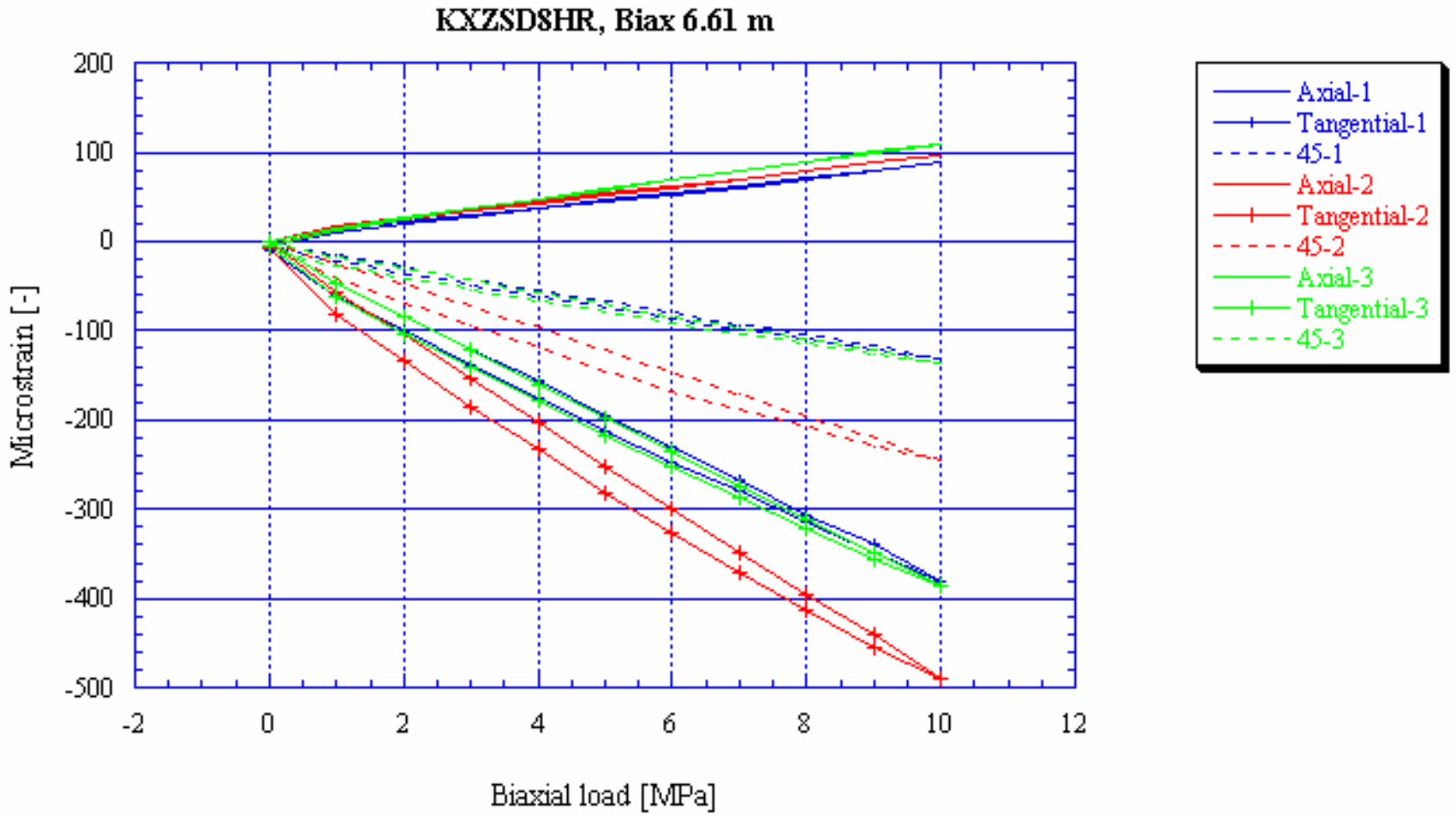
KXZSD8HR, Biax 6.61 m
Microstrain [-]
200
100
0
-100
-200
-300
-400
-500
-2
0
2
4
6
8
10
12
Biaxial load [MPa]
Axial-1
Tangential-1
45-1
Axial-2
Tangential-2
45-2
Axial-3
Tangential-3
45-3

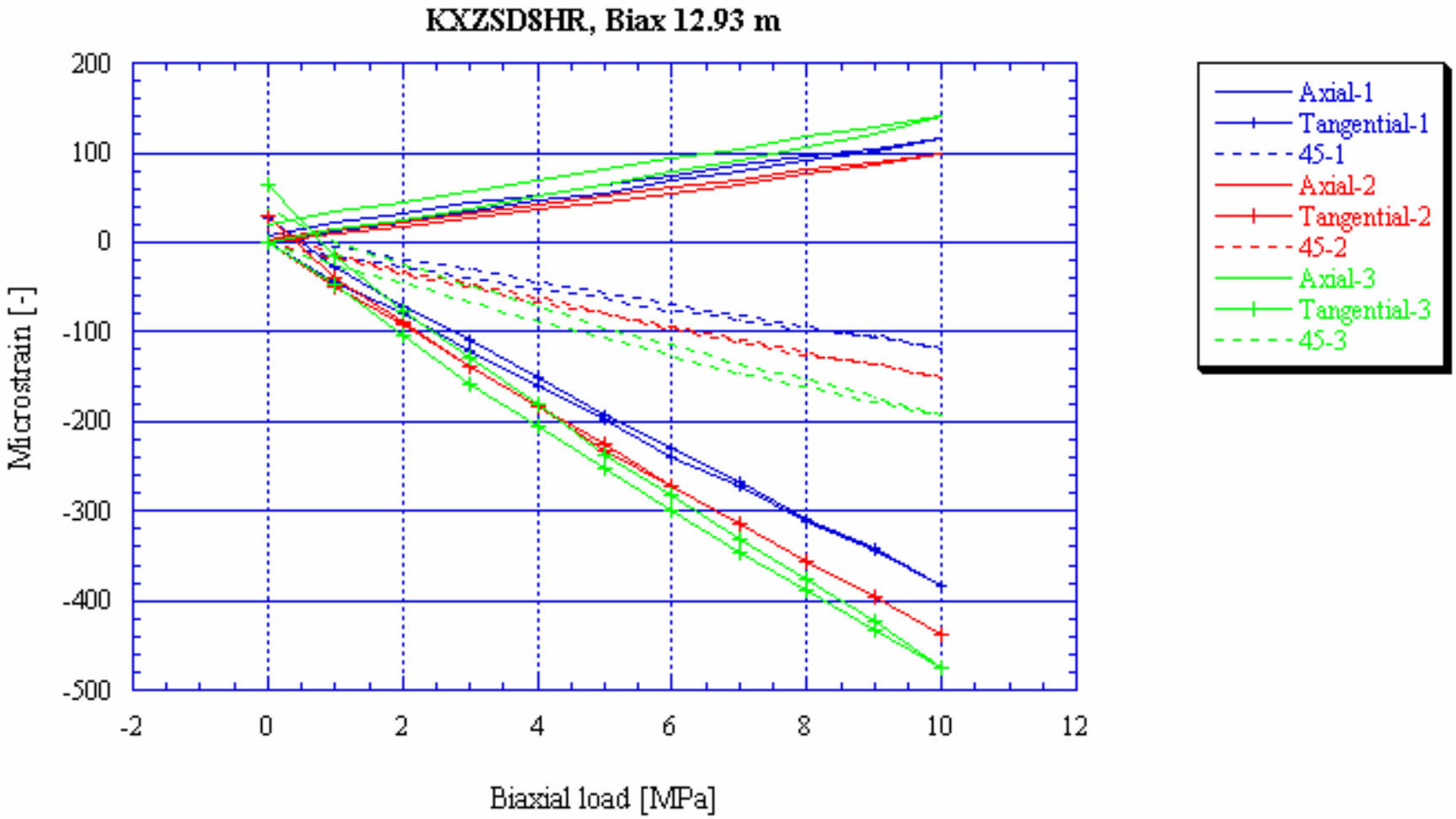
KXZSD8HR, Biax 12.93 m
Microstrain [-]
200
100
0
-100
-200
-300
-400
-500
-2
0
2
4
6
8
10
12
Biaxial load [MPa]
Axial-1
Tangential-1
45-1
Axial-2
Tangential-2
45-2
Axial-3
Tangential-3
45-3

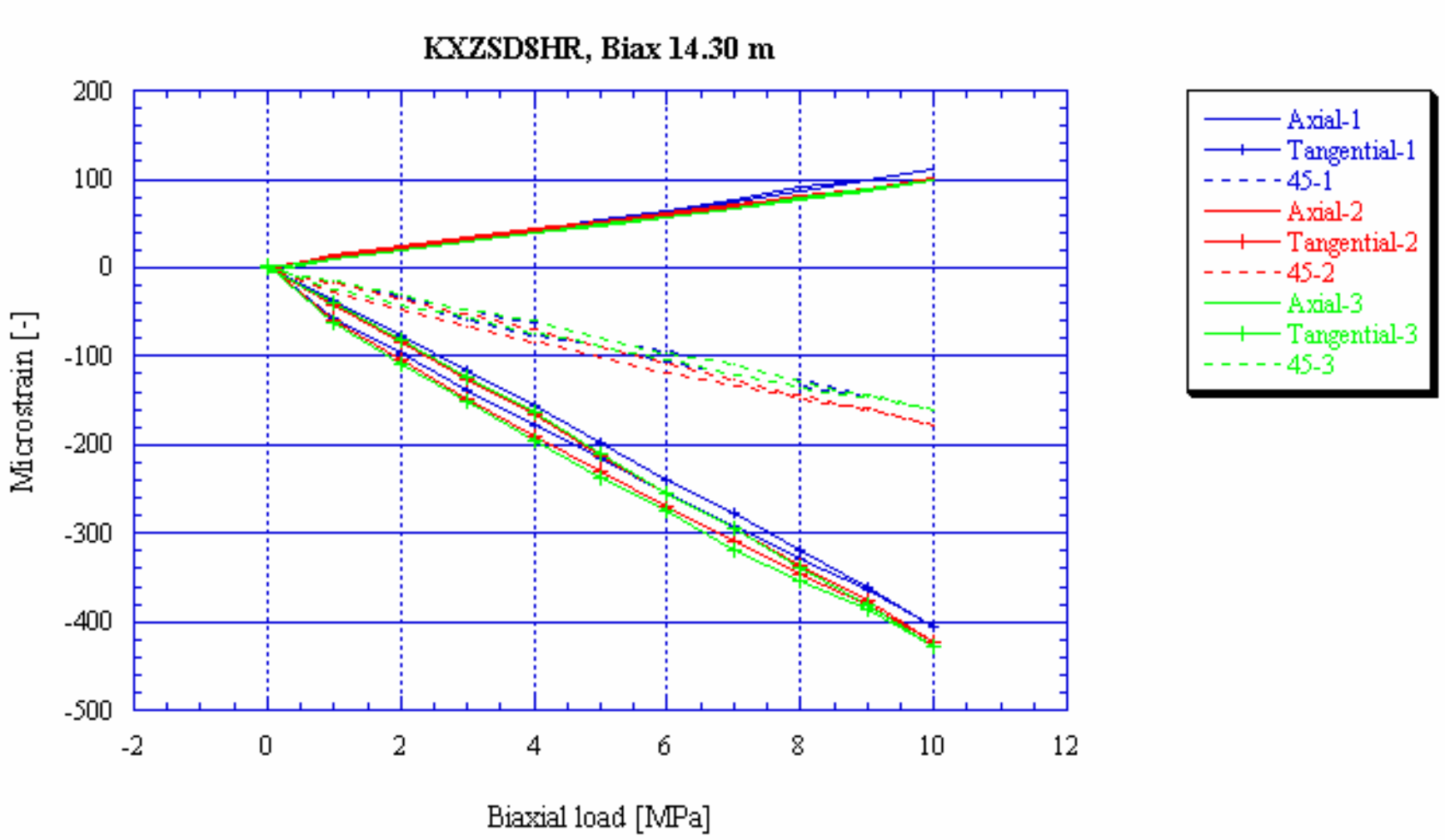
KXZSD8HR, Biax 14.30 m
Microstrain [-]
200
100
0
-100
-200
-300
-400
-500
-2
0
2
4
6
8
10
12
Biaxial load [MPa]
Axial-1
Tangential-1
45-1
Axial-2
Tangential-2
45-2
Axial-3
Tangential-3
45-3

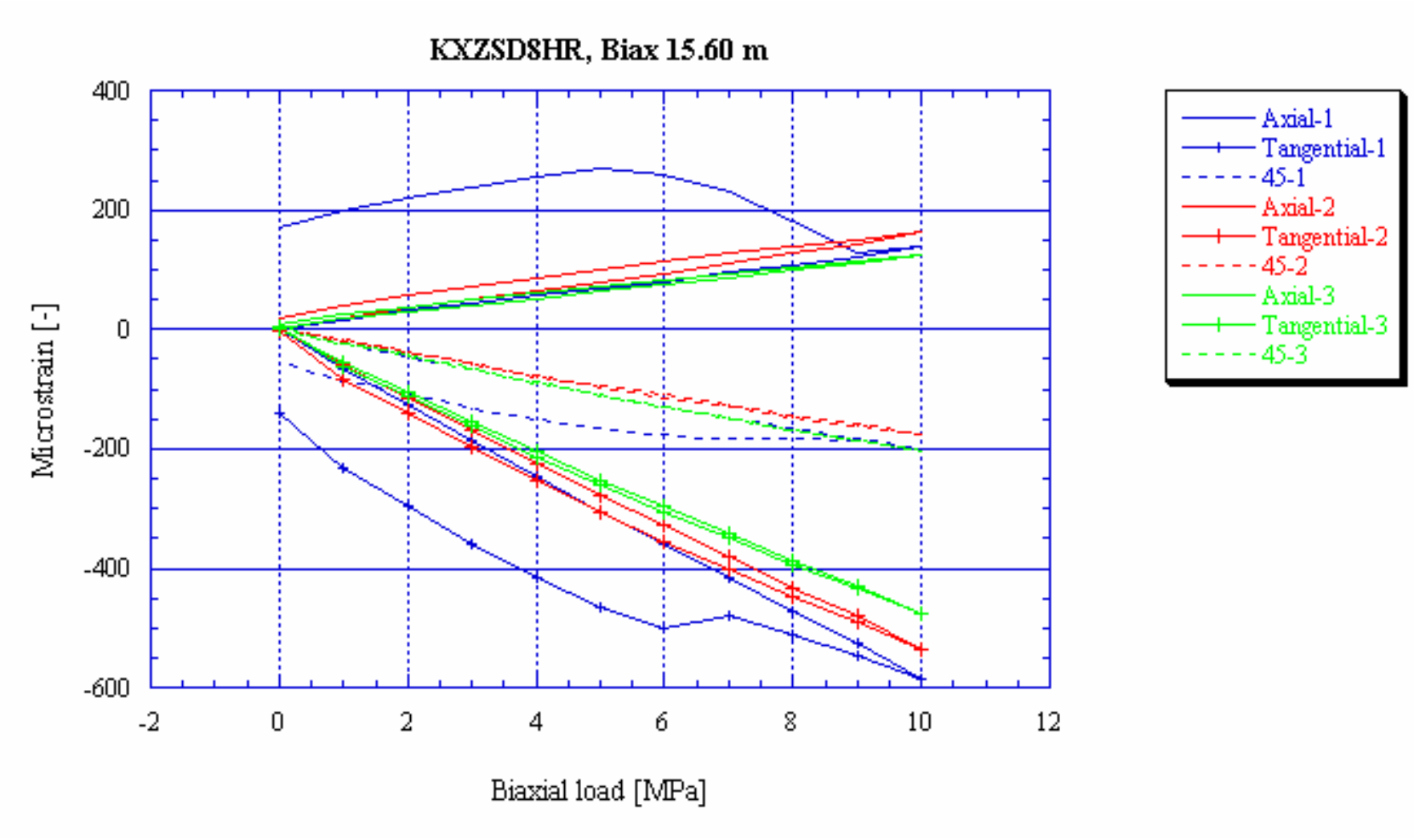
KXZSD8HR, Biax 15.60 m
Microstrain [-]
400
200
0
-200
-400
-600
-2
0
2
4
6
8
10
12
Biaxial load [MPa]
Axial-1
Tangential-1
45-1
Axial-2
Tangential-2
45-2
Axial-3
Tangential-3
45-3

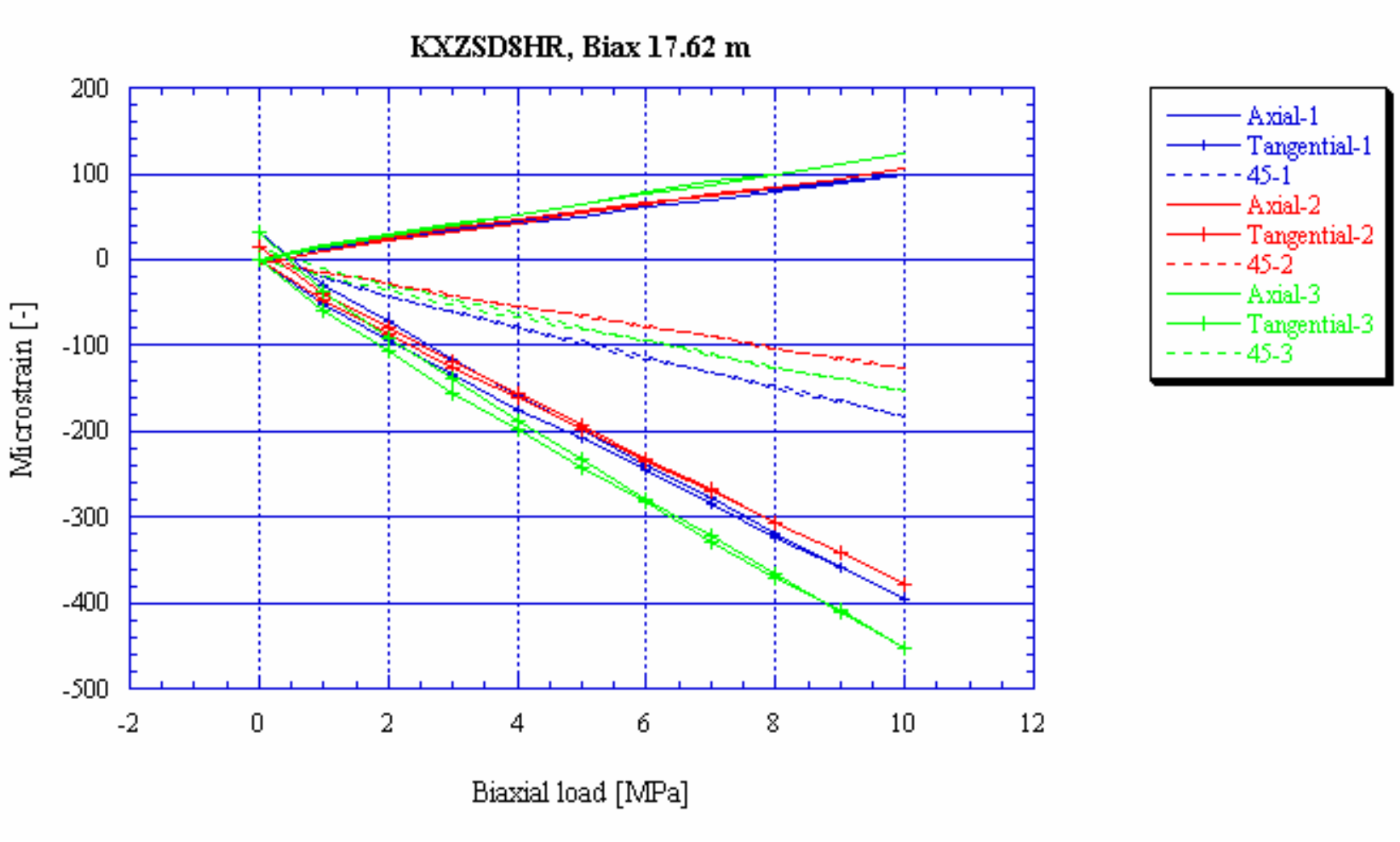
KXZSD8HR, Biax 17.62 m
Microstrain [-]
200
100
0
-100
-200
-300
-400
-500
-2
0
2
4
6
8
10
12
Biaxial load [MPa]
Axial-1
Tangential-1
45-1
Axial-2
Tangential-2
45-2
Axial-3
Tangential-3
45-3

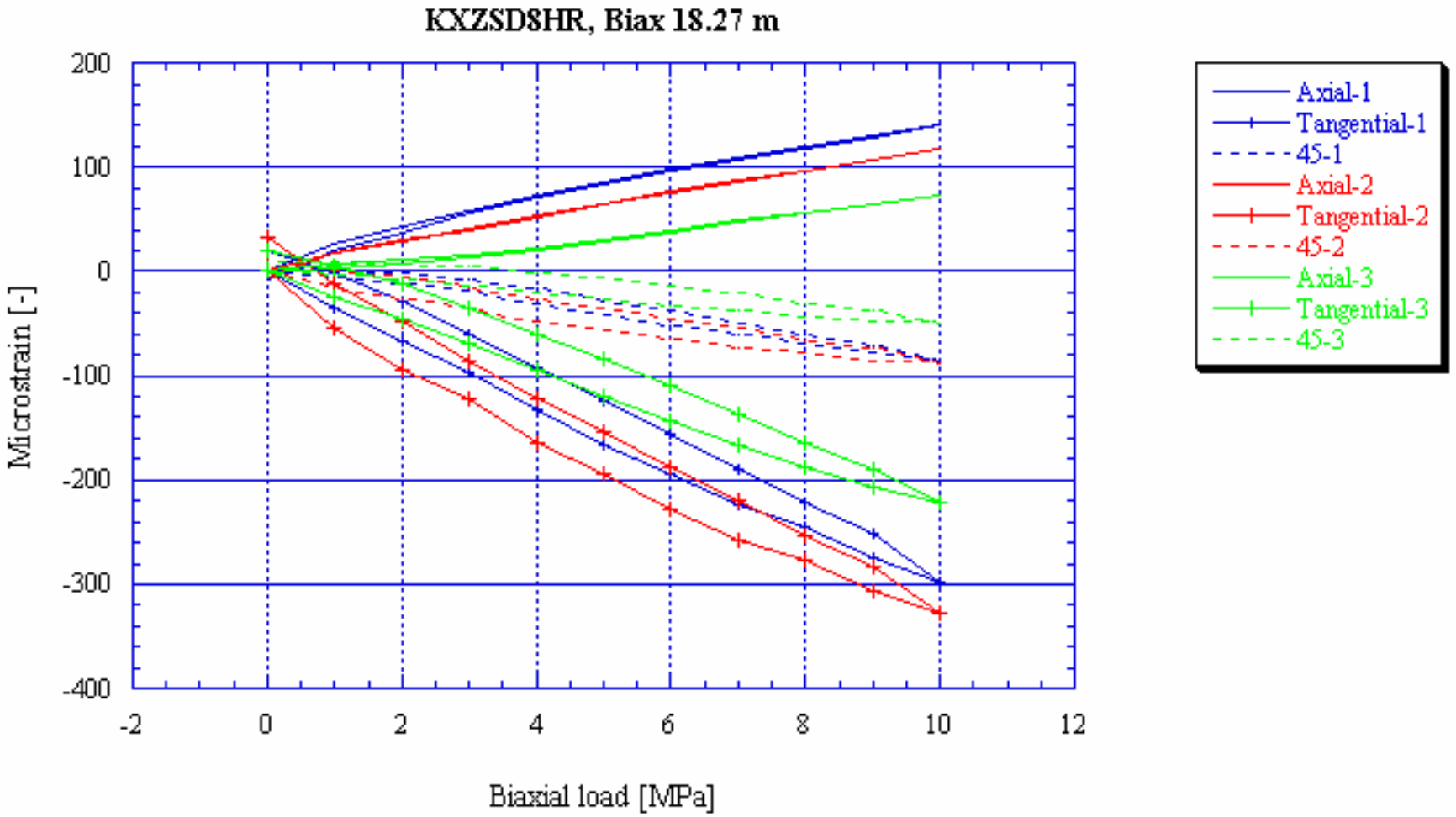
KXZSD8HR, Biax 18.27 m
Microstrain [-]
200
100
0
-100
-200
-300
-400
-2
0
2
4
6
8
10
12
Biaxial load [MPa]
Axial-1
Tangential-1
45-1
Axial-2
Tangential-2
45-2
Axial-3
Tangential-3
45-3

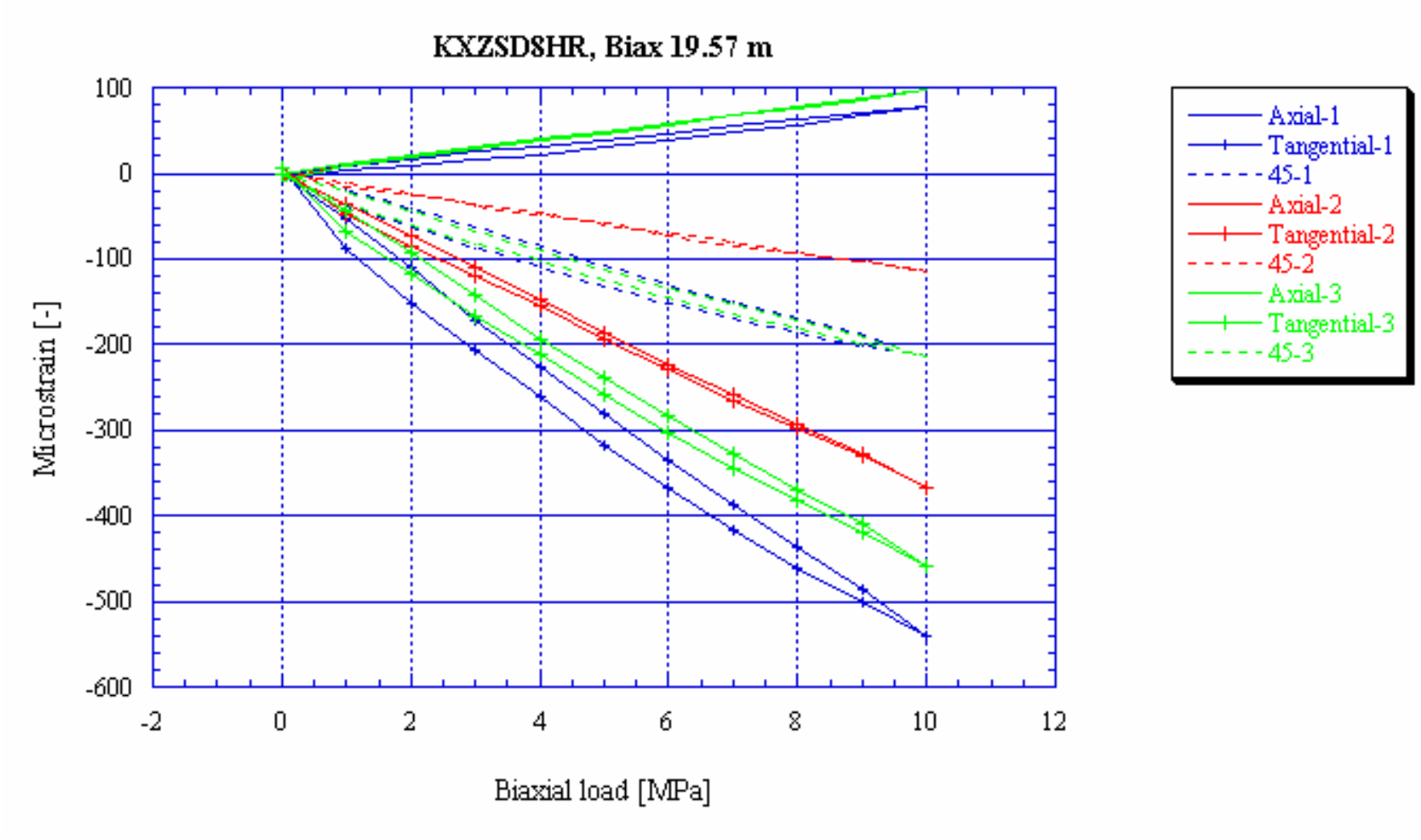
KXZSD8HR, Biax 19.57 m
Microstrain [-]
100
0
-100
-200
-300
-400
-500
-600
-2
0
2
4
6
8
10
12
Biaxial load [MPa]
Axial-1
Tangential-1
45-1
Axial-2
Tangential-2
45-2
Axial-3
Tangential-3
45-3

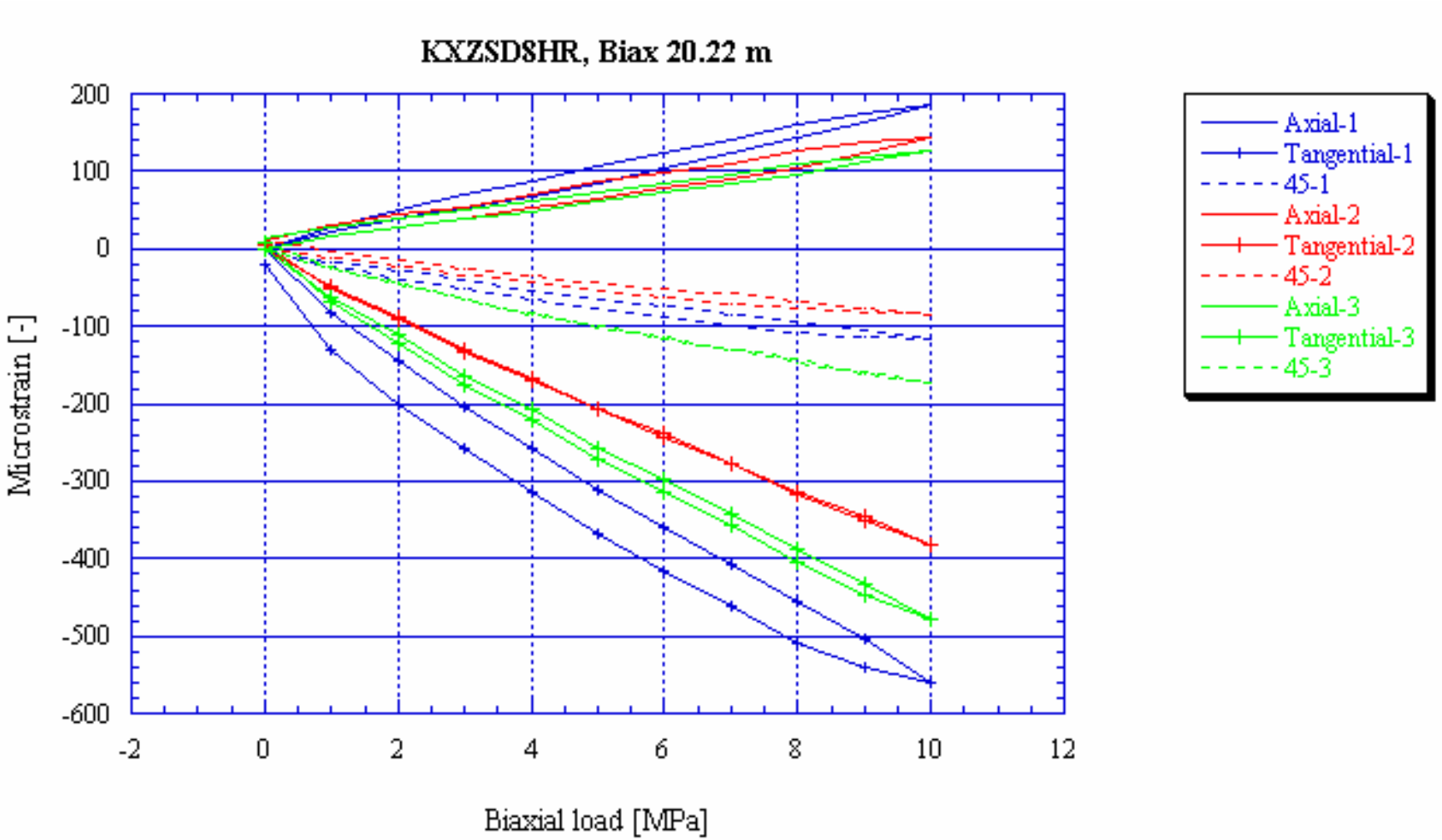
KXZSD8HR, Biax 20.22 m
Microstrain [-]
200
100
0
-100
-200
-300
-400
-500
-600
-2
0
2
4
6
8
10
12
Biaxial load [MPa]
Axial-1
Tangential-1
45-1
Axial-2
Tangential-2
45-2
Axial-3
Tangential-3
45-3

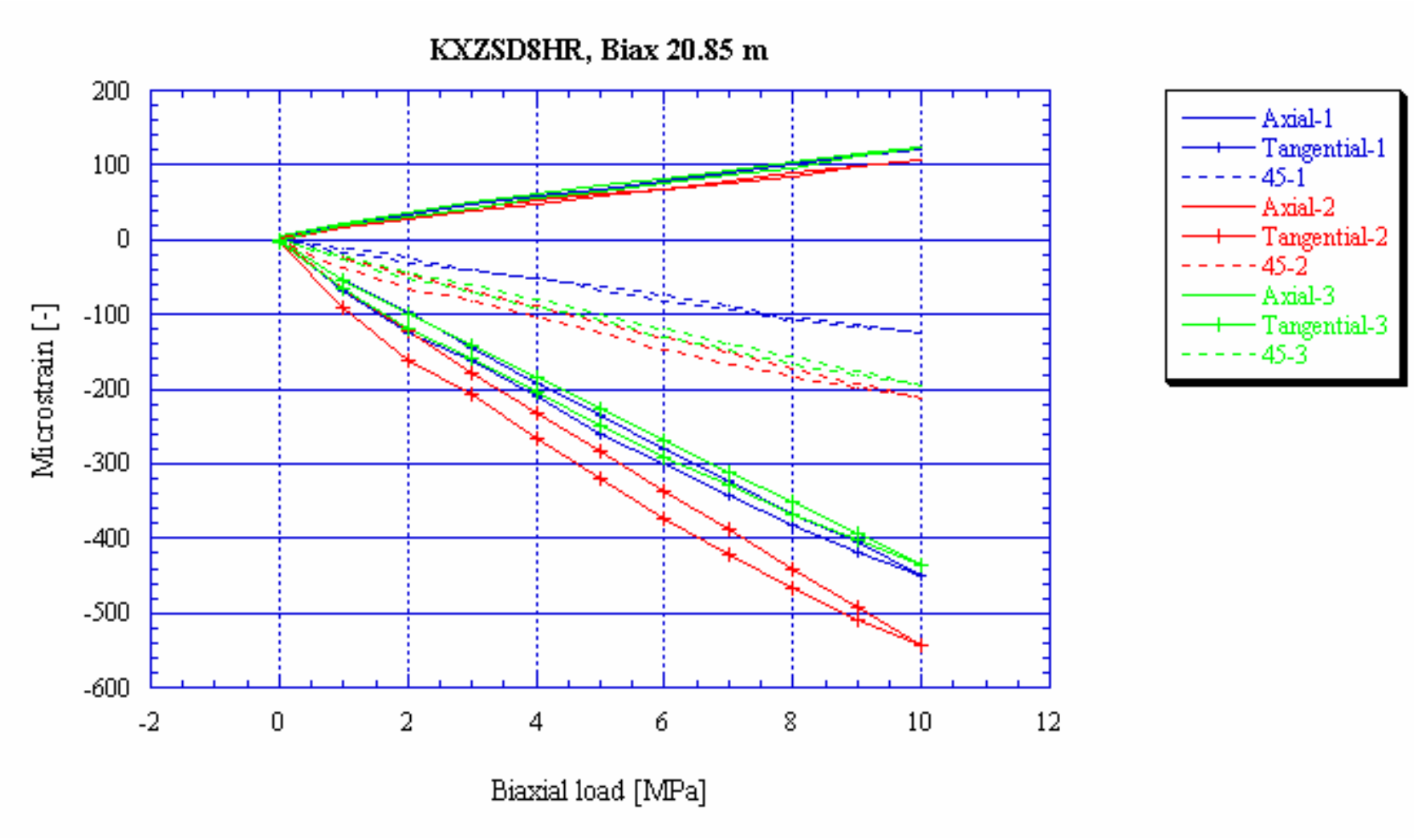
KXZSD8HR, Biax 20.85 m
Microstrain [-]
200
100
0
-100
-200
-300
-400
-500
-600
-2
0
2
4
6
8
10
12
Biaxial load [MPa]
Axial-1
Tangential-1
45-1
Axial-2
Tangential-2
45-2
Axial-3
Tangential-3
45-3

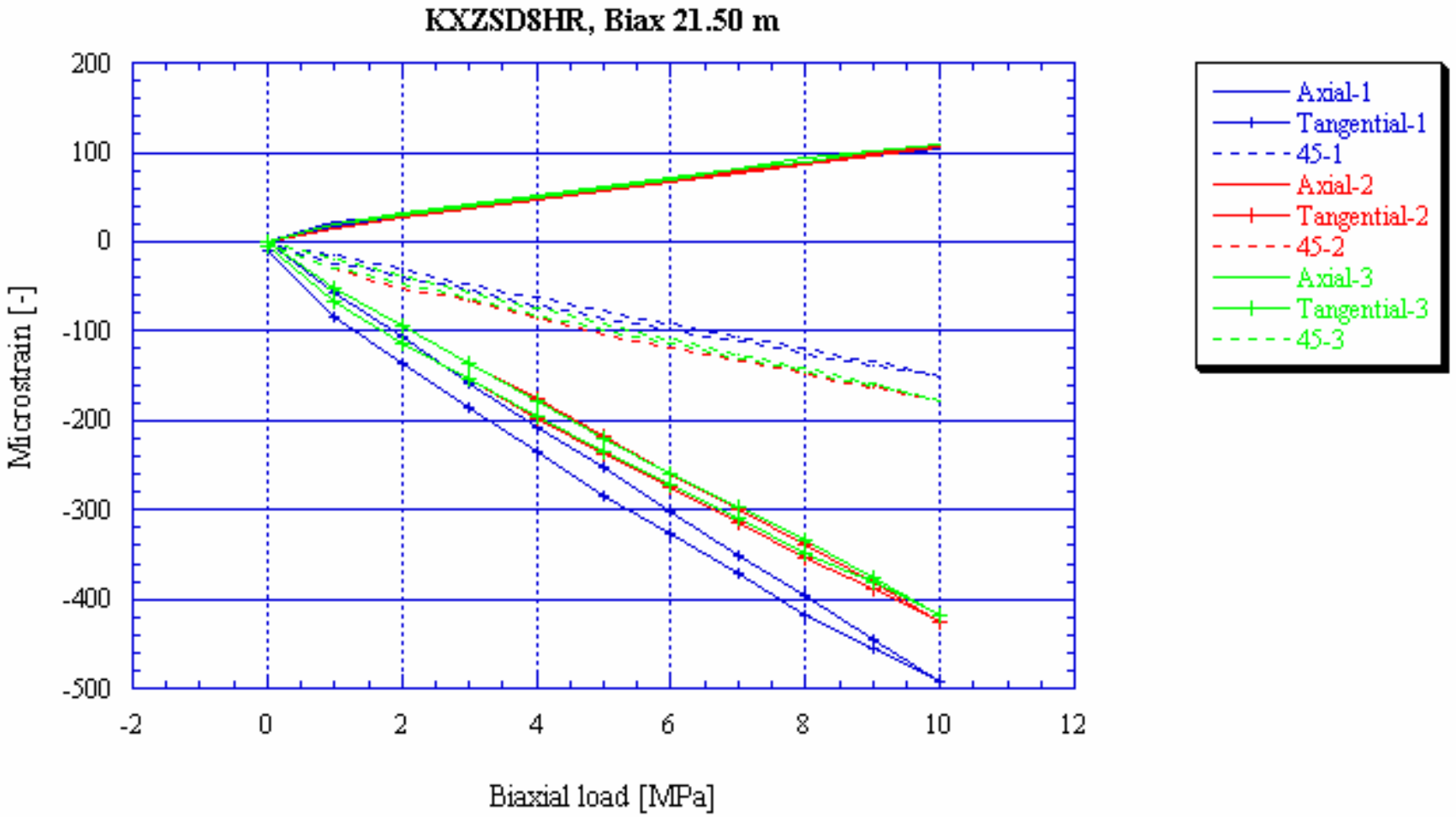
KXZSD8HR, Biax 21.50 m
Microstrain [-]
200
100
0
-100
-200
-300
-400
-500
-2
0
2
4
6
8
10
12
Biaxial load [MPa]
Axial-1
Tangential-1
45-1
Axial-2
Tangential-2
45-2
Axial-3
Tangential-3
45-3

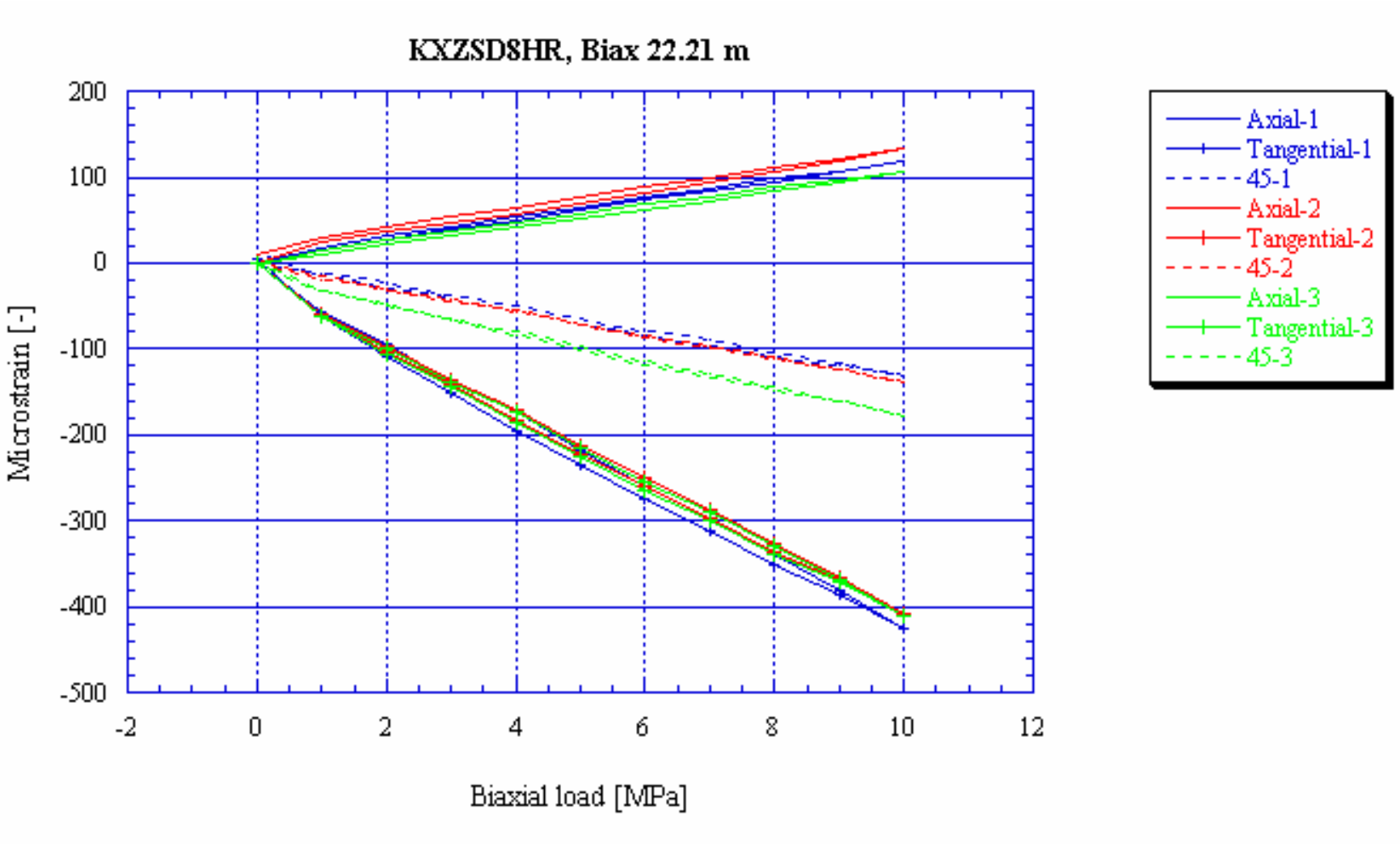
KXZSD8HR, Biax 22.21 m
Microstrain [-]
200
100
0
-100
-200
-300
-400
-500
-2
0
2
4
6
8
10
12
Biaxial load [MPa]
Axial-1
Tangential-1
45-1
Axial-2
Tangential-2
45-2
Axial-3
Tangential-3
45-3

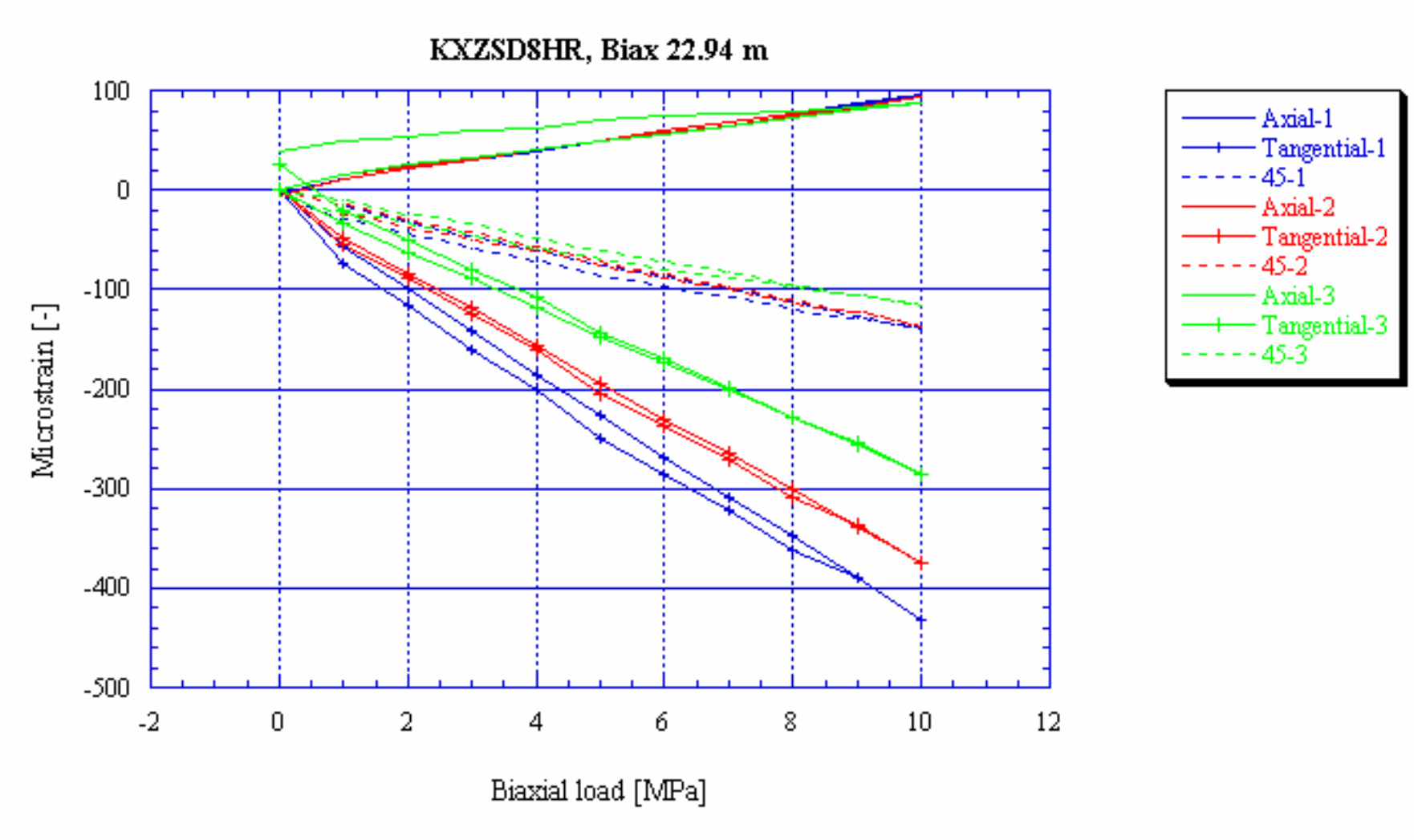
KXZSD8HR, Biax 22.94 m
Microstrain [-]
100
0
-100
-200
-300
-400
-500
-2
0
2
4
6
8
10
12
Biaxial load [MPa]
Axial-1
Tangential-1
45-1
Axial-2
Tangential-2
45-2
Axial-3
Tangential-3
45-3

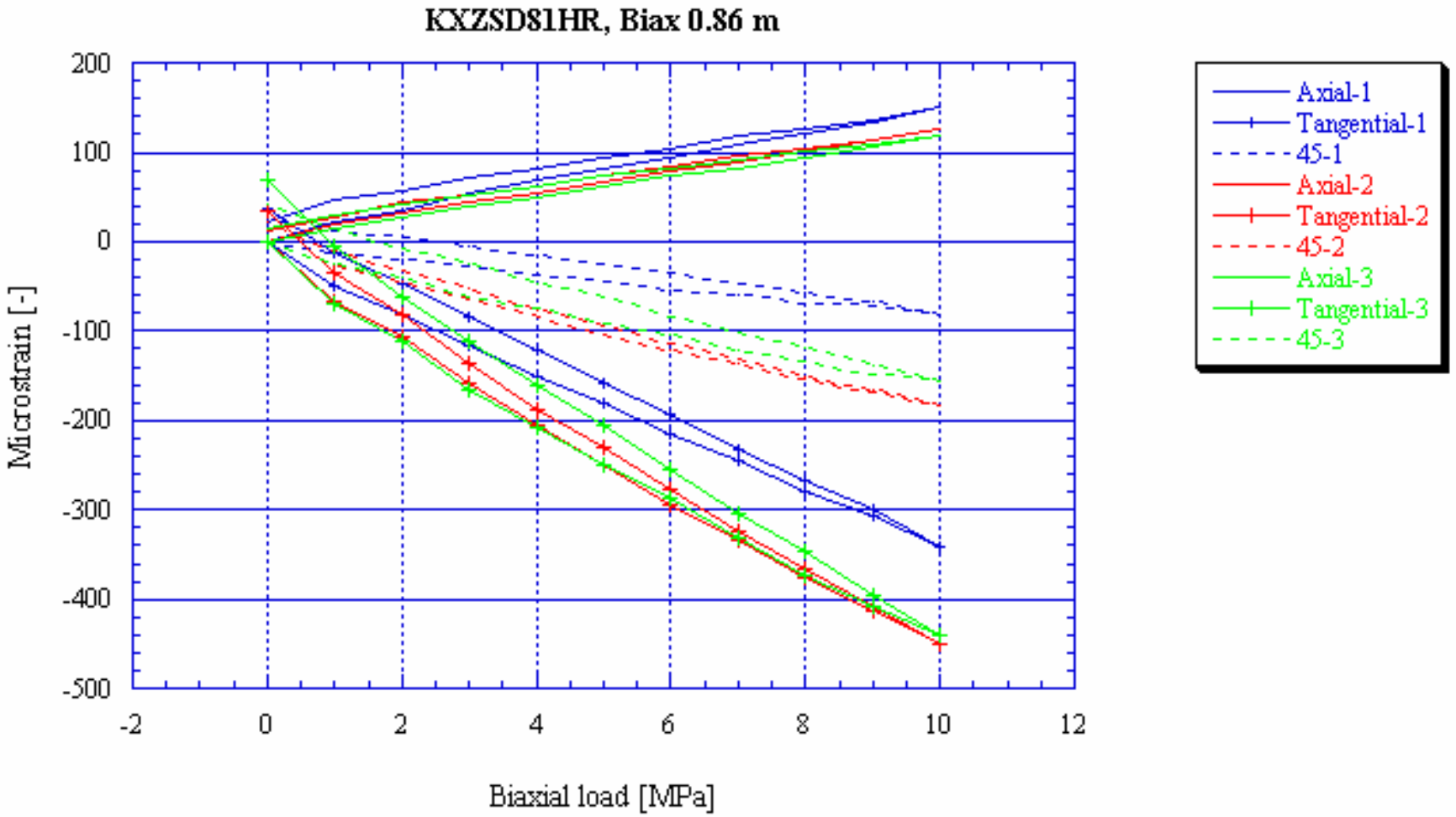
KXZSD81HR, Biax 0.86 m
Microstrain [-]
200
100
0
-100
-200
-300
-400
-500
-2
0
2
4
6
8
10
12
Biaxial load [MPa]
Axial-1
Tangential-1
45-1
Axial-2
Tangential-2
45-2
Axial-3
Tangential-3
45-3

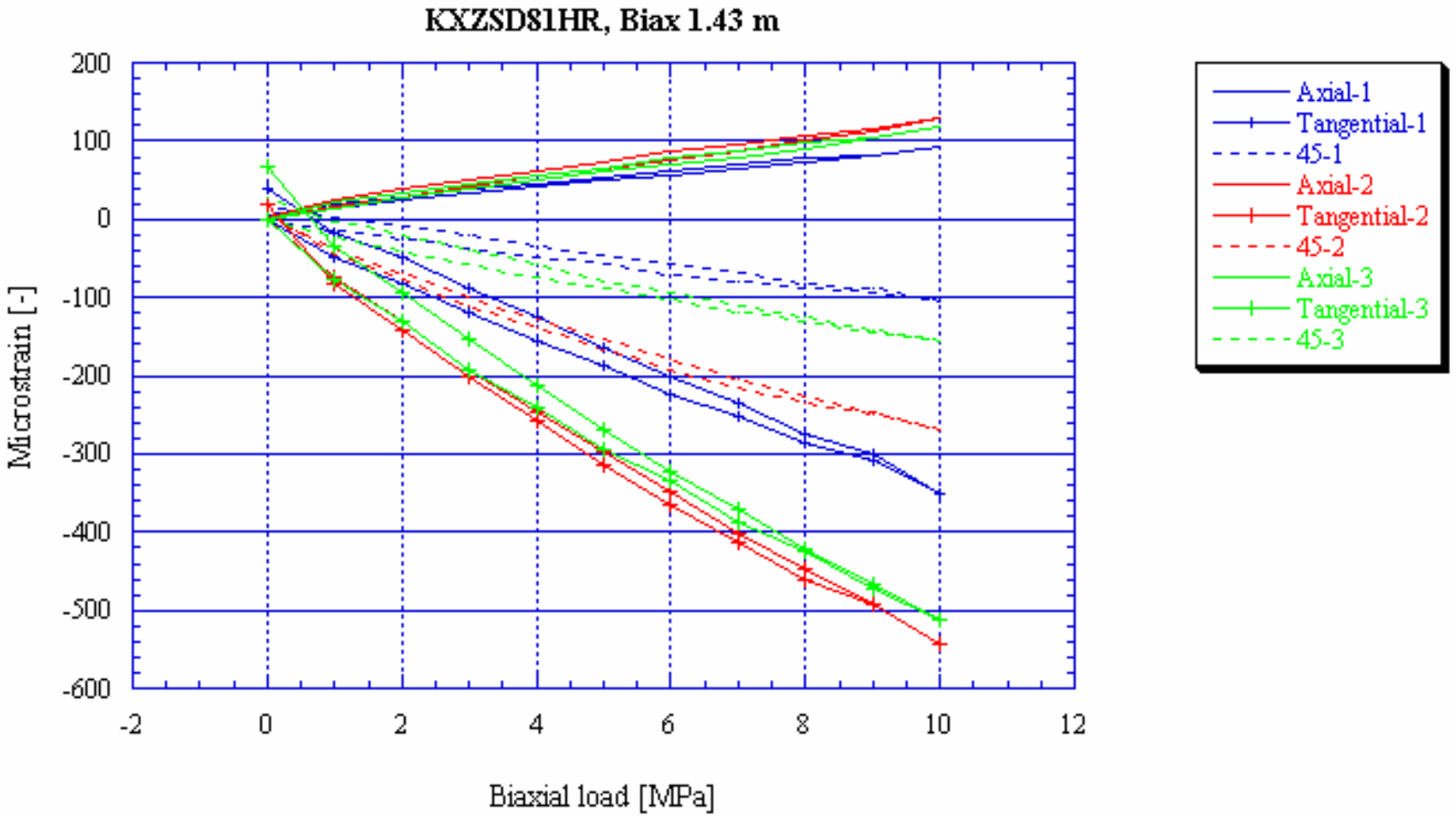
KXZSD81HR, Biax 1.43 m
Microstrain [-]
200
100
0
-100
-200
-300
-400
-500
-600
-2
0
2
4
6
8
10
12
Biaxial load [MPa]
Axial-1
Tangential-1
45-1
Axial-2
Tangential-2
45-2
Axial-3
Tangential-3
45-3

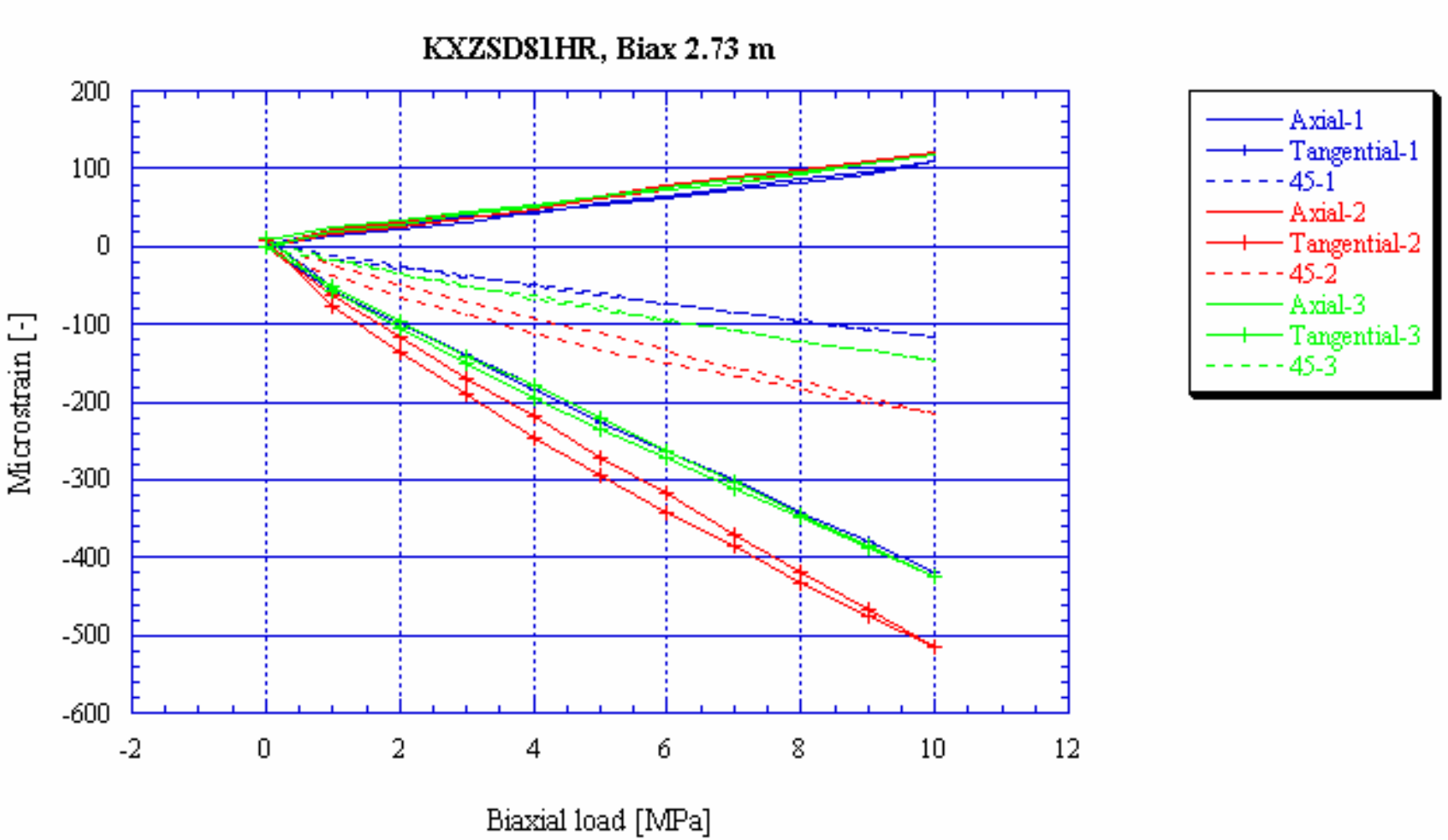
KXZSD81HR, Biax 2.73 m
Microstrain [-]
200
100
0
-100
-200
-300
-400
-500
-600
-2
0
2
4
6
8
10
12
Biaxial load [MPa]
Axial-1
Tangential-1
45-1
Axial-2
Tangential-2
45-2
Axial-3
Tangential-3
45-3

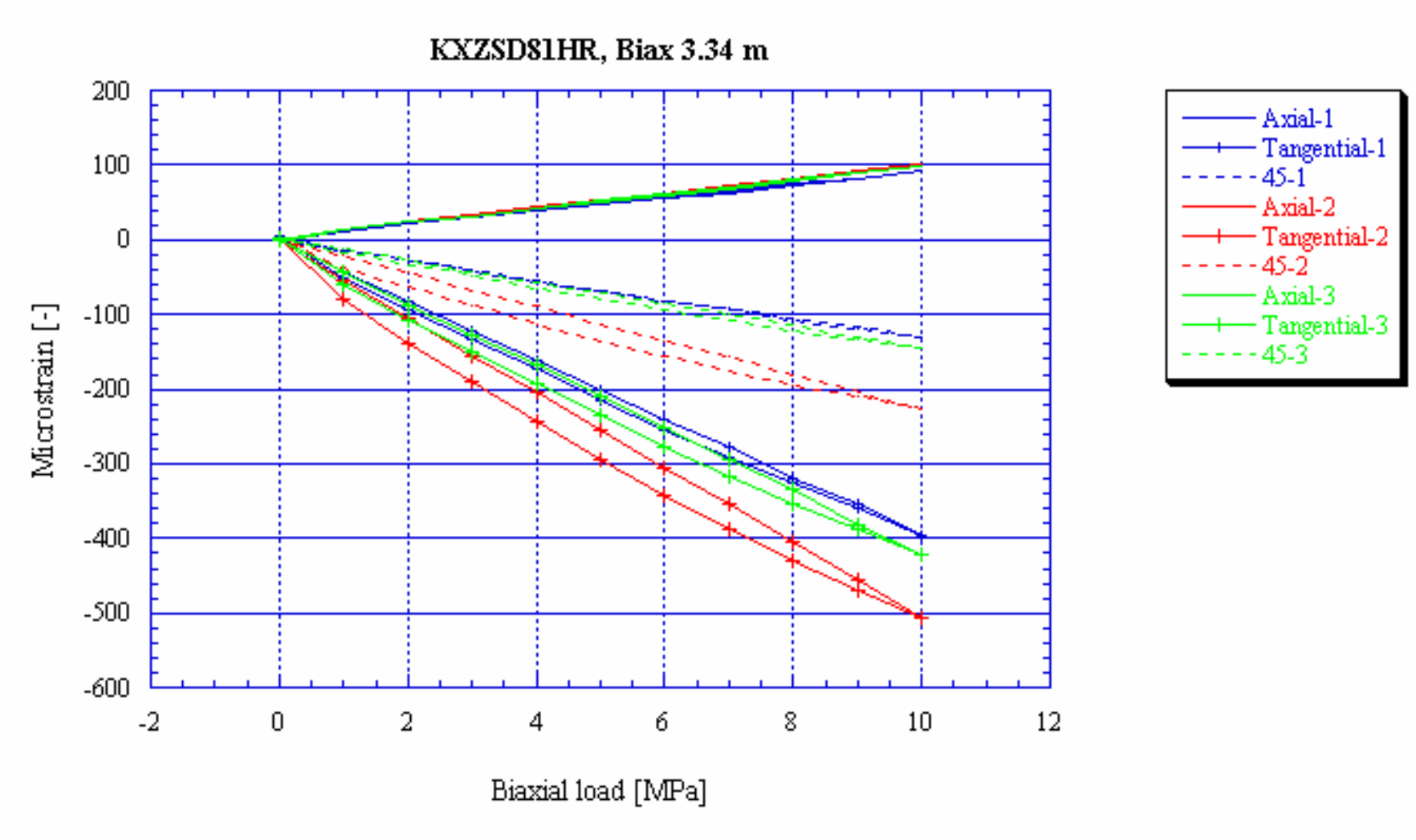
KXZSD81HR, Biax 3.34 m
Microstrain [-]
200
100
0
-100
-200
-300
-400
-500
-600
-2
0
2
4
6
8
10
12
Biaxial load [MPa]
Axial-1
Tangential-1
45-1
Axial-2
Tangential-2
45-2
Axial-3
Tangential-3
45-3

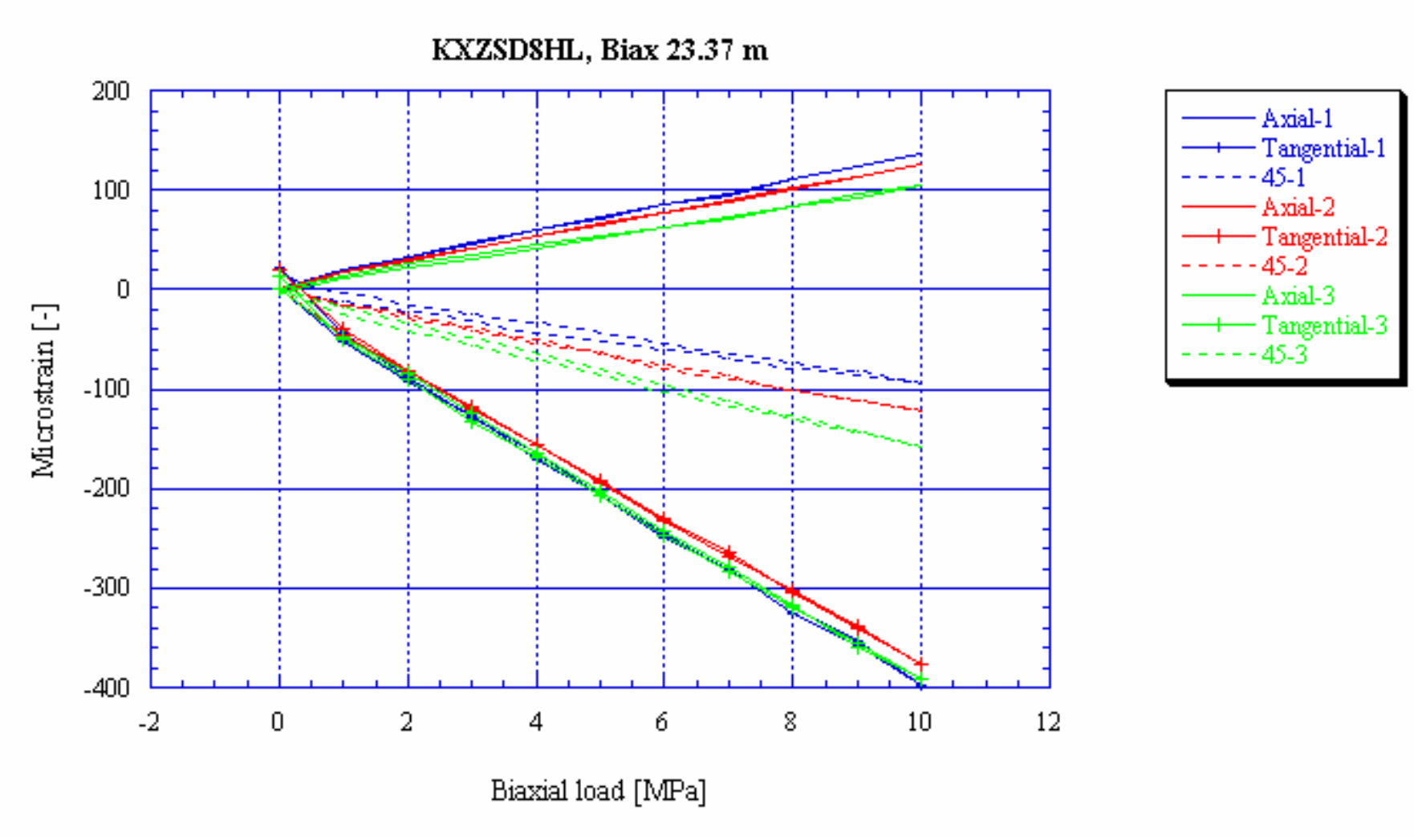
KXZSD8HL, Biax 23.37 m
Microstrain [-]
200
100
0
-100
-200
-300
-400
-2
0
2
4
6
8
10
12
Biaxial load [MPa]
Axial-1
Tangential-1
45-1
Axial-2
Tangential-2
45-2
Axial-3
Tangential-3
45-3

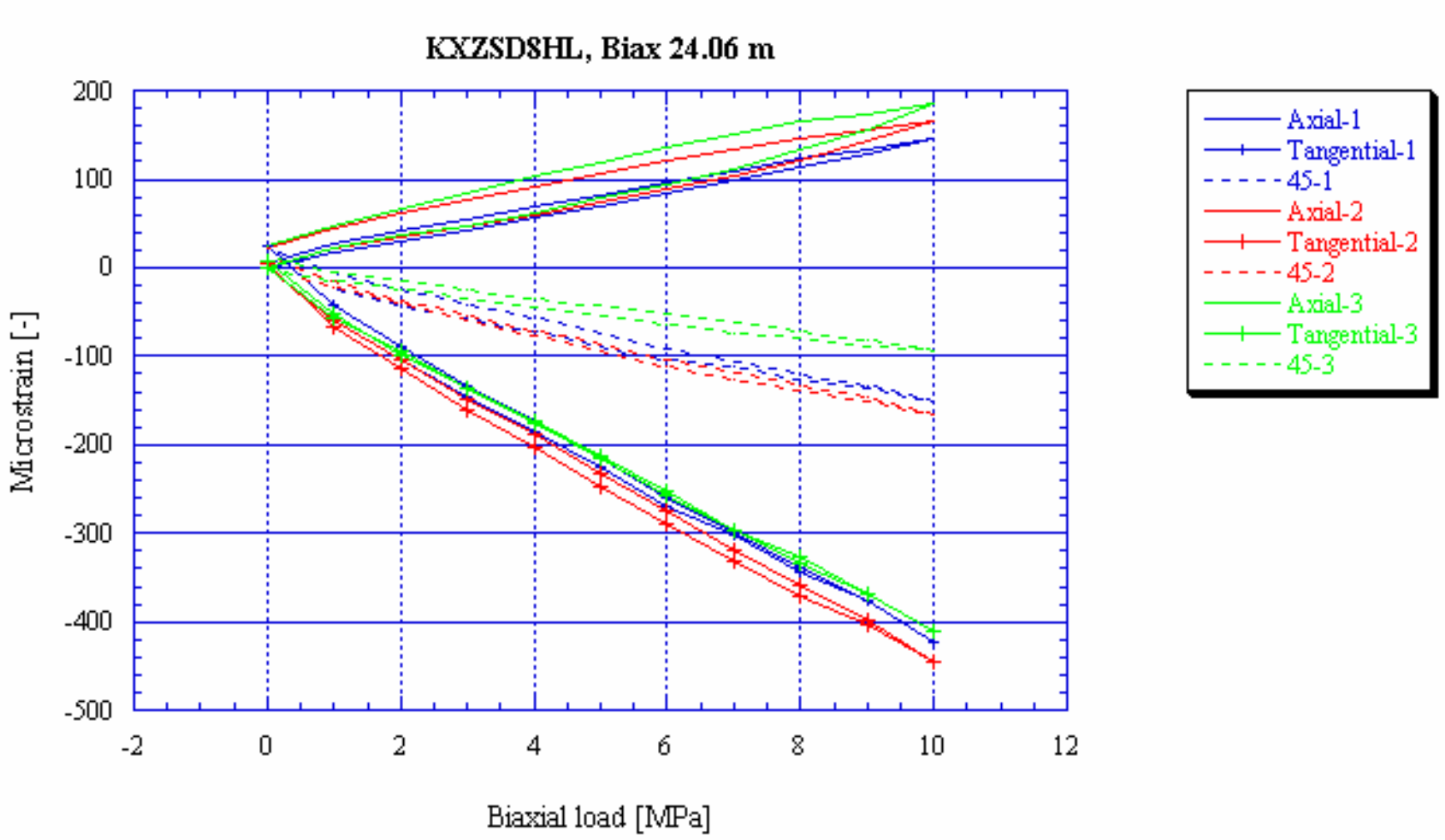
KXZSD8HL, Biax 24.06 m
Microstrain [-]
200
100
0
-100
-200
-300
-400
-500
-2
0
2
4
6
8
10
12
Biaxial load [MPa]
Axial-1
Tangential-1
45-1
Axial-2
Tangential-2
45-2
Axial-3
Tangential-3
45-3

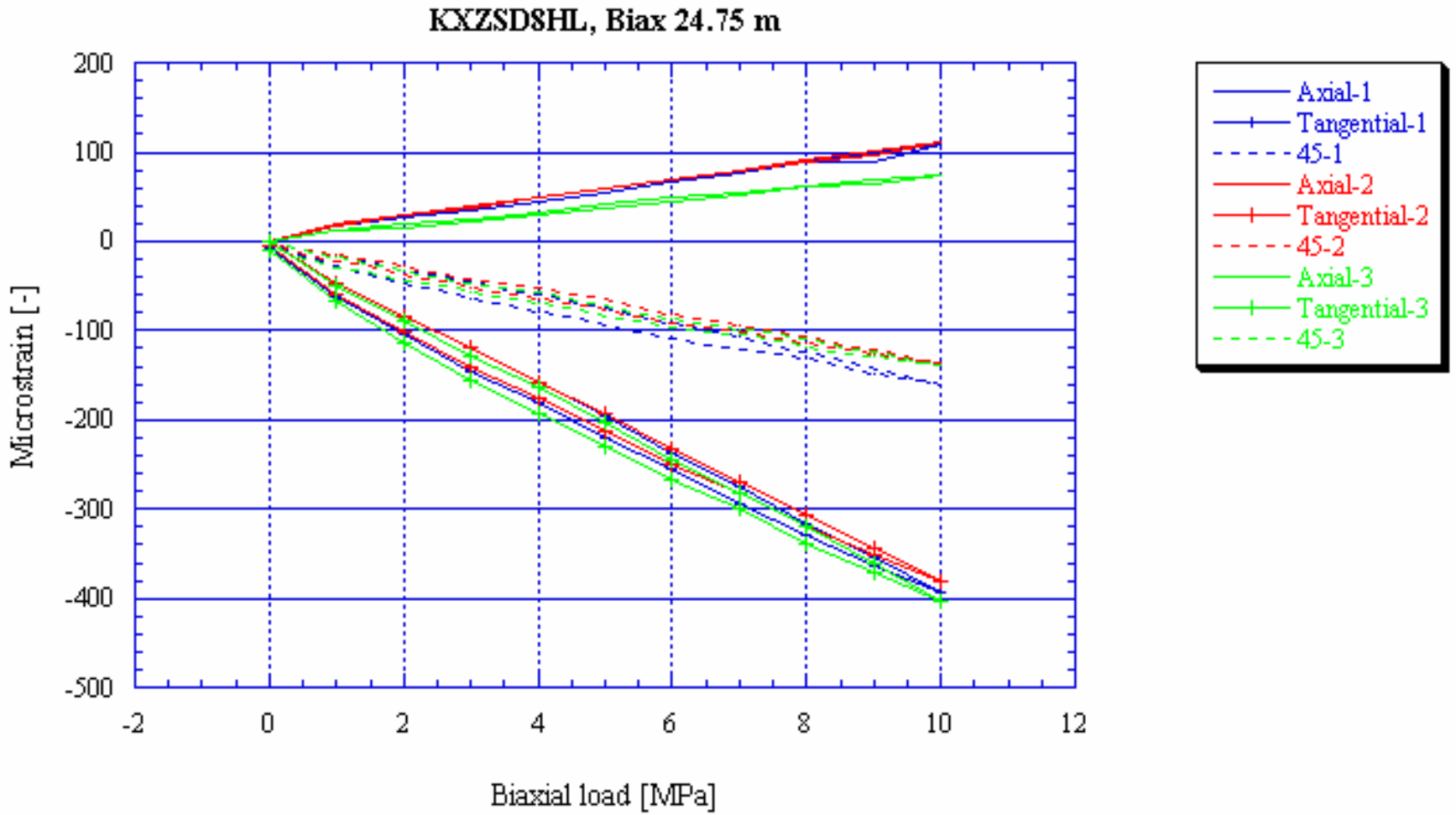
KXZSD8HL, Biax 24.75 m
Microstrain [-]
200
100
0
-100
-200
-300
-400
-500
-2
0
2
4
6
8
10
12
Biaxial load [MPa]
Axial-1
Tangential-1
45-1
Axial-2
Tangential-2
45-2
Axial-3
Tangential-3
45-3

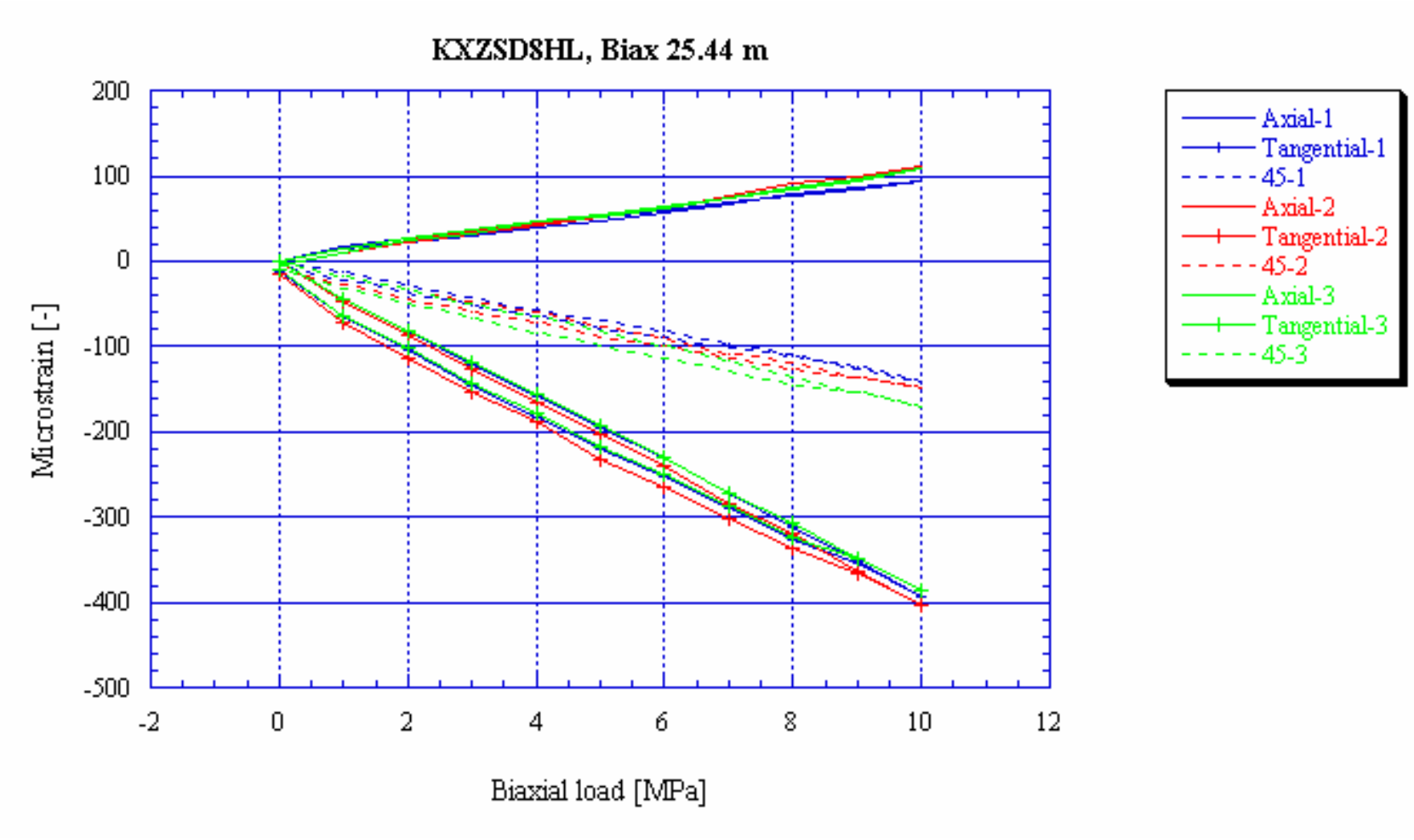
KXZSD8HL, Biax 25.44 m
Microstrain [-]
200
100
0
-100
-200
-300
-400
-500
-2
0
2
4
6
8
10
12
Biaxial load [MPa]
Axial-1
Tangential-1
45-1
Axial-2
Tangential-2
45-2
Axial-3
Tangential-3
45-3

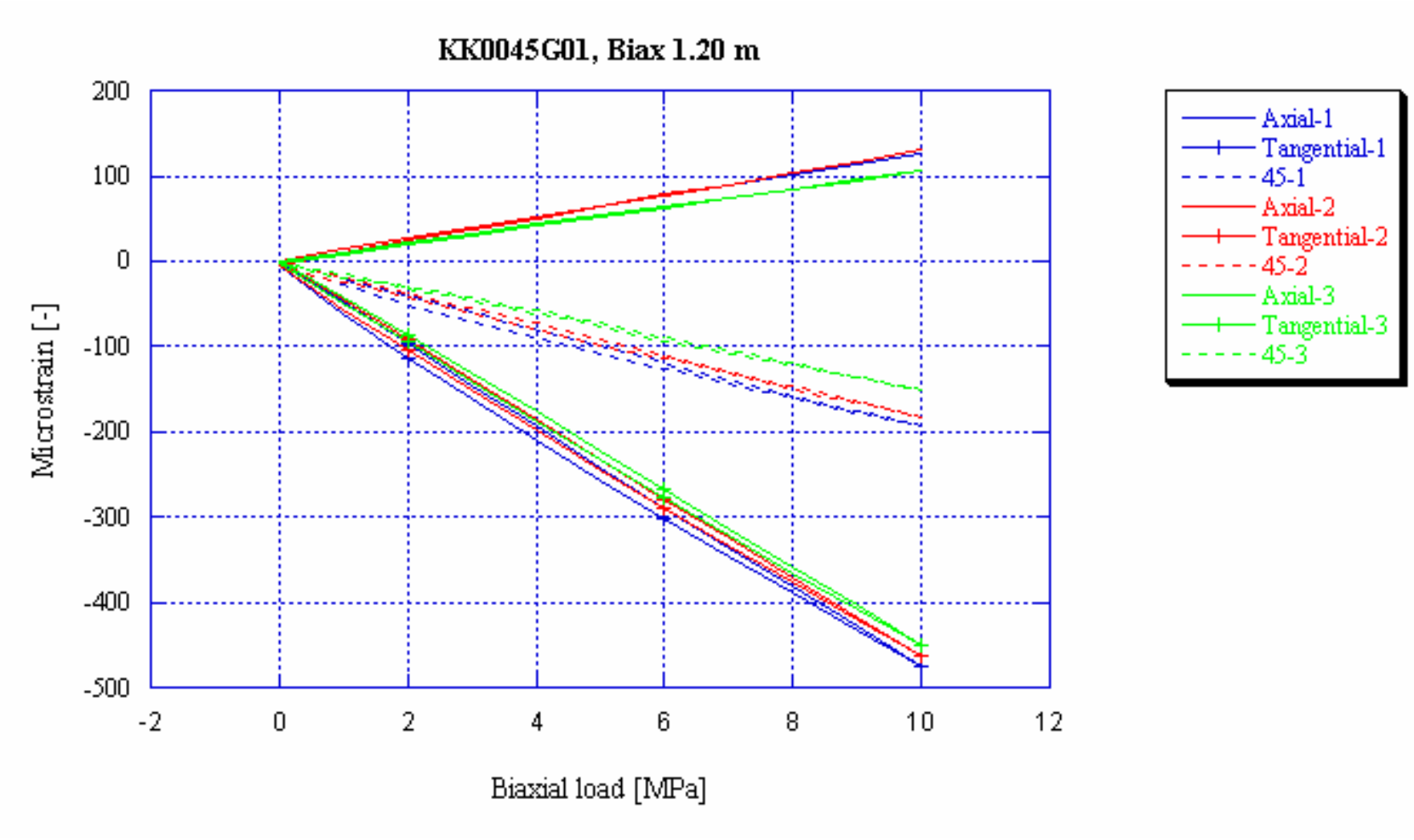
KK0045G01, Biax 1.20 m
Microstrain [-]
200
100
0
-100
-200
-300
-400
-500
-2
0
2
4
6
8
10
12
Biaxial load [MPa]
Axial-1
Tangential-1
45-1
Axial-2
Tangential-2
45-2
Axial-3
Tangential-3
45-3

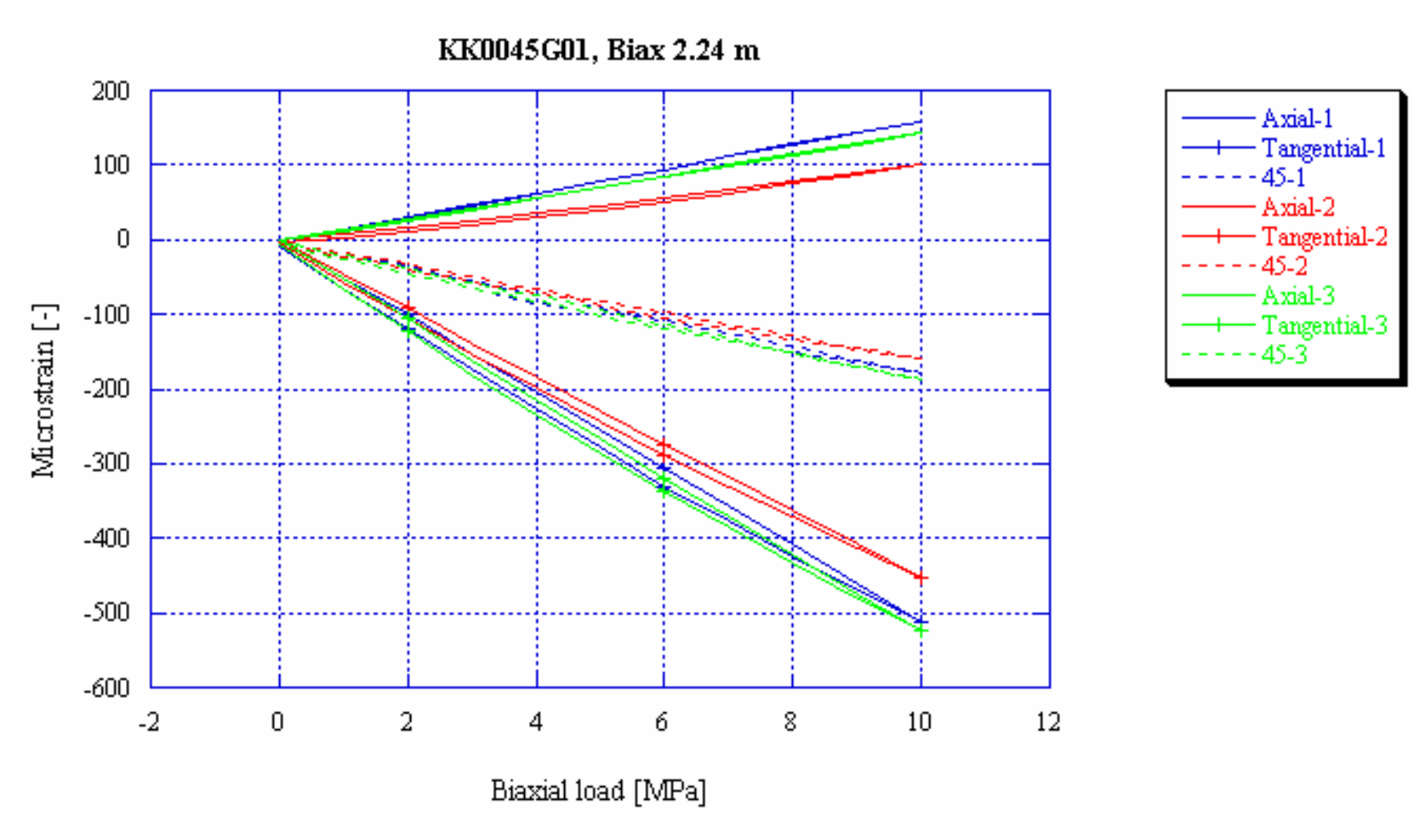
KK0045G01, Biax 2.24 m
Microstrain [-]
200
100
0
-100
-200
-300
-400
-500
-600
-2
0
2
4
6
8
10
12
Biaxial load [MPa]
Axial-1
Tangential-1
45-1
Axial-2
Tangential-2
45-2
Axial-3
Tangential-3
45-3

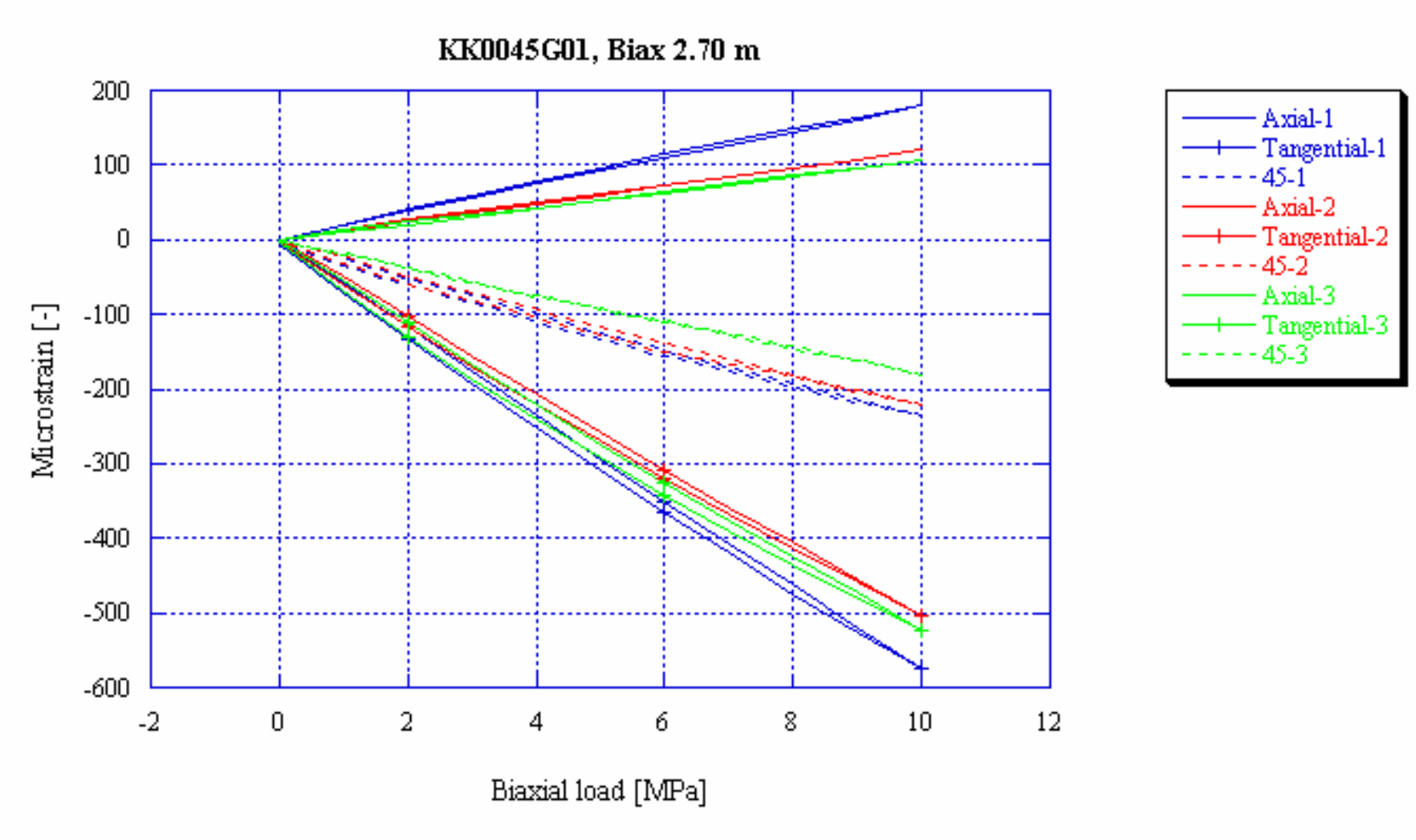
KK0045G01, Biax 2.70 m
Microstrain [-]
200
100
0
-100
-200
-300
-400
-500
-600
-2
0
2
4
6
8
10
12
Biaxial load [MPa]
Axial-1
Tangential-1
45-1
Axial-2
Tangential-2
45-2
Axial-3
Tangential-3
45-3

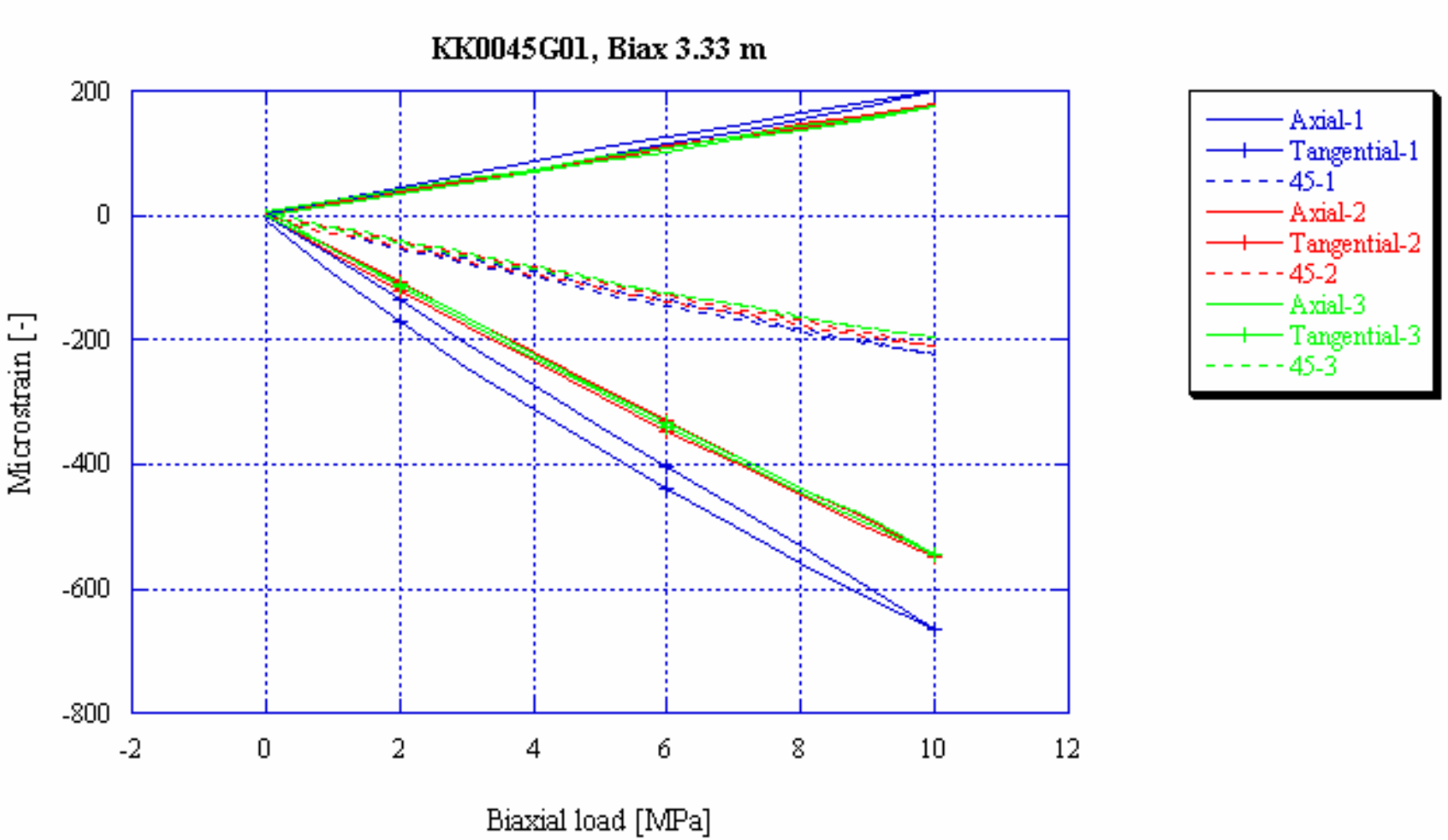
KK0045G01, Biax 3.33 m
Microstrain [-]
200
0
-200
-400
-600
-800
-2
0
2
4
6
8
10
12
Biaxial load [MPa]
Axial-1
Tangential-1
45-1
Axial-2
Tangential-2
45-2
Axial-3
Tangential-3
45-3

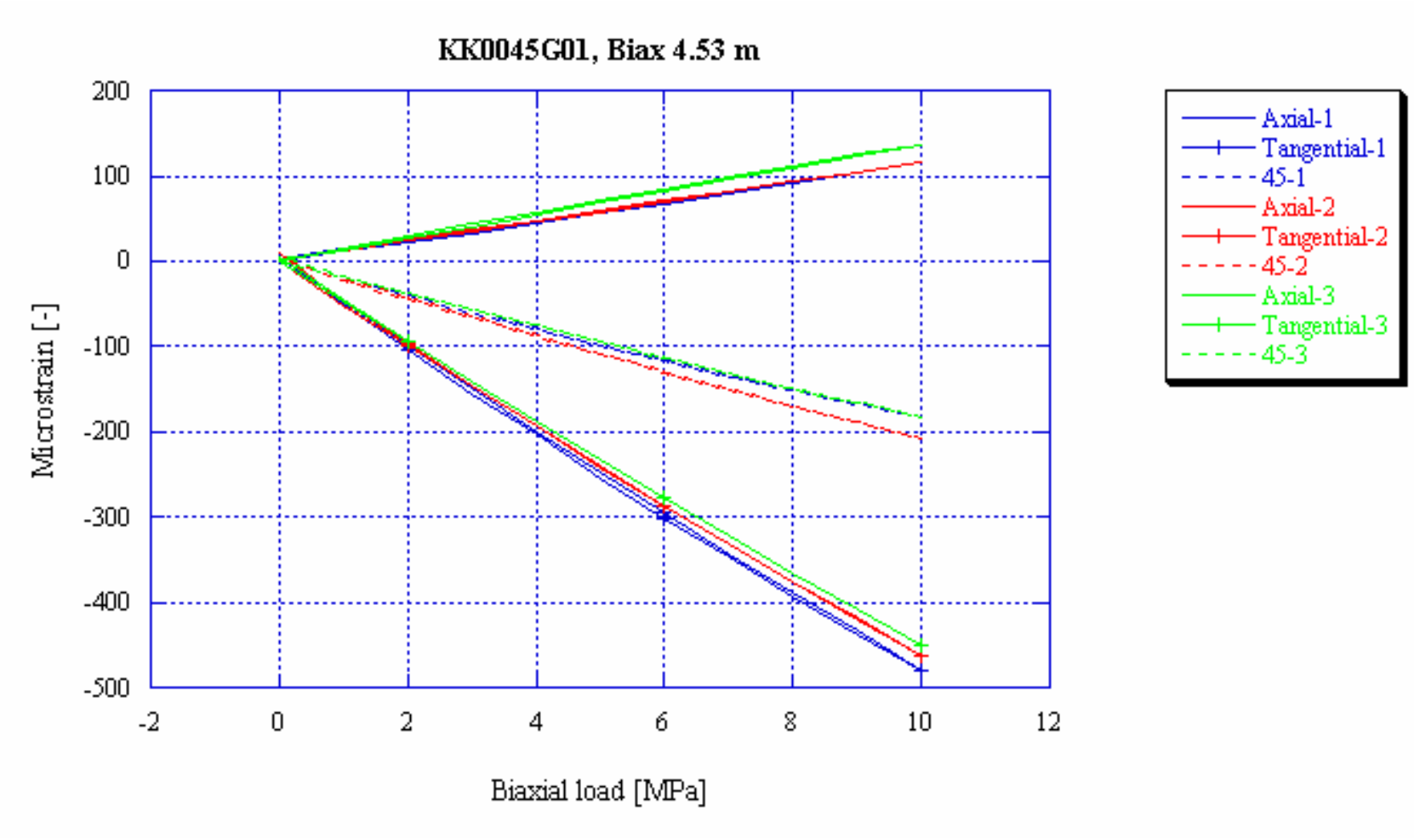
KK0045G01, Biax 4.53 m
Microstrain [-]
200
100
0
-100
-200
-300
-400
-500
-2
0
2
4
6
8
10
12
Biaxial load [MPa]
Axial-1
Tangential-1
45-1
Axial-2
Tangential-2
45-2
Axial-3
Tangential-3
45-3

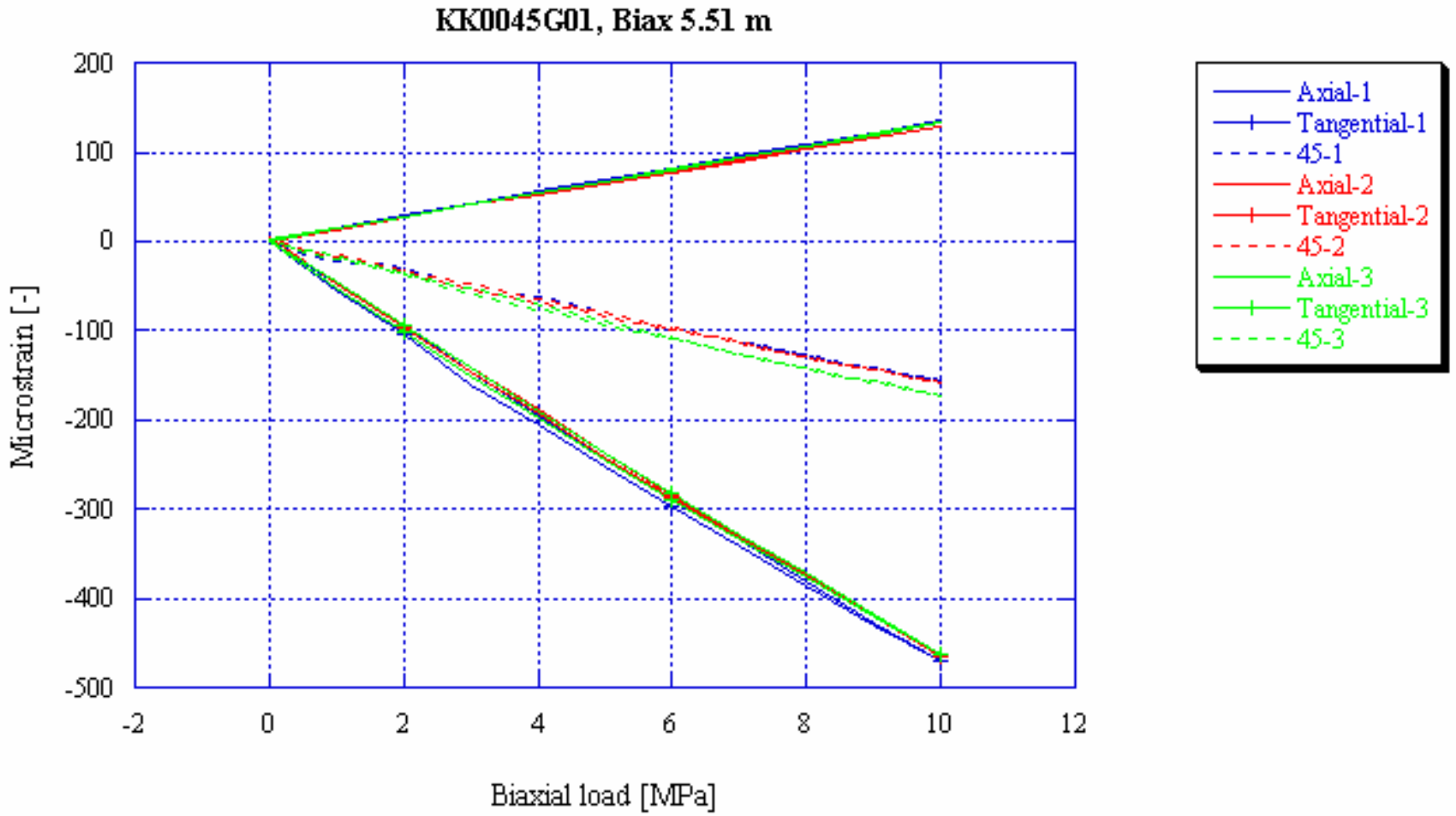
KK0045G01, Biax 5.51 m
Microstrain [-]
200
100
0
-100
-200
-300
-400
-500
-2
0
2
4
6
8
10
12
Biaxial load [MPa]
Axial-1
Tangential-1
45-1
Axial-2
Tangential-2
45-2
Axial-3
Tangential-3
45-3

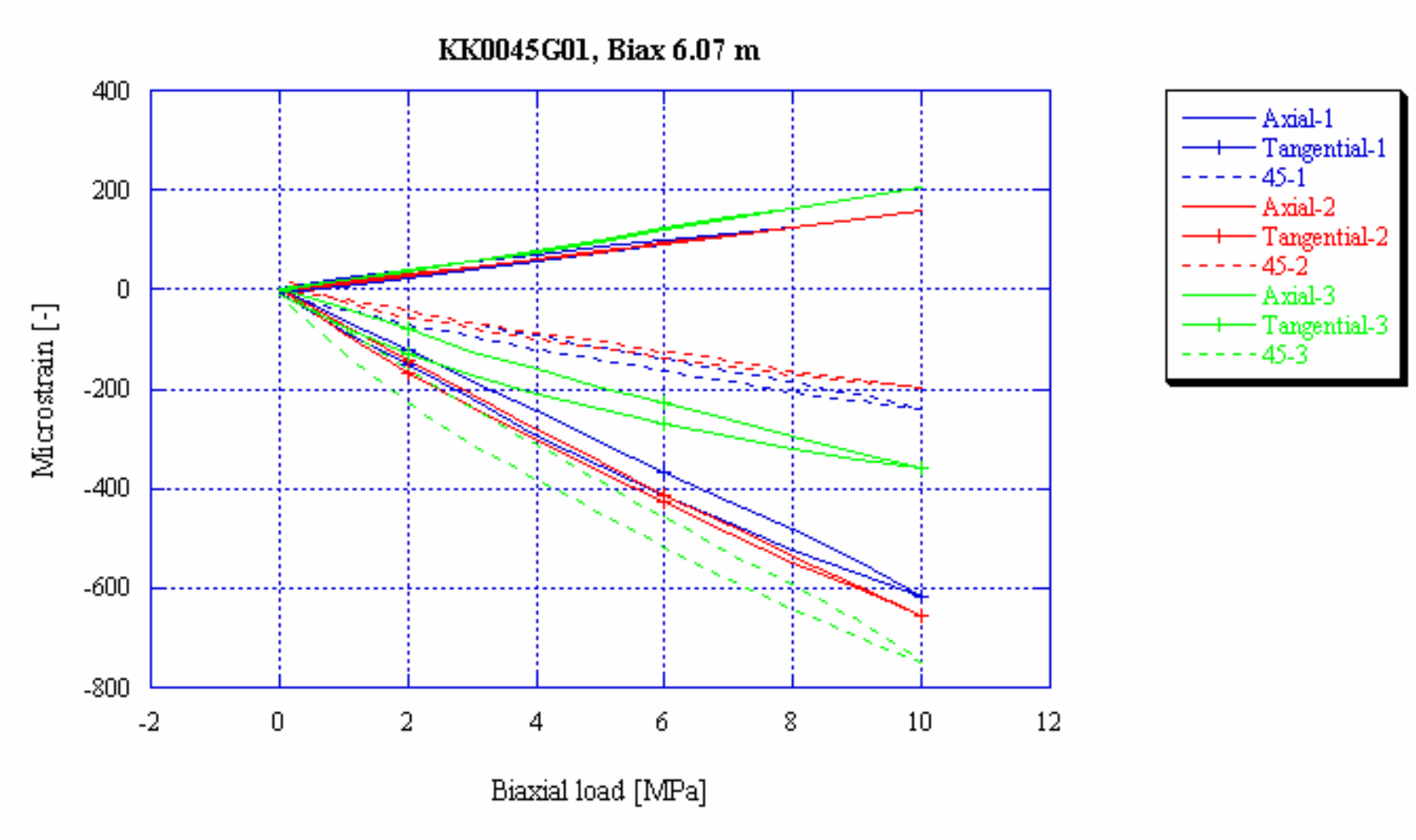
KK0045G01, Biax 6.07 m
Microstrain [-]
400
200
0
-200
-400
-600
-800
-2
0
2
4
6
8
10
12
Biaxial load [MPa]
Axial-1
Tangential-1
45-1
Axial-2
Tangential-2
45-2
Axial-3
Tangential-3
45-3

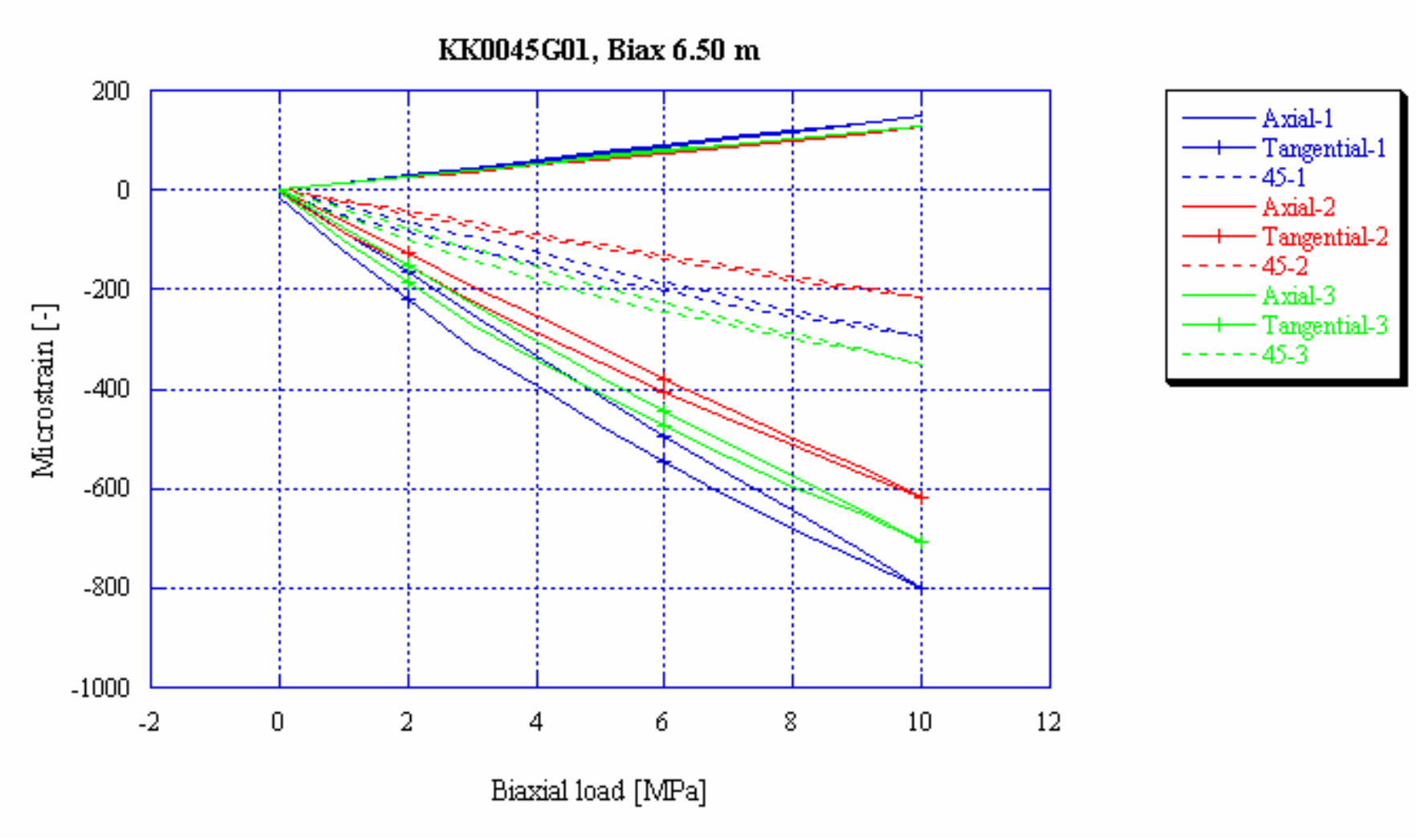
KK0045G01, Biax 6.50 m
Microstrain [-]
200
0
-200
-400
-600
-800
-1000
-2
0
2
4
6
8
10
12
Biaxial load [MPa]
Axial-1
Tangential-1
45-1
Axial-2
Tangential-2
45-2
Axial-3
Tangential-3
45-3

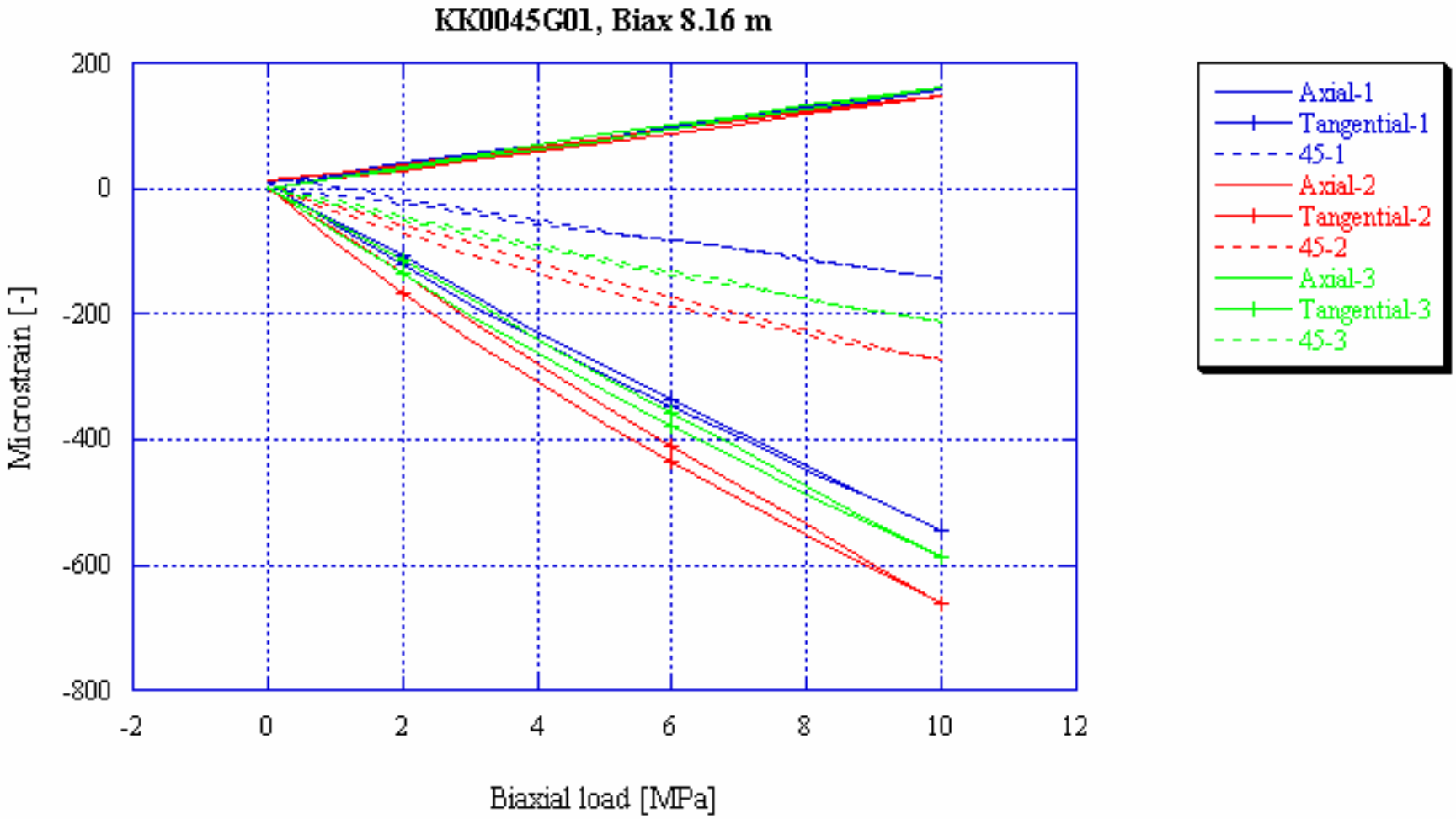
KK0045G01, Biax 8.16 m
Microstrain [-]
200
0
-200
-400
-600
-800
-2
0
2
4
6
8
10
12
Biaxial load [MPa]
Axial-1
Tangential-1
45-1
Axial-2
Tangential-2
45-2
Axial-3
Tangential-3
45-3

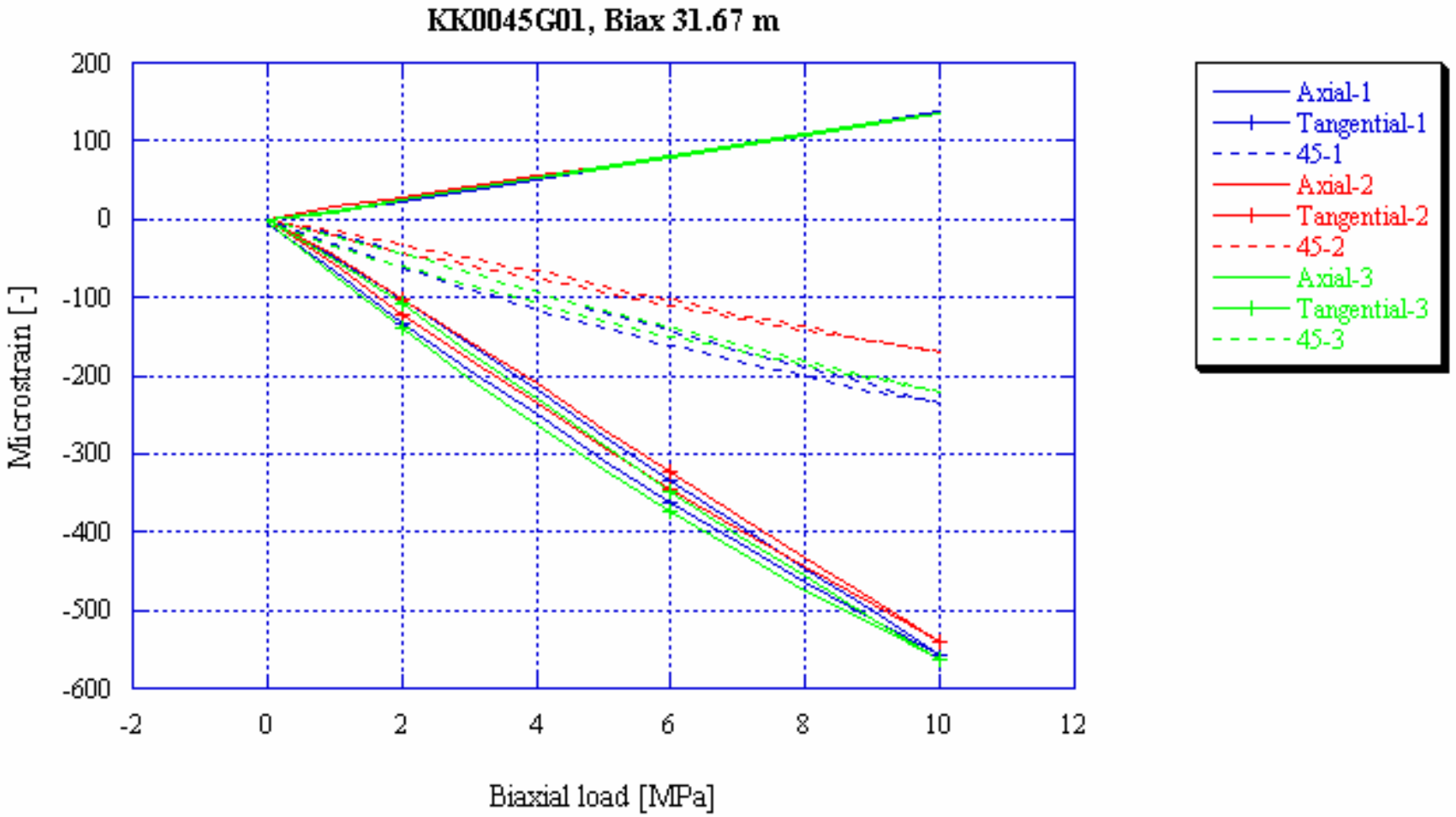
KK0045G01, Biax 31.67 m
Microstrain [-]
200
100
0
-100
-200
-300
-400
-500
-600
-2
0
2
4
6
8
10
12
Biaxial load [MPa]
Axial-1
Tangential-1
45-1
Axial-2
Tangential-2
45-2
Axial-3
Tangential-3
45-3

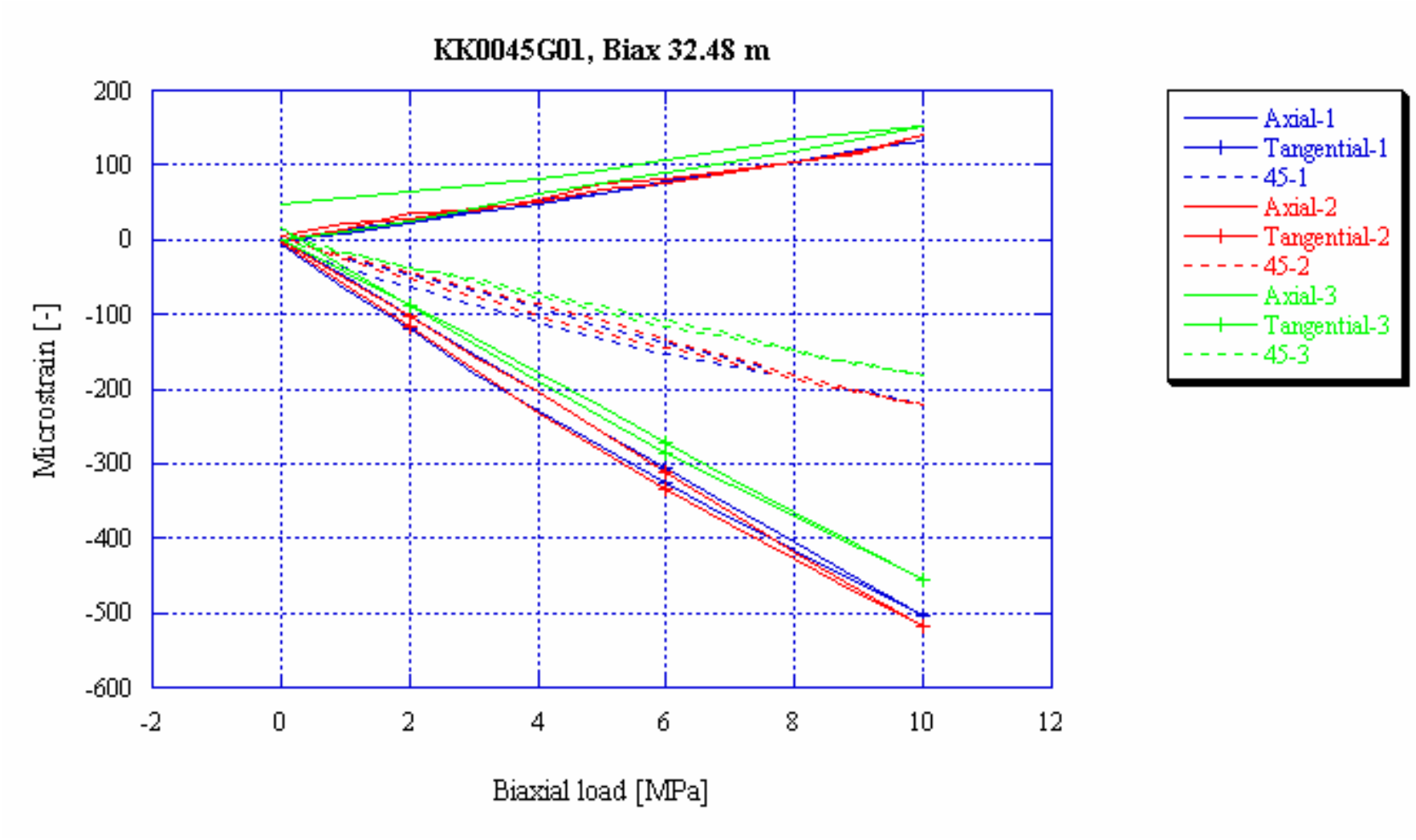
KK0045G01, Biax 32.48 m
Microstrain [-]
200
100
0
-100
-200
-300
-400
-500
-600
-2
0
2
4
6
8
10
12
Biaxial load [MPa]
Axial-1
Tangential-1
45-1
Axial-2
Tangential-2
45-2
Axial-3
Tangential-3
45-3

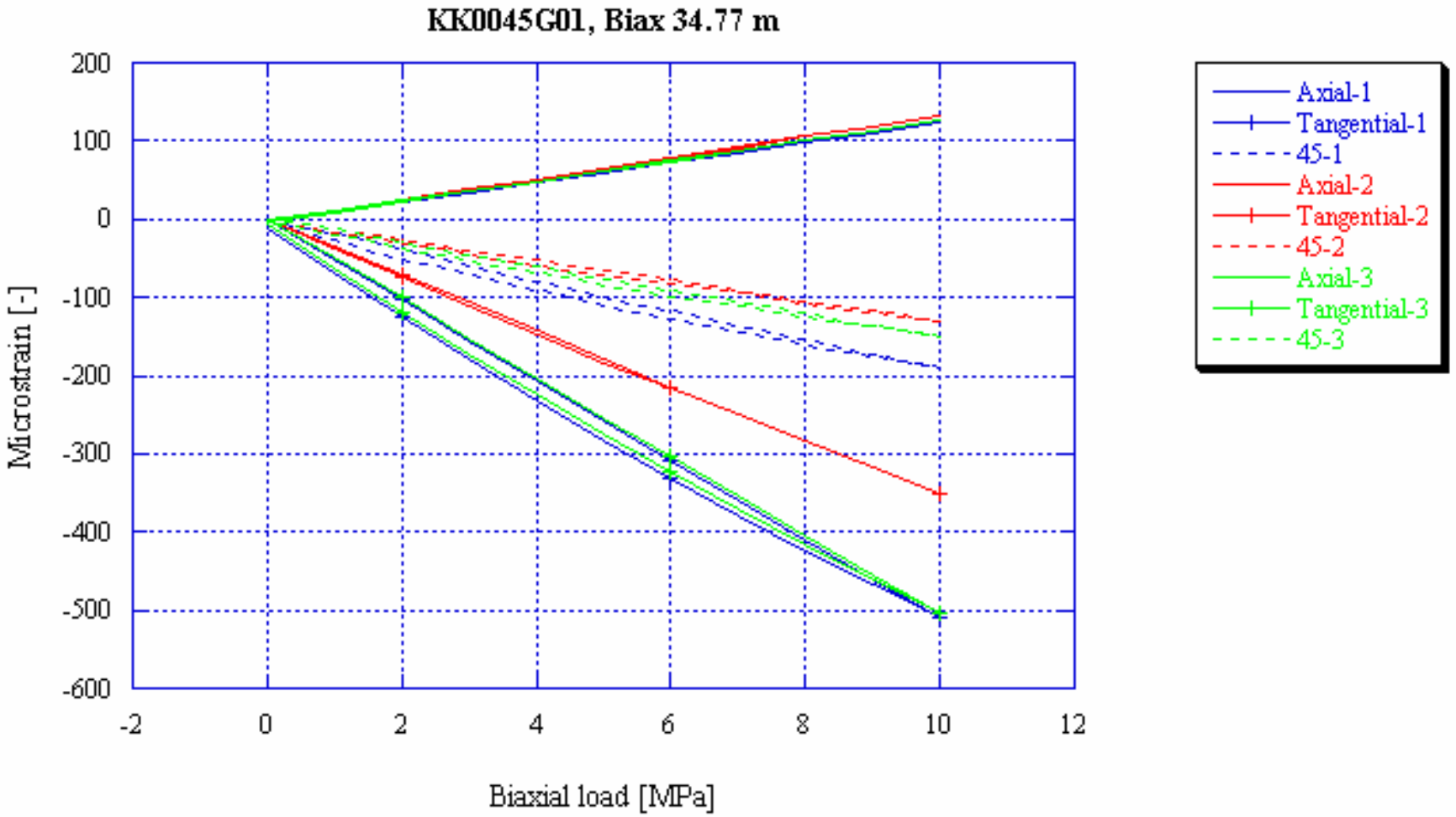
KK0045G01, Biax 34.77 m
Microstrain [-]
200
100
0
-100
-200
-300
-400
-500
-600
-2
0
2
4
6
8
10
12
Biaxial load [MPa]
Axial-1
Tangential-1
45-1
Axial-2
Tangential-2
45-2
Axial-3
Tangential-3
45-3

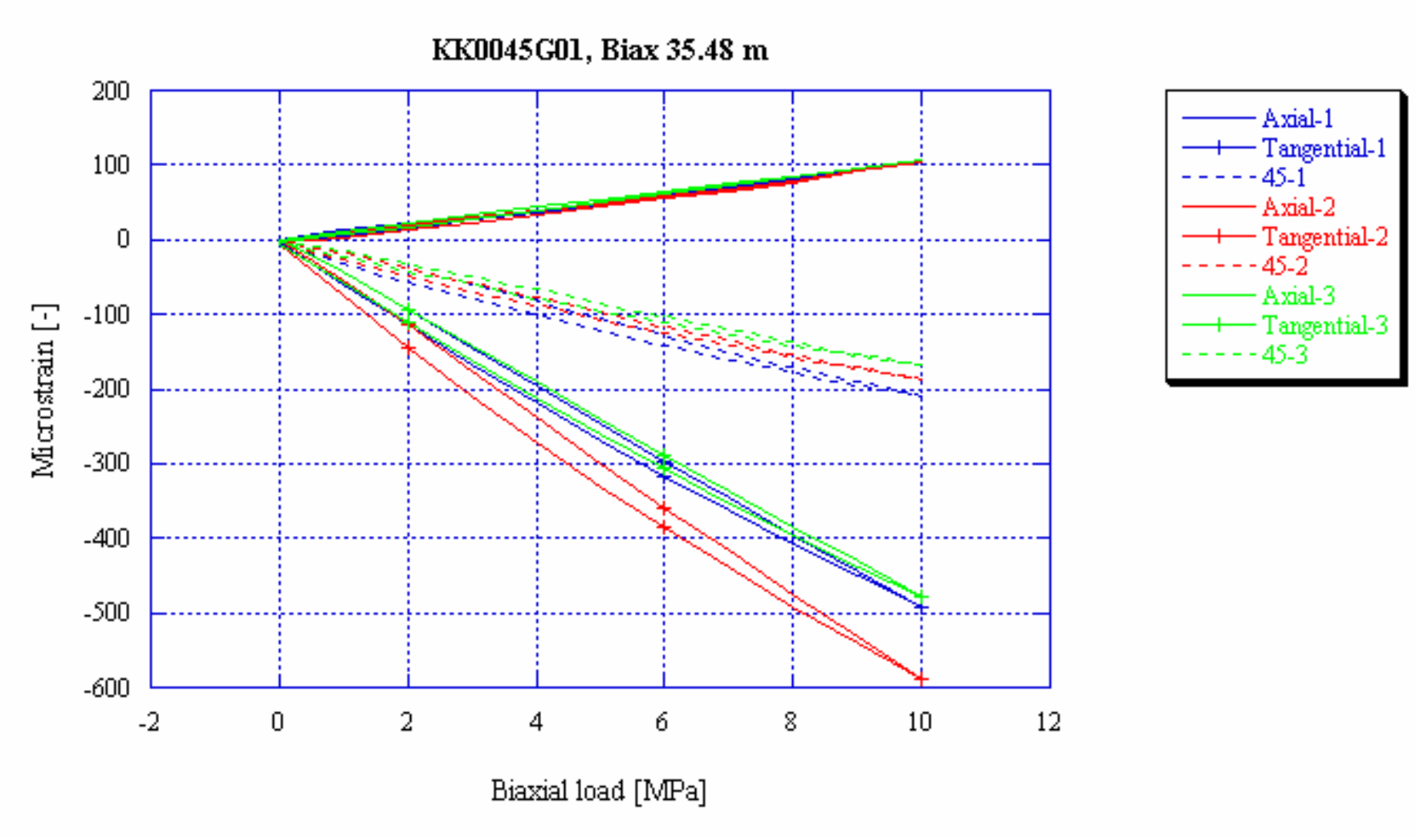
KK0045G01, Biax 35.48 m
Microstrain [-]
200
100
0
-100
-200
-300
-400
-500
-600
-2
0
2
4
6
8
10
12
Biaxial load [MPa]
Axial-1
Tangential-1
45-1
Axial-2
Tangential-2
45-2
Axial-3
Tangential-3
45-3

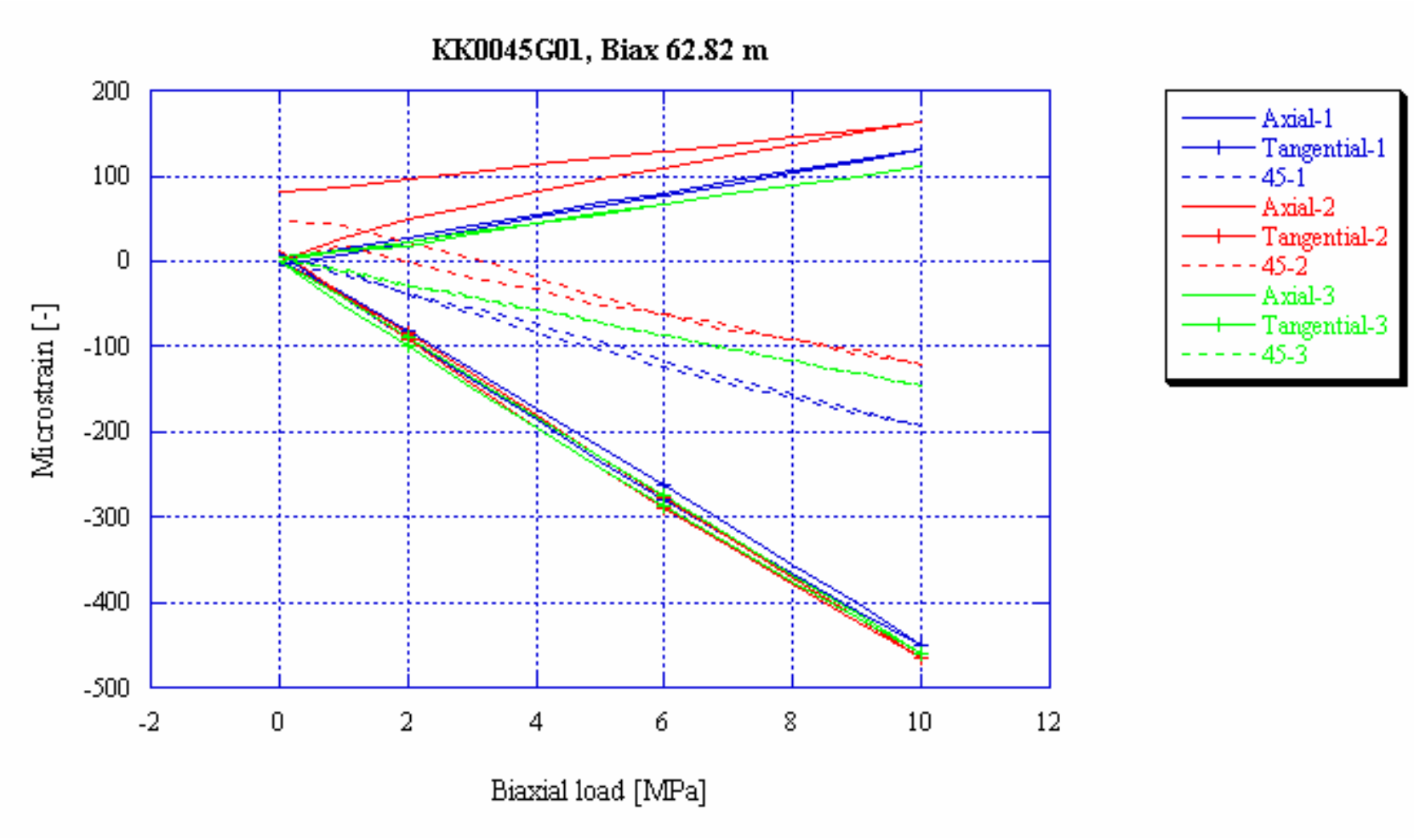
KK0045G01, Biax 62.82 m
Microstrain [-]
200
100
0
-100
-200
-300
-400
-500
-2
0
2
4
6
8
10
12
Biaxial load [MPa]
Axial-1
Tangential-1
45-1
Axial-2
Tangential-2
45-2
Axial-3
Tangential-3
45-3

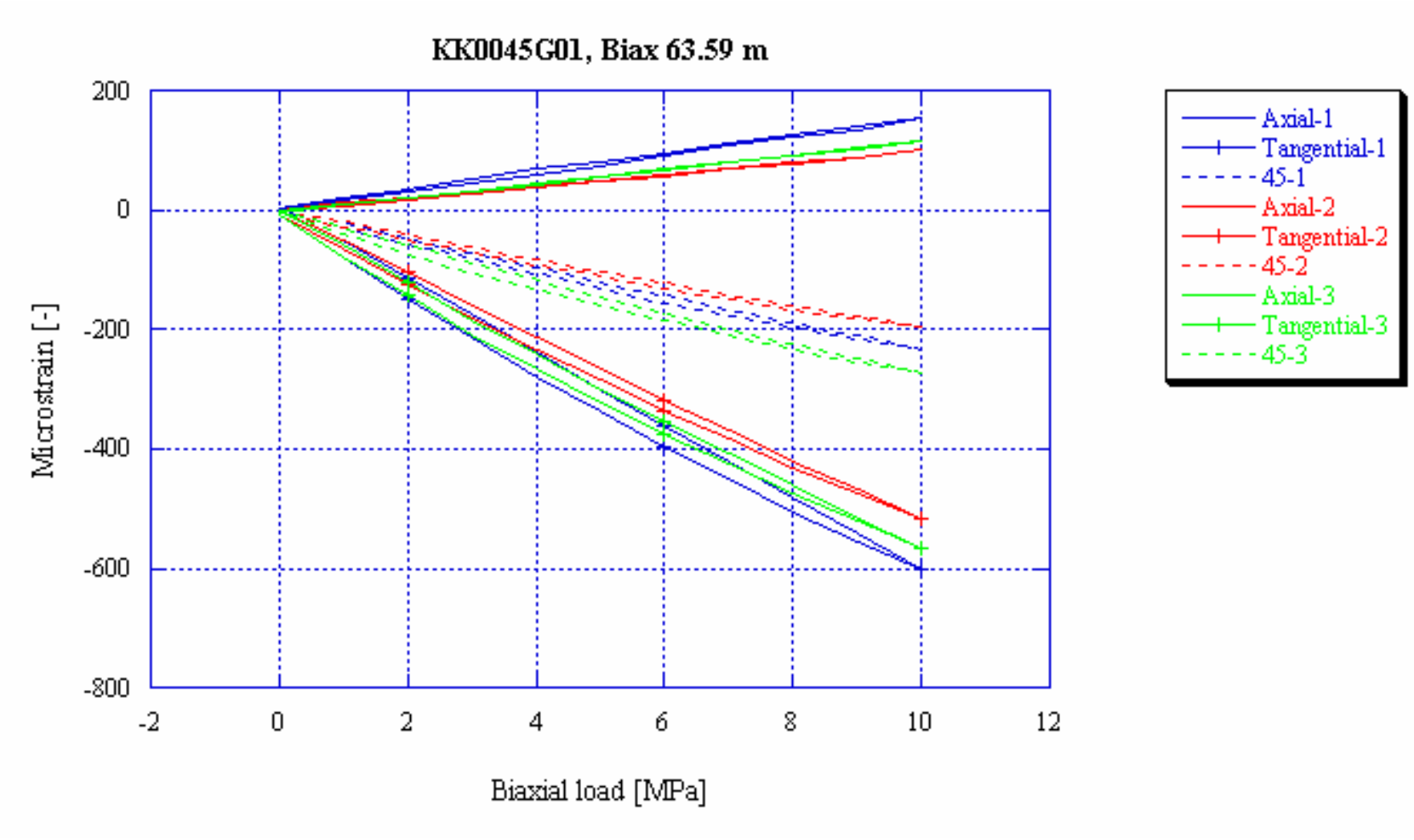
KK0045G01, Biax 63.59 m
Microstrain [-]
200
0
-200
-400
-600
-800
-2
0
2
4
6
8
10
12
Biaxial load [MPa]
Axial-1
Tangential-1
45-1
Axial-2
Tangential-2
45-2
Axial-3
Tangential-3
45-3

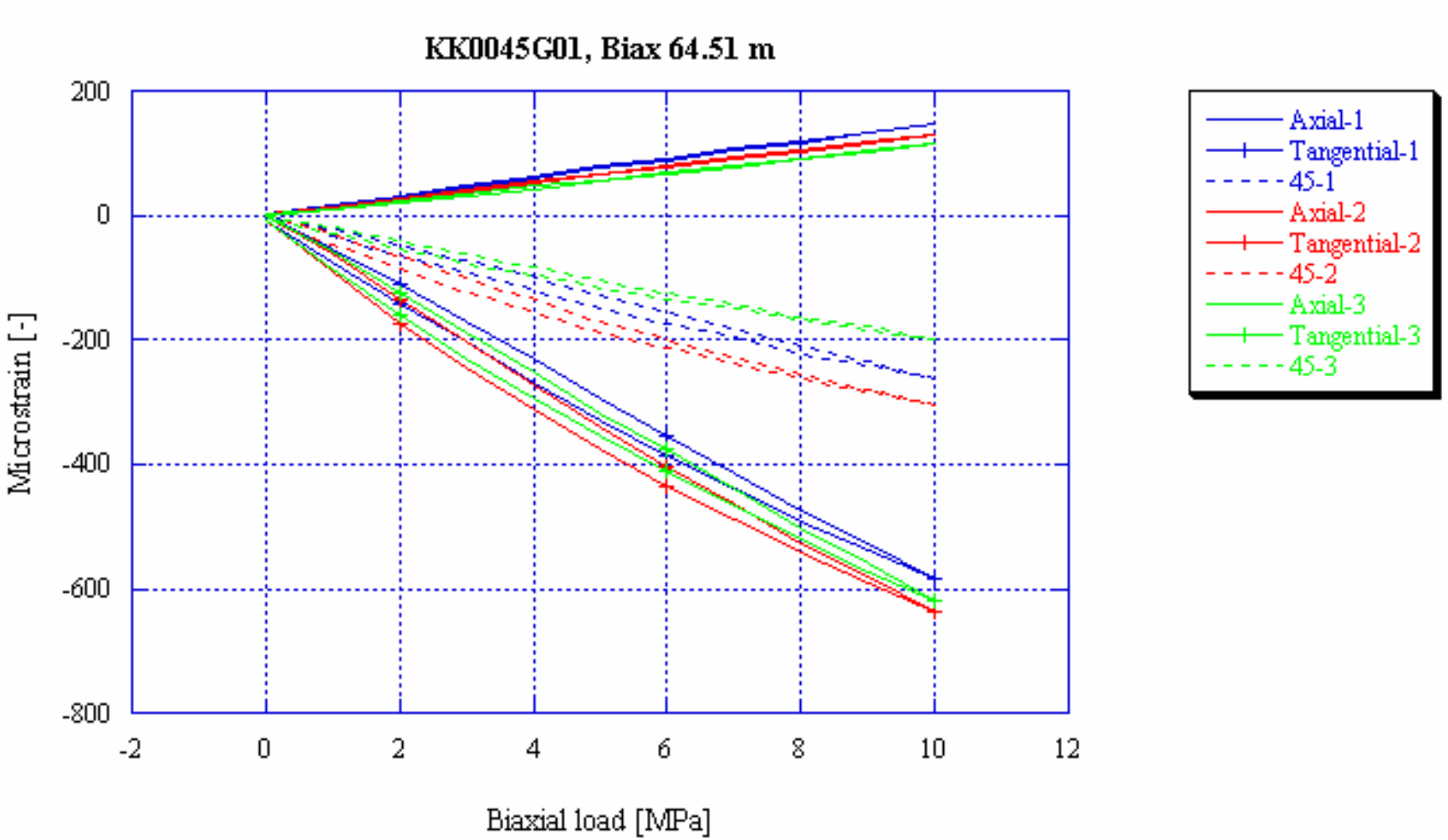
KK0045G01, Biax 64.51 m
Microstrain [-]
200
0
-200
-400
-600
-800
-2
0
2
4
6
8
10
12
Biaxial load [MPa]
Axial-1
Tangential-1
45-1
Axial-2
Tangential-2
45-2
Axial-3
Tangential-3
45-3

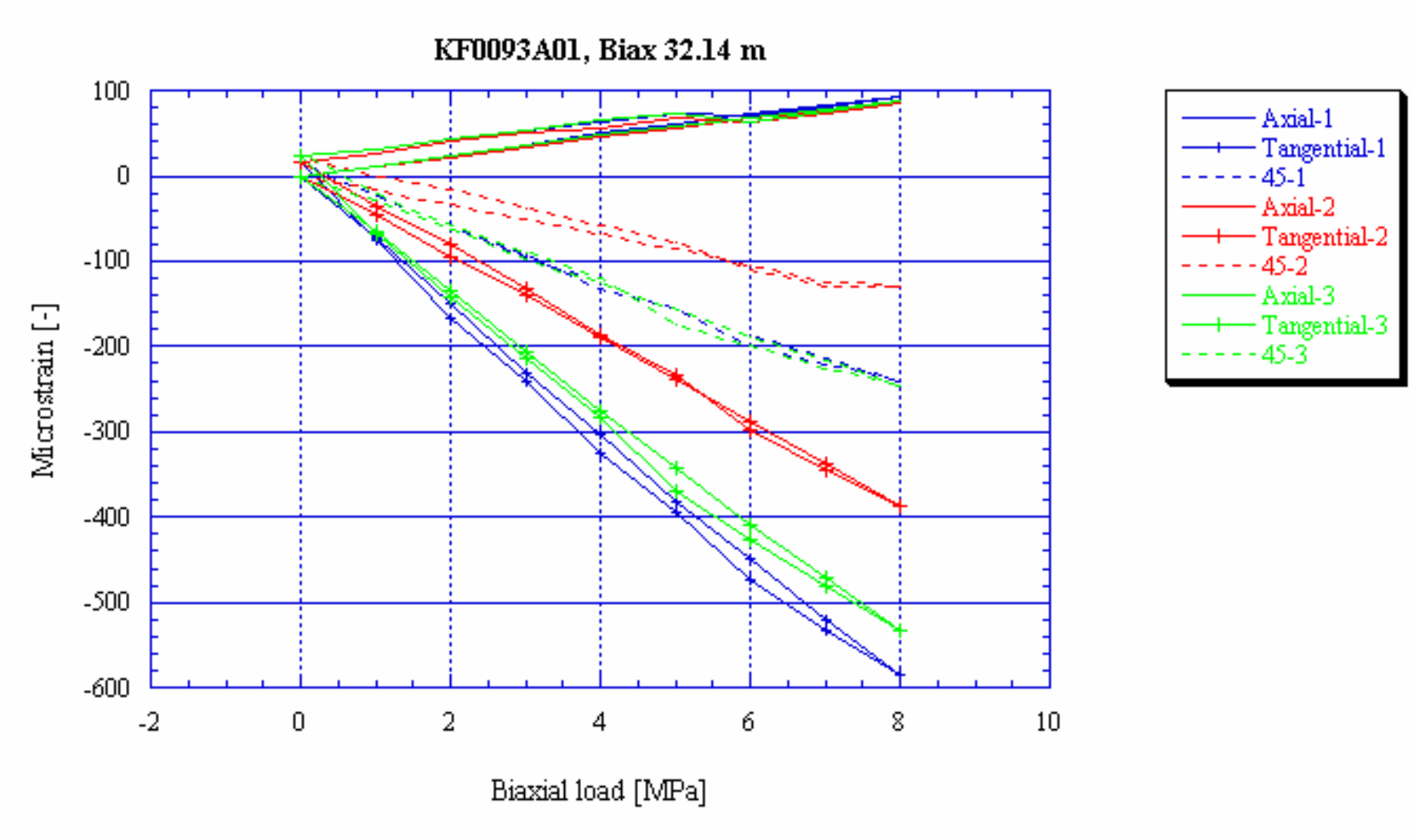
KF0093A01, Biax 32.14 m
Microstrain [-]
100
0
-100
-200
-300
-400
-500
-600
-2
0
2
4
6
8
10
Biaxial load [MPa]
Axial-1
Tangential-1
45-1
Axial-2
Tangential-2
45-2
Axial-3
Tangential-3
45-3

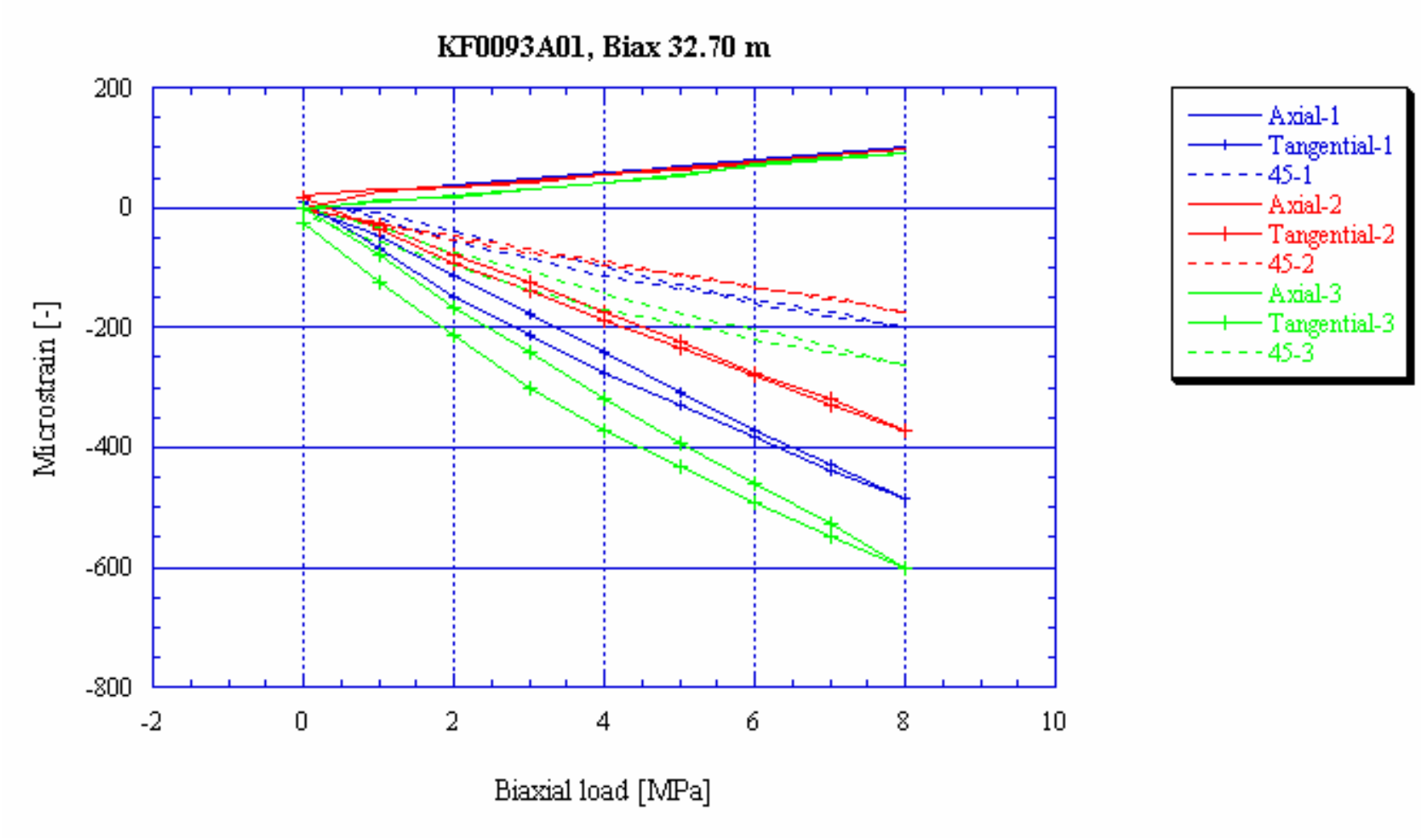
KF0093A01, Biax 32.70 m
Microstrain [-]
200
0
-200
-400
-600
-800
-2
0
2
4
6
8
10
Biaxial load [MPa]
Axial-1
Tangential-1
45-1
Axial-2
Tangential-2
45-2
Axial-3
Tangential-3
45-3

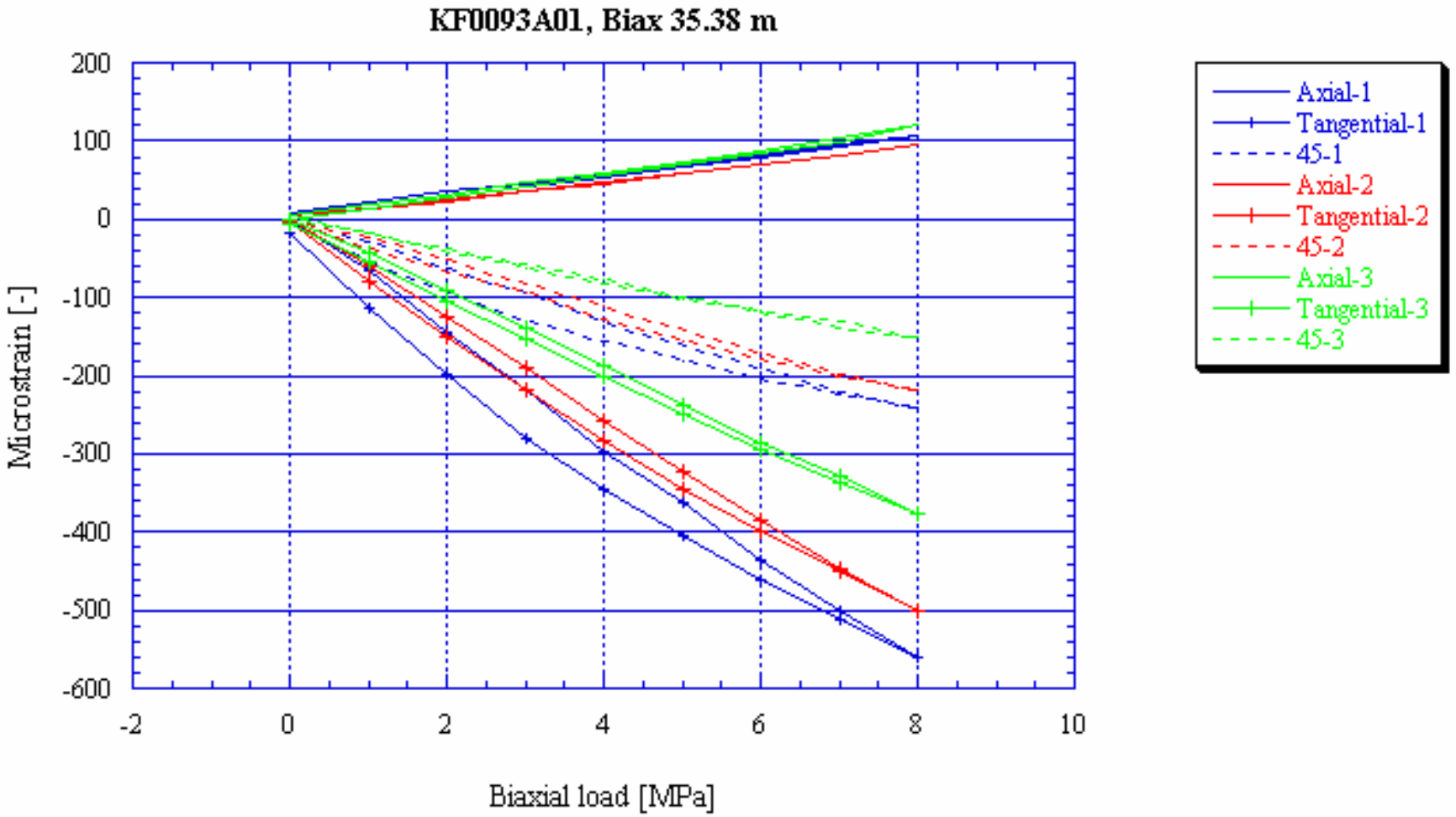
KF0093A01, Biax 35.38 m
Microstrain [-]
200
100
0
-100
-200
-300
-400
-500
-600
-2
0
2
4
6
8
10
Biaxial load [MPa]
Axial-1
Tangential-1
45-1
Axial-2
Tangential-2
45-2
Axial-3
Tangential-3
45-3

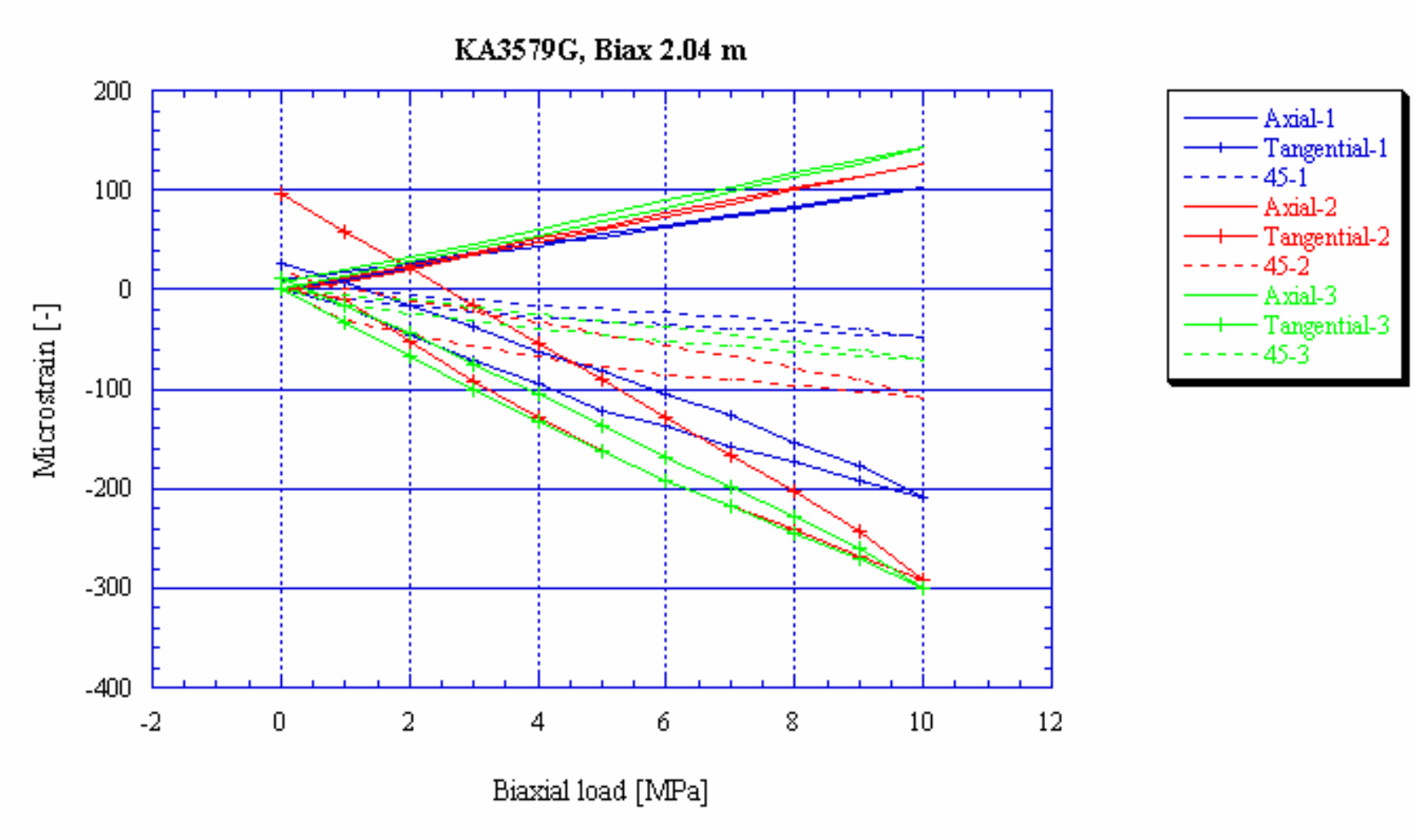
KA3579G, Biax 2.04 m
Microstrain [-]
200
100
0
-100
-200
-300
-400
-2
0
2
4
6
8
10
12
Biaxial load [MPa]
Axial-1
Tangential-1
45-1
Axial-2
Tangential-2
45-2
Axial-3
Tangential-3
45-3

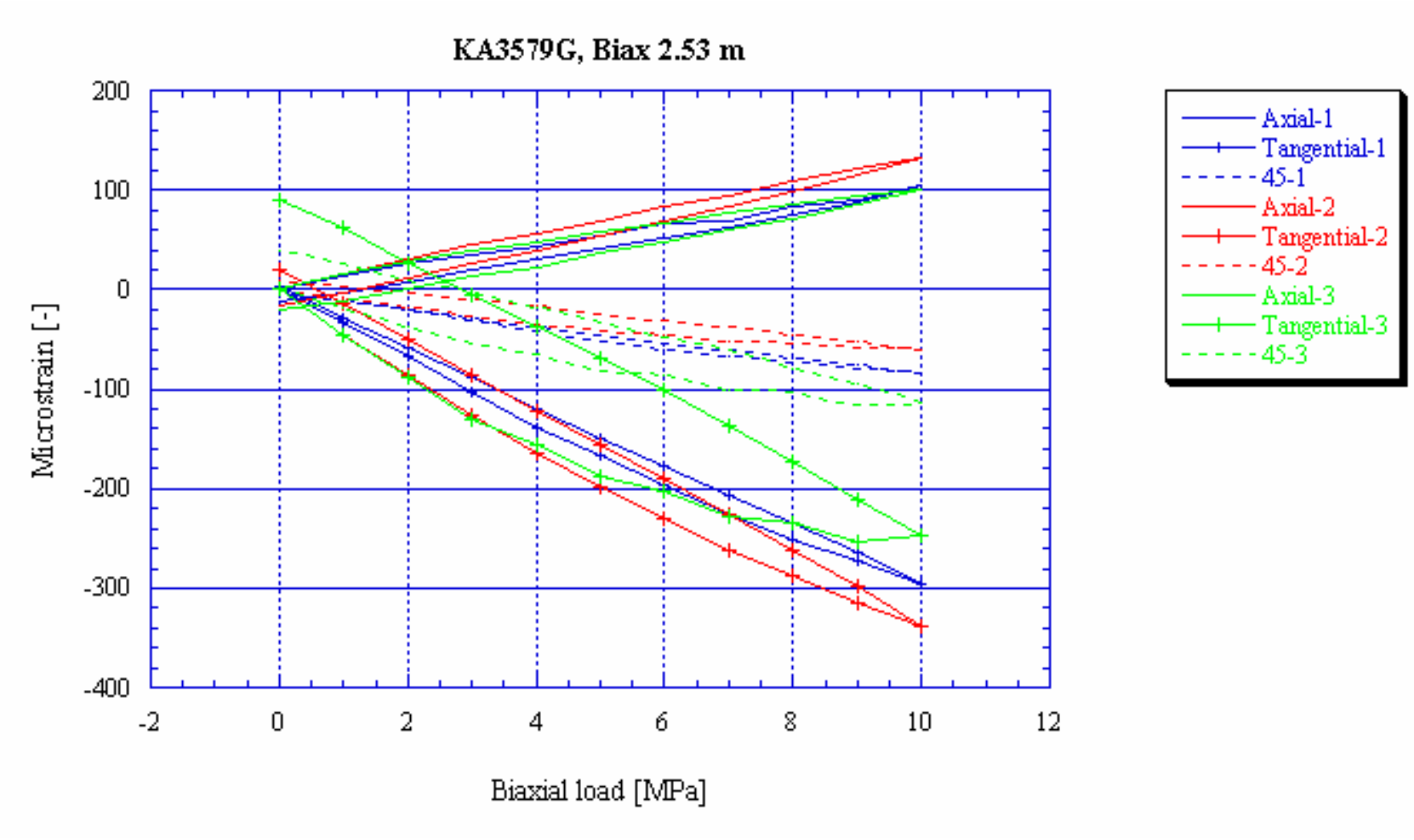
KA3579G, Biax 2.53 m
Microstrain [-]
200
100
0
-100
-200
-300
-400
-2
0
2
4
6
8
10
12
Biaxial load [MPa]
Axial-1
Tangential-1
45-1
Axial-2
Tangential-2
45-2
Axial-3
Tangential-3
45-3

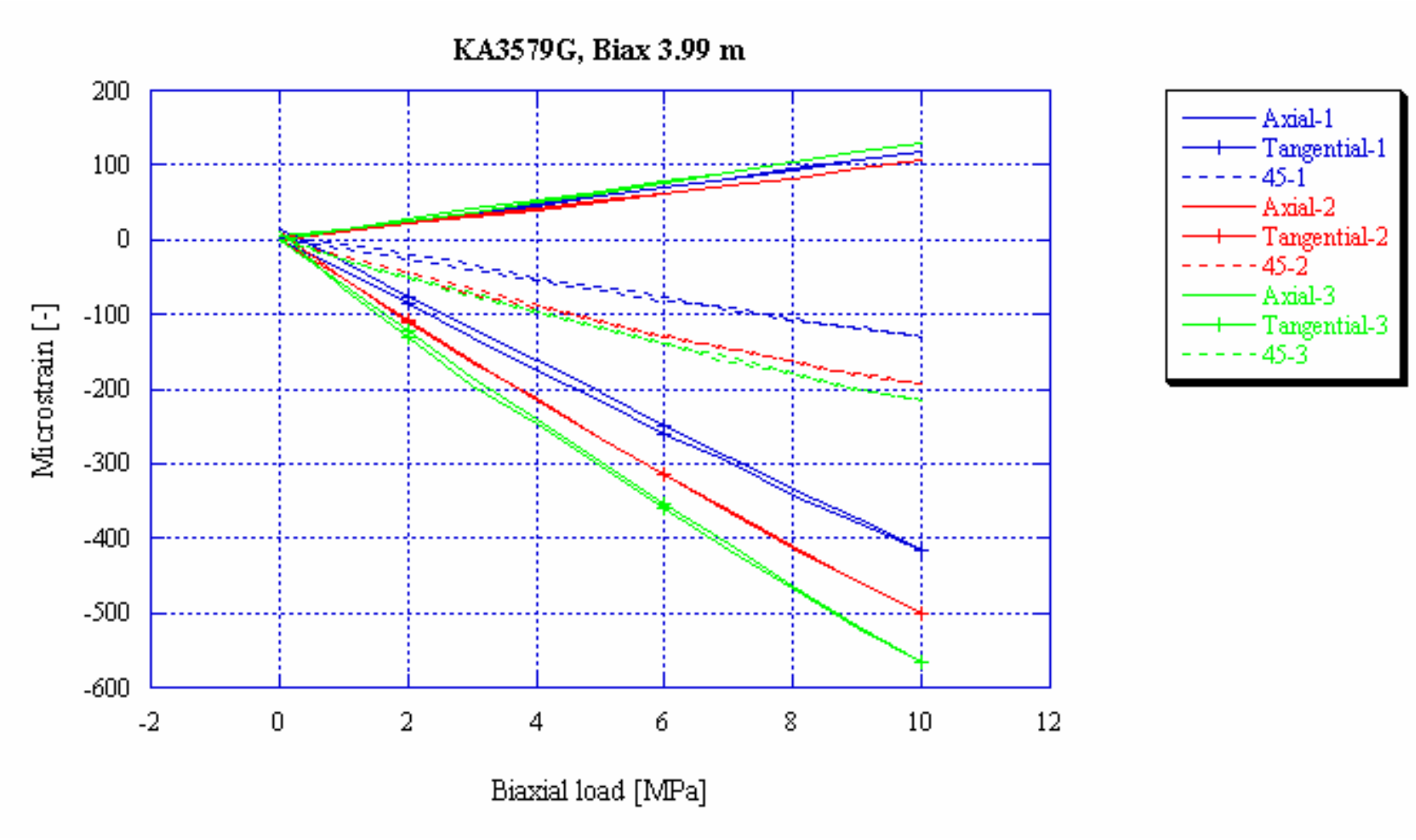
KA3579G, Biax 3.99 m
Microstrain [-]
200
100
0
-100
-200
-300
-400
-500
-600
-2
0
2
4
6
8
10
12
Biaxial load [MPa]
Axial-1
Tangential-1
45-1
Axial-2
Tangential-2
45-2
Axial-3
Tangential-3
45-3

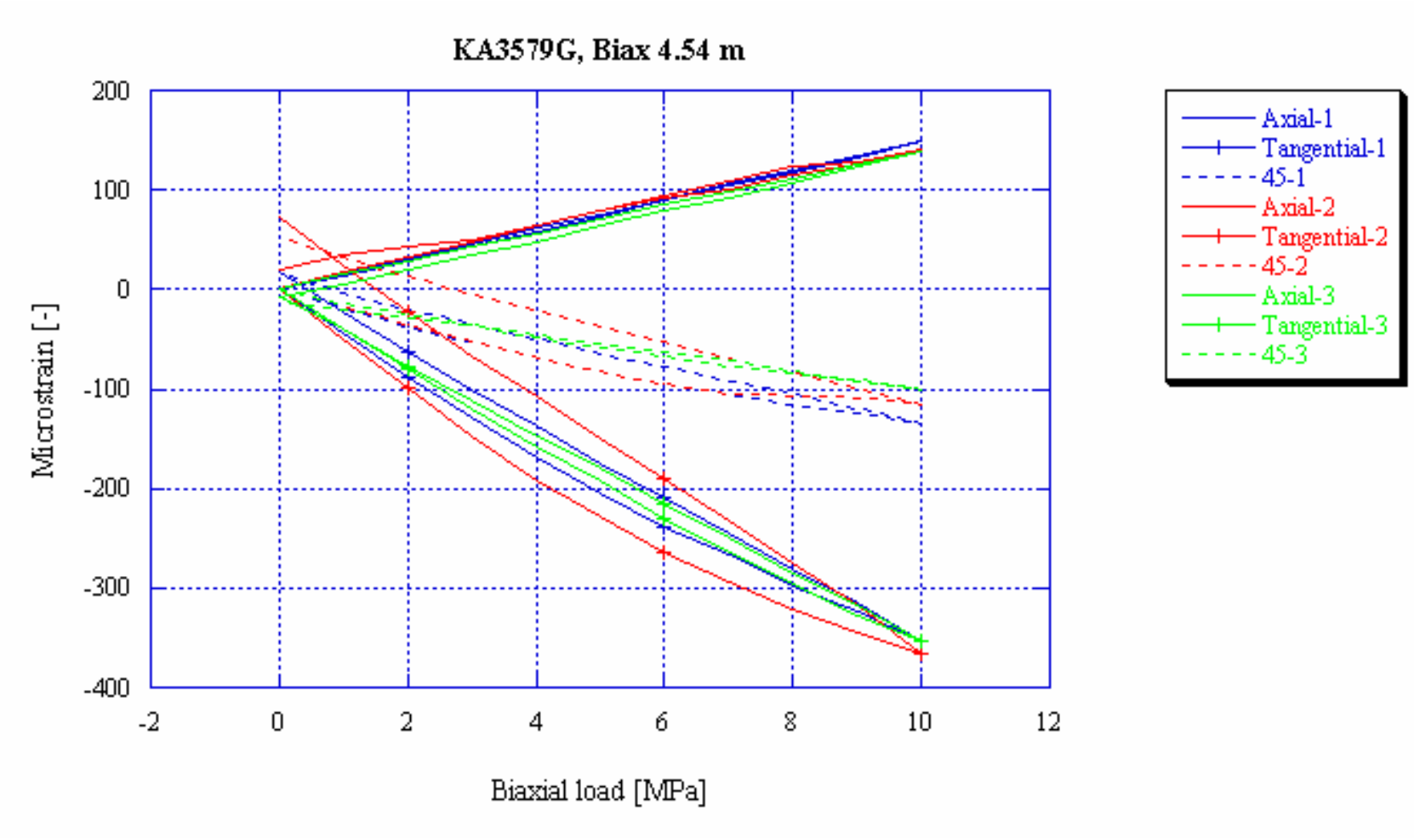
KA3579G, Biax 4.54 m
Microstrain [-]
200
100
0
-100
-200
-300
-400
-2
0
2
4
6
8
10
12
Biaxial load [MPa]
Axial-1
Tangential-1
45-1
Axial-2
Tangential-2
45-2
Axial-3
Tangential-3
45-3

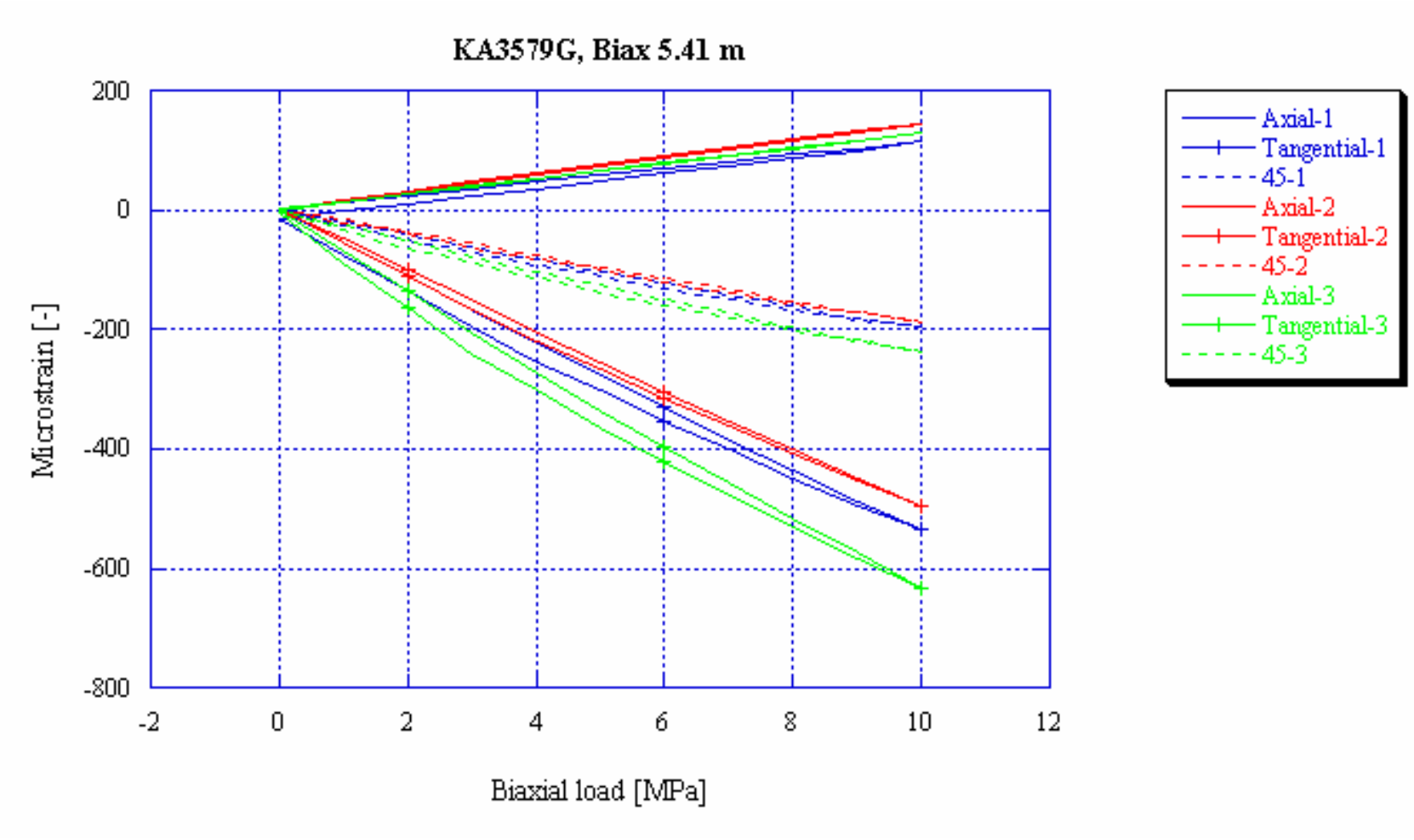
KA3579G, Biax 5.41 m
Microstrain [-]
200
0
-200
-400
-600
-800
-2
0
2
4
6
8
10
12
Biaxial load [MPa]
Axial-1
Tangential-1
45-1
Axial-2
Tangential-2
45-2
Axial-3
Tangential-3
45-3

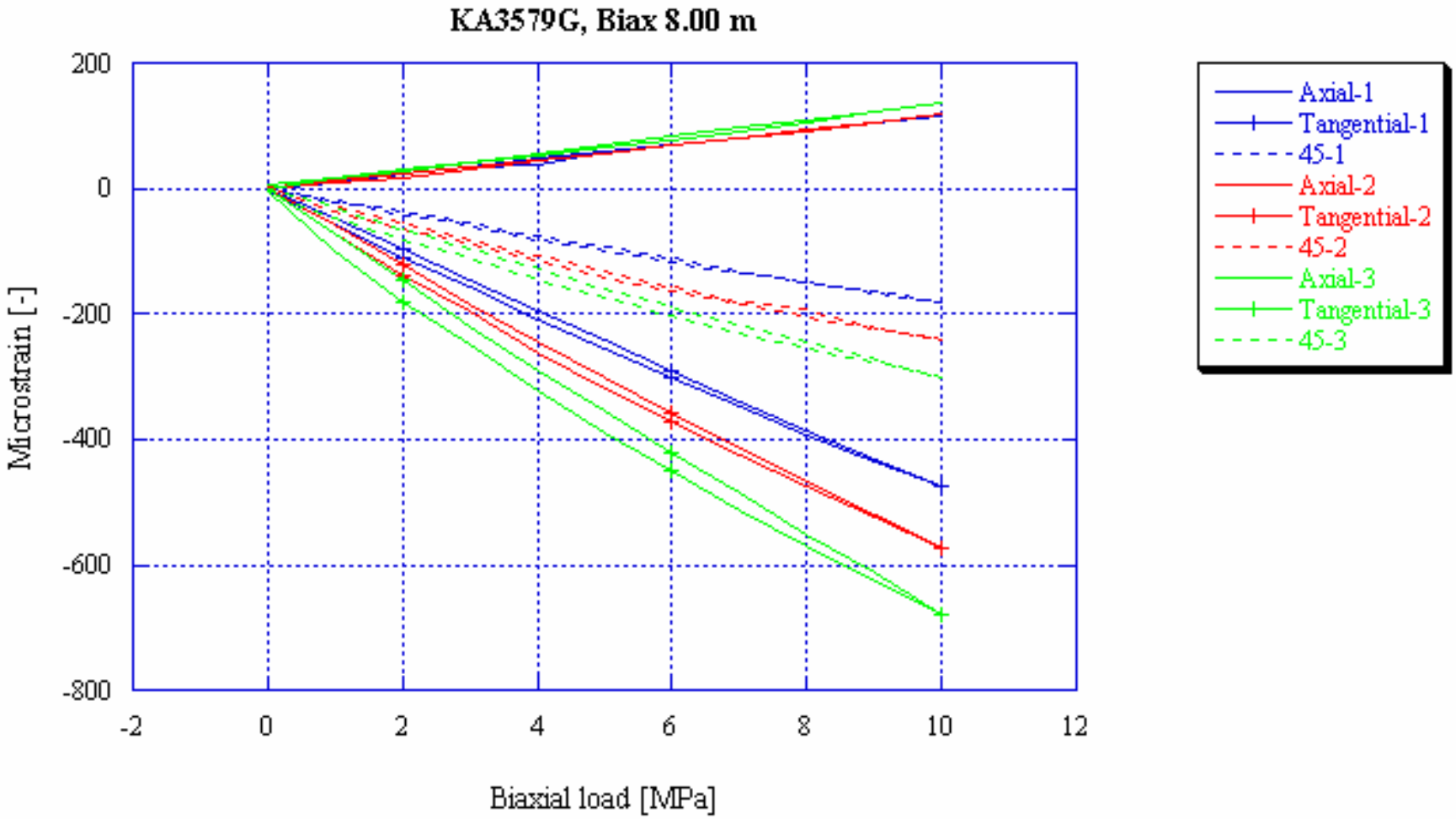
KA3579G, Biax 8.00 m
Microstrain [-]
200
0
-200
-400
-600
-800
-2
0
2
4
6
8
10
12
Biaxial load [MPa]
Axial-1
Tangential-1
45-1
Axial-2
Tangential-2
45-2
Axial-3
Tangential-3
45-3

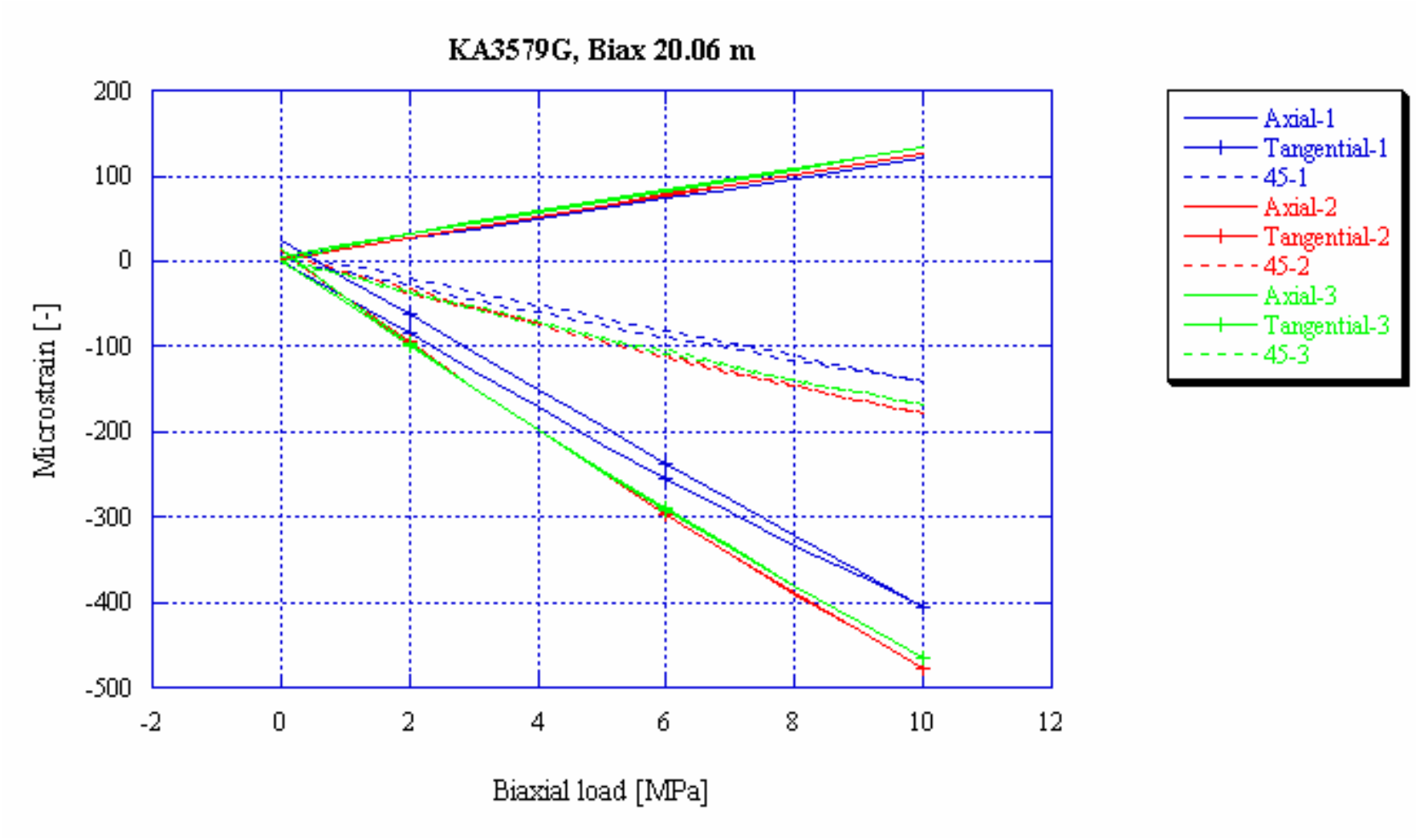
KA3579G, Biax 20.06 m
Microstrain [-]
200
100
0
-100
-200
-300
-400
-500
-2
0
2
4
6
8
10
12
Biaxial load [MPa]
Axial-1
Tangential-1
45-1
Axial-2
Tangential-2
45-2
Axial-3
Tangential-3
45-3

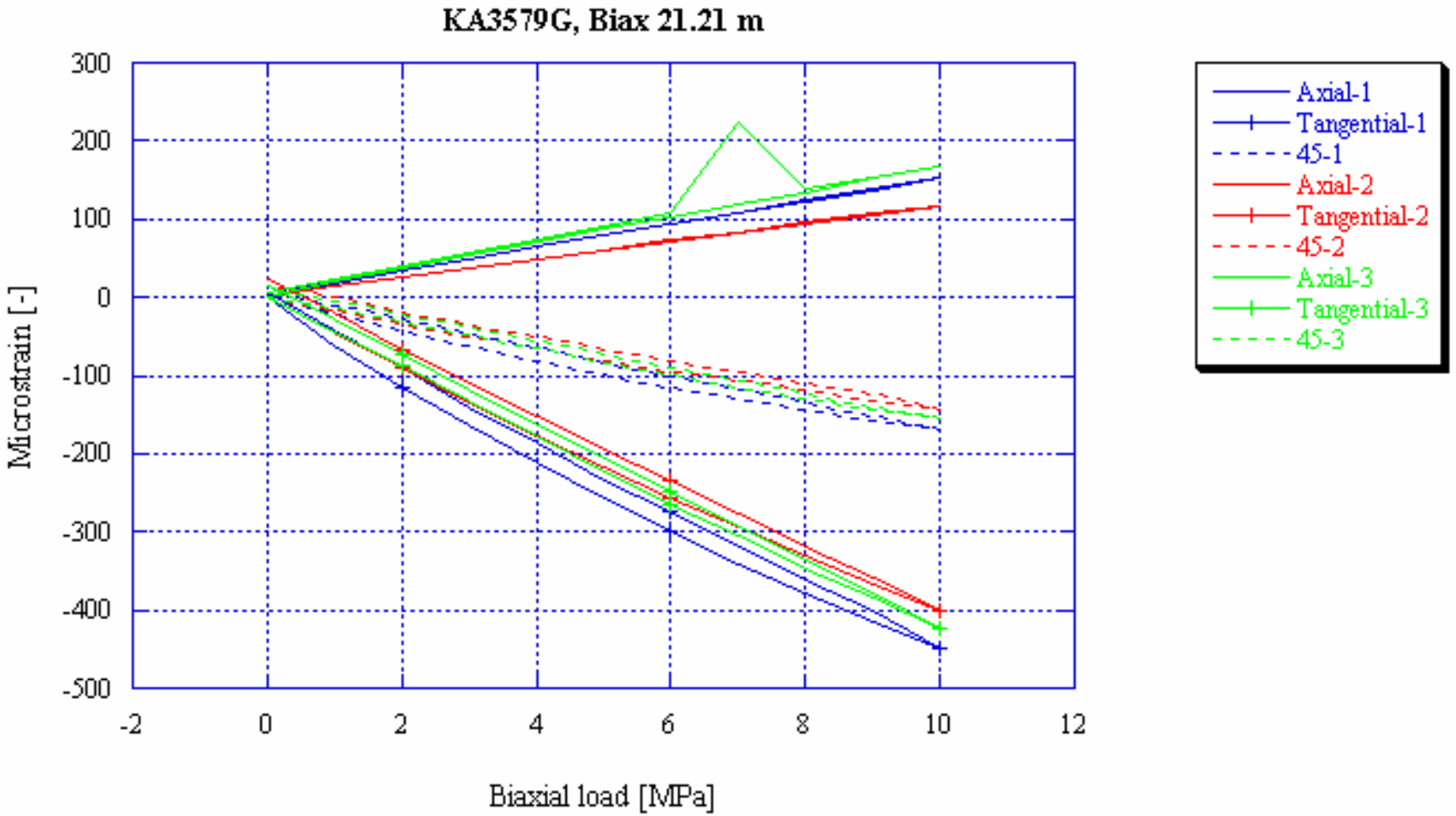
KA3579G, Biax 21.21 m
Microstrain [-]
300
200
100
0
-100
-200
-300
-400
-500
-2
0
2
4
6
8
10
12
Biaxial load [MPa]
Axial-1
Tangential-1
45-1
Axial-2
Tangential-2
45-2
Axial-3
Tangential-3
45-3

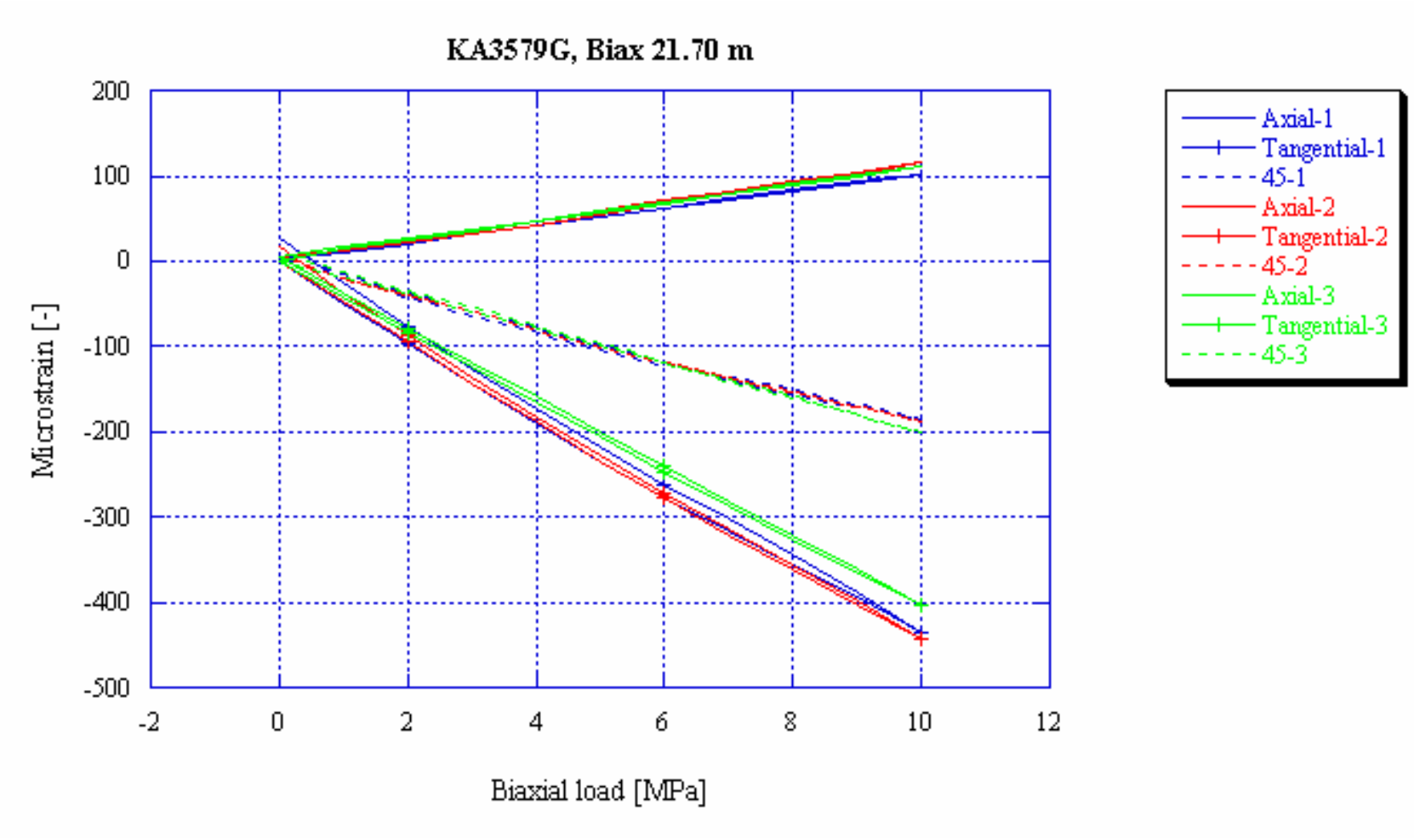
KA3579G, Biax 21.70 m
Microstrain [-]
200
100
0
-100
-200
-300
-400
-500
-2
0
2
4
6
8
10
12
Biaxial load [MPa]
Axial-1
Tangential-1
45-1
Axial-2
Tangential-2
45-2
Axial-3
Tangential-3
45-3

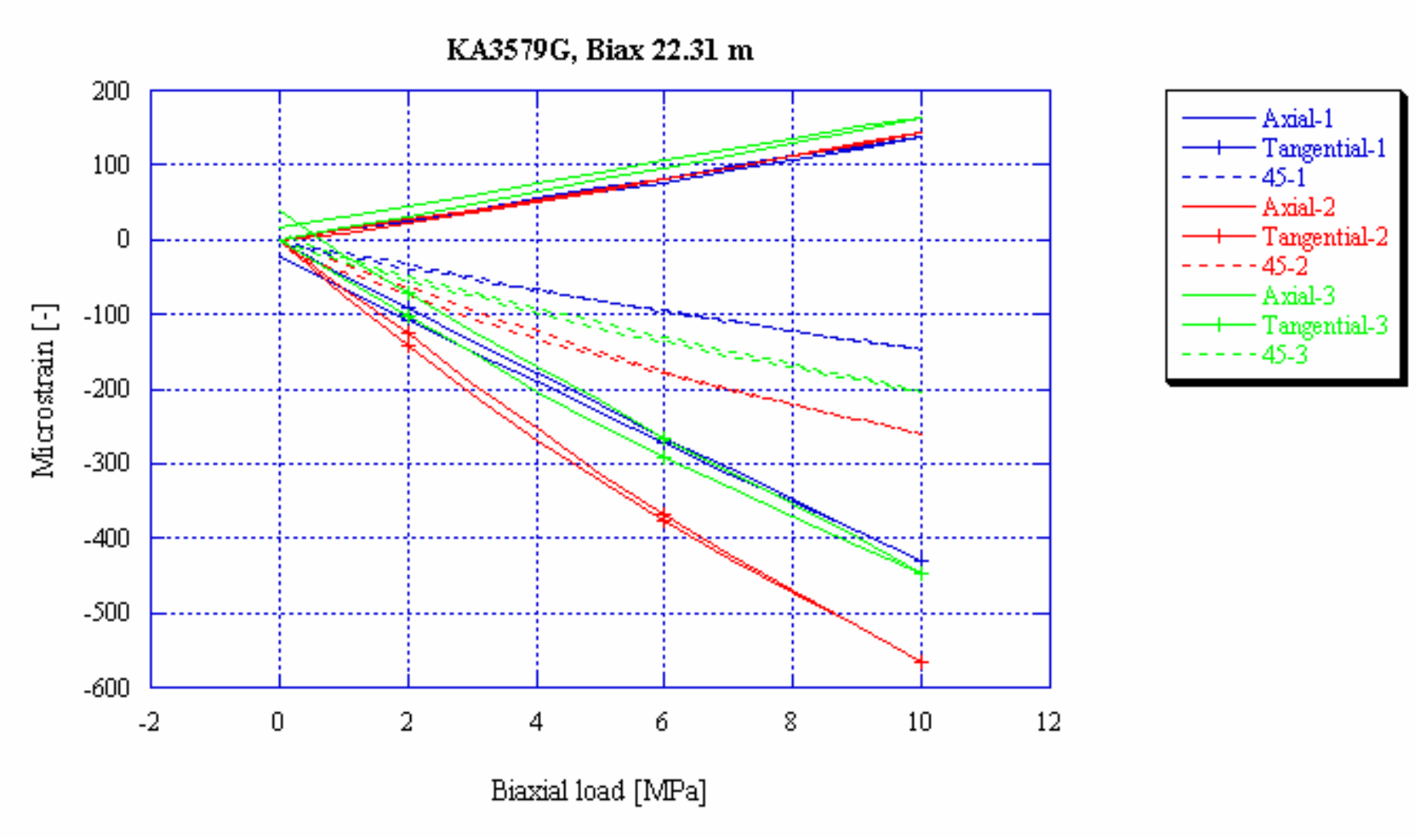
KA3579G, Biax 22.31 m
Microstrain [-]
200
100
0
-100
-200
-300
-400
-500
-600
-2
0
2
4
6
8
10
12
Biaxial load [MPa]
Axial-1
Tangential-1
45-1
Axial-2
Tangential-2
45-2
Axial-3
Tangential-3
45-3

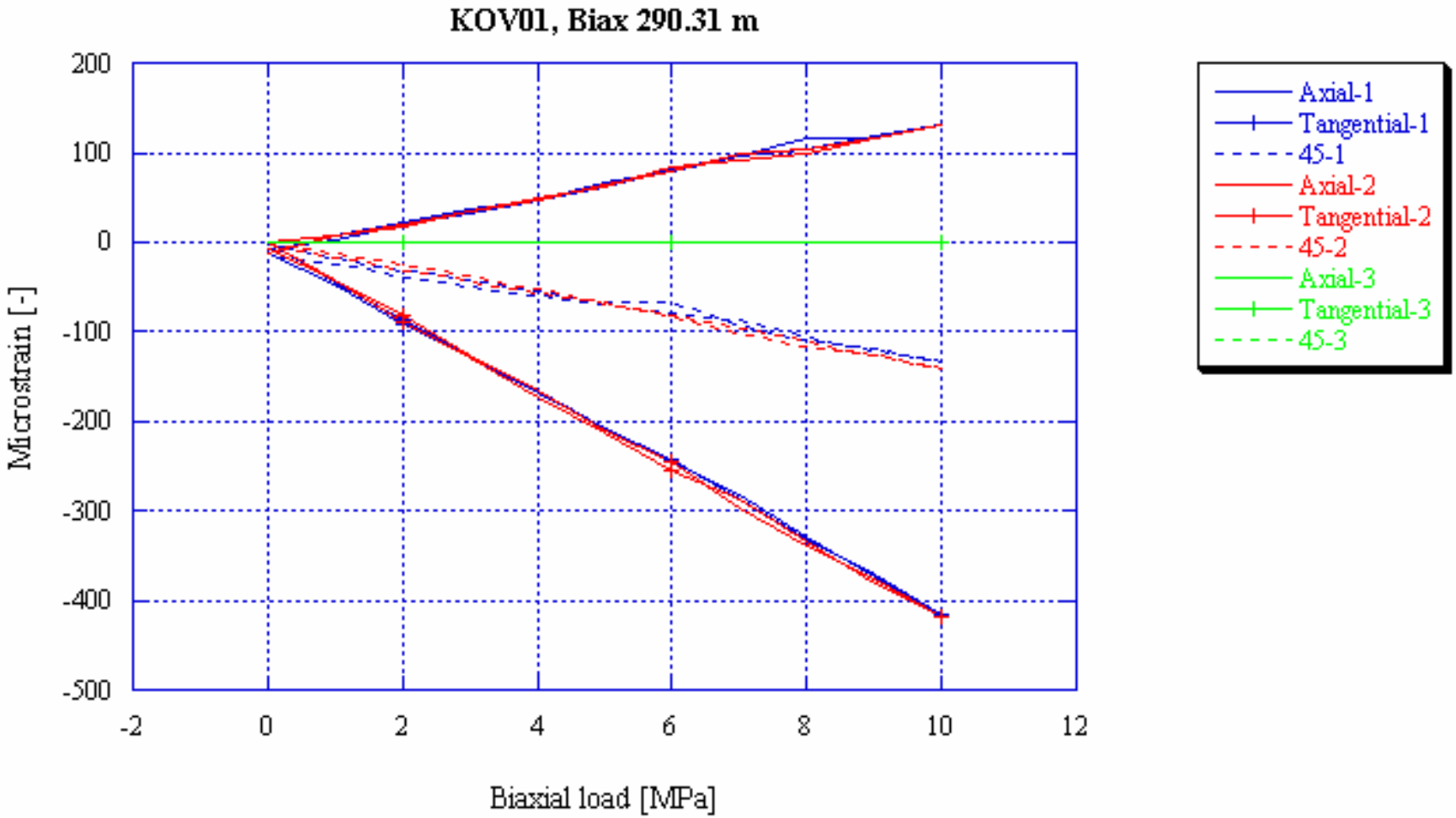
KOV01, Biax 290.31 m
Microstrain [-]
200
100
0
-100
-200
-300
-400
-500
-2
0
2
4
6
8
10
12
Biaxial load [MPa]
Axial-1
Tangential-1
45-1
Axial-2
Tangential-2
45-2
Axial-3
Tangential-3
45-3

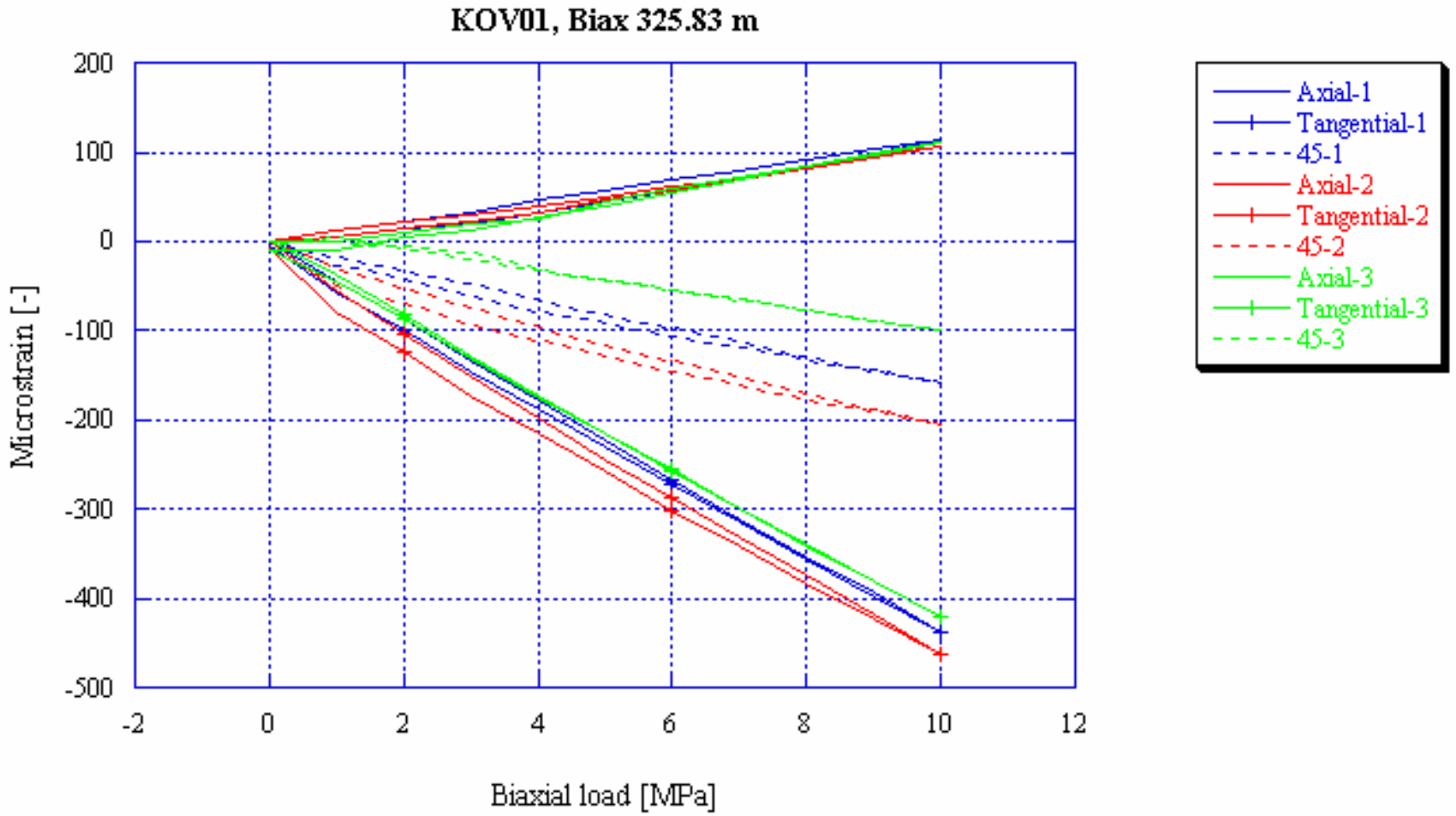
KOV01, Biax 325.83 m
Microstrain [-]
200
100
0
-100
-200
-300
-400
-500
-2
0
2
4
6
8
10
12
Biaxial load [MPa]
Axial-1
Tangential-1
45-1
Axial-2
Tangential-2
45-2
Axial-3
Tangential-3
45-3

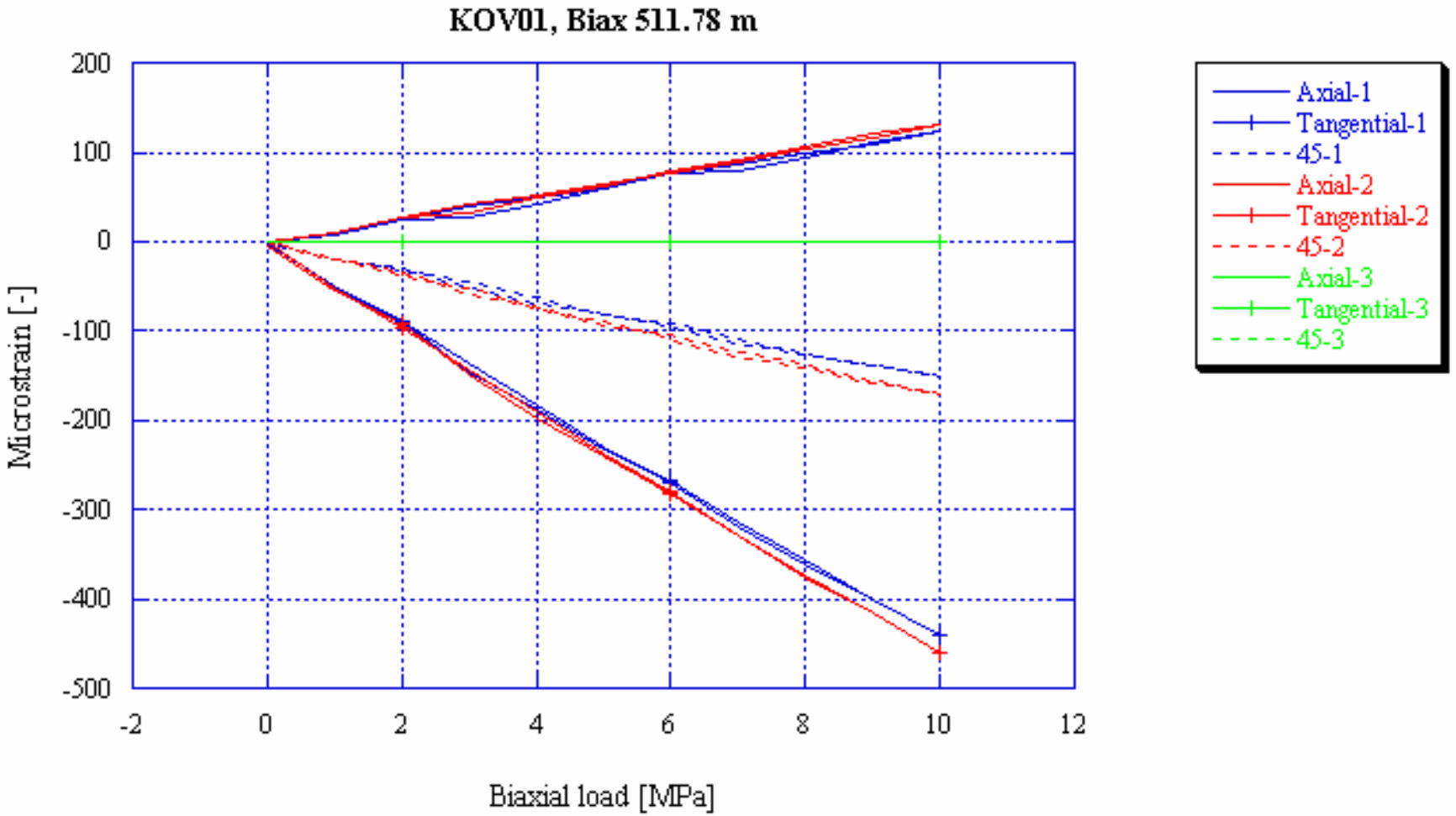
KOV01, Biax 511.78 m
Microstrain [-]
200
100
0
-100
-200
-300
-400
-500
-2
0
2
4
6
8
10
12
Biaxial load [MPa]
Axial-1
Tangential-1
45-1
Axial-2
Tangential-2
45-2
Axial-3
Tangential-3
45-3

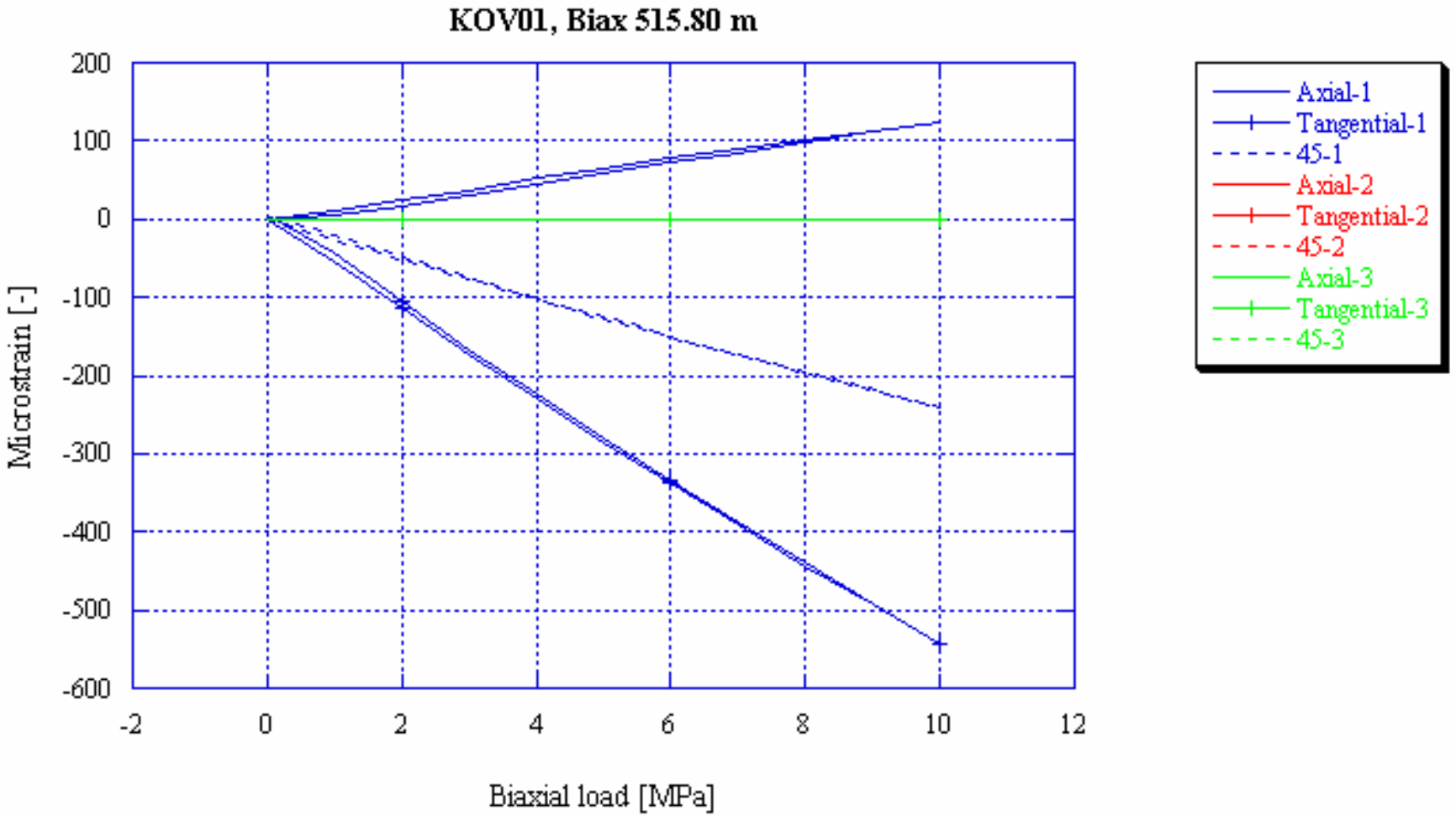
KOV01, Biax 515.80 m
Microstrain [-]
200
100
0
-100
-200
-300
-400
-500
-600
-2
0
2
4
6
8
10
12
Biaxial load [MPa]
Axial-1
Tangential-1
45-1
Axial-2
Tangential-2
45-2
Axial-3
Tangential-3
45-3

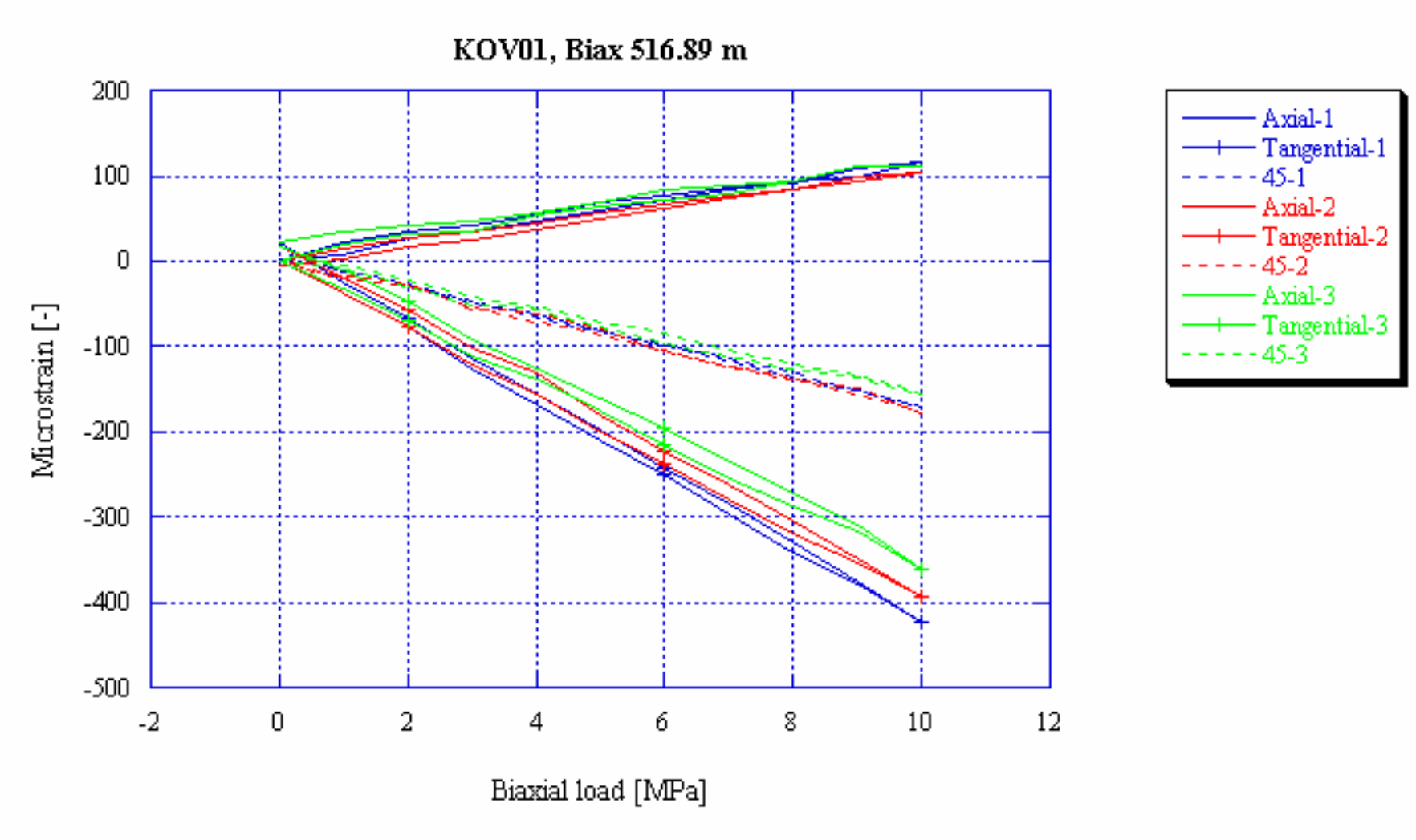
KOV01, Biax 516.89 m
Microstrain [-]
200
100
0
-100
-200
-300
-400
-500
-2
0
2
4
6
8
10
12
Biaxial load [MPa]
Axial-1
Tangential-1
45-1
Axial-2
Tangential-2
45-2
Axial-3
Tangential-3
45-3

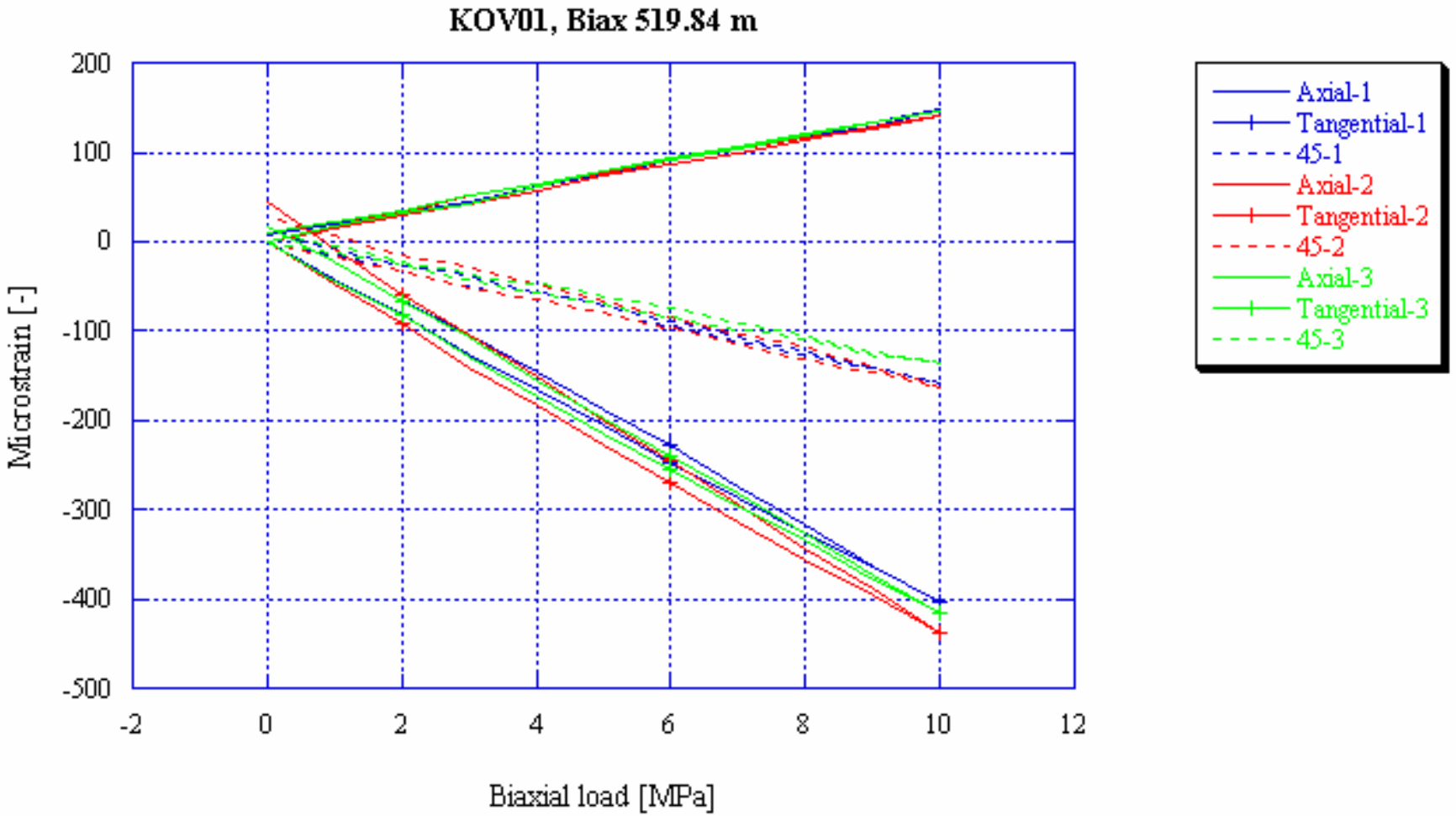
KOV01, Biax 519.84 m
Microstrain [-]
200
100
0
-100
-200
-300
-400
-500
-2
0
2
4
6
8
10
12
Biaxial load [MPa]
Axial-1
Tangential-1
45-1
Axial-2
Tangential-2
45-2
Axial-3
Tangential-3
45-3

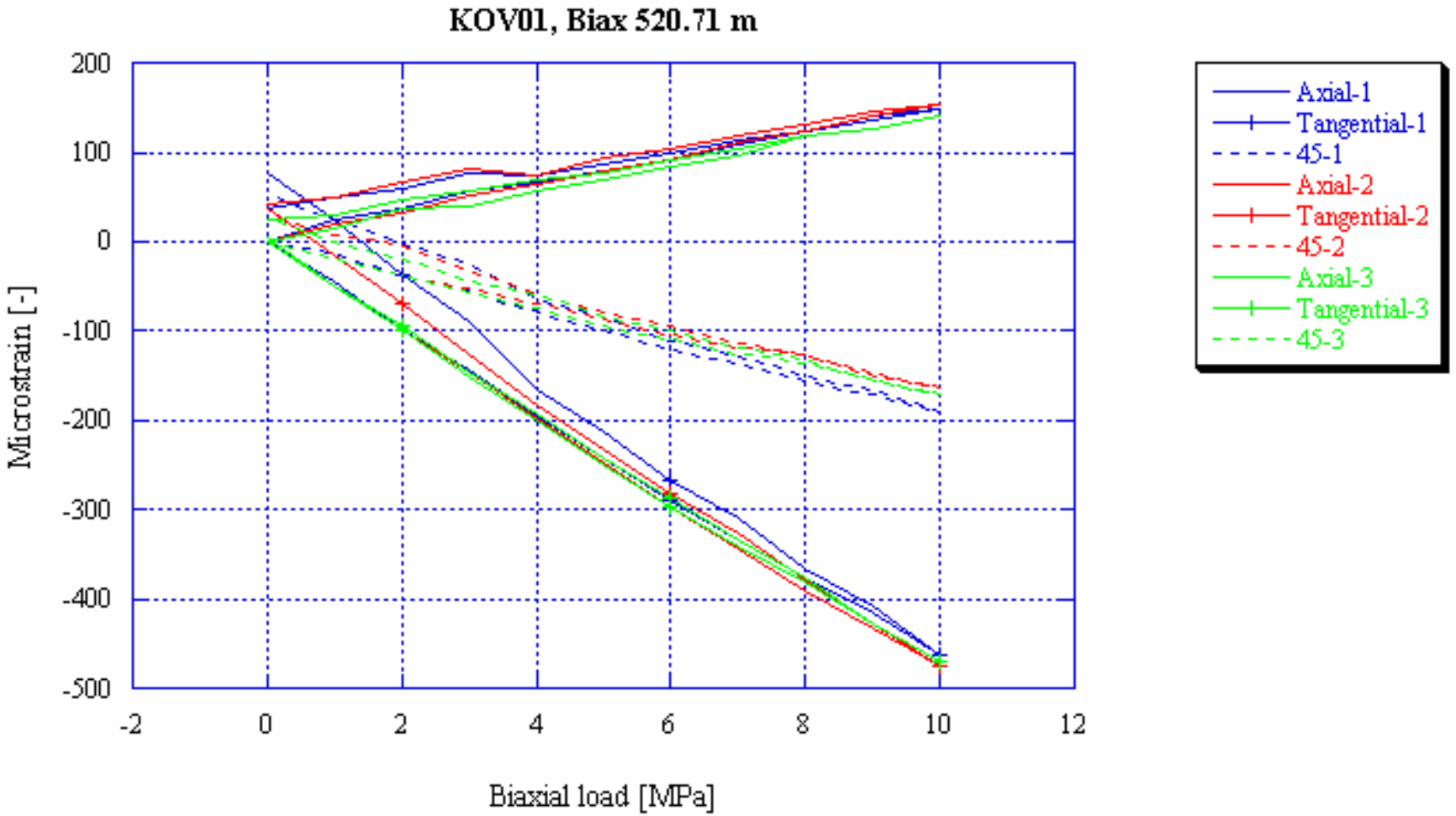
KOV01, Biax 520.71 m
Microstrain [-]
200
100
0
-100
-200
-300
-400
-500
-2
0
2
4
6
8
10
12
Biaxial load [MPa]
Axial-1
Tangential-1
45-1
Axial-2
Tangential-2
45-2
Axial-3
Tangential-3
45-3

Appendix 5

Evaluated strains, elastic parameters and their standard deviation

A5.1 General about overcoring data from the Borre Probe

The following results from the overcoring data analysis are based on viewing the data as individual measurement points. Consequently, no attempts have been made to combine measurement points from a single or from multiple boreholes. Note that SD^{ind} includes all data, i.e. also strain gauges that are likely to be erroneous or questionable. Data rejected by the Chauvenet's criterion are indicated by ^{C}.

A5.2 Borehole KAS05

Raw stress data has not been found for borehole KAS05

A5.3 Borehole KXZSD8HR

Table A5-1. Results from re-analysis of overcoring strains in borehole KXZSD8HR. The published results are presented in brackets. Gauges/rosettes that are of questionable quality are in italic font. ^{T} indicates that the strain data have been temperature corrected. The standard deviations for single measurement points are also given.

Depth	Microstrains [-]								
	Rosette 1			Rosette 2			Rosette 3		
[m]	Ax.	Tang.	45°	Ax.	Tang.	45°	Ax.	Tang.	45°
1.29	*69*^{T} (62)	*123*^{T} (219)	*67*^{T} (40)	*74*^{T} (60)	*79*^{T} (126)	*92*^{T} (165)	*73*^{T} (65)	*63*^{T} (45)	*64*^{T} (32)
1.66	*-71*^{C} (94)	*119* (430)	*59* (242)	*71* (97)	*168* (215)	*169* (211)	*64* (91)	*-21* (-35)	*34* (35)
2.40	36 (35)	123 (258)	45 (84)	*54* (72)	*64* (75)	*69* (64)	*54* (69)	*52* (-4)	*48* (49)
3.18	-	264	197	-	235	249	-	-33	119
4.07	*60* (76)	*289* (354)	*136* (178)	*112* (111)	*166* (222)	*95* (106)	*149* (199)	*-65* (-38)	*82* (176)
5.96	177 (197)	481 (522)	354 (372)	200 (220)	153 (168)	128 (144)	195 (214)	103 (111)	241 (252)
6.61	69 (84)	197 (286)	127 (146)	104 (124)	238 (434)	180 (313)	*558*^{C} (104)	*109* (44)	*64* (16)
12.28	58 (138)	137 (235)	121 (174)	243 (289)	475 (633)	805 (940)	272 (395)	218 (343)	236 (292)
12.93	207 (218)	375 (408)	184 (203)	223 (243)	99 (118)	128 (145)	*279* (306)	*58* (71)	*349* (357)
13.59	*43* (109)	*20* (49)	*-32* (-1)	*67* (130)	*103* (208)	*96* (191)	*-22* (-22)	*-30* (27)	*-11* (33)
14.30	210 (251)	142 (181)	98 (121)	203 (239)	372 (408)	351 (383)	209 (241)	88 (106)	199 (222)

Depth	**Microstrains [-]**								
	Rosette 1			**Rosette 2**			**Rosette 3**		
[m]	Ax.	Tang.	45°	Ax.	Tang.	45°	Ax.	Tang.	45°
15.60	195 (164)	157 (124)	205 (171)	314[C] (283)	94 (66)	191 (161)	204 (172)	532 (501)	396 (363)
16.96	- 	- 	- 	*84* (59)	*270* (279)	*277* (257)	*50* (36)	*360* (367)	*384* (389)
17.62	142 (165)	39 (50)	-52 (-52)	152 (177)	331 (358)	314 (334)	182 (215)	146 (175)	261 (286)
18.27	*-76*[C] (-54)	*75* (100)	*-71* (-64)	*60* (86)	*-18* (-5)	*128* (145)	*70* (73)	*109* (106)	*64* (83)
18.92	*59* (218)	*4* (159)	*5* (149)	*15* (210)	*23* (183)	*12* (179)	*0* (159)	*-95* (103)	*13* (188)
19.57	*162* (185)	*141* (156)	*297* (304)	180 (189)	265 (264)	147 (148)	162 (165)	304 (298)	192 (192)
20.22	203 (216)	256 (266)	112 (108)	170 (181)	410 (426)	226 (232)	201 (206)	305 (309)	212 (213)
20.85	109 (142)	281 (305)	183 (202)	115 (138)	23 (38)	-38 (-26)	79[C] (126)	250 (287)	347 (381)
21.50	74 (85)	39 (49)	126 (139)	75 (82)	124 (136)	-28 (-18)	45[C] (83)	303 (349)	257 (284)
22.21	34 (50)	50 (68)	132 (148)	29 (48)	228 (257)	-9 (10)	38 (57)	207 (234)	203 (227)
22.94	77 (74)	92 (102)	242 (243)	88 (88)	441 (454)	144 (137)	*-45*[C] (81)	*210* (191)	*131* (129)
	SD^{gauge} [-]								
1.29	*15*	*9*	*11*	*12*	*9*	*9*	*14*	*9*	*9*
1.66	*8*	*15*	*16*	*4*	*4*	*3*	*7*	*7*	*6*
2.40	11	7	7	*12*	*7*	*11*	*13*	*6*	*12*
3.18	*50*[I]	29	28	*50*[I]	23	46	*50*[I]	31	16
4.07	*7*	*11*	*9*	*10*	*8*	*9*	*11*	*9*	*12*
5.96	2	2	2	2	2	3	1	1	1
6.61	13	12	8	11	15	15	*105*	*52*	*64*
12.28	4	15	15	2	8	10	35	9	27
12.93	2	4	3	2	2	2	*6*	*4*	*7*
13.59	*7*	*6*	*6*	*5*	*9*	*6*	*7*	*8*	*8*
14.30	3	3	2	3	3	2	5	2	3
15.60	2	3	3	4	2	3	4	3	3
16.96	-	-	-	*5*	*3*	*3*	*3*	*7*	*5*
17.62	3	2	3	2	2	1	1	4	2
18.27	*5*	*9*	*3*	*12*	*7*	*10*	*16*	*5*	*12*
18.92	*7*	*3*	*4*	*5*	*2*	*4*	*2*	*3*	*4*
19.57	*3*	*5*	*4*	3	2	1	1	1	1
20.22	2	1	1	2	2	2	2	1	1
20.85	1	2	2	3	2	1	3	3	2
21.50	1	2	2	3	2	2	1	4	2
22.21	2	3	2	2	2	1	2	2	2
22.94	3	4	3	1	1	2	*15*	*34*	*6*
[m]	**$SD^{diff,\ ind}$ [-]**								
1.29	*8*	*9*	*9*	*9*	*9*	*9*	*7*	*7*	*7*
1.66	*34*	*13*	*11*	*4*	*4*	*4*	*7*	*7*	*7*
2.40	3	3	3	*1*	*1*	*0*	*2*	*2*	*2*
3.18	*9*[I]	9[I]	9[I]	*16*[I]	31[I]	41[I]	*18*[I]	18[I]	18[I]
4.07	*14*	*3*	*16*	*2*	*2*	*2*	*3*	*3*	*3*
5.96	7	1	1	3	3	3	5	5	5

Depth	**Microstrains [-]**								
	Rosette 1			**Rosette 2**			**Rosette 3**		
[m]	Ax.	Tang.	45°	Ax.	Tang.	45°	Ax.	Tang.	45°
6.61	8	19	171	1	1	1	*3*	*3*	*3*
12.28	61	0	10	17	17	17	34	34	34
12.93	11	6	13	1	1	1	*3*	*3*	*3*
13.59	*6*	*14*	*16*	*1*	*1*	*1*	*3*	*3*	*3*
14.30	0	3	1	1	1	1	3	3	3
15.60	16	24	13	2	2	2	3	3	3
16.96	-	-	-	-	-	-	-	-	-
17.62	7	3	7	1	1	1	2	2	2
18.27	*32*	*14*	*17*	*0*	*0*	*0*	*1*	*1*	*1*
18.92	*10*	*4*	*9*	*1*	*1*	*1*	*2*	*2*	*2*
19.57	*3*	*3*	*3*	1	1	1	2	2	2
20.22	12	1	11	8	8	8	16	16	16
20.85	0	2	10	2	2	2	5	5	5
21.50	2	3	7	1	1	1	2	2	2
22.21	1	3	0	1	1	1	2	2	2
22.94	9	13	32	3	3	3	*6*	*6*	*6*
[m]	**SD^{ind} [-]**								
1.29	*23*	*18*	*20*	*21*	*18*	*18*	*21*	*16*	*16*
1.66	*42*	*28*	*27*	*8*	*8*	*7*	*14*	*14*	*13*
2.40	14	10	10	*13*	*8*	*11*	*15*	*8*	*14*
3.18	*59*[1]	38[1]	37[1]	*66*[1]	54[1]	87[1]	*68*[1]	49[1]	34[1]
4.07	*21*	*14*	*25*	*12*	*10*	*11*	*14*	*12*	*15*
5.96	9	3	3	5	5	6	6	6	6
6.61	21	31	179	12	16	16	*108*	*55*	*67*
12.28	65	15	25	19	25	27	69	43	61
12.93	13	10	16	3	3	3	*9*	*7*	*10*
13.59	*13*	*20*	*22*	*6*	*10*	*7*	*10*	*11*	*11*
14.30	3	6	3	4	4	3	8	5	6
15.60	18	27	16	6	4	5	7	6	6
16.96	-	-	-	-	-	-	-	-	-
17.62	10	5	10	3	3	2	2	6	4
18.27	*37*	*23*	*20*	*12*	*7*	*10*	*17*	*6*	*13*
18.92	*17*	*7*	*13*	*6*	*3*	*4*	*4*	*5*	*6*
19.57	*6*	*8*	*7*	4	3	2	3	3	3
20.22	14	2	12	10	10	10	18	17	17
20.85	1	4	12	5	4	3	8	8	7
21.50	3	5	9	4	3	3	3	6	4
22.21	3	6	2	3	3	2	4	4	4
22.94	12	17	35	4	4	5	*21*	*40*	*12*

[1] in measurement point 3.18 m was calculated using the average value of the axial gauges in 2.40 and 4.07 m, i.e. with 78 με, and the SD^{gauge} was set to 50 με. Measurement points 13.59, 18.27, and 18.92 indicate very low stresses probably due to imperfect gluing. Measurement point 16.96 m has one malfunctioning rosette, i.e. SD^{ind} is not possible to calculate.

Table A5-2. Results from re-analysis of biaxial tests in borehole KXZSD8HR. Values in brackets include erroneous strain gauges and asterisk indicates questionable result.

Depth	Elastic parameters			
[m]	E^{ind}	δE^{ind}	υ^{ind}	$\delta\upsilon^{ind}$
1.29	55.4*	8.8*	0.31*	0.03*
1.66	60.2*	16.3*	0.36*	0.09*
2.40	72.2 (65.4)	1.2 (5.2)	0.28 (0.23)	0.01 (0.05)
3.18	-	-	-	-
4.07	54.3*	10.5*	0.18*	0.11*
5.96	61.1	9.3	0.24	0.02
6.61	62.1 (64.4)	9.0 (8.0)	0.21 (0.23)	0.02 (0.04)
12.28	-	-	-	-
12.93	61.3 (63.2)	0.6 (5.9)	0.23 (0.28)	0.01 (0.04)
13.59	-	-	-	-
14.30	64.0	2.0	0.24	0.02
15.60	50.4*	6.5*	0.27*	0.05*
16.96	-	-	-	-
17.62	66.3	5.3	0.27	0.01
18.27	102.3*	19.6*	0.41*	0.08*
18.92	-	-	-	-
19.57	65.8 (60.1)	8.6 (10.9)	0.23 (0.20)	0.03 (0.06)
20.22	55.0 (56.7)	1.6 (10.7)	0.27 (0.33)	0.01 (0.05)
20.85	55.7	6.0	0.25	0.04
21.50	59.9	5.0	0.24	0.02
22.21	64.1 (64.7)	1.7 (1.7)	0.27 (0.29)	0.01 (0.03)
22.94	66.6 (76.1)	5.6 (15.0)	0.23 (0.26)	0.02 (0.05)

The shallow data is replaced by the average of 2.40, 5.96 and 6.61 m, i.e. with E=65.1 GPa and ν=0.24; 12.28 m is replaced by the data at 12.93 m; 13.59 m is replaced by the average of 12.93 and 14.30 m, i.e. with E=65.0 GPa and ν=0.26; 15.60 and 16.96 m is replaced by the average of 14.30 and 17.62 m, i.e. with E=58.2 GPa and ν=0.28; 18.27 and 18.92 m is replaced by the average of 17.62 and 19.57 m, i.e. with E=66.1 GPa and ν=0.25.

A5.4 Borehole KXZSD81HR

Table A5-3. Results from re-analysis of overcoring strains in borehole KXZSD81HR. The published results are presented in brackets. Gauges/rosettes that are of questionable quality are in italic font. The standard deviations for single measurement points are also given.

Depth	Microstrains [-]								
	Rosette 1			Rosette 2			Rosette 3		
[m]	Ax.	Tang.	45°	Ax.	Tang.	45°	Ax.	Tang.	45°
0.86	*2* (74)	*596* (618)	*97* (127)	*42* (59)	*420* (427)	*302* (317)	83 (90)	-119 (-146)	5 (-11)
1.43	53 (77)	248 (424)	108 (206)	*159*[C] (163)	*131* (128)	*107* (95)	*63* (82)	*-54* (-68)	*23* (32)
2.73	139 (135)	499 (500)	289 (285)	117 (114)	48 (46)	42 (40)	155 (152)	124 (123)	203 (199)
3.34	82[C] (98)	410 (477)	225 (272)	156 (162)	39 (43)	68 (71)	116 (131)	130 (164)	197 (210)
[m]	SD^{gauge} [-]								
0.86	*12*	*23*	*5*	*3*	*2*	*1*	*4*	*3*	*4*
1.43	2	7	4	*5*	*4*	*7*	*2*	*3*	*3*
2.73	1	1	1	2	1	1	1	1	1
3.34	2	4	4	3	2	3	1	2	2
[m]	$SD^{diff, ind}$ [-]								
0.86	*9*	*4*	*18*	*4*	*4*	*4*	*8*	*8*	*8*
1.43	11	25	7	*2*	*2*	*2*	*5*	*5*	*5*
2.73	1	6	6	0	0	0	1	37	1
3.34	13	12	2	1	1	1	2	2	2
[m]	SD^{ind} [-]								
0.86	*21*	*27*	*23*	*7*	*6*	*5*	*12*	*11*	*12*
1.43	13	32	11	*7*	*6*	*9*	*7*	*8*	*8*
2.73	2	7	7	2	1	1	2	38	2
3.34	15	16	6	4	3	4	3	4	4

Table A5-4. Results from re-analysis of biaxial tests in borehole KXZSD81HR. Values in brackets include erroneous strain gauges.

Depth	Elastic parameters			
[m]	E^{ind}	δE^{ind}	υ^{ind}	$\delta\upsilon^{ind}$
0.86	60.7 (68.4)	0.4 (10.0)	0.28 (0.34)	0.01 (0.09)
1.43	79.1 (59.9)	2.1 (14.5)	0.28 (0.25)	0.01 (0.02)
2.73	59.3	6.2	0.26	0.02
3.34	60.6	7.0	0.26	0.04

A5.5 Borehole KXZSD8HL

Table A5-5. Results from re-analysis of overcoring strains in borehole KXZSD8HL. The published results are presented in brackets. Gauges/rosettes that are of questionable quality are in italic font. ^{T} indicates that the strain data have been temperature corrected. The standard deviations for single measurement points are also given.

Depth	Microstrains [-]								
	Rosette 1			Rosette 2			Rosette 3		
[m]	Ax.	Tang.	45°	Ax.	Tang.	45°	Ax.	Tang.	45°
23.37	*111*^{T} (150)	*144*^{T} (223)	*166*^{T} (243)	*254*^{T,C} (162)	*96*^{T} (242)	*42*^{T} (50)	*133*^{T} (174)	*56*^{T} (37)	*182*^{T} (201)
24.06	*2*^{C} (200)	*-105* (223)	*209* (364)	*127* (198)	*-49* (224)	*130* (129)	205 (195)	114 (122)	82 (88)
24.75	168^{C} (192)	196 (216)	215 (234)	207 (218)	175 (184)	68 (86)	215 (253)	99 (110)	283 (308)
25.44	224 (236)	281 (288)	137 (142)	251 (256)	359 (360)	160 (440)	212 (217)	138 (143)	169 (168)
[m]	**SD^{gauge} [-]**								
23.37	*6*	*7*	*12*	*235*	*268*	*13*	*4*	*3*	*3*
24.06	*45*	*47*	*12*	*10*	*12*	*2*	1	2	3
24.75	1	1	1	1	1	1	1	1	1
25.44	1	2	1	1	2	1	2	1	2
[m]	**$SD^{diff, ind}$ [-]**								
23.37	*18*	*30*	*11*	*0*	*0*	*0*	*1*	*1*	*1*
24.06	*50*	*8*	*18*	*13*	*13*	*13*	26	26	26
24.75	11	2	5	1	1	1	3	3	3
25.44	8	17	4	10	10	10	20	20	20
[m]	**SD^{ind} [-]**								
23.37	24	37	23	*235*	*268*	*13*	5	4	4
24.06	*95*	*55*	*30*	*23*	*25*	*15*	27	28	29
24.75	12	3	6	2	2	2	4	4	4
25.44	9	19	5	11	12	11	22	21	22

Table A5-6. Results from re-analysis of biaxial tests in borehole KXZSD8HL. Values in brackets include erroneous strain gauges and asterisk indicates questionable result.

Depth	Elastic parameters			
[m]	E^{ind}	δE^{ind}	υ^{ind}	$\delta\upsilon^{ind}$
23.37	68.5	0.8	0.26	0.01
24.06	63.1*	2.7*	0.40*	0.05*
24.75	64.5	2.0	0.25	0.05
25.44	64.8	1.8	0.26	0.02

*is replaced by the average of 23.37, 24.75 and 25.44 m, i.e. with E=65.6 GPa and ν=0.27.

A5.6 Borehole KK0045G01

Table A5-7. Results from re-analysis of overcoring strains in borehole KK0045G01. The published results are presented in brackets. Gauges/rosettes that are of questionable quality are in italic font. ^{T} indicates that the strain data have been temperature corrected. The standard deviations for single measurement points are also given.

Depth	Microstrains [-]								
	Rosette 1			Rosette 2			Rosette 3		
[m]	Ax.	Tang.	45°	Ax.	Tang.	45°	Ax.	Tang.	45°
1.20	-105^{T} (-109)	392^{T} (375)	70^{T} (71)	-89^{T} (-109)	273^{T} (249)	35^{T} (16)	-72^{T,C} (-109)	1700^{T} (1691)	923^{T} (907)
2.24	-37^{T} (-79)	17^{T} (-13)	1^{T} (-34)	-21^{T,C} (-76)	488^{T} (482)	263^{T} (249)	-37^{T} (-72)	679^{T} (652)	272^{T} (234)
2.70	85^{T} (61)	432^{T} (405)	326^{T} (328)	*70*^{T} (50)	*691*^{T} (640)	115^{T} (89)	66^{T} (39)	261^{T} (235)	321^{T} (295)
3.33	-24^{T} (-43)	-26^{T} (-32)	-38^{T} (-54)	-54^{T,C} (-45)	541^{T} (513)	240^{T} (220)	-26^{T} (-47)	702^{T} (661)	409^{T} (380)
4.12	2^{T} (-4)	266^{T} (253)	145^{T} (168)	*4*^{T} (0)	*208*^{T} (253)	*257*^{T} (230)	*222*^{T,C} (-2)	*652*^{T} (624)	*150*^{T} (164)
4.53	99^{T} (68)	299^{T} (312)	146^{T} (119)	88^{T} (82)	667^{T} (668)	425^{T} (407)	*-55*^{T,C} (75)	*249*^{T} (383)	*88*^{T} (268)
4.97	*1345*^{T} (85)	*766*^{T} (754)	*666*^{T} (634)	*899*^{T,C} (85)	*686*^{T} (652)	*1444*^{T} (-469)	*1472*^{T} (85)	*198*^{T} (192)	*711*^{T} (762)
5.51	*-283*^{T} (82)	*227*^{T} (757)	*-240*^{T} (192)	94^{T} (96)	413^{T} (379)	101^{T} (65)	105^{T} (68)	166^{T} (128)	247^{T} (220)
6.07	105^{T} (65)	139^{T} (98)	78^{T} (35)	158^{T,C} (70)	803^{T} (765)	321^{T} (283)	115^{T} (75)	567^{T} (515)	529^{T} (465)
6.50	*42*^{T} (34)	*147*^{T} (109)	*71*^{T} (81)	62^{T} (34)	390^{T} (371)	227^{T} (195)	*-65*^{T,C} (34)	*757*^{T} (758)	*383*^{T} (394)
8.16	*-333*^{TC} (38)	638^{T} (668)	178^{T} (226)	*34*^{T} (38)	*74*^{T} (90)	*167*^{T} (154)	79^{T} (38)	156^{T} (119)	156^{T} (116)
31.67	*44*^{T,1} (82)	*427*^{T,1} (368)	*590*^{T,1} (593)	212^{T,1} (202)	1144^{T,1} (1082)	572^{T,1} (542)	*212*^{T,1} (195)	*415*^{T,1} (312)	*30*^{T,1} (38)
32.48	*39*^{T} (88)	*98*^{T} (347)	*227*^{T} (272)	*-130*^{T,C} (72)	*267*^{T} (490)	*-68*^{T} (-47)	*2*^{T} (55)	*898*^{T} (716)	*658*^{T} (658)
34.77	156^{T} (144)	234^{T} (226)	12^{T} (-5)	*61*^{T,C} (132)	*391*^{T} (538)	*546*^{T} (620)	131^{T} (119)	594^{T} (601)	269^{T} (265)
35.48	77^{T} (91)	*496* (566)	114^{T} (139)	127^{T} (132)	*494* (518)	309^{T} (338)	*206*^{C} (112)	75^{T} (151)	297^{T} (308)
62.82	*7* (21)	*-1* (44)	*181* (184)	*-13*^{C} (16)	*868* (1004)	*313* (444)	*3* (10)	*450* (550)	*196* (195)
63.59	113^{T} (158)	400^{T} (456)	109^{T} (113)	137^{T} (150)	815^{T} (910)	593^{T} (655)	167^{T} (166)	216^{T} (376)	290^{T} (340)
64.51	*74* (230)	*951*^{T} (1093)	*1031*^{T} (1030)	*60*^{T} (208)	*593*^{T} (689)	*371*^{T} (381)	*76*^{T} (186)	*484*^{T} (508)	*76*^{T} (46)
	SD^{gauge} [-]								
1.20	1	2	1	1	2	1	1	1	1
2.24	2	2	2	4	6	3	1	2	2
2.70	2	2	2	*9*	*12*	5	2	4	2
3.33	1	1	1	2	2	2	1	3	4
4.12	6	3	14	*6*	*3*	*1*	*34*	*12*	*7*
4.53	1	2	1	5	2	2	*40*	*25*	*67*

Depth	Microstrains [-]								
	Rosette 1			Rosette 2			Rosette 3		
[m]	Ax.	Tang.	45°	Ax.	Tang.	45°	Ax.	Tang.	45°
4.97	*5*	*1*	*1*	*1*	*1*	*5*	*5*	*2*	*5*
5.51	*55*	*75*	*73*	5	3	1	1	2	2
6.07	2	1	1	2	2	1	2	2	2
6.50	*2*	*4*	*6*	3	3	1	*11*	*7*	*11*
8.16	*41*	7	10	*24*	*46*	*29*	2	2	1
31.67	*11*	*10*	*5*	2	2	2	*65*	*21*	*38*
32.48	*29*	*10*	*70*	*90*	*25*	*21*	*91*	*85*	*91*
34.77	1	2	2	*13*	*14*	*6*	2	7	11
35.48	3	*8*	6	3	*11*	4	*17*	5	7
62.82	*61*	*10*	*32*	*22*	*11*	*31*	*10*	*2*	*6*
63.59	6	7	3	2	7	5	2	4	2
64.51	*39*	*57*	*13*	*23*	*12*	*18*	*81*	*60*	*41*
[m]	**$SD^{diff, ind}$ [-]**								
1.20	5	1	6	1	1	1	2	2	2
2.24	1	4	1	0	0	0	1	1	1
2.70	5	0	1	*2*	*2*	*2*	3	3	3
3.33	2	8	1	2	2	2	4	4	4
4.12	20	19	53	*5*	*5*	*5*	*9*	*9*	*9*
4.53	19	15	32	1	1	1	*1*	*1*	*1*
4.97	*30*	*118*	*73*	*5*	*5*	*5*	*10*	*10*	*10*
5.51	*76*	*50*	*54*	9	9	9	19	19	19
6.07	6	11	3	1	1	0	1	1	1
6.50	*9*	*16*	*27*	1	1	1	*1*	*1*	*1*
8.16	*93*	29	44	*7*	*7*	*7*	13	13	13
31.67	*18*	*13*	*13*	2	2	2	*5*	*5*	*5*
32.48	*14*	*42*	*2*	*9*	*9*	*9*	*17*	*17*	*17*
34.77	12	20	3	*2*	*2*	*2*	3	3	3
35.48	19	*3*	24	1	*1*	1	*1*	1	1
62.82	*1*	*5*	*0*	*1*	*1*	*1*	*2*	*2*	*2*
63.59	11	3	7	3	3	3	5	5	5
64.51	*12*	*17*	*11*	*13*	*13*	*13*	*27*	*27*	*27*
	SD^{ind} [-]								
1.20	6	3	7	2	3	2	3	3	3
2.24	3	6	3	4	6	3	2	3	3
2.70	7	2	3	*11*	*14*	*7*	5	7	5
3.33	3	9	2	4	4	4	5	7	8
4.12	26	22	67	*11*	*8*	*6*	*43*	*21*	*16*
4.53	20	17	33	6	3	3	*41*	*26*	*68*
4.97	*35*	*119*	*74*	*6*	*6*	*10*	*15*	*12*	*15*
5.51	*131*	*125*	*127*	14	12	10	20	21	21
6.07	8	12	4	3	3	1	3	3	3
6.50	*11*	*20*	*33*	4	4	2	*12*	*8*	*12*
8.16	*134*	36	54	*31*	*53*	*36*	15	15	14
31.67	*29*	*23*	*18*	4	4	4	*70*	*26*	*43*
32.48	*43*	*52*	*72*	*99*	*34*	*30*	*108*	*102*	*108*
34.77	13	22	5	*15*	*16*	*8*	5	10	14
35.48	22	*11*	30	4	*12*	5	*18*	6	8
62.82	*62*	*15*	*32*	*23*	*12*	*32*	*12*	*4*	*8*
63.59	17	10	10	5	10	8	7	9	7
64.51	*51*	*74*	*24*	*36*	*25*	*31*	*108*	*87*	*68*

[1] indicates that the data has been corrected for rotation of rosette (only 31.67 m).

Table A5-8. Results from re-analysis of biaxial tests in borehole KK0045G01. Values in brackets include erroneous strain gauges and asterisk indicates questionable result.

Depth	Elastic parameters			
[m]	E^{ind}	δE^{ind}	υ^{ind}	$\delta\upsilon^{ind}$
1.20	66.7	1.8	0.26	0.02
2.24	63.2 (62.0)	5.2 (4.5)	0.26 (0.26)	0.02 (0.04)
2.70	58.0 (57.2)	1.1 (3.5)	0.20 (0.25)	0.01 (0.05)
3.33	52.4*	5.4*	0.32*	0.01’
4.12	-	-	-	-
4.53	65.0 (66.0)	1.5 (2.0)	0.25 (0.26)	0.01 (0.03)
4.97	-	-	-	-
5.51	66.2 (65.7)	0.5 (0.9)	0.28 (0.28)	0.01 (0.01)
6.07	45.7* (58.9*)	1.7* (17.3*)	0.24* (0.34*)	0.01* (0.15*)
6.50	49.3* (43.2*)	1.0* (5.2*)	0.20* (0.19*)	0.01* (0.01*)
8.16	53.9* (51.2*)	2.5* (4.5’)	0.28* (0.26*)	0.01* (0.03*)
31.67	55.8 (55.2)	1.5 (1.7)	0.24 (0.24)	0.01 (0.01)
32.48	59.9 (62.4)	1.3 (4.0)	0.26 (0.29)	0.01 (0.05)
34.77	60.6 (70.0)	1.1 (14.2)	0.24 (0.29)	0.01 (0.07)
35.48	64.2 (59.5)	1.1 (5.8)	* (0.20)	* (0.02)
62.82	67.0*	1.1*	0.30*	0.06*
63.59	53.8	3.8	0.21	0.03
64.51	49.2*	2.3*	0.21*	0.03*

The points at 3.33 and 4.12 m is replaced by the average of 2.70 and 4.53 m, i.e. with E=61.5 GPa and ν=0.23; 4.97 m is replaced by the average of 4.53 and 5.51 m, i.e. with E=65.6 GPa and ν=0.27; points at 6.07, 6.50 and 8.16 m is replaced by the data at 5.51m; the Poisson’s ratio in 35.48 is replaced by the average of the data at the 30 m level, i.e. with ν=0.25; the elastic parameters for the 60 m level is set equal to the result at 63.59 m.

A5.7 Borehole KF0093A01

Table A5-9. Results from re-analysis of overcoring strains in borehole KF0093A01. The published results are presented in brackets. Gauges/rosettes that are of questionable quality are in italic font. The standard deviations for single measurement points are also given.

Depth	Microstrains [-]								
	Rosette 1			Rosette 2			Rosette 3		
[m]	Ax.	Tang.	45°	Ax.	Tang.	45°	Ax.	Tang.	45°
32.14	*250* (364)	*165* (331)	*347* (491)	*119*[C] (364)	*530* (949)	*75* (211)	*337* (364)	*107* (243)	*403* (606)
32.70	*292* (344)	*217* (444)	*407* (603)	*163*[C] (344)	*529* (903)	*102* (249)	*350* (344)	*-38* (32)	*239* (353)
35.38	358[C] (330)	67 (145)	18 (131)	202 (330)	506 (548)	406 (438)	*187* (330)	*137* (247)	*314* (436)
[m]	SD^{gauge} [-]								
32.14	*2*	*4*	*5*	*2*	*8*	*3*	*1*	*2*	*8*
32.70	*12*	*16*	*12*	*7*	*17*	*11*	*6*	*2*	*6*
35.38	3	6	2	5	4	3	*17*	*539*	*11*
[m]	$SD^{diff, ind}$ [-]								
32.14	*2*	*41*	*31*	*3*	*3*	*3*	*5*	*5*	*5*
32.70	*8*	*35*	*28*	*0*	*4*	*0*	*1*	*1*	*1*
35.38	36	16	21	0	0	0	*1*	*1*	*1*
[m]	SD^{ind} [-]								
32.14	*4*	*45*	*36*	*5*	*11*	*6*	*6*	*7*	*13*
32.70	*20*	*51*	*40*	*7*	*21*	*11*	*7*	*3*	*7*
35.38	39	22	23	5	4	3	*18*	*540*	*12*

Table A5-10. Results from re-analysis of biaxial tests in borehole KF0093A01. Values in brackets include erroneous strain gauges.

Depth	Elastic parameters			
[m]	E^{ind}	δE^{ind}	υ^{ind}	$\delta\upsilon^{ind}$
32.14	51.7 (49.4)	13.3 (10.9)	0.18 (0.17)	0.04 (0.03)
32.70	51.7	12.6	0.21	0.06
35.38	44.6 (51.1)	3.7 (10.6)	0.18 (0.22)	0.01 (0.06)

Note that the biaxial test was conducted with maximum pressure of 8 MPa.

A5.8 Borehole KA3579G

Table A5-11. Results from re-analysis of overcoring strains in borehole KA3579G. The published results are presented in brackets. Gauges/rosettes that are of questionable quality are in italic font. [T] indicates that the strain data have been temperature corrected. The standard deviations for single measurement points are also given.

Depth	Microstrains [-]								
	Rosette 1			Rosette 2			Rosette 3		
[m]	Ax.	Tang.	45°	Ax.	Tang.	45°	Ax.	Tang.	45°
2.04	-6 (-16)	585 (639)	319 (334)	-30 (-36)	-135 (-147)	-207[C] (-219)	2 (-6)	544 (600)	302 (344)
2.53	-64[T] (8)	701[T] (796)	281[T] (339)	-37[T] (-48)	115[T] (111)	-21[T] (-27)	70[T,C] (67)	-201[T] (-242)	-3[T] (-20)
3.99	-38[C] (12)	917 (926)	272 (203)	15 (23)	421 (439)	358 (370)	-1 (1)	-55 (-153)	41 (22)
4.54	49 (4)	528 (494)	88 (91)	*-661*[C] (22)	*-677* (-153)	*-547* (-177)	4 (25)	700 (750)	653 (705)
5.41	*632*[C] (100)	*20* (675)	*124* (126)	55 (50)	930 (921)	706 (697)	149 (151)	56 (48)	69 (58)
8.00	86[T] (75)	669[T] (689)	269[T] (274)	65[T] (63)	673[T] (708)	523[T] (528)	*37*[T] (64)	*-46*[T] (211)	*120*[T] (103)
20.06	36 (60)	603 (622)	318 (333)	26[C] (47)	1009 (1013)	512 (550)	*36* (31)	*68* (23)	*64* (62)
21.21	-9 (-4)	867 (902)	454 (477)	-13 (-14)	184 (178)	-11 (41)	*50*[C] (90)	*346* (435)	*271* (276)
21.70	61 (62)	423 (423)	267 (261)	25 (21)	311 (312)	249 (253)	56 (56)	1364 (1427)	802 (833)
22.31	*-90*[C] (82)	*612* (785)	*329* (393)	50 (66)	806 (843)	542 (562)	97 (95)	94 (93)	55 (52)
[m]	SD^{gauge} [-]								
2.04	4	9	5	2	2	3	2	4	3
2.53	3	6	5	3	4	3	4	9	4
3.99	9	4	8	3	3	2	1	6	6
4.54	8	9	3	*108*	*99*	*52*	4	6	5
5.41	*218*	*188*	*12*	3	3	3	4	1	4
8.00	2	3	2	1	3	3	*21*	*23*	*10*
20.06	9	2	1	7	9	6	*15*	*10*	*3*
21.21	2	3	3	1	1	1	7	13	6
21.50	2	1	1	1	1	1	4	11	12
22.31	*36*	*29*	*8*	2	3	2	1	1	1
	$SD^{diff, ind}$ [-]								
2.04	4	4	7	2	2	2	5	5	5
2.53	17	8	28	1	1	1	3	3	3
3.99	12	6	1	2	2	2	3	3	3
4.54	76	161	61	*8*	*8*	*8*	16	16	16
5.41	*119*	*74*	*42*	1	1	1	2	2	2
8.00	1	6	15	6	6	6	13	13	13
20.06	1	2	1	0	0	0	*0*	*0*	*0*
21.21	6	7	7	0	0	0	*0*	*0*	*0*
21.50	3	15	4	7	7	7	15	15	15
22.31	*42*	*5*	*21*	5	5	5	10	10	10

Depth	Microstrains [-]								
	Rosette 1			Rosette 2			Rosette 3		
[m]	Ax.	Tang.	45°	Ax.	Tang.	45°	Ax.	Tang.	45°
[m]	SD^{ind} [-]								
2.04	8	13	12	4	4	5	7	9	8
2.53	20	14	33	4	5	4	7	12	7
3.99	21	10	9	5	5	4	4	9	9
4.54	84	170	64	*116*	*107*	*60*	20	22	21
5.41	*337*	*262*	*54*	4	4	4	*6*	*3*	*6*
8.00	3	9	17	7	9	9	*24*	*36*	*23*
20.06	10	4	2	7	9	6	*15*	*10*	*3*
21.21	8	10	10	1	1	1	*7*	*13*	*6*
21.50	5	16	5	8	8	8	19	26	27
22.31	*78*	*34*	*29*	7	8	7	11	11	11

Table A5-12. Results from re-analysis of biaxial tests in borehole KA3579G. Values in brackets include erroneous strain gauges and asterisk indicates questionable result.

Depth	Elastic parameters			
[m]	E^{ind}	δE^{ind}	υ^{ind}	$\delta\upsilon^{ind}$
2.04	125.5*	23.6*	0.49*	0.03*
2.53	109.4*	18.4*	0.38*	0.03*
3.99	63.1	9.1	0.24	0.03
4.54	87.6* (87.6)	0.6* (1.5)	0.40* (0.40)	0.02* (0.02)
5.41	54.6 (55.1)	7.5 (6.1)	0.25 (0.23)	0.05 (0.05)
8.00	58.5 (53.8)	6.1 (8.5)	0.22 (0.21)	0.02 (0.02)
20.06	70.4 (68.8)	6.7 (5.8)	0.28 (0.28)	0.02 (0.02)
21.21	72.5 (72.6)	4.7 (3.7)	0.32 (0.35)	0.02 (0.05)
21.50	72.7	3.2	0.26	0.02
22.31	61.7 (64.9)	8.8 (8.5)	0.31 (0.31)	0.07 (0.06)

*is replaced by the average of 3.99, 5.41 and 8.00 m, i.e. with E=58.7 GPa and ν=0.24.

A5.9 Borehole KOV01

Table A5-13. Results from re-analysis of overcoring strains in borehole KOV01. The published results are presented in brackets. Gauges/rosettes that are of questionable quality are in italic font. The standard deviations for single measurement points are also given.

Depth	Microstrains [-]								
	Rosette 1			Rosette 2			Rosette 3		
[m]	Ax.	Tang.	45°	Ax.	Tang.	45°	Ax.	Tang.	45°
290.31	*22* (20)	*-9* (-56)	*118* (74)	*7* (20)	*203* (165)	*-27* (-57)	*79*[C] (20)	*233* (205)	*143* (130)
325.83	22 (5)	435 (480)	40 (52)	40 (5)	30 (36)	-47 (-35)	-42[C] (5)	879 (930)	777 (714)
511.78	*67*[C] (-82)	*1028* (1059)	*496* (484)	*-131* (-82)	*363* (318)	*107* (75)	*-138* (-82)	*-99* (-187)	*-138* (-162)
514.79	*-82* (-138)	*270* (-71)	*-148* (-209)	*-81* (-98)	*476* (428)	*300* (257)	*-145* (-212)	*1259* (1157)	*569* (480)
515.80	-18 (-54)	1475 (1416)	839 (795)	-25 (-14)	390 (340)	155 (92)	-10 (-5)	262 (241)	148 (102)
516.89	*-41* (-49)	*41* (7)	*91* (-13)	*-62* (-39)	*116* (104)	*134* (93)	*129* (12)	*783* (747)	*442* (371)
519.84	*-53* (-29)	*726* (704)	*485* (451)	*-59* (-104)	*-100* (83)	*-71* (-96)	*-20* (-53)	*526* (505)	*220* (198)
520.71	*52* (8)	*-83* (-27)	*10* (-39)	*63* (8)	*693* (671)	*539* (496)	*-35*[C] (8)	*724* (680)	*309* (217)
527.46	16[C] (90)	162 (171)	182 (181)	97 (90)	147 (130)	161 (169)	*155* (90)	*803* (981)	*378* (426)
[m]	**SD^{gauge} [-]**								
290.31	*6*	*7*	*6*	*5*	*6*	*3*	*4*	*8*	*6*
325.83	11	9	7	6	7	4	3	9	5
511.78	*15*	*9*	*5*	*7*	*7*	*5*	*3*	*10*	*8*
514.79	*36*	*35*	*19*	*6*	*7*	*10*	*13*	*14*	*9*
515.80	2	6	4	6	8	6	2	4	9
516.89	*3*	*9*	*16*	*4*	*8*	*19*	*20*	*9*	*12*
519.84	*6*	*4*	*5*	*4*	*7*	*4*	*3*	*5*	*3*
520.71	*4*	*10*	*6*	*33*	*17*	*7*	*4*	*5*	*8*
527.46	3	8	5	3	5	4	*5*	*16*	*8*
[m]	**$SD^{diff,\ ind}$ [-]**								
290.31	*3*	*8*	*16*	*1*	*1*	*1*	*2*	*2*	*2*
325.83	2	8	19	3	3	3	7	7	7
511.78	*48*	*18*	*21*	*3*	*3*	*3*	*6*	*6*	*6*
514.79	*12*	*12*	*9*	*5*	*5*	*5*	*9*	*9*	*9*
515.80	4	6	1	4	4	4	8	8	8
516.89	*23*	*30*	*33*	*7*	*7*	*7*	*14*	*14*	*14*
519.84	*8*	*10*	*3*	*5*	*5*	*5*	*9*	*9*	*9*
520.71	*3*	*7*	*26*	*6*	*6*	*6*	*11*	*11*	*11*
527.46	26	1	21	1	1	1	*2*	*2*	*2*
[m]	**SD^{ind} [-]**								
290.31	*9*	*15*	*22*	*6*	*7*	*4*	*6*	*10*	*8*
325.83	13	17	26	9	10	7	10	16	11
511.78	*63*	*27*	*26*	*10*	*10*	*8*	*9*	*16*	*14*
514.79	*48*	*47*	*28*	*11*	*12*	*15*	*22*	*23*	*18*
515.80	6	12	5	10	12	10	10	12	17

Depth	Microstrains [-]								
	Rosette 1			Rosette 2			Rosette 3		
[m]	Ax.	Tang.	45°	Ax.	Tang.	45°	Ax.	Tang.	45°
516.89	*26*	*39*	*49*	*11*	*15*	*26*	*34*	*23*	*26*
519.84	*14*	*14*	*8*	*9*	*12*	*9*	*12*	*14*	*12*
520.71	*7*	*17*	*32*	*39*	*23*	*13*	*15*	*16*	*19*
527.46	29	9	26	4	6	5	*7*	*18*	*10*

Table A5-14. Results from re-analysis of biaxial tests in borehole KOV01. Values in brackets include erroneous strain gauges.

Depth	Elastic parameters			
[m]	E^{ind}	δE^{ind}	υ^{ind}	$\delta\upsilon^{ind}$
290.31	74.0	0.7	0.30* (0.32)	0.02
325.83	69.4	3.3	0.24	0.02
511.78	67.9	1.7	0.28	0.01
514.79	68.3	1.8	0.28	0.02
515.80	56.6	0.30	0.23	0.01
516.89	76.9	3.2	0.27	0.01
519.84	74.4	2.6	0.30* (0.35)	0.02
520.71	65.8	1.2	0.30* (0.32)	0.02
527.46	68.3	1.8	0.28	0.02

Values in brackets is exchanged by υ=0.30. The points at 514.79 and 527.46 m is replaced by the average of the 500 m level, i.e. with E=68.3 GPa and ν=0.28.

Appendix 6

Results from calculation of stresses using standard least squares method

A6.1 General about the stress calculation

The results from the stress calculation are based on viewing the data as individual measurement points. Further, strain gauges have only been excluded based on the empirical Chauvenet's criterion; thus, gauges that are likely to be erroneous and are of questionable quality are still included. Consequently, the results should only be regarded as a comparison with the original result, which is based on a different analysis method.

A6.2 Borehole KAS05

Raw stress data has not been found for borehole KAS05

A6.3 KXZSD8HR

Table A6-1. Results from stress calculation using re-analyzed strain data in borehole KXZSD8HR. The published results are presented in brackets. Gauges/rosettes that are of questionable quality are in italic font. ^{T} indicates that the strain data have been temperature corrected.

Borehole depth [m]	Principal stress magnitudes [MPa]			orientations [°N/°]			Elastic parameters [GPa]	[-]
	σ_1	σ_2	σ_3	σ_1	σ_2	σ_3	E	υ
1.29^{T}	*6.5* (9.6)	*4.0* (4.9)	*2.9* (3.1)	*152/5* (169/29)	*262/75* (331/60)	*61/14* (75/8)	65.1 (68)	0.24 (0.30)
1.66	*7.4* (17.6)	*4.8* (14.1)	*1.8* (4.7)	*299/38* (279/68)	*181/30* (148/15)	*65/37* (53/16)	65.1 (83)	0.24 (0.30)
2.40	*5.7* (6.1)	*3.8* (4.3)	*2.6* (2.8)	*318/41* (315/67)	*142/49* (158/21)	*50/2* (65/8)	72.2 (73)	0.28 (0.23)
4.07	*9.9* (12.6)	*8.4* (10.7)	*1.1* (2.0)	*344/35* (346/19)	*142/53* (134/68)	*246/11* (252/11)	65.1 (63)	0.24 (0.24)
5.96	17.1 (23.5)	13.6 (18.3)	5.6 (7.7)	334/10 (333/12)	153/80 (155/78)	244/0 (63/0)	61.1 (74)	0.24 (0.27)
6.61	*8.3* (15.8)	*7.1* (13.4)	*5.0* (8.3)	*319/49* (330/58)	*126/40* (148/32)	*222/6* (239/1)	62.1 (71)	0.21 (0.26)
12.93	*20.2* (24.0)	*10.0* (12.4)	*3.5* (5.0)	*302/5* (304/5)	*40/57* (41/55)	*209/33* (211/34)	61.3 (66)	0.23 (0.27)
14.30	18.3 (21.5)	11.3 (13.0)	5.4 (6.8)	337/3 (336/3)	68/8 (66/6)	228/81 (220/83)	64.0 (65)	0.24 (0.25)
15.60	18.4 (17.1)	14.8 (13.3)	6.1 (4.9)	325/8 (325/8)	233/14 (232/14)	85/74 (84/73)	58.2 (57)	0.28 (0.28)
17.62	16.6 (19.5)	10.8 (12.4)	3.3 (4.1)	343/20 (343/18)	184/69 (187/70)	76/7 (75/8)	66.3 (70)	0.27 (0.26)
18.92	(18.4)	(8.7)	(6.8)	(329/6)	(64/43)	(232/46)	(72)	(0.27)

Borehole depth [m]	Principal stress magnitudes [MPa]			orientations [°N/°]			Elastic parameters [GPa]	[-]
	σ_1	σ_2	σ_3	σ_1	σ_2	σ_3	E	υ
19.57	*17.1* (21.0)	*11.4* (13.3)	*6.6* (8.5)	*303/5* (306/6)	*196/76* (197/76)	*34/13* (37/13)	65.8 (74)	0.23 (0.27)
20.22	14.8 (20.9)	11.5 (15.8)	8.7 (11.9)	331/3 (331/4)	66/60 (67/58)	239/30 (238/32)	55.0 (71.0)	0.27 (0.30)
20.85	12.3 (15.6)	7.8 (10.1)	2.8 (4.4)	170/38 (347/35)	166/52 (160/55)	258/2 (255/4)	55.7 (61)	0.25 (0.28)
21.50	10.0 (11.9)	6.5 (8.2)	1.8 (2.5)	158/35 (161/35)	268/26 (271/26)	26/44 (29/44)	59.9 (64)	0.24 (0.25)
22.21	10.6 (12.5)	5.1 (6.5)	2.1 (3.7)	122/40 (124/37)	259/42 (266/46)	11/23 (18/20)	64.1 (66)	0.27 (0.29)
22.94	*15.2* (14.9)	*9.9* (9.1)	*3.9* (4.0)	*104/30* (104/29)	*308/58* (311/58)	*200/10* (201/12)	66.6 (72)	0.23 (0.25)

Borehole depth [m]	Horizontal stress magnitudes [MPa]			orientations [°N]
	σ_H	σ_h	σ_v	σ_H
1.29[T]	*6.5* (8.5)	*3.0* (3.2)	*4.1* (6.6)	*152* (122)
1.66	*6.1* (14.4)	*3.2* (5.7)	*4.9* (16.3)	*138* (142)
2.40	*4.9* (5.5)	*2.6* (1.5)	*4.4* (7.6)	*139* (144)
4.07	*9.4* (12.4)	*1.4* (2.3)	*8.2* (10.6)	*157* (163)
5.96	17.0 (23.3)	5.6 (7.7)	13.5 (18.6)	154 (153)
6.61	*7.6* (14.1)	*5.0* (8.3)	*7.5* (14.7)	*133* (136)
12.93	*20.1* (23.9)	*5.4* (7.4)	*7.1* (10.3)	*121* (123)
14.30	18.2 (21.4)	11.2 (12.9)	5.6 (6.9)	157 (156)
15.60	18.2 (16.8)	14.2 (12.7)	7.3 (5.7)	149 (149)
17.62	16.0 (18.8)	3.4 (4.3)	11.0 (13.0)	165 (164)
18.92	(18.3)	(7.8)	(7.9)	(148)
19.57	*17.1* (20.9)	*6.8* (8.8)	*11.4* (13.1)	*124* (126)
20.22	14.8 (20.9)	9.4 (13.0)	10.6 (14.8)	150 (150)
20.85	10.6 (13.8)	2.8 (4.4)	8.8 (12.0)	169 (166)
21.50	8.3 (10.0)	4.7 (6.0)	6.6 (6.6)	137 (138)
22.21	8.2 (10.2)	2.8 (4.1)	7.4 (8.2)	113 (118)
22.94	*13.8* (13.5)	*4.2* (4.3)	*10.5* (10.2)	*108* (108)

A6.4 KXZSD81HR

Table A6-2. Results from stress calculation using re-analyzed strain data in borehole KXZSD81HR. The published results are presented in brackets. Gauges/rosettes that are of questionable quality are in italic font.

Borehole depth [m]	Principal stress magnitudes [MPa]			orientations [°N/°]			Elastic parameters [GPa]	[-]
	σ_1	σ_2	σ_3	σ_1	σ_2	σ_3	E	υ
0.86	*18.4* (21.8)	*6.2* (9.2)	*2.2* (2.6)	*302/77* (304/75)	*171/9* (161/12)	*79/10* (69/9)	60.7 (68)	0.28 (0.30)
1.43	*9.7* (11.5)	*6.8* (9.3)	*1.4* (1.2)	*299/68* (310/75)	*160/17* (155/14)	*66/13* (64/6)	*79.1* (65)	*0.28* (0.25)
2.73	13.4 (14.5)	11.9 (12.9)	3.5 (3.8)	333/55 (332/57)	162/35 (162/32)	69/5 (69/5)	59.3 (64)	0.26 (0.27)
3.34	13.0 (14.5)	10.2 (12.1)	3.7 (4.4)	323/42 (312/60)	174/44 (165/26)	68/16 (68/15)	60.6 (66)	0.26 (0.23)

Borehole depth [m]	Horizontal stress magnitudes [MPa]			orientations [°N]
	σ_H	σ_h	σ_v	σ_H
0.86	*6.5* (9.8)	*2.6* (3.0)	*17.1* (20.8)	*165* (156)
1.43	*7.1* (9.4)	*1.9* (1.3)	*9.0* (11.2)	*154* (153)
2.73	12.4 (13.3)	3.5 (3.8)	12.7 (14.0)	159 (158)
3.34	11.7 (12.6)	4.2 (5.0)	10.9 (13.4)	155 (156)

A6.5 KXZSD8HL

Table A6-3. Results from stress calculation using re-analyzed strain data in borehole KXZSD8HL. The published results are presented in brackets. Gauges/rosettes that are of questionable quality are in italic font. ^{T} indicates that the strain data have been temperature corrected.

Borehole depth [m]	Principal stress magnitudes [MPa]			orientations [°N/°]			Elastic parameters [GPa]	[-]
	σ_1	σ_2	σ_3	σ_1	σ_2	σ_3	E	υ
23.37^{T}	*12.4* (18.2)	*5.9* (9.5)	*3.5* (5.1)	*331/26* (325/35)	*222/34* (200/39)	*91/45* (80/32)	68.5 (70)	0.26 (0.30)
24.06	*15.0* (19.7)	*3.7* (9.1)	*-0.53* (7.2)	*329/26* (345/19)	*182/58* (250/16)	*68/17* (122/65)	*65.6* (65)	*0.27* (0.30)
24.75	18.6 (20.2)	8.1 (9.1)	5.2 (5.9)	339/21 (339/20)	206/61 (208/61)	77/19 (77/20)	64.5 (66)	0.25 (0.25)
25.44	18.4 (23.3)	12.0 (12.1)	7.2 (9.2)	315/12 (343/25)	59/47 (92/35)	215/40 (226/44)	64.8 (66)	0.26 (0.26)

Borehole depth [m]	Horizontal stress magnitudes [MPa]			orientations [°N]
	σ_H	σ_h	σ_v	σ_H
23.37^{T}	*10.9* (15.0)	*4.9* (6.7)	*5.5* (11.2)	*156* (154)
24.06	*12.8* (18.4)	*-0.1* (8.9)	*4.6* (8.7)	*152* (166)
24.75	17.2 (18.8)	5.6 (6.4)	8.5 (10.1)	161 (161)
25.44	18.0 (21.0)	9.3 (10.9)	5.6 (12.7)	132 (160)

A6.6 KK0045G01

Table A6-4. Results from stress calculation using re-analyzed strain data in borehole KK0045G01. The published results are presented in brackets. Gauges/rosettes that are of questionable quality are in italic font. [T] indicates that the strain data have been temperature corrected. [1] indicates that the data has been corrected for rotation of rosette (only 31.67 m).

Borehole depth [m]	Principal stress magnitudes [MPa]			orientations [°N/°]			Elastic parameters [GPa]	[-]
	σ_1	σ_2	σ_3	σ_1	σ_2	σ_3	E	υ
2.24[T]	19.8 (17.5)	6.4 (4.9)	4.3 (0.8)	117/5 (128/5)	207/3 (218/1)	328/84 (318/85)	63.2 (59)	0.26 (0.24)
2.70[T]	*21.1* (18.8)	*11.3* (9.8)	*5.8* (5.2)	*301/28* (312/28)	*41/19* (51/17)	*161/55* (169/56)	58.0 (54)	0.20 (0.24)
3.33[T]	20.4 (17.3)	6.2 (6.8)	4.6 (4.0)	298/5 (311/5)	30/20 (44/25)	195/70 (210/64)	61.5 (54)	0.23 (0.30)
4.12[T]	*18.1* (15.3)	*8.6* (7.4)	*3.2* (3.9)	*114/19* (125/17)	*15/23* (32/12)	*250/59* (270/69)	61.5 (54)	0.23 (0.24)
4.53[T]	*19.5* (20.1)	*12.0* (14.6)	*9.7* (11.1)	*104/15* (122/7)	*238/69* (24/50)	*10/15* (217/40)	65.0 (64)	0.25 (0.26)
5.51[T]	*11.4* (24.1)	*10.5* (11.0)	*-4.5* (8.3)	*98/31* (116/27)	*177/18* (344/52)	*242/53* (220/24)	66.2 (63)	0.28 (0.27)
6.07[T]	28.3 (17.2)	16.9 (8.6)	11.4 (4.6)	300/25 (311/23)	74/56 (63/41)	200/22 (200/40)	66.2 (51)	0.28 (0.28)
6.50[T]	*22.2* (14.2)	*11.9* (5.5)	*9.3* (5.1)	*130/2* (322/0)	*32/79* (232/35)	*221/11* (52/55)	66.2 (45)	0.28 (0.19)
8.16[T]	*19.0* (15.1)	*8.1* (6.4)	*4.3* (3.2)	*306/24* (320/18)	*91/61* (105/68)	*209/15* (226/12)	66.2 (53)	0.28 (0.29)
31.67[T,1]	*29.9*	*25.8*	*8.1*	*60/34*	*297/39*	*175/33*	55.8	0.24
34.77[T]	*21.9* (26.1)	*15.5* (17.3)	*6.6* (8.9)	*140/44* (135/39)	*24/24* (19/28)	*275/36* (264/38)	60.6 (66)	0.24 (0.26)
35.48[T]	20.0 (18.1)	14.8 (12.3)	5.1 (5.0)	136/33 (132/29)	14/40 (19/36)	251/33 (251/41)	64.2 (56)	0.25 (0.17)
62.82	*19.9* (28.4)	*8.7* (13.9)	*2.0* (5.9)	*109/9* (107/2)	*10/44* (15/51)	*221/45* (199/39)	53.8 (65)	0.21 (0.26)
63.59[T]	20.6 (23.6)	14.6 (16.8)	7.8 (10.4)	117/24 (118/23)	354/51 (2/45)	221/29 (226/36)	53.8 (55)	0.21 (0.20)
64.51	*29.9* (33.4)	*18.0* (20.3)	*8.3* (12.2)	*109/31* (107/34)	*9/15* (0/24)	*257/55* (242/46)	53.8 (55)	0.21 (0.19)

Borehole depth [m]	Horizontal stress magnitudes [MPa]			orientations [°N]
	σ_H	σ_h	σ_v	σ_H
2.24[T]	19.7 (17.4)	6.4 (4.9)	4.4 (0.9)	117 (128)
2.70[T]	*18.0* (15.9)	*10.5* (9.2)	*9.7* (8.7)	114 (126)
3.33[T]	20.3 (17.2)	6.0 (6.3)	4.9 (4.6)	118 (131)
4.12[T]	*16.7* (14.3)	*7.6* (7.2)	*5.6* (5.1)	*118* (127)
4.53[T]	*19.0* (20.0)	*9.8* (12.5)	*12.4* (13.3)	*103* (123)
5.51[T]	*10.7* (21.3)	*5.4* (8.9)	*0.8* (13.3)	*148* (118)
6.07[T]	26.2 (15.6)	12.2 (6.5)	18.1 (8.3)	117 (126)
6.50[T]	*22.2* (14.2)	*9.4* (5.4)	*11.8* (5.2)	*130* (142)
8.16[T]	*17.2* (14.2)	*4.5* (3.3)	*9.6* (7.1)	*124* (139)
31.67[T,I]	*28.2*	*13.7*	*21.9*	*81*
34.77[T]	*17.5* (21.4)	*10.8* (13.2)	*15.5* (17.7)	*170* (154)
35.48[T]	18.0 (16.2)	8.4 (8.6)	13.5 (10.5)	153 (146)
62.82	*19.5* (28.4)	*5.4* (9.0)	*5.7* (10.8)	*111* (108)
63.59[T]	19.5 (22.3)	9.5 (12.8)	14.0 (15.7)	124 (126)
64.51	*24.8* (27.8)	*16.8* (18.0)	*14.6* (20.1)	*119* (119)

A6.7 KF0093A01

Table A6-5. Results from stress calculation using re-analyzed strain data in borehole KF0093A01. The published results are presented in brackets. Gauges/rosettes that are of questionable quality are in italic font.

Borehole depth [m]	Principal stress magnitudes [MPa]			orientations [°N/°]			Elastic parameters [GPa]	[-]
	σ_1	σ_2	σ_3	σ_1	σ_2	σ_3	E	υ
32.14	*23.0* (32.5)	*7.5* (13.8)	*4.6* (8.7)	*296/31* (295/38)	*82/54* (84/48)	*195/16* (192/16)	51.7 (51)	0.18 (0.19)
32.70	*22.9* (36.0)	*8.7* (17.7)	*3.4* (8.9)	*297/29* (298/37)	*101/61* (102/51)	*203/7* (202/8)	51.7 (60)	0.21 (0.23)
35.38	*12.6* (23.2)	*9.7* (14.2)	*2.5* (6.9)	*285/11* (296/10)	*21/31* (32/30)	*178/57* (190/58)	*44.6* (53)	*0.18* (0.22)

Borehole depth [m]	Horizontal stress magnitudes [MPa]			orientations [°N]
	σ_H	σ_h	σ_v	σ_H
32.14	*18.7* (25.3)	*4.9* (9.2)	*11.4* (20.4)	*114* (111)
32.70	*19.7* (29.2)	*3.5* (9.1)	*11.8* (24.3)	*116* (115)
35.38	*12.4* (22.8)	*7.6* (12.3)	*4.9* (9.2)	*98* (113)

A6.8 KA3579G

Table A6-6. Results from stress calculation using re-analyzed strain data in borehole KA3579G. The published results are presented in brackets. Gauges/rosettes that are of questionable quality are in italic font. [T] indicates that the strain data have been temperature corrected.

Borehole depth [m]	Principal stress magnitudes [MPa]			orientations [°N/°]			Elastic parameters [GPa]	[-]
	σ_1	σ_2	σ_3	σ_1	σ_2	σ_3	E	υ
2.04	17.5 (21.9)	5.3 (7.5)	1.9 (1.1)	297/0 (297/1)	207/56 (205/53)	27/34 (28/37)	58.7 (67)	0.24 (0.27)
2.53[T]	14.4 (18.9)	1.8 (5.3)	-3.8 (-4.2)	302/3 (301/3)	206/57 (203/71)	34/33 (32/19)	58.7 (67)	0.24 (0.27)
3.99	25.3 (26.1)	6.1 (5.3)	5.1 (2.5)	310/16 (311/19)	155/72 (186/59)	42/7 (49/24)	63.1 (63)	0.24 (0.24)
4.54	(26.7)	(6.8)	(2.4)	(297/24)	(177/48)	(42/32)	(67)	(0.27)
5.41	*20.9* (26.1)	*12.7* (10.6)	*2.8* (8.1)	*325/18* (299/23)	*128/72* (174/54)	*233/5* (41/26)	54.6 (55)	0.25 (0.23)
8.00	*22.8* (26.7)	*10.5* (14.8)	*6.6* (13.1)	*300/17* (303/18)	*172/64* (50/42)	*36/20* (196/43)	58.5 (66)	0.22 (0.27)
20.06	*32.2* (34.5)	*14.8* (17.6)	*11.3* (11.4)	*296/1* (115/1)	*34/85* (10/86)	*206/5* (205/4)	70.4 (73)	0.28 (0.30)
21.21	*27.2* (29.0)	*14.3* (15.1)	*7.8* (11.0)	*129/0* (126/0)	*220/50* (216/60)	*39/40* (36/30)	72.5 (73)	0.32 (0.30)
21.70	41.9 (43.7)	20.1 (20.5)	15.7 (15.8)	111/2 (111/2)	218/82 (215/81)	21/8 (20/9)	72.7 (73)	0.26 (0.26)
22.31	*25.9* (30.4)	*16.3* (18.2)	*10.9* (12.7)	*126/10* (121/10)	*262/76* (252/76)	*34/10* (29/11)	61.7 (65)	0.31 (0.30)

Borehole depth [m]	Horizontal stress magnitudes [MPa]			orientations [°N]
	σ_H	σ_h	σ_v	σ_H
2.04	17.5 (21.9)	3.0 (3.4)	4.2 (5.1)	117 (117)
2.53[T]	14.3 (18.8)	-2.1 (-3.2)	0.2 (4.3)	122 (122)
3.99	23.9 (23.9)	5.1 (3.0)	7.6 (7.0)	130 (132)
4.54	(23.3)	(3.8)	(8.8)	(119)
5.41	*20.2* (23.8)	*2.8* (8.7)	*13.4* (12.4)	*144* (121)
8.00	*21.8* (25.5)	*7.1* (13.9)	*11.1* (15.1)	*121* (122)
20.06	*32.2* (34.5)	*11.4* (11.4)	*14.7* (17.5)	*116* (115)
21.21	*27.2* (29.0)	*10.5* (12.0)	*11.6* (14.1)	*129* (126)
21.70	41.8 (43.6)	15.8 (15.9)	20.0 (20.5)	111 (111)
22.31	*25.5* (30.1)	*11.0* (12.9)	*16.4* (18.3)	*126* (120)

A6.9 KOV01

Table A6-7. Results from stress calculation using re-analyzed strain data in borehole KOV01. The published results are presented in brackets. Gauges/rosettes that are of questionable quality are in italic font.

Borehole depth [m]	Principal stress magnitudes [MPa]			orientations [°N/°]			Elastic parameters [GPa]	[-]
	σ_1	σ_2	σ_3	σ_1	σ_2	σ_3	E	υ
290.31	*10.4* (7.6)	*6.2* (3.6)	*-0.0* (-1.8)	*4/48* (5/50)	*247/23* (247/21)	*141/33* (143/32)	*74.0* (66)	*0.30* (0.21)
325.83	30.0 (28.0)	8.1 (7.8)	6.8 (4.9)	295/26 (298/21)	29/9 (39/26)	137/62 (174/55)	*69.4* (66)	*0.24* (0.21)
511.78	*26.7* (25.7)	*2.6* (0.8)	*-0.8* (0.1)	*308/3* (309/2)	*38/6* (174/88)	*193/84* (39/2)	*67.9* (66)	*0.28* (0.26)
514.79	*34.2* (26.1)	*14.8* (4.8)	*2.0* (-3.7)	*321/4* (135/1)	*54/41* (45/34)	*226/49* (226/56)	*68.3* (60)	*0.28* (0.22)
515.80	33.1 (30.8)	10.4 (8.8)	9.0 (6.9)	289/0 (288/1)	19/46 (19/37)	199/44 (197/54)	56.6 (56)	0.23 (0.22)
516.89	*24.0* (22.3)	*9.9* (5.7)	*4.4* (2.1)	*124/2* (124/2)	*225/77* (11/85)	*34/12* (214/5)	*76.9* (79)	*0.27* (0.28)
519.84	*26.5* (25.7)	*7.3* (10.9)	*5.3* (4.0)	*296/6* (300/8)	*50/74* (37/36)	*205/14* (200/51)	*74.4* (77)	*0.30* (0.30)
520.71	*27.8* (25.7)	*14.2* (9.4)	*7.7* (7.3)	-/- (-/-)	-/- (-/-)	-/- (-/-)	*65.8* (66)	*0.30* (0.30)
527.46	*23.6* (26.3)	*16.1* (13.2)	*6.9* (6.1)	*241/5* (242/1)	*103/83* (142/83)	*332/5* (332/7)	*68.3* (66)	*0.28* (0.25)

Borehole depth [m]	Horizontal stress magnitudes [MPa]			orientations [°N]
	σ_H	σ_h	σ_v	σ_H
290.31	*7.3* (4.6)	*2.6* (0.5)	*3.2* (1.4)	*39* (40)
325.83	25.6 (25.1)	8.0 (7.2)	7.5 (8.5)	114 (117)
511.78	*26.6* (25.7)	*2.6* (0.1)	*-0.0* (0.8)	*128* (129)
514.79	*34.1* (26.1)	*9.2* (2.2)	*8.1* (-1.1)	*140* (135)
515.80	33.1 (30.8)	9.7 (8.1)	10.3 (7.6)	109 (108)
516.89	*23.9* (22.3)	*4.6* (2.1)	*10.7* (5.7)	*124* (124)
519.84	*26.2* (25.3)	*5.4* (8.3)	*7.2* (6.9)	*117* (119)
520.71	*27.0* (24.8)	*8.2* (8.0)	*14.0* (9.6)	- (-)
527.46	*23.5* (26.3)	*7.0* (6.2)	*15.9* (13.1)	61 (62)